Forest ecosystems in mountain regions: conditions, risks and impacts

Edited by
Lucian Dinca, Miglena Zhiyanski and Hongxu Wei

Published in
Frontiers in Forests and Global Change

About Frontiers

Frontiers is more than just an open access publisher of scholarly articles: it is a pioneering approach to the world of academia, radically improving the way scholarly research is managed. The grand vision of Frontiers is a world where all people have an equal opportunity to seek, share and generate knowledge. Frontiers provides immediate and permanent online open access to all its publications, but this alone is not enough to realize our grand goals.

Frontiers journal series

The Frontiers journal series is a multi-tier and interdisciplinary set of open-access, online journals, promising a paradigm shift from the current review, selection and dissemination processes in academic publishing. All Frontiers journals are driven by researchers for researchers; therefore, they constitute a service to the scholarly community. At the same time, the *Frontiers journal series* operates on a revolutionary invention, the tiered publishing system, initially addressing specific communities of scholars, and gradually climbing up to broader public understanding, thus serving the interests of the lay society, too.

Dedication to quality

Each Frontiers article is a landmark of the highest quality, thanks to genuinely collaborative interactions between authors and review editors, who include some of the world's best academicians. Research must be certified by peers before entering a stream of knowledge that may eventually reach the public – and shape society; therefore, Frontiers only applies the most rigorous and unbiased reviews. Frontiers revolutionizes research publishing by freely delivering the most outstanding research, evaluated with no bias from both the academic and social point of view. By applying the most advanced information technologies, Frontiers is catapulting scholarly publishing into a new generation.

What are Frontiers Research Topics?

Frontiers Research Topics are very popular trademarks of the *Frontiers journals series*: they are collections of at least ten articles, all centered on a particular subject. With their unique mix of varied contributions from Original Research to Review Articles, Frontiers Research Topics unify the most influential researchers, the latest key findings and historical advances in a hot research area.

Find out more on how to host your own Frontiers Research Topic or contribute to one as an author by contacting the Frontiers editorial office: frontiersin.org/about/contact

Forest ecosystems in mountain regions: conditions, risks and impacts

Topic editors

Lucian Dinca — National Institute for Research and Development in Silviculture INCDS, Romania

Miglena Zhiyanski — Forest Research Institute, Bulgarian Academy of Sciences, Bulgaria

Hongxu Wei — Northeast Institute of Geography and Agroecology, Chinese Academy of Sciences (CAS), China

Table of
contents

Check for updates

Genetic legacy of southern Middle Siberian mountain and foothill populations of Scots pine (*Pinus sylvestris* L.): Diversity and differentiation

Marina Sheller[1,2]*, Endre György Tóth ⓘ [3], Elena Ciocîrlan[2],
Pavel Mikhaylov[1], Andrey Tatarintsev[1], Sergey Kulakov[1,4],
Nadezhda Kulakova[1], Natalia Melnichenko[1], Aleksey Ibe[5],
Tatyana Sukhikh[5] and Alexandru Lucian Curtu[2]

[1]Scientific Laboratory of Forest Health, Reshetnev Siberian State University of Science and Technology,
Krasnoyarsk, Russia, [2]Faculty of Silviculture and Forest Engineering, Transilvania University of Brasov,
Brasov, Romania, [3]Forest Research Institute (FRI), University of Sopron (UOS), Sárvár, Hungary,
[4]Sukachev Institute of Forest SB RAS, Federal Research Center, Krasnoyarsk Science Center SB RAS,
Krasnoyarsk, Russia, [5]Branch of the Russian Centre of Forest Health − Centre of Forest Health of
Krasnoyarsk krai, Krasnoyarsk, Russia

Scots pine (*Pinus sylvestris* L.) is a widespread and economically important tree species in Eurasia. Southern Siberian, Scots pine mountain and foothills forests are especially valuable natural objects that help to stabilize environmental conditions. Due to the associated impact of natural and anthropogenic factors, the habitats of the species in southern Siberia are constantly shrinking. In this regard, the study of genetic diversity and structure of Scots pine forests in southern Siberia is very relevant. Here, we studied the genetic diversity and structure of eight Scots pine populations located in southern Middle Siberia (Russia). A high level of genetic diversity (H_E=0.518) was detected in the studied populations. No recent bottleneck effect, isolation by distance or isolation-by-environment were detected. Most genetic diversity was found within populations, while only 7% of genetic diversity occurred among populations. Both STRUCTURE analysis and UPGMA clustering showed two genetic groups. Two populations from the Minusink basin and a population from the Western Sayan Mts. formed the first group and the second group was composed of the other populations from Kuznetsk Alatau Mts., Central Tuva basin and Todzha basin. Our findings suggest that the studied Scots pine populations originate from different gene pools. The pattern of genetic diversity revealed by our study may be useful for the elaboration of conservation measures of genetic resources of Scots pine in southern Middle Siberia.

KEYWORDS

Scots pine, *Pinus sylvestris* L., nuclear microsatellite markers (nSSR), genetic diversity, genetic structure, Middle Siberia

1. Introduction

Genetic diversity is recognized as one of three basic components of biodiversity, i.e., the genes, species and ecosystems (Hoban et al., 2020). It plays an important role in species adaption to changing climate, habitats, and biotic interactions (Spielman et al., 2004). Furthermore, it helps to maintain ecosystem functions, stability and services (Hoban et al., 2020). The

characterization of genetic diversity pattern within species and among populations is a fundamental requirement for the establishment of programs aimed at biodiversity preservation (Belletti et al., 2017).

Scots pine (*Pinus sylvestris* L.) is one of the most widespread conifers in the world, which has great economic and ecological importance (Floran et al., 2011). Within its vast distribution, Scots pine grows in various soil and climatic conditions. It forms over 20 geographical races and about 100 forms and varieties (Ekart et al., 2014). A significant part of its range is located on the territory of Siberia where permafrost and forest fires determine the northern and southern boundaries of the species' area of distribution. At the same time, the impact of fires has not only negative, but also positive consequences; it ensures the removal of ground cover that prevents the germination of pine seeds, as well as the mineralization of sandy and gravelly soils (Sannikov, 1992; Pimenov, 2015). In the south of Siberia, pine forests are classified as especially valuable natural objects that stabilize environmental conditions. The maximum spectrum of adaptive variations for Scots pine is observed in this part of the region. Relict morpho-and genotypes of Scots pine can still be preserved in the south of Siberia (Pimenov, 2015). In Asia, Scots pine growing in the south of 52°N was identified as a steppe Scots pine variety (*Pinus sylvestris* var. *mongholica* Litv.) (The Plant List, 2023; World Flora Online, 2023), which most often known as Syn.: *P. s. ssp. Kulundensis* (Pravdin, 1964). *P. s.* var. *mongholica* is exceptionally resistant to adverse conditions and, growing on the sandy shores of salt lakes, can tolerate slight salinization of the soil (Zvereva, 2017). In the southern border of the species` distribution range in Siberia Scots pine forms island-like and ribbon-like forests and due to the structure and location features, they can serve as important objects for studying such processes as isolation, selection, genetic drift, mutation and inbreeding (Novikova and Zhamyansuren, 2012).

In recent decades, due to the combined effect of natural and anthropogenic factors, the dieback of coniferous forests in the south of Siberia has become catastrophic (Bazhina, 2010; Pavlov et al., 2011). For instance, by the end of the last century, due to root rot damage, as well as wind damage, forest fire, sanitary cuttings, Minusinsk pine forests (Minusinsk basin) suffered on an area of 28 thousand hectares (Tatarintsev et al., 2015). Over the past decade, in Khamar-Daban mountain range (the south of Lake Baikal) 40% of Siberian stone pine (*Pinus sibirica* Du Tour) forests has died because of bacterial infection caused by *Erwinia* sp. and *Pseudomonas* sp. and damages caused by *Dendrolimus sibiricus* Tschetw (Stavnikov, 2013; Voronin et al., 2013). Furthermore, since 1970s, there has been an intensive dieback of Siberian fir (*Abies sibirica* Ledeb.) in the mountains of Southern Siberia (Khamar Daban Mts., Western and Eastern Sayan Mts.) (Tretyakova et al., 2008). In this regard, the study of genetic diversity and structure of coniferous forests in the south of Siberia is very relevant.

Population genetic studies of Scots pine based on isoenzyme, chloroplast DNA markers show the evidence of genetic heterogeneity of pine populations in the south of Siberia (Sannikov and Petrova, 2012; Ekart et al., 2014; Semerikov et al., 2014). This is mainly due to the island type of the species' range in the steppes of Southern Transbaikalia, Northern Mongolia and its mountainous island type in the mountains of Southern Siberia and the Amur region (Sannikov and Petrova, 2012).

In this study, we used nuclear SSR markers to explore the genetic diversity and structure of Scots pine populations in southern Middle Siberia. Specifically, we aimed to: (a) assess the patterns of genetic

diversity within and among populations, (b) test whether genetic differentiation is related to climatic variables.

2. Materials and methods

2.1. Plant material

Initially, 210 Scots pine individuals were sampled from eight populations located in southern Middle Siberia (Russia) on a vast territory covering the mountain and foothill forests of the Western Sayan Mts., Kuznetsk Alatau Mts. and forest-steppe and steppe landscapes of the Minusinsk basin, Todzha basin and Central Tuva basin (Table 1; Figure 1). Due to amplification failures, the number of studied individuals was reduced to 169.

2.2. DNA extraction and microsatellite analysis

Total genomic DNA was isolated according to the CTAB method (Doyle and Doyle, 1990). The quality and quantity of the extracted DNA was measured with a Nanodrop 8,000 spectrophotometer (Thermo Fisher Scientific, United States), then adjusted to a concentration of 10 ng/µL. Seven nuclear microsatellite primers were selected: Psyl16, Psyl42, Psyl44, Psyl57 (Sebastiani et al., 2012); PtTX2146 (Elsik et al., 2000); lw_isotig04306, lw_isotig07383 (Fang et al., 2014). All primers were combined into two multiplex sets: set 1 consisted of Psyl44, Psyl57 and lw_isotig04306; set 2 comprised of Psyl16, Psyl42, PtTX2146, and lw_isotig07383. Reverse primers were labelled with a fluorescent dye. Polymerase chain reaction (PCR) was performed in a 10 µL reaction volume using Qiagen Multiplex PCR Kits (Qiagen, Germany) under the manufacturer's instructions. Amplification was performed in a Corbett thermal cycler (Corbett Research, Australia) with the following cycling parameters: an initial denaturation at 95°C for 5 min, followed by 32 cycles of denaturation at 95°C for 30 s, annealing at 58°C for 90 s, extension at 72°C for 50 s and a final extension at 72°C for 7 min. Then, the amplified fragments were run on a GenomeLab GeXP genetic analyzer (Beckman Coulter, Fullerton, CA) with an internal size standard. Genotyping was

TABLE 1 Geographic location of eight Scots pine populations in southern Middle Siberia.

Pop ID	Locality	N	Latitude/ Longitude	Altitude (m)
SAR-1	Kuznetsk Alatau Mts.	29	55.00/89.40	550–560
SAR-2	Kuznetsk Alatau Mts.	26	54.87/89.22	500–520
PER-1	Minusinsk basin	20	53.28/92.00	294–295
PER-2	Minusinsk basin	20	53.28/91.97	286–288
KER	Western Sayan Mts.	20	52.12/92.23	707–710
TOD	Todzha basin	18	52.72/95.74	860–980
BAL-1	Central Tuva basin	22	51.08/95.09	970–1,060
BAL-2	Central Tuva basin	24	51.02/95.28	880–890

Sample size (N).
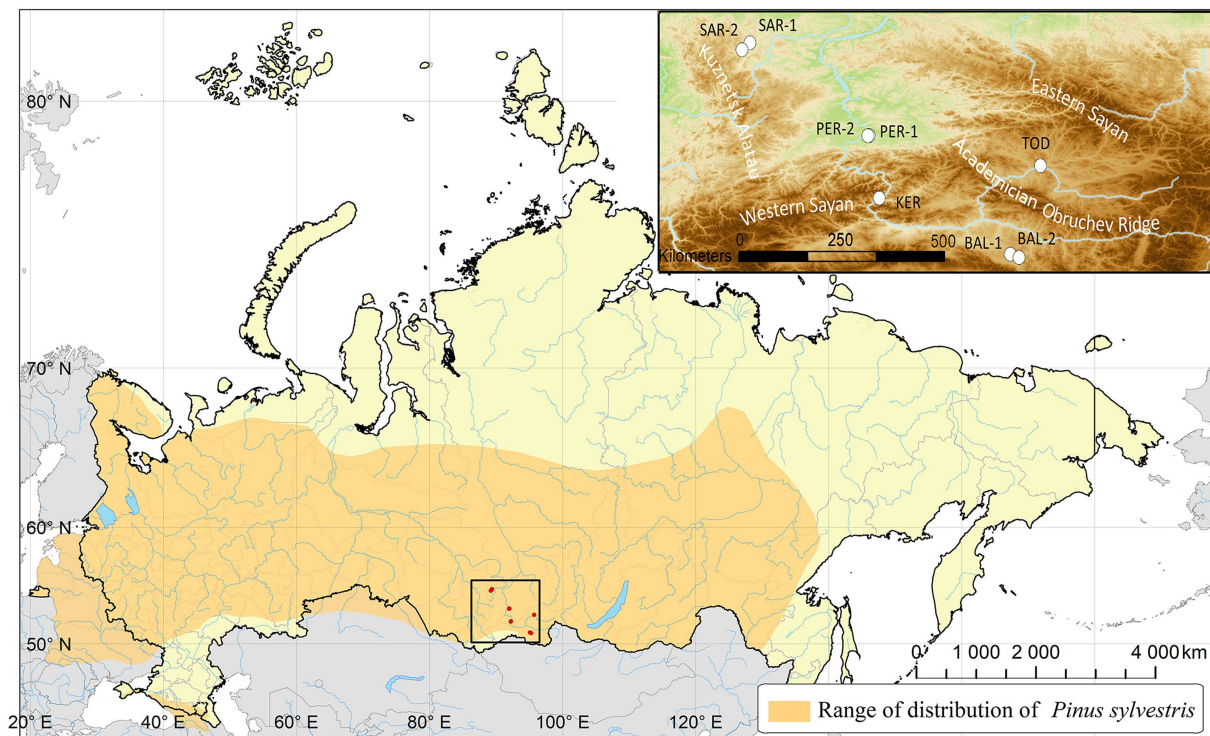
FIGURE 1
Location of the studied Scots pine populations in southern Middle Siberia.

performed with the GenomeLab GeXP software (Version 10.2, Beckman Coulter, Fullerton, CA).

2.3. Data analysis

Genetic diversity per locus and population was estimated by using GenAlEx v. 6.5 software (Peakall and Smouse, 2006). The number of alleles (N_A); number of effective alleles (N_E); inbreeding coefficient of an individual relative to the subpopulation (F_{IS}); inbreeding coefficient of an individual relative to the total population (F_{IT}); genetic differentiation coefficient (F_{ST}); observed heterozygosity (H_O); expected heterozygosity (H_E) were calculated. The allelic richness (A_R) was computed in R (R Core Team, 2013) using the "hierfstat" package (Goudet, 2005). Presence of null alleles and possible genotyping errors was checked using Micro-Checker software (Van Oosterhout et al., 2006). No evidence of null alleles or genotyping errors was found in the populations.

BOTTLENECK software v.1.2.02 (Piry et al., 1999) was used to test for recent population bottlenecks on the basis of the infinite allele model (IAM). Statistical significance was determined by two-tailed Wilcoxon signed-rank test with 1,000 iterations.

Analysis of molecular variance (AMOVA) was performed using the software GenAlEx v. 6.5. The significance of differences was tested by 999 permutations. The unweighted pair-group method with arithmetic mean (UPGMA) was applied to perform cluster analysis on the Nei's genetic distances data (Nei, 1978) and a Principal Coordinates Analysis (PCoA) was conducted using the "FactoMineR"

package in R (Lê et al., 2008) to compare genetic differentiation among populations.

A Bayesian clustering approach implemented in STRUCTURE v.2.3.4 was used to estimate the number of clusters in the nSSR dataset (Pritchard et al., 2000). The analysis was performed with an admixture model with correlated allele frequencies and a LOCPRIOR setup. K value was set to 1–10 with a burn-in period of 100,000 iterations followed by 500,000 Monte Carlo Markov repetitions. Twenty repetitions were set for each run. The number of clusters was estimated using ΔK parameter according to Evanno et al. (2005) using the STRUCTURE HARVESTER program (Earl and Vonholdt, 2012). To average the results of the replicated runs, the CLUMPP software v.1.1.2. was used (Jakobsson and Rosenberg, 2007).

SAMOVA software v.2.0 (Dupanloup et al., 2002) was used to identify groups of populations that are maximally differentiated from each other. Runs were conducted with the number of groups set from two to seven, performing 100 independent simulated annealing processes. The maximum F_{CT} value was chosen as the indicator of the best grouping.

Followed by the detection of genetic clusters, Genetic Landscape Shape Interpolation analysis was carried out, as implemented in Alleles in Space (Miller, 2005), to produce a surface plot that shows major genetic discontinuities, indicating probable contact areas between the detected genetic clusters. On the surface plot, positive peaks indicate areas with high genetic discontinuities (high genetic distances) and negative peaks represent of areas with genetic similarities (low genetic distances).

To detect the presence of isolation by distance (IBD), the correlation between geographical distances and genetic distances between population pairs was tested with Mantel test (Mantel, 1967). The test was performed with the "adegenet" R package with 1,000 bootstrap replicates (Jombart, 2008).

To test whether climatic variation contributed to the patterns of genetic differentiation, i.e., to test the isolation-by-environment (IBE) hypothesis (Wang and Bradburd, 2014), three different approaches were taken. First, in addition to the genetic and geographic distances calculated for IBD, Euclidean climatic distances were calculated from recent (c. 1950–2000) climate data using 19 bioclimatic variables (Supplementary Table S1) which were extracted from the global climate layer data using a grid size of 30 arc-seconds and downloaded from the WorldClim v.1.4 database.[1] After, genetic, geographic, and the climatic distances were used in Mantel, partial-Mantel and MMRR (Multiple Matrix Regression with Randomization) regression analyses. The partial-Mantel test was conducted using the "vegan" package (Oksanen et al., 2022), while the MMRR carried out using the custom script of Wang (2013). The MMRR R script is deposited in the Dryad Data Repository under DOI:10.5061/dryad.kt71r.

3. Results

Using seven nuclear microsatellite loci, we identified a total of 49 alleles in the 169 individuals (Supplementary Table S2). The average number of alleles per locus (N_A) was seven. F_{IS} ranged from -0.055 (Psyl42) to 0.249 (Psyl44). The values of genetic differentiation (F_{ST}) varied in the range between 0.028 (lw_isotig07383) to 0.111 (Psyl42).

The mean number of alleles present per population varied from 3.571 (BAL-2) to 5.143 (PER-1 and SAR-1) (Table 2). Effective number of alleles (N_E) ranged between 2.191 in KER population and 2.910 in PER-2 population, with an average of 2.517 per population. Shannon Information Index (I) varied from 0.891 (BAL-1) to 1.118 (PER-2) population. The BAL-2 population had the lowest values for allelic richness ($A_R = 3.571$) and PER-1 population had the highest value ($A_R = 4.764$). The values of expected heterozygosity (H_E) ranged from 0.472 (BAL-1) to 0.565 (PER-2). The inbreeding coefficient (F_{IS}) values were between -0.161 and 0.229, but in general placed around zero in most of the populations. The value of the number of migrants per generation was high ($Nm = 5.690$) indicates high gene flow between populations. The ratio of observed and expected heterozygosity was balanced (mean H_O: $H_E = 0.510$: 0.518).

The population stability analysis revealed no evidence for recent bottlenecks in the studied populations.

We performed AMOVA among and within Scots pine populations (Supplementary Table S3) and the results showed that the genetic variation among populations was 7%, whereas most of genetic variation occurred within populations (93%, $p < 0.001$).

The matrix of pairwise F_{ST} values (Figure 2A) revealed that the highest differentiation apparent between KER, PER-1, PER-2 and SAR-1, SAR-2 and BAL-1 populations, while the lowest between KER, PER-1, PER-2 populations. Similarly, the UPGMA clustering indicated two groups. The first group consisted of PER-1, PER-2 and KER populations and the second group was composed of the five remaining Scots pine populations (Figure 2B).

The Bayesian STRUCTURE analysis revealed two Scots pine gene pools in the south of Middle Siberia (Figure 3), based on the Mean L(K) (±SD) and ΔK values. Group I included PER-1, PER-2 and KER populations, whereas Group II included all remaining populations.

Principal Coordinates Analysis (PCoA) based on the F_{ST} values identified two major groups (Supplementary Figure S1) at Dim. 1 vs. Dim. 2, explaining jointly 74.01% of the total variation for the nSSR markers. One group included populations from the Minusinsk basin (PER-1 and PER-2) and the Western Sayan Mts. (KER). The second group contained five populations from the Kuznetsk Alatau Mts. (SAR-1 and SAR-2), the Central Tuva basin (BAL-1 and BAL-2) and the Todzha Basin (TOD). The second and third axes (Dim. 2 vs. Dim. 3) explained much less, only 31.69% of the total variation and grouped SAR-1 and SAR-2 with PER-1 and PER-2 populations.

Genetic Landscape Spatial Interpolation has detected a significant barrier to gene flow in the form of a genetic discontinuity in the contact zone between the genetic lineages in this region (Figure 4). The estimation of the contribution of genotypes in each population showed that the PER-1, PER-2 and KER populations contained a higher proportion of genotypes originated from the Minusinsk basin, compared to other samples from the Kuznetsk Alatau Mts. (SAR-1 and SAR-2), the Central Tuva basin (BAL-1 and BAL-2) and the Todzha basin (TOD).

Spatial analysis of molecular variance (SAMOVA) produced values of F_{CT} ranging from 0.0305 ($K = 3$) to a maximal value of 0.03336 ($K = 6$), which indicated number 6 to be the preferred number of genetically homogenous clusters for the whole dataset (Supplementary Table S4). The six defined clusters contained the following populations: (I) PER-1 and PER-2; (II) BAL-1; (III) BAL-2; (IV) SAR-1 and SAR-2; (V) KER; (VI) TOD.

We further analyzed the correlation between genetic distance and geographic distance for the studied populations using the Mantel test. The results showed no correlation between genetic differentiation and geographical distance among Scots pine populations ($R^2 = 0.043$, $p = 0.163$). In addition, none of the matrix regression approaches (Mantel, partial-Mantel, and MMRR) to investigate IBE, were able to find significant relationships between the genetic, geographic and climatic distances (Supplementary Table S5).

4. Discussion

Forest fragmentation is constantly increasing in southern Siberia due to intensive logging, livestock grazing, as well as drought-and fire-related forest declines, and has been detected for many forest species (Wirth et al., 1999; González de Andrés et al., 2022). Fragmentation of forest landscapes causes isolation, and poses genetic and ecological threats to populations (Gustafson et al., 2010; Khansaritoreh et al., 2018; Erasmi et al., 2021). Conservation and rational use of Siberian forest genetic resources is one of the most important environmental and economic tasks. The effectiveness of solving this problem depends on the degree of knowledge of forest genetic resources. Unfortunately, despite some success, Siberian forest genetic resources have not been studied enough (Tarakanov and Krutovsky, 2016). Here, we assessed the genetic diversity and structure of eight southern Siberian Scots pine populations.

---

1 http://www.worldclim.org/

TABLE 2 Genetic statistics averaged across seven microsatellite loci for each Scots pine population.

Population		N_A	N_E	I	A_R	H_O	H_E	F_{IS}	Bottleneck
KER	Mean	4.143	2.191	0.909	3.861	0.443	0.474	0.066	0.563
		(±0.595)	(±0.317)	(±0.174)	(±0.588)	(±0.087)	(±0.089)	(±0.043)	
PER-1	Mean	5.143	2.655	1.094	4.764	0.543	0.535	−0.013	0.688
		(±0.800)	(±0.444)	(±0.208)	(±0.783)	(±0.108)	(±0.099)	(±0.065)	
PER-2	Mean	4.857	2.910	1.118	4.510	0.421	0.565	0.229	0.578
		(±0.670)	(±0.587)	(±0.202)	(±0.686)	(±0.086)	(±0.094)	(±0.079)	
SAR-1	Mean	5.143	2.740	1.069	4.255	0.557	0.534	−0.011	0.688
		(±0.705)	(±0.458)	(±0.203)	(±0.565)	(±0.122)	(±0.105)	(±0.058)	
SAR-2	Mean	4.571	2.579	1.037	4.179	0.495	0.522	0.049	0.078
		(±0.685)	(±0.452)	(±0.199)	(±0.635)	(±0.098)	(±0.098)	(±0.051)	
BAL-1	Mean	4.286	2.209	0.891	3.768	0.552	0.472	−0.161	0.688
		(±0.474)	(±0.362)	(±0.164)	(±0.488)	(±0.096)	(±0.083)	(±0.045)	
TOD	Mean	4.571	2.632	1.061	4.352	0.571	0.538	−0.056	0.813
		(±0.528)	(±0.398)	(±0.188)	(±0.559)	(±0.105)	(±0.096)	(±0.038)	
BAL-2	Mean	3.571	2.217	0.918	3.571	0.500	0.506	0.075	0.078
		(±0.429)	(±0.272)	(±0.126)	(±0.463)	(±0.092)	(±0.063)	(±0.119)	
Total mean		4.536	2.517	1.012	4.158	0.510	0.518	0.022	
		(±0.216)	(±0.143)	(±0.062)	(±0.596)	(±0.034)	(±0.031)	(±0.027)	

N_A, number of alleles; N_E, number of effective alleles; I, Shannon Information Index; A_R, allelic richness; Ho, observed heterozygosity; H_E, expected heterozygosity; F_{IS}, fixation index; ±, standard deviation.

FIGURE 2
Heatmap of pairwise Fst (Nei, 1978) values (A) and bootstrapped UPGMA tree (B) of the eight Scots pine populations investigated.
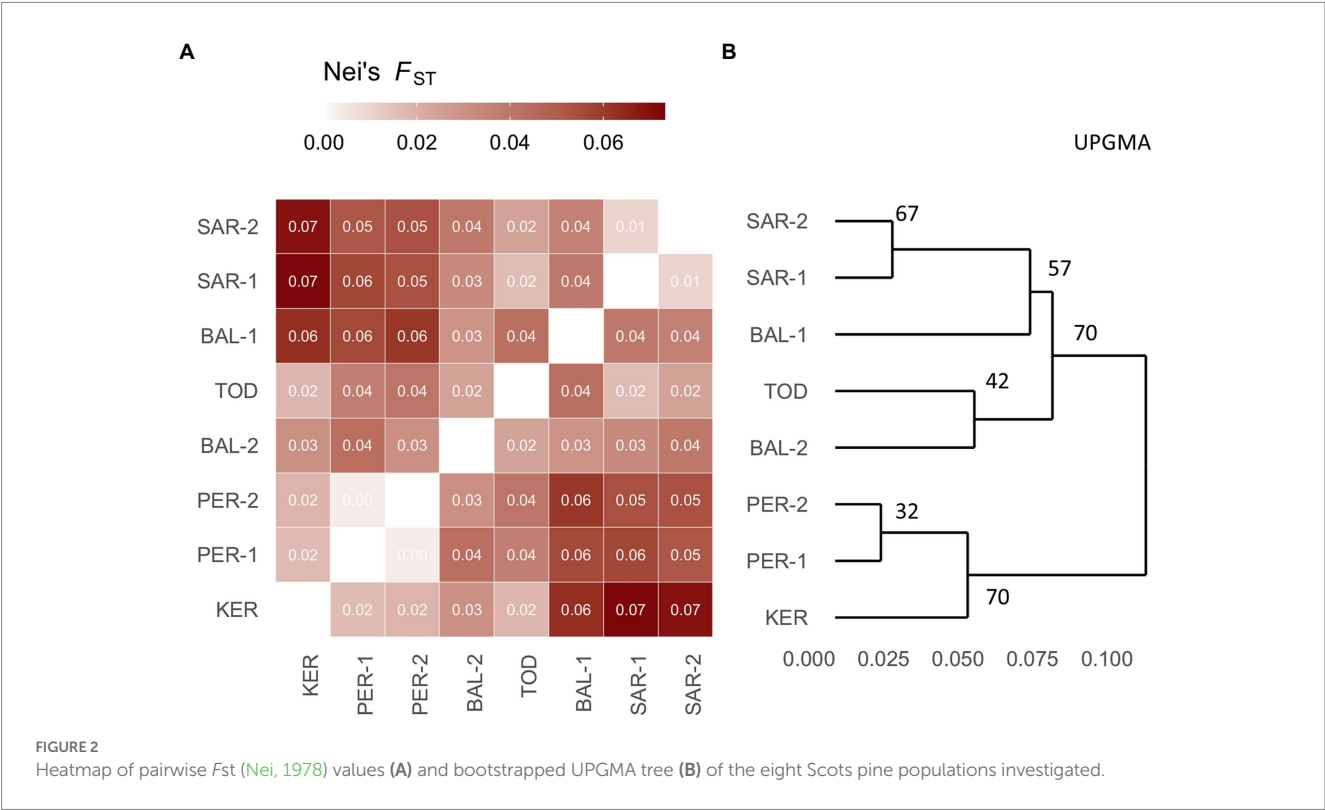
Our results showed that, despite the detectable effects of fragmentation, the level of genetic diversity in Scots pine populations in southern Middle Siberia is high ($H_E = 0.518$) and is similar to the other Scots pine populations in Middle Siberia ($H_E = 0.514$) (Sheller et al., 2023). At the same time, our estimates are lower than those observed in other studies of Scots pine from Italy ($H_E = 0.81$) (Scalfi et al., 2009), Romania and Hungary ($H_E = 0.55$) (Bernhardsson et al., 2016), Turkey ($H_E = 0.772$) (Bilgen and Nuray, 2017), and Lithuania
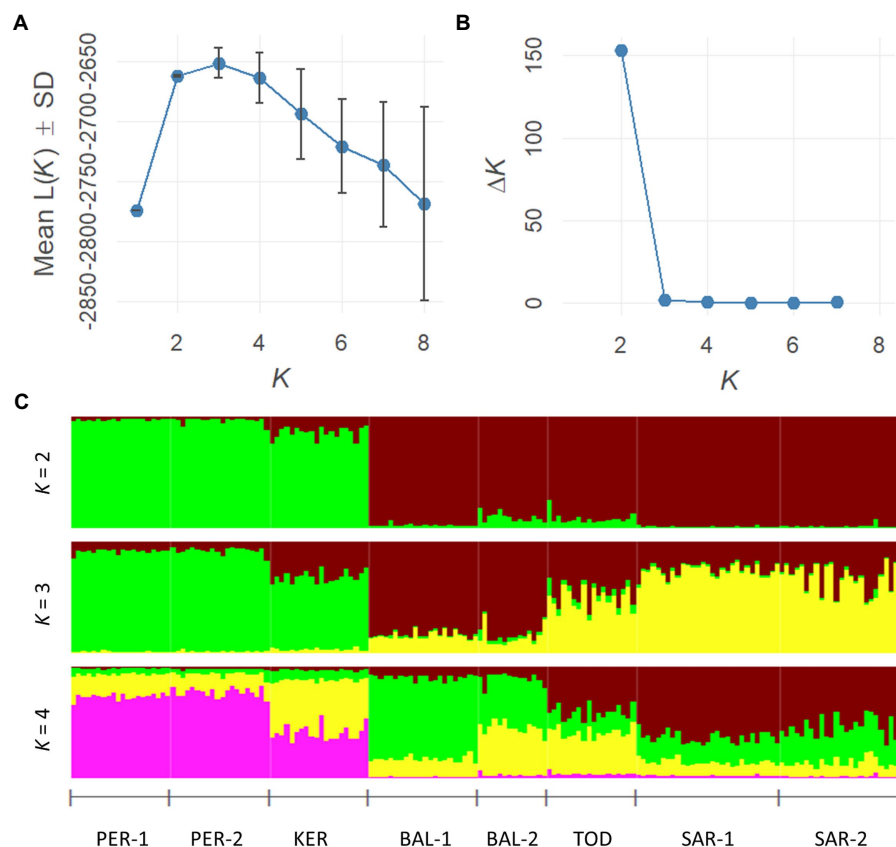
FIGURE 3
Estimation of the best subpopulation numbers based on Mean L(K) (±SD) and ΔK values **(A,B)**. Genetic structural plot of eight Scots pine populations (acronyms are as in Table 1) **(C)**.
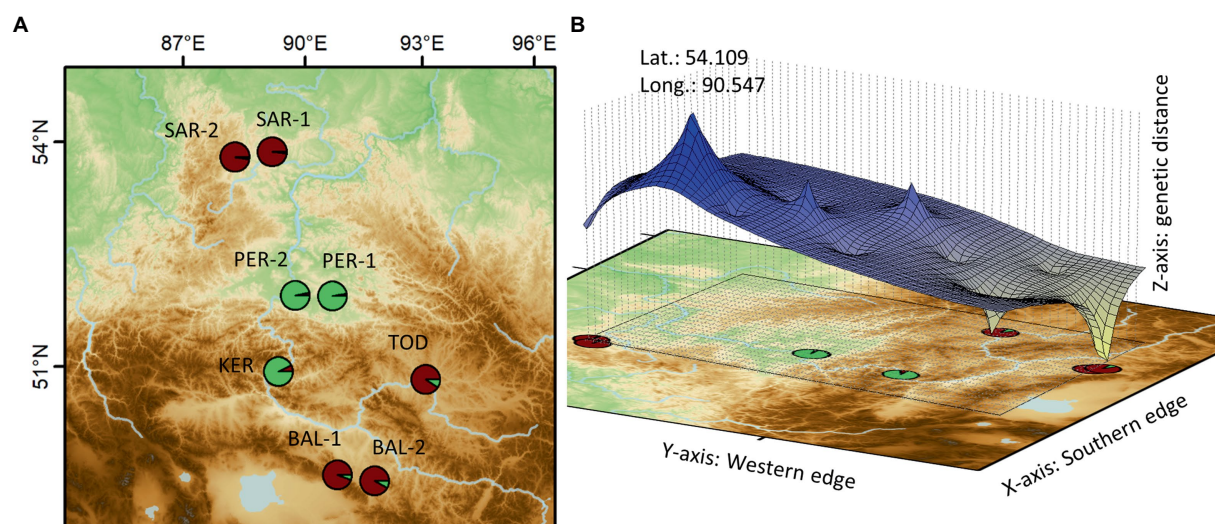
FIGURE 4
Spatial extent of the detected genetic clusters **(A)** and the genetic discontinuity revealed by the Genetic Landscape Shape Interpolation analysis **(B)** (for the acronyms, see Table 1).

($H_E = 0.59$) (Kavaliauskas et al., 2022). The highest level of genetic diversity and allelic richness were detected in PER-2 and PER-1 populations ($H_E = 0.565$ and $A_R = 4.764$ respectively) located in the

Minusinsk basin. PER-1 and PER-2 populations represent geographically isolated pine forests, which are unique in their origin and ecological functions (Polyakova, 2008; Tatarintsev et al., 2015).

The Minusinsk basin populations are distributed on the territory of the National Park "Sushenshky Forest," which is specially protected natural area of national importance. The extrazonal ribbon-like Scots pine forests are particularly valuable natural objects of the National Park "Sushenshky Forest" (Pate, 2020). The obtained results indicate the need to maintain the genetic variability of these valuable Scots pine forests in the Minusinsk basin. In the study by Ekart et al., 2014 the highest values of heterozygosity (Ho and H_E) were also found in Scots pine population from the Minusinsk basin.

Gene flow is one of the most important factors that maintains genetic diversity and improves population fitness and/or adaptive potential and decrease extinction probability especially in small populations (Berthaud et al., 2001; O'Connell et al., 2007). We detected high number of migrants (Nm) indicating substantial gene flow among the studied populations, also the ration of expected and observed heterozygosity was balanced, indicating neither inbreeding nor isolation-breaking effects. This hypothesis was further supported by the inbreeding coefficient, with an overall mean of $F_{IS} = 0.022$, which generally indicated random mating of individuals.

However, toward the south the pattern of genetic diversity changes, and considerably lower levels of genetic diversity were found. Expected heterozygosity and allelic richness in two southernmost populations, BAL-1 and BAL-2, were $H_E = 0.472$ and $A_R = 3.571$, respectively. These populations are located in the Central Tuva basin and belong to Balgazyn relict pine forest. It is possible that the adverse effects of the extremely continental climate of Central Asia and the anthropogenic factors in the area of the Balgazyn pine forest, which is steadily shrinking, contributed to the decreased diversity. For instance, due to fires, natural forests decreased by four times in the last 25 years (1988–2014) (Kuular et al., 2015). Decrease of population size, due to fires and logging, diseases and environmental pollution leads to the reduction of genetic diversity (Ellstrand and Elam, 1993). In the study by Sheller et al. (2021) the lowest level of chloroplast DNA haplotype diversity was also detected in one of the Balgazyn Scots pine populations, confirming the need the conservation of these genetic resources.

Our estimate on total genetic variation occurring among populations showed a 7% applying AMOVA, which is considerably high, by taking into account the relatively short geographical distances among some of the populations (from 3 to 593 km). In similar microsatellite studies, but on a larger geographical scales, Shuvaev et al. (2022) found a F_{ST} value of only 0.026 in Scots pine populations in Krasnoyarsk region (Middle Siberia) and Sheller et al. (2023) found a F_{ST} value of 0.097 among distant Scots pine populations in Russia. Based on allozyme analysis, Sannikov and Petrova (2012) revealed that the genetic differentiation of Scots pine populations in the southern part of the range (south of 52°–53° latitude) in Central and Eastern Siberia is 2–4 times higher than in the contiguous forest zone. By decomposing our F_{ST} value among populations, based on pairwise estimates, majority of differentiation was found between populations located in the Kuznetsk Alatau Mts. (SAR-1 and SAR-2), the Minusinsk basin (PER-1 and PER-2), and the Western Sayan (KER).

The results obtained through the utilization of regression approaches (Mantel, partial-Mantel, MMRR) did not reveal a significant association between genetic differentiation and either geographic or climatic distances. This finding suggests that genetic differentiation may be attributed to past demographic events, rather than the specific environmental conditions of the region where the population resides.

Our Bayesian and the spatial clustering approaches (STRUCTURE and SAMOVA) were consistent with the F_{ST} estimates. The STRUCTURE analysis divided the studied populations into two main groups ($K = 2$), with PER-1, PER-2 and KER forming one group and the remaining five populations forming another group. The Minusinsk basin and the Western Sayan populations (PER-1, PER-2 and KER) wedged among the members of the other genetic group. However, toward the south they showed mixing, albeit at an extremely low proportion. This was evident also on our pairwise F_{ST} estimates, because lower F_{ST} values were typical here than toward the north, in the direction of the West Siberian Plain. We assume that this genetic differentiation across the landscape provided evidence of a contact zone of distinct genetic lineages, and a sharp boundary limiting gene flow, of a wedged population group. The genetic specificity of many population groups in marginal parts of the species' distribution range was also observed in Iberia, Transcaucasia, Asia Minor and Eastern Siberia (Prus-Glowacki and Stephan, 1994; Sinclair et al., 1999; Sannikov et al., 2005; Cheddadi et al., 2006; Naydenov et al., 2007; Pihäjärvi et al., 2008; Dering et al., 2017, 2021; Sheller et al., 2023). At the same time, a significant homogeneity of populations was revealed within certain regions of Scandinavia, Central, Western and Eastern Europe, Siberia (Goncharenko et al., 1993; Zhelev et al., 1994; Sinclair et al., 1999; Robledo-Arnuncio et al., 2005; Cheddadi et al., 2006; Pihäjärvi et al., 2008; Semerikov et al., 2018; Sheller et al., 2021, 2023).

It should be noted, as an interesting fact, that SAMOVA indicated six different groups, and dissected the population groups in the same order as F_{ST} decreases. First separated the Minusinsk basin and the Western Sayan populations (PER-1, PER-2, and KER), from the remaining ones, and so on. This shows that the primary barrier to restriction of gene flow is located here. Our Genetic Landscape Spatial Interpolation concurs with this, having identified a significant barrier to gene flow in the form of a genetic discontinuity in the contact zone between the genetic lineages in this region.

However, this pattern changes as we move toward the south. It is known, that an increase in F_{ST} indicates a decrease in number of migrants (Nm) and vice versa (Whitlock and McCauley, 1999). In line with this, we observed that there was less differentiation to the south, potentially indicating increased gene flow. Historical and contemporary gene flow between genetic lineages, of the same species, has been described in many species (McDermott and McDonald, 1993; Ottenburghs, 2020), and it has been known to cause introgression (i.e., admixture), through hybridization and backcrossing (Petit and Excoffier, 2009). However, in this case increased genetic diversity is expected (Pazouki et al., 2016; Dering et al., 2017). In contrast, our observations revealed a discrepancy in the southern populations. Despite the notable degree of differentiation, the level of genetic diversity was found to be low, for example in BAL-1 and BAL-2 (described above). It is plausible that these populations are relict, since the legacy of long-term isolation is characterized by low genetic diversity. Such relict populations generally harbor low levels of allelic and haplotypic variation, have limited adaptive potential for range expansion and increased risk of extinction (Rinaldi et al., 2019; Urbaniak et al., 2019; Méndez-Cea et al., 2023). However, to rule out misclassification of these southern populations, further investigations targeting past demography, gene flow and introgression are required.

5. Conclusion

In our study, we assessed the genetic diversity and population structure of eight Scots pine populations in southern Middle Siberia using seven nuclear SSR markers. The study has revealed genetic heterogeneity of Scots pine populations near the southern boundaries of the species distribution in Middle Siberia. Despite fragmentation, the studied populations preserved high genetic diversity. The highest level of genetic diversity and allelic richness was detected in two populations from the Minusinsk basin while the lowest level of genetic diversity and allelic richness was found in two southernmost populations, which belong to a relict Balgazyn pine forest in the Central Tuva basin. However, to confirm a relictary status of Balgazyn pine forest additional studies should be carried out. Two clustering methods showed that the Minusinsk basin and the Western Sayan populations formed a distinct genetic group. The pattern of genetic diversity suggests a different origin of the studied Scots pine populations. However, further investigation is needed to study the evolutionary history of Scots pine populations in southern Siberia.

Data availability statement

The original contributions presented in the study are included in the article/Supplementary material, further inquiries can be directed to the corresponding author.

Author contributions

MS and AC designed the experiment. EC performed laboratory work. MS and ET analyzed the data. MS wrote the manuscript. ET reviewed and edited the manuscript. SK, AT, NK, AI, TS, NM, and PM collected the samples. All authors contributed to the article and approved the submitted version.

Conflict of interest

The authors declare that the research was conducted in the absence of any commercial or financial relationships that could be construed as a potential conflict of interest.

Publisher's note

All claims expressed in this article are solely those of the authors and do not necessarily represent those of their affiliated organizations, or those of the publisher, the editors and the reviewers. Any product that may be evaluated in this article, or claim that may be made by its manufacturer, is not guaranteed or endorsed by the publisher.

Supplementary material

The Supplementary material for this article can be found online at: https://www.frontiersin.org/articles/10.3389/ffgc.2023.1152850/full#supplementary-material

References

Bazhina, E. V. (2010). On the factors of Abies sibirica drying in the southern Siberia mountains. *News Irkutsk State Univ.* 3, 20–25.

Belletti, P., Ferrazzini, D., Ducci, F., De Rogatis, A., and Mucciarelli, M. (2017). Genetic diversity of Italian populations of Abies alba. *Dendrobiology* 77, 147–159. doi: 10.12657/denbio.077.012

Bernhardsson, C., Floran, V., Ganea, S. L., and García-Gil, M. R. (2016). Present genetic structure is congruent with the common origin of distant scots pine populations in its Romanian distribution. *For. Ecol. Manag.* 361, 131–143. doi: 10.1016/j.foreco.2015.10.047

Berthaud, J., Clément, J. C., Emperaire, L., Louette, D., Pinton, F., Sanou, J., et al. (2001). "The role of local level gene flow in enhancing and maintaining genetic diversity" in *Broadening the genetic base of crop production*. eds. H. D. Cooper, C. Spillane and T. Hodgkin (New York, NY: CABI Publishing in Association with FAO and IPGRI), 81–103.

Bilgen, B. B., and Nuray, K. (2017). Genetic diversity among *Pinus sylvestris* L. populations and its implications for genetic conservation: Comparison of nuclear and chloroplast microsatellite markers. *Fresenius Environ. Bull.* 26, 6873–6881.

Cheddadi, R., Vendramin, G. G., Litt, T., François, L., Kageyama, M., Lorentz, S., et al. (2006). Imprints of glacial refugia in the modern genetic diversity of *Pinus sylvestris*. *Glob. Ecol. Biogeogr.* 15, 271–282. doi: 10.1111/j.1466-822X.2006.00226.x

Dering, M., Baranowska, M., Beridze, B., Chybicki, I. J., Danelia, I., Iszkuło, G., et al. (2021). The evolutionary heritage and ecological uniqueness of scots pine in the Caucasus ecoregion is at risk of climate changes. *Sci. Rep.* 11:22845. doi: 10.1038/s41598-021-02098-1

Dering, M., Kosiński, P., Wyka, T. P., Pers-Kamczyc, E., Boratyński, A., Boratyńska, K., et al. (2017). Tertiary remnants and Holocene colonizers: Genetic structure and phylogeography of scots pine reveal higher genetic diversity in young boreal than in relict Mediterranean populations and a dual colonization of Fennoscandia. *Divers. Distrib.* 23, 540–555. doi: 10.1111/ddi.12546

Doyle, J. J., and Doyle, J. L. (1990). Isolation of plant DNA from fresh tissue. *Focus* 12, 13–15.

Dupanloup, I., Schneider, S., and Excoffier, L. (2002). A simulated annealing approach to define the genetic structure of populations. *Mol. Ecol.* 11, 2571–2581. doi: 10.1046/j.1365-294X.2002.01650.x

Earl, D. A., and Vonholdt, B. M. (2012). Structure harvester: A website and program for visualizing STRUCTURE output and implementing the Evanno method. *Conserv. Genet. Resour.* 4, 359–361. doi: 10.1007/s12686-011-9548-7

Ekart, A. K., Larionova, A. Y., Kravchenko, A. N., Tikhonova, I. V., Zatsepina, K. G., Tarakanov, V. V., et al. (2014). Genetic diversity and differentiation of scots pine populations in southern Siberia and Mongolia. *Contemp. Probl. Ecol.* 7, 52–59. doi: 10.1134/S1995425514010041

Ellstrand, N. C., and Elam, D. R. (1993). Population genetic consequences of small population size: Implications for plant conservation. *Annu. Rev. Ecol. Syst.* 24, 217–242. doi: 10.1146/annurev.es.24.110193.001245

Elsik, C. G., Minihan, V. T., Hall, S. E., Scarpa, A. M., and Williams, C. G. (2000). Low-copy microsatellite markers for *Pinus taeda* L. *Genome* 43, 550–555. doi: 10.1139/g00-002

Erasmi, S., Klinge, M., Dulamsuren, C., Schneider, F., and Hauck, M. (2021). Modelling the productivity of Siberian larch forests from Landsat NDVI time series in fragmented forest stands of the Mongolian forest-steppe. *Environ. Monit. Assess.* 193, 1–18. doi: 10.1007/s10661-021-08996-1

Evanno, G., Regnaut, S., and Goudet, J. (2005). Detecting the number of clusters of individuals using the software STRUCTURE: A simulation study. *Mol. Ecol.* 14, 2611–2620. doi: 10.1111/j.1365-294X.2005.02553.x

Fang, P., Niu, S., Yuan, H., Li, Z., Zhang, Y., Yuan, L., et al. (2014). Development and characterization of 25 454 EST-SSR markers in *Pinus sylvestris* var. mongolica (Pinaceae). *Appl. Plant Sci.* 2:455. doi: 10.3732/apps.1300057

Floran, V., Sestras, R. E., and Garcia-Gil, M. R. (2011). Organelle genetic diversity and Phylogeography of scots pine (*Pinus sylvestris* L.). *Not. Bot. Horti Agrobot. Cluj-Napoca* 39, 317–322. doi: 10.15835/nbha3916103

Goncharenko, G. G., Silin, A. E., and Padutov, V. E. (1993). Investigation of the genetic structure and level of differentiation in *Pinus sylvestris* L. in central and regional populations of Eastern Europe and Siberia. *Genetics* 29, 2019–2037.

González de Andrés, E., Shestakova, T. A., Scholten, R. C., Delcourt, C. J., Gorina, N. V., and Camarero, J. J. (2022). Changes in tree growth synchrony and resilience in Siberian *Pinus sylvestris* forests are modulated by fire dynamics and ecohydrological conditions. *Agric. For. Meteorol.* 312:108712. doi: 10.1016/j.agrformet.2021.108712

Goudet, J. (2005). Hierfstat, a package for R to compute and test hierarchical F-statistics. *Mol. Ecol. Notes* 5, 184–186. doi: 10.1111/j.1471-8286.2004.00828.x

Gustafson, E. J., Shvidenko, A. Z., Sturtevant, B. R., and Scheller, R. M. (2010). Predicting global change effects on forest biomass and composition in south-central Siberia. *Ecol. Appl.* 20, 700–715. doi: 10.1890/08-1693.1

Hoban, S., Bruford, M., D'Urban, J. J., Lopes-Fernandes, M., Heuertz, M., Hohenlohe, P. A., et al. (2020). Genetic diversity targets and indicators in the CBD post-2020 global biodiversity framework must be improved. *Biol. Conserv.* 248:108654. doi: 10.1016/j.biocon.2020.108654

Jakobsson, M., and Rosenberg, N. A. (2007). CLUMPP: A cluster matching and permutation program for dealing with label switching and multimodality in analysis of population structure. *Bioinformatics* 23, 1801–1806. doi: 10.1093/bioinformatics/btm233

Jombart, T. (2008). Adegenet: An R package for the multivariate analysis of genetic markers. *Bioinformatics* 24, 1403–1405. doi: 10.1093/bioinformatics/btn129

Kavaliauskas, D., Danusevičius, D., and Baliuckas, V. (2022). New insight into genetic structure and diversity of scots pine (*Pinus sylvestris* L.) populations in Lithuania based on nuclear, chloroplast and mitochondrial DNA markers. *Forests* 13:1179. doi: 10.3390/f13081179

Khansaritoreh, E., Schuldt, B., and Dulamsuren, C. (2018). Hydraulic traits and tree-ring width in Larix sibirica Ledeb. as affected by summer drought and forest fragmentation in the Mongolian forest steppe. *Ann. For. Sci.* 75, 1–12.

Kuular, H. B., Namzyn, S. A., and Hertek, S. B. (2015). Monitoring of the Balgazyn forest according to remote sensing data. News of higher educational institutions. *Geodesy Aerial Photogr.* 3, 67–72.

Lê, S., Josse, J., and Husson, F. (2008). FactoMineR: An R package for multivariate analysis. *J. Stat. Softw.* 25, 1–18. doi: 10.18637/jss.v025.i01

Mantel, N. A. (1967). The detection of disease clustering and a generalized regression approach. *Cancer Res.* 27, 209–220.

McDermott, J. M., and McDonald, B. A. (1993). Gene flow in plant pathosystems. *Annu. Rev. Phytopathol.* 31, 353–373. doi: 10.1146/annurev.py.31.090193.002033

Méndez-Cea, B., García-García, I., Gazol, A., Camarero, J. J., de Andrés, E. G., Colangelo, M., et al. (2023). Weak genetic differentiation but strong climate-induced selective pressure toward the rear edge of mountain pine in North-Eastern Spain. *Sci. Total Environ.* 858:159778. doi: 10.1016/j.scitotenv.2022.159778

Miller, M. P. (2005). Alleles in space (AIS): computer software for the joint analysis of interindividual spatial and genetic information. *J. Hered.* 96, 722–724. doi: 10.1093/jhered/esi119

Naydenov, K., Senneville, S., Beaulieu, J., Tremblay, F., and Bousquet, J. (2007). Glacial variance in Eurasia: Mitochondrial DNA evidence from scots pine for a complex heritage involving genetically distinct refugia at mid-northern latitudes and in Asia minor. *BMC Evol. Biol.* 7, 233–235. doi: 10.1186/1471-2148-7-233

Nei, M. (1978). Estimation of average heterozygosity and genetic distance from a small number of individuals. *Genetics* 89, 583–590. doi: 10.1093/genetics/89.3.583

Novikova, T. N., and Zhamyansuren, S. (2012). Scotch pine seed quality variability near southern limits of its spread in Siberia and Mongolia. *Bull. KrasSAU* 4, 102–107.

O'Connell, L. M., Mosseler, A., and Rajora, O. P. (2007). Extensive long-distance pollen dispersal in a fragmented landscape maintains genetic diversity in white spruce. *J. Hered.* 98, 640–645. doi: 10.1093/jhered/esm089

Oksanen, J., Blanchet, F.G., Friendly, M., Kindt, R., Legendre, P., McGlinn, D., et al. (2022). Package 'vegan': community ecology package. Available at: https://cran.r-project.org/web/packages/vegan/index.html

Ottenburghs, J. (2020). Ghost introgression: Spooky gene flow in the distant past. *BioEssays* 42:2000012. doi: 10.1002/bies.202000012

Pate, E. Y. (2020) *Stories of the Shushensky forest.* Verkhny Tagil: Ural Provincial Publishing House, 207.

Pavlov, I. N., Barabanova, O. A., and Ageev, A. A. (2011). Resistance reduction of fir-cedar forests of eastern Sayan Mountains to root pathogens. *Russ. For. J.* 4, 40–45.

Pazouki, L., Shanjani, P. S., Fields, P. D., Martins, K., Suhhorutšenko, M., Viinalass, H., et al. (2016). Large within-population genetic diversity of the widespread conifer *Pinus sylvestris* at its soil fertility limit characterized by nuclear and chloroplast microsatellite markers. *Eur. J. For. Res.* 135, 161–177. doi: 10.1007/s10342-015-0928-5

Peakall, R., and Smouse, P. E. (2006). GenAlEx 6: Genetic analysis in excel. Population genetic software for teaching and research. *Mol. Ecol. Notes* 6, 288–295. doi: 10.1111/j.1471-8286.2005.01155.x

Petit, R. J., and Excoffier, L. (2009). Gene flow and species delimitation. *Trends Ecol. Evol.* 24, 386–393. doi: 10.1016/j.tree.2009.02.011

Pihäjärvi, T., Salmela, M. J., and Savolainen, O. (2008). Colonization routes of *Pinus sylvestris* inferred from distribution of mitochondrial DNA variation. *Tree Genet. Genomes* 4, 247–254. doi: 10.1007/s11295-007-0105-1

Pimenov, A.V. (2015). *Biodiversity of the scots pine (Pinus sylvestris L.) in contrasting ecotopes of the south of Siberia.* dissertation/doctoral thesis. Krasnoyarsk: Sukachev Forest Institute of the Siberian Branch of the Russian Academy of Sciences.

Piry, S., Luikart, G., and Cornuet, J. M. (1999). BOTTLENECK: A computer program for detecting recent reductions in the effective population size using allele frequency data. *J. Hered.* 90, 502–503. doi: 10.1093/jhered/90.4.502

Polyakova, M. A. (2008). Vegetation of ribbon forests of the Minusinsk basin. dissertation/PhD thesis. Novosibirsk: Central Botanical Garden SB RAS.

Pravdin, L. F. (1964). *Scots pine.* Moscow: Nauka.

Pritchard, J., Stephens, M., and Donnelly, P. (2000). Inference of population structure using multilocus genotype data. *Genetics* 155, 945–959. doi: 10.1093/genetics/155.2.945

Prus-Glowacki, W., and Stephan, B. R. (1994). Genetic variation of *Pinus sylvestris* from Spain in relation to other European populations. *Silvae Genet.* 43, 7–14.

R Core Team. (2013). *R: A language and environment for statistical computing.* Vienna: R Foundation for Statistical Computing.

Rinaldi, R., Cafasso, D., Strumia, S., Cristaudo, A., Sebastiani, F., and Fineschi, S. (2019). The influence of a relict distribution on genetic structure and variation in the Mediterranean tree, Platanus orientalis. *AoB Plants.* 11:plz002. doi: 10.1093/aobpla/plz002

Robledo-Arnuncio, J. J., Collada, C., Alia, R., and Gil, L. (2005). Genetic structure of montane isolates of *Pinus sylvestris* L. in a Mediterranean refugial area. *Biogeographica* 32, 595–605. doi: 10.1111/j.1365-2699.2004.01196.x

Sannikov, S. N. (1992). *Ecology and geography of natural renewal of scots pine.* Nauka: Moscow.

Sannikov, S. N., and Petrova, I. V. (2012). Phylogenogeography and genotaxonomy of *Pinus sylvestris* L. populations. *Ecology* 4, 252–260.

Sannikov, S. N., Petrova, I. V., Sannikova, N. S., and Philippova, T. V. (2005). Gradient genogeographic analysis of *Pinus sylvestris* L. populations in Europe. *Ecology* 6, 415–420.

Scalfi, M., Piotti, A., Rossi, M., and Piovani, P. (2009). Genetic variability of Italian southern scots pine (*Pinus sylvestris* L.) populations: The rear edge of the range. *Eur. J. Forest Res.* 128, 377–386. doi: 10.1007/s10342-009-0273-7

Sebastiani, F., Pinzauti, F., Kujala, S. T., González-Martínez, S. C., and Vendramin, G. G. (2012). Novel polymorphic nuclear microsatellite markers for *Pinus sylvestris* L. *Conserv. Genet. Resour.* 4, 231–234. doi: 10.1007/s12686-011-9513-5

Semerikov, V. L., Semerikova, S. A., Dymshakova, O. S., Zatsepina, K. G., Tarakanov, V. V., Tikhonova, I. V., et al. (2014). Microsatellite loci polymorphism of chloroplast DNA of scots pine (*Pinus sylvestris* L.) in Asia and Eastern Europe. *Russ. J. Genet.* 50, 577–585. doi: 10.1134/S1022795414040127

Semerikov, V., Semerikova, S., Putintseva, J., Tarakanov, V., Tikhonova, I., Vidyakin, A., et al. (2018). Colonization history of scots pine in Eastern Europe and North Asia based on mitochondrial DNA variation. *Tree Genet. Genomes* 14, 1–7. doi: 10.1007/s11295-017-1222-0

Sheller, M., Ciocîrlan, E., Mikhaylov, P., Kulakov, S., Kulakova, N., Ibe, A., et al. (2021). Chloroplast DNA diversity in populations of *P. sylvestris* L. from Middle Siberia and the Romanian Carpathians. *Forests* 12:1757. doi: 10.3390/f12121757

Sheller, M., Tóth, E. G., Ciocîrlan, E., Mikhaylov, P., Kulakov, S., Kulakova, N., et al. (2023). Genetic diversity and population structure of scots pine (*Pinus sylvestris* L.) in middle Siberia. *Forests* 14:119. doi: 10.3390/f14010119

Shuvaev, D. N., Ibe, A. A., Shcherba, Y. E., Sukhikh, T. V., Shilkina, E. A., Sheller, M. A., et al. (2022). Molecular genetic characteristics of scots pine populations in Krasnoyarsk region by panel of 15 nuclear microsatellite loci. *Forestry* 5, 530–539.

Sinclair, W. T., Morman, J. D., and Ennos, R. A. (1999). The postglacial history of scots pine (*Pinus sylvestris* L.) in western Europe: Evidence from mitochondrial DNA variation. *Mol. Ecol.* 8, 83–88. doi: 10.1046/j.1365-294X.1999.00527.x

Spielman, D., Brook, B. W., and Frankham, R. (2004). Most species are not driven to extinction before genetic factors impact them. *Proc. Natl. Acad. Sci. U. S. A.* 101, 15261–15264. doi: 10.1073/pnas.0403809101

Stavnikov, D. (2013). Analysis of sanitary and forest pest status of forests in republic of Buryatia. *Environ. Manage. Cadastres* 31, 67–73.

Tarakanov, V. V., and Krutovsky, K. V. (2016). Conservation of Siberian forest genetic resources: A brief review of the materials of the IV international meeting (Barnaul, august 24-29, 2015). *Sib. For. J.* 5, 7–11.

Tatarintsev, A. I., Kalenskaya, O. P., and Bublikov, A. G. (2015). On the issue of root rot infestation of pine forests of the Minusinsk basin. *Conif. Boreal Zone* 5, 240–247.

The Plant List. (2023). Available at: (http://www.theplantlist.org/).

Tretyakova, I. N., Bazhina, E. V., Pakharkova, N. V., and Storozhev, V. N. (2008). The condition of fir-cedar forests of the Ergaki Nature Park and their fluorescent diagnostics. *Conif. Boreal Zone* 3, 237–243.

Urbaniak, L., Wojnicka-Półtorak, A., Celiński, K., Lesiczka, P., Pawlaczyk, E., and Aučina, A. (2019). Genetic resources of relict populations of *Pinus sylvestris* (L.) in Western Carpathians assessed by chloroplast microsatellites. *Biologia* 74, 1077–1086. doi: 10.2478/s11756-019-00255-6

Van Oosterhout, C., Weetman, D., and Hutchinson, W. F. (2006). Estimation and adjustment of microsatellite null alleles in nonequilibrium populations. *Mol. Ecol. Notes* 6, 255–256. doi: 10.1111/j.1471-8286.2005.01082.x

Voronin, V. I., Morozova, T. I., Stavnikov, D. Y., Nechesov, I. A., Oskolkov, V. A., Buyantuev, V. A., et al. (2013). Bacterial damage of Siberian stone pine forests in the Baikal region. *Forestry* 3, 39–41.

Wang, I. J. (2013). Examining the full effects of landscape heterogeneity on spatial genetic variation: A multiple matrix regression approach for quantifying geographic and ecological isolation. *Evolution* 67, 3403–3411. doi: 10.1111/evo.12134

Wang, I. J., and Bradburd, G. S. (2014). Isolation by environment. *Mol. Ecol.* 23, 5649–5662. doi: 10.1111/mec.12938

Whitlock, M. C., and McCauley, D. E. (1999). Indirect measures of gene flow and migration: FST$\neq$ 1/(4Nm+ 1). *Heredity* 82, 117–125. doi: 10.1038/sj.hdy.6884960

Wirth, C., Schulze, E. D., Schulze, W., von Stunzner-Karbe, D., Ziegler, W., Miljukova, I. M., et al. (1999). Above-ground biomass and structure of pristine Siberian scots pine forests as controlled by competition and fire. *Oecologia* 121, 66–80. doi: 10.1007/s004420050908

World Flora Online (2023). Available at: http://www.worldfloraonline.org. (Accessed January 21, 2023).

Zhelev, P., Longauer, R., Paule, L., and Gömöry, D. (1994). Genetic variation of the indigenous scots pine (*Pinus sylvestris* L.) population from the Rhodopi mountains. *Nauka-za-go-rata.* 31, 68–76.

Zvereva, G. K. (2017). Structural adaptation of chlorophyll parenchyma of *Pinus sylvestris* L. needles in the south of Western Siberia. In Proceedings of the 16th International Scientific and Practical Conference, Barnaul, Russia, 2017 Jun 5–8.

Floristic composition, life history traits and phytogeographic distribution of forest vegetation in the Western Himalaya

Shiekh Marifatul Haq[1]*, Aadil Abdullah Khoja[2], Fayaz A. Lone[3], Muhammad Waheed[4], Rainer W. Bussmann[1,5], Eman A. Mahmoud[6] and Hosam O. Elansary[7]*

[1]Department of Ethnobotany, Institute of Botany, Ilia State University, Tbilisi, Georgia, [2]Department of Botany, Glocal University Saharanpur, Saharanpur, India, [3]Department of Botany, Government Degree College (Women), Kupwara, India, [4]Department of Botany, University of Okara, Okara, Pakistan, [5]Department of Botany, Institute of Life Sciences, State Museum of Natural History, Karlsruhe, Germany, [6]Department of Food Industries, Faculty of Agriculture, Damietta University, Damietta, Egypt, [7]Department of Plant Production, College of Food and Agriculture Sciences, King Saud University, Riyadh, Saudi Arabia

Introduction: Scientific documentation of the qualitative forest vegetation parameters of a biogeographical area provides baseline information to guide conservation strategies and design policies for biodiversity management regulations.

Methods: We present one of the most comprehensive qualitative vegetation analyses to evaluate the entire structure and function of an ecosystem in the remote northern part of the Kashmir Himalaya, India. Several multivariate ecological community analyses were conducted after determining the presence of plant species in the various habitats using a random sampling technique.

Results: In total, 155 plant species belonging to 120 genera and 49 families occurred in the area. Asteraceae was the largest family (12% of plant species) followed by Rosaceae (11%). The patterns of species distribution across families were uneven, with 50% of the species belonging to only 7 families, and 23 families being monotypic. In terms of functional groups, the herbaceous growth form dominated. Therophytes were the dominant life form, indicating that the vegetation was disturbed. According to the phytogeographical research, 65% of the species documented in the study area were native, 15% were invasive, 14% naturalized, and 5% being casual. The majority (30%) of exotic species were reported along roadsides. Of all the species found, 39% grew in their natural habitats, such as forests, and 11% were scattered along roadsides. Plant species were grouped in five different clusters based on their floristic similarity. According to the estimated diversity indices, natural forest has the greatest values for Shannon's and Simpson's index. We found that the study area serves as the natural habitat for several significant, endangered medicinal plants, including *Arnebia benthamii, Bergenia ciliata, Delphinium roylei, Gentiana kurroo, Phytolacca acinosa, Saussurea costus*, and *Trillium govanianum*. Therefore, we recommend that human intervention in natural regeneration efforts be prioritized in these habitats to increase the population of these species.

Conclusion: Examining species features from the perspective of functional groups contributes to our understanding of the ecological aspects of the flora. It may also be useful in developing management plans to ensure long-term management of forest landscapes in this remote Himalayan region.

Introduction

Floristic diversity is an important element of ecosystems (Hua et al., 2022). This diversity includes the plant species diversity of a particular area representing the local flora of a given area (Qian et al., 2021). Taxonomy is concerned with their identification and classification of species (Barkley et al., 2004). Floristic and taxonomic studies provide efficient information about different aspects of an ecosystem, including nomenclature, distribution, ecology and utility of plant species of an area (Grime et al., 2014; Haq et al., 2022d). While information on plants of many regions has long been available online via checklists (Safidkon et al., 2003), comprehensive floristic studies are still necessary to document the whole plant diversity of any geographic region (Noss, 1983). Lack of such studies strongly limits the scientific inquiry into plants (Kier et al., 2005), and is needed to ultimately understand how plant communities are structured and distributed.

Among the various ecological attributes of plant communities, floristic composition and ecological diversity are the most important ones that are influenced by a variety of biotic and abiotic factors (Khan et al., 2018; Solefack et al., 2018). The understanding of linkages among plants diversity and its ecological functions is critical for understanding the adjustment of plant communities, and how they adopt toward specific habitats (Rahman et al., 2019a; Altaf et al., 2022). Lifeform and habit are the two important physiognomic features that are being widely used while investigating vegetation (Haq et al., 2019). Studying functional plant traits of a given region is an important tool that helps in understanding the relationship between environmental variables and plant community structure and distribution, ultimately revealing the biological functions of individual species in a community (Vakhlamova et al., 2016).

The Himalayan Mountain Range is a prominent biogeographic ecoregion that shows great variation in topography and climate, and thus harbors significant plant diversity (Olson et al., 2001). This mountain ecosystem has been recognized as a global biodiversity hotspot due to its significant biodiversity and huge endemism (Myers et al., 2000). The Kashmir Himalaya, part of Indian Himalayan Region, has been considered as a promising floristic region with high endemism (Mahar et al., 2009). Nonetheless, many remote areas of this biodiversity-rich region have not received much attention as far as floristic and ecological investigations are concerned, which is especially the case of remote mountains region in Kashmir Himalayas. The capability and productivity of the Himalayan forest ecosystem have decreased as a result of numerous stressors, including anthropogenic factors (such as over-exploitation of forest resources and the spread of invasive species), environmental (climate, slope, soil), fire incidences, and declining biological diversity (Haq et al., 2020). Floristic and ecological studies are crucial to advancing our understanding of the distribution and composition of plant communities in biodiversity hotspots. It is crucial and most effective to record qualitative forest vegetation parameters in order to preserve floristic diversity in the future and utilize biological resources sustainably. Keeping this in view, we focused on the following objectives: (i) to record the floristic composition of the vegetation in the region. (ii) What are the patterns of the emergent ecological traits groups in the flora in this region (iii) to find out the contribution of native and alien elements in the region vegetation and (iv) to find out the forest species pool shows habitat filtering in the region.

Given the ecological and economic significance of the forest vegetation under consideration, the findings of this study can guide sustainable biodiversity management and habitat restoration, particularly in invaded habitats in this Himalayan region, with global implications.

Materials and methods

Research area

The study area one of the remotest Tehsil of District Bandipore, Jammu and Kashmir, India. The Gurez valley is situated in the high-altitude Kashmir Himalaya, about 86 kms from Bandipore and 146 kms from the regions summer capital (Srinagar) (**Figure 1**). The Gurez valley is at an altitude of ranges from 2,400 to 3,500 masl and is mostly inhabited by Pahari and Gujjar tribes. The study area includes fifteen Panchayats (village administrative units) with about 30,000 inhabitants. Dawar is known as the main town in the area. Due to heavy snowfall (approx. 1.5–1.8 m), the area remains disconnected from the rest of the region for about 6 months a year, as Razdan Pass is completely closed in the winter. It has a dry and mild climate. The valley is vital for wildlife tourism because it is surrounded by high mountains and steep gorges that are drained by the Kishanganga River. It also supports a variety of vegetation, dense forests, and a wealth of species.

Field survey

Frequent surveys were conducted to obtain a better understanding of the research area and field data were collected during in various expeditions 2019–2021. Sites for the floristic studies were chosen using a random sampling technique to guarantee that plant species from various habitats had an equal chance of being sampled. The quadrat method was used to record

FIGURE 1
Map of study area **(A)** India **(B)** Jammu and Kashmir **(C)** Bandipora district and point showing the Gurez Valley in the Kashmir Himalaya, India (generated using ArcGIS version,10.5).
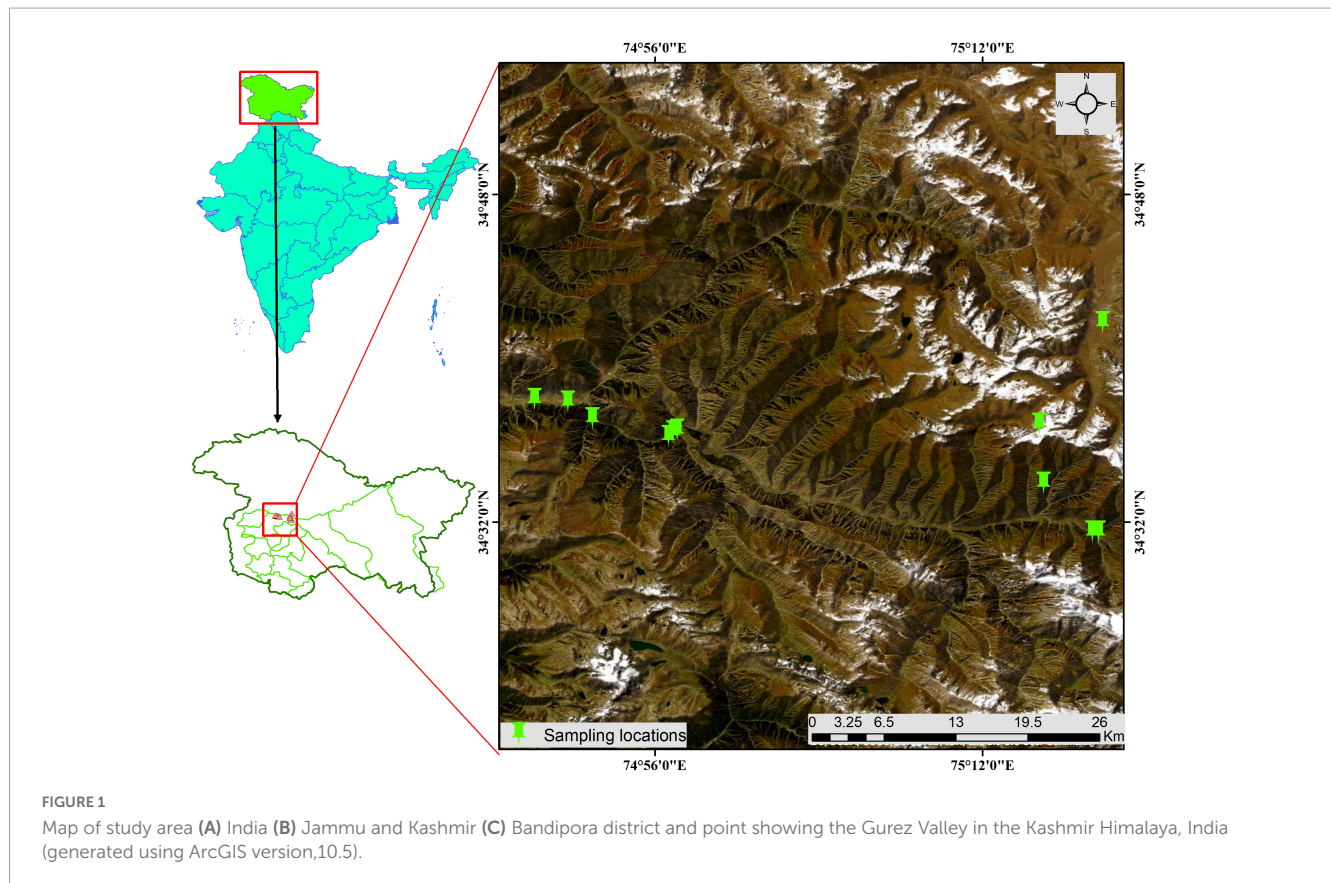
floristic composition and functional characteristics to improve vegetation documentation (Haq et al., 2020). We set up 36 0.1 ha plots for field sampling across different habitats in the study area. Within each 0.1 ha plot, two 5 m^2 plots were placed in opposite corners estimate shrub diversity. For the herbaceous layer, 5 plots of size 1 m^2 were laid (4 in each corner 0.1 ha plot and one in the center). In total, 32 plots for trees, 64 (2 plots × 32 = 64) plots for shrubs and 160 (5 plots × 32 = 160) plots for herbs were sampled in the present study. Field data about each specimen of plant material was meticulously recorded during field studies. In order to serve as herbarium voucher specimens, plant specimens were collected from the field, identified using taxonomic literature, and then authenticated by comparing the plant specimens with material in the KASH herbarium. Ecological traits (like Raunkiaer's life-form, plant habit, phyto-geographical, life span) of each species were recorded during sampling, following Raunkiaer (1934), and Pérez-Harguindeguy et al. (2016). Furthermore, habitat characteristics of each plant species were categorized as Dry slope (DS), Moist places (MP), Natural forest (FR), Shady places (SP), Riparian vegetation (RV), Rock crevice (RC), Roadside (RS), Crop fields (CF), Vegetable garden (VG) (**Plate 1**). The range of native phyto-geographically reported plant specimens was acquired by using secondary sources like manuals, Flora and specified internet web pages (GRIN: Germplasm Resource Information Network).[1] Based on the available data, all plant specimens were categorized into native and exotic species.

---

1   www.efloras.org

Data analysis

To investigate the relationships between ecological variables and plant compositions, heat map and clustering analysis were employed (Rahman et al., 2019a; Haq et al., 2021d). The heat map displayed the distribution of species using presence/absence data, and the clustering algorithm grouped species with similar habitat categories. The Sørensen (1948) similarity coefficient based on presence/absence data was used to identify significant differences among different habitat types and microclimatic similarities (Dalirsefat et al., 2009). In order to identify hypothetical variables (components) that explain the majority of the variance in our multidimensional data, Non-Metric Multidimensional Scaling (NMDS) was utilized. The contribution of various Raunkiaer's life forms was visualized using chord diagrams generated with the circlize package (Gu et al., 2014). Subsequently, we computed three diversity indices, namely, species richness, Shannon and Simpson, based on presence/absence of species for all habitats, and all plots and analyses were performed using R software version 4.0.0 (R Core Team, 2020).

Results

Floristic composition and distribution

Based on the present investigation, 155 plant species from 120 genera and 49 families were reported in the current study area (**Table 1**). The distribution of the species among the 49 families was
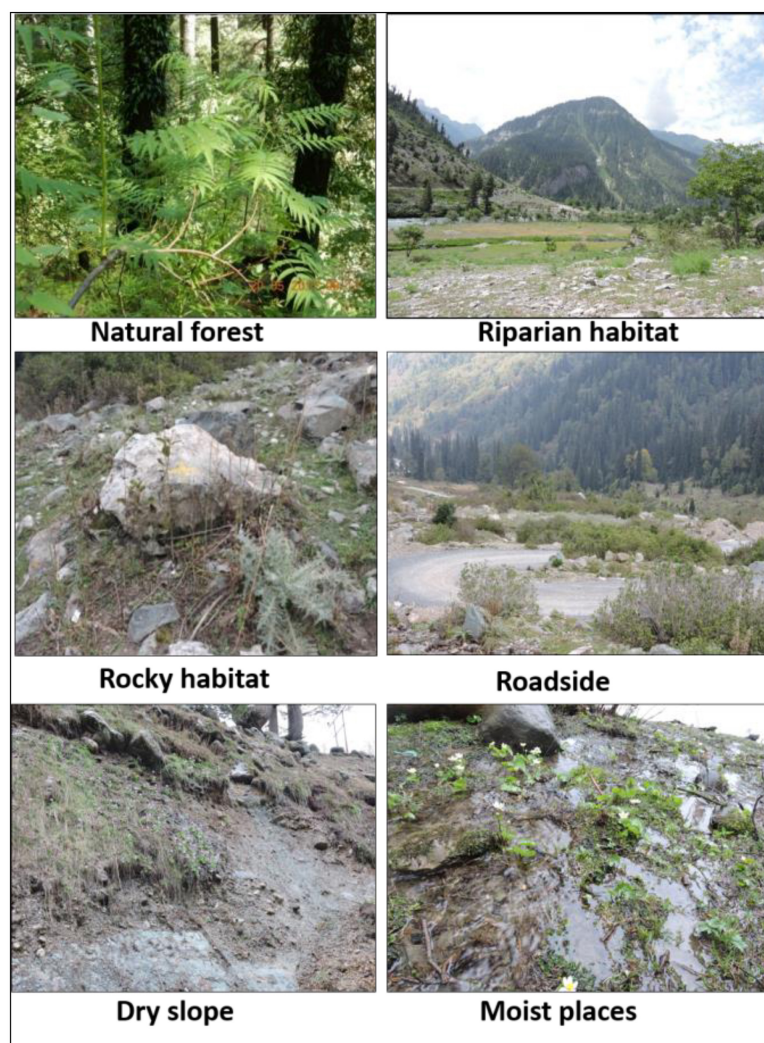
PLATE 1
Representation of different habitats in the study area.

unequal; just 7 families held half of the species, while 42 families held the other half. 23 families were monotypic (**Figure 2**). The top five plant families were Asteraceae (19 species, or 12% of all species), Rosaceae (17 species, or 11% of all species), Lamiaceae (15 species, or 10%), Ranunculaceae (10 species, or 6%), and Apiaceae (8 species, or 5%) (**Table 1**).

Species distribution among growth form types

In the current study, the highest number of plant species (111) were herbaceous plants (72% of all species), followed by 21 tree species (13%), 15 shrubs (10%), four climbers (3%), and four sub-shrubs (2%) (**Table 1**). Most of the tree species growing in the valley were deciduous (e.g., *Aesculus indica, Acer caesium, Betula utilis, Celtis australis, Prunus armeniaca, Prunus cornuta, Populus nigra,* and *Ulmus villosa*). A few coniferous tree species (e.g., *Abies pindrow, Cedrus deodara, Picea smithiana, Pinus wallichiana,* and *Taxus wallichiana*) were also reported. Shrubs included

Rosa webbiana, Berberis lyceum, Rubus ulmifolius, Parrotiopsis jacquemontiana, and *Indigofera heterantha.* Important medicinal herbs reported from the valley were *Ajuga parviflora, Bergenia ciliate, Delphinium roylei, Gentiana kurroo, Heracleum candicans, Phytolacca acinosa, Saussurea costus, Taraxacum officinale,* and *Trillium govanianum* (**Table 1**). The representative plants species documented in the different habitats of the study area are shown in **Plate 2**.

Species distribution among life-form traits

About 35% of the species (54 species) were therophytes which constituted the dominant life form, followed by 29 species of hemicryptophytes (19%), chamaephytes and geophytes with 15 species each (10%), megaphanerophytes with 13 species (8%), nanophanerophytes with 12 species (8%), cryptophytes and mesophanerophytes with 7 species each (4%), microphanerophytes with 2 species (1%), and parasitic forms with a single species (1%)

TABLE 1 Floristic composition and life span traits of the forest vegetation in Gurez Valley of Kashmir Himalaya, India.

Family	Scientific name	Habitat#	Altitude (m)	Nativity**	Invasion status	Growth form	Raunkiaer life-form*	Life cycle	Abbreviation of plant used
Acoraceae	*Acorus calamus* L (4225-KASH)	MP	2,000–2,200	N	RN	Herb	CRP	Perennial	Aco.cal
Apiaceae	*Bunium persicum* (Boiss.) B. Fedtsch. (2974-KASH)	DS, RS	2,000–2,500	N	RN	Herb	GEO	Perennial	Bun.per
	Bupleurum falcatum L. (8075-KASH)	DS, RS	2,500–3,200	E	NT	Herb	HCP	Perennial	Bup.fal
	Chaerophyllum reflexum Aitch. (8095-KASH)	FR, MP	2,000–2,500	N	RN	Herb	HCP	Perennial	Cha.ref
	Ferula jaeschkeana Vatke (8015-KASH)	DS, MP	2,200–2,500	N	RN	Herb	HCP	Perennial	Fer.jae
	Heracleum candicans Wall. ex DC. (3446-KASH)	FR, MP	2,000–2,800	N	RN	Herb	HCP	Perennial	Her.can
	Pleurospermum candollei (DC.) Benth. ex C.B. Clarke	FR, DS	2,200–2,600	N	RN	Herb	HCP	Perennial	Ple.can
	Selinum conioides (Lange) E.H.L. Krause (8118-KASH)	DS, RS	3,000–3,500	E	NT	Herb	HCP	Perennial	Sel.con
Asteraceae	*Achillea millefolium* L (4097-KASH)	CF, DS, RS	2,000–2,800	N	RN	Herb	CHA	Perennial	Ach.mil
	Anaphalis royleana DC. (3808-KASH)	DS, RC	2,700–3,200	N	NT	Herb	HCP	Annual	Ana. Roy
	Anthemis cotula L. (4244-KASH)	RS, CF	2,000–2,500	E	IN	Herb	THE	Annual	Ant.cot
	Artemisia absinthium L. (4224-KASH)	RS, CF	2,000–2,500	E	IN	Herb	THE	Perennial	Art.abs
	Artemisia japonica Thunb (8092-KASH)	FR, DS	2,200–2,500	N	RN	Herb	HCP	Perennial	Art.jap
	Artemisia martima L. (8045-KASH)	FR, DS	2,400–2,800	N	RN	Shrub	NOP	Perennial	Art.mar
	Artemisia rutifolia Spreng. (8062-KASH)	DS, FR	2,200–2,600	N	RN	Herb	HCP	Perennial	Art.rut
	Artemisia vulgaris L. (4210-KASH)	DS, FR	2,000–2,500	N	RN	Shrub	CHA	Perennial	Art.vul
	Aster thomsonii C.B. Clarke (8067-KASH)	SP, FR	2,800–3,000	N	RN	Herb	THE	Perennial	Ast.tho
	Calendula officinalis L (8046-KASH)	RS	2,000–2,500	E	IN	Herb	THE	Annual	Call.off
	Centaurea iberica Trevir. ex Spreng. (4084-KASH)	RS, DS	2,000–2,400	E	IN	Herb	THE	Perennial	Cen.ibe
	Cichorium intybus L. (4222-KASH)	MP, RS	2,000–2,400	N	RN	Herb	THE	Perennial	Cic.int
	Galinsoga parviflora Cav. (8064-KASH)	RS, FR	2,000–2,500	E	IN	Herb	THE	Annual	Gal.par
	Inula racemosa Hook. f.(8119-KASH)	FR, SP	2,800–3,200	N	RN	Herb	THE	Perennial	Inu.rac
	Saussurea costus (Falc.) Lipschitz (4211-KASH)	FR, SP	2,800–3,200	N	RN	Herb	CHA	Annual	Sau.cos
	Saussurea sacra Edgew. (8128-KASH)	FR, SP	2,800–3,200	N	RN	Herb	CHA	Perennial	Sau.sac
	Senecio chrysanthemoides DC. (4102-KASH)	RS, MP	2,000–2,900	E	CS	Herb	THE	Perennial	Sen.chr
	Taraxacum officinale Wigg. (6259-KASH)	DS, FR	2,000–2,500	E	IN	Herb	CHA	Annual	Tar.off
Asparagaceae	*Asparagus officinalis* L. (8125-KASH)	FR, SP	2,200–2,700	E	NT	Climber	CRP	Perennial	Asp.off
	Polygonatum acuminatifolium Kom. (4230-KASH)	FR, SP	2,000–2,400	E	NT	Herb	GEO	Perennial	Pol.cum
Amaranthaceae	*Amaranthus caudatus* L. (4217-KASH)	RS, CF	2,000–2,400	E	IN	Herb	THE	Annual	Ama.cau
	Amaranthus retroflexus L.(6244-KASH)	RS, CF	2,000–2,400	E	NT	Herb	THE	Annual	Ama.ret
	Amaranthus spinosus L. (3361-KASH)	RS, CF	2,000–2,400	E	NT	Herb	THE	Annual	Ama.spi
	Chenopodium album L. (4805-KASH)	RS, CF	2,000–2,500	E	IN	Herb	THE	Annual	Che.alb
	Chenopodium botrys L. (4089-KASH)	DS, RS	2,000–2,500	N	RN	Herb	THE	Annual	Che.bot
Balsaminaceae	*Impatiens glandulifera* Royle (2989-KASH)	RV, FR	2,000–2,400	N	RN	Herb	THE	Annual	Imp.gla
Berberidaceae	*Berberis lycium* Royle (4101-KASH)	FR, DS	2,100–2,600	N	RN	Shrub	NOP	Perennial	Ber.lyc

(Continued)

TABLE 1 (Continued)

Family	Scientific name	Habitat#	Altitude (m)	Nativity**	Invasion status	Growth form	Raunkiaer life-form*	Life cycle	Abbreviation of plant used
Betulaceae	*Betula utilis* D. Don (4105-KASH)	FR	2,800–3,300	N	RN	Tree	MSP	Perennial	Bet.uti
Boraginaceae	*Arnebia benthamii* Wall. ex G. Don (4096-KASH)	RC, FR	3,000–3,300	N	RN	Herb	HCP	Annual	Arn.ben
	Cynoglossum wallichii var. *glochidiatum* (Wall. ex Benth.) Kazmi (4083-KASH)	DS, FR	2,000–2,500	N	RN	Herb	THE	Biennial	Cyn.wal
	Pseudomertensia echioides Riedl (8085-KASH)	FR	2,300–2,800	N	RN	Herb	THE	Perennial	Pse.ech
Brassicaceae	*Brassica juncea* (L.) Czern (4086-KASH)	RS, DS, CF	2,000–2,400	E	NT	Herb	THE	Annual	Bra.jun
Cannabaceae	*Celtis australis* L. (3380-KASH)	FR	2,000–2,500	E	IN	Tree	MGP	Perennial	Cel.aus
Campanulaceae	*Codonopsis rotundifolia* Benth. (7093-KASH)	FR, MP	2,200–2,700	N	RN	Herb	HCP	Perennial	Cod.rot
Caryophyllaceae	*Dianthus angulatus* Royle (4229-KASH)	DS, FR	2,000–2,400	N	RN	Herb	THE	Perennial	Dia.ang
	Gypsophila cerastioides D. Don (8073-KASH)	FR, MP	2,600–3,000	N	RN	Herb	HCP	Perennial	Gyp.cer
	Silene conoidea L. (7101-KASH)	FR, SP	2,700–2,900	N	RN	Herb	THE	Annual	Sil.con
	Silene vulgaris Garcke (3441-KASH)	FR, SP	2,000–2,600	N	RN	Herb	THE	Perennial	Sil.vul
	Stellaria media L. (4249-KASH)	MP, FR	2,000–2,700	N	RN	Herb	THE	Annual	Ste.med
Caprifoliaceae	*Valeriana pyrolifolia* Decne.(4221-KASH)	MP, SP	2,000–2,700	N	RN	Herb	GEO	Perennial	Val.pyr
	Viburnum grandiflorum Wall. ex DC (4241-KASH)	FR	2,000–3,000	N	RN	Shrub	NOP	Perennial	Vib.gra
Convolvulaceae	*Cuscuta reflexa* Roxb. (4082-KASH)	RS	2,000–2,400	E	IN	Climber	PAR	Perennial	Cus.ref
Datiscaceae	*Datisca cannabina* L. (4235-KASH)	FR, DS	2,000–2,500	N	RN	Herb	HCP	Perennial	Dat.can
Dioscoreaceae	*Dioscorea deltoidea* Wall. ex Griseb. (6237-KASH)	FR, SP	2,200–2,600	N	RN	Climber	HCP	Perennial	Dio.del
Euphorbiaceae	*Euphorbia helioscopia* L (4237-KASH)	MP, FR	2,000–2,400	E	IN	Herb	THE	Annual	Eup.hel
	Euphorbia wallichii Hook. f. (4216-KASH)	MP, FR	2,700–3,100	N	RN	Herb	THE	Perennial	Eup.wal
Fabaceae	*Astragalus grahamianus* Benth.(3805-KASH)	DS, RS	2,200–2,600	N	RN	Sub-shrub	CHA	Perennial	Ast.gra
	Lathyrus emodi (Wall. ex Fritsch) Fritsch ex T. Durand and B.D. Jacks. (3806-KASH)	FR, SP	2,300–2,600	N	RN	Herb	THE	Perennial	Lat.emo
	Indigofera heterantha Brandis (4221-KASH)	DS, FR	2,000–2,700	N	RN	Shrub	NOP	Perennial	Ind.het
	Medicago polymorpha L. (4232-KASH)	DS, FR	2,000–2,500	E	NT	Herb	THE	Perennial	Med.pol
	Oxytropis sericea Nutt. (8062-KASH)	FR, DS	2,100–2,400	E	IN	Herb	HCP	Perennial	Oxy.ser
Fumariaceae	*Corydalis govianiana* Wall. (3810-KASH)	RC, SP, FR	2,300–2,900	N	RN	Herb	GEO	Perennial	Cor.gov
Gentianaceae	*Gentiana kurroo* Royle (8066-KASH)	FR, SP	2,000–2,500	N	RN	Herb	THE	Perennial	Gen.kur
	Swertia petiolata Royle (7094-KASH)	RV, FR	2,700–3,000	N	RN	Herb	GEO	Perennial	Swe.pet
Geraniaceae	*Geranium pratense* L. (4098-KASH)	FR, SP	2,800–3,200	N	RN	Herb	THE	Perennial	Ger.pra
	Geranium wallichianum D. Don (4112-KASH)	FR, SP	2,000–2,700	N	RN	Herb	CHA	Perennial	Ger.wal
Hamamelidaceae	*Parrotiopsis jacquemontiana* Rehder (6258-KASH)	DS, FR	2,200–2,700	N	RN	Shrub	NOP	Perennial	Par.jac
Juglandaceae	*Juglans regia* L. (8053-KASH)	DS, CF	2,000–2,800	N	RN	Tree	MSP	Perennial	Jug.reg
Lamiaceae	*Ajuga parviflora* Benth. (4095-KASH)	FR, SP	2,000–2,500	N	RN	Herb	HCP	Annual	Aju.par
	Dracocephalum nutans L. (6261-KASH)	FR, SP	2,100–2,400	E	NT	Herb	CHA	Perennial	Dra.nut

(Continued)

TABLE 1 (Continued)

Family	Scientific name	Habitat#	Altitude (m)	Nativity**	Invasion status	Growth form	Raunkiaer life-form*	Life cycle	Abbreviation of plant used
	Leucas lanata Benth. (6240-KASH)	FR, MP	2,200–2,500	N	RN	Herb	THE	Perennial	Leu.lan
	Mentha arvensis L. (4234-KASH)	FR, RV	2,000–2,400	E	RN	Herb	GEO	Perennial	Men.arv
	Mentha longifolia L. (4251-KASH)	RV, FR	2,000–2,600	E	IN	Herb	GEO	Perennial	Men.lon
	Nepeta connata Royle ex Benth. (6233-KASH)	FR, MP	2,000–2,400	N	RN	Herb	THE	Perennial	Nep.con
	Nepeta erecta (Royle ex Benth.) Benth. (6241-KASH)	FR, MP	2,100–2,500	N	RN	Herb	THE	Perennial	Nep.ere
	Nepeta govaniana (Wall. ex Benth.) Benth. (8047-KASH)	FR, MP	2,200–2,500	N	RN	Herb	THE	Perennial	Nep.gov
	Nepeta laevigata (D. Don) Hand.-Mazz. (8056-KASH)	FR, MP	2,000–2,500	N	RN	Herb	THE	Perennial	Nep.lae
	Nepeta linearis Royle ex Benth. (8046-KASH)	FR, MP	2,200–2,600	N	RN	Herb	THE	Perennial	Nep.lin
	Prunella vulgaris L. (4254-KASH)	RV, RS	2,000–2,500	E	IN	Herb	THE	Perennial	Pru.vul
	Salvia hains Royle ex Bentham (8049-KASH)	FR, RC	2,700–2,900	N	RN	Herb	THE	Biennial	Sal.hai
	Salvia moorcroftiana Wall. ex Benth. (6256-KASH)	RS, DS	2,000–2,500	N	RN	Herb	CHA	Perennial	Sal.moo
	Thymus linearis Benth. (4107-KASH)	DS, FR, RS	2,000–3,000	N	RN	Sub-shrub	HCP	Perennial	Thy.lin
	Thymus serpyllum L. (8055-KASH)	DS, RS	2,400–2,800	E	NT	Sub shrub	HCP	Annual	Thy.ser
Liliaceae	*Allium cepa* L. (3813-KASH)	CF, VG	2,000–2,500	E	NT	Herb	GEO	Perennial	All.cep
	Fritillaria roylei Hook. f. 4086-KASH)	FR, MP	3000–3400	N	RN	Herb	GEO	Perennial	Fri.roy
Malvaceae	*Lavatera cashemiriana* Cambess. (4099-KASH)	FR, SP	2,300–2,700	N	RN	Herb	CHA	Perennial	Lav.cas
	Malva neglecta Wallr. (4114-KASH)	VG, FR	2,000–2,600	E	IN	Herb	THE	Perennial	Mal.neg
Melanthiaceae	*Trillium govanianum* Wall. (6230-KASH)	FR, SP	2,200–3,000	N	RN	Herb	THE	Perennial	Tri.gov
Oxalidaceae	*Oxalis corniculata* L. (4113-KASH)	SP, VG,RS	2,000–3,500	E	IN	Herb	THE	Perennial	Oxa.cor
Papaveraceae	*Meconopsis latifolia* (Prain) Prain (7093-KASH)	FR, MP	2,800–3,100	N	RN	Herb	HCP	Perennial	Mec.lat
Primulaceae	*Androsace rotundifolia* Hardw.(4240-KASH)	DS, FR	2,700–3,200	N	RN	Herb	CRP	Perennial	And.rot
	Anagallis arvensis L. (4239-KASH)	SP, FR	2,000–2,700	N	RN	Herb	HCP	Perennial	Ana.arv
	Primula denticulata Sm. (3810-KASH)	FR	2,100–2,700	N	RN	Herb	GEO	Perennial	Pri.den
Pinaceae	*Abies pindrow* Royle (2965-KASH)	FR	2,300–3,100	N	RN	Tree	MGP	Perennial	Abi.pin
	Cedrus deodara G. Don (4228-KASH)	FR	2,000–2,400	N	RN	Tree	MGP	Perennial	Ced.deo
	Pinus wallichiana A.B. Jacks. (4227-KASH)	FR	2,000–3,000	N	RN	Tree	MGP	Perennial	Pin.wal
	Picea smithiana Boiss. (2967-KASH)	FR	2,200–2,900	N	RN	Tree	MGP	Perennial	Pic.smi
Phytolaccaceae	*Phytolacca acinosa* Roxb. (4253-KASH)	FR, SP	2,200–2,600	N	RN	Herb	GEO	Perennial	Phy.aci
Plantaginaceae	*Veronica laxa* Benth. (3809-KASH)	FR	2,100–2,900	N	RN	Herb	CRP	Perennial	Ver.lax
	Veronica beccabunga L. (4210-KASH)	MP, RS	2,200–2,600	E	CS	Herb	HCP	Perennial	Ver.bec
Poaceae	*Poa bulbosa* L. (4230-KASH)	CF, FR, VG	2,000–2,400	E	IN	Herb	THE	Perennial	Poa.bul
	Poa pratensis L. (4235-KASH)	CF, FR, VG,	2,000–2,600	E	IN	Herb	HCP	Perennial	Poa.pra
	Stipa sibirica Lam. (4236-KASH)	DS, FR	2,200–2,700	N	RN	Herb	HCP	Perennial	Sti.sib
Polygonaceae	*Polygonum viviparum* L. (8066-KASH)	RS, DS	2,200–2,600	E	IN	Herb	THE	Perennial	Pol.viv

(Continued)

TABLE 1 (Continued)

Family	Scientific name	Habitat#	Altitude (m)	Nativity**	Invasion status	Growth form	Raunkiaer life-form*	Life cycle	Abbreviation of plant used
	Rheum emodi Wall.ex Meissn. (4212-KASH)	RC, FR	2,700–3,200	N	RN	Herb	GEO	Perennial	Rhe.emo
	Rumex dentatus L. (4247-KASH)	RS, DS	2,000–2,500	N	RN	Herb	THE	Annual	Rum.den
Pteridaceae	*Pteris cretica* L. (8073-KASH)	MP, FR	2,000–2,600	E	CS	Herb	HCP	Perennial	Pte.cre
Saxifragaceae	*Bergenia ciliata* (Haw) Sternb. (4213-KASH)	RC, FR	2,400–3,100	N	RN	Herb	CRP	Perennial	Ber.cil
	Bergenia stracheyi (Hook. f. and Thomson) Engl. (2973-KASH)	RC, FR	2,500–3,200	N	RN	Herb	CRP	Perennial	Ber.str
Sapindaceae	*Acer caesium* Wall. ex Brandis (6261-KASH)	FR	2,200–2,700	N	RN	Tree	MGP	Perennial	Ace.cae
	Aesculus indica Hook. (4111-KASH)	FR	2,200–2,800	N	RN	Tree	MGP	Perennial	Aes. Ind
Salicaceae	*Populus alba* L. (6262-KASH)	CF	2,000–2,400	E	NT	Tree	MSP	Perennial	Pop.alb
	Populus ciliata Wall. ex Royle (6234-KASH)	CF, FR	2,000–2,500	E	IN	Tree	MSP	Perennial	Pop.cil
	Populus nigra L. (6235-KASH)	DS, CF	2,000–2,600	N	RN	Tree	MSP	Perennial	Pop.nig
	Salix denticulata Andersson (6239-KASH)	MP, FR	2,700–3,200	N	RN	Tree	MSP	Perennial	Sal.den
Sambucaceae	*Sambucus wightiana* Wall. ex Wt. and Arn. (6243-KASH)	RS, DS	2,200–2,900	N	RN	Sub-shrub	THE	Perennial	Sam.wig
Scrophulariaceae	*Euphrasia aristulata* Penn. (6248-KASH)	FR, DS	2,200–2,500	N	RN	Herb	THE	Annual	Eup.ari
	Picrorhiza kurroa Royle ex Benth. (6246-KASH)	FR, SP	2,000–2,500	N	RN	Herb	HCP	Perennial	Pic.kur
	Verbascum thapsus L. (4242-KASH)	RS, DS	2,000–2,800	N	RN	Herb	HCP	Perennial	Ver.tha
Simaroubaceae	*Ailanthus altissima* Swingle.	DS	2,000–2,400	E	NT	Tree	MGP	Perennial	Ail.alt
Solanaceae	*Atropa acuminata* Royle ex Lindl. (4252-KASH)	FR, SP	2,200–2,800	N	RN	Herb	THE	Perennial	Atr.acu
	Datura stramonium L. (4085-KASH)	RS	2,000–2,400	E	IN	Herb	THE	Annual	Dat.str
	Hyoscyamus niger L. (4106-KASH)	RS	2,200–2,700	E	NT	Herb	CRP	Biennial	Hyo.nig
	Solanum tuberosum L. (8092-KASH)	CF, VG	2,000–2,400	E	NT	Herb	GEO	Perennial	Sol.tub
Ranunculaceae	*Aquilegia fragrans* Benth. (8082-KASH)	FR, SP	2,500–2,900	N	RN	Herb	CHA	Perennial	Aqu.fra
	Aconitum chasmanthum Stapf ex Holmes (4109-KASH)	DS, RC	3,000–3,200	N	RN	Herb	HCP	Perennial	Aco.cha
	Aconitum heterophyllum Wall. ex Royle (4094-KASH)	FR	2,700–3,200	N	RN	Herb	CHA	Perennial	Aco.het
	Clematis montana Buch. -Ham. ex DC. (8120-KASH)	FR	2,200–2,500	N	RN	Climber	CHA	Perennial	Cle.mon
	Delphinium roylei Munz (7106-KASH)	FR, MP	2,000–2,600	N	RN	Herb	THE	Perennial	Del.roy
	Ranunculus palmatifidus Riedl (7104-KASH)	MP, FR, SP	2,000–2,600	N	RN	Herb	GEO	Perennial	Ran.pal
	Ranunculus hirtellus Royle (7105-KASH)	MP, SP, CF	2,700–3,000	N	RN	Herb	THE	Perennial	Ran.hir
	Ranunculus laetus Wall. ex Hook. (7118-KASH)	CF, FR,RS	2,000–2,500	E	IN	Herb	GEO	Perennial	Ran.lae
	Ranunculus sceleratus L. (8117-KASH)	RV, RS	2,200–2,600	E	CS	Herb	THE	Annual	Ran.sce
	Thalictrum cultratum Wall. (8115-KASH)	FR	2,300–2,700	N	RN	Herb	CHA	Perennial	Tha.cul
Rosaceae	*Cotoneaster affinis* Lindl. (8125-KASH)	FR	2,600–3,100	N	RN	Shrub	MGP	Perennial	Cot.aff
	Cotoneaster nummularius Fisch. and C.A. Mey. (8070-KASH)	RS	2,000–2,800	E	NT	Shrub	NOP	Perennial	Cot.num

(Continued)

TABLE 1   (Continued)

Family	Scientific name	Habitat#	Altitude (m)	Nativity**	Invasion status	Growth form	Raunkiaer life-form*	Life cycle	Abbreviation of plant used
	Crataegus songarica K. Koch (3381-KASH)	FR	2,000–2600	N	RN	Tree	MCP	Perennial	Cra.son
	Filipendula vestita (Wall. ex G. Don.) Maxim.	FR, SP	2200–2,600	N	RN	Shrub	CHA	Perennial	Fil.ves
	Fragaria nubicola (Lindl. ex Hook. f.) Lacaita (4087-KASH)	FR, DS	2,000–3,000	N	RN	Herb	HCP	Perennial	Fra.nub
	Malus domestica Borkh. (4248-KASH)	CF	2,000–2,500	N	RN	Tree	MGP	Perennial	Mal.dom
	Potentilla multifida L. (7088-KASH)	RS, DS	2,200–2,800	E	IN	Herb	HCP	Perennial	Pot.mul
	Potentilla nepalensis Hook. (7098-KASH)	DS, RS	2,200–2,500	E	NT	Herb	THE	Perennial	Pot.nep
	Prunus avium L.(7101-KASH)	CF	2,000–2,600	E	CS	Tree	MGP	Perennial	Pru.avi
	Prunus cornuta Steud. (3431-KASH)	FR	2,300–2,800	N	RN	Tree	MGP	Perennial	Pru.cor
	Prunus persica Batsch (8059-KASH)	CF	2,000–2,500	E	CS	Tree	MCP	Perennial	Pru.per
	Rosa indica L. (8084-KASH)	FR, SP	2,000–2,400	N	RN	Shrub	NOP	Perennial	Ros.ind
	Rosa webbiana Wall. ex Royle (6245-KASH)	DS, FR	2,000–2,800	N	RN	Shrub	NOP	Perennial	Ros.web
	Rubus ellipticus Sm. (6255-KASH)	FR, DS	2,000–2,600	N	RN	Shrub	NOP	Perennial	Rub.ell
	Rubus niveus Thunb. (6252-KASH)	FR, DS	2,400–2,900	N	RN	Shrub	NOP	Perennial	Rub.niv
	Rubus ulmifolius Schott (6252-KASH)	FR, DS	2,000–2,500	E	CS	Shrub	NOP	Perennial	Rub.ulm
	Sorbaria tomentosa Rehder (8086-KASH)	FR	2,400–3,000	N	NT	Shrub	NOP	Perennial	Sor.tom
Taxaceae	*Taxus wallichiana* Zucc.(8094-KASH)	FR	2,400–2,700	N	RN	Tree	MSP	Perennial	Tax.wal
Ulmaceae	*Ulmus villosa* Brandis ex Gamble (8091-KASH)	FR, CF	2,000–2,500	N	RN	Tree	MGP	Perennial	Ulm.vil
Urticaceae	*Urtica dioica* L. (4219-KASH)	RS, DS	2,000–3,100	E	NT	Herb	THE	Perennial	Urt.dio
Verbenaceae	*Verbena officinalis* L. (4117-KASH)	MP, RS	2,000–2,500	E	IN	Herb	THE	Perennial	Ver.off
Violaceae	*Viola canescens* Wall. ex Roxb. (3458-KASH)	FR, SP	2,000–2,500	N	RN	Herb	THE	Perennial	Vio.can
	Viola odorata L. (3462-KASH)	FR, SP	2,000–2,600	E	NT	Herb	THE	Perennial	Vio.odo

*THE, therophytes; HCP, hemicryptophytes; MGP, magaphanerophytes; NOP, nanophanerophytes; CHA, chamaephytes; GEO, geophytes; MSP, mesophanerophytes; CRP, cryptophytes; MCP, microphanerophytes; PAR, parasitic. **N = native, E = exotic. #Dry slope (DS), Moist places (MP), Natural forest (FR), Shady places (SP), Riparian vegetation (RV), Rock crevice (RC), Roadside (RS), Crop fields (CF), Vegetable garden (VG), Regional native (RN), Naturalized (NT), Invasive (IN), Casual (CS).

(Figure 3). Majority of the plant species (129) in the studied valley were represented by perennials (83%) followed by annuals with 23 species (15%), and biennials with three species (2%). According to the phyto-geographical research, 65% of the species documented in the study area were native, with the remaining 15% being invasive, 14% being naturalized, and 5% being casual (Figure 4 and Table 1). The majority (30%) of exotic species were reported on the roadside, followed by natural forests (23%), crop fields (17%), dry slopes (16%), shady areas (5%), moist places, and riparian zones (4% each).

Habitat-wise distribution

Of all species encountered 39% grew in the natural forests, 17% on dry slopes, 11% in shady places, 10% in moist places, 2% in riparian zones, 3% in rock crevices, and the remaining species were dispersed in highly distributed habitats, e.g., 11% along roadsides, 6% in crop fields, and 1% in vegetables gardens

(Table 1 and Plate 2). Based on their floristic similarity, cluster analysis identified five clusters of various habitat types (Figure 5). Natural forests made up the first cluster, dry slopes and roadside vegetation made up the second, wet and shady areas made up the third, crop fields and vegetable gardens made up the fourth, and riparian vegetation and rock crevices made up the fifth (Figure 5).

Similar to this, the NMDS revealed significant variation in habitat types, with some species groups having a stronger association with particular habitat types than others (Figure 6). In the biplot, five clusters of habitats based on species presence/absence can be identified: dry slope; natural forest; roadside; moist places and rocky crevice; and crop fields, riparian vegetation, shady places, and vegetable gardens. The major plant species richness was detected in rich and optimally moisturized natural forest habitats and middle richness in moist places as well as less distributed habitations.

According to the estimated diversity indices, Natural forest had the greatest values for all three indices (Table 2). Shannon's
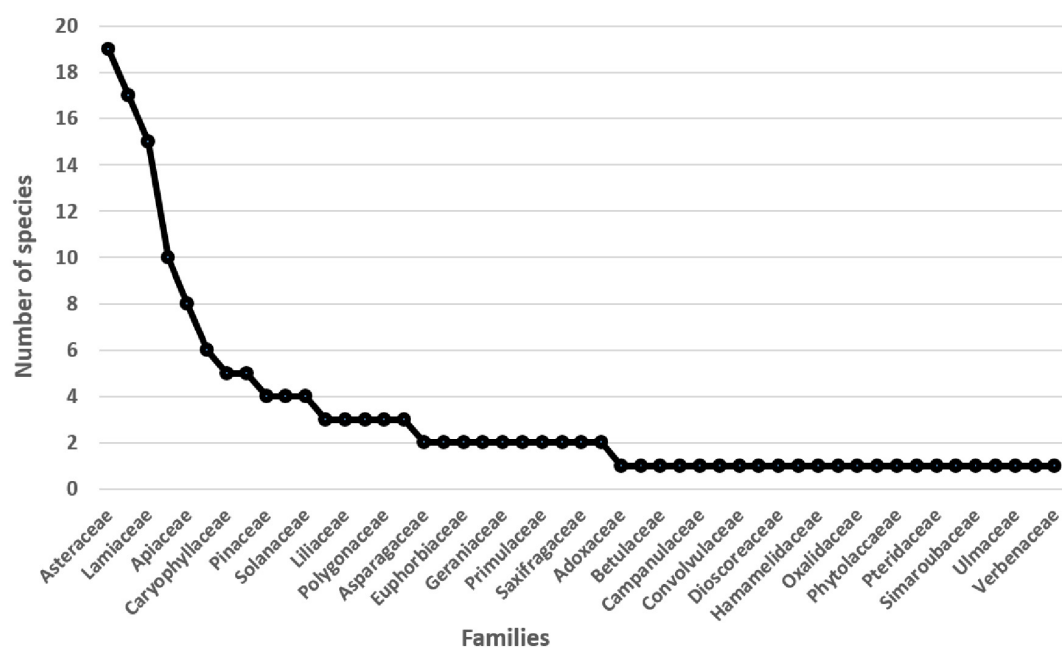
FIGURE 2
Species- family relationship of documented species in the study area.

index for this habitat was 4.73, and Simpson's was 0.99. There were 113 species present. After that, Dry slope and Shady areas held 46 and 31 specie (3.83 and 3.43 for Shannon index, and 0.98 and 0.97 for Simpson index, respectively) (Table 2) lowest values were recorded for Rock crevice and Vegetable garden (Table 2).

Discussion

In this study, we provide an in-depth evaluation of the qualitative vegetation of remote region of Kashmir Himalaya. The study revealed (i) 155 plant species belonging to 120 genera and 49 families, with (ii) an uneven distribution within families, with 50% of the species belonging to just 7 families and 23 families being monotypic. (iii) Therophytes were the most prevalent form of life, showing that the vegetation was disturbed (iv) Exotic species made up the remaining 35% and most exotic plants were found along roadsides. Finally, (v) natural forests scored the highest values for all three estimated diversity indices, compared to other human-modified habitats. Vegetation analysis helps to develop a comprehensive image of the plant communities of a particular region (Chhetri and Shrestha, 2019). Assessing the floristic diversity of hotspots of biodiversity is essential to understand the conservation status of these areas, which have a significant role in making the conservation strategies as well as policies. The vegetation of region was found to be very diverse due to ecological zonation, different microhabitats, and topographic features. 49 families and 155 species were found in the current investigation. In comparison to past studies conducted in other Himalayan locations (Qureshi and Bhatti, 2010; Semwal et al., 2010; Shaheen and Qureshi, 2011; Dangwal et al., 2012; Singh

and Rawat, 2012) the number of plant species recorded in the current research area was higher. Numerous interrelated factors, including elevation, regional climate, topography, competition, regional species pool, regional species dynamics, and human activity have an impact on the regional patterns of species richness (Rahman et al., 2020; Mitchell et al., 2023). However, Khan et al. (2012) reported a higher number of plant species (198) from the Naran valley forest of Pakistan Himalaya but distributed in a lower number of families (68) when compared to our study. Similarly, Verma and Kapoor (2011) reported 160 vascular plant species belongs to 51 families from Ropa-Giavung valley in the cold deserts of District Kinnaur, Himachal Pradesh, India (also see Manzoor et al., 2016; Haq et al., 2022d; Ullah et al., 2022). However, at the region level the species richness of our study was comparatively higher than report in previous studies from Kashmir Himalayas (Bhat et al., 2014). Thus, the slight but predictable fluctuation in species number might be attributed to both abiotic environmental and biotic causes. Apart from elevation, microhabitats that reflect or predict vegetation patterns across landscapes. Together with the previously described findings, our findings demonstrate that while various studies have analyzed the floristic composition of the Himalayan region, each micro-region has unique functional groups that can significantly affect the structuring of the local plant community. Our study showed a smaller number of species than several other studies, but had a larger number of families, which may also represent an important result for the analysis of biodiversity in these regions. Asteraceae, Rosaceae, Lamiaceae, Ranunculaceae, and Apiaceae were reported as the families with the largest number of plant species. Due to wide range of ecological amplitudes, the plant species of Asteraceae are varied in habitats (Rahman et al., 2019a; Rashid et al., 2021; Waheed et al., 2022). Similar findings were observed by Haq et al. (2021d) in Kashmir Himalaya, India and Rahman et al. (2018) in Manoor
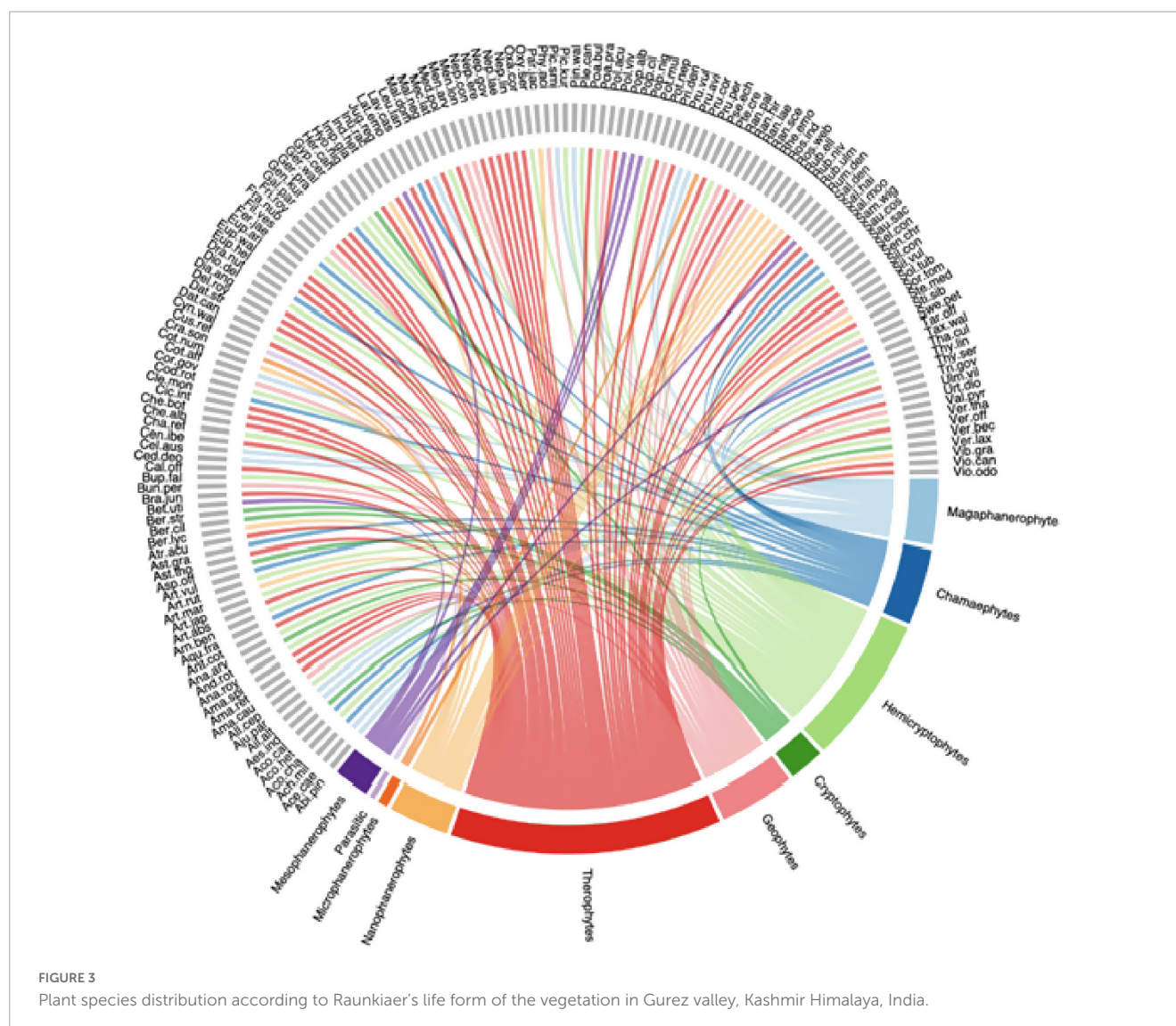
PLATE 2
Representative plant species growing in different habitats of the study area.

valley, Pakistan. Many researchers have reported Asteraceae as the dominant family from different regions (Verma and Kapoor, 2011; Hussain et al., 2015; Ali et al., 2016; Amjad et al., 2017; Khan et al., 2018; Rahman et al., 2019a). This demonstrates the family's strong capacity for adaptation to a variety of environments and temperatures. Additionally, in agreement with our findings, two other studies—Suyal et al. (2010) in the Garhwal Himalaya, India, and Khan et al. (2015) in Kabal (Swat), Pakistan—reported Lamiaceae as the dominant family.

The current study emphasizes the uneven distribution of plant species throughout families, with 23 families being identified as monotypic. The large variety of families, which revealed a varied distribution of flora in the area, is explained by variances in microhabitat, morphological features, life duration, and dynamic ecological niche (Haq et al., 2022a; Khoja et al., 2022). The diversity and structure of these plant communities can be influenced by various abiotic and biotic factors, which has also been shown by earlier research in the Western Himalayan region, and some species and/or families may not be as able to inhabit particular habitats as

others (Rahman et al., 2018). The growth form of trees had higher proportion (13%) than shrubs (10%), an expression of a functioning forest ecosystem (Khan et al., 2015). The present results agreed with Khan et al. (2015), who found that a large diversity of microhabitats was favorable to tree species in the region. The findings of Sharma and Raina (2018) from other Himalayan forests further support these findings. Herbaceous species (111) were the dominant habit similar to other areas of the Northwestern Himalaya (Dar and Sundarapandian, 2016; Rahman et al., 2019b; Haq et al., 2021a; Nafeesa et al., 2021). Previous research in the Western Himalayan region has shown that certain species and/or families rarely have the same ability to occupy specific habitats as others, where varied abiotic and biotic effects can alter the diversity and organization of these plant communities (Haq et al., 2021b; Nafeesa et al., 2021).

It has been observed that the most promising approaches for predicting the species composition of any forest communities revolves around their functional traits. Therefore, studying functional groups usually provides clear information on the direct physiological adaptations of plant communities to particular

FIGURE 3
Plant species distribution according to Raunkiaer's life form of the vegetation in Gurez valley, Kashmir Himalaya, India.

environments conditions (Haq et al., 2019). The most common life form class were therophytes, followed by hemicryptophytes, magaphanerophytes, chamaephytes, and geophytes. Such biological variety represents the adaptation of plant species to the climatic factors (Khan et al., 2018). Hemi-cryptophytes predominate in the study area due to the cold and mountainous climate. In general, they withstand water scarcity by remaining dry or developing physiological, morphological, and anatomical traits that allow them to tolerate water loss. The fact that therophytes were found as the dominant life form in the studied area, which indicates high biotic disturbance levels on the habitat via grazing, human settlements, agricultural practices, and road constructions, since this life form is commonly associated with the unfavorable dry environmental condition, resulting in adopted strategies for their survival (Vakhlamova et al., 2016). The current findings agreed with Asim et al. (2016), Rahman et al. (2018, 2019b), Wali et al. (2022) who also documented the dominance of therophytes in the respective research areas. The high biotic disturbance significantly alters composition of the herbaceous layer and favored the abundant growth of alien annual weedy species such as such as *Anthemis cotula, Amaranthus caudatus, Centaurea iberica,*

Datura stramonium, and *Galinsoga parviflora*, all of which are therophytes (Haq et al., 2021d). The second most prevalent type of life was hemicryptophytes. The association of hemicryptophytes with a cold, mountainous climate is a likely explanation for their predominance (Shimwell, 1971). Because of the soil and climate in the subalpine zones, chamaephytes are more common (Khan et al., 2018). Some habitats are more suited to plant development than others based on the diversity of species found in the forest environments of different geographic regions (Medvecká et al., 2018). Comparing natural forest habitats to other types of habitat, the current study found that natural forest environments harbored the highest diversity of species. However, anthropogenic disturbances are fragmenting, destroying, and degrading natural forest habitats, which is affecting the composition and layout of forest communities including in this area of the Himalayan region (Chakraborty et al., 2017; Rahman et al., 2022). Qureshi and Bhatti (2010), who recorded the highest number of plant species in natural forest habitats from Pakistan, provide additional support for our findings. Moreover, the resemblance in the plant species pool in human modified habitats provides an evidence toward the indication of
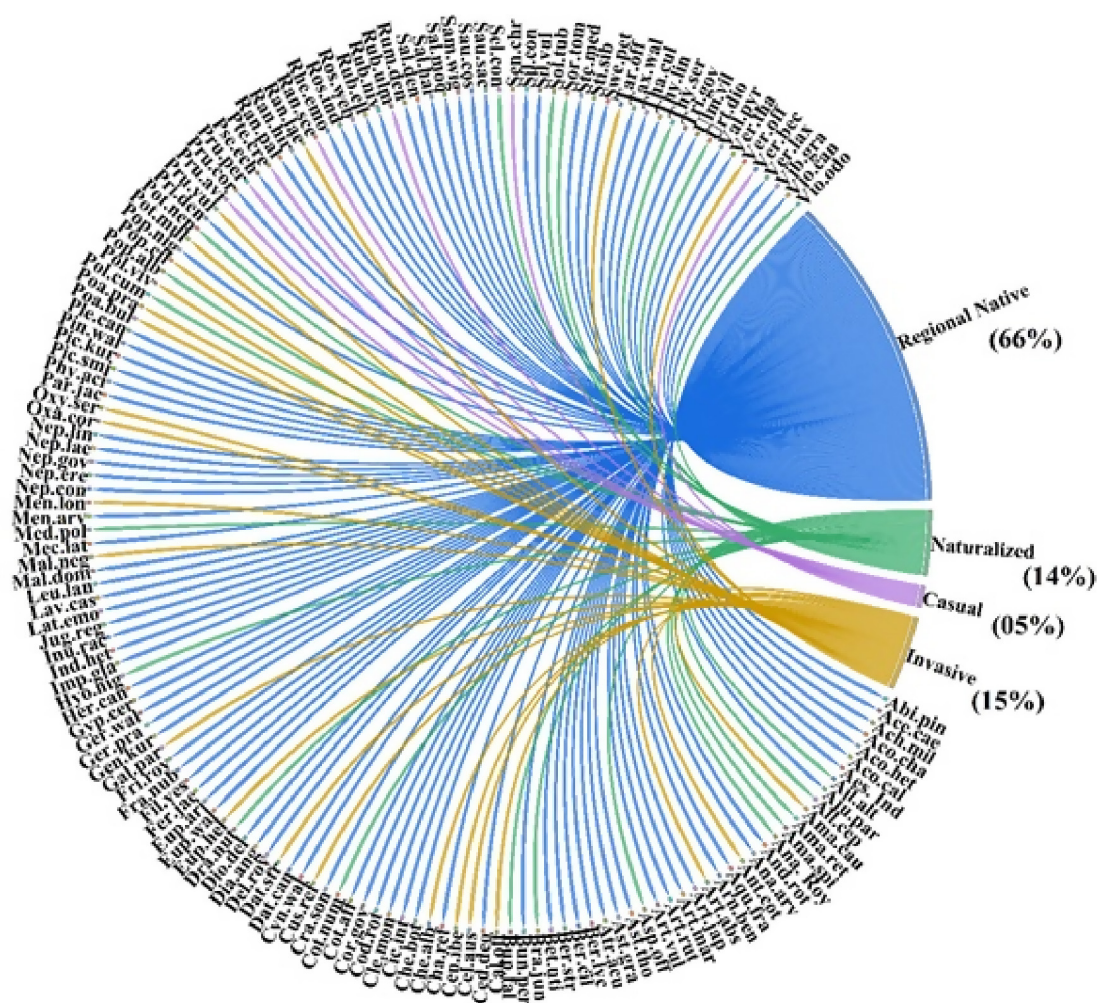
FIGURE 4
Plant species distribution according to nativity range of the vegetation in Gurez valley, Kashmir Himalaya, India.

ecological filtration that occurs in the region (Gardner et al., 2009). Anthropogenic disturbances common in this Himalayan region include overgrazing, deforestation, over-exploitation and fragmentation of natural intact forests due to linear development such as road networks and transmission lines (Haq et al., 2022b). Out of the total reported plant species, 35% were exotic, mostly in human modified habitats. Such numbers are comparable with those documented by Kohli et al. (2004) from the forests of Himachal Pradesh of Indian Himalayas. The most common invasive species growing in forest ecosystems of Jammu and Kashmir included trees like *Aesculus indica, Ailanthus altissima, Juglans regia, Populus ciliate,* subshrub *Sambucus wightiana,* and herbs such as *Anthemis cotula, Amaranthus caudatus, Centaurea iberica* and *Datura stramonium* (Haq et al., 2019, 2023b). The invasion of plant species is typically facilitated by disturbance because it overwhelms environmental and physical barriers. The parameters that cause the disturbances have been seen to be able to filter the makeup of a community and affect species concurrence by altering resource and safe spot availability (Davis et al., 2000; Haq et al., 2022c, 2023a). Generally, those species having wide niches and can pass via these filters and likely to overrun newly

ecosystems after these are disturbed (Dukes and Mooney, 1999). Furthermore, invasions of exotics into forests might be facilitated by the incursion of other plant species generating conditions that encourage other invasive plant species over native species (Niu et al., 2007). When alien species invade a newly range, innate plant species, adaptation to the new environment, is sometimes evacuated (van Boheemen et al., 2019). The vegetation composition variations rise via a variety of procedure sensuing the disappearance of the diversity of plant species such as communities change from native desired plant species to monospecific positions of the invasive plant species (Pérez-Ramos et al., 2019; Haq et al., 2021c). Invasive species have broad consequences in affecting potential management to decrease the effects of climate changes (Kraft et al., 2015).

Implications for forest management and policy

According to our findings, 35% of plant species were deemed to be alien, indicating that a large number of non-native species

FIGURE 5
Heat map based on Sørensen's (1948) similarity index of plant species in Gurez valley, Kashmir Himalaya, India.

have spread to the inaccessible and isolated Himalaya region. We discovered a high percentage of exotic species (such as *Aesculus indica, Ailanthus altissima, Sambucus wightiana, Anthemis cotula, Amaranthus caudatus, Centaurea iberica,* and *Datura stramonium*) in disturbed forest habitats such as roadsides, and we propose that tunnels, rather than roads, are the best opinions of connectivity in fragile mountain ecosystems. The elements

that threaten biodiversity must be minimized in order to keep ecosystems operating and their members intact. Regulations that limit alien species like *Anthemis cotula, Artemisia absinthium, Bupleurum falcatum, Cuscuta reflexa, Galinsoga parviflora,* and *Senecio chrysanthemoides,* introductions, and boost recovery, such as modifying structure through enhanced species regeneration and planting native species (*Abies pindrow, Cedrus deodara,*
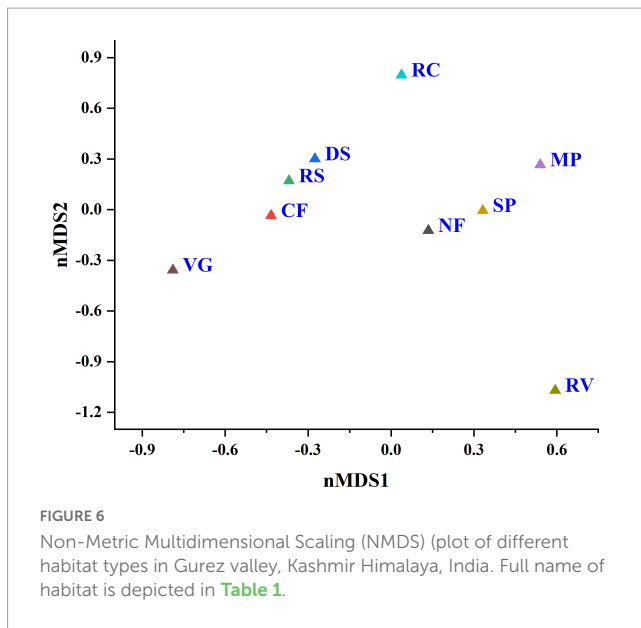
FIGURE 6
Non-Metric Multidimensional Scaling (NMDS) (plot of different habitat types in Gurez valley, Kashmir Himalaya, India. Full name of habitat is depicted in **Table 1**.

TABLE 2 Variation of diversity indices between habitat types in Gurez valley, Kashmir Himalaya, India.

Habitats	Richness	Shannon	Simpson
Crop fields	22	3.09	0.95
Dry slopes	46	3.83	0.98
Moist places	27	3.30	0.96
Natural forests	113	4.73	0.99
Riparian vegetation	12	2.48	0.92
Roadsides	29	3.37	0.97
Rock crevices	9	2.20	0.89
Shady places	31	3.43	0.97
Vegetable gardens	9	2.20	0.89

Pinus roxburghii, P. wallichiana, Taxus wallichiana, Betula utilis, Ulmus villosa, Trillium govanianum, Ajuga parviflora). We found that the study area serves as the natural habitat for several significant, endangered medicinal plants, including *Arnebia benthamii, Bergenia ciliata, Delphinium roylei, Gentiana kurroo, Phytolacca acinosa, Saussurea costus,* and *Trillium govanianum.* Therefore, we recommend that human intervention in natural regeneration efforts be prioritized in these habitats to increase the population of these species. Finally, existing knowledge of threats to the forest flora can be used to guide management in the face of future climate change. The forest management strategy could be organized so that potential hazards (like forest fragmentation, invasion of exotic species) are addressed before they become a problem. Furthermore, the majority of species recovery initiatives should focus on managing forest restoration in human modified habitats through by planting and reseeding native species like*, Ulmus villosa, Betula utilis, Aconitum heterophyllum, Trillium govanianum, Fritillaria roylei, Arnebia benthamii,* to lessen susceptibility to future threats in the landscape.

Conclusion

The identification of areas with a high value for biodiversity and the prioritization of these areas for conservation are crucial for preserving biodiversity. The present investigation described qualitative vegetation characteristics in a remote region of the Kashmir Himalaya. The dominance of few families, especially the Asteraceae, is a result of actual and potential dominating invaders in zones with significant disturbance. Therophytes emerged to be the primary form of life in the research area. The presence of a large fraction of therophytes indicates major anthropogenic disruptions. The study examined how environmental factors affect plant communities and placed special emphasis on the idea of habitat filtration as it relates to plant species' abiotic tolerance. Furthermore, by examining species features from a functional groups standpoint, it may be possible to predict an ecosystem functionality more accurately. The study's findings suggest that decision-makers and planners should place a greater emphasis on ecologically sustainable development in forest landscapes, considering species composition and the preservation of ecosystem function. Similar approaches should undoubtedly ensure that development activities do not contribute to biodiversity loss in fragile ecosystems.

Data availability statement

The original contributions presented in this study are included in the article/supplementary material, further inquiries can be directed to the corresponding authors.

Author contributions

SH, FL, and AK collected the data. SH and MW analyzed and interpreted the data and results. SH wrote initial draft of the manuscript. SH, RB, EM, HE, and FL revised the manuscript. All authors read and approved the final manuscript.

Conflict of interest

The authors declare that the research was conducted in the absence of any commercial or financial relationships that could be construed as a potential conflict of interest.

Publisher's note

All claims expressed in this article are solely those of the authors and do not necessarily represent those of their affiliated organizations, or those of the publisher, the editors and the reviewers. Any product that may be evaluated in this article, or claim that may be made by its manufacturer, is not guaranteed or endorsed by the publisher.

References

Ali, A., Badshah, L., Hussain, F., and Shinwari, Z. K. (2016). Floristic composition and ecological characteristics of plants of Chail valley, district Swat, Pakistan. *Pak. J. Bot.* 48, 1013–1026.

Altaf, A., Haq, S. M., Shabnum, N., and Jan, H. A. (2022). Comparative assessment of phyto diversity in Tangmarg Forest division in Kashmir Himalaya, India. *Acta Ecol. Sin.* 42, 609–615. doi: 10.1016/j.chnaes.2021.04.009

Amjad, M. S., Arshad, M., Page, S., Qureshi, R., and Mirza, S. N. (2017). Floristic composition, biological spectrum and phenological pattern of vegetation in the subtropical forest of Kotli District, AJK, Pakistan. *Pure Appl. Biol.* 6, 426–447. doi: 10.19045/bspab.2017.60043

Asim, Z. I., Haq, F, Iqbal, A. (2016). Phenology, life form and leaf spectra of the vegetation of Kokarai valley, district swat. *J. Bio. Environ. Sci.* 9, 23–31.

Barkley, T. M., DePriest, P., Funk, V., Kiger, R. W., Kress, W. J., and Moore, G. (2004). Linnaean nomenclature in the 21st Century: A report from a workshop on integrating traditional nomenclature and phylogenetic classification. *Taxon* 53, 153–158. doi: 10.2307/4135501

Bhat, F., Mahajan, D. M., Sayyed, MRG, Bhat, A. (2014). Phytosociological measurements and vegetation analysis along an altitudinal gradient of Lolab valley (Kashmir Himalaya. India). *WCS's Natl. J. Inter. Res.* 1, 1–13.

Chakraborty, A., Ghosh, A., Sachdeva, K., and Joshi, P. K. (2017). Characterizing fragmentation trends of the Himalayan forests in the Kumaon region of Uttarakhand, India. *Ecol. Inform.* 38, 95–99. doi: 10.1016/j.ecoinf.2016.12.006

Chhetri, N. B. K., and Shrestha, K. K. (2019). Floristic diversity and important value indices of tree species in lower Kanchenjunga Singhalila Ridge Eastern Nepal. *Am. J. Plant Sci.* 10, 248–263. doi: 10.4236/ajps.2019.101019

Dalirsefat, S. B., da Silva, A., Meyer, and Mirhoseini, S. Z. (2009). Comparison of similarity coefficients used for cluster analysis with amplified fragment length polymorphism markers in the silkworm *Bombyx mori*. *J. Insect Sci.* 9, 1–8. doi: 10.1673/031.009.7101

Dangwal, L. R., Singh, T., Singh, A., and Sharma, A. (2012). Plant diversity assessment in relation to disturbances in subtropical chirpine forest of the western Himalaya of district Rajouri, J&K, India. *Int. J. Plant Anim. Environ. Sci.* 2, 206–213.

Dar, J. A., and Sundarapandian, S. (2016). Patterns of plant diversity in seven temperate forest types of Western Himalaya, India. *J. Asia Pac. Biodivers.* 9, 280–292. doi: 10.1016/j.japb.2016.03.018

Davis, M. A., Grime, J. P., and Thompson, K. (2000). Fluctuating resources in plant communities: A general theory of invasibility. *J. Ecol.* 88, 528–534. doi: 10.1046/j.1365-2745.2000.00473.x

Dukes, J. S., and Mooney, H. A. (1999). Does global change increase the success of biological invaders?. *Trends Ecol. Evol.* 14, 135–139. doi: 10.1016/S0169-5347(98)01554-7

Gardner, T. A., Barlow, R., Chazdon, R. M., Ewers, C. A., Harvey, C. A., Peres, C., et al. (2009). Prospects for tropical forest biodiversity in a human-modified world. *Ecol. Lett.* 12, 561–582. doi: 10.1111/j.1461-0248.2009.01294.x

Grime, J. P., Hodgson, J. G., and Hunt, R. (2014). *Comparative plant ecology: A functional approach to common British species*. Berlin: Springer.

Gu, Z., Gu, L., Eils, R., Schlesner, M., and Brors, B. (2014). circlize implements and enhances circular visualization in R. *Bioinformatics* 30, 2811–2812. doi: 10.1093/bioinformatics/btu393

Haq, S. M., Calixto, E. S., and Kumar, M. (2020). Assessing biodiversity and productivity over a small-scale gradient in the protected forests of Indian Western Himalayas. *J. Sustain.* 40, 675–694. doi: 10.1080/10549811.2020.1803918

Haq, S. M., Lone, F. A., Kumar, M., Calixto, E. S., Waheed, M., Casini, R., et al. (2023b). Phenology and diversity of weeds in the agriculture and horticulture cropping systems of Indian Western Himalayas: Understanding implications for agro-ecosystems. *Plants* 12:1222. doi: 10.3390/plants12061222

Haq, S. M., Waheed, M., Khoja, A. A., Amjad, M. S., Bussmann, R. W., Ali, K., et al. (2023a). Measuring forest health at stand level: A multi-indicator evaluation for use in adaptive management and policy. *Ecol. Indicat.* 150:110225. doi: 10.1016/j.ecolind.2023.110225

Haq, S. M., Malik, Z. A., and Rahman, I. U. (2019). Quantification and characterization of vegetation and functional trait diversity of the riparian zones in protected forest of Kashmir Himalaya, India. *Nord. J. Bot.* 37:11. doi: 10.1111/njb.02438

Haq, S. M., Calixto, E. S., Rashid, I., and Khuroo, A. A. (2021d). Human-driven disturbances change the vegetation characteristics of temperate forest stands: A case study from Pir Panchal mountain range in Kashmir Himalaya. *Trees For. People* 6:100134. doi: 10.1016/j.tfp.2021.100134

Haq, S. M., Shah, A. A., Yaqoob, U., and Hassan, M. (2021a). Floristic quality assessment index of the Dagwan stream in Dachigam National Park of Kashmir Himalaya. *Proc. Natl. Acad. Sci. India Sec B Biol. Sci.* 91, 657–664. doi: 10.1007/s40011-021-01247-w

Haq, S. M., Yaqoob, U., Calixto, E. S., Kumar, M., Rahman, I. U., Hashem, A., et al. (2021b). Long-term impact of transhumance pastoralism and associated disturbances in high-altitude forests of Indian Western Himalaya. *Sustainability* 13:12497. doi: 10.3390/su132212497

Haq, S. M., Hamid, M., Lone, F. A., and Singh, B. (2021c). Himalayan hotspot with alien weeds: A case study of biological spectrum, phenology, and diversity of weedy plants of high-altitude Mountains in District Kupwara of J&K Himalaya, India. *Proc. Natl. Acad. Sci. India Sec. B Biol. Sci.* 91, 139–152. doi: 10.1007/s40011-020-01219-6

Haq, S. M., Khan, I., Malik, Z. A., and Singh, B. (2022d). "Plant diversity and species distribution pattern across the Pir Panjal mountain forest range in the Western Himalayas." in *Biodiversity, conservation and sustainability in Asia: Volume 2: Prospects and challenges in south and middle Asia*, eds M. Öztürk, S. M. Khan, V. Altay, R. Efe, D. Egamberdieva, F. O. Khassanov (Cham: Springer International Publishing), 67–84.

Haq, S. M., Waheed, M., Bussmann, R. W., and Arshad, F. (2022a). Vegetation composition and ecological characteristics of the forest in the Shawilks Mountain Range from Western Himalayas. *Acta Ecol. Sin*. doi: 10.1016/j.chnaes.2022.10.008

Haq, S. M., Yaqoob, U., Hamid, S., Hassan, M., Bashir, F., Waheed, M., et al. (2022b). Localized impact of livestock settlements on vegetation patterns in fir forests of Kashmir Himalaya. *Acta Ecol. Sin.* 42, 407–416. doi: 10.1016/j.chnaes.2022.07.004

Haq, S. M., Amjad, M. S., Waheed, M., Bussmann, R. W., and Proæków, J. (2022c). The floristic quality assessment index as ecological health indicator for forest vegetation: A case study from Zabarwan Mountain Range, Himalayas. *Ecol. Indic.* 145:109670. doi: 10.1016/j.ecolind.2022.109670

Hua, F., Bruijnzeel, L. A., Meli, P., Martin, P. A., Zhang, J., Nakagawa, S., et al. (2022). The biodiversity and ecosystem service contributions and trade-offs of forest restoration approaches. *Science* 376, 839–844. doi: 10.1126/science.abl4649

Hussain, F., Shah, S. S., Badshah, L., and Durrani, M. J. (2015). Diversity and ecological characteristics of flora of Mastuj valley, district Chitral, Hindukush range, Pakistan. *Pak. J. Bot.* 47, 495–510.

Khan, S. M., Page, S., Ahmad, H., Shaheen, H., and Harper, D. M. (2012). Vegetation dynamics in the Western Himalayas, diversity indices and climate change. *Sci. Tech. Dev.* 31, 232–243.

Khan, W., Khan, S. M., and Ahmad, H. (2015). Altitudinal variation in plant species richness and diversity at Thandiani sub forests division, Abbottabad, Pakistan. *JBES* 7, 46–53.

Khan, W., Khan, S. M., Ahmad, H., Alqarawi, A. A., Shah, G. M., Hussain, M., et al. (2018). Life forms, leaf size spectra, regeneration capacity and diversity of plant species grown in the Thandiani forests, district Abbottabad, Khyber Pakhtunkhwa, Pakistan. *Saudi J. Biol. Sci.* 25, 94–100. doi: 10.1016/j.sjbs.2016.11.009

Khoja, A. A., Haq, S. M., Majeed, M., Hassan, M., Waheed, M., Yaqoob, U., et al. (2022). Diversity, ecological and traditional knowledge of pteridophytes in the western Himalayas. *Diversity* 14:628. doi: 10.3390/d14080628

Kier, G., Mutke, J., Dinerstein, E., Ricketts, T. T., Küper, W., Kreft, H., et al. (2005). Global patterns of plant diversity and floristic knowledge. *J. Biogeogr.* 32, 1107–1116. doi: 10.1111/j.1365-2699.2005.01272.x

Kohli, R. K., Dogra, K. S., Batish, D. R., and Singh, H. P. (2004). Impact of invasive plants on the structure and composition of natural vegetation of Northwestern Indian Himalayas1. *Weed Technol.* 18, 1296–1300. doi: 10.1614/0890-037X(2004)018[1296:IOIPOT]2.0.CO;2

Kraft, N. J., Adler, P. B., Godoy, O., James, E. C., Fuller, S., and Levine, J. M. (2015). Community assembly, coexistence and the environmental filtering metaphor. *Funct. Ecol.* 29, 592–599. doi: 10.1111/1365-2435.12345

Mahar, G., Dhar, U., Rawal, R. S., and Bhatt, I. D. (2009). Implications of location specific data and their usefulness in conservation planning: An example from Indian Himalayan Region (IHR). *Biodivers. Conserv.* 18, 1273–1286. doi: 10.1007/s10531-008-9450-0

Manzoor, M., Riaz, A., Iqbal, Z., and Mian, A. (2016). Biodiversity of Pir Lasura National Park, Azad Jammu and Kashmir, Pakistan. *Sci. Tech. Dev.* 82, 182–196.

Medvecká, J., Jarolímek, I., Hegedüšová, K., Škodová, I., Bazalová, D., Botková, K., et al. (2018). Forest habitat invasions–Who with whom, where and why. *For. Ecol. Manag.* 409, 468–478. doi: 10.1016/j.foreco.2017.08.038

Mitchell, J. C., Kashian, D. M., Chen, X., Cousins, S., Flaspohler, D., Gruner, D. S., et al. (2023). Forest ecosystem properties emerge from interactions of structure and disturbance. *Front. Ecol. Environ.* 21:14–23. doi: 10.1002/fee.2589

Myers, N., Mittermeier, R. A., Mittermeier, C. G., Da Fonseca, G. A., and Kent, J. (2000). Biodiversity hotspots for conservation priorities. *Nature* 403, 853–858. doi: 10.1038/35002501

Nafeesa, Z., Haq, S. M., Bashir, F., Gaus, G., Mazher, M., Anjum, M., et al. (2021). Observations on the floristic, life-form, leaf-size spectra and habitat diversity of vegetation in the Bhimber hills of Kashmir Himalayas. *Acta Ecol. Sin.* 41, 228–234. doi: 10.1016/j.chnaes.2021.03.003

Niu, H. B., Liu, W. X., Wan, F. H., and Liu, B. (2007). An invasive aster (*Ageratina adenophora*) invades and dominates forest understories in China: Altered soil microbial communities facilitate the invader and inhibit natives. *Plant Soil* 294, 73–85. doi: 10.1007/s11104-007-9230-8

Noss, R. F. (1983). A regional landscape approach to maintain diversity. *BioScience* 33, 700–706. doi: 10.2307/1309350

Olson, D. M., Dinerstein, E., Wikramanayake, E. D., Burgess, H. D., Powell, G. V., and Underwood, C. E. (2001). Terrestrial ecoregions of the world: A new map of life on earth a new global map of terrestrial ecoregions provides an innovative tool for conserving biodiversity. *BioScience* 51, 933–938. doi: 10.1641/0006-3568(2001)051[0933:TEOTWA]2.0.CO;2

Pérez-Harguindeguy, N., Diaz, S., Garnier, E., Lavorel, S., Poorter, H., Jaureguiberry, P., et al. (2016). Corrigendum to: New handbook for standardised measurement of plant functional traits worldwide. *Aust. J. Bot.* 64, 715–716. doi: 10.1071/BT1 2225_CO

Pérez-Ramos, I. M., Matías, L., Gómez-Aparicio, L., and Godoy, O. (2019). Functional traits and phenotypic plasticity modulate species coexistence across contrasting climatic conditions. *Nat. Commun.* 10:2555. doi: 10.1038/s41467-019-10453-0

Qian, H., Zhou, Y., Zhang, J., Jin, Y., Deng, T., and Cheng, S. (2021). A synthesis of botanical informatics for vascular plants in Africa. *Ecol. Inform.* 64:101382. doi: 10.1016/j.ecoinf.2021.101382

Qureshi, R., and Bhatti, G. R. (2010). Floristic inventory of PAI Forest, Nawab Shah, Sindh, Pakistan. *Pak. J. Bot.* 42, 2215–2224.

R Core Team (2020). *A language and environment for statistical computing*. Vienna: R Foundation for Statistical Computing.

Rahman, I. U., Afzal, A., Iqbal, Z., Abd Allah, E., Alqarawi, A. A., Calixto, E. S., et al. (2019a). Role of multivariate approaches in floristic diversity of Manoor Valley (Himalayan Region), Pakistan. *Appl. Ecol. Environ. Res.* 17, 1475–1498. doi: 10.15666/aeer/1702_14751498

Rahman, I. U., Calixto, E. S., Afzal, A., Iqbal, Z., Ali, N., Ijaz, F., et al. (2019b). "Advanced multivariate and computational approaches in agricultural studies," in *Essentials of bioinformatics*, Vol. III, eds K. Hakeem, N. Shaik, B. Banaganapalli, and R. Elango (Cham: Springer), 93–102. doi: 10.1007/978-3-030-193 18-8_5

Rahman, I. U., Afzal, A., Iqbal, Z., Bussmann, R. W., Alsamadany, H., Calixto, E. S., et al. (2020). Ecological gradients hosting plant communities in Himalayan subalpine pastures: Application of multivariate approaches to identify indicator species. *Ecol. Inform.* 60:101162. doi: 10.1016/j.ecoinf.2020.101162

Rahman, I. U., Afzal, A., Iqbal, Z., Ijaz, F., Ali, A., Asif, M., et al. (2018). First insights into the floristic diversity, biological spectra and phenology of Manoor Valley, Pakistan. *Pak. J. Bot.* 5, 1113–1124.

Rahman, I. U., Hart, R. E., Ijaz, F., Afzal, A., Iqbal, Z., and Calixto, E. S. (2022). Environmental variables drive plant species composition and distribution in the moist temperate forests of Northwestern Himalaya, Pakistan. *PLoS One* 17:e0260687. doi: 10.1371/journal.pone.0260687

Rashid, I., Haq, S. M., Lembrechts, J. J., Khuroo, A. A., Pauchard, A., and Dukes, J. S. (2021). Railways redistribute plant species in mountain landscapes. *J. Appl. Ecol.* 58, 1967–1980. doi: 10.1111/1365-2664.13961

Raunkiaer, C. (1934). *The life forms of plants and statistical geographical*. Oxford: Clarendon Press, 632.

Safidkon, F., R. Kalvandi, M. Atri and M.M. Barazandeh. (2003). Contribution for the characterization of *Thymus eriocalyx* chemotypes. *Int. Mag. Cosmet. Fragr.*

Semwal, D. P., Uniyal, P. L., and Bhatt, A. B. (2010). Structure, composition and dominance–diversity relations in three forest types of a part of Kedarnath Wildlife Sanctuary, Central Himalaya, India. *Not. Sci.* 2, 128–132. doi: 10.15835/nsb234655

Shaheen, H., and Qureshi, R. A. (2011). Vegetation types of Sheosar Lake and surrounding landscape in Deosai Plains of North Pakistan, Western Himalayas. *J. Med. Plant Res.* 5, 599–603.

Sharma, J., and Raina, A. K. (2018). Quantitative analysis, distributional pattern and species diversity of woody plant species of Lamberi Forest Range, Rajouri, J&K, India. *J. Nat. Appl. Sci.* 10, 522–527. doi: 10.31018/jans.v10i1.1661

Shimwell, D. W. (1971). *The description and classification of vegetation*. London: Sedgwick and Jackson, 322.

Singh, G., and Rawat, G. S. (2012). "Depletion of oak (*Quercus* spp.) forests in the western Himalaya: Grazing, fuelwood and fodder collection," in *Global perspectives on sustainable forest management*, ed. C. A. Okia (Crotia: Intech publisher), 29–42. doi: 10.5772/33554

Solefack, M. C. M., Fedoung, E. F., and Temgoua, L. F. (2018). Factors determining floristic composition and functional diversity of plant communities of Mount Oku forests, Cameroon. *Asia Pac. Biodivers.* 11, 284–293. doi: 10.1016/j.japb.2018.03.005

Sørensen, T. (1948). A method of establishing groups of equal amplitude in plant sociology based on similarity of species content and its application to analyses of the vegetation on Danish commons. *Videnski Selskab Biologiske Skrifter* 5, 1–34.

Suyal, S., Sharma, C. M., Gairola, S., Ghildiyal, S., Rana, C., Butola, D. S. (2010). Phyto diversity (angiosperms and gymnosperms) in Chaurangikhal forest of Garhwal Himalaya, Uttarakhand, India. *Indian J. Sci. Tech.* 3, 267–275. doi: 10.17485/ijst/2010/v3i3.2

Ullah, U., Rahim, F., Jan, H. A., Haq, S. M., Wali, S., and Filimban, F. Z. (2022). A survey of the floristic composition of the Kambat Valley, District Dir Lower, Northern Pakistan. *Acta Ecol. Sin.* doi: 10.1016/j.chnaes.2022.08.002

Vakhlamova, T., Rusterholz, H. P., Kanibolotskaya, Y., and Baur, B. (2016). Effects of road type and urbanization on the diversity and abundance of alien species in roadside verges in Western Siberia. *Plant Ecol.* 217, 241–252. doi: 10.1007/s11258-016-0565-1

van Boheemen, L. A., Atwater, D. Z., and Hodgins, K. A. (2019). Rapid and repeated local adaptation to climate in an invasive plant. *New Phytol.* 222, M614–M627. doi: 10.1111/nph.15564

Verma, R. K., and Kapoor, K. S. (2011). Plant species diversity in Ropa-Giavung valley in cold deserts of District Kinnaur, Himachal Pradesh. *Biol. Forum Int. J.* 3, 34–43.

Waheed, M., Haq, S. M., Arshad, F., Bussmann, R. W., Iqbal, M., Bukhari, N. A., et al. (2022). Grasses in semi-arid lowlands—community composition and spatial dynamics with special regard to the influence of edaphic factors. *Sustainability* 14:14964. doi: 10.3390/su142214964

Wali, S., Jan, H. A., Haq, S. M., Calixto, E. S., Bussmann, R. W., and Rahim, F. (2022). Phyto-ecological study of the forests of Shishi Koh Valley, Chitral, Pakistan. *Vegetos* 35, 1024–1035. doi: 10.1007/s42535-022-00379-2

Influence of snowpack on forest water stress in the Sierra Nevada

Stefano Casirati[1]*, Martha H. Conklin[2] and Mohammad Safeeq[2,3]

[1]School of Engineering and Environmental Systems Graduate Program, University of California, Merced, Merced, CA, United States, [2]Civil and Environmental Engineering, University of California, Merced, Merced, CA, United States, [3]Division of Agriculture and Natural Resources, University of California, Davis, Davis, CA, United States

Higher global temperatures and intensification of extreme hydrologic events, such as droughts, can lead to premature tree mortality. In a Mediterranean climate like California, the seasonality of precipitation is out of sync with the peak growing season. Seasonal snowpack plays a critical role in reducing this mismatch between the timing of water input to the root zone and the peak forest water use. A loss of snowpack, or snow droughts, during warmer years, increases the asynchrony between water inputs and the peak of forest water use, intensifying water stress and tree mortality. Therefore, we hypothesize that the montane vegetation response to interannual climate variability in a Mediterranean climate is regulated by the snowpack. We tested this hypothesis using the 2012−2015 drought as a natural experiment. Regional Generalized Additive Models (GAMs) were used to infer and quantify the role of snowpack on forest water stress. The models simulate the Normalized Difference Infrared Index (NDII) as a proxy of forest water stress using water deficit (as seasonality index), location, slope, and aspect. The GAMs were trained using 75% of the data between 2001 and 2014. The remaining 25% of the data were used for validation. The model was able to simulate forest water stress for 2015 and 2016 across the northern, central, and southern Sierra Nevada with a range of R^2 between 0.80 and 0.84. The simulated spatial patterns in forest water stress were consistent with those captured by the USDA Forest Service Aerial Detection Survey. Our findings suggest that the failure of a reduced snowpack in mitigating water deficit exacerbates forest water stress and tree mortality. Variations in water and surface energy budget across an elevational gradient play a critical role in modulating the vegetation response. These results provide insights into the importance of the Sierra Nevada snowpack under a warming climate. The models can aid forest managers to identify future forest water stress and tree die-off patterns.

KEYWORDS

drought, forest, waterstress, tree mortality, snow, water deficit

Highlights

- Snowpack loss increases forest water stress and tree mortality.
- Trade-offs between water and energy availability across the landscape modulate the vegetation response.
- This study provides a predictive tool for identifying forest vulnerability to snowpack losses.

1. Introduction

Mediterranean mountainous ecosystems, such as Sierra Nevada forests in California, USA, are characterized by cold, wet winters and hot, dry summers. Precipitation (P) occurs mostly between October and May when water demand is low, asynchronous with the peak summer growing season (May–September). The temporal offsets between evapotranspiration demand and water inputs highlight the importance of above-ground snowpack storage and subsurface soil water storage in supporting forest ecosystems during the growing season (Garcia and Tague, 2015).

Droughts can intensify tree water stress and elevate the risks of tree mortality, particularly when coupled with higher temperatures (McDowell et al., 2008; Allen et al., 2015). Large precipitation deficits combined with remarkably warmer temperatures in 2014 and 2015 intensified the drought in California leading to a massive forest die-off (Williams et al., 2015; Bales et al., 2018; Goulden and Bales, 2019; Restaino et al., 2019). However, Sierra Nevada forests' response to drought is highly variable between water- and energy-limited regions (Das et al., 2013; Paz-Kagan et al., 2017). A temperature rise increases the vapor pressure deficit, causing more water stress in water-limited areas than in energy-limited areas (Allen et al., 2015; Bales et al., 2018).

Terrestrial water storage in the form of snowpack is particularly vulnerable to global warming and droughts. An increase in temperature influences the fraction of precipitation that falls as snow during the winter season, and the position of the rain–snow transition in the landscape, reducing the subsurface storage recharge through snowmelt during the spring and early summer (Garcia and Tague, 2015; Meixner et al., 2016). This loss of above-ground storage limits recharge to the root zone during the dry season (Barnett et al., 2005; Garcia and Tague, 2015). Even though Mediterranean forests are well adapted to hot and dry summers, high interannual and interseasonal precipitation variability can often induce water stress conditions (Tague et al., 2019). A reduction in water storage, both surface and subsurface, available to the vegetation during part of the growing season and extreme variations in evapotranspiration demand resulting from warmer temperatures and heatwaves are important contributors to forest ecosystem water stress (Allen et al., 2015; Garcia and Tague, 2015). Severe tree water stress conditions are known to trigger mechanisms of hydraulic failure, carbon starvation, and increased vulnerability to biotic agents, all of which contribute to tree mortality (McDowell et al., 2008). Recent studies have linked the 2012–2015 tree die-off in the Sierra Nevada to multi-year drying of the deep root zone water storage under below-normal precipitation and excessive warming (Goulden and Bales, 2019) along with increased competition for water due to an increase in tree density caused by an extensive fire suppression over the last century (Young et al., 2016; Fettig et al., 2019).

Declines in mountain snowpack have been observed in the last century across Western North America (Mote et al., 2005) as the precipitation phase continues to shift toward more rain instead of snow (Knowles et al., 2006; Safeeq et al., 2015). In the Sierra Nevada, the snowpack is expected to decline by as much as ~45% by the year 2050 (Siirila-Woodburn et al., 2021). Warmer atmospheric rivers are expected to produce more rain than snow

(Siirila-Woodburn et al., 2021). Snow accumulation modulates the water availability in water-limited mid-elevations and is linked to forest productivity (Trujillo et al., 2012). Hence, in a warmer climate, the contribution of snowpack storage supporting forest ecosystems during the growing season will be reduced. In addition, future precipitation events will likely be more extreme but less frequent (Bedsworth et al., 2018; Swain et al., 2018). Therefore, the soil would dry earlier in the spring, the dry summer conditions will last longer, and warmer temperatures will further intensify summer droughts (Thorne et al., 2015; Swain et al., 2018). The exceptionally warm and dry droughts of the years 2014 and 2015, characterized by low snowpack, can be considered a likely analog for future climate and water supply scenarios (Dettinger and Anderson, 2015; Mann and Gleick, 2015).

Normalized Difference Infrared Index (NDII) (Kimes et al., 1981; Hardisky et al., 1983; Yilmaz et al., 2008), frequently called Normalized Difference Moisture Index (NDMI, Wilson and Sader, 2002), has been often used to map tree water stress and forest die-off. NDII showed a strong correlation with water balance, such as Precipitation (P)–Evapotranspiration (ET), and with the dead trees detected by the USDA Forest Service Aerial Detection Survey (ADS, U.S. Forest Service, 2016) in the Sierra Nevada (Goulden and Bales, 2019). However, the role of water delivery by snowmelt during late spring and early summer in regulating forest water stress has not yet been fully understood. Here, we utilized the 2012–2015 tree mortality episode in the Sierra Nevada as a natural experiment to investigate the role of snowpack in modulating the patterns of forest water stress and die-off. We hypothesize that the vegetation response to interannual variability in a Mediterranean climate is regulated by the snowpack dynamics. In the absence of snowpack storage, subsurface soil water storage alone may not be enough to support summer forest water demands.

The study was organized according to the following steps: (I) collect and assemble existing spatial climate datasets and register them at the same spatial scale (coordinate reference system and spatial resolution); (II) calculate water deficit using a spatial water balance approach; (III) analyze vegetation responses to water deficit across the elevation gradient; and (IV) build, train, and test a set Generalized Additive Models (GAMs) and use them to simulate 2015 and 2016 NDII.

2. Methods

2.1. Study area

We focused the study on the western slope of the Sierra Nevada mountains in California (Figure 1). To better capture the climate and geologic variability, the study area was further divided into three regions: Northern Sierra (NS), Central Sierra (CS), and Southern Sierra (SS) (Figure 1A). This analysis focused on drought-sensitive evergreen forests (Figure 1B).

Northern Sierra is characterized by moderate elevation (elevation range from 42 to 3,071 m_{asl}, mean = 1,274 m_{asl}) and underlying volcanic and metamorphic rocks (Irwin, 1990). The average (2000–2016) annual precipitation and mean daily
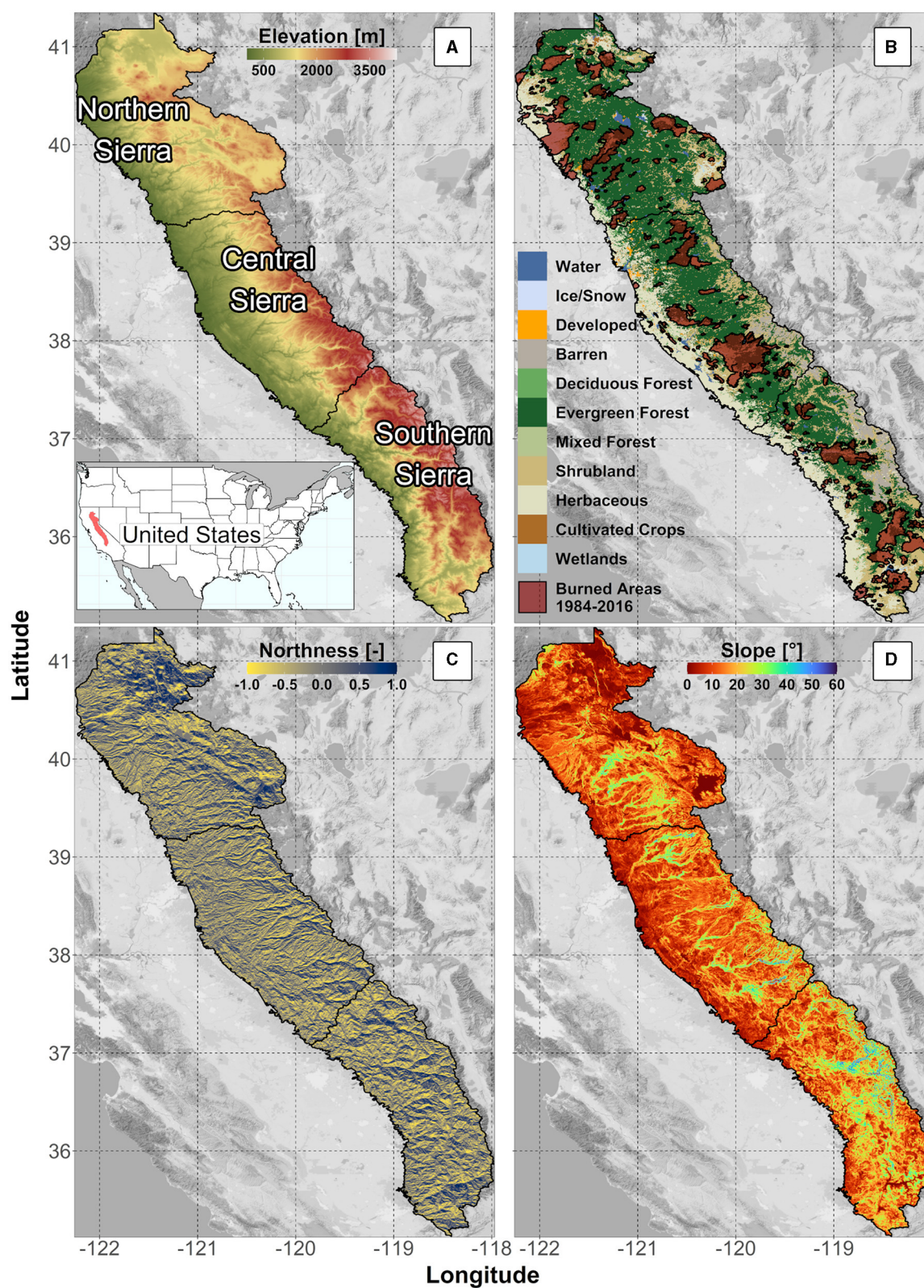
FIGURE 1
Sierra Nevada's study area and landscape characteristics: **(A)** study area's regions: northern, central, and southern Sierra, with elevation in meters above the sea level; **(B)** land cover classes from NLCD2011 and burned areas obtained from MTBS; **(C)** northness (North = 1, South = −1); **(D)** slope in degrees [°].
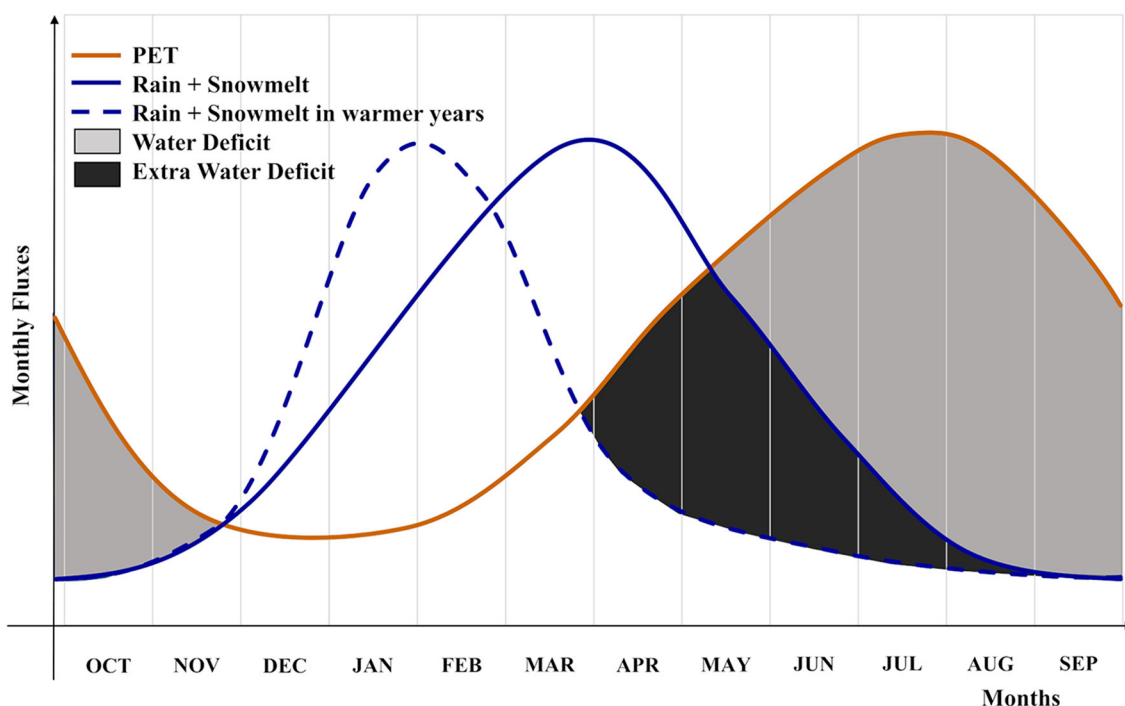
FIGURE 2
Conceptual diagram including the monthly potential evapotranspiration (PET, orange line); monthly water inputs (monthly rain + monthly snowmelt) in a water year characterized by an average snowpack (blue continuous line), and in a water year with a reduced snowpack (blue dashed line). Water deficit (gray areas) represents the negative difference between water inputs and potential evapotranspiration. A reduction in the snowpack, with a consequent failure in delivering the water during the spring and early summer, involves an increase in water deficit [extra water deficit (dark-gray area)].

temperature over the NS region were 1,149 mm/yr and 10.7°C, respectively. CS is characterized by a slightly steeper elevation gradient (elevation range from 51 to 3,807 m_{asl}, mean = 1,259 m_{asl}) and by the presence of metamorphic and granitic rocks (Irwin, 1990). The precipitation averaged over the CS was 1,076 mm/yr, and the mean temperature was 11.7°C between 2000 and 2016. SS is characterized by a higher elevation (elevation range from 1,346 to 4,033 m_{asl}, mean = 1,837 m_{asl}) and by the predominance of granitic rocks (Irwin, 1990). The 2000–2016 precipitation averaged over the SS was 768 mm/yr, and the 2000–2016 average mean temperature was 9.3°C. As evident, the amount of precipitation and average temperature decrease along the north–south gradient, causing more of that precipitation to fall as snow (Bales et al., 2006).

The ecosystems in the study area follow the elevational gradient. At low elevations below approximately 1,200 m_{asl}, the lower montane blue oak-foothill pine woodland and savanna are dominant. This system is characterized by species, such as California foothill pines (*Pinus sabiniana*), oaks, and other broadleaf trees and shrubs. Low- and mid-elevations, ranging from approximately 600 to 1,800 m_{asl} in the NS and 800 to 1,600 m_{asl} in the CS and SS, are dominated by dry-mesic mixed conifer forests, like Douglas firs (*Pseudotsuga menziesii*), ponderosa pines (*Pinus ponderosa*), and California incense cedars (*Calocedrus decurrens*). Mesic mixed conifer forests dominate the mid-elevation region (1,400–2,500 m_{asl}), which has an average annual precipitation of 1,000–1,500 mm, with roughly half falling as snow. This elevation

region is characterized by conifers such as white firs (*Abies concolor*), California incense cedars (*C. decurrens*), and sugar pines (*P. lambertiana*), with limited areas dominated by Giant Sequoias (*Sequoiadendron giganteum*). Ponderosa pine (*P. ponderosa*) and jeffrey pine (*P. jeffreyi*) forests can be found at higher elevations (2,200–3,000 m_{asl}), while red fir (*A. magnifica*) forests can be found mostly in areas with deep, drained soils that heavily rely on snowpack. At elevations above 3,000 m_{asl}, the subalpine lodgepole pine (*P. contorta*) is dominant (Comer et al., 2003; U.S. Geological Survey, 2016; Supplementary Figure S1).

2.2. Spatial datasets

2.2.1. Digital elevation model, land cover, and fire masks

The study area was delineated using ~30 m (1 arc-second, Figure 1A) digital elevation model (DEM, U.S. Geological Survey, 2017) and the HUC-8 watershed boundaries from the USGS Watershed Boundary Dataset, WBD (U.S. Geological Survey, 2020). We performed a terrain analysis, using TauDEM (Tarboton, 2005) and R (R Core Team, 2021), and obtained northness (North/South) and slope (Figures 1C, D).

We used land cover data from the National Land Cover Database (NLCD 2011; Dewitz, 2014) and the GAP/LANDFIRE National Terrestrial Ecosystems (U.S. Geological Survey, 2016), respectively, to select all the pixels with evergreen forests

TABLE 1 Ecological systems used in defining the two-year cumulative Water Deficit (WD) smooths in the GAM model.

Region	GAP/landfire description	Percentage of pixels
Northern Sierra	Mediterranean California mesic mixed conifer forest and woodland	51%
	Mediterranean California dry-mesic mixed conifer forest and woodland	17%
	California montane jeffrey pine-ponderosa pine woodland	7%
	Mediterranean California lower montane black oak-conifer forest and woodland	7%
	Other	18%
	Total	**100%**
Central Sierra	Mediterranean California mesic mixed conifer forest and woodland	35%
	California lower montane blue oak-foothill pine woodland and savanna	20%
	Mediterranean California dry-mesic mixed conifer forest and woodland	20%
	Sierra Nevada subalpine lodgepole pine forest and woodland	6%
	Other	19%
	Total	**100%**
Southern Sierra	Mediterranean California mesic mixed conifer forest and woodland	25%
	Sierra Nevada subalpine lodgepole pine forest and woodland	22%
	Mediterranean California red fir forest	13%
	California lower montane blue oak-foothill pine woodland and savanna	10%
	Other	30%
	Total	**100%**

(Figure 1B) and to identify the most common plant communities. Monitoring Trends in Burn Severity (MTBS, Eidenshink et al., 2007) burned area polygons (Figure 1B) were used to mask and exclude all areas where a fire occurred between 1984 and 2016 from the further analysis. Additional information is reported in the Supplementary material (section "land cover and fire masks").

2.2.2. Precipitation and temperatures

We obtained daily total precipitation (mm/day) and daily maximum and minimum temperatures (°C) from the parameter-elevation regressions on the independent slopes model (PRISM, Daly et al., 1994) at 30 arcsec (∼800 m) resolution from 2000 to 2016. We aggregated the daily rasters to obtain the monthly average temperatures (T_m) and monthly total precipitation (P_m). P_m and T_m were then spatially downscaled from 30 arcsec (∼800 m) to 0.005 degrees (∼500 m) resolution using the downscaling method from Zimmermann and Roberts (2001) and Lute and Abatzoglou (2020). Additional information on the downscaling method is reported in the Supplementary material (section "precipitation and temperatures downscaling method").

2.2.3. Monthly potential evapotranspiration

We calculated monthly potential evapotranspiration (PET_m) for each pixel, using the modified Hamon approach (1963) (adopted by Dingman, 2002; Fellows and Goulden, 2016; Roche et al., 2020): first, monthly potential evapotranspiration was

estimated using the original Hamon (1963) model as follows:

$$PET_{Hamon} = 29.8 * n * L * \left(\frac{E_{sat}}{T_m + 273.2} \right) \qquad (1)$$

where L is the median day length (hours) (obtained using *insol* R package; Corripio, 2021); n is the number of days in the month; T_m is the monthly average temperature; and E_{sat} is the saturated vapor pressure (kPa) calculated as $E_{sat} = 0.611 * exp\left(\frac{17.3 * T_m}{T_m + 237.3} \right)$. Subsequently, PET_{Hamon} values were adjusted using a scaling factor of 1.265 to minimize the bias (Fellows and Goulden, 2016) as follows:

$$PET_m = 1.265 * PET_{Hamon} \qquad (2)$$

2.2.4. Snow water equivalent

We obtained daily snow water equivalent (SWE) (2000–2016) from the Sierra Nevada snow reanalysis dataset (Margulis et al., 2015, 2016). We used changes in daily SWE (ΔSWE) to estimate monthly snow accumulation ($\sum SWE_+$) and monthly snowmelt output ($\sum SWE_-$). Sublimation losses and snow redistribution were not considered. In the event of a discrepancy between P_m and $\sum SWE_+$, we adjusted the P_m to match the differences between the two datasets. For each month m, if the total precipitation was less than the snow accumulation, we adjusted the total precipitation to match the snow accumulation.

TABLE 2 Average values of climate and forest water stress variables for each region obtained considering all the unburned evergreen forest pixels.

Average values	1: Northern Sierra			2: Central Sierra			3: Southern Sierra		
	2000−2016	2007−2008	2012−2015	2000−2016	2007−2008	2012−2015	2000−2016	2007−2008	2012−2015
T avg (°C)	10.7	10.5	11.4	11.7	11.7	12.4	9.3	9.2	9.9
Tot PPT (mm)	1,149	846	921	1,076	792	795	768	558	461
Snow Acc. (mm)	267	255	139	333	310	181	432	395	223
NDII (−)	0.254	0.257	0.251	0.204	0.203	0.197	0.123	0.126	0.108
Tot PPT– Snow Acc. (mm)	882	591	782	743	482	614	336	163	238
Δ Tot PPT (%)	-	−26%	−20%	-	−26%	−26%	-	−27%	−40%
Δ Tot PPT–Snow Acc. (%)	-	−33%	−11%	-	−35%	−17%	-	−51%	−29%
Δ Snow Acc. (%)	-	−4%	−48%	-	−7%	−46%	-	−9%	−48%
Δ NDII (%)	-	2%	−1%	-	−1%	−4%	-	2%	−12%

The percentage change (%) is calculated over the 2000–2016 mean.

2.2.5. Water deficit

We used the seasonality index (Leibowitz et al., 2011; Wigington et al., 2012) to explore and analyze seasonal water availability and its effect on vegetation. A monthly water surplus (S_m) can be estimated as follows:

$$S_m = P_m - PET_m - SWE_m \qquad (3)$$

where ΔSWE_m is the monthly variation in snow water equivalent estimated as the difference between snow accumulation and melt (i.e., $\sum SWE_+ - \sum SWE_-$). Equation (3) accounts for the seasonality of water inputs and water demands. We defined water surplus (WS) when $S_m > 0$ and water deficit (WD) when $S_m < 0$. We calculated the yearly WD as the sum of the monthly WD for each water year. For clarity, we reversed the sign of the WD to have positive values.

We focused on the WD months to emphasize the importance of water released through snowmelt during the growing season (Figure 2). During a warmer year, a snowpack loss will reduce the water available for the vegetation during the dry summer season, inducing an additional WD. The extra WD, triggered by snowpack loss, is additionally exacerbated by an increase in evaporative demand (not reported in the conceptual Figure 2). In this study, we did not account for lateral flow and subsurface water storage.

2.2.6. Forest water stress

Normalized Difference Infrared Index (NDII) is a spectral index sensitive to vegetation canopy water content (Ceccato et al., 2002; Davidson et al., 2006). NDII is correlated with the canopy water content in different forest types (Cheng, 2007). We obtained near-infrared reflectance (NIR) and short-wave infrared reflectance (SWIR) values from MODIS/Terra 8-Day L3 Global 500 m (MOD09A1 Version 6; Vermote, 2015), from 2001 to 2016. Conversions from sinusoidal projection to NAD 83 were performed using the *MODIStsp* R package (Busetto and Ranghetti, 2016).

NDII was computed using the formula:

$$NDII = \frac{NIR - SWIR}{NIR + SWIR} \qquad (4)$$

Monthly NDII was obtained as the median of 8-day NDII. The 8-day NDII values were masked for clouds by excluding all the pixels with state quality assessment flags different than "*clear.*" Pixels with poor data quality were flagged as missing. While spring NDII reflects year-to-year variations in perennial evergreen and deciduous vegetation, it also includes the peak of grasses and spring deciduous vegetation productivity. Late summer season NDII is better suited to isolate the interannual response of evergreen forests (Goulden and Bales, 2019). Therefore, late summer season NDII (hereafter NDII) was calculated as an average of August, September, and October NDII.

2.3. Analysis

2.3.1. Progression of the drought

We performed an exploratory analysis to investigate the time series of average temperatures, precipitation,
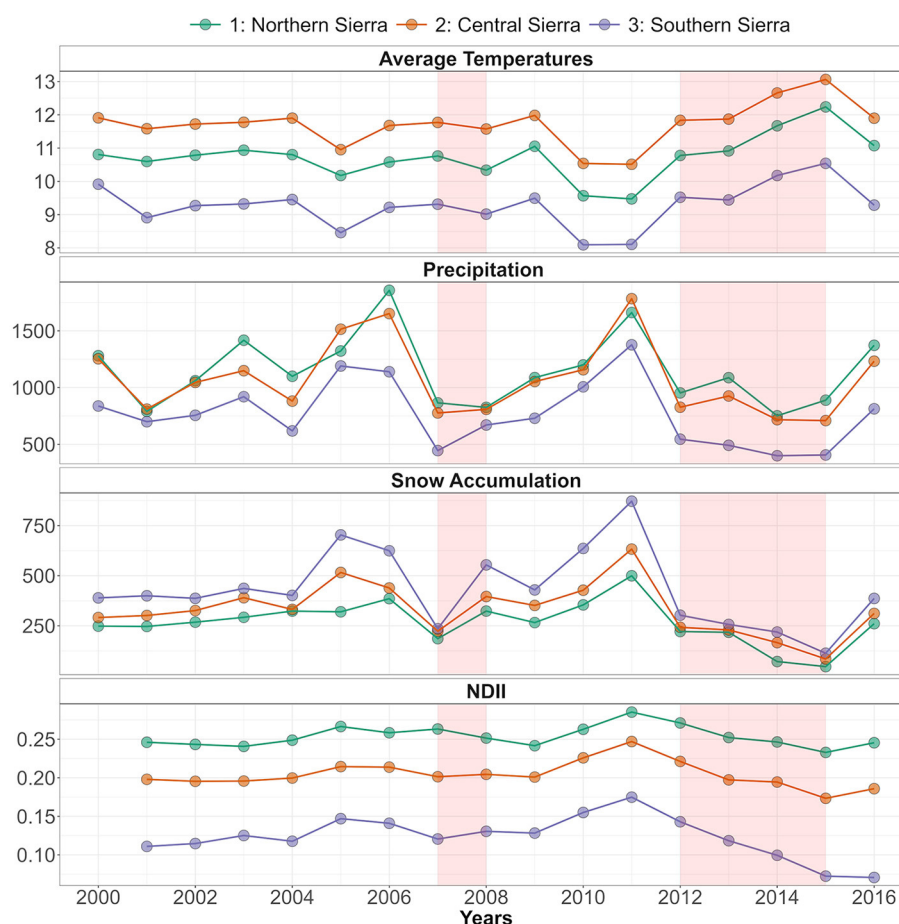
FIGURE 3
Time series of average temperatures, precipitation, and snow accumulation, from 2000 to 2016, and Normalized Difference Infrared Index (NDII), from 2001 to 2016, across the three study regions (NS, CS, and SS). The 2007−2008 and the 2012−2015 droughts are highlighted in red.

and snow accumulation, from 2000 to 2016, and NDII, from 2001 to 2016, for each Sierra Nevada study region (i.e., NS, CS, and SS). Consequently, we analyzed the spatial patterns of cumulative water deficit and the changes in NDII between each year from 2012 to 2016 and the pre-drought conditions, from the 2009–2011 average NDII.

2.3.2. Role of snow on water deficit

Statistical analysis was performed for each Sierra Nevada study region (i.e., NS, CS, and SS) and at six predefined elevation bands ($<$1,000; 1,000–1,500; 1,500–2,000; 2,000–2,500; 2,500–3,000; and $\geq$3,000 m_{asl}). We used the *lmg* (Lindeman et al., 1980) relative importance analysis (*ralaimpo* R package; Groemping, 2006) to quantify the individual contribution (i.e., partition-explained variance) of snowmelt and potential evapotranspiration to water deficit in the linear regression equation, across the elevation bands. Additionally, 95% bootstrap confidence intervals for relative importance were obtained using 1,000 realizations.

2.3.3. Role of water deficit on NDII

We analyzed how NDII is related to water deficit to inspect regional vegetation-elevation patterns. We obtained the yearly averages for each region of NDII (response variable) and WD (explanatory variable), and we built a linear model. Accordingly, we obtained the yearly averages for each region and elevation band, and we performed an analysis of variance (ANOVA) to investigate whether the introduction of the elevation bands as an additive term significantly improved the model. Finally, we investigated the statistical significance of the interaction terms, followed by a regression coefficient pairwise comparison between the elevation bands.

2.3.4. Model building

We developed a set of three generalized additive models (GAMs) to analyze the spatiotemporal effects of multiyear cumulative water deficit on vegetation response. GAMs (Hastie and Tibshirani, 1986) are a semi-parametric extension of generalized linear models (Aalto et al., 2012; Crockett and Westerling, 2017) with a linear predictor involving a sum of smooth functions of covariates. We built separate models for NS, CS, and SS using the
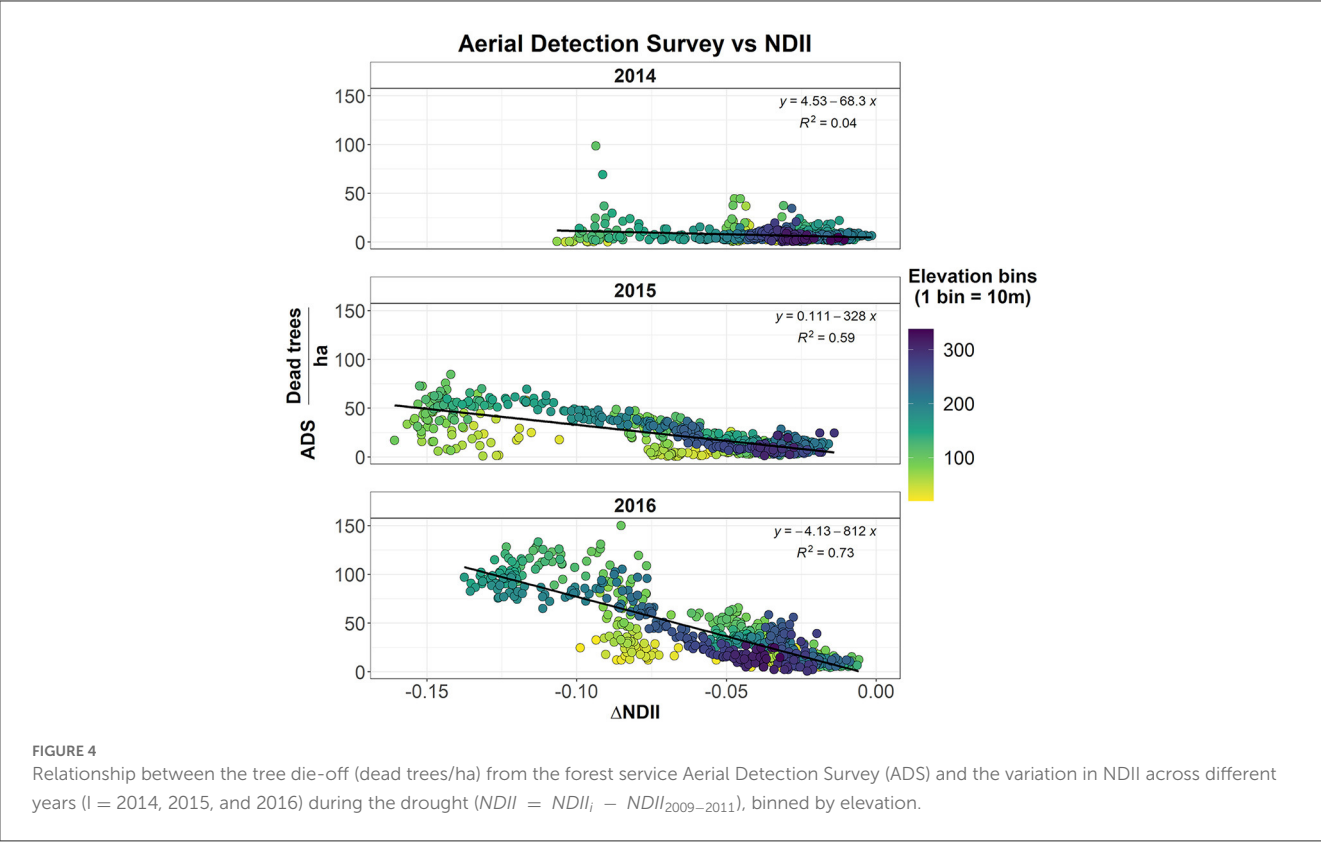
FIGURE 4
Relationship between the tree die-off (dead trees/ha) from the forest service Aerial Detection Survey (ADS) and the variation in NDII across different years (I = 2014, 2015, and 2016) during the drought ($NDII = NDII_i - NDII_{2009-2011}$), binned by elevation.
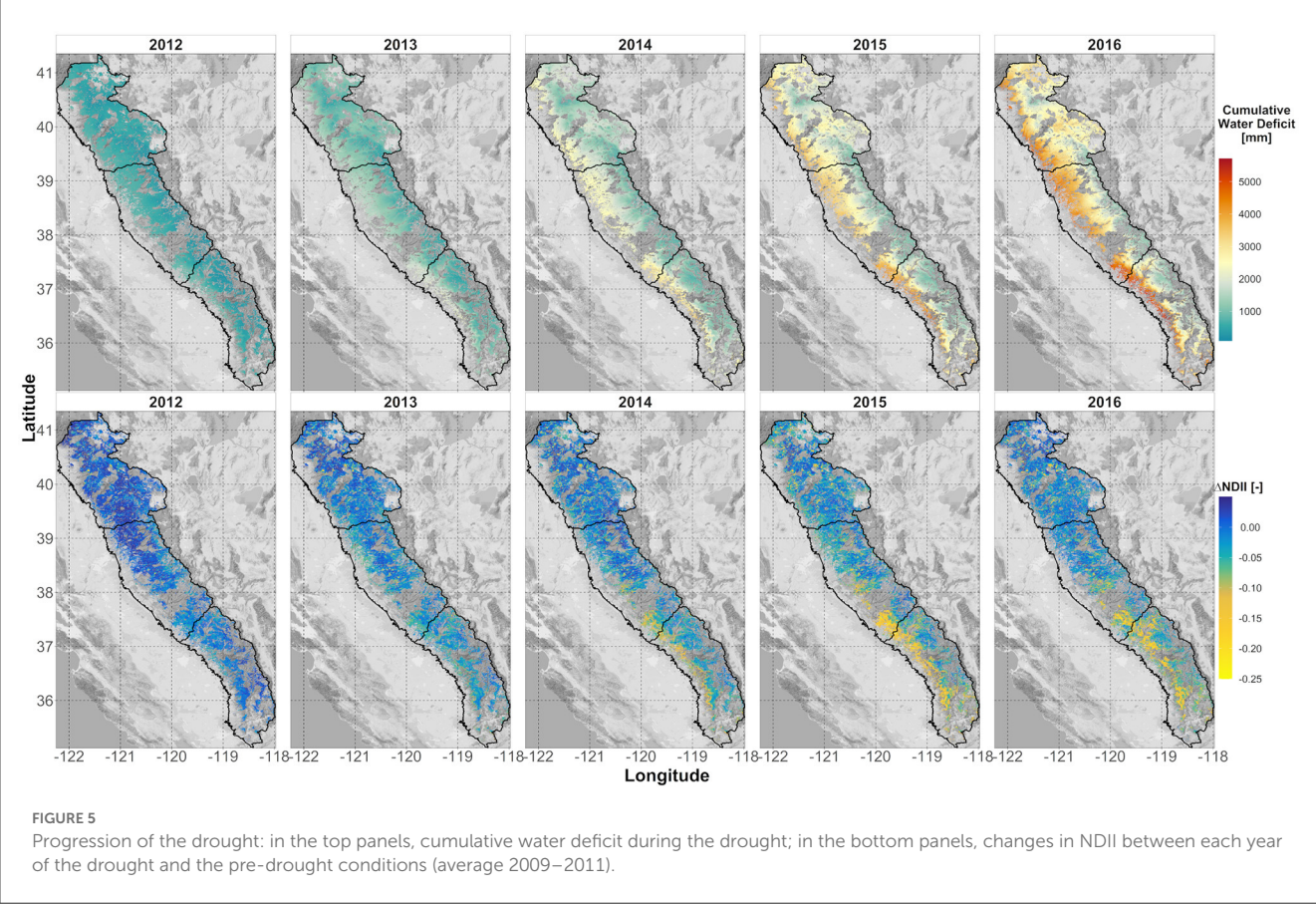
FIGURE 5
Progression of the drought: in the top panels, cumulative water deficit during the drought; in the bottom panels, changes in NDII between each year of the drought and the pre-drought conditions (average 2009−2011).

FIGURE 6
Relationship between NDII and water deficit across northern, central, and southern Sierra. Each dot represents the yearly average of each region.

"Generalized Additive Models for very large datasets" R function (BAM function from *mgcv* package in R (Wood et al., 2014; Wood, 2017; Li and Wood, 2019).

We included four sets of smooth functions s_i in the models (Supplementary Figures S2–S4): The first set of smooth functions includes the 2-year cumulative water deficit for five plant communities' classes and accounts for the multi-year disturbance effect. The plant communities' classes include the four most common terrestrial ecological systems in each region (Table 1), while the fifth class ("other") includes all the remaining evergreen forest pixels. Water deficit is strongly correlated (Pearson's correlation $r > |0.6|$) with many climatic and landscape variables. These variables are, therefore, redundant and excluded from the model. The choice of a 2-year cumulative water deficit is based on model evaluation using Akaike's and the Bayesian information criteria. The second smooth function includes latitude (*lat*) and longitude (*long*) and accounts for spatial locations and spatial correlation between neighboring pixels; the third smooth function includes slope to account for differences between steep and flat areas; the fourth smooth function includes northness to account for the differences in water demands between sunny south-faced slopes and shady north-faced slopes. These smooth functions were used to estimate the vegetation response as NDII index. For each region, the model has the following structure:

$$NDII = \beta_0 + s_{1,j}\left(cumulative\ WD\right) + s_2\left(lat,\ long\right) + s_3\left(slope\right)$$
$$+ s_4\left(northness\right) + \varepsilon \tag{5}$$

where *NDII* is the response, β_0 is the intercept, s_i are smooth functions estimated by fast stable restricted maximum likelihood (fREML), and *lat*, *long*, 2-year cumulative water deficit (*cumulative WD*) for each of the five plant community classes *j*, *slope*, and *northness* are explanatory variables. We selected generalized additive models with separated terms to distinguish the influence of location, slope, northness, and 2-year cumulative WD on NDII. We used thin-plate splines that are particularly suited to interpolate climatic data (Hong et al., 2005; Aalto et al., 2012), to estimate smooth functions based on a scaled *t* distribution to account for heavy-tailed data (Wood et al., 2016). The models were fit to 75% of the data from 2000 to 2014, leaving the

remaining 25% for validation. Consequently, we applied three increasing perturbations (+100 mm, +500 mm, and +800 mm) to the average (2002–2014) 2-year cumulative WD to test the model sensitivity of vegetation moisture response (NDII). We then used the models to simulate 2015–2016 NDII given a 2-year cumulative WD and checked simulation performance. Post-checks on the autocorrelation of model residuals were also performed. Finally, we created a set of maps for forest water stress, defined as NDII anomalies ($NDII_{anomalies} = NDII_{simulated} - NDII_{\overline{2009:2011}}$).

3. Results

3.1. Progression of the 2012–2015 drought

During the 2012–2015 drought, the average precipitation declined by −20% in the NS, −26% in the CS, and −40% in the SS, compared to the 2000–2016 average (Table 2). Additionally, the 2012–2015 drought was also characterized by warmer temperatures (+0.7°C in the NS, +0.6°C in the CS, and +0.7°C in the SS). The snow accumulation declined to its lowest levels [139 mm in the NS (−48%), 181 mm in the CS (−46%), and 223 mm in the SS (−48%)]. Accordingly, the NDII decreased substantially, all but at a varying rate between NS (−1%), CS (−4%), and SS (−12%), compared to the 2000–2016 average (Table 2, Figure 3). As a comparison, the 2007–2008 drought had a similar change in precipitation (−26% in the NS, −26% in the CS, and −27% in the SS). However, the duration of this drought was shorter with slightly cooler temperatures than the 2000–2016 average and thus by a modest snow accumulation decrease (−4% in the NS, −7% in the CS, and −9% in the SS). The average 2007–2008 NDII was higher in the NS (+2%) and the SS (+2%) and slightly lower in the CS (−1%) (Table 2, Supplementary Figure S5). The relationship between the change in NDII during th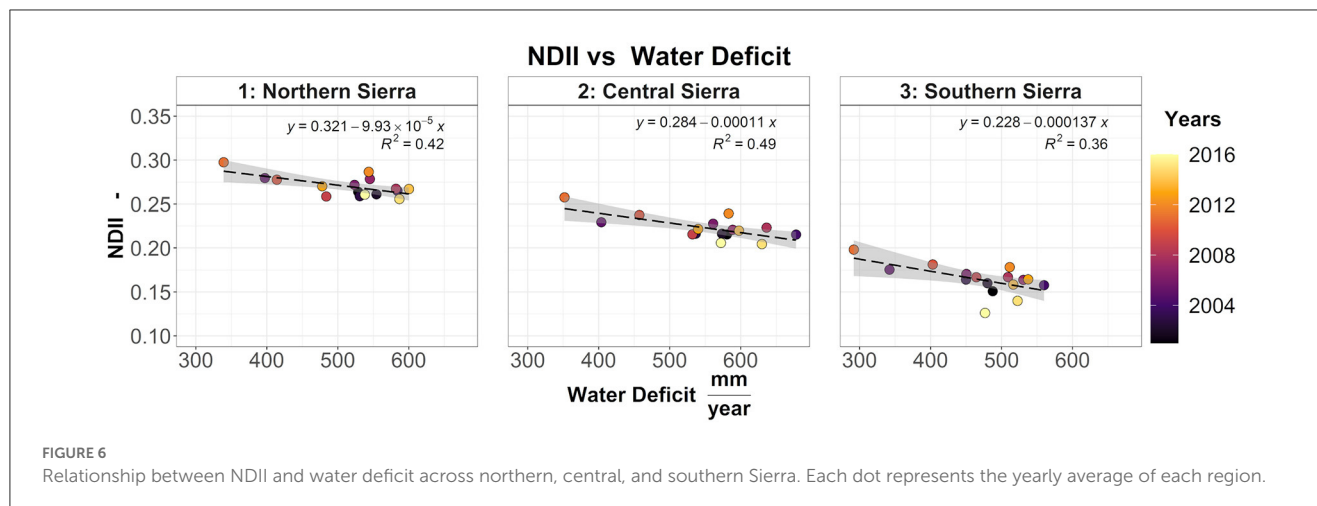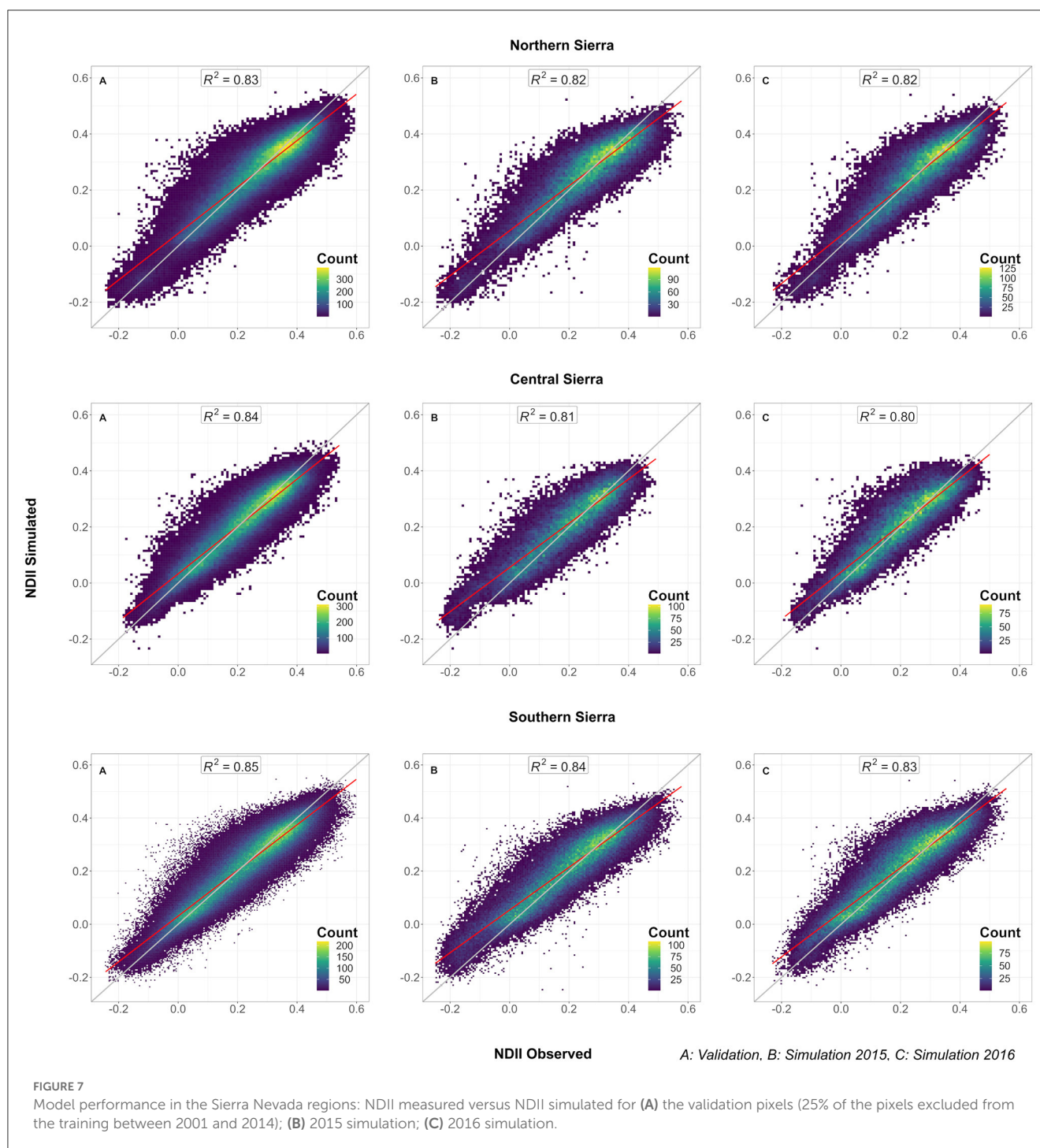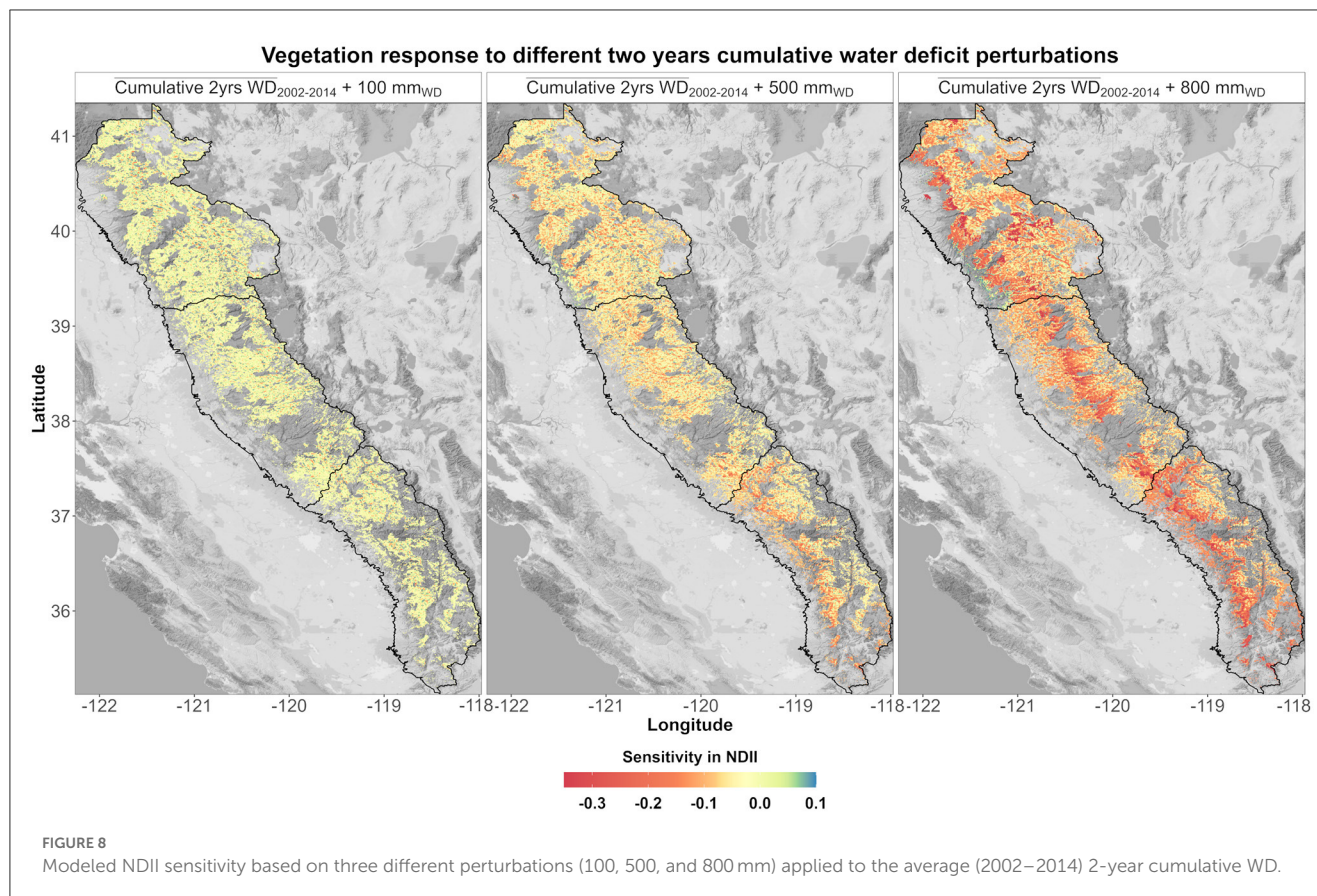e drought and the tree die-off (dead trees/ha) from the Forest Service Aerial Detection Survey (ADS) showed a moderate–strong correlation (Figure 4). The strength of the correlation increased as the drought progressed. In addition, NDII and basal area are related through a linear-log function ($R^2 = 0.35$, *p*-value < 0.001, Supplementary Figure S6) (GNN dataset; LEMMA group, 2015).

FIGURE 7
Model performance in the Sierra Nevada regions: NDII measured versus NDII simulated for **(A)** the validation pixels (25% of the pixels excluded from the training between 2001 and 2014); **(B)** 2015 simulation; **(C)** 2016 simulation.

Spatial patterns of cumulative water deficit severely increased during the drought years. Mid- and low-elevation forests exhibited higher cumulative water deficit, particularly in the SS, where the increase was more severe. The progressive decline in NDII across time is coherent with the cumulative water deficit increase, particularly in SS, which was more affected by tree mortality episodes. However, visual acuity shows a discrepancy between NDII and cumulative water deficit in the NS and the CS (Figure 5). Contrary to the SS, the increased water deficit in the NS and CS in 2015 and 2016 did not correspond to a severe decrease in the NDII.

3.1.1. Role of snowpack

Water deficit has been used to investigate how the loss of snowpack and the increase in evaporative demand aggravated the asynchrony between water inputs and forest water demands. The relative importance analysis showed that snowmelt explained most of the variation of water deficit in the SS (43%), while in the NS and CS, PET was the dominant variable. Across the elevation gradient over the entire study area, the contribution of snowmelt to the water deficit increased with elevation, becoming the

FIGURE 8
Modeled NDII sensitivity based on three different perturbations (100, 500, and 800 mm) applied to the average (2002−2014) 2-year cumulative WD.

most important variable approximately 2,000–2,500 m_{asl} (Supplementary Figure S7).

3.1.2. Role of water deficit on NDII

The regional yearly average vegetation moisture (NDII) decreased from north to south, driven by an increase in WD (Figure 6). However, across the elevation gradient, NDII is non-linearly related to the yearly water deficit (Supplementary Figure S8). Higher elevation pixels (>2,500 m_{asl}) are contradistinguished by lower NDII and lower water deficit. Conversely, lower elevation pixels (<1,000 m_{asl} for central and southern Sierra) are characterized by lower NDII and higher water deficit. Mid-elevation pixels are characterized by higher NDII and moderate water deficit. For each elevation band, an increase in water deficit resulted in a reduction in vegetation water content (negative regression coefficient). For all three regions, the contribution of elevation as an additive term is significant (p-value < 0.05). However, when the interaction term was included in the linear model, only a few elevation bands resulted significantly. The following pairwise comparison indicated no significant difference between the regression coefficients at different elevation bands. The same analysis was repeated using the cumulative 2-year water deficit (Supplementary Figure S9). In the southern Sierra, the 1,000–1,500 m_{asl} regression coefficients resulted significantly different compared to the band <1,000 m_{asl} (p-value $= 0.01$) and the 3,000–4,035 m_{asl} (p-value $= 0.02$)

regression coefficients. All the remaining regression coefficients resulted not significantly different.

3.2. Predicting vegetation water stress with generalized additive models

The models showed a robust performance in predicting vegetation moisture (NDII). For the southern Sierra, the coefficients of determination (R^2) were 0.85, 0.84, and 0.83, respectively, for model validation, 2015 simulation, and 2016 simulation (Figure 7) and the *RMSEs* were 0.051, 0.069, and 0.071, respectively. Although the model had a slight tendency in overestimating the measured MODIS NDII in 2015 and 2016, most of the NDII simulations were consistent with the measured NDII (filled with lighter colors). The models can detect the distribution of the most productive region at mid-elevation [i.e., northern, central, and southern Sierra (Supplementary Figures S2–S4)]. In addition, the model captured an important partial effect of the 2-year cumulative water deficit for each ecological system, as well as a moderate partial effect of the slope and the northness.

3.3. Model sensitivity analysis

A 100-mm increase in the average 2-year cumulative WD was not translated in a conspicuous estimated vegetation
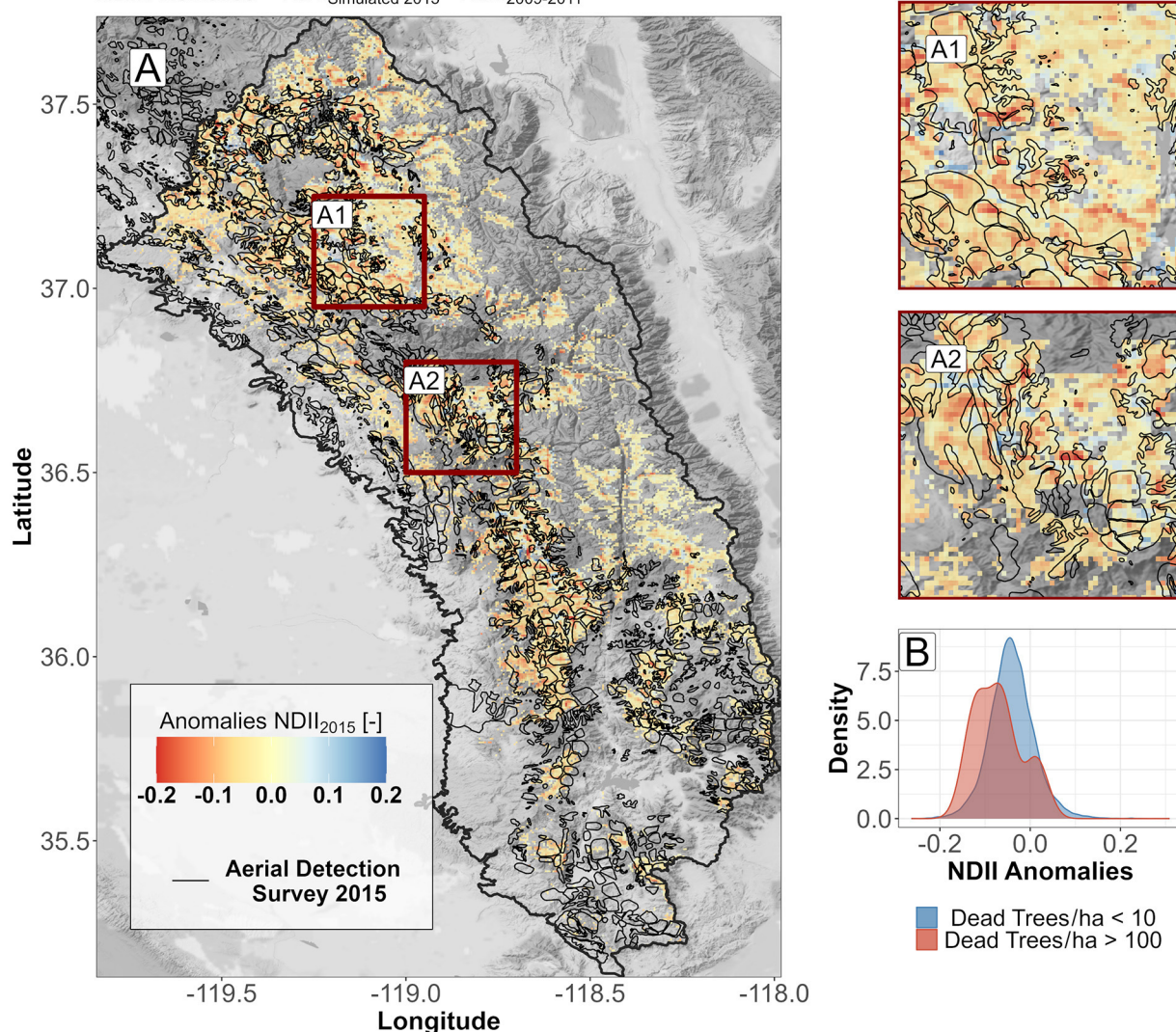
FIGURE 9
(A) Spatial patterns of dead trees from the Aerial Detection Survey (ADS) and anomalies in NDII for the year 2015 in the southern Sierra. A zoom into boxes A1 and A2 highlights the overlay between the ADS and the more severe simulated anomalies in NDII. **(B)** Comparison between density plots of anomalies in NDII for the year 2015 in the southern Sierra: In blue, pixels are characterized by low/undetected tree mortality (<10 dead trees/ha); in red, pixels are characterized by severe tree mortality (>100 dead trees/ha).

moisture variation (±0.05) (Figure 8). A 500-mm perturbation caused a decrease in vegetation moisture response with spatial patterns mostly located in the SS middle-elevation forests. An 800-mm perturbation was translated into a severe decrease in vegetation moisture response across the mid-elevation forests in all the regions. Some low- and high-elevation areas were still insensitive to 2-year cumulative WD perturbations. The model sensitivity was analyzed by region and ecological system (Supplementary Figure S10). By increasing the perturbation, differences in each ecological system are evident. An 800-mm perturbation caused the most severe decrease in vegetation moisture response in the NS dry-mesic mixed conifer forests and the CC and SS mesic mixed conifer forests.

3.4. Forecast maps and spatial patterns of forest water stress

The prediction of vegetation moisture (NDII) combining 2-year cumulative water deficits for each ecological system, slope, northness, and geographical coordinates allowed us to inspect the spatial pattern of forest water stress in relation to the Forest Service Aerial Detection Survey polygons. The water stress has been determined as $NDII_{anomalies}$ defined as the difference between the simulated NDII for 2015 and 2016, estimated using cumulative WD and generalized additive models, and the average late summer season NDII for the period 2009–2011 (non-drought conditions). The resulting map (Figure 9) showed, for the SS region, an agreement between the spatial patterns of water stress and the 2015

Aerial Detection Survey. The difference between low tree mortality (<10 dead trees/ha) and severe tree mortality (>100 dead trees/ha) was statistically significant (Wilcoxon rank-sum test, p-value = 0.049). Maps related to the NS and CS and 2016 SS are reported in the Supplementary Figures S11–S15.

4. Discussion

Our findings suggest that snowpack loss, associated with an increase in temperatures, exacerbates vegetation water stress and consequent tree mortality episodes. The water availability necessary to maintain xylem functionality and photosynthesis is constrained by the terrestrial water storage (snowpack and subsurface water storage) and by the ability of vegetation to access it (Bales et al., 2018; Klos et al., 2018). The snowpack recharges the root zone water storage more efficiently than rain (Earman et al., 2006; Meixner et al., 2016) and provides the water necessary for the vegetation in spring and early summer when precipitation is low or absent. We used WD as a seasonal index to account for the differences in time and magnitude between water inputs and water demand. WD indicates the negative difference between monthly water inputs and monthly potential evapotranspiration (PET). The water delivered by the snowpack alleviates the WD and aids the subsurface storage in sustaining the vegetation during the growing season. Furthermore, variations in the snowpack, snowmelt timing, and temperatures directly modulate the water deficit, as confirmed by the high correlation between snowmelt and PET. As the drought propagates, an increase in WD occurred in the whole Sierra Nevada. Mid- and low-elevation forests exhibit higher cumulative water deficit across time. The increase in cumulative water deficit was particularly high in the southern Sierra region (Figure 5), which was the most affected by the 2012–2016 tree mortality episodes (U.S. Forest Service, 2016). However, in the northern and central Sierra, the increase in the cumulative deficit was not translated into vegetation water stress and tree mortality as severely as in the southern Sierra. This can be explained by the higher subsurface water available in the northern and central Sierra, as shown in previous studies (Fellows and Goulden, 2016).

Additionally, water and energy gradients across the elevation profile play a key role in the spatial distributions of forest water stress. At mid-elevation, previous studies indicate that ET is about equal to PET (Fellows and Goulden, 2016). The average yearly water deficit (pre-drought 2000–2011) in the southern Sierra for the conifer forests at mid-elevation (1,500–2,000 m_{asl}) was 528 mm ($q_{0.25}$ = 438 mm, $q_{0.75}$ = 607 mm). These average conditions (pre-drought) indicate that the WD was satisfied by the subsurface water storage, and it is consistent with the conifers' water withdrawal from the belowground estimated by Fellows and Goulden (2016) (30 years mean soil water drawdown of the conifers at 1,500 m_{asl} of ~400 mm ± ~100 mm). The 2-year cumulative WD (during dry years) at the mid-elevation region is consistent with the estimated subsurface water storage of 140 cm at the 1,100 m_{asl} Southern Sierra Critical Zone Observatory (SSCZO) site by Klos et al. (2018) and with the cumulative P-ET drought equilibrium of ~1,500 mm at mid-elevation obtained by Goulden and Bales (2019). At mid-elevation, NDII is higher, which indicates higher moisture content in leaves. Our study indicates that NDII and basal area are

related through a linear-log function (Supplementary Figure S6). Furthermore, NDII is positively correlated with both NDVI and LAI (Goulden and Bales, 2019). Hence, the higher sensitivity (Figure 8 and Supplementary Figure S8) of the Southern Sierra NDII to the 2-year cumulative water deficit at mid-elevation indicates the higher vulnerability of the denser mid-elevation forests, consistent with Young et al. (2016) and Fettig et al. (2019).

The regional generalized additive models were trained to capture how forest moisture (NDII) varies in the landscape (using a combination of latitude, longitude, slope, and northness) based on a 2-year cumulative WD by different ecological systems, which is the unique independent variable considered that varies through time. The model results show robustness in simulating forest moisture (NDII) between regions (northern, central, and southern Sierra) and between simulated years (2015 and 2016). Our findings suggest that the difference between evaporative demand and water inputs (i.e., WD) can be used to estimate forest water stress, as NDII. The simulated anomalies in forest moisture (NDII) were reflected in the Forest Service Aerial Detection Survey (ADS) in 2015 and 2016 (Figure 9, Supplementary Figures S11–S15).

Tree species can respond differently to variations in the water balance (Hinckley et al., 1978). Some species can tolerate a larger spectrum of water availability (Lutz et al., 2010) and have different regulation strategies during dry conditions (McDowell et al., 2008). A previous study showed that across the elevation gradient, tree mortality was species-specific (Paz-Kagan et al., 2017). The inclusion of the different smooth functions in the model training helps to identify in space how pixels characterized by different vegetation composition, forest structure, and average water available respond to different levels of water deficit. Our results suggest that in the CS and SS, the mesic mixed conifer forest and the dry-mesic mixed conifer forest are the most vulnerable to cumulative water deficit variations (Supplementary Figure S10). The tree species characterizing these ecological systems are consistent with the trees least tolerant to drought reported by Kocher and Harris, 2007.

4.1. Limitations and uncertainties

Possible limitations and sources of uncertainties in this study can be identified in the following. First, the difference in the original resolution between the spatial datasets (PRISM ~800 m, MODIS ~500 m, NLCD 2011 30 m, GAP/LANDFIRE 30 m, DEM 30 m, and SWE ~90 m) may lead to inaccuracies in water deficit calculations. However, PET used in the water deficit calculation can be useful to overcome the non-availability of independent ET measurements. Second, there are temporal differences between the Aerial Detection Surveys and late summer season NDII (ADS performed during July–August 2015 and May 2016, while the late summer season NDII was derived as an average of MODIS scenes from August, September, and October). Third, in this study, we did not consider non-drought-related tree mortality (i.e., bark beetle). However, tree defenses weakened by the drought, and the consequent increase in insects and pathogens, may induce a lag in tree mortality (Das et al., 2013; Young et al., 2016). Fourth, due to the typology of the chosen statistical model, we did not account

for streamflow, lateral water redistribution, and subsurface flow. This may lead to forest moisture underestimation in valleys and overestimation in runoff generation areas.

4.2. Future implications

Increases in tree mortality episodes, wildfire extent, and wildfire severity have been linked to temperature increases and lower precipitation (Crockett and Westerling, 2017). Future model projections indicate a decline and even disappearance in some parts of the snowpack in the Sierra Nevada by the end of the century (Siirila-Woodburn et al., 2021). Consequently, an increase in the summer water deficit will likely involve an increase in forest vulnerability, water stress, tree mortality, and severe wildfire risks. Higher elevation regions may be affected as well. Some locations, due to the low water storage, heavily rely on lateral flows and snowpack accumulation to support ET. The vegetation response to variations in water and energy availability will affect streamflow generation as well (Safeeq and Hunsaker, 2016). Forest management can contribute to partially mitigating such risks. A reduction in forest density can enhance forest health, increase streamflow (Tague et al., 2019), restore forest-fire resilient conditions (McKelvey and Johnston, 1992), and eventually maximize the trade-off between snow accumulation and snow ablation (Broxton et al., 2020).

5. Conclusion

We evaluated and simulated using linear regressions and regional Generalized Additive Models (GAMs) how temperature and seasonal snowpack variations can affect NDII as a proxy of forest water stress. We used water deficit as a seasonality index to inspect the critical role of mountain snowpack in reducing the mismatch between the timing of water input to the root zone and the peak forest water use under the Mediterranean climate of the Sierra Nevada. Our findings suggest that a loss of snowpack will increase the water deficit, which will lead to higher forest water stress. However, the availability of subsurface storage or lower evaporative demand can modulate the vegetation response to changes in snowpack. Consistent with previous studies, the response of the denser mid-elevation forests in the proximity of the rain–snow transition zone is more sensitive to water deficit variations. This suggests a snowpack dependence in satisfying ET requirements. We simulated forest water stress for 2015 and 2016 for the different regions (i.e., northern, central, and southern Sierra) with a range of R^2 between 0.80 and 0.84. The predicted spatial patterns in forest water stress were comparable with the tree die-off detected by the USDA Forest Service Aerial Detection Survey. These results can

provide insight into the importance of the Sierra Nevada snowpack in a warming climate and make predictions on vulnerable areas.

Data availability statement

Publicly available datasets were analyzed in this study. This data can be found here: PRISM: https://prism.oregonstate.edu/, Sierra Nevada Snow Reanalysis: https://margulis-group.github.io/data/. Questions regarding the datasets should be directed to SC, scasirati@ucmerced.edu.

Author contributions

SC: conceptualization, methodology, investigation, analysis, visualization, writing—original draft, writing—review, and editing. MC and MS: supervision, conceptualization, resources, investigation, review, and editing. All authors contributed to the article and approved the submitted version.

Funding

Conflict of interest

The authors declare that the research was conducted in the absence of any commercial or financial relationships that could be construed as a potential conflict of interest.

Publisher's note

All claims expressed in this article are solely those of the authors and do not necessarily represent those of their affiliated organizations, or those of the publisher, the editors and the reviewers. Any product that may be evaluated in this article, or claim that may be made by its manufacturer, is not guaranteed or endorsed by the publisher.

Supplementary material

The Supplementary Material for this article can be found online at: https://www.frontiersin.org/articles/10.3389/ffgc.2023.1181819/full#supplementary-material

References

Aalto, J., Pirinen, P., Heikkinen, J., and Venäläinen, A. (2012). Spatial interpolation of monthly climate data for Finland: comparing the performance of kriging and generalized additive models. *Theor. Appl. Climatol.* 112, 99–111. doi: 10.1007/s00704-012-0716-9

Allen, C. D., Breshears, D. D., and McDowell, N. G. (2015). On underestimation of global vulnerability to tree mortality and forest die-off from hotter drought in the Anthropocene. *Ecosphere* 6, art129. doi: 10.1890/ES15-00 203.1

Bales, R. C., Goulden, M. L., Hunsaker, C. T., Conklin, M. H., Hartsough, P. C., O'Geen, A. T., et al. (2018). Mechanisms controlling the impact of multi-year drought on mountain hydrology. *Scient. Rep.* 8, 1. doi: 10.1038/s41598-017-19007-0

Bales, R. C., Molotch, N. P., Painter, T. H., Dettinger, M. D., Rice, R., and Dozier, J. (2006). Mountain hydrology of the western United States. *Water Resour. Res.* 42, 8. doi: 10.1029/2005WR004387

Barnett, T. P., Adam, J. C., and Lettenmaier, D. P. (2005). Potential impacts of a warming climate on water availability in snow-dominated regions. *Nature* 438, 303–309. doi: 10.1038/nature04141

Bedsworth, L., Cayan, D., Franco, G., Fisher, L., and Ziaja, S. (2018). *Statewide Summary Report.* California's Fourth Climate Change Assessment. Publication number: SUMCCCA4-2018-013

Broxton, P. D., Leeuwen, W. J. D., and Biederman, J. A. (2020). Forest cover and topography regulate the thin, ephemeral snowpacks of the semiarid Southwest United States. *Ecohydrology* 13, 4. doi: 10.1002/eco.2202

Busetto, L., and Ranghetti, L. (2016). *MODIStsp*: An R package for automatic preprocessing of MODIS Land Products time series. *Comput. Geosci.* 97, 40–48. doi: 10.1016/j.cageo.2016.08.020

Ceccato, P., Gobron, N., Flasse, S., Pinty, B., and Tarantola, S. (2002). Designing a spectral index to estimate vegetation water content from remote sensing data: Part 1. *Remote Sens. Environ.* 82, 188–197. doi: 10.1016/S0034-4257(02)00037-8

Cheng, Y.-B. (2007). Relationships between Moderate Resolution Imaging Spectroradiometer water indexes and tower flux data in an old growth conifer forest. *J. Appl. Rem. Sens.* 1, 013513. doi: 10.1117/1.2747223

Comer, P., Faber-Langendoen, D., Evans, R., Gawler, S., Josse, C., Kittel, G., et al. (2003). *Ecological systems of the United States: a working classification of US terrestrial systems.* Arlington, VA: NatureServe.

Corripio, J. G. (2021). *insol: Solar Radiation. R package version 1.2.2.* Available online at: https://CRAN.R-project.org/package=insol (accessed July 31, 2022).

Crockett, J. L., and Westerling, A. L. (2017). Greater temperature and precipitation extremes intensify western U.S. droughts, wildfire severity, and sierra nevada tree mortality. *J. Clim.* 31, 341–354. doi: 10.1175/JCLI-D-17-0254.1

Daly, C., Neilson, R. P., and Phillips, D. L. (1994). A statistical-topographic model for mapping climatological precipitation over mountainous terrain. *J. Appl. Meteorol.* 33, 140–158. doi: 10.1175/1520-0450(1994)033<0140:ASTMFM>2.0.CO;2

Das, A. J., Stephenson, N. L., Flint, A., Das, T., and van Mantgem, P. J. (2013). Climatic correlates of tree mortality in water- and energy-limited forests. *PLoS ONE* 8, e69917. doi: 10.1371/journal.pone.0069917

Davidson, A., Wang, S., and Wilmshurst, J. (2006). Remote sensing of grassland–shrubland vegetation water content in the shortwave domain. *Int. J. Appl. Earth Observ. Geoinform.* 8, 225–236. doi: 10.1016/j.jag.2005.10.002

Dettinger, M. D., and Anderson, M. L. (2015). Storage in California's reservois and snowpack in this time of drought. *San Francisco Estuary Watershed Sci.* 13, 2. doi: 10.15447/sfews.2015v13iss2art1

Dewitz, J. (2014). *National Land Cover Database (NLCD) 2011 Land Cover Conterminous United States [Data set].* U.S. Geological Survey.

Dingman, S. L. (2002). *Physical Hydrology.* 2nd Edn. Upper Saddle River, NJ: Prentice Hall.

Earman, S., Campbell, A. R., Phillips, F. M., and Newman, B. D. (2006). Isotopic exchange between snow and atmospheric water vapor: Estimation of the snowmelt component of groundwater recharge in the southwestern United States. *J. Geophys. Res.* 111, D9. doi: 10.1029/2005JD006470

Eidenshink, J., Schwind, B., Brewer, K., Zhu, Z.-L., Quayle, B., and Howard, S. (2007). A project for monitoring trends in burn severity. *Fire Ecol.* 3, 3–21. doi: 10.4996/fireecology.0301003

Fellows, A. W., and Goulden, M. L. (2016). Mapping and understanding dry season soil water drawdown by California montane vegetation. *Ecohydrology* 10, e1772. doi: 10.1002/eco.1772

Fettig, C. J., Mortenson, L. A., Bulaon, B. M., and Foulk, P. B. (2019). Tree mortality following drought in the central and southern Sierra Nevada, California, U.S. *Forest Ecol. Manage.* 432, 164–178. doi: 10.1016/j.foreco.2018.09.006

Garcia, E. S., and Tague, C. L. (2015). Subsurface storage capacity influences climate–evapotranspiration interactions in three western United States catchments. *Hydrol. Earth Syst. Sci.* 19, 4845–4858. doi: 10.5194/hess-19-4845-2015

Goulden, M. L., and Bales, R. C. (2019). California forest die-off linked to multi-year deep soil drying in 2012–2015 drought. *Nat. Geosci.* 12, 632–637. doi: 10.1038/s41561-019-0388-5

Groemping, U. (2006). Relative Importance for Linear Regression in R: The Package relaimpo. *J. Stat. Softw.* 17, 1–27. doi: 10.18637/jss.v017.i01

Hamon, W. (1963). Computation of direct runoff amounts from storm rainfall. *Int. Assoc. Sci. Hydrol. Publ.* 63, 52–62.

Hardisky, M. A., Klemas, V., and Smart, R. M. (1983). The influence of soilsalinity, growth form, and leaf moisture on the spectral radiance of Spartina alterniflora canopies. *Photogram. Eng. Rem. Sens.* 49, 77–83.

Hastie, T., and Tibshirani, R. (1986). Generalized additive models. *Stat. Sci.* 1, 3. doi: 10.1214/ss/1177013604

Hinckley, T. M., Lassoie, J. P., and Running, S. W. (1978). Temporal and spatial variations in water status of forest trees. *Forest Sci.* 24, 1–72.

Hong, Y., Nix, H. A., Hutchinson, M. F., and Booth, T. H. (2005). Spatial interpolation of monthly mean climate data for China. *Int. J. Climatol.* 25, 1369–1379. doi: 10.1002/joc.1187

Irwin, W. P. (1990). "Geology and plate-tectonic development," in R. E. Wallace, ed., *The San Andreas Fault System: U.S. Geological Survey Professional* 61–80. Available online at: https://pubs.usgs.gov/pp/1990/1515/

Kimes, D. S., Markham, B. L., Tucker, C. J., and McMurtrey, J. E. III. (1981). Temporal relationships between spectral response and agronomic variables of a corn canopy. *Remote Sens. Environ.* 11, 401–411. doi: 10.1016/0034-4257(81)90037-7

Klos, P. Z., Goulden, M. L., Riebe, C. S., Tague, C. L., O'Geen, A. T., Flinchum, B. A., et al. (2018). Subsurface plant-accessible water in mountain ecosystems with a Mediterranean climate. *WIREs Water* 5, 3. doi: 10.1002/wat2.1277

Knowles, N., Dettinger, M. D., and Cayan, D. R. (2006). Trends in Snowfall versus Rainfall in the Western United States. *J. Climate* 19, 4545–4559. doi: 10.1175/JCLI3850.1

Kocher, S. D., and Harris, R. (2007). *Forest Stewardship Series 5: Tree Growth and Competition.* University of California, Agriculture and Natural Resources. doi: 10.3733/ucanr.8235

Leibowitz, S. G., Wigington, J,r,., P. J., Comeleo, R. L., and Ebersole, J. L. (2011). A temperature-precipitation-based model of thirty-year mean snowpack accumulation and melt in Oregon, USA. *Hydrol. Proces.* 26, 741–759. doi: 10.1002/hyp.8176

LEMMA group (2015). *GNN structure (species-size) maps.* Available online at: http://lemma.forestry.oregonstate.edu/data/structure-maps (accessed May 17, 2017).

Li, Z., and Wood, S. N. (2019). Faster model matrix crossproducts for large generalized linear models with discretized covariates. *Stat. Comput.* 30, 19–25. doi: 10.1007/s11222-019-09864-2

Lindeman, R. H., Merenda, P. F., and Gold, R. Z. (1980). *Introduction to Bivariate and Multivariate Analysis.* Glenview, IL: Scott, Foresman.

Lute, A. C., and Abatzoglou, J. T. (2020). Best practices for estimating near-surface air temperature lapse rates. *Int. J. Climatol.* 41, S1. doi: 10.1002/joc.6668

Lutz, J. A., van Wagtendonk, J. W., and Franklin, J. F. (2010). Climatic water deficit, tree species ranges, and climate change in Yosemite National Park. *J. Biogeogr.* 37, 936–950. doi: 10.1111/j.1365-2699.2009.02268.x

Mann, M. E., and Gleick, P. H. (2015). "Climate change and California drought in the 21st century," in *Proceedings of the National Academy of Sciences* 112, 3858–3859. doi: 10.1073/pnas.1503667112

Margulis, S. A., Cortés, G., Girotto, M., and Durand, M. (2016). A landsat-era sierra nevada snow reanalysis (1985–2015). *J. Hydrometeorol.* 17, 1203–1221. doi: 10.1175/JHM-D-15-0177.1

Margulis, S. A., Girotto, M., Cortés, G., and Durand, M. (2015). A particle batch smoother approach to snow water equivalent estimation. *J. Hydrometeorol.* 16, 1752–1772. doi: 10.1175/JHM-D-14-0177.1

McDowell, N., Pockman, W. T., Allen, C. D., Breshears, D. D., Cobb, N., Kolb, T., et al. (2008). Mechanisms of plant survival and mortality during drought: why do some plants survive while others succumb to drought? *New Phytol.* 178, 719–739. doi: 10.1111/j.1469-8137.2008.02436.x

McKelvey, K. S., and Johnston, J. D. (1992). "Historical perspectives on forests of the Sierra Nevada and the transverse ranges of southern California; forest conditions at the turn of the century," in *The California spotted owl: a technical assessment of its current status* (Albany, CA: Pacific Southwest Research Station, Forest Service, U.S. Department of Agriculture) 225–246.

Meixner, T., Manning, A. H., Stonestrom, D. A., Allen, D. M., Ajami, H., Blasch, K. W., et al. (2016). Implications of projected climate change for groundwater recharge in the western United States. *J. Hydrol.* 534, 124–138. doi: 10.1016/j.jhydrol.2015.12.027

Mote, P. W., Hamlet, A. F., Clark, M. P., and Lettenmaier, D. P. (2005). Declining mountain snowpack in western North America. *Bull. Am. Meteorol. Soc.* 86, 39–50. doi: 10.1175/BAMS-86-1-39

Paz-Kagan, T., Brodrick, P. G., Vaughn, N. R., Das, A. J., Stephenson, N. L., Nydick, K. R., et al. (2017). What mediates tree mortality during drought in the southern Sierra Nevada? *Ecol. Applic.* 27, 2443–2457. doi: 10.1002/eap.1620

R Core Team (2021). *R: A Language and Environment for Statistical Computing. Vienna, Austria.* Available online at: https://www.R-project.org (accessed July 31, 2022).

Restaino, C., Young, D. J. N., Estes, B., Gross, S., Wuenschel, A., Meyer, M., et al. (2019). Forest structure and climate mediate drought-induced tree mortality in forests of the Sierra Nevada, USA. *Ecol. Appl.* 29, e01902. doi: 10.1002/eap.1902

Roche, J. W., Ma, Q., Rungee, J., and Bales, R. C. (2020). Evapotranspiration Mapping for Forest Management in California's Sierra Nevada. *Front. Forests Global Change* 3, 69. doi: 10.3389/ffgc.2020.00069

Safeeq, M., and Hunsaker, C. T. (2016). Characterizing runoff and water yield for headwater catchments in the southern sierra nevada. *JAWRA J. Am. Water Resour. Assoc.* 52, 1327–1346. doi: 10.1111/1752-1688.12457

Safeeq, M., Shukla, S., Arismendi, I., Grant, G. E., Lewis, S. L., and Nolin, A. (2015). Influence of winter season climate variability on snow-precipitation ratio in the western United States. *Int. J. Climatol.* 36, 3175–3190. doi: 10.1002/joc.4545

Siirila-Woodburn, E. R., Rhoades, A. M., Hatchett, B. J., Huning, L. S., Szinai, J., Tague, C., et al. (2021). A low-to-no snow future and its impacts on water resources in the western United States. *Nat. Rev. Earth Environ.* 2, 800–819. doi: 10.1038/s43017-021-00219-y

Swain, D. L., Langenbrunner, B., Neelin, J. D., and Hall, A. (2018). Increasing precipitation volatility in twenty-first-century California. *Nat. Clim. Change* 8, 427–433. doi: 10.1038/s41558-018-0140-y

Tague, C. L., Moritz, M., and Hanan, E. (2019). The changing water cycle: The eco-hydrologic impacts of forest density reduction in Mediterranean (seasonally dry) regions. *WIREs Water* 6, 4. doi: 10.1002/wat2.1350

Tarboton, D. G. (2005). Terrain analysis using digital elevation models (TauDEM). *Utah State Univ. Logan* 3012, 2018.

Thorne, J. H., Boynton, R. M., Flint, L. E., and Flint, A. L. (2015). The magnitude and spatial patterns of historical and future hydrologic change in California's watersheds. *Ecosphere* 6, art24. doi: 10.1890/ES14-00300.1

Trujillo, E., Molotch, N. P., Goulden, M. L., Kelly, A. E., and Bales, R. C. (2012). Elevation-dependent influence of snow accumulation on forest greening. *Nat. Geosci.* 5, 705–709. doi: 10.1038/ngeo1571

U.S. Forest Service (2016). *U.S. Forest Service Pacific Southwest Region Forest Health Protection Aerial Detection Survey.* Available online at: https://www.fs.usda.gov/detail/r5/forest-grasslandhealth/?cid=fsbdev3_046696 (accessed December 8, 2021).

U.S. Geological Survey (2016). *GAP/LANDFIRE National Terrestrial Ecosystems 2011: U.S.* Geological Survey data release.

U.S. Geological Survey (2017) *1 Arc-second Digital Elevation Models (DEMs) - USGS National Map 3DEP Downloadable Data Collection.* U.S. Geological Survey.

U.S. Geological Survey (2020). *USGS watershed boundary dataset (WBD) for 2-digit Hydrologic unit - 18 (published 20201204).* U.S. Geological Survey (USGS).

Vermote, E. (2015). *MOD09A1 MODIS/Terra Surface Reflectance 8-Day L3 Global 500m SIN Grid V006 [Data set].* NASA EOSDIS Land Processes DAAC.

Wigington, P. J., Leibowitz, S. G., Comeleo, R. L., and Ebersole, J. L. (2012). Oregon Hydrologic Landscapes: A Classification Framework1. *JAWRA J. Am. Water Resour. Assoc.* 49, 1, 163–182. doi: 10.1111/jawr.12009

Williams, A. P., Seager, R., Abatzoglou, J. T., Cook, B. I., Smerdon, J. E., and Cook, E. R. (2015). Contribution of anthropogenic warming to California drought during 2012–2014. *Geophys. Res. Lett.* 42, 6819–6828. doi: 10.1002/2015GL064924

Wilson, E. H., and Sader, S. A. (2002). Detection of forest harvest type using multiple dates of Landsat TM imagery. *Remote Sens. Environ.* 80, 385–396. doi: 10.1016/S0034-4257(01)00318-2

Wood, S. N. (2017). *Generalized Additive Models.* Chapman and Hall/CRC. doi: 10.1201/9781315370279

Wood, S. N., Goude, Y., and Shaw, S. (2014). Generalized additive models for large data sets. *J. R. Stat. Soc.* 64, 139–155. doi: 10.1111/rssc.12068

Wood, S. N., Pya, N., and Säfken, B. (2016). Smoothing Parameter and Model Selection for General Smooth Models. *J. Am. Stat. Assoc.* 111, 1548–1563. doi: 10.1080/01621459.2016.1180986

Yilmaz, M. T., Hunt, E. R. Jr., and Jackson, T. J. (2008). Remote sensing of vegetation water content from equivalent water thickness using satellite imagery. *Remote Sens. Environ.* 112, 2514–2522. doi: 10.1016/j.rse.2007.11.014

Young, D. J. N., Stevens, J. T., Earles, J. M., Moore, J., Ellis, A., Jirka, A. L., et al. (2016). Long-term climate and competition explain forest mortality patterns under extreme drought. *Ecol. Lett.* 20, 78–86. doi: 10.1111/ele.12711

Zimmermann, N. E., and Roberts, D. W. (2001). *Final report of the MLP climate and biophysical mapping project.* Swiss Federal Research Institute WSL/Utah State University Birmensdorf, Switzerland/Logan, USA 18.

Accuracy and inter-cloud precision of low-cost mobile LiDAR technology in estimating soil disturbance in forest operations

Gabriel Osei Forkuo and Stelian Alexandru Borz*

Department of Forest Engineering, Forest Management Planning and Terrestrial Measurements, Faculty of Silviculture and Forest Engineering, Transilvania University of Braşov, Braşov, Romania

Forest operations can cause long-term soil disturbance, leading to environmental and economic losses. Mobile LiDAR technology has become increasingly popular in forest management for mapping and monitoring disturbances. Low-cost mobile LiDAR technology, in particular, has attracted significant attention due to its potential cost-effectiveness, ease of use, and ability to capture high-resolution data. The LiDAR technology, which is integrated in the iPhone 13–14 Pro Max series, has the potential to provide high accuracy and precision data at a low cost, but there are still questions on how this will perform in comparison to professional scanners. In this study, an iPhone 13 Pro Max equipped with SiteScape and 3D Scanner apps, and the GeoSlam Zeb Revo scanner were used to collect and generate point cloud datasets for comparison in four plots showing variability in soil disturbance and local topography. The data obtained from the LiDAR devices were analyzed in CloudCompare using the Iterative Closest Point (ICP) and Least Square Plane (LSP) methods of cloud-to-cloud comparisons (C2C) to estimate the accuracy and intercloud precision of the LiDAR technology. The results showed that the low-cost mobile LiDAR technology was able to provide accurate and precise data for estimating soil disturbance using both the ICP and LSP methods. Taking as a reference the point clouds collected with the Zeb Revo scanner, the accuracy of data derived with SiteScape and 3D Scanner apps varied from RMS = 0.016 to 0.035 m, and from RMS = 0.017 to 0.025 m, respectively. This was comparable to the precision or repeatability of the professional LiDAR instrument, Zeb Revo (RMS = 0.019−0.023 m). The intercloud precision of the data generated with SiteScape and 3D Scanner apps varied from RMS = 0.015 to 0.017 m and from RMS = 0.012 to 0.014 m, respectively, and were comparable to the precision of Zeb Revo measurements (RMS = 0.019−0.023 m). Overall, the use of low-cost mobile LiDAR technology fits well to the requirements to map and monitor soil disturbances and it provides a cost-effective and efficient way to gather high resolution data, which can assist the sustainable forest management practices.

1. Introduction

Forest operations can have a significant impact on soil structure and health (Ampoorter et al., 2010, 2012; Koreň et al., 2015). These changes can adversely affect soil fertility, water retention capacity, nutrient cycling, and vegetation growth (Frey et al., 2009; Tavankar et al., 2017; Dudáková et al., 2020). Therefore, monitoring soil disturbance is essential to mitigate its effects on forest ecosystems (Nikooy et al., 2020; Mohieddinne et al., 2022), meaning that estimates on its extent, severity and dynamics are critical for the effective forest management and conservation efforts (Tavankar et al., 2017; Nikooy et al., 2020). Traditionally, the estimation of soil disturbance has been done through manual measurements and visual assessments (Nichol and Wong, 2005; Frankl et al., 2011) which can be time-consuming, labor-intensive (Sharma, 2018), costly, and prone to errors. Additionally, these methods may not capture spatial and temporal variability in soil disturbance due to their limited coverage (Coleman, 2005; Cécillon et al., 2009; Sharma, 2018).

There are several harvesting systems used under the mountainous conditions (Heinimann, 2000, 2004; Pentek et al., 2008). Although in sloped terrains cable yarding should be preferred (Heinimann, 2000, 2004; Heinimann et al., 2001; Pentek et al., 2008; Spinelli et al., 2021) due to its low impact to the ground, this kind of technology still accounts for a small share in the European countries (Heinimann et al., 2001; Spinelli et al., 2013; Böhm and Kanzian, 2022). The alternatives are ground-based extraction systems which usually include either a forwarder (Pentek et al., 2008; Visser and Stampfer, 2015) or a skidder (Pentek et al., 2008; Jaafari et al., 2014). Their use comes at the expense of some soil impact such as compaction and rutting (Cambi et al., 2015, 2016, 2017; Pierzchała et al., 2016). In some cases, extraction is done by skidding after building bladed skid roads (Vinson et al., 2017) which, in time, may be affected by erosion (Shishiuchi, 1993; Brown et al., 2013), meaning that soil particles are washed, and the ruts become more prominent (Brown et al., 2013; Vinson et al., 2017).

LiDAR is an optical device that utilizes lasers in measuring the distances and positions of objects (Stovall et al., 2017; Elhashash et al., 2022). It gives precise individual point measurements on a 3D object, with the collective measurements providing information about the object's shape and surface characteristics (Elhashash et al., 2022). It is highly accurate, quick, provides dense 3D information, and can penetrate sparse objects like canopies (Stovall et al., 2017; Elhashash et al., 2022). Hence, Stovall et al. (2017) and Wilkes et al. (2017) have proposed that LiDAR is a feasible method to offer fast, precise, and non-invasive assessments of forest biophysical characteristics. According to Beland et al. (2019), it is crucial in LiDAR-based research to make decisions about the type of LiDAR platform that is best for extracting the necessary information, the provider who will conduct the survey, the protocols that will be used for the survey, and the tools and processing methods that will be used to transform raw LiDAR data into useful information. The five main LiDAR platforms used in forest research are airborne laser scanning (ALS) from manned aircraft, unmanned aerial vehicle (UAV) laser scanning (ULS), terrestrial laser scanning (TLS) from a stationary ground platform, mobile laser scanning (MLS) from a moving ground platform, and spaceflight lidar

(SLS) (Akay et al., 2009; Beland et al., 2019; Talbot and Astrup, 2021).

The use of LiDAR platforms in studies on forest ecosystem management has been around since the 1960s and 1970s (Nitoslawski et al., 2021). Nevertheless, Dassot et al. (2011) and Mohan et al. (2017) report that it is still one of the most widely used tools for forest research and management. It is frequently combined with other remote sensing techniques, such as satellite imaging (Ke et al., 2010; Tigges et al., 2013), to evaluate tree characteristics and forest structure. LiDAR methods are frequently used in conjunction with laser scanning methods for land or airborne platforms for forest inventory. For instance, MLS has been used in several forestry applications, including non-destructive estimation, forest inventory, canopy mapping, crown projection, and evacuation planning (Novo et al., 2020; Shao et al., 2020). Similarly, UAV has been used in tree growth models, forest inventory, economic and ecological stand value, monitoring and detection of forest fires, and assessment of forest structure and characteristics (Milas et al., 2018; Krause et al., 2019). TLS has also been used for automatic tree detection, leaf and wood separation, assessment of forest structure and characteristics, automated processing chains, and forest inventories (Cabo et al., 2018; Vicari et al., 2019; Wang et al., 2020). According to Dassot et al. (2011) and Heinzel and Koch (2011), ALS can be used for a variety of forestry research tasks, such as forest inventory, tree crown delineation, assessment of forest parameters and structure, 3D data collection, ecological research, transpiration, habitat diversity, and flood modeling. Spatial resolution, occlusion, and coverage are the three key opposing features of these five different types of LiDAR platforms, which make it easier to comprehend the advantages and drawbacks of each type of platform and choose the best option for a particular research application (Beland et al., 2019).

For measuring soil impacts using contemporary technology, several methods, including proximal, mobile, and low-cost remote sensing, have been proposed recently (Talbot and Astrup, 2021), but little research has been done on their suitability for use in research trials or the possibility of use in operational forestry settings. Proximal remote sensing is a quick and non-intrusive imaging technique that involves briefly and closely positioning the target object beneath the camera's lens to get information on its transmittance or reflectance (Doetterl et al., 2013; Nansen and Strand, 2018). According to Talbot and Astrup (2021), proximal sensing technologies are becoming more and more common in a variety of environmental sciences sectors, including the measurement of ground surfaces to analyze how tracked and wheeled machinery affects the displacement of forest soil. Doetterl et al. (2013) claim that proximal soil sensors can measure soil parameters rapidly, precisely, more inexpensively, and directly in the field, giving the data a more accurate representation of the soil there, while Liu et al. (2019) describe the mobile laser scanning (MLS) system as a kinematic platform that includes a laser scanner, inertial measurement unit (IMU), GPS receiver, and other equipment mounted on a mobile platform. The MLS system makes it easy, efficient, and precise to create 3D point clouds of the immediate surroundings, which are useful for a wide range of applications, such as 3D landscape visualization for planning and simulations for environmental management (Vallet and Mallet, 2016; Liu et al., 2019). On the other hand, low-cost LiDAR is described as a cost-effective and cost-efficient industrial

quality sensor technology that reconsiders the use, robustness, and flexibility of sensor technology (Jeong et al., 2018).

Regarding mobile LiDAR applications, Astrup et al. (2016) evaluated the use of two low-cost 2D LiDAR scanners, each installed vertically on the rear forwarder bunk, while Salmivaara et al. (2018) mounted a robust 2D sensor on both a harvester and forwarder. Both studies addressed the use of mobile and low-cost LiDAR scanning platforms in soil impact assessment. Still, there are very few examples of low-cost LiDAR technology applications in forest management in high-impact journals (Nitoslawski et al., 2021). Recent developments in technology have enabled the integration of sensor systems, such as 3D Time-of-Flight and laser scanning, onto mobile devices, enhancing augmented reality capabilities and supporting terrestrial/mobile LiDAR-based soil characterization and modeling (Apple Inc., 2021a, 2022; Samsung Group, 2023). According to Silver (2019), as smartphone use increases internationally, crowdsourcing and citizen science-based research on forest ecology may become more practical and trustworthy. The accuracy, precision, and repeatability of smartphones as a tool for citizen-based environmental research and monitoring, however, is still uncertain (Andrachuk et al., 2019).

Currently, there are several apps that may be installed and used on low-cost, proximal-sensing mobile platforms, such as Trnio (Trnio Inc, 2014), Scandy Pro (Scandy, 2016), Heges App (Simonik, 2018), Capture 3D (Matterport Inc, 2018), Polycam (Polycam Inc, 2017), Canvas (Occipital Inc, 2018), 3D Scanner App (Laan Labs, 2011), and SiteScape (Trimble Inc, 2009; Corke, 2021; SiteScape FARO Solution, 2023). These can be used to scan various objects of interest for recreational and professional purposes (Gregurić, 2022; Hullette et al., 2023). Some of these are coming at a subscription low-cost while some are for free. Gollob et al. (2021) evaluated eight applications on forest inventory plots and found that three of them, namely 3D Scanner, Polycam, and SiteScape were suitable for use under forest environments.

Usually, the collected point clouds require some post-processing in external software. Among the existing options, CloudCompare (Girardeau-Montaut, 2015, 2016) has been extensively used in point-cloud based research (Girardeau-Montaut et al., 2005; Ahmad Fuad et al., 2018). C2C (cloud-to-cloud comparison) has been proved to be a powerful tool for evaluating the accuracy and precision of LiDAR data (Girardeau-Montaut et al., 2005; Lague et al., 2013; Kharroubi et al., 2022). Zhang et al. (2015) demonstrated the effectiveness of a weighted anisotropic ICP algorithm through experiments on a dataset of a forested area and a coastal beach, showing that the algorithm can detect subtle changes in the environment that are missed by the other methods. This method compares two-point clouds captured from the same area but using different sensors, scanning platforms or time frames. In the context of mapping and estimating soil disturbance in forest operations, this method can be used to compare low-cost mobile LiDAR technology with high-end LiDAR systems used for accurate soil disturbance estimation. In comparison to other methods such as ground-based measurements or aerial photography, the C2C provides a more comprehensive and accurate assessment of LiDAR data (Ahmad Fuad et al., 2018; Cheng et al., 2018). Besides, ground-based measurements are limited in coverage, while aerial photography may not capture the fine details necessary for accurate soil disturbance mapping and monitoring (Coleman, 2005; Cécillon et al., 2009; Sharma, 2018).

Therefore, the cloud-to-cloud comparison method may provide a useful alternative for checking the capabilities of low-cost mobile LiDAR systems.

According to Carter et al. (2012), recent advancements in LiDAR mapping systems and the technology that enables them have allowed scientists and mapping specialists to investigate natural environments on a range of scales with greater accuracy, precision, repeatability and flexibility than ever before. Accuracy is the degree to which a measurement is near to the correct or true value of that measurement, while precision of a measurement system refers to how closely repeated measurements (that are repeated under the same conditions) agree with one another (Teller, 2013; McLain et al., 2018). However, precision is independent of accuracy and therefore, a measurement can be accurate but not precise, precise but not accurate, not accurate and not precise, or both accurate and precise (Dodge, 2008; Teller, 2013; Glen, 2023). On the other hand, repeatability is the variance in measurement obtained by a measuring instrument or device used by a single appraiser or operator measuring the characteristics of the same part multiple times (Nakagawa and Schielzeth, 2010; McLain et al., 2018). The ability to evaluate repeatability enables the comparison of a specific result or collection of data to a measurement that was obtained under identical conditions using the same tool or device in a short amount of time (McLain et al., 2018). Thus, a new piece of equipment and the testing methodology that goes with it must be accurate, precise, repeatable, or reproducible from operator to operator, in order to have confidence in a method and prevent disputes between researchers (Downing, 2004; McLain et al., 2018).

Concerning the relevance of this study, accuracy is one of the main justifications for using LiDAR data. According to Akay et al. (2009), LiDAR is an accurate and economical approach for gathering data over large areas. As a result, choosing the necessary degree of data accuracy and recording the level attained are crucial steps in both data collection and utilization (Carter et al., 2012). According to Nitoslawski et al. (2021), researchers have found that despite the increasing digitalization of our world, there hasn't been enough research conducted on the uses and effects of new digital tools in forestry research. Thus, ensuring accurate and high-quality data is one of the main challenges associated with applying various digital technologies to manage forest ecosystems (Nitoslawski et al., 2021). Additionally, documenting and validating data accuracy and precision is necessary to increase data utility and assure proper and widespread use (Carter et al., 2012).

Conducting a study to estimate the accuracy and precision of low-cost mobile LiDAR technology for estimating soil disturbance is important because one can ascertain the repeatability of results which is critical for ensuring that they are valid and can be replicated by others. In this regard, Vogt et al. (2021) assert that the scanning accuracy of a 3D scanner determines both its potential applications and usability. In forestry, it is common for studies to be place-, scale- and time-variant. As such, ensuring that the LiDAR data remains consistent and accurate is essential for their success. By conducting a repeatable study, researchers can assess the variability of LiDAR data and investigate the sources of error, which are factors that may impact the accuracy of the soil disturbance estimates (Kedron and Frazier, 2022). This information can then be used to refine and improve the LiDAR technology, leading to more accurate and reliable estimates in the future (Kedron and Frazier, 2022), which will correctly inform

decision-making in forest operations. Several studies demonstrate the potential of LiDAR technology for forest operations and soil research (Akay et al., 2009; Salmivaara et al., 2018; Foldager et al., 2019; Mohieddinne et al., 2022). The repeatability of studies also shows the importance of rigorous data collection and processing protocols in ensuring the validity and reliability of the results (Kedron and Frazier, 2022).

The purpose of this study was to estimate the scanning accuracy, precision, and repeatability of an iPhone 13 Pro Max (Apple Inc., 2021b) equipped with SiteScape and the 3D Scanner App utilizing a set of LiDAR point clouds collected from the 3D scanning of soil disturbance in forest operations. As a benchmark for cloud-to-cloud comparisons with the iPhone scans, LiDAR point clouds obtained with the GeoSlam Zeb Revo scanner were used to estimate scan accuracy. The research hypothesis for this study was that the iPhone 13 Pro Max equipped with SiteScape and the 3D Scanner App can produce LiDAR point clouds that are comparable in accuracy, precision, and repeatability to those obtained with the GeoSlam Zeb Revo scanner for measuring soil disturbance in forest operations.

2. Materials and methods

2.1. Description of the study area

The study area was located near the Răcădău River in Brasov County, Romania, at the geographical coordinates of approximately 45° 37′ 27″ N and 25° 45′ 46″ E. The location is covered by a mixed stand in which some old skidding roads were present, on which four sample plots (Table 1) were established. The site's altitude ranges from roughly 700 to 720 m above sea level, and the dominant tree species found in the area are the European beech (*Fagus sylvatica* L.), Silver fir (*Abies alba* Mill.), and Norway spruce [*Picea abies* (L.) H. Karst]. During the data collection period, the weather was characterized by light to moderate rainfall and temperatures which varied between 6 and 11°C. Dry leaves and organic matter covered all the sample plots, which were chosen to reflect variations in terrain, slope, and rut depths (Table 1). The skid roads were very old and most likely they were used by cable skidders in the past to extract the wood from the area following selective felling. The ruts were exposed to weathering and erosion over time, resulting in different depths and shapes. The ruts varied in depth, from shallow to approximately 30 cm, while the slope of the plots was between 15 and 22° (Table 1 and Figure 1). The ruts found on the sample plots were not new, but the effect of time and weather factors since there was a long time from the last use of these skid roads for timber extraction. Nevertheless, these roads are still used by the local people seeking leisure in the area.

Data collection process was implemented in April 2022. The sample plots were rectangular in shape (Figure 1), measuring approximately 2 by 10 m and were geographically positioned using a handheld GPS receiver. Ten ground control points (GCP) were used in each plot, placed on their boundary and spaced at approximately 2 m each other (Figure 1), so as to form a grid overlapped on the boundary of each sample plot. GCPs were in the form of white plastic spheres, measuring 10 cm in diameter, attached to black stands, which were inserted vertically into the soil

so as the top of each sphere was located at approximately 30 cm above the ground. These spheres were marked in advance on the sides with numbers from 1 to 10 by the use of a black permanent marker.

2.2. Acquisition and processing of LiDAR data

Two mobile LiDAR-based devices were used for scanning, namely the GeoSLAM Zeb-Revo (GeoSLAM Ltd et al., 2017) and the iPhone 13 Pro Max (Apple Inc., Cupertino, CA, USA, 2021). SiteScape and 3DScanner App were installed on the iPhone platform and used to collect the point clouds. The steps involved in the data collection process are illustrated in Figure 2. The scanning procedures used for the Zeb Revo were adapted to those used in earlier studies (Ryding et al., 2015; Gollob et al., 2021; Marra et al., 2022), meaning that the operator walked slowly around the edge of each sample plot, following a closed path while remaining about 1.5 m away from the boundary. This approach aimed to ensure that the entire area was scanned and to minimize position accuracy drifts and scanner range noise. After each scanning process and based on external control, the device automatically processed and saved the point cloud data on a USB stick. For the mobile phone and associated apps, scans were done at medium-density (MD), for which the clouds showed a good representation of the ground. The LiDAR sensor collected the 3D point cloud data as the operator walked along the plot's axis. In each plot, two scans were taken by the Zeb Revo device; the iPhone platform was used to take two scans by 3D Scanner app, and another two by the SiteScape app. After each measurement day, the point clouds produced by both LiDAR platforms were transferred into a computer. Table 2 describes the point cloud datasets and their corresponding settings used in the C2C and data analyses.

Point clouds produced by scans had various sizes after pre-processing. Typically, the ZR files had between approximately 1.0 and 1.7 million points, SA between approximately 0.2 and 0.8 million points and SS between approximately 0.7 and 2.3 million points, respectively.
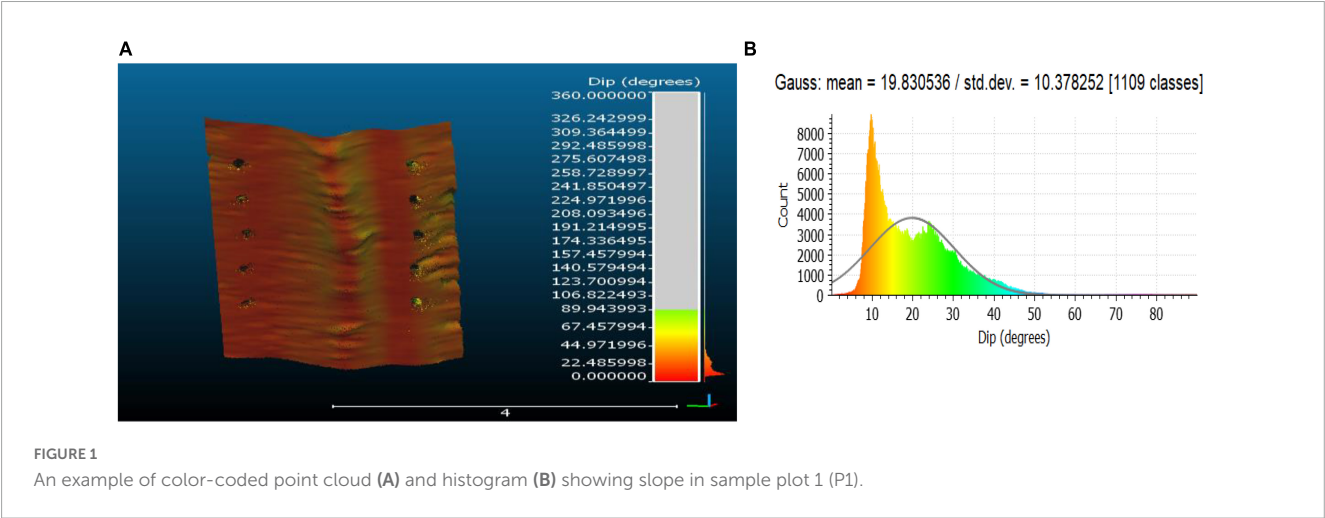
2.3. Cloud-to-cloud comparisons (C2C) of the point clouds

2.3.1. Point-cloud pre-processing and processing

The Cloud-to-Cloud comparison method (C2C) computes the distances between two LiDAR point clouds, and is a widely used technique (Ahmad Fuad et al., 2018). The C2C method compares a reference point cloud generated from a highly accurate surveying method to a test point cloud generated from the LiDAR system under test. This is done by aligning and comparing the point clouds to identify any discrepancies or potential errors in the data, and to estimate the accuracy and precision of the LiDAR system under test (Lague et al., 2013; Ahmad Fuad et al., 2018; Kharroubi et al., 2022). The accuracy and precision of the low-cost LiDAR platforms used for mobile scanning were estimated in this study using the C2C approach. Feature-based and Iterative Closest Point (ICP) options were combined as a part of the coarse-to-fine (C2F)

TABLE 1 Description of the sample plots.

Name	Coordinates	Slope (deg.)		Leaf coverage (%)	Mean rut depth (m)		State
		Mean	Standard deviation		Mean	Standard deviation	
P1	45° 37′ 20.5″ N, 25° 35′ 44.7″ E	19.83	± 10.38	70	0.313	± 0.056	Moist
P2	45° 37′ 17.9″ N, 25° 35′ 43.0″ E	15.20	± 11.11	80	0.122	± 0.015	Moist
P3	45° 37′ 20.6″ N, 25° 35′ 46.0″ E	19.60	± 16.57	90	0.152	± 0.036	Moist
P4	45° 37′ 19.0″ N, 25° 35′ 42.0″ E	21.84	± 18.17	90	0.135	± 0.039	Moist

FIGURE 1
An example of color-coded point cloud **(A)** and histogram **(B)** showing slope in sample plot 1 (P1).

registration strategy (Besl and McKay, 1992; Cheng et al., 2018). The feature-based method was used to identify the corresponding ground control points (GCPs) between the test and reference point clouds and align them accordingly as an initial coarse registration, while the ICP algorithm was used to find the closest point pair between the two-point clouds and align them together in a fine registration (Besl and McKay, 1992; Cheng et al., 2018). Cheng et al. (2018) claim that the fine registration approach is used to alter the results of coarse registration to acquire a satisfactory starting position. This is the main justification for using the two options in this study. Nevertheless, due to the iterative nature of point cloud registration, the ICP technique is slower in identifying connected points between two-point clouds and less effective at registering large, high-density point cloud files (Cheng et al., 2018).

In this study, C2C involved five stages: raw point cloud data pre-processing and processing, point cloud alignment, point cloud fine-registration, cloud-to-cloud distance computation, and surface deviation analysis in CloudCompare software (version 2.12 beta; Girardeau-Montaut, 2015). CloudCompare is a widely used software for point cloud processing, analysis, and visualization (Girardeau-Montaut, 2015; Ahmad Fuad et al., 2018). It provides a range of tools for cleaning, segmentation, filtering, aligning, registering, computing distances, and comparing point clouds (Biber and Strasser, 2003; Ahmad Fuad et al., 2018; Kharroubi et al., 2022). The raw point cloud data pre-processing and

processing involved cleaning and segmentation. The point clouds were first imported from the LiDAR scans in a LAZ file format (.laz) (Thomson, 2018). The raw point cloud data acquired from all the mobile LiDAR scanning platforms were then processed by cleaning the 3D point cloud using the noise filter tool in CloudCompare, which removes unnecessary data associated with the scanned surface (Ahmad Fuad et al., 2018). After cleaning the clouds, the data were segmented using the interactive segmentation tool (Girardeau-Montaut, 2015), exported, and saved in PLY MESH (.ply) file format (Thomson, 2018). According to Rajendra et al. (2014), point cloud pre-processing and processing involve converting the initial raw LiDAR-derived point cloud into a final deliverable. For the purposes of this study, the final deliverables were fully cleaned and segmented LiDAR scans of the soil surfaces for the C2C.

2.3.2. Alignment of the processed LiDAR-derived point cloud

The ground control points (GCPs) found on each of the two clouds were first selected and then used for alignment (Maté-González et al., 2022). Iterative Closest Point (ICP), a popular approach that iteratively discovers the transformation parameters that minimize the distance between matching points in the two clouds, was used in CloudCompare to align pairs of point clouds (Besl and McKay, 1992). A rotation, translation,
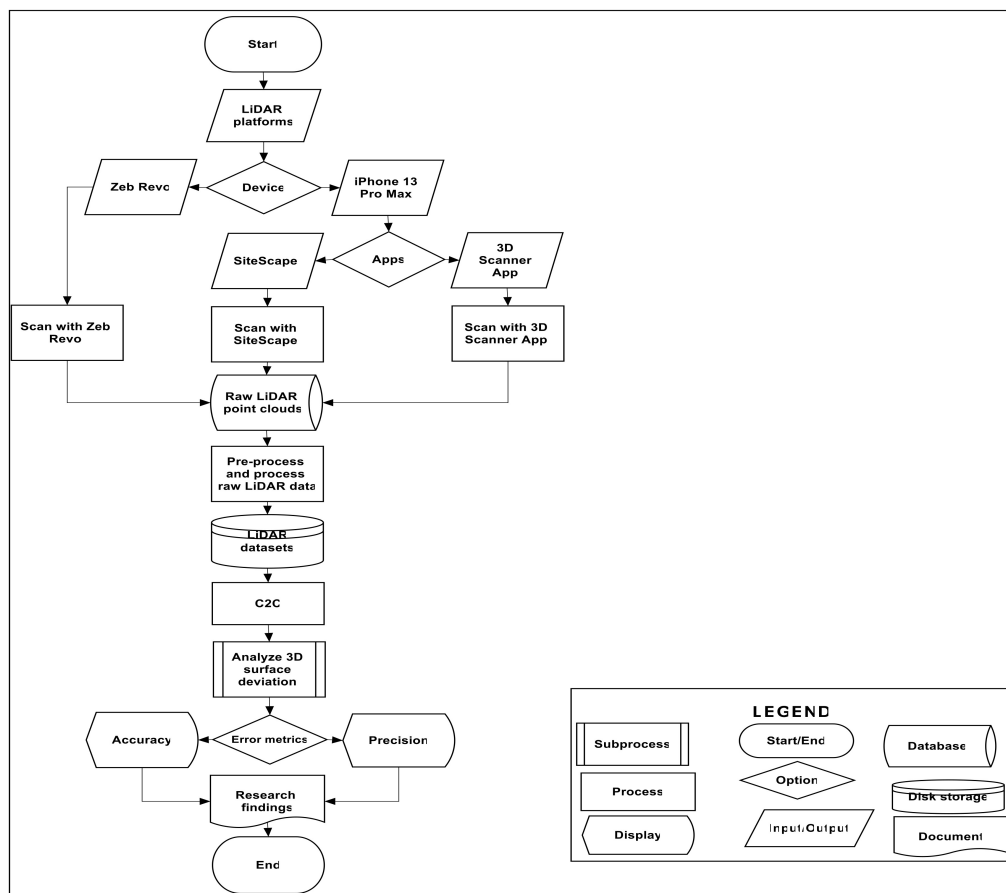
FIGURE 2
Flow chart of LiDAR data collection, processing, analysis and cloud-to-cloud comparison in CloudCompare software. Designed with ClickCharts diagram flowchart software Version 6.98. © NCH software.

and scaling factor make up the rigid transformation. The objective was to identify the transformation parameters that would best align the point clouds (Besl and McKay, 1992). To create a statistically fair comparison, all point clouds used in the C2C were subsampled to 50,000 points (Costantino et al., 2022). Once the optimal transformation parameters were found, the clouds were aligned, and the registration process was complete. Then the RMS values, mean distance, and their standard deviations were recorded. The alignment quality was then assessed using various tools provided by CloudCompare, including color-coded deviation maps, distance histograms, and visualization of the aligned clouds. These tools enabled the evaluation of the accuracy and precision of the alignment and refinement of the alignment parameters if necessary. **Figure 3** shows the ICP alignment process and results provided by the CloudCompare software. Typically, a satisfactory beginning position is initially attained using the point cloud alignment approach, and then registration is fine-tuned using the fine registration method (Biber and Strasser, 2003; Cheng et al., 2018).

2.3.3. Fine registration

The ICP registration method was used for the fine registration of the datasets. This method iteratively matches points in two datasets to find the optimal transformation that aligns the datasets (Segal et al., 2009). The ability to automatically complete the ICP registration process is provided by the CloudCompare program (Ahmad Fuad et al., 2018). However, the value for the point sample unit and the number of iterations were specified prior to starting the ICP registration procedure. **Figure 4** shows an example of the CloudCompare's results and the ICP registration options.

The registration method consisted of several steps, including point selection, point matching, transformation estimation, and transformation refinement. The first step was to select a subset of points from the two datasets. Here again, all point clouds used in the ICP method were those subsampled to 50,000 points (**Figure 4B**). These points were used as the initial correspondence between the two datasets. The point matching step involved finding the closest points in the second dataset for each point in the first dataset. This was done using the more robust Point-to-Plane distance measure (Rusinkiewicz and Levoy, 2001). For the accuracy and precision analyses, the number of iterations of the algorithm was fixed to the default value of 20, the optimum threshold for minimizing the root mean square (RMS) difference was 1.0 E-05 m, and the theoretical overlap was set 100% (**Figure 4A**). Following the establishment of the correspondences, the transformation estimation process involved determining the transformation that would best align the two datasets. This

TABLE 2 Description of the datasets used in the C2C and data analyses.

Abbreviation	Dataset
SA1	1st LiDAR-derived point cloud data based on 3D scanner App. Scanning settings: advanced, low area, medium density. Export: medium density. Collected in each plot.
SA2	2nd LiDAR-derived point cloud data based on 3D scanner App. Scanning settings: advanced, low area, medium density. Export: medium density. Collected in each plot.
SS1	1st LiDAR-derived point cloud data based on SiteScape. Scanning settings: maximum area, medium density. Export: medium density. Collected in each plot.
SS2	2nd LiDAR-derived point cloud data based on SiteScape. Scanning settings: maximum area, medium density. Export: medium density. Collected in each plot.
ZR1	1st LiDAR-derived point cloud data based on GeoSlam Zeb Revo. Scanning settings: as provided by device. Export: as provided by the dedicated software. Collected in each plot.
ZR2	2nd LiDAR-derived point cloud data based on GeoSlam Zeb Revo. Scanning settings: as provided by device. Export: as provided by the dedicated software. Collected in each plot.

transformation was rigid, consisting of a rotation, a translation, and scale factor (Ahmad Fuad et al., 2018; Cheng et al., 2018). A least-square optimization was used to compute the transformation, minimizing the distance between equivalent points in the two datasets (Besl and McKay, 1992; Cheng et al., 2018).

Following the initial transformation, the transformation refinement step iteratively refined the transformation by repeating the point selection, point matching, and transformation estimation steps. The refinement process continued until convergence criteria were met, such as the change in the transformation parameters or the distance between corresponding points falling below a certain threshold. To align the two datasets, the approach iteratively matched points in each of the two datasets before computing the best rigid transformation (Zhang, 1994; Zhang et al., 2015).

To estimate the accuracy of the low-cost LiDAR technology in this study, the point clouds collected by SiteScape and 3D Scanner App were compared against those collected by Zeb Revo, using the Zeb Revo LiDAR point clouds as reference point clouds. For simplicity, the comparisons were done for each plot by matching the repetitions taken by iPhone with those taken by Zeb Revo, namely SA1 against ZR1, SS1 against ZR1, SA2 against ZR2 and SS2 against ZR2. Furthermore, the precision of each LiDAR platform was estimated in each plot by comparing the first repetition against the second one taken by the same platform and software, namely SA1 against SA2, SS1 against SS2 and ZR1 against ZR2. The RMS values, mean distances and their standard deviations were recorded once the registration process was complete.

2.3.4. Cloud-to-cloud distance computation and surface deviation analysis

The 3D surface deviation analysis was carried out using CloudCompare software with the C2C distance computation

method (Zhang, 1994; Zhang et al., 2015; Ahmad Fuad et al., 2018). The software first estimates the results for the distance computation between the chosen datasets using the reference dataset and the compared dataset. Local surface model option from the local modeling menu of the CloudCompare was chosen to increase the accuracy of analysis. Computation was done by the Least Square Plane C2C distance with the default values. The appropriate Octree level value for the process was automatically determined (Zhang, 1994; Zhang et al., 2015; Ahmad Fuad et al., 2018). By activating the data in the layer panel, it was simple to see the resulting 3D surface deviation that was displayed and saved in the test datasets.

The outcome of the 3D surface deviation analysis was then used to identify any alterations resulting from the differences in the compared LiDAR datasets. The CloudCompare software comes equipped with a color scale that displays the value of the C2C distance computation to provide a better understanding of the result. The aligned and registered point clouds were then compared using various metrics, such as the root mean square (RMS), mean distances, and their standard deviations. The RMS error is the square root of the mean square error (MSE) between two clouds (Chai and Draxler, 2014; Brassington, 2017). These metrics help quantify the differences between the point clouds and provide insight into the accuracy and precision of the LiDAR data. However, the C2C distance computation process using CloudCompare software was susceptible to errors, such as the inclusion of unnecessary point cloud data that did not belong to the computed surfaces. To mitigate this for the low-cost LiDAR datasets, the point cloud cleaning and segmentation tools were used. Additionally, the most suitable filtering method was used to produce the point clouds datasets that only belonged to the soil surface (Ahmad Fuad et al., 2018). It is important to note that the accuracy of the analysis was improved by carefully selecting the appropriate filtering methods and settings.

3. Results and discussion

3.1. Accuracy of low-cost derived point clouds

The results on the accuracy of low-cost mobile LiDAR scans using the C2C in the studied plots are summarized in Figure 5 and Table 3. Figure 5 gives only a limited amount of information on the accuracy comparisons. For more graphical information, see the Supplementary material. For the comparison of SS1 against ZR1 in Plot 1 (Figure 5), these metrics were computed on 47,372 points out of 50,000 subsampled from approximately 1.37 million sampling units of the SS test point cloud (Figures 5A, C). The results indicated that the mean distance was 0.010 m, with standard deviation of 0.009 (Figure 5E). Additionally, the final RMS errors during point cloud alignment and fine registration were 0.030 and 0.093 m, respectively (Table 3). For the C2C of SA1 against ZR1 point clouds in the same sample plot (Figures 5B, D, F), however, the metrics were computed on 46,828 points out of the 50,000 points selected from 337,086 sampling points of the SA test point cloud (Figures 5B, D). The results indicated that the mean distance was 0.004 m at a standard deviation of 0.005 (Figure 5F). Moreover, the final RMS error of the registration phase was 0.018 m, while the
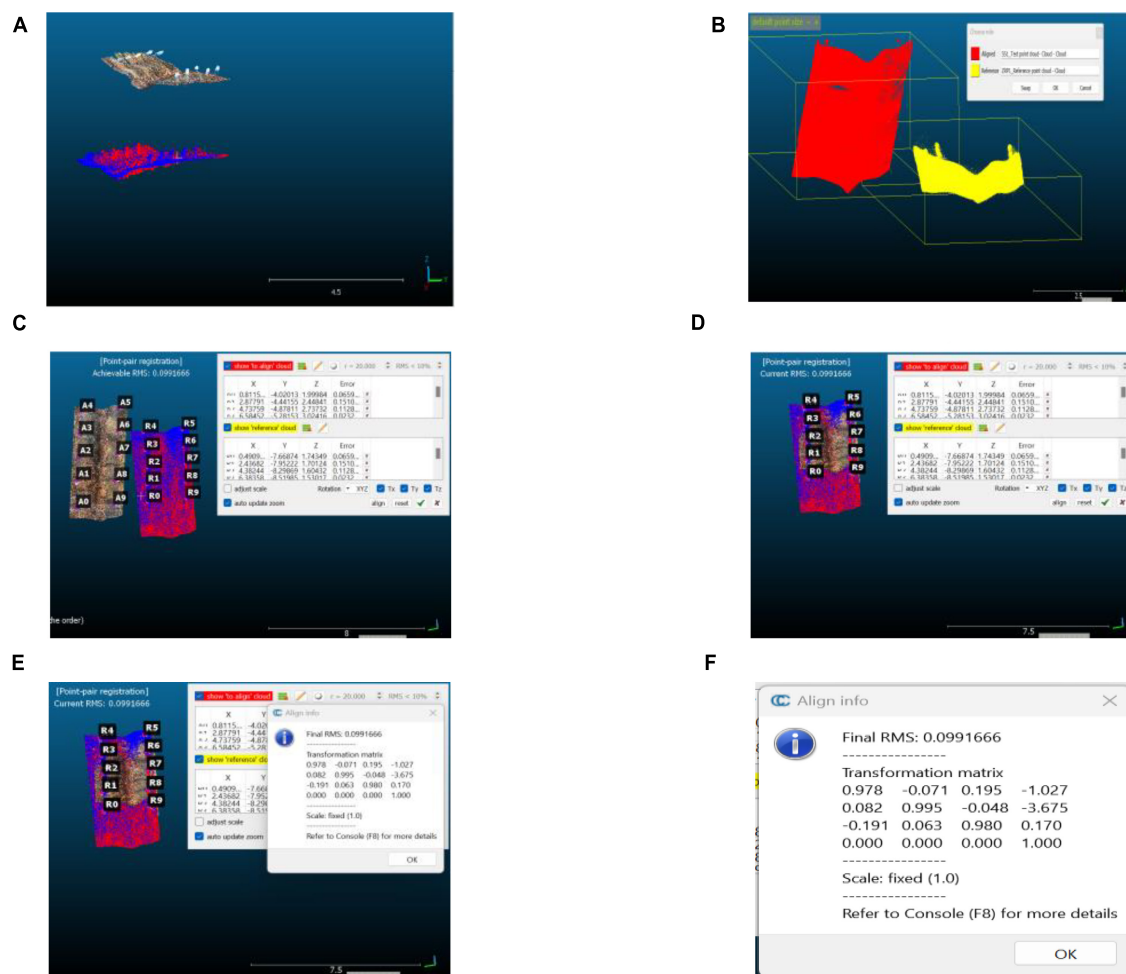
FIGURE 3
An example of ICP alignment and results using low-cost LiDAR-derived data collected by SiteScape (compared) and Zeb Revo (reference) point clouds for Plot 1: **(A)**−the point clouds before role selection, **(B)**−the selected test and reference point clouds, **(C)**−the point clouds ready for alignment after GCP picking, **(D)**−the aligned point clouds, **(E)**−the aligned point clouds with the alignment information, **(F)**−the alignment information on the final RMS error and transformation matrix.

final RMS error obtained during the alignment phase was 0.042 m (Table 3).

Similar results on accuracy were obtained in the remaining C2Cs of SS and SA against the ZR reference point cloud. Table 3 provides a summary of all the results on accuracy of the LiDAR scans with SS and SA by considering the sample plot under question, RMS error obtained at the alignment and registration phases, as well as the mean and standard deviation of distance calculations between point clouds. As shown, the SA had lower RMS errors, mean distances and standard deviations compared to the SS, indicating that it may be more accurate in measuring distances with better repeatability. From these results, the range of final RMS errors of SS vs. ZR was 0.016–0.035 m (Range = 0.019 m). Additionally, the average final RMS error of SS vs. ZR was 0.023 m. In terms of the mean cloud-to-cloud absolute distance, the values varied from 0.004 to 0.039 m (Range = 0.035 m). The corresponding the standard deviation values varied from 0.003 to 0.081 (Range = 0.078). However, the average cloud-to-cloud distance and average standard deviation of SS vs. ZR were 0.016 m and 0.032, respectively.

For SA vs. ZR, the final RMS errors varied from 0.017–0.025 m (Range = 0.007 m). Moreover, the average final RMS error of SA vs. ZR comparisons was 0.020 m; the mean distance varied from 0.004 to 0.042 m (Range = 0.038 m). The corresponding standard deviation varied from 0.006 to 0.081 (Range = 0.075). However, the average cloud-to-cloud absolute distance and average standard deviation values of SA vs. ZR comparisons were 0.011 m and 0.021, respectively.

Overall, both SA and SS produced relatively accurate point clouds with low RMS errors, but SA appeared to have a slight edge in terms of consistency (repeatability) and smaller errors. The overall average final RMS error for SS was slightly higher than the overall average for SA (0.023 vs. 0.020 m). Besides, the SA has a slightly lower average mean distance and standard deviation compared to the SS, indicating that on average, the SA may be slightly more accurate than SS for cloud-to-cloud comparisons using the ZR as the reference point cloud. The results also suggest that the SA has less variability in its measurements than the SS and therefore greater repeatability by comparing the average standard deviations (0.021 vs. 0.032 m). The difference in accuracy between
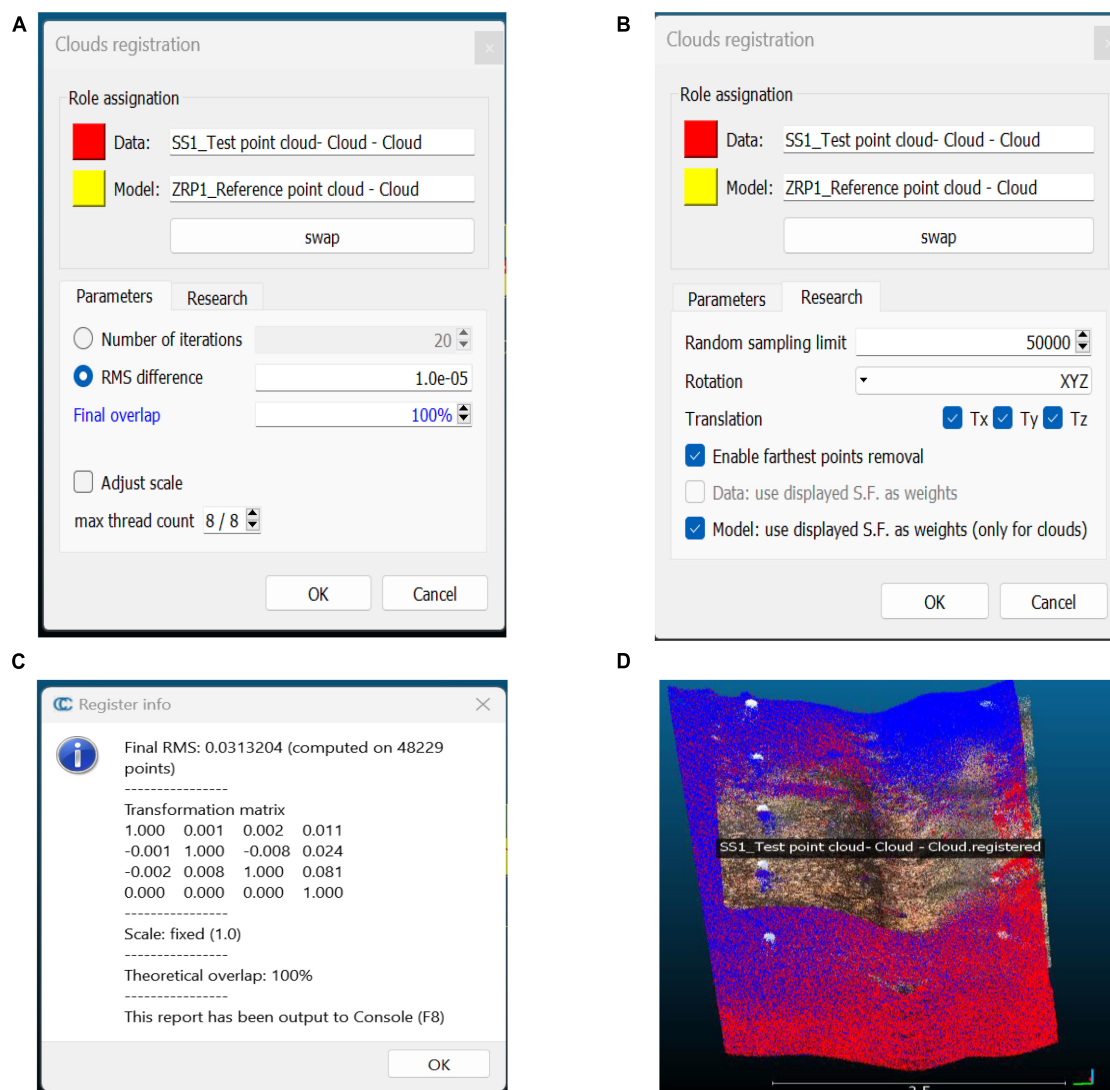
FIGURE 4
An example of ICP registration and results using low-cost LiDAR-derived data collected by SiteScape (compared) and Zeb Revo (reference) point cloud for Plot 1: **(A)**—the number of iterations and final overlap, **(B)**—the default number of sampling points, **(C)**—the final RMS error and the transformation matrix, **(D)**—the registered point cloud.

the two apps is relatively small, so it may not be a significant difference and thus suggesting that both apps are comparable in terms of overall accuracy.

3.2. Intercloud precision of the LiDAR-derived point clouds

Figure 6 and Table 4 show the results of the precision of low-cost mobile LiDAR scans. Figure 6 shows the results graphically only for the sample plot 1. The rest of the graphical results are given in the Supplementary material. The final RMS errors, mean distance, and standard deviation were used to evaluate the precision of the scans during both the alignment and registration phases. For instance, the comparison of SS1 and SS2 in Plot 1 (Figure 6) was based on 46,091 points out of 50,000 points subsampled from

approximately 1.37 million of sampling units of SS test point cloud (Figures 6A, D). The results indicated that the mean distance was 0.006 m at a standard deviation of 0.009 m (Figure 6G). The final RMS error in registration was 0.017 m, whereas the final RMS error obtained during the alignment phase was 0.074 m (Table 4). Similarly, the statistical metrics for the C2C of SA1 and SA2 in the same sample plot 1 (Figure 6) were computed on 44,378 points out of 50,000 subsampled from approximately 0.83 million sampling units of the SA test point cloud (Figures 6B, E). The mean distance was 0.005 m with a standard deviation of 0.014 m (Figure 6H). Additionally, the final RMS error at fine registration was estimated at 0.012 m, whilst the final RMS error at the alignment phase was 0.039 m (Table 4). Regarding ZR1 and ZR2 C2C in the same sample plot 1 (Figure 6), the metrics were computed on 39,273 points out of 50,000 points selected from approximately 1.23 million sampling units of the ZR test point cloud (Figures 6C, F). The mean distance was 0.057 m, and the standard deviation was 0.185 m (Figure 6I);

TABLE 3 Summary statistics of C2C showing the accuracy of the LiDAR scans.

Plot	Compared point clouds	Final RMS Error (m)		Mean cloud-to-cloud distance (m)	Standard deviation
		Alignment	Registration		
P1	SS1 vs. ZR1	0.093	0.030	0.010	0.009
	SS2 vs. ZR2	0.105	0.033	0.012	0.012
	SA1 vs. ZR1	0.042	0.018	0.004	0.005
	SA2 vs. ZR2	0.058	0.030	0.021	0.025
P2	SS1 vs. ZR1	0.104	0.035	0.012	0.012
	SS2 vs. ZR2	0.033	0.018	0.004	0.006
	SA1 vs. ZR1	0.045	0.018	0.004	0.003
	SA2 vs. ZR2	0.078	0.017	0.005	0.016
P3	SS1 vs. ZR1	0.037	0.019	0.005	0.007
	SS2 vs. ZR2	0.023	0.019	0.005	0.006
	SA1 vs. ZR1	0.045	0.020	0.006	0.006
	SA2 vs. ZR2	0.035	0.020	0.007	0.010
P4	SS1 vs. ZR1	0.057	0.016	0.039	0.080
	SS2 vs. ZR2	0.069	0.016	0.042	0.081
	SA1 vs. ZR1	0.088	0.025	0.028	0.040
	SA2 vs. ZR2	0.042	0.016	0.024	0.055

the final RMS error at fine registration was estimated at 0.019 m, while the final RMS error obtained during the alignment phase was 0.053 m (Table 4). A summary of all the comparisons is presented in Table 4.

The results presented in Table 4 show the final RMS errors at point cloud alignment and registration, and the mean C2C (cloud-to-cloud) absolute distances and their standard deviations of the point clouds generated by the iPhone 13 Pro Max (Apple Inc., 2021b) equipped with SS and SA and the professional mobile LIDAR platform of ZR for the four sample plots. From these results, the final RMS error values at fine registration when comparing ZR1 with ZR2 varied from 0.019 to 0.023 m (Range = 0.004 m). Additionally, the average final RMS error of ZR1 vs. ZR2 was 0.021 m. In terms of the range of values for the mean distance and standard deviation for ZR1 vs. ZR2, the mean distance varied from 0.005 to 0.201 m (Mean distance range = 0.197 m), and the standard deviation varied from 0.008 to 0.441 (Standard deviation range = 0.028). Similarly, the average cloud-to-cloud distance and standard deviation of these comparisons were 0.074 and 0.181 m, respectively.

For the comparison between SS1 and SS2, the final RMS error values varied from 0.015 to 0.017 m (Range = 0.002). The average RMS error of SS1 vs. SS2 was 0.017 m. Furthermore, the mean distance varied from 0.006 to 0.011 m (Mean distance range = 0.004 m), while the standard deviation varied from 0.009 to 0.037 m (Standard deviation range = 0.028); the average cloud-to-cloud distance was 0.008 m with a standard deviation of 0.023 m. Regarding the comparison between SA1 and SA2, the final RMS error values varied from 0.012 to 0.014 m (Range = 0.002 m). Moreover, the average RMS error of SA1 vs. SA2 was 0.013 m. Additionally, the mean distance ranged

from 0.001 to 0.008 m (Mean distance range = 0.007), and the standard deviation ranged from 0.001 to 0.014 m (Standard deviation range = 0.012). However, the average cloud-to-cloud distance and standard deviation of these comparisons were 0.004 and 0.009 m, respectively.

Generally, these results suggest that the precision of the low-cost mobile LiDAR technology in estimating soil disturbance in forest operations is high. The final RMS errors, mean distances and standard deviations observed during the C2C comparison were generally low, indicating a high degree of precision. However, the results also show that the final RMS errors during the alignment phase were higher than during the registration phase. Overall, these results suggest that the SA app installed on the iPhone was the best option in terms of precision and consistency (repeatability).

3.3. Discussion

This study aimed to estimate the accuracy and precision of the low-cost mobile LiDAR technology in estimating soil disturbance in forest operations using a cloud-to-cloud comparison approach (C2C), and on that basis, to give indications on repeatability. Regarding the metrics for estimating the accuracy and precision in this study, the RMS error and standard deviation are very similar statistical measures of variability (accuracy, precision, and repeatability) used in LiDAR research (Carter et al., 2012). However, studies show that the two values will be equal in a non-biased data set, when the error is normally distributed above and below zero (Carter et al., 2012). The closer the average RMS error values to zero, the better the performance, as it indicates a smaller deviation from the actual values (Girardeau-Montaut et al., 2005;
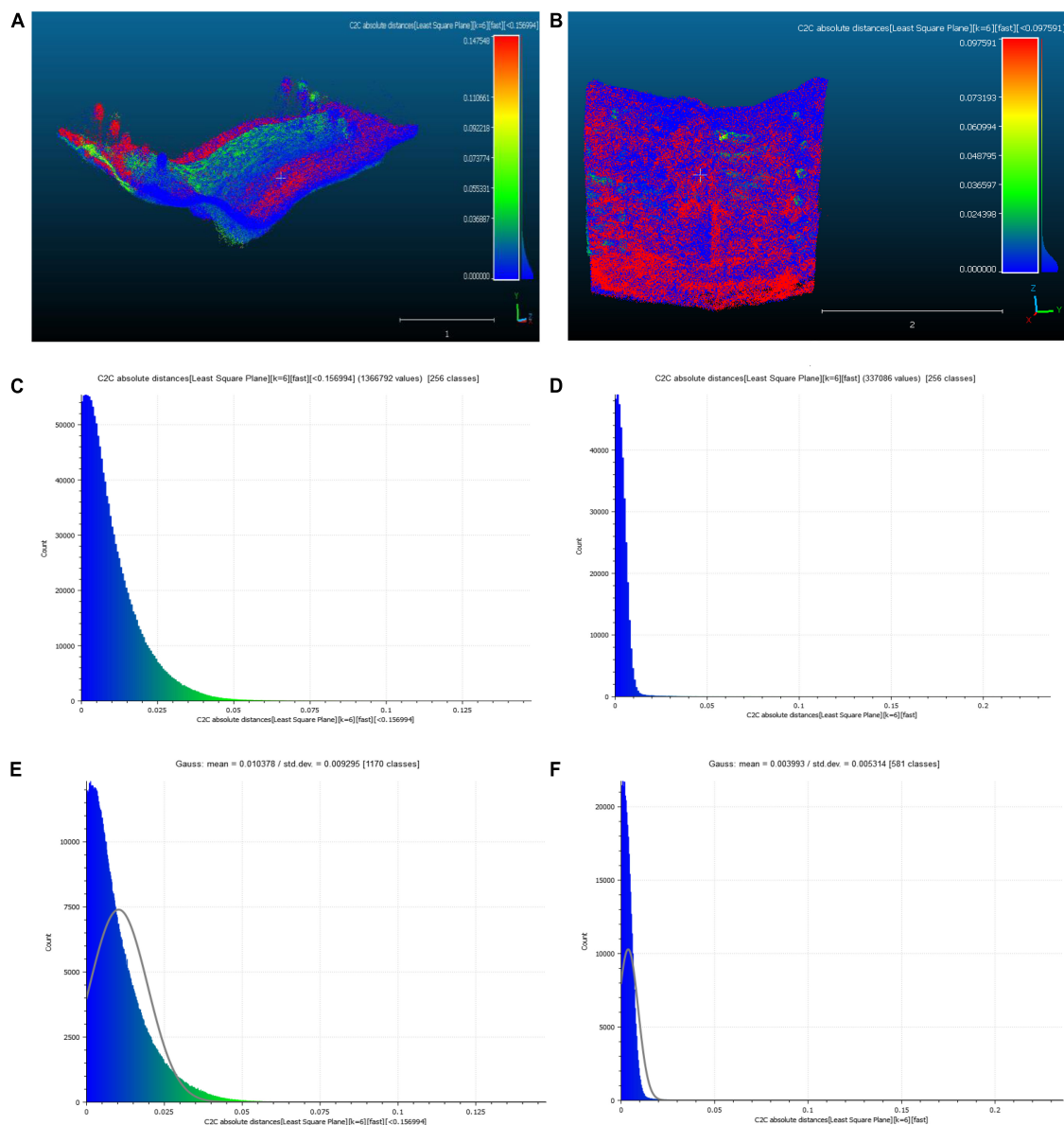
FIGURE 5
An example of accuracy in terms of observed differences between SS1 and ZR1 in Plot 1 **(A,C,E)** and between SA1 and ZR1 in Plot 1 **(B,D,F)**: **(A,B)**—color-coded deviation map of absolute distances, **(C,D)**—histogram of absolute distances, **(E,F)**—histogram of the mean distance and standard deviation.

Ahmad Fuad et al., 2018). Similarly, the lower the average cloud-cloud distance values, the better the accuracy and precision of the scanning device and technology used (Girardeau-Montaut et al., 2005; Ahmad Fuad et al., 2018). According to MacMillan et al. (2023), the standard deviation provides a sense of how close the complete collection of data is to the average value; data sets with modest standard deviations contain precisely organized data, while those with big standard deviations have data dispersed throughout a wide range of values. For example, if the standard deviation of a measurement is very small, it means that repeating that measurement will give similar results. Thus, lower values of the average standard deviation in this study indicate less variability in the precision and accuracy of the scanning devices and therefore greater repeatability.

In this study, the final alignment and registration RMS errors represent the error in aligning the SS and SA scan point clouds and registering them to the reference ZR point cloud, respectively. These errors were used to quantify the difference between test and reference point clouds, and subsequently estimate the accuracy and precision. These values gave us an idea of the variability of the registration and alignment accuracy and precision for each application and device. Nonetheless, the average standard deviation values showed how much the scanned data was spread out from the mean cloud-to-cloud distances, which were used to assess the repeatability of this method. Additionally, the mean cloud-to-cloud distance is the average displacement between the SS or SA point clouds and the reference model of ZR in each plot, which also gave us
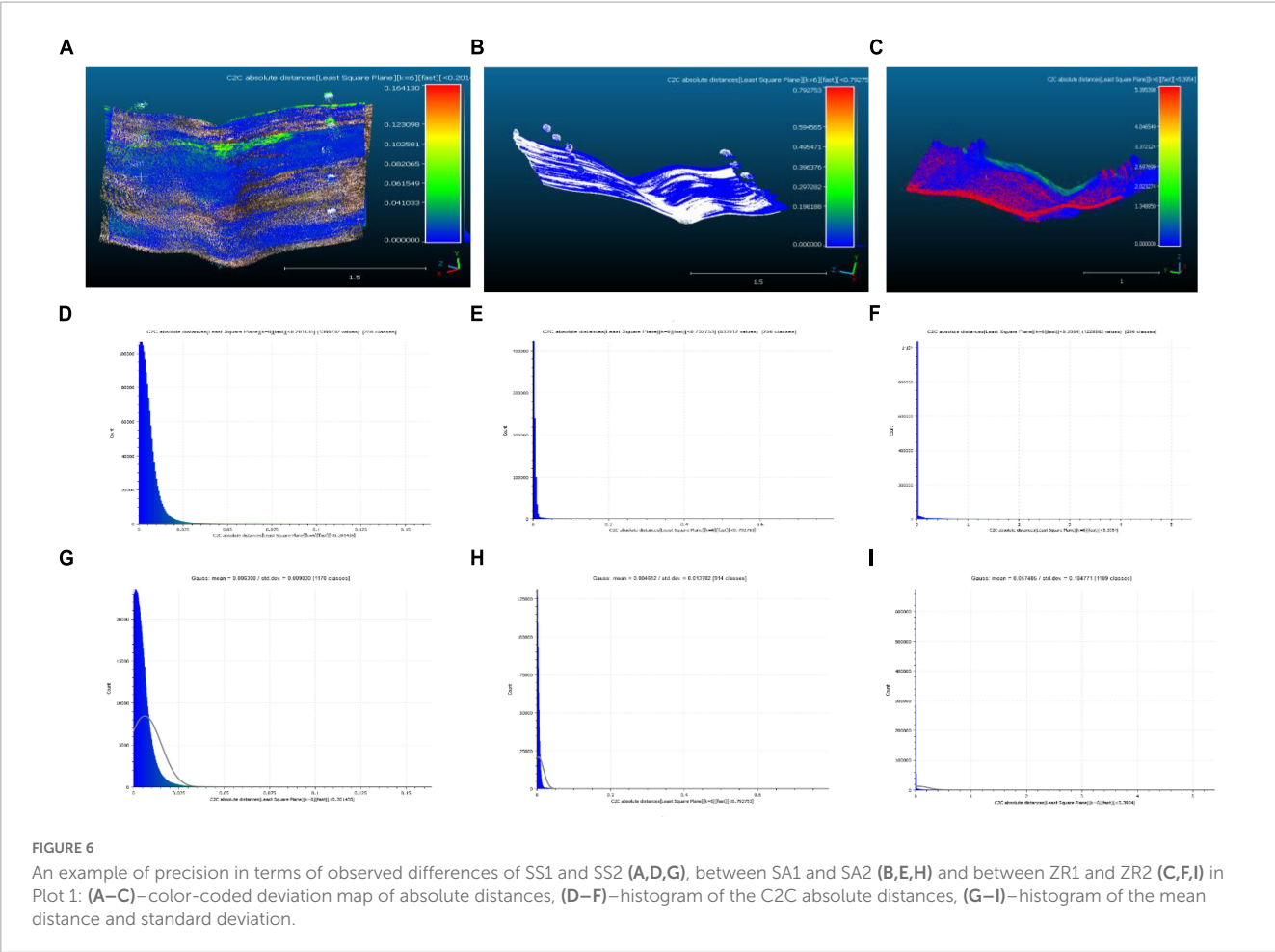
FIGURE 6

An example of precision in terms of observed differences of SS1 and SS2 **(A,D,G)**, between SA1 and SA2 **(B,E,H)** and between ZR1 and ZR2 **(C,F,I)** in Plot 1: **(A−C)**−color-coded deviation map of absolute distances, **(D−F)**−histogram of the C2C absolute distances, **(G−I)**−histogram of the mean distance and standard deviation.

TABLE 4 Summary statistics of C2C showing the precision of the LiDAR scans.

Plot	C2C	Final RMS Error (m)		Mean cloud-to-cloud distance (m)	Standard deviation
		Alignment	Registration		
P1	ZR1 vs. ZR2	0.053	0.019	0.057	0.185
P2	ZR1 vs. ZR2	0.063	0.019	0.005	0.008
P3	ZR1 vs. ZR2	0.074	0.023	0.031	0.092
P4	ZR1 vs. ZR2	0.266	0.020	0.201	0.441
P1	SS1 vs. SS2	0.074	0.017	0.006	0.009
P2	SS1 vs. SS2	0.073	0.016	0.007	0.017
P3	SS1 vs. SS2	0.056	0.015	0.011	0.037
P4	SS1 vs. SS2	0.073	0.016	0.007	0.026
P1	SA1 vs. SA2	0.039	0.012	0.005	0.014
P2	SA1 vs. SA2	0.139	0.014	0.008	0.011
P3	SA1 vs. SA2	0.047	0.012	0.002	0.006
P4	SA1 vs. SA2	0.016	0.014	0.001	0.001

an idea of the accuracy and precision of the low-cost mobile LiDAR technology.

Overall, the performance of each application in terms of accuracy varied plot wise. SA consistently had the smallest final RMS error values, indicating that it was more accurate in capturing

the geometry of the reference model. However, SA had considerably higher final RMS error values, especially in P4, which suggests that it may have some limitations in capturing more complex geometries (see **Supplementary material**). SS had the lowest overall mean cloud-to-cloud distance and standard deviation in P2.

However, it had considerably larger final RMS error values in P1 and P4, suggesting that it is less accurate in capturing certain types of geometries. Similarly, based on the ranges of RMS errors, SA performed slightly better in terms of accuracy compared to SS. SA had a narrower range of RMS errors, which means that the errors varied less between different test point clouds. In contrast, SS had a wider range of RMS errors, indicating that its accuracy varied more between different test point clouds. However, SA's RMS errors were generally smaller than SS's RMS errors. SA's lowest RMS error (0.017 m) was smaller than both of SS's RMS errors, and SA's highest RMS error (0.025 m) was still smaller than SS's highest RMS error (0.035 m). This suggests that SA may be more consistently accurate across different test conditions, while SS may be less predictable in terms of accuracy.

In general, the registration error was smaller than the alignment error across all plots for all applications, suggesting that the registration process was generally more accurate. Overall, these results suggest that both applications can be useful for capturing 3D geometry of soil disturbance in forest operations. However, the accuracy of each application may vary based on the complexity of the soil geometry being captured as well as the complexity of space surrounding the sample plots. Further research could focus on identifying the limitations of each application and developing methods for improving the accuracy of 3D scanning.

Based on the average (mean) distance and standard deviation, SA had a slightly lower average mean distance and standard deviation compared to SS, indicating that it may be slightly more accurate. Overall, the average standard deviations for both apps were relatively low, indicating that they may have good repeatability on average. However, the standard deviations for some of the individual comparisons were relatively large (e.g., SS2 vs. ZR2 in P4 with a standard deviation of 0.081 and SA2 vs. ZR2 in P2 with a standard deviation of 0.016), indicating a lower repeatability in those cases. This suggests that while the studied apps may have good repeatability on average, there are some individual cases where the results could be less reliable. It is possible that this is due to differences in the underlying algorithms or hardware used by each application and device (Gollob et al., 2020, 2021). Further analysis, such as statistical testing or confidence interval estimation, could be used to better understand the variability of the results and their implications for the application being studied. Besides, comparing the average standard deviation values with the average RMS error values, it is evident that for all applications and plots, the standard deviation values were significantly lower. This suggests a good consistency and repeatability in the measurements, and a low uncertainty in the obtained results (Downing, 2004; Nakagawa and Schielzeth, 2010).

The overall accuracy and performance of each application and device may vary depending on the specific use, precision of the data, and other factors. Based on the results of this study, it appears that both applications can achieve a reasonable level of accuracy for cloud-to-cloud comparisons. Therefore, the choice of a given application may ultimately depend on other factors such as precision, user preferences, cost, and ease of use (Wang and Qi, 2021).

Similarly, the study found that the precision of SS, SA, and ZR point clouds was high. The ranges in the descriptive statistics indicated the variability in the final RMS error values, mean cloud-to-cloud absolute distances, and their standard deviation values for each application and device across all four plots; they shown that comparisons between SA1 and SA2 had the least variability in RMS error values, while the ZR1 vs. ZR2 comparisons had the highest variability. Moreover, the SA1 vs. SA2 C2C had the lowest range of values for both mean distance and standard deviation, indicating that the SA application was a consistent (repeatable) and reliable option. The ZR1 vs. ZR2 C2C had the highest range of values for both mean distance and standard deviation, indicating that ZR was the least consistent (repeatable) option. The SS1 vs. SS2 C2C falls somewhere in between with moderate performance in terms of precision and consistency (repeatability).

However, the range alone does not provide enough information about the overall precision; the average of the final RMS error values, mean distance and standard deviation may give a more accurate representation. Consequently, both the range and the average values were combined in the overall evaluation of the performance of the LiDAR platforms. From the results, SA1 vs. SA2 C2C had the lowest average RMS error (0.013 m), indicating that 3D Scanner app was the most precise option. The SA1 vs. SA2 had also the lowest average mean distance (0.004 m), and standard deviation value (0.009), indicating that 3D Scanner app was the most consistent (repeatable) option. On the other hand, the ZR1 vs. ZR2 C2C had the highest average RMS error (0.021 m), which suggests that it was the least precise option. Moreover, the ZR1 vs. ZR2 has the highest average mean distance (0.074 m), and the highest standard deviation (0.181), which suggests that this option was the least consistent (repeatable).

There is limited information available on similar studies for direct comparisons of these findings. For instance, SiteScape is supposed to enable users to easily take 3D scans that are accurate to within ± 1 inch, on average (Corke, 2021). Findings of this study are consistent with some previous research that also used LiDAR systems and/or C2C comparison methods to estimate the accuracy and precision of LiDAR technology. For instance, Milenković et al. (2015) evaluated the accuracy and potential of terrestrial laser scanning (TLS) for soil surface roughness assessment. Their study found that TLS provided highly accurate measurements of soil surface roughness with a mean difference of 0.52 mm between TLS data and ground truth measurements. Furthermore, Mikita et al. (2022) investigated the use of different types of laser scanning methods, including the iPhone 12 Pro Max LiDAR scanning apps, for assessing damage to forest road wearing courses. The study found that the root mean square error (RMSE) of the iPhone LiDAR scanning method was 0.023 m and the coefficient of variation (CV) for the vertical accuracy of the iPhone LiDAR scanning method was 0.25%. They compared these values to those obtained using a terrestrial laser scanner (TLS) and a mobile laser scanning system (MLS). They found that the RMSEs and CVs of the iPhone LiDAR scanning method were comparable to those of the TLS and MLS, indicating that the iPhone LiDAR scanning method can provide accurate and precise measurements. Additionally, the study suggested that the iPhone apps have the potential to streamline the data acquisition process and reduce costs compared to traditional terrestrial laser scanning methods. Similarly, Luetzenburg et al. (2021) evaluated the Apple iPhone 12 Pro LiDAR for its potential application in geosciences. The study found a mean horizontal error of 0.03 m and a mean vertical error of 0.05 m in a vegetation-dominated environment, making it suitable for high-resolution topographic mapping applications.

Additionally, Jaboyedoff et al. (2009) used terrestrial laser scanning for the characterization of retrogressive landslides in sensitive clay and rotational landslides in riverbanks, finding that this method was highly accurate and precise for monitoring landslide movement and deformation. The study reported accuracy values generally less than 5 cm and precision values ranging from 1 to 2 cm. Ahmad Fuad et al. (2018) also found that the Iterative Closest Point (ICP) registration method and the Least Square Plane cloud-to-cloud distance approach were more accurate than other methods for spotting changes in 3D landslide surfaces utilizing Mobile Laser Scanning data between two periods.

In general, the quality of the scan would depend on various factors such as the type of soil, its moisture content, and the texture but when it comes to scanning soil, one important consideration is the resolution of the scanner (Jaboyedoff et al., 2009; Milenković et al., 2015). According to a study by Milenković et al. (2015), the accuracy of laser scanning for soil surface roughness measurement was affected by the point density of the laser scanner. TLS was also found to have high spatial resolution and could be used as a valuable tool for monitoring soil erosion and other environmental changes (Milenković et al., 2015). Similarly, a study by Jaboyedoff et al. (2009) found that increasing the point density resulted in a significant reduction of the error in comparisons between terrestrial laser scanning datasets which was approximately 3 to 6 cm in their study. Therefore, a higher resolution scanner is likely to provide more accurate results when scanning soil surfaces. Another factor that could have affected the accuracy and precision of the low-cost LiDAR scans in this study was the presence of vegetation or other objects on the soil surface (Salmivaara et al., 2018). Several studies indicated that the presence of small vegetation and litter on the soil surface caused errors in the determination of soil surface elevation and roughness, compaction and rutting using LiDAR and TLS methods (Milenković et al., 2015; Salmivaara et al., 2018; Mohieddinne et al., 2022). According to Magtalas et al. (2016), the meter level distances and standard deviations in their study were produced by the fact that both point clouds' whole contents including vegetation were used to calculate the cloud-to-cloud distance when they employed distance computations to further compare their findings. However, the descriptive statistics they used to assess accuracy and precision reduced when the C2C was performed on non-vegetation point clouds using the same procedure. Thus, the vegetation growing on the soil's surface, which exhibited elevation differences of a few meters between the two datasets, might be the source of the meter level deviations (Magtalas et al., 2016). The accuracy and precision values from their study cannot, however, be directly compared to those from this study, because their technique of assessing the accuracy and precision differs from that used herein. Thus, further research is necessary to explore the effects of vegetation on the accuracy and precision of these low-cost LiDAR systems.

Despite being a useful method for analyzing LiDAR data, the C2C has important limitations in its use (Girardeau-Montaut et al., 2005; Cheng et al., 2018; Kharroubi et al., 2022). One of the main limitations is the assumption that the point clouds being compared are of the same geographic location. The comparisons may be inaccurate if there are any variations in the position or orientation of the point clouds during scanning (Girardeau-Montaut et al., 2005; Lague et al., 2013; Kharroubi et al., 2022). Additionally, the accuracy and precision of the cloud-to-cloud comparison method

depend on the quality and resolution of the point clouds generated by the LiDAR systems (Cheng et al., 2018; Kharroubi et al., 2022). The C2C method is not robust to changes in point density and point cloud noise (Girardeau-Montaut et al., 2005; Lague et al., 2013), which may affect the accuracy and precision of the results. The accuracy of the method can be reduced if the clouds from different LiDAR systems have different point densities (Cheng et al., 2018; Kharroubi et al., 2022). These problems were addressed in this study by modeling the soil surfaces locally to prevent problems with density change.

Moreover, this study is constrained by the small sample size because it only included four rectangular plots, each measuring around 20 m². More studies may be necessary to evaluate the suitability of this technology in different forested landscapes. Furthermore, the studies cited in this research paper are case studies and may not be generalizable to other locations or forest types. As such, additional research may be necessary to test the applicability of low-cost mobile LiDAR technology in other forested areas. In addition, the cost of high-end LiDAR systems for soil disturbance estimation may not be justifiable for small-scale forest operations. The potential benefits of low-cost mobile LiDAR technology for these operations may be limited by their accuracy and dependence on mobile platforms.

Numerous studies demonstrate that attaining accurate results with low-cost LiDAR technology depends on several variables, including the calibration parameters of the LiDAR platform components, the underlying point cloud density, the scanning settings, and the data processing methods used. Therefore, it is necessary to keep exploring new low-cost LiDAR technologies as they appear. Future studies might consider integrated low-cost LiDAR systems that can potentially offer enhanced capture options with a greater spatial resolution and a longer effective range in forest environments. Additionally, increasing plot coverage while maintaining low operational costs can potentially be achieved by designing and implementing a multiplatform LiDAR sensor solution using Apple's iPhones. For instance, the use of selfie sticks in future research can potentially increase plot coverage and point cloud capture. Moreover, incorporating a multiple-iPhone strategy for the capturing of LiDAR point clouds may be able to shorten the time required for data collection. However, future studies should assess how quickly (time efficiency) point cloud data can be captured and processed using low-cost LiDAR technology. Besides, it will be necessary for extra caution to be taken in using the point picking tool in CloudCompare to ensure that the exact centers of the GCPs are hit to ensure proper alignment and subsequent registration of the point clouds.

Additionally, both the procedures and protocols used in low-cost LiDAR scanning and the experience of the operator are relevant factors that can impact the quality (accuracy, precision, and repeatability) of the resulting LiDAR data (Rathore, 2017). Several studies suggest that that optimizing the scanning procedure, by carefully planning the survey area, selecting appropriate scanning parameters and designing efficient scan paths, choosing the scanning pattern and processing of the data collected are essential steps in the process and can improve the quality of the data while reducing costs (Rathore, 2017; Wang and Menenti, 2021). The experience of the operator is also critical in ensuring the quality of data collected by low-cost LiDAR systems. An experienced operator can anticipate problems that may arise during

the survey and adjust the scanning plan accordingly. Additionally, an experienced operator can make a significant difference in the accuracy of the data collected, particularly in areas with dense vegetation cover by understanding the limitations of the technology and taking appropriate corrective actions.

4. Conclusion

This study aimed to evaluate the accuracy and precision of three LiDAR options for estimating small-scale soil disturbance in forest operations. The three LiDAR options used can generate highly accurate and precise point clouds for small-scale soil disturbance estimation. The cloud-to-cloud distances (C2C) between the point clouds were generally small, indicating a high degree of similarity and agreement between the different options. However, some differences in accuracy and precision may exist between these options depending on the specific test conditions. Additionally, the precision of the LiDAR scans generated by the three options was generally good for all plots tested. The C2C distances between point clouds generated from the same option were also small, indicating a high degree of repeatability and consistency of the LiDAR scans for small-scale soil mapping. Overall, the study suggests that LiDAR scans generated by the three options are highly accurate and precise for small-scale soil disturbance mapping. Additional research is necessary to further validate the applicability of low-cost mobile LiDAR technology for mapping and monitoring forested landscapes.

Data availability statement

The raw data supporting the conclusions of this article will be made available by the authors, without undue reservation.

Author contributions

SB: conceptualization, supervision, and project administration. GF and SB: methodology, formal analysis, writing—original draft, writing–review and editing, resources, and funding acquisition. GF: data curation, validation, visualization, and investigation. Both authors contributed to the article and approved the submitted version.

Funding

Acknowledgments

Conflict of interest

The authors declare that the research was conducted in the absence of any commercial or financial relationships that could be construed as a potential conflict of interest.

Publisher's note

All claims expressed in this article are solely those of the authors and do not necessarily represent those of their affiliated organizations, or those of the publisher, the editors and the reviewers. Any product that may be evaluated in this article, or claim that may be made by its manufacturer, is not guaranteed or endorsed by the publisher.

Supplementary material

The Supplementary Material for this article can be found online at: https://www.frontiersin.org/articles/10.3389/ffgc.2023.1224575/full#supplementary-material

References

Ahmad Fuad, N., Yusoff, A. R., Ismail, Z., and Majid, Z. (2018). Comparing the performance of point cloud registration methods for landslide monitoring using mobile laser scanning data. *ISPRS Arch.* 42, 11–16. doi: 10.5194/isprs-archives-XLII-4-W9-11-2018

Akay, A. E., Oğuz, H., Karas, I. R., and Aruga, K. (2009). Using LiDAR technology in forestry activities. *Environ. Monit. Assess.* 151, 117–125. doi: 10.1007/s10661-008-0254-1

Ampoorter, E., de Schrijver, A, van Nevel, L, Martin Hermy, M., et al. (2012). Impact of mechanized harvesting on compaction of sandy and clayey forest soils: Results of a meta-analysis. *Ann. For. Sci.* 69, 533–542. doi: 10.1007/s13595-012-0199-y

Ampoorter, E., Van Nevel, L., De Vos, B., Hermy, M., and Verheyen, K. (2010). Assessing the effects of initial soil characteristics, machine mass and traffic intensity on forest soil compaction. *For. Ecol. Manag.* 260, 1664–1676.

Andrachuk, M., Marschke, M., Hings, C., and Armitage, D. (2019). Smartphone technologies supporting community-based environmental monitoring and implementation: A systematic scoping review. *Biol. Conserv.* 237, 430–442.

Apple Inc. (2021a). *Apple unveils iPhone 13 Pro and iPhone 13 Pro Max – more pro than ever before*. Available online at: https://www.apple.com/ro/newsroom/2021/09/apple-unveils-iphone-13-pro-and-iphone-13-pro-max-more-pro-than-ever-before/ (accessed May 13, 2023).

Apple Inc. (2021b). *iPhone 13 Pro and 13 Pro Max – technical specifications*. Available online at: https://www.apple.com/by/iphone-13-pro/specs/ (accessed April 28, 2023).

Apple Inc. (2022). *Apple introduces gorgeous new green finishes for the iPhone 13 lineup*. Available online at: https://www.apple.com/ro/newsroom/2022/03/apple-introduces-gorgeous-new-green-finishes-for-the-iphone-13-lineup/ (accessed May 10, 2023).

Astrup, R., Nowell, T., and Talbot, B. (2016). *Deliverable D3.3. The OnTrack monitor – A report on the results of extensive field testing in participating countries. OnTrack – Innovative solutions for the future of wood supply. H2020-EU.3.2.1.4. - Sustainable forestry*. Available online at: https://cordis.europa.eu/project/id/728029 (accessed May 7, 2023).

Beland, M., Parker, G., Sparrow, B., Harding, D., Chasmer, L., Phinn, S., et al. (2019). On promoting the use of lidar systems in forest ecosystem research. *For. Ecol. Manag.* 450:117484. doi: 10.1016/j.foreco.2019.117484

Besl, P. J., and McKay, N. D. (1992). A method for registration of 3-D shapes. *IEEE Trans. Pattern Anal. Mach. Intell.* 14, 239–256. doi: 10.1109/34.121791

Biber, P., and Strasser, W. (2003). "The normal distributions transform: A new approach to laser scan matching," in *Proceedings of the 2003 IEEE/RSJ international conference on intelligent robots and systems (IROS 2003)*, Las Vegas, NV: IEEE, 2743–2748. doi: 10.1109/IROS.2003.1249285

Böhm, S., and Kanzian, C. (2022). A review on cable yarding operation performance and its assessment. *Int. J. For. Eng.* 34, 229–253. doi: 10.1080/14942119.2022.2153505

Brassington, G. (2017). "Mean absolute error and root mean square error: Which is the better metric for assessing model performance?," in *Proceedings of the EGU general assembly conference abstracts*, Vienna, 3574.

Brown, K. R., Aust, W. M., and McGuire, K. J. (2013). Sediment delivery from bare and graveled forest road stream crossing approaches in the Virginia piedmont. *For. Ecol. Manag.* 310, 836–846. doi: 10.1016/j.foreco.2013.09.031

Cabo, C., Ordóñez, C., López-Sánchez, C. A., and Armesto, J. (2018). Automatic dendrometry: Tree detection, tree height and diameter estimation using terrestrial laser scanning. *Int. J. Appl. Earth Obs. Geoinf.* 69, 164–174. doi: 10.1016/j.jag.2018.01.011

Cambi, M., Certini, G., Neri, F., and Marchi, E. (2015). The impact of heavy traffic on forest soils: A review. *For. Ecol. Manag.* 338, 124–138.

Cambi, M., Grigolato, S., Neri, F., Picchio, R., and Marchi, E. (2016). Effects of forwarder operation on soil physical characteristics: A case study in the Italian alps. *Croat. J. For. Eng.* 37, 233–239.

Cambi, M., Hoshika, Y., Mariotti, B., Paoletti, E., Picchio, R., Venanzi, R., et al. (2017). Compaction by a forest machine affects soil quality and *Quercus robur* L. seedling performance in an experimental field. *For. Ecol. Manag.* 384, 406–414.

Carter, J., Schmid, K., Waters, K., Betzhold, L., Hadley, B., Mataosky, R., et al. (2012). *Lidar 101: An introduction to LiDAR technology, data, and applications*. Washington, DC: National oceanic and atmospheric administration (NOAA).

Cécillon, L., Barthès, B. G., Gomez, C., Ertlen, D., Génot, V., Hedde, M., et al. (2009). Assessment and monitoring of soil quality using near-infrared reflectance spectroscopy (NIRS). *Eur. J. Soil Sci.* 60, 770–784. doi: 10.1111/j.1365-2389.2009.01178.x

Chai, T., and Draxler, R. R. (2014). Root mean square error (RMSE) or mean absolute error (MAE)? - Arguments against avoiding RMSE in the literature. *Geosci. Model Dev.* 7, 1247–1250. doi: 10.5194/gmd-7-1247-2014

Cheng, L., Chen, S., Liu, X., Xu, H., Wu, Y., Li, M., et al. (2018). Registration of laser scanning point clouds: A review. *Sensors* 18, 1641. doi: 10.3390/s18051641

Coleman, D. C. (2005). "Vital soil: Function, value and properties," in *Developments in soil science*, Vol. 29, eds P. Doelman and H. Eijsackers (Amsterdam: Elsevier), doi: 10.1016/j.agrformet.2005.09.003

Corke, G. (2021). *SiteScape: LiDAR scanning on the iPhone/iPad*. Available online at: https://aecmag.com/reality-capture-modelling/sitescape-lidar-scanning-on-the-iphone-ipad/ (accessed May 4, 2023).

Costantino, D., Vozza, G., Pepe, M., and Alfio, V. S. (2022). Smartphone LiDAR technologies for surveying and reality modelling in urban scenarios: Evaluation methods, performance and challenges. *Appl. Syst. Innov.* 5, 63. doi: 10.3390/asi5040063

Dassot, M., Constant, T., and Fournier, M. (2011). The use of terrestrial LiDAR technology in forest science: Application fields, benefits and challenges. *Ann. For. Sci.* 68, 959–974. doi: 10.1007/s13595-011-0102-2

Dodge, Y. (2008). *The concise encyclopedia of statistics*. Berlin: Springer Science & Business Media, doi: 10.1007/978-0-387-32833-1

Doetterl, S., Stevens, A., Van Oost, K., and Van Wesemael, B. (2013). Soil organic carbon assessment at high vertical resolution using closed-tube sampling and Vis-NIR spectroscopy. *Soil Sci Soc Am J.* 77, 1430–1435. doi: 10.2136/sssaj2012.0410n

Downing, S. M. (2004). Reliability: On the reproducibility of assessment data. *Med. Educ.* 38, 1006–1012. doi: 10.1111/j.1365-2929.2004.01932.x

Dudáková, Z., Allman, M., Merganič, J., and Merganičová, K. (2020). Machinery-induced damage to soil and remaining forest stands - Case study from Slovakia. *Forests* 11:1289. doi: 10.3390/f11121289

Elhashash, M., Albanwan, H., and Qin, R. (2022). A review of mobile mapping systems: From sensors to applications. *Sensors* 22, 4262. doi: 10.3390/s22114262

Foldager, F. F., Pedersen, J. M., Haubro Skov, E., Evgrafova, A., and Green, O. (2019). Lidar-based 3d scans of soil surfaces and furrows in two soil types. *Sensors* 19:661. doi: 10.3390/s19030661

Frankl, A., Nyssen, J., De Dapper, M., Haile, M., Billi, P., Munro, R. N., et al. (2011). Linking long-term gully and river channel dynamics to environmental change using repeat photography (Northern Ethiopia). *Geomorphology* 129, 238–251. doi: 10.1016/j.geomorph.2011.02.018

Frey, B., Kremer, J., Rüdt, A., Sciacca, S., Matthies, D., and Lüscher, P. (2009). Compaction of forest soils with heavy logging machinery affects soil bacterial community structure. *Eur. J. Soil Biol.* 45, 312–320. doi: 10.1016/j.ejsobi.2009.05.006

GeoSLAM Ltd, Ruddington, and Nottinghamshire (2017). *ZEB-REVO user manual v3.0.0*. Available online at: https://download.geoslam.com (accessed April 18, 2023).

Girardeau-Montaut, D. (2015). *CloudCompare - 3D point cloud and mesh processing software. Open-Source Project, 197*. Available online at: https://scholar.google.co.uk/citations?user=d3cx1qsAAAAJ&hl=en (Accessed May 8, 2023).

Girardeau-Montaut, D. (2016). *CloudCompare. France: EDF R&D Telecom ParisTech, 11*. Available online at: https://scholar.google.com/citations?user=d3cx1qsAAAAJ&hl=fr (Accessed May 1, 2023).

Girardeau-Montaut, D., Roux, M., Marc, R., and Thibault, G. (2005). Change detection on points cloud data acquired with a ground laser scanner. *Int. Arch. Photogramm. Remote Sens. Spat. Inf. Sci.* 36:W19.

Glen, S. (2023). *Accuracy and precision: Definition, examples. StatisticsHowTo.com*. Available online at: https://www.statisticshowto.com/accuracy-and-precision/ (accessed May 9, 2023).

Gollob, C., Ritter, T., Kraßnitzer, R., Tockner, A., and Nothdurft, A. (2021). Measurement of forest inventory parameters with Apple iPad Pro and integrated LiDAR technology. *Remote Sens.* 13:3129. doi: 10.3390/rs13163129

Gollob, C., Ritter, T., and Nothdurft, A. (2020). Comparison of 3D point clouds obtained by terrestrial laser scanning and personal laser scanning on forest inventory sample plots. *Data* 5:103. doi: 10.3390/data5040103

Gregurić, L. (2022). *The best LiDAR scanner apps of 2022*. Available online at: https://all3dp.com/2/best-lidar-scanner-app/ (accessed May 11, 2023).

Heinimann, H. R. (2000). "Forest operations under mountainous conditions,"In *Forests in sustainable mountain development: A state of knowledge report for 2000*, Wallingford: CABI Publishing, 224–234.

Heinimann, H. R. (2004). "Harvesting| forest operations under mountainous conditions," in *Encyclopedia of forest sciences*, eds J. Evans and J. A. Youngquist (Cambridge, MA: Elsevier Academic Press), 279–285. doi: 10.1016/B0-12-145160-7/00011-9

Heinimann, H. R., Stampfer, K., Loschek, J., and Caminada, L. (2001). "Perspectives on central European cable yarding systems," in *Proceedings of the International mountain logging and 11th pacific northwest skyline symposium*, Seattle, WA, 268–279.

Heinzel, J., and Koch, B. (2011). Exploring full-waveform LiDAR parameters for tree species classification. *Int. J. Appl. Earth Obs. Geoinf.* 13, 152–160. doi: 10.1016/j.jag.2010.09.010

Hullette, T., Ghadge, P., and Ali, A. (2023). *The best 3D scanner apps of 2023 (iPhone & Android)*. Available online at: https://all3dp.com/2/best-3d-scanner-app-iphone-android-photogrammetry/ (accessed May 11, 2023).

Jaafari, A., Najafi, A., and Zenner, E. K. (2014). Ground-based skidder traffic changes chemical soil properties in a mountainous Oriental beech (Fagus orientalis Lipsky) forest in Iran. *J. Terramechanics* 55, 39–46. doi: 10.1016/j.jterra.2014.06.001

Jaboyedoff, M., Demers, D., Locat, J., Locat, A., Locat, P., Oppikofer, T., et al. (2009). Use of terrestrial laser scanning for the characterization of retrogressive landslides in sensitive clay and rotational landslides in river banks. *Can. Geotech. J.* 46, 1379–1390. doi: 10.1139/T09-073

Jeong, N., Hwang, H., and Matson, E. T. (2018). "Evaluation of low-cost LiDAR sensor for application in indoor uav navigation," in *Proceedings of the 2018 IEEE sensors applications symposium (SAS)*, Seoul: IEEE, 1–5. doi: 10.1109/SAS.2018.8336719

Ke, Y., Quackenbush, L. J., and Im, J. (2010). Synergistic use of QuickBird multispectral imagery and LiDAR data for object-based forest species classification. *Remote Sens. Environ.* 114, 1141–1154. doi: 10.1016/j.rse.2010.01.002

Kedron, P., and Frazier, A. E. (2022). How to improve the reproducibility, replicability, and extensibility of remote sensing research. *Remote Sens.* 14:5471. doi: 10.3390/rs14215471

Kharroubi, A., Poux, F., Ballouch, Z., Hajji, R., and Billen, R. (2022). Three-dimensional change detection using point clouds: A review. *Geomatics* 2, 457–485. doi: 10.3390/geomatics2040025

Koreň, M., Slančík, M., Suchomel, J., and Dubina, J. (2015). Use of terrestrial laser scanning to evaluate the spatial distribution of soil disturbance by skidding operations. *iForest* 8, 386–393. doi: 10.3832/ifor1165-007

Krause, S., Sanders, T. G. M., Mund, J. P., and Greve, K. (2019). UAV-based photogrammetric tree height measurement for intensive forest monitoring. *Remote Sens.* 11:758. doi: 10.3390/rs11070758

Laan Labs (2011). *3D Scanner App.* Available online at: https://laanlabs.com/ (accessed May 4, 2023).

Lague, D., Brodu, N., and Leroux, J. (2013). Accurate 3D comparison of complex topography with terrestrial laser scanner: Application to the Rangitikei canyon (N-Z). *ISPRS J. Photogramm. Remote Sens.* 82, 10–26. doi: 10.1016/j.isprsjprs.2013.04.009

Liu, W., Li, Z., Sun, S., Malekian, R., Ma, Z., and Li, W. (2019). Improving positioning accuracy of the mobile laser scanning in GPS-denied environments: An experimental case study. *IEEE Sens. J.* 19, 10753–10763. doi: 10.1109/JSEN.2019. 2929142

Luetzenburg, G., Kroon, A., and Bjørk, A. A. (2021). Evaluation of the Apple iPhone 12 Pro LiDAR for an application in geosciences. *Sci. Rep.* 11:22221. doi: 10.1038/ s41598-021-01763-9

MacMillan, A., Preston, D., Wolfe, J., Yu, S., and Yu, S. (2023). "13.1: Basic statistics mean, median, average, standard deviation, z-scores, and p-value," in *Chemical process dynamics and controls*, ed. University of Michigan Engineering Controls Group, 2009 (Ann Arbor, MI: University of Michigan).

Magtalas, M. S. L. Y., Aves, J. C. L., and Blanco, A. C. (2016). Georeferencing UAS derivatives through point cloud registration with archived lidar datasets. *ISPRS Ann. Photogramm. Remote Sens. Spatial Inf. Sci.* 4:195. doi: 10.5194/isprs-annals-IV-2-W1-195-2016

Marra, E., Laschi, A., Fabiano, F., Foderi, C., Neri, F., Mastrolonardo, G., et al. (2022). Impacts of wood extraction on soil: Assessing rutting and soil compaction caused by skidding and forwarding by means of traditional and innovative methods. *Eur. J. For. Res.* 141, 71–86. doi: 10.1007/s10342-021-01420-w

Maté-González, M. Á, Di Pietra, V., and Piras, M. (2022). Evaluation of different LiDAR technologies for the documentation of forgotten cultural heritage under forest environments. *Sensors* 22:6314. doi: 10.3390/s22166314

Matterport Inc (2018). *Capture 3D.* Available online at: https://matterport.com/ (accessed May 4, 2023).

McLain, K. W., Bumblauskas, D. P., White, D. J., and Gransberg, D. D. (2018). Comparative analysis of repeatability and reproducibility of compaction testing. *J. Struct. Integrity Maint.* 3, 106–113. doi: 10.1080/24705314.2018.1461545

Mikita, T., Krausková, D., Hrůza, P., Cibulka, M., and Patočka, Z. (2022). Forest road wearing course damage assessment possibilities with different types of laser scanning methods including new iPhone LiDAR scanning apps. *Forests* 13:1763. doi: 10.3390/f13111763

Milas, A. S., Cracknell, A. P., and Warner, T. A. (2018). Drones - The third generation source of remote sensing data. *Int. J. Remote Sens.* 39, 7125–7137. doi: 10.1080/01431161.2018.1523832

Milenković, M., Pfeifer, N., and Glira, P. (2015). Applying terrestrial laser scanning for soil surface roughness assessment. *Remote Sens.* 7, 2007–2045. doi: 10.3390/ rs70202007

Mohan, M., Silva, C. A., Klauberg, C., Jat, P., Catts, G., Cardil, A., et al. (2017). Individual tree detection from unmanned aerial vehicle (UAV) derived canopy height model in an open canopy mixed conifer forest. *Forests* 8:340. doi: 10.3390/f809 0340

Mohieddinne, H., Brasseur, B., Gallet-Moron, E., Lenoir, J., Spicher, F., Kobaissi, A., et al. (2022). Assessment of soil compaction and rutting in managed forests through an airborne LiDAR technique. *Land Degrad. Dev.* 34, 1558–1569. doi: 10.1002/ldr.4553

Nakagawa, S., and Schielzeth, H. (2010). Repeatability for Gaussian and non-Gaussian data: A practical guide for biologists. *Biol. Rev.* 85, 935–956. doi: 10.1111/ j.1469-185X.2010.00141.x

Nansen, C., and Strand, M. R. (2018). Proximal remote sensing to non-destructively detect and diagnose physiological responses by host insect larvae to parasitism. *Front. Physiol.* 9:1716. doi: 10.3389/fphys.2018.01716

Nichol, J., and Wong, M. S. (2005). Satellite remote sensing for detailed landslide inventories using change detection and image fusion. *Int. J. Remote Sens.* 26, 1913–1926. doi: 10.1080/01431160512331314047

Nikooy, M., Tavankar, F., Naghdi, R., Ghorbani, A., Jourgholami, M., and Picchio, R. (2020). Soil impacts and residual stand damage from thinning operations. *Int. J. For. Eng.* 31, 126–137. doi: 10.1080/14942119.2020.1744954

Nitoslawski, S. A., Wong-Stevens, K., Steenberg, J. W. N., Witherspoon, K., Nesbitt, L., Konijnendijk, et al. (2021). The digital forest: Mapping a decade of knowledge on technological applications for forest ecosystems. *Earth's Future* 9:e2021EF002123. doi: 10.1029/2021EF002123

Novo, A., González-Jorge, H., Martínez-Sánchez, J., and Lorenzo, H. (2020). Canopy detection over roads using mobile LiDAR data. *Int. J. Remote Sens.* 41, 1927–1942. doi: 10.1080/01431161.2019.1678077

Occipital Inc (2018). *Canvas.* Available online at: https://canvas.io/ (accessed May 4, 2023).

Pentek, T., Poršinsky, T., Šušnjar, M., Stankić, I., Nevečerel, H., and Šporčić, M. (2008). Environmentally sound harvesting technologies in commercial forests in the area of Northern Velebit–functional terrain classification. *Period. Biol.* 110, 127–135.

Pierzchała, M., Talbot, B., and Astrup, R. (2016). Measuring wheel ruts with close-range photogrammetry. *Forestry* 89, 383–391. doi: 10.1093/forestry/cpw009

Polycam Inc (2017). *Polycam.* Available online at: https://polycam.ai/ (accessed May 4, 2023).

Rajendra, Y. D., Mehrotra, S. C., Kale, K. V., Manza, R. R., Dhumal, R. K., Nagne, A. D., et al. (2014). Evaluation of partially overlapping 3D point cloud's registration by using ICP variant and CloudCompare. *ISPRS Arch.* 40:891. doi: 10.5194/isprsarchives-XL-8-891-2014

Rathore, F. (2017). *Techniques, protocols, application 3D scanning/geomatics ".* P2Endure Research Project. Available online at: https://www.p2endure-project.eu/ en/results/PublishingImages/d1-3/D1.5_Techniques%20protocols%20application% 203D%20scanning.pdf (accessed May 11, 2023).

Rusinkiewicz, S., and Levoy, M. (2001). "Efficient variants of the ICP algorithm," in *Proceedings of the third international conference on 3-D digital Imaging and modeling*, Quebec City, QC: IEEE, 145–152. doi: 10.1109/IM.2001.924423

Ryding, J., Williams, E., Smith, M. J., and Eichhorn, M. P. (2015). Assessing handheld mobile laser scanners for forest surveys. *Remote Sens.* 7, 1095–1111. doi: 10.3390/rs70101095

Salmivaara, A., Miettinen, M., Finér, L., Launiainen, S., Korpunen, H., Tuominen, S., et al. (2018). Wheel rut measurements by forest machine-mounted LiDAR sensors - Accuracy and potential for operational applications? *Int. J. For. Eng.* 29, 1–12. doi: 10.1080/14942119.2018.1419677

Samsung Group (2023). *Galaxy Z Fold4.* Available online at: https://www.samsung. com/global/galaxy/galaxy-z-fold4/ accessed May 12, 2023).

Scandy, L. (2016). *Scandy Pro.* Available online at: https://www.scandy.co/ (accessed May 4, 2023).

Segal, A., Haehnel, D., and Thrun, S. (2009). "Generalized-ICP," in *Robotics: Science and Systems V*, eds J. Trinkle, Y. Matsuoka, and J. A. Castellanos (Cambridge, MA: MIT Press), 435–442. doi: 10.15607/RSS.2009.V.021

Shao, J., Zhang, W., Mellado, N., Wang, N., Jin, S., Cai, S., et al. (2020). SLAM-aided forest plot mapping combining terrestrial and mobile laser scanning. *ISPRS J. Photogramm. Remote Sens.* 163, 214–230. doi: 10.1016/j.isprsjprs.2020.03.008

Sharma, V. (2018). *Methods and techniques for soil moisture monitoring.* Available online at: https://wyoextension.org/publications/html/B1331/ (accessed April 25, 2023).

Shishiuchi, M. (1993). Optimal skid trail spacing for small vehicles in thinning. *J. For. Eng.* 5, 29–34. doi: 10.1080/08435243.1993.10702652

Silver, L. (2019). *Smartphone ownership is growing rapidly around the world, but not always equally.* Available online at: https://www.pewresearch.org/global/2019/02/ 05/smartphone-ownership-is-growing-rapidly-around-the-world-but-not-always-equally/ (accessed May 10, 2023).

Simonik, M. (2018). *Heges – the iOS 3D Scanner app | using FaceID or LiDAR to make scans.* Available online at: https://hege.sh/ (accessed May 4, 2023).

SiteScape FARO Solution (2023). *SiteScape - LiDAR 3D scanning for construction.* Available online at: https://www.sitescape.ai/ (accessed May 4, 2023).

Spinelli, R., Magagnotti, N., Cosola, G., Labelle, E. R., Visser, R., and Erber, G. (2021). The effect of yarding technique on yarding productivity and cost: Conventional single-hitch suspension vs. horizontal double-hitch suspension. *Croat. J. For. Eng.* 42, 369–380. doi: 10.5552/crojfe.2021.886

Spinelli, R., Magagnotti, N., and Facchinetti, D. (2013). Logging companies in the European mountains: An example from the Italian Alps. *Int. J. For. Eng.* 24, 109–120. doi: 10.1080/14942119.2013.838376

Stovall, A. E., Vorster, A. G., Anderson, R. S., Evangelista, P. H., and Shugart, H. H. (2017). Non-destructive aboveground biomass estimation of coniferous trees using terrestrial LiDAR. *Remote Sens Environ.* 200, 31–42. doi: 10.1016/j.rse.2017.08.013

Talbot, B., and Astrup, R. (2021). A review of sensors, sensor-platforms and methods used in 3D modelling of soil displacement after timber harvesting. *Croat. J. For. Eng.* 42, 149–164. doi: 10.5552/crojfe.2021.837

Tavankar, F., Bonyad, A. E., Nikooy, M., Picchio, R., Venanzi, R., and Calienno, L. (2017). Damages to soil and tree species by cable-skidding in Caspian forests of Iran. *For. Syst.* 26:e009. doi: 10.5424/fs/2017261-09100

Teller, P. (2013). The concept of measurement-precision. *Synthese* 190, 189–202. doi: 10.1007/s11229-012-0141-8

Thomson, C. (2018). *Common 3D point cloud file formats & solving interoperability issues.* Available online at: https://info.vercator.com/blog/what-are-the-most-common-3d-point-cloud-file-formats-and-how-to-solve-interoperability-issues (accessed April 18, 2023).

Tigges, J., Lakes, T., and Hostert, P. (2013). Urban vegetation classification: Benefits of multitemporal RapidEye satellite data. *Remote Sens. Environ.* 136, 66–75. doi: 10.1016/j.rse.2013.05.001

Trimble Inc (2009). *SiteScape app.* Available online at: https://www.trimble.com/ (accessed May 4, 2023).

Trnio Inc (2014). *Trnio.* Available online at: https://www.trnio.com/ (accessed May 4, 2023).

Vallet, B., and Mallet, C. (2016). "Urban scene analysis with mobile mapping technology," in *Land surface remote sensing in Urban and Coastal Areas*, eds N. Baghdadi and M. Zribi (Amsterdam: Elsevier), 63–100.

Vicari, M. B., Disney, M., Wilkes, P., Burt, A., Calders, K., and Woodgate, W. (2019). Leaf and wood classification framework for terrestrial LiDAR point clouds. *Methods Ecol Evol.* 10, 680–694. doi: 10.1111/2041-210X.13144

Vinson, J. A., Barrett, S. M., Aust, W. M., and Bolding, M. C. (2017). Suitability of soil erosion models for the evaluation of bladed skid trail BMPs in the southern Appalachians. *Forests* 8:482. doi: 10.3390/f8120482

Visser, R., and Stampfer, K. (2015). Expanding ground-based harvesting onto steep terrain: A review. *Croat. J. For. Eng.* 36, 321–331.

Vogt, M., Rips, A., and Emmelmann, C. (2021). Comparison of iPad Pro® 's LiDAR and TrueDepth capabilities with an industrial 3D scanning solution. *Technologies* 9:25. doi: 10.3390/technologies9020025

Wang, C., and Qi, H. (2021). Influencing factors of acceptance and use behavior of mobile health application users: Systematic review. *Healthcare* 9:357. doi: 10.3390/healthcare9030357

Wang, D., Momo Takoudjou, S., and Casella, E. (2020). LeWoS: A universal leaf?wood classification method to facilitate the 3D modelling of large tropical trees using terrestrial LiDAR. *Methods Ecol. Evol.* 11, 376–389. doi: 10.1111/2041-210X.13342

Wang, Z., and Menenti, M. (2021). Challenges and opportunities in Lidar remote sensing. *Front. Remote Sens.* 2:641723. doi: 10.3389/frsen.2021.641723

Wilkes, P., Lau, A., Disney, M., Calders, K., Burt, A., de Tanago, J. G., et al. (2017). Data acquisition considerations for terrestrial laser scanning of forest plots. *Remote Sens. Environ.* 196, 140–153. doi: 10.1016/j.rse.2017.04.030

Zhang, X., Glennie, C., and Kusari, A. (2015). Change detection from differential airborne lidar using a weighted anisotropic iterative closest point algorithm. *IEEE J. Sel. Top. Appl. Earth Obs. Remote Sens.* 99, 1–9. doi: 10.1109/JSTARS.2015.2398317

Zhang, Z. (1994). Iterative point matching for registration of free-form curves and surfaces. *Int. J. Comput. Vis.* 13, 119–152. doi: 10.1007/BF01427149

Assessment of above ground biomass and soil organic carbon in the forests of Nepal under climate change scenario

Rajesh Malla[1,2]*, Prem Raj Neupane[2,3] and Michael Köhl[2]

[1]Forest Research and Training Centre (FRTC), Pokhara, Nepal, [2]Center for Earth Systems Research and Sustainability (CEN) and IWS-World Forestry, University of Hamburg, Hamburg, Germany, [3]Friends of Nature, Nepal (FON), Kathmandu, Nepal

Introduction: Many factors, such as climate, topography, forest management, or tree/forest attributes, influence soil organic carbon (SOC) and above-ground tree biomass (AGTB). This study focuses on assessing relationship between various predictor variables and response variables (SOC and AGTB) in the perspective of climate change scenario. The study was conducted throughout in Nepal using forest resource assessment data (2010−2014).

Methods: Our study applied a random forest model to assess the status of SOC and AGTB under future climate change scenarios using 19 bioclimatic variables accompanied by other variables such as altitude, aspect, basal area, crown cover development status, distance to settlement forest types, number of trees, macro-topography, management regime, physiographic zones, slope, and soil depth. The study used 737 (70%) samples as a training data for model development while 312 (30%) samples as a testing data for model validation.

Results and discussion: The respective RMSE, RMSE% and adjusted R^2 of the Random Forest Model for SOC estimation were found to be 9.53 ton/ha, 15% and 0.746 while same for the AGTB were 37.55 ton/ha, 21.74% and 0.743. Particularly, changes in temperature and precipitation showed an effect on the amount of SOC and AGTB in the projected scenario i.e., CMIP6, SSP2 4.5 for 2040−2060. The study found the amount of SOC decreased by 3.85%, while AGTB increased by 2.96% in the projected scenario. The proposed approach which incorporates the effect of bioclimatic variables can be a better option for understanding the dynamics of SOC and AGTB in the future using climatic variables.

KEYWORDS

biomass, carbon, climate change, random forest model, Nepal, precipitation, temperature

1. Introduction

Forest ecosystems are the largest carbon reservoirs storing ∼2 billion tons of CO_2 per year (UNDESA and UNFFS, 2021). The 2006 Intergovernmental Panel on Climate Change (IPCC) guidelines for the national greenhouse gas inventories indicate three major carbon pools (biomass, dead organic matter, and soil) in the forest ecosystem (Eggleston et al., 2006; IPCC, 2006). Most of the forest carbon is found in soil organic matter (45%) followed by living biomass (44%) i.e., above-ground tree biomass (AGTB) and root biomass and remaining in dead organic matter, i.e., in dead wood and litter (FAO, 2020).

Several climatic and edaphic factors influence forest carbon storage (Hofhansl et al., 2020). AGTB is influenced by altitude (Powell et al., 2010; Van der Laan et al., 2014; Rajput et al., 2017), temperature and precipitation (Yan et al., 2015), water availability, soil nitrogen content, and tree cover (Requena Suarez et al., 2021). Similarly, soil organic carbon (SOC) is affected by the amount of above-ground litter fall and root turnover (Andivia et al., 2016), temperature and precipitation (Sun et al., 2019), soil conditions and vegetation (Reyna-Bowen et al., 2019), species diversity (Gamfeldt et al., 2013), soil properties and moisture (Hounkpatin et al., 2018), altitude (Zinn et al., 2018), slope aspect, and soil depths (Zhu et al., 2017).

Climate change is contributing to global warming due to the steady increase in temperature since the 1960s (NOAA, 2023). It is projected to increase the severity of impacts in both the natural and human systems (IPCC, 2023). Climate change, rising temperature particularly, in the future has shown to have a negative effect on AGTB (Larjavaara et al., 2021; Li Y. et al., 2022) and SOC (Kirschbaum, 2000; Zhao et al., 2021) while a positive effect of the rising temperature on AGTB and SOC has also been studied under different climate change scenarios (Fu et al., 2017; Azian et al., 2022). The carbon sink of the forest is sensitive to CO_2 emission change resulting from increasing temperature, hydrological changes, and forest dynamics (Hubau et al., 2020).

Efficient estimation of above ground biomass and soil organic carbon is crucial for the study of carbon dynamics in forest ecosystems. Different assessment methods for the estimation of AGTB and SOC have been carried out. The 2006 IPCC guidelines have provisioned simple to robust method for the estimation of above and below carbon in Tier 1, Tier 2 and Tier 3 categories (IPCC, 2006). Design-based estimation (using ground-based sample plots) is one of the most used approaches for estimating AGTB and SOC (DFRS, 2014, 2015a,b; DFRS/FRA, 2014). Though it provides the precise evaluation of changes (stand structure, tree attributes) due to small standard error (Schadauer and Gabler, 2007), it is time-consuming, less cost-effective and difficult to implement in poorly accessible forest areas (Köhl et al., 2011; Kandel, 2013). Alternatively, a regression model (model-based estimation) has been used for the estimation of AGTB and SOC (Tian et al., 2014; Mohd Zaki et al., 2016; Pokhre, 2018; Li et al., 2019; Malla et al., 2022) that allows more flexibility to provide estimates outside the sample plots (Ståhl et al., 2016). Thus, model based estimation (regression model) is cost-effective and also able to estimate target variables of poorly accessible areas.

Recently, several studies have used a machine learning method such as random forest model (RFM) and gradient boosting (GB) for the prediction of AGTB and SOC (Powell et al., 2010; John et al., 2020; Lee et al., 2020; Li et al., 2020; López-Serrano et al., 2020; Nguyen and Kappas, 2020; Vorster et al., 2020). The RFM model uses machine learning algorithms for classification and regression based on decision trees (Jin et al., 2020). It is appropriate for large datasets with large numbers of variables, non-linear responses, both continuous and categorical variables and is less affected by the multicollinearity problem (Lu et al., 2016). Several studies found RFM superior to the regression model in terms of lowering mean squared error (Hounkpatin et al., 2018; Zhu et al., 2020; Xie et al., 2021), handling non-linear relations

(Pahlavan Rad et al., 2014; Hengl et al., 2015), and indifference of assumptions of having probability distribution (normality) and no multicollinearity among independent variables (Lu et al., 2016; López-Serrano et al., 2016). Moreover, RFM does not require several numbers of sample plots, as in the case of design-based estimation, thus it is cost-effective. It can also estimate the target variable of the poorly accessible area in the presence of readily available independent variables (i.e., temperature, precipitation, slope, altitude, etc.).

Previous studies have used spectral values of satellite images as an independent variable to predict a response variable such as AGTB and SOC in the past period (Powell et al., 2010; Vicharnakorn et al., 2014; Angelopoulou et al., 2019; López-Serrano et al., 2020; Zhu et al., 2020; Kumar et al., 2022). However, the response of AGTB and SOC against change in climatic variables (temperature and precipitation) in the future has been lacking in the national scenario in Nepal. The influence of temperature and precipitation on the quantity of AGTB and SOC (Mehta et al., 2014; Bennett et al., 2020; Saimun et al., 2021) helps estimate these target variables in future climate change scenarios. Therefore, this study aims to answer the questions (1) Which are the variables (topographic, forest variables and climatic) significant to influence AGTB and SOC? (2) Are these variables likely to contribute to the amount of AGTB and SOC under the climate change scenario? The study covered all the forest covers of Nepal using forest resource assessment data. A RFM was used to better examine the influence of climatic, topographic and forest variables on the amount of AGTB and SOC. The research will improve our understanding of how climate change affects AGTB and SOC in the forests.

2. Materials and methods

2.1. Study area

For this study, we selected Nepal (Map 1) as a study site due to its varied site conditions. In Nepal, hilly region occupies a higher chunk of the land (∼86% of the total land area) while lowland (less than 300 m altitude) occupies only 14%. Wide altitudinal variations (<300–8,848 m), resulting in diverse climatic conditions, have produced different physiographic zones, i.e., Terai and Siwalik (lowlands), Mid-hills, High mountains and High *Himal* (LRMP, 1986), which influence the composition of flora and fauna (HMGN/MFSC, 2002). Stainton (1972) classified 35 forest types in Nepal that were further broadly categorized into 10 major groups based on the altitudinal range (HMGN/MFSC, 2002).

The climate of Nepal varies seasonally. For the last 30 years (1991–2020), the average monthly temperature ranges from ∼5°C in January to ∼18°C in July, whereas average rainfall ranges from ∼20 mm in November to ∼340 mm in July (ADB and WB, 2021). Nepal is likely to experience a higher rate of warming in two future periods (2016–2045 and 2036–2065) compared to the reference period, i.e., 1981 to 2010 (GoN/MoFE, 2021) and spatiotemporal changes in precipitation over the period from 1981 to 2010 (Karki et al., 2017). Diverse current and future climatic conditions within comparatively small areas (Dawadi, 2017) make Nepal an ideal place to study the effects of climate change on forests.
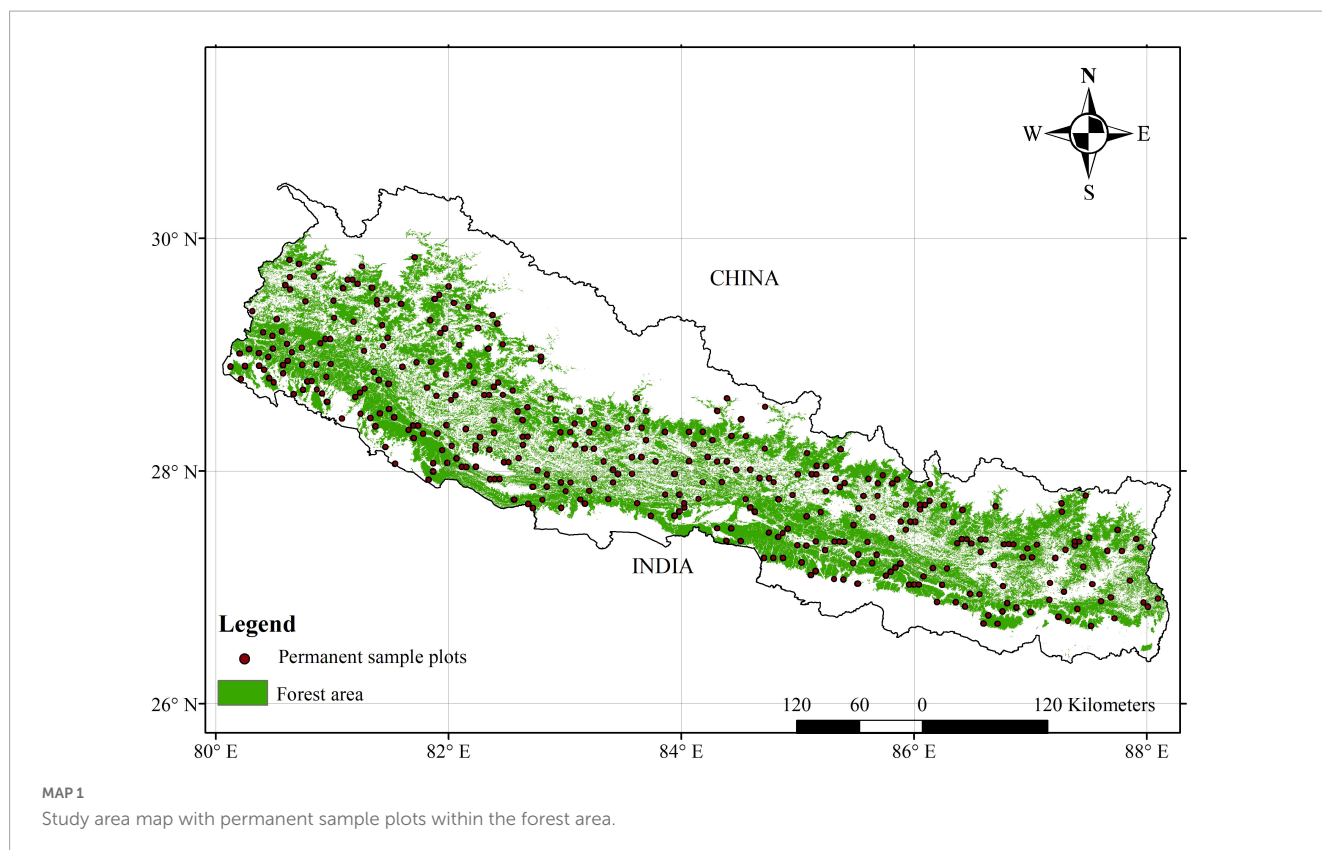
2.2. Data collection

The primary data used in this study were obtained from the third national forest inventory (NFI), which was carried out during 2010–2014. The NFI adopted a two-phase systematic sampling design, composed of 450 clusters containing 1,553 Permanent Sample Plots (PSPs)-after excluding inaccessible PSPs - in the real ground (See **Figure 1**). Data were collected only from the accessible PSPs (slope up to 100 % or 45°). On the sample plots tree related attributes such as diameter at breast height (DBH) and tree height were recorded for the analysis of growing stock, above ground tree biomass and carbon. The third NFI is the first assessment in Nepal that collected soil samples to analyze the SOC of the forests. Four soil pits were established in a cardinal direction in each PSP to collect soil samples. At each cardinal direction, soil pits of appropriate size were dug within the 2 m * 2 m area size at a 21 m distance from the PSP center. In each soil pit, soil samples were collected from three different horizons (1–10 cm, 10–20 cm, and 20–30 cm) up to the depth of 30 cm and were mixed together resulting in 3 soil samples representing three different soil horizons in each PSP (DFRS/FRA, 2014).

Besides forest inventory data, the study used 19 bioclimatic variables representing historic data (near current) representing average figures for the years 1970–2000 at 30 arc sec (~1 km²) resolution (Fick and Hijmans, 2017). The study also used future climate data from the WorldClim data set[1] at 30 arc sec (~1 km²) resolution. representing Couple Modeled Inter-comparison Project

Phase 6 (CMIP6) based on shared socio-economic pathways (SSP2 4.5) scenario from 2041 to 2060 (i.e., 2050 on average) with resulting global warming of 1.6 –2.5°C (IPCC, 2021). We used this scenario in the study because it is an intermediate scenario among five prescribed by Intergovernmental Panel on Climate Change (IPCC) and is based on the current level of CO_2 emission until the middle of the century.

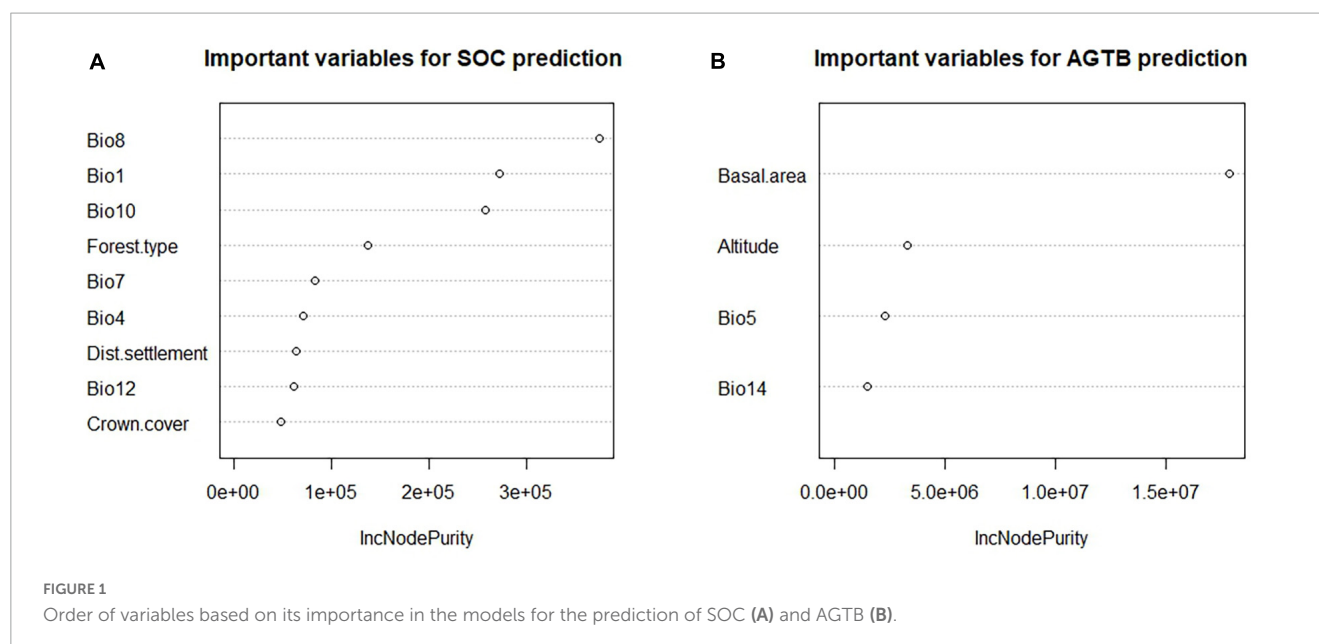## 2.3. Soil organic carbon analysis

Altogether 1,049 PSPs out of 1,553 PSPs were used for SOC analysis. Data from 504 PSPs were removed for one or more of the factors: inappropriateness of the site condition e.g., presence of rock or boulder instead of soil, and missing data for important variables such as aspect, distance to settlement, etc. The Black wet combustion method (Walkley and Black, 1934) was applied in the Nepalese Department of Forest Research and Survey (DFRS) soil laboratory to analyze the SOC content. In addition, dry combustion and LECO CHN Analyzer were used in the Metla Soil Laboratory, Finland, to assure the quality of the laboratory test.

2.4. Above ground tree biomass analysis

Above-ground tree biomass was also estimated from the same PSPs used for SOC analysis. DBH of the tree greater than 5 cm was recorded from the PSPs. The stem volume of the tree was calculated using the equation given by Sharma and Pukkala (1990a).

$$\ln(v) = a + b * \ln(d) + c * \ln(h) \qquad (1)$$

FIGURE 1
Order of variables based on its importance in the models for the prediction of SOC **(A)** and AGTB **(B)**.

where,

ln = Natural logarithm to the base 2.71828,

d = DBH in cm.

h = Total tree height in m.

a, b and c are parameters of the volume equation (**Annex 1**).

To get stem volume in a cubic meter, the model estimation must be divided by 1,000. According to Sharma and Pukkala (1990b), the air-dried wood densities of the tree species range from 352 kg/m^3 for *Trewia nudiflora L.* to 960 kg/m^3 for *Acacia catechu* (L.F.) wild.

In order to estimate AGTB, firstly stem biomass was calculated using following equation.

$$Stem\ biomass\ =\ Volume * Density \quad\quad (2)$$

where,

Volume = Stem volume (m^3).

Density = Air-dried wood density (kg/m^3).

Branch biomass and foliage biomass of the trees were calculated using branch-to-stem and foliage-to-stem ratios, respectively based on tree species and three classes of the size of the stem (small = < 28 cm, medium = 28–53 cm and large = > 53 cm) at diameter at breast height (Sharma and Pukkala, 1990a). Finally, above ground tree biomass (AGTB) of each tree in the PSPs was calculated by using an equation (3). The individual tree biomass (Kg/m^3) within PSP was calculated and it was further converted into ton/ha using the plot expansion factor.

$$AGTB\ =\ Stem\ biomass + Branch\ biomass + Foliage\ biomass \quad (3)$$

2.5. Partition of data set

In order to have independent data sets for model development and model testing, the data were partitioned into two sets A total of 737 (70%) samples were used as training data and 312 (30%) were used as test data. The partitioning of the data was done by using the *createDataPartition* function in the "caret" package

(Kuhn, 2008), which splits data randomly into two different subsets with different proportions.

2.6. Variables selection

Altogether 36 variables were identified for modeling purposes (**Table 1**). Out of these 36 variables, we conducted variable selection based on the importance of the variables in the model. To select the important variables, the function *VSURF* from the R package "VSURF" (Genuer et al., 2010) was used. This package selects important predictor variables for the model by step-wise analysis i.e., threshold, interpretation and prediction. Finally, the selected predictor variables were applied in the model development.

2.7. Estimation of SOC and AGTB using random forest model

Estimation of the SOC and AGTB was conducted (including all predictor variables and only important predictor variables) using a random forest model (RFM) by a function *randomForest* under the "randomForest" package in R software (version 4.2.1). RFM is a machine learning tool using bootstrap aggregating to develop models with an improved prediction (Jin et al., 2020). It is based on two parameters i.e., Number of predictor variables (Mtree) and the number of decision trees (Ntree). The random selection of predictor variables and the records in the data set to generate one decision tree helps to achieve higher accuracy in subsequent iterations. In this way, the RFM function generates many decision trees and averages to give an estimation for the response variable. Averaging a large number of decision trees helps to increase accuracy. Moreover, RFM generates *IncNodePurity* which is a total decrease in node impurities when splitting the predictor variables. An increase in the *IncNodePurity* value of the predictor variables

TABLE 1 Variables to be used for the modeling of SOC and AGTB under random forest model.

Variables		Type	Unit	Source
Topographic Variables	Altitude	Numerical	m	FRA, 2010–2014
	Slope	Numerical	degree	
	Aspect	Numerical	degree	
Forest related variables	Crown cover	Numerical	Percent	
	Basal area	Numerical	m^2/ha	
	Number of trees	Numerical	No./ha	
	Above ground tree biomass	Numerical	Ton/ha	
	Development status (4 types)	Categorical	–	
	Distance to settlement	Numerical	m	
	Physiographic zone (5 types)	Categorical	–	
	Macro-topography (6 types)	Categorical	–	
	Forest type (16 types)	Categorical	–	
	Management regime (9 types)	Categorical	–	
	Soil depth (5 types)	Categorical	–	
	Origin (4 types)	Categorical	–	
	Organic layer (5 types)	Categorical	–	
	Soil organic carbon	Numerical	Ton/ha	
Bioclimatic variables	Bio1 = Annual Mean Temperature	Numerical	^{0}C	World clim data 1970–2000
	Bio2 = Mean Diurnal Range (Mean of monthly (max temp - min temp))	Numerical	^{0}C	
	Bio3 = Isothermality (BIO2/BIO7) (× 100)	Numerical	^{0}C	
	Bio4 = Temperature Seasonality (standard deviation × 100)	Numerical	^{0}C	
	Bio5 = Max Temperature of Warmest Month	Numerical	^{0}C	
	Bio6 = Min Temperature of Coldest Month	Numerical	^{0}C	
	Bio7 = Temperature Annual Range (Bio5-Bio6)	Numerical	^{0}C	
	Bio8 = Mean Temperature of Wettest Quarter	Numerical	^{0}C	
	Bio9 = Mean Temperature of Driest Quarter	Numerical	^{0}C	
	Bio10 = Mean Temperature of Warmest Quarter	Numerical	^{0}C	
	Bio11 = Mean Temperature of Coldest Quarter	Numerical	^{0}C	
	Bio12 = Annual Precipitation	Numerical	mm	
	Bio13 = Precipitation of Wettest Month	Numerical	mm	
	Bio14 = Precipitation of Driest Month	Numerical	mm	
	Bio15 = Precipitation Seasonality (Coefficient of Variation)	Numerical	mm	
	Bio16 = Precipitation of Wettest Quarter	Numerical	mm	
	Bio17 = Precipitation of Driest Quarter	Numerical	mm	
	Bio18 = Precipitation of Warmest Quarter	Numerical	mm	
	Bio19 = Precipitation of Coldest Quarter	Numerical	mm	

indicates the higher importance of the variables. Furthermore, the partial dependence plot was plotted using the *partialPlot* function under the "randomForest" package in the R program.

The plot shows the marginal effects of predictor variables on the response variable in the model (Friedman, 2001). It is generally used to evaluate whether the relationship between the

predictor and response variable is linear, non-linear, or more complex.

2.8. Model validation

Observed data (test data) was plotted against predicted data (model output) to see their relationship for visual interpretation. Moreover, RMSE, RMSE% and R^2 value was calculated to determine the efficiency of the model developed using the *rmse* function ("ModelMetrics" package), *rmse_per* function ("forestmangr" package) and *summary* function in the R program. The RMSE and RMSE% were calculated as follows.

$$RMSE = \sqrt{\sum_{i=1}^{n} \frac{(\hat{y}_i - y_i)^2}{n}} \qquad (4)$$

$$RMSE\% = \frac{RMSE}{\bar{y}_i} \times 100 \qquad (5)$$

Where,

$\hat{y}i$ = the predicted SOC or AGTB on the ith plot,

yi = the observed SOC or AGTB on the ith plot,

$\bar{y}_i$ = the average value of SOC or AGTB.

n = Number of samples.

3. Results

3.1. Variables used in the model

Altogether 35 independent variables were used for the prediction of SOC or AGTB in the study. Of which, nine variables were selected for the prediction of SOC (Bio1, Bio4, Bio7, Bio8, Bio10, Bio12, Forest type, Distance to settlement and Crown cover) and four variables for the prediction of AGTB (Basal area, Altitude, Bio5 and Bio14).

3.2. Variables importance in the model

The selected 9 and 4 Predictor variables for estimating SOC and AGTB, respectively showed different importance values in the models. The predictor variable "Bio8" was found to be the most important variable for the prediction of SOC followed by Bio1, Bio10, Forest type, Bio7, Bio4, Distance to settlement, Bio12 and Crown cover (Figure 1A) whereas Basal area showed its importance highest for the prediction of AGTB followed by Altitude, Bio5, and Bio14 (Figure 1B).

3.3. SOC and AGTB estimation

The random forest model was run in two ways. Firstly, all 35 predictor variables (RFM1 and RFM3) were used in the model (RMF1 and RMF3) for the estimation of SOC and AGTB. Secondly, only predictor variables with high-importance values were used in the model (RFM2 and RFM4) for the same estimation (Table 2). The root mean square error (RMSE), RMSE% and coefficient of

determination (R^2) were found similar for using all 35 predictor variables and using only 9 predictor variables for the estimation of SOC. On the other hand, the performance of the model for the estimation of AGTB was found slightly better while using 35 predictor variables compared to 4 predictor variables (Table 2).

3.4. Relation between number of decision trees and error in the model

The number of decision trees (or "trees") in the Random forest model represents the number of sub-samples selected randomly from the original data set. Increasing the number of decision trees helps to reduce the error in the model. The error was sharply reduced when the number of sub-samples selected from the sample population increased from 1 to 100 and slowed down afterward in both the SOC (Figure 2A) and AGTB (Figure 2B) models.

3.5. Accuracy assessment

Model performance varied in the estimation of SOC (RFM2) and AGTB (RFM4) using test data. RMSE% was found lower in the estimation of SOC as compared to the estimation of AGTB (Table 3).

Moreover, the degree of fitness of the model calculated from the predicted value against the observed value for the estimation of SOC was found to be strong i.e., $R^2 = 0.759$ and the relation was found significant ($p < 0.05$) (Figure 3A). A similar degree of fitness was also found in the case of AGTB estimation i.e., $R^2 = 0.762$ and ($p < 0.05$) (Figure 3B).

3.6. Partial dependence plots (Response plots)

Partial dependence plots for each important predictor variable were plotted for both SOC (RFM2) and AGTB (RFM4) models. Our study found that the response variable SOC responded positively with Crown cover, Distance to settlement and Bio12, and responded negatively with Bio1, Bio7, Bio8 and Bio10, whereas it responded both ways (non-linear relation) with Bio4.

An increase in distance to settlement from the forests up to 8,000 m contributed to the increase in SOC, while for longer distances no effect on SOC was found. Similarly, an increase in crown cover and Bio12 also contributed to the increase in SOC. Furthermore, Bio1, Bio8 and Bio10 did not contribute to SOC up to the temperature of 12, 17, and 19°C, respectively. However, the increase in temperature after those limits contributed to a decrease in SOC. In contrast, Bio4 contributed to a decrease in SOC up to 500 mm and afterward, it contributed to an increase in SOC. Lastly, The comparison of forest types revealed that 1, 11, and 17 contributed more to SOC than the other forest types (Figure 4).

Above-ground tree biomass responded differently with the four predicted variables (Basal area, Altitude, Bio5 and Bio14). Basal area and Bio5 showed a positive relation with AGTB, while Bio14 and Altitude showed both positive and negative (Figure 5). Basal area up to 80 m^2/ha of the forests increased AGTB, and then the

TABLE 2   Summary of the models for the estimation of SOC and AGTB.

Model	Response variable	No. of predictor variable	Ntry	Mtry	RMSE	RMSE%	R^2
RFM1	SOC	35	500	12	9.53	15.00	0.746
RFM2	SOC	9	500	3	10.66	16.77	0.742
RFM3	AGTB	35	500	12	37.55	18.51	0.779
RFM4	AGTB	4	500	2	44.10	21.74	0.743

In the Table, Ntry, number of trees to grow, Mtry, number of variables randomly sampled as candidates at each split, RMSE, root mean square error, R^2, coefficient of determination.
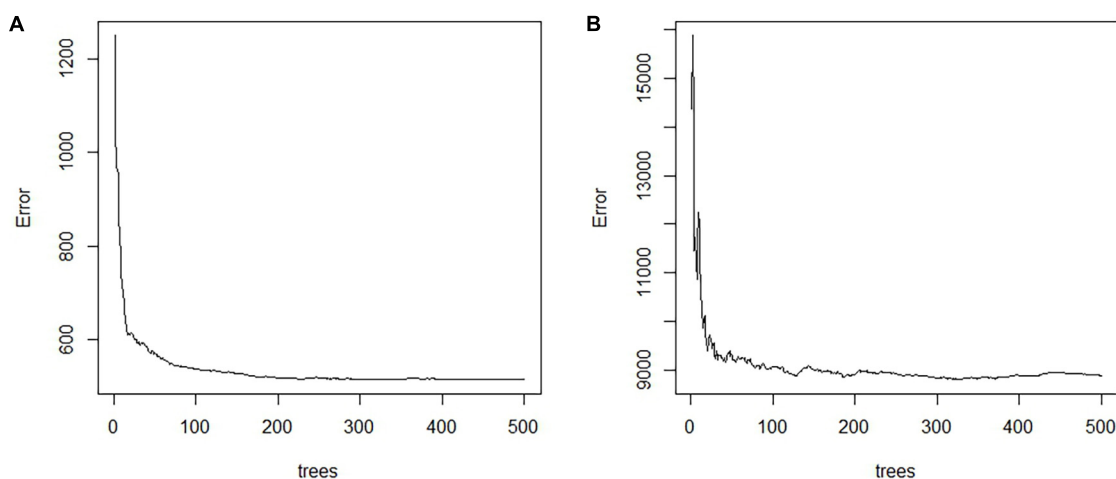
FIGURE 2
Reduction of error as the increase of number of decision trees ("trees") in the RFM2 and RMF4 models for the estimation of SOC **(A)** and AGTB **(B)**, respectively. "Trees" is a number of sub samples selected randomly from the sample population.

amount of AGTB stayed more or less stable, while an increase in Bio5 further increased AGTB. In contrast, altitude and Bio14 decreased AGTB up to 2,000 m and 7 mm, respectively, and after those limits, these variables increased AGTB.

3.7. Amount of soil organic carbon (SOC) and above ground tree biomass (AGTB) using climate change scenario (CMIP6, SSP2 4.5 for 2050)

The CMIP, SSP2 4.5 scenario showed an effect of climate change on SOC and AGTB, assuming other predictors to be the same. An average SOC stock of 63.6 tons/ha was found in the near current period, while it would decrease to 61.15 tons/ha in the future scenario. Unlikely, an average AGTB would increase to 210.57 tons/ha in the future scenario compared to the near current period (204.51 ton/ha). Our result shows that the amount of SOC would likely decrease by 3.85% while AGTB would likely increase by 2.96% in the future climate change scenario (**Table 4**).

The SOC and AGTB were plotted over the individual PSP. The blue lines in both figures represent SOC/ATGB in the near current period (1970–2000) whereas red lines represent them in the future scenario (2040–2060). The blue line has exceeded the red line indicating decreasing trend of SOC in the future scenario (**Figure 6A**). But, for the amount of AGTB, a red line has

TABLE 3   Error assessment of the models (RFM2 and RFM4) developed to predict soil organic carbon (SOC) and above ground tree biomass (AGTB).

Errors	SOC	AGTB
RMSE	20.32	90.11
RMSE %	32.63	44.44

RMSE, root mean square error and RMSE%, root mean square error percentage.

exceeded the blue line indicating the trend of AGTB in the future (**Figure 6B**).

4. Discussion

4.1. Performance of the random forest models

A random forest model has been used in this study to estimate SOC and AGTB in the current and future climate change scenario. The RFM has been popular and considered to produce better accuracy than the multiple linear regression (Powell et al., 2010; Hounkpatin et al., 2018). The multiple linear regression approach is though popular, it does not well capture the complex relationships between the forest variables; and soil-landscape relationships subject to non-linear dynamics (Grimm et al., 2008; Chen et al., 2012). The coefficient of determination (R^2 value) produced by
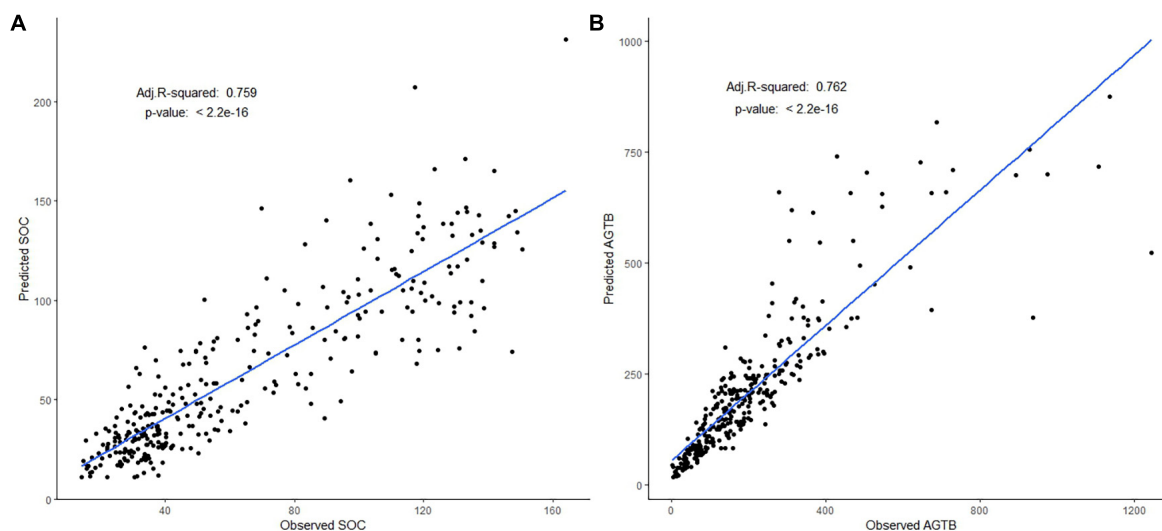
FIGURE 3
Validation of the models for Soil organic carbon (SOC) prediction **(A)** and Above ground tree biomass (AGTB) prediction **(B)** using predicted data and observed data with the help of independent data set.
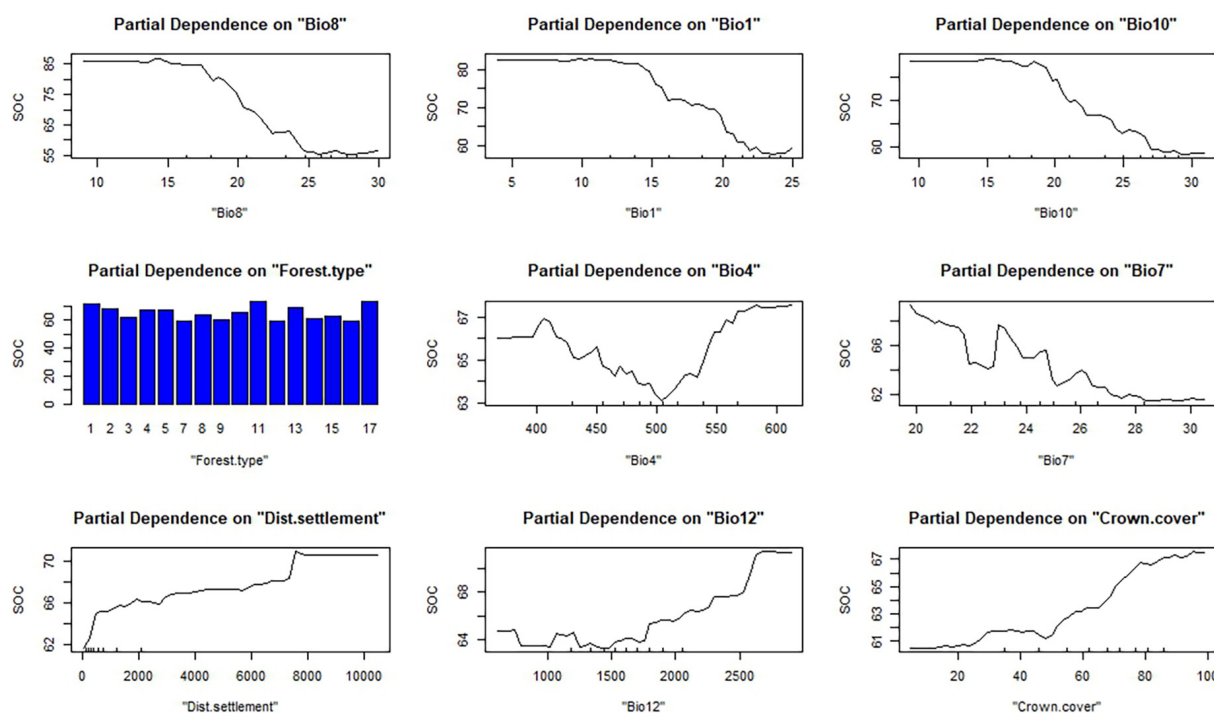

FIGURE 4
Predictor variables responding to Soil organic carbon (SOC) in the partial dependence plot of the random forest model (RFM2) where forest type represented by 1 = Abies spectabilis forest, 2 = Betula utilis forest, 3 = Cedrus deodara forest, 4 = Cupressus torulosa forest, 5 = Junifer wallichiana forest, 7 = Acacia catechu/Dalbergia sisso forest, 8 = Lower mixed hardwood (LMH) forest, 9 = Pinus roxburghii forest, 10 = Pinus wallichiana forest, 11 = Quercus sps forest, 12 = Shorea robusta forest, 13 = Picea smithiana forest, 14 = Shorea robusta TMH forest, 15 = Tsuga dumusa forest,16 = Terai mixed hardwood (TMH) forest, 17 = Upper mixed hardwood (UMH) forest.

our model for the estimation of AGTB is found strong, i.e., 0.74, which is higher than or similar to the other previous studies that used different predictor variables to predict AGTB using RFM (Powell et al., 2010; López-Serrano et al., 2020; Nguyen and Kappas, 2020; Li Z. et al., 2022). Similarly, the RMSE percent of the AGTB

model in our study is slightly higher than the results reported by Musthafa and Singh (2022), Wai et al. (2022) and slightly lower than result of Zhu et al. (2020). These studies completely used other predictors (Image pixel value, age, crown density etc.) compared to our studies (especially temperature and precipitation). Moreover,
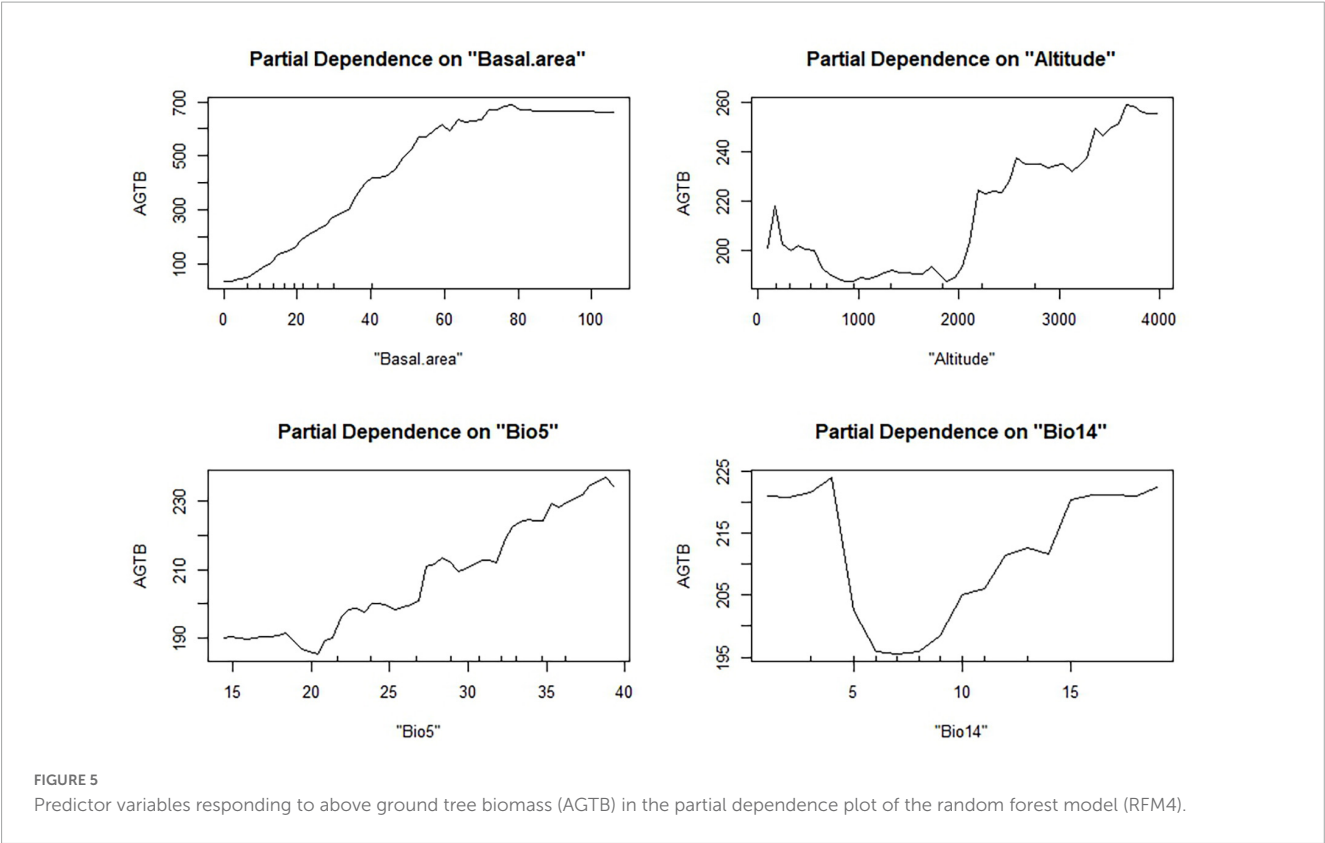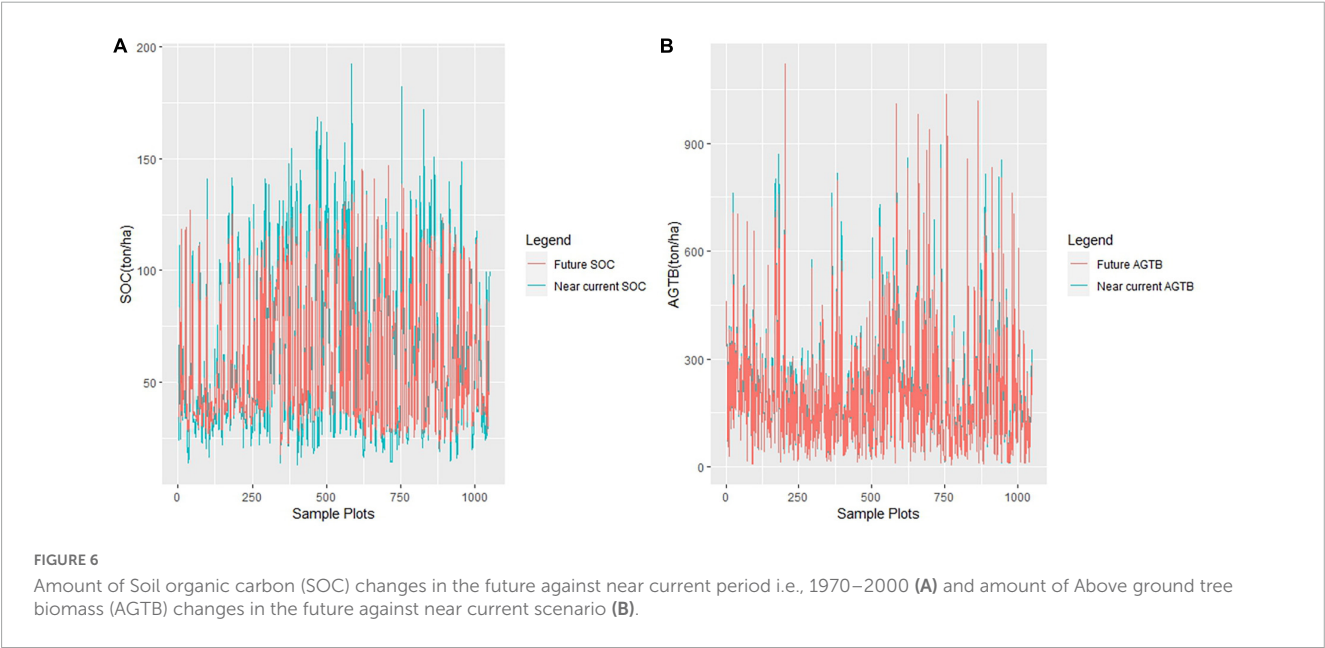
FIGURE 5
Predictor variables responding to above ground tree biomass (AGTB) in the partial dependence plot of the random forest model (RFM4).

TABLE 4   Changes in the amount of soil organic carbon (SOC) and above ground tree biomass (AGTB) in the near current period (1970−2000) and future scenario (2040−2060).

Response variables	Near current period (1970−2000)			Future scenario (2040−2060)			Loss/Gain
	Min	Mean	Max	Min	Mean	Max	
SOC (ton/ha)	12.54	63.6	194.97	18.22	61.15	172.4	−3.85%
AGTB (ton/ha)	5.56	204.51	1121.42	6.04	210.57	1100.14	+2.96%

FIGURE 6
Amount of Soil organic carbon (SOC) changes in the future against near current period i.e., 1970−2000 **(A)** and amount of Above ground tree biomass (AGTB) changes in the future against near current scenario **(B)**.

R^2 and RMSE% of the model for the estimation of SOC is smaller and higher, respectively than other studies (Hounkpatin et al., 2018; Lee et al., 2020). The possible reason could be the use of different independent variables in those studies than our study.

If we compare the estimated quantity of SOC and AGTB of the Random forest model with the forest resource assessment result (DFRS, 2015c) based on design based estimation, the quantity is found similar. The estimated average of SOC (63.6 ton/ha) in this study is 4.9% lower than the forest resource assessment result (66.88 ton/ha) whereas the average of AGTB (204.51 ton/ha) is 5.14% higher than the forest inventory result (i.e., 194.51 ton/ha). Though number of samples used in the model is lower than the samples used in design based approach, the Random forest model seems to be capable to produce better accuracy.

4.2. Factors influencing above ground tree biomass (AGTB)

Based on the previous studies, altitude, stand characteristics (tree age, density), slope, aspect, temperature and precipitation affect the AGTB (Powell et al., 2010; Van der Laan et al., 2014; Yan et al., 2015; Zhang et al., 2016; Rajput et al., 2017; Shen et al., 2018). Similar to the other studies (Wang et al., 2017; Bennett et al., 2020; Larjavaara et al., 2021), our study reports the effect of climate attributes on AGTB, particularly due to the maximum temperature of the warmest month (Bio5) and precipitation of the driest month (Bio14).

The RFM used in this study helps understand AGTB as functions of predictors such as altitude and climatic variables. Previous studies also used RFM to estimate AGTB, but were confined to a few predictor variables such as image pixel value, canopy height, topography, vegetation indices, and texture feature (Li Z. et al., 2022; Musthafa and Singh, 2022; Wai et al., 2022).

Our model shows an increase of AGTB under future climate change scenarios, a finding that is consistent with the results reported by Day et al. (2008), Saeed et al. (2019), Wang et al. (2019). Temperature is the most determining climatic factor that helps in accumulation of tree biomass particularly in the growth season (Devi et al., 2020). Similarly, an increase in precipitation in the driest months (Bio14) helps increase AGTB by lengthening the growing season that supports plant growth (Vaganov et al., 1999). Our results show a positive effect of Bio14 and warmer in the summer (similar to Bio5) with AGTB is consistent with the study conducted by Lewis et al. (2013), Devi et al. (2020), Noguchi et al. (2022). Unlike the forests in Nepal, rising temperature is likely to decrease above-ground biomass in the old-growth tropical forests (Larjavaara et al., 2021).

4.3. Factors influencing soil organic carbon (SOC)

Nine predictor variables, including topographic variables, climatic variables, forest types, distance to settlement and crown cover, are important to influence SOC distribution. Previous studies also report similar influencing variables for SOC, topography (altitude, slope and aspect), above-ground biomass, basal area,

canopy cover, climate and forest types (Kara et al., 2008; Song et al., 2012; Mohammad and Rasel, 2013; Liu et al., 2016; Bangroo et al., 2017; Chaturvedi and Sun, 2018; Jakšić et al., 2021; Shapkota and Kafle, 2021). Apart from other variables, distance to settlement has also an effect on SOC. Our result shows that an increase in distance to settlement- which is likely to reduce human disturbances- results increase in SOC stock (Figure 4). SOC distribution is likely to be more in the area with less human disturbance (Mehta et al., 2008; Eshaghi Rad et al., 2018). Human disturbance such as logging and tree harvest result in a decrease in soil carbon and organic matter (Latty et al., 2004; Moreno et al., 2007).

Our study shows the mean temperature of the wettest quarter (Bio8) as a major predictor variable to estimate SOC in particular. In general, climatic variables are dominating other variables for the prediction of SOC. Similar to our study, previous studies have reported the effect of climate (temperature and precipitation) on SOC (Chen et al., 2015; Alani et al., 2017; Sun et al., 2019; Odebiri et al., 2020; Fang et al., 2022). But, other studies also found altitude as a major variable for SOC prediction (Dieleman et al., 2013; Odebiri et al., 2020). This is also true because altitude though does not directly influence SOC but is an indicator of various climatic functions that govern different vegetation and soil formation processes (Hanawalt and Wittaker, 1976). Thus, altitude can be used as a proxy of climatic variables (Malla et al., 2022).

Furthermore, our model shows a decrease in SOC amount in the future climate change scenario which is similar to the finding reported by Dimobe et al. (2018). Owing to global warming, surface temperature will continue to increase, at least, until 2050 under all emission scenarios (IPCC, 2021). The result shows an increase in temperature (in the future scenario) leads to a decrease in SOC amount, which is supported by other studies (Liu et al., 2021; Zhao et al., 2021). The possible reason could be an increase of soil microbial decomposition due to higher temperature resulting less SOC amount (Dong et al., 2021; Song et al., 2021). Similarly, the negative association of precipitation (in the future scenario) with SOC in our result is similar to the result reported by Alani et al. (2017). The higher amount of precipitation possibly causes to leach dissolved organic carbon of the soil resulting less SOC accumulation.

4.4. Implications of the study

4.4.1. Model implications

Our model shows the effect of climatic variables, topographic variables, forest variables, and distance to settlements on the amount of SOC and AGTB. Particularly, climatic variables (temperature and precipitation) have a direct relation with the formation process of SOC and AGTB. Mean annual precipitation is a driver of the amount of SOC and AGTB (Mehta et al., 2014). Precipitation influences soil moisture and hydrological processes (Heisler and Weltzin, 2006) which is an important factor in SOC cycling (Aanderud et al., 2010) and affects AGTB through functional traits (Cheng et al., 2021). Similarly, temperature also affects the amount of SOC (Zinn et al., 2018; Zhang et al., 2021) and the amount of AGTB (Poudel et al., 2011; Larjavaara et al., 2021). An increase in temperature helps soil microbial decomposition resulting in higher carbon emission or lower SOC

accumulation (Dong et al., 2021; Song et al., 2021) whereas warming temperature enhances tree growth resulting in an increase in AGTB (Way and Oren, 2010).

However, most of the previous studies were focused on forest inventory data accompanied by satellite imageries to estimate AGTB and SOC of the latest period (Angelopoulou et al., 2019; López-Serrano et al., 2020). But for the future prediction of AGTB and SOC under climate change scenario, projected bioclimatic variables are necessary as input variables to produce a precise result. These projected bioclimatic variables have been widely used in species distribution modeling, and habitat suitability under different climate change scenarios (Fyllas et al., 2022; Khan et al., 2022; Shrestha et al., 2022) however, the use of these variables have been very limited for SOC prediction (Liu et al., 2021; Zhao et al., 2021).

Inclusion of Bio2 and Bio6 bioclimatic variables with inventory data helps estimate AGTB and SOC, respectively in a better way. Readily available bioclimatic variables not only improve the performance of the model but also reduce the cost of the model. Combining bioclimatic variables with other variables for the prediction of SOC and AGTB can be a viable option to understand the present scenario.

Moreover, using easily available projected bioclimatic variables under different climate change scenarios see text footnote 1 has benefited us in getting a better understanding the trend of SOC and AGTB in the future. Thus, our model shows an advantage over previous model to assess AGTB and SOC in the future climate change scenario using freely available climatic data.

4.4.2. Implications to Nepal

The forest policy of Nepal emphasizes managing forest resources largely through community participation. Almost half of the total forests have been managed under the broad regime of community-based forest management (Ghimire and Lamichhane, 2020). After the involvement of local people in forest resource management, Nepal has received positive changes in the forest condition. The forest cover of Nepal has been in an increasing trend reported by different assessments, i.e., 29% (DFRS, 1999), 40.36% (DFRS, 2015c), 41.69% (FRTC, 2022). Despite these facts, our model shows the amount of SOC is likely to be decreased in the future, whereas there will be a slight gain in the AGTB. In order to increase SOC in the future, the result highlights the need of management intervention to reduce forest degradation and deforestation through sustainable forest management in all the forests of Nepal to deal with climate change impact.

5. Conclusion

Climatic variables (temperature and precipitation) show an effect on the amount of SOC and AGTB in the future climate change scenario. However, the effect of climate on the SOC and AGTB is opposite (positive with AGTB while negative with SOC). Therefore, management intervention through sustainable forest management is crucial in all forest types to maintain SOC level in the future climate change scenario.

Our study proposed an approach for estimating the AGTB and SOC of Nepal using forest inventory data combined with world climate data (bioclimatic variables). Integrating readily available bioclimatic variables along with other predictor variables helps estimate SOC and AGTB in the near current and future scenario, leading to a better understanding of AGTB and SOC dynamics.

Data availability statement

The datasets presented in this article are not readily available because data sets are available from Forest Research and Training Center, Kathmandu, Nepal upon the request of the researchers, students or institutions. Requests to access the datasets should be directed to Forest Research and Training Center, info@frtc.gov.np.

Author contributions

RM contributes on data acquisition, data analysis and drafting manuscript. PN and MK contribute from draft stage to the final stage of the manuscripts. All authors discussed and revised the manuscript and read and approved the final manuscript.

Funding

Acknowledgments

Conflict of interest

The authors declare that the research was conducted in the absence of any commercial or financial relationships that could be construed as a potential conflict of interest.

Publisher's note

All claims expressed in this article are solely those of the authors and do not necessarily represent those of their affiliated organizations, or those of the publisher, the editors and the reviewers. Any product that may be evaluated in this article, or claim that may be made by its manufacturer, is not guaranteed or endorsed by the publisher.

References

Aanderud, Z. T., Richards, J. H., Svejcar, T., and James, J. J. (2010). A shift in seasonal rainfall reduces soil organic carbon storage in a cold desert. *Ecosystems* 13, 673–682. doi: 10.1007/s10021-010-9346-1

ADB and WB (2021). *Climate Risk Country Profile: Nepal*. Mandaluyong: ADB.

Alani, R., Odunuga, S., Andrew-Essien, N., Appia, Y., and Muyiolu, K. (2017). Assessment of the effects of temperature, precipitation and altitude on greenhouse gas emission from soils in Lagos metropolis. *J. Environ. Protect.* 08, 98–107. doi: 10.4236/jep.2017.81008

Andivia, E., Rolo, V., Jonard, M., Formánek, P., and Ponette, Q. (2016). Tree species identity mediates mechanisms of top soil carbon sequestration in a Norway spruce and European beech mixed forest. *Ann. For. Sci.* 73, 437–447. doi: 10.1007/s13595-015-0536-z

Angelopoulou, T., Tziolas, N., Balafoutis, A., Zalidis, G., and Bochtis, D. (2019). Remote sensing techniques for soil organic carbon estimation: A review. *Remote Sens.* 11, 1–18. doi: 10.3390/rs11060676

Azian, M., Nizam, M., Nik-Norafida, N., Ismail, P., Samsudin, M., and Noor-Farahanizan, Z. (2022). Projection of soil carbon changes and forest productivity for 100 years in Malaysia using dynamic vegetation model Lund-Potsdam-Jena. *J. Trop. For. Sci.* 34, 275–284. doi: 10.26525/jtfs2022.34.3.275

Bangroo, S. A., Najar, G. R., and Rasool, A. (2017). Effect of altitude and aspect on soil organic carbon and nitrogen stocks in the Himalayan Mawer Forest Range. *Catena* 158, 63–68. doi: 10.1016/j.catena.2017.06.017

Bennett, A. C., Penman, T. D., Arndt, S. K., Roxburgh, S. H., and Bennett, L. T. (2020). Climate more important than soils for predicting forest biomass at the continental scale. *Ecography* 43, 1692–1705. doi: 10.1111/ecog.05180

Chaturvedi, S. S., and Sun, K. (2018). Soil organic carbon and carbon stock in community forests with varying altitude and slope aspect in Meghalaya, India. *Glob. Change Biol.* 7:6.

Chen, G., Hay, G. J., and St-Onge, B. (2012). A GEOBIA framework to estimate forest parameters from lidar transects, Quickbird imagery and machine learning: A case study in Quebec, Canada. *Int. J. Appl. Earth Observ. Geoinf.* 15, 28–37. doi: 10.1016/j.jag.2011.05.010

Chen, X., Zhang, D., Liang, G., Qiu, Q., Liu, J., Zhou, G., et al. (2015). Effects of precipitation on soil organic carbon fractions in three subtropical forests in southern China. *J. Plant Ecol.* 9, 10–19. doi: 10.1093/jpe/rtv027

Cheng, H., Gong, Y., and Zuo, X. (2021). Precipitation variability affects aboveground biomass directly and indirectly via plant functional traits in the desert steppe of Inner Mongolia, Northern China. *Front. Plant Sci.* 12:674527. doi: 10.3389/fpls.2021.674527

Dawadi, B. (2017). Climatic records and linkage along an altitudinal gradient in the southern slope of Nepal Himalaya. *J. Nepal Geol. Soc.* 53, 47–56. doi: 10.3126/jngs.v53i0.23804

Day, T. A., Ruhland, C. T., and Xiong, F. S. (2008). Warming increases aboveground plant biomass and C stocks in vascular-plant-dominated Antarctic tundra. *Glob. Change Biol.* 14, 1827–1843. doi: 10.1111/j.1365-2486.2008.01623.x

Devi, N. M., Kukarskih, V. V., Galimova, ÀA., Mazepa, V. S., and Grigoriev, A. A. (2020). Climate change evidence in tree growth and stand productivity at the upper treeline ecotone in the Polar Ural Mountains. *For. Ecosyst.* 7:7. doi: 10.1186/s40663-020-0216-9

DFRS/FRA (2014). *Terai forests of Nepal*. Kathmandu: Department of Forest Research and Survey.

DFRS (1999). *Forest resources of Nepal (1987–1998)*. Kathmandu: Department of Forest Research and Survey.

DFRS (2014). *Churia forests of Nepal (2011-2013)*. Kathmandu: Department of Forest Research and Survey.

DFRS (2015a). *High mountains and high Himalaya forests of Nepal*. Kathmandu: Department of Forest Research and Survey.

DFRS (2015b). *Middle mountains forests of Nepal: Forest resource assessment (FRA)*. Kathmandu: Department of Forest Research and Survey.

DFRS (2015c). *State of Nepal's forests*. Kathmandu: Department of Forest Research and Survey (DFRS).

Dieleman, W. I. J., Venter, M., Ramachandra, A., Krockenberger, A. K., and Bird, M. I. (2013). Soil carbon stocks vary predictably with altitude in tropical forests: Implications for soil carbon storage. *Geoderma* 20, 59–67. doi: 10.1016/j.geoderma.2013.04.005

Dimobe, K., Kouakou, J. L. N., Tondoh, J. E., Zoungrana, B. J. B., Forkuor, G., and Ouédraogo, K. (2018). Predicting the potential impact of climate change on carbon stock in semi-arid West African Savannas. *Land* 7:124. doi: 10.3390/land7040124

Dong, X., Liu, C., Ma, D., Wu, Y., Man, H., Wu, X., et al. (2021). Organic carbon mineralization and bacterial community of active layer soils response to short-term warming in the great Hing'an Mountains of Northeast China. *Front. Microbiol.* 12:802213. doi: 10.3389/fmicb.2021.802213

Eggleston, S., Buendia, L., Miwa, K., Negara, T., and Tanabe, K. (2006). *2006 IPCC guidelines for national greenhouse gas inventories*. Hayama: Institute for Global Environmental Strategies.

Eshaghi Rad, J., Valadi, G., Salehzadeh, O., and Maroofi, H. (2018). Effects of anthropogenic disturbance on plant composition, plant diversity and soil properties in oak forests, Iran. *J. For. Sci.* 64, 358–370. doi: 10.17221/13/2018-JFS

Fang, X., Lin Zhu, Y., Di Liu, J., Ping Lin, X., Zhao Sun, H., Hao Tan, X., et al. (2022). Effects of moisture and temperature on soil organic carbon decomposition along a vegetation restoration gradient of subtropical China. *Forests* 13, 1–16. doi: 10.3390/f13040578

FAO (2020). *Global forest resource assessment 2020:Main report*. Rome: FAO, doi: 10.4324/9781315184487-1

Fick, S. E., and Hijmans, R. J. (2017). WorldClim 2: New 1-km spatial resolution climate surfaces for global land areas. *Int. J. Climatol.* 37, 4302–4315. doi: 10.1002/joc.5086

Friedman, J. H. (2001). Greedy function approximation: A gradient boosting machine. *Ann. Stat.* 29, 1189–1232. doi: 10.1214/aos/1013203451

FRTC (2022). *National Land Cover Monitoring System of Nepal*. Kathmandu: Forest Research and Training Center.

Fu, L., Lei, X., Hu, Z., Zeng, W., Tang, S., Marshall, P., et al. (2017). Integrating regional climate change into allometric equations for estimating tree aboveground biomass of Masson pine in China. *Ann. For. Sci.* 74:42. doi: 10.1007/s13595-017-0636-z

Fyllas, N. M., Koufaki, T., Sazeides, C. I., Spyroglou, G., and Theodorou, K. (2022). Potential impacts of climate change on the habitat suitability of the dominant tree species in Greece. *Plants* 11:1616. doi: 10.3390/plants11121616

Gamfeldt, L., Snäll, T., Bagchi, R., Jonsson, M., Gustafsson, L., Kjellander, P., et al. (2013). Higher levels of multiple ecosystem services are found in forests with more tree species. *Nat. Commun.* 4:2328. doi: 10.1038/ncomms2328

Genuer, R., Poggi, J. M., and Tuleau-Malot, C. (2010). Variable selection using random forests. *Pattern Recogn. Lett.* 31, 2225–2236. doi: 10.1016/j.patrec.2010.03.014

Ghimire, P., and Lamichhane, U. (2020). Community based forest management in Nepal: Current status, successes and challenges. *Grassroots J. Natl. Resour.* 3, 16–29. doi: 10.33002/nr2581.6853.03022

GoN/MoFE (2021). *Third National Communication to the United Nations*. Kathmandu: Ministry of Forest and Soil Conservation (MFSC).

Grimm, R., Behrens, T., Märker, M., and Elsenbeer, H. (2008). Soil organic carbon concentrations and stocks on Barro Colorado Island — Digital soil mapping using Random Forests analysis. *Geoderma* 146, 102–113. doi: 10.1016/j.geoderma.2008.05.008

Hanawalt, R. B., and Wittaker, R. H. (1976). Altitudinally coordinated patterns of soils and vegetation in the San Jacinto Mountains, California. *Soil Sci.* 121, 114–124. doi: 10.1097/00010694-197602000-00007

Heisler, J. L., and Weltzin, J. F. (2006). Variability matters: Towards a perspective on the influence of precipitation on terrestrial ecosystems. *N. Phytol.* 172, 189–192. doi: 10.1111/j.1469-8137.2006.01876.x

Hengl, T., Heuvelink, G. B. M., Kempen, B., Leenaars, J. G. B., Walsh, M. G., Shepherd, K. D., et al. (2015). Mapping soil properties of Africa at 250 m resolution: Random forests significantly improve current predictions. *PLoS One* 10:e0125814. doi: 10.1371/journal.pone.0125814

HMGN/MFSC (2002). *Nepal biodiversity strategy*. Kathmandu: Ministry of Forests and Soil Conservation.

Hofhansl, F., Chacón-Madrigal, E., Fuchslueger, L., Jenking, D., Morera-Beita, A., Plutzar, C., et al. (2020). Climatic and edaphic controls over tropical forest diversity and vegetation carbon storage. *Sci. Rep.* 10:5066. doi: 10.1038/s41598-020-61868-5

Hounkpatin, O. K. L., Op, de Hipt, F., Bossa, A. Y., Welp, G., and Amelung, W. (2018). Soil organic carbon stocks and their determining factors in the Dano catchment (Southwest Burkina Faso). *Catena* 166, 298–309. doi: 10.1016/j.catena.2018.04.013

Hubau, W., Lewis, S. L., Phillips, O. L., Affum-Baffoe, K., Beeckman, H., Cuní-Sanchez, A., et al. (2020). Asynchronous carbon sink saturation in African and Amazonian tropical forests. *Nature* 579, 80–87. doi: 10.1038/s41586-020-2035-0

IPCC (2006). *2006 IPCC Guidelines for National Greenhouse Gas Inventories*. Geneva: IPCC.

IPCC (2021). *Climate Change 2021: The physical science basis – Summary for the Policymakers (Working Group I)*. Geneva: IPCC.

IPCC (2023). *AR6 Sythesis report: Climate change 2023*. Geneva: IPCC.

Jakšić, S., Ninkov, J., Milić, S., Vasin, J., Živanov, M., Jakšić, D., et al. (2021). Influence of slope gradient and aspect on soil organic carbon content in the region of Niš, Serbia. *Sustainability* 13:8332. doi: 10.3390/su13158332

Jin, Z., Shang, J., Zhu, Q., Ling, C., Xie, W., and Qiang, B. (2020). " RFRSF: Employee Turnover Prediction Based on Random Forests and Survival Analysis," in *Proceedings of the Lecture Notes in Computer Science (Including Subseries Lecture Notes in Artificial Intelligence and Lecture Notes in Bioinformatics)*, Amsterdam.

John, K., Isong, I. A., Kebonye, N. M., Ayito, E. O., Agyeman, P. C., and Afu, S. M. (2020). Using machine learning algorithms to estimate soil organic carbon variability with environmental variables and soil nutrient indicators in an alluvial soil. *Land* 9, 1–20. doi: 10.3390/land9120487

Kandel, P. (2013). Monitoring above-ground forest biomass: A comparison of cost and accuracy between LiDAR assisted multisource programme and field-based forest resource assessment in Nepal. *Banko Janakari* 23, 12–22. doi: 10.3126/banko.v23i1.9463

Kara, Ö, Bolat, I., Çakiroğlu, K., and Öztürk, M. (2008). Plant canopy effects on litter accumulation and soil microbial biomass in two temperate forests. *Biol. Fertil. Soils* 45, 193–198. doi: 10.1007/s00374-008-0327-x

Karki, R., Hasson, S., Schickhoff, U., Scholten, T., and Böhner, J. (2017). Rising precipitation extremes across Nepal. *Climate* 5:10004. doi: 10.3390/cli5010004

Khan, A. M., Li, Q., Saqib, Z., Khan, N., Habib, T., Khalid, N., et al. (2022). MaxEnt modelling and impact of climate change on habitat suitability variations of economically important Chilgoza Pine (Pinus gerardiana Wall.) in South Asia. *Forests* 13, 1–23. doi: 10.3390/f13050715

Kirschbaum, M. U. F. (2000). Will changes in soil organic carbon act as a positive or negative feedback on global warming? *Biogeochemistry* 48, 21–51. doi: 10.1023/A: 1006238902976

Köhl, M., Lister, A., Scott, C. T., Baldauf, T., and Plugge, D. (2011). Implications of sampling design and sample size for national carbon accounting systems. *Carbon Bal. Manage.* 6, 1–20. doi: 10.1186/1750-0680-6-10

Kuhn, M. (2008). Building predictive models in R using the caret package. *J. Stat. Softw.* 28, 1–26. doi: 10.18637/jss.v028.i05

Kumar, M., Kumar, A., Thakur, T. K., Sahoo, U. K., Kumar, R., Konsam, B., et al. (2022). Soil organic carbon estimation along an altitudinal gradient of Chir-pine forests of Garhwal Himalaya, India: A Field Inventory to Remote Sensing Approach. *Land Degrad. Dev.* 33, 3387–3400. doi: 10.1002/ldr.4393

Larjavaara, M., Lu, X., Chen, X., and Vastaranta, M. (2021). Impact of rising temperatures on the biomass of humid old-growth forests of the world. *Carbon Bal. Manage.* 16, 1–9. doi: 10.1186/s13021-021-00194-3

Latty, E. F., Canham, C. D., and Marks, P. L. (2004). The effects of land-use history on soil properties and nutrient dynamics in northern hardwood forests of the Adirondack Mountains. *Ecosystems* 7, 193–207. doi: 10.1007/s10021-003-0157-5

Lee, S., Lee, S., Shin, J., Yim, J., and Kang, J. (2020). Assessing the carbon storage of soil and litter from national forest inventory data in South Korea. *Forests* 11, 1–15. doi: 10.3390/f11121318

Lewis, S. L., Sonké, B., Sunderland, T., Begne, S. K., Lopez-Gonzalez, G., van der Heijden, G. M. F., et al. (2013). Above-ground biomass and structure of 260 African tropical forests. *Philos. Trans. R. Soc. B: Biol. Sci.* 368:295. doi: 10.1098/rstb.2012.0295

Li, C., Li, Y., and Li, M. (2019). Improving forest aboveground biomass (AGB) estimation by incorporating crown density and using Landsat 8 OLI images of a subtropical forest in western Hunan in central China. *Forests* 10:104. doi: 10.3390/f10020104

Li, Y., Li, M., Li, C., and Liu, Z. (2020). Forest aboveground biomass estimation using Landsat 8 and Sentinel-1A data with machine learning algorithms. *Sci. Rep.* 10, 1–12. doi: 10.1038/s41598-020-67024-3

Li, Y., Li, M., and Wang, Y. (2022). Forest aboveground biomass estimation and response to climate change based on remote sensing data. *Sustainability* 14:14222. doi: 10.3390/su142114222

Li, Z., Bi, S., Hao, S., and Cui, Y. (2022). Aboveground biomass estimation in forests with random forest and Monte Carlo-based uncertainty analysis. *Ecol. Indic.* 142:109246. doi: 10.1016/j.ecolind.2022.109246

Liu, W., Zhu, M., Li, Y., Zhang, J., Yang, L., and Zhang, C. (2021). Assessing soil organic carbon stock dynamics under future climate change scenarios in the middle Qilian mountains. *Forests* 12:1698. doi: 10.3390/f12121698

Liu, Y., Li, S., Sun, X., and Yu, X. (2016). Variations of forest soil organic carbon and its influencing factors in east China. *Ann. For. Sci.* 73, 501–511. doi: 10.1007/s13595-016-0543-8

López-Serrano, P. M., Corral-Rivas, J. J., Díaz-Varela, R. A., Álvarez-González, J. G., and López-Sánchez, C. A. (2016). Evaluation of radiometric and atmospheric correction algorithms for aboveground forest biomass estimation using landsat 5 TM data. *Remote Sens.* 8:369. doi: 10.3390/rs8050369

López-Serrano, P. M., Domínguez, J. L. C., Corral-Rivas, J. J., Jiménez, E., López-Sánchez, C. A., and Vega-Nieva, D. J. (2020). Modeling of aboveground biomass with landsat 8 oli and machine learning in temperate forests. *Forests* 11, 1–18. doi: 10.3390/f11010011

LRMP (1986). *Summary report: Land resources mapping project*. Nepal: HMGN and Kenting Earth Sciences.

Lu, D., Chen, Q., Wang, G., Liu, L., Li, G., and Moran, E. (2016). A survey of remote sensing-based aboveground biomass estimation methods in forest ecosystems. *Int. J. Digit. Earth* 9, 63–105. doi: 10.1080/17538947.2014.990526

Malla, R., Neupane, P. R., and Köhl, M. (2022). Modelling soil organic carbon as a function of topography and stand variables. *Forests* 13:1391. doi: 10.3390/f13091391

Mehta, D. V. K., Sullivan, P. J., Walter, M. T., Krishnaswamy, J., and DeGloria, S. D. (2008). Impacts of disturbance on soil properties in a dry tropical forest in Southern India. *Ecohydrology* 1, 161–175. doi: 10.1002/eco.15

Mehta, N., Pandya, N. R., Thomas, V. O., and Krishnayya, N. S. R. (2014). Impact of rainfall gradient on aboveground biomass and soil organic carbon dynamics of forest covers in Gujarat, India. *Ecol. Res.* 29, 1053–1063. doi: 10.1007/s11284-014-1192-8

Mohammad, S., and Rasel, M. (2013). Effect of elevation and above ground biomass (AGB) on Soil Organic Carbon (SOC): A remote sensing based approach in Chitwan District, Nepal. *Int. J. Sci. Eng. Res.* 4, 1546–1553.

Mohd Zaki, N. A., Abd Latif, Z., Suratman, M. N., and Zainal, M. Z. (2016). Aboveground biomass and carbon stocks modelling using non-linear regression model. *IOP Conf. Ser. Earth Environ. Sci.* 37:12030. doi: 10.1088/1755-1315/37/1/012030

Moreno, G., Obrador, J. J., and García, A. (2007). Impact of evergreen oaks on soil fertility and crop production in intercropped dehesas. *Agric. Ecosyst. Environ.* 119, 270–280. doi: 10.1016/j.agee.2006.07.013

Musthafa, M., and Singh, G. (2022). Improving forest above-ground biomass retrieval using multi-Sensor L- and C- Band SAR data and multi-temporal spaceborne LiDAR Data. *Front. For. Glob. Change* 5:822704. doi: 10.3389/ffgc.2022.822704

Nguyen, T. D., and Kappas, M. (2020). Estimating the aboveground biomass of an evergreen broadleaf forest in Xuan Lien Nature Reserve, Thanh Hoa, Vietnam, using SPOT-6 data and the random forest algorithm. *Int. J. For. Res.* 2020:13. doi: 10.1155/2020/4216160

NOAA (2023). *NOAA National Centers for Environmental information, Climate at a Glance: Global Time Series, published March 2023*. Washington, DC: NOAA.

Noguchi, M., Hoshizaki, K., Matsushita, M., Sugiura, D., Yagihashi, T., Saitoh, T., et al. (2022). Aboveground biomass increments over 26 years (1993–2019) in an old-growth cool-temperate forest in northern Japan. *J. Plant Res.* 135, 69–79. doi: 10.1007/s10265-021-01358-5

Odebiri, O., Mutanga, O., Odindi, J., Peerbhay, K., Dovey, S., and Ismail, R. (2020). Estimating soil organic carbon stocks under commercial forestry using topo-climate variables in KwaZulu-Natal, South Africa. *S. Afr. J. Sci.* 116, 2–9. doi: 10.17159/sajs.2020/6339

Pahlavan Rad, M. R., Toomanian, N., Khormali, F., Brungard, C. W., Komaki, C. B., and Bogaert, P. (2014). Updating soil survey maps using random forest and conditioned Latin hypercube sampling in the loess derived soils of northern Iran. *Geoderma* 234, 97–106. doi: 10.1016/j.geoderma.2014.04.036

Pokhre, S. (2018). Assessment of above ground biomass and fire risk zonation in selected forest areas of Ludhikhola watershed, Gorkha Nepal. *Remote Sens. Land* 2, 47–64. doi: 10.21523/gcj1.18020104

Poudel, B. C., Sathre, R., Gustavsson, L., Bergh, J., Lundström, A., and Hyvönen, R. (2011). Effects of climate change on biomass production and substitution in north-central Sweden. *Biomass Bioenergy* 35, 4340–4355. doi: 10.1016/j.biombioe.2011.08.005

Powell, S. L., Cohen, W. B., Healey, S. P., Kennedy, R. E., Moisen, G. G., Pierce, K. B., et al. (2010). Quantification of live aboveground forest biomass dynamics with Landsat time-series and field inventory data: A comparison of empirical modeling approaches. *Remote Sensing Environ.* 114, 1053–1068. doi: 10.1016/j.rse.2009.12.018

Rajput, B. S., Bhardwaj, D. R., and Pala, N. A. (2017). Factors influencing biomass and carbon storage potential of different land use systems along an elevational gradient in temperate northwestern Himalaya. *Agrofor. Syst.* 91, 479–486. doi: 10.1007/s10457-016-9948-5

Requena Suarez, D., Rozendaal, D. M. A., De Sy, V., Gibbs, D. A., Harris, N. L., Sexton, J. O., et al. (2021). Variation in aboveground biomass in forests and woodlands in Tanzania along gradients in environmental conditions and human use. *Environ. Res. Lett.* 16, abe960. doi: 10.1088/1748-9326/abe960

Reyna-Bowen, L., Lasota, J., Vera-Montenegro, L., Vera-Montenegro, B., and Błońska, E. (2019). Distribution and factors influencing organic carbon stock in mountain soils in Babia Góra National Park, Poland. *Appl. Sci.* 9:1253. doi: 10.3390/app9153070

Saeed, S., Yujun, S., Beckline, M., Chen, L., Zhang, B., Ahmad, A., et al. (2019). Forest edge effect on biomass carbon along altitudinal gradients in Chinese Fir (*Cunninghamia lanceolata*): A study from Southeastern China. *Carbon Manage.* 10, 11–22. doi: 10.1080/17583004.2018.1537517

Saimun, M. S. R., Karim, M. R., Sultana, F., and Arfin-Khan, M. A. S. (2021). Multiple drivers of tree and soil carbon stock in the tropical forest ecosystems of Bangladesh. *Trees For. People* 5:100108. doi: 10.1016/j.tfp.2021.100108

Schadauer, K., and Gabler, K. (2007). Some approaches and designs of sample-based National Forest Inventories. *Austrian J. For. Sci.* 124, 105–133.

Shapkota, J., and Kafle, G. (2021). Variation in soil organic carbon under different forest types in Shivapuri Nagarjun National Park, Nepal. *Scientifica* 2021:1382687. doi: 10.1155/2021/1382687

Sharma, E. R., and Pukkala, T. (1990a). *Volume equations and biomass prediction of forest trees in Nepal*. Nepal: Forest Survey and Statistics Division.

Sharma, E. R., and Pukkala, T. (1990b). *Volume tables for forest trees of Nepal*. Nepal: Forest Survey and Statistics Division.

Shen, A., Wu, C., Jiang, B., Deng, J., Yuan, W., Wang, K., et al. (2018). Spatiotemporal variations of aboveground biomass under different terrain conditions. *Forests* 9:778. doi: 10.3390/f9120778

Shrestha, U. B., Lamsal, P., Ghimire, S. K., Shrestha, B. B., Dhakal, S., Shrestha, S., et al. (2022). Climate change– induced distributional change of medicinal and aromatic plants in the Nepal Himalaya. *Ecol. Evolut.* 12:e9204. doi: 10.1002/ece3. 9204

Song, B., Niu, S., Zhang, Z., Yang, H., Li, L., and Wan, S. (2012). Light and heavy fractions of soil organic matter in response to climate warming and increased precipitation in a temperate steppe. *PLoS One* 7:e33217. doi: 10.1371/journal.pone. 0033217

Song, Y., Liu, C., Song, C., Wang, X., Ma, X., Gao, J., et al. (2021). Linking soil organic carbon mineralization with soil microbial and substrate properties under warming in permafrost peatlands of Northeastern China. *CATENA* 203:105348. doi: 10.1016/j.catena.2021.105348

Ståhl, G., Saarela, S., Schnell, S., Holm, S., Breidenbach, J., Healey, S. P., et al. (2016). Use of models in large-area forest surveys: Comparing model-assisted, model-based and hybrid estimation. *For. Ecosyst.* 3:5. doi: 10.1186/s40663-016-0064-9

Stainton, J. D. A. (1972). *Forests of Nepal. In Taxon*. London: John Murray, doi: 10.2307/1218063

Sun, X., Tang, Z., Ryan, M. G., You, Y., and Sun, O. J. (2019). Changes in soil organic carbon contents and fractionations of forests along a climatic gradient in China. *For. Ecosyst.* 6, 1–12. doi: 10.1186/s40663-019-0161-7

Tian, X., Li, Z., Su, Z., Chen, E., van der Tol, C., Li, X., et al. (2014). Estimating montane forest above-ground biomass in the upper reaches of the Heihe River Basin using Landsat-TM data. *Int. J. Remote Sensing* 35, 7339–7362. doi: 10.1080/01431161. 2014.967888

UNDESA and UNFFS. (2021). *The Global Forest Goals Report*. New York City, NY: United Nations Department of Economic and Social Affairs.

Vaganov, E. A., Hughes, M. K., Kirdyanov, A. V., Schweingruber, F. H., and Silkin, P. P. (1999). Influence of snowfall and melt timing on tree growth in subarctic Eurasia. *Nature* 400, 149–151. doi: 10.1038/22087

Van der Laan, C., Verweij, P. A., Quiñones, M. J., and Faaij, A. P. C. (2014). Analysis of biophysical and anthropogenic variables and their relation to the regional spatial variation of aboveground biomass illustrated for North and East Kalimantan, Borneo. *Carbon Bal. Manage.* 9:8. doi: 10.1186/s13021-014-0008-z

Vicharnakorn, P., Shrestha, R. P., Nagai, M., Salam, A. P., and Kiratiprayoon, S. (2014). Carbon stock assessment using remote sensing and forest inventory data in Savannakhet, Lao PDR. *Remote Sens.* 6, 5452–5479. doi: 10.3390/rs6065452

Vorster, A. G., Evangelista, P. H., Stovall, A. E. L., and Ex, S. (2020). Variability and uncertainty in forest biomass estimates from the tree to landscape scale: The role of allometric equations. *Carbon Bal. Manage.* 15, 1–20. doi: 10.1186/s13021-020-00143-6

Wai, P., Su, H., and Li, M. (2022). Estimating aboveground biomass of two different forest types in Myanmar from sentinel-2 data with machine learning and geostatistical algorithms. *Remote Sens.* 14:2146. doi: 10.3390/rs14092146

Walkley, A., and Black, I. A. (1934). An examination of the degtjareff method for determining soil organic matter, and a proposed modification of the chromic acid titration method. *Soil Sci.* 37, 29–38. doi: 10.1097/00010694-193401000-00003

Wang, W. J., He, H. S., Thompson, F. R., Fraser, J. S., and Dijak, W. D. (2017). Changes in forest biomass and tree species distribution under climate change in the northeastern United States. *Landsc. Ecol.* 32, 1399–1413. doi: 10.1007/s10980-016-0429-z

Wang, W. J., Thompson, F. R., He, H. S., Fraser, J. S., Dijak, W. D., and Jones-Farrand, T. (2019). Climate change and tree harvest interact to affect future tree species distribution changes. *J. Ecol.* 107, 1901–1917. doi: 10.1111/1365-2745.13144

Way, D. A., and Oren, R. (2010). Differential responses to changes in growth temperature between trees from different functional groups and biomes: A review and synthesis of data. *Tree Physiol.* 30, 669–688. doi: 10.1093/treephys/tpq015

Xie, X., Wu, T., Zhu, M., Jiang, G., Xu, Y., Wang, X., et al. (2021). Comparison of random forest and multiple linear regression models for estimation of soil extracellular enzyme activities in agricultural reclaimed coastal saline land. *Ecol. Indic.* 120:106925. doi: 10.1016/j.ecolind.2020.106925

Yan, F., Wu, B., and Wang, Y. (2015). Estimating spatiotemporal patterns of aboveground biomass using Landsat TM and MODIS images in the Mu Us Sandy Land, China. *Agric. For. Meteorol.* 200, 119–128. doi: 10.1016/j.agrformet.2014.09.010

Zhang, H., Song, T., Wang, K., Yang, H., Yue, Y., Zeng, Z., et al. (2016). Influences of stand characteristics and environmental factors on forest biomass and root–shoot allocation in southwest China. *Ecol. Engineer.* 91, 7–15. doi: 10.1016/j.ecoleng.2016.01. 040

Zhang, Y., Ai, J., Sun, Q., Li, Z., Hou, L., Song, L., et al. (2021). Soil organic carbon and total nitrogen stocks as affected by vegetation types and altitude across the mountainous regions in the Yunnan Province, south-western China. *Catena* 196:104872. doi: 10.1016/j.catena.2020.104872

Zhao, F., Wu, Y., Hui, J., Sivakumar, B., Meng, X., and Liu, S. (2021). Projected soil organic carbon loss in response to climate warming and soil water content in a loess watershed. *Carbon Bal. Manage.* 16:24. doi: 10.1186/s13021-021-00187-2

Zhu, M., Feng, Q., Qin, Y., Cao, J., Li, H., and Zhao, Y. (2017). Soil organic carbon as functions of slope aspects and soil depths in a semiarid alpine region of Northwest China. *Catena* 152, 94–102. doi: 10.1016/j.catena.2017.01.011

Zhu, Y., Feng, Z., Lu, J., and Liu, J. (2020). Estimation of forest biomass in Beijing (China) using multisource remote sensing and forest inventory data. *Forests* 11, 1–17. doi: 10.3390/f11020163

Zinn, Y. L., Andrade, A. B., Araujo, M. A., and Lal, R. (2018). Soil organic carbon retention more affected by altitude than texture in a forested mountain range in Brazil. *Soil Res.* 56, 284–295. doi: 10.1071/SR17205

ANNEX

ANNEX 1 Parameters a, b, and c of the volume equation i.e.,
$\ln(v) = a + b*\ln(d) + c*\ln(h)$.

Species	a	b	c
Abies pindrow	−2.4453	1.7220	1.0757
Acacia catechu	−2.3256	1.6476	1.0552
Adina cordifolia	−2.5626	1.8598	0.8783
Albizia spp.	−2.4284	1.7609	0.9662
Alnus nepalensis	−2.7761	1.9006	0.9428
Anogeissus latifolia	−2.2720	1.7499	0.9174
Bombax malabaricum	−2.3865	1.7414	1.0063
Cedrela toona	−2.1832	1.8679	0.7569
Dalbergia sisso	−2.1959	1.6567	0.9899
Eugenia jambolana	−2.5693	1.8816	0.8498
Hymenodictyon excelsum	−2.5850	1.9437	0.7902
Lagerstroemia parviflora	−2.3411	1.7246	0.9702
Michelia champaca	−2.0152	1.8555	0.7630
Pinus roxburghii	−2.9770	1.9235	1.0019
Pinus wallichiana	−2.8195	1.7250	1.1623
Quercus spp.	−2.3600	1.9680	0.7469
Schima wallichii	−2.7385	1.8155	1.0072
Shorea robusta	−2.4554	1.9026	0.8352
Terminalia tomentosa	−2.4616	1.8497	0.8800
Trewia nudiflora	−2.4585	1.8043	0.9220
Tsuga spp.	−2.5293	1.7815	1.0369
Miscellaneous in Terai	−2.3993	1.7836	0.9546
Miscellaneous in Hills	−2.3204	1.8507	0.8223

Vulnerability of northern rocky mountain forests under future drought, fire, and harvest

Jeffrey E. Stenzel[1]*, Crystal A. Kolden[1], Polly C. Buotte[2],
Kristina J. Bartowitz[3,4], Eric W. Walsh[5] and Tara W. Hudiburg[4]

[1]Management of Complex Systems, University of California Merced, Merced, CA, United States, [2]Energy and Resources Group, University of California, Berkeley, Berkeley, CA, United States, [3]American Forests, Washington, DC, United States, [4]Department of Forest, Rangeland, and Fire Sciences, University of Idaho, Moscow, ID, United States, [5]Manomet, Plymouth, MA, United States

Novel climate and disturbance regimes in the 21st century threaten to increase the vulnerability of some western U.S. forests to loss of biomass and function. However, the timing and magnitude of forest vulnerabilities are uncertain and will be highly variable across the complex biophysical landscape of the region. Assessing future forest trajectories and potential management impacts under novel conditions requires place-specific and mechanistic model projections. Stakeholders in the high-carbon density forests of the northern U.S. Rocky Mountains (NRM) currently seek to understand and mitigate climate risks to these diverse conifer forests, which experienced profound 20th century disturbance from the 1910 "Big Burn" and timber harvest. Present forest management plan revisions consider approaches including increases in timber harvest that are intended to shift species compositions and increase forest stress tolerance. We utilize CLM-FATES, a dynamic vegetation model (DVM) coupled to an Earth Systems Model (ESM), to model shifting NRM forest carbon stocks and cover, production, and disturbance through 2100 under unprecedented climate and management. Across all 21st century scenarios, domain forest C-stocks and canopy cover face decline after 2090 due to the interaction of intermittent drought and fire mortality with declining Net Primary Production (NPP) and post-disturbance recovery. However, mid-century increases in forest vulnerability to fire and drought impacts are not consistently projected across climate models due to increases in precipitation that buffer warming impacts. Under all climate scenarios, increased harvest regimes diminish forest carbon stocks and increase period mortality over business-as-usual, despite some late-century reductions in forest stress. Results indicate that existing forest carbon stocks and functions are moderately persistent and that increased near-term removals may be mistimed for effectively increasing resilience.

KEYWORDS

forest, climate change, modeling, vulnerability, drought, fire, management, carbon

Introduction

Temperate conifer forests are among the most carbon-dense forests globally (Hudiburg et al., 2009, 2019; Thurner et al., 2014; Smith et al., 2019) and are responsible for most of the western North American carbon sink (Schimel et al., 2002). Drought and fire are endemic across much of this region. However, the magnitude of these disturbances has increased in recent decades (Zhao and Running, 2010; Schwalm et al., 2012; Abatzoglou and Williams, 2016; Buotte et al., 2019) due to increased soil and atmospheric aridity, historic harvest impacts, excessive fuels from fire suppression, and human ignitions (Higuera and Abatzoglou, 2021). These shifts have increased the vulnerability of landscape carbon sinks and myriad ecosystem services (Walsh and Hudiburg, 2021). Forest vulnerability to changing drought and wildfire regimes varies among trees, species, and populations (VanderWeide and Hartnett, 2011; Lutz et al., 2012; Evans et al., 2016) due to the interaction between legacies from past disturbance (Hudiburg et al., 2017; Bartowitz et al., 2019) and hotter and drier growing seasons (Allen et al., 2010).

Increasing natural and anthropogenic disturbance in regions of productive, high carbon density forests (Law et al., 2018) has accelerated the need for improved understanding of western U.S. landscape trajectories in the 21st century (Case et al., 2021). Evaluating potential outcomes, however, requires quantifying ecological metrics at appropriate spatiotemporal scales and quantifying trade-offs between management approaches (Hudiburg et al., 2019). Much recent forest management literature emphasizes the need for species composition shifts and density reductions through active management such as harvest and prescribed fire to create more resilient forests (Prichard et al., 2021). Whether or not such actions will successfully decrease forest vulnerability while minimizing carbon losses at landscape scales and across the complex subregions of the western U.S. remains largely untested (Bartowitz et al., 2022). Given the long-term observations needed to empirically confirm the consequences of intertwined novel climate, disturbance, and forest management strategies (Nagy et al., 2021; Muthukrishnan et al., 2022), robust, process-based methods are presently needed to quantify and assess these complex potential outcomes across landscapes and through time (Anderegg et al., 2022). Due to the rapidly changing environmental conditions governing forest growth, mortality, and carbon balance, mechanistic models that explicitly represent forest processes (i.e., photosynthesis, hydraulic limitation, carbon allocation, changes to water use efficiency, prognostic fire events, forest structure, etc.) must be utilized to better predict potential trajectories of forest vulnerability and resulting carbon fluxes of proposed management plans.

Much previous regional-scale forest modeling has utilized two broad categories of models, each with limitations in projecting vegetation responses to novel conditions. First, the land components of earth systems models (ESMs) have represented mechanistic biophysics and biogeochemistry at soil-plant-atmosphere surfaces (Bonan, 2008, 2019), but have historically represented site vegetation via aggregated pools and fluxes of mass (e.g., Hudiburg et al., 2013). Previous studies using ESMs at the scale of western U.S. forests have derived forest vulnerability indicators from model outputs such as site carbon

fluxes (e.g., NPP; Buotte et al., 2019), yet their lack of modeled individual mortality and canopy gap formation has meant that key structural feedbacks (e.g., functional gaps, demographics) to projection outcomes were absent. Second, vegetation demographic models (VDMs) have represented structural and compositional shifts of individuals, cohorts, and successional patches across grid cells via mortality and growth (Scheiter et al., 2013). VDMs can lack the spatial scale and biogeophysical dynamics of ESMs, while employing simple empirical representations of essential plant processes (Hanbury-Brown et al., 2022). More recently, coupling of VDMs with ESMs has enabled progress towards regional modeling experiments that fuse mechanistic surface exchanges with ecosystem demographic resolution (Fisher et al., 2018; Fisher and Koven, 2020). These coupled models can enable essential sub-grid cell vegetation heterogeneity via cohorts of trees across variably disturbed patches within the land models of ESMs.

The U.S. Northern Rocky Mountain (NRM) ecoregion (Omernik and Griffith, 2014) represents a important, sparsely studied and carbon dense forested domain (Walsh and Hudiburg, 2021) on which to test advances in coupled forest-disturbance modeling is the western U.S. The NRM contains over 100,000 km^2 of predominantly conifer forests in northern Idaho, Montana, and Washington that have experienced profound 20th and 21st century changes to composition and structure from harvest, insects, pathogens, wildfire, and fire suppression (Bollenbacher et al., 2014; Ramsfield et al., 2016). The NRM was notably the primary region of the 1910 "Big Burn," in which over 1.2 million hectares of wildland burned (Koch, 1942, 1978; Bartowitz et al., 2022). The 1910 fires shaped both NRM forest structure as well as the subsequent fire suppression policies of the nascent United States Forest Service (USFS), which contributed to large reductions in regional burned area by the latter portion of the 20th century (Arno et al., 2000; Gibson and Morgan, 2005; Walsh and Hudiburg, 2021). NRM forests are also imprinted with the legacy of 20th century timber harvest, which ultimately increased tree density and homogenized forest composition with early 20th century selective harvest (i.e., "high grading") followed by even aged, regeneration harvest methods (e.g., clear cutting) (USDA, 2015, 2019).

Critically, much of the present-day NRM region has been identified as a high priority for carbon storage reserves due to higher carbon density than drier regions of the western U.S. and moderate vulnerability to drought and fire mortality (Buotte et al., 2020; Law et al., 2022). However, a warming climate, increased wildfire activity (Parks and Abatzoglou, 2020), and lack of species tolerant to fire, drought, and pathogens relative to the past (Evangelista et al., 2011; Stevens-Rumann et al., 2017; Turner et al., 2019), have led to concern regarding regional 21st century forest vulnerability and continued ability to provide ecosystem services, including the ability of forests to sequester and store carbon (Henne et al., 2021; Walsh and Hudiburg, 2021). In this context, recent national forest land management plan revisions and draft revisions within the NRM aim to reduce forest vulnerability via changes to species composition and density, in part via increased even-aged timber harvests (i.e., harvests that remove the majority of overstory trees) (USDA, 2015, 2019). Increased harvests are incorporated into plans to reduce forest density and sharply increase the prevalence of planted fire, drought, or pathogen-tolerant species (e.g., ponderosa pine, western white pine, and western larch over Douglas fir and mesic mixed conifers). Notably, the draft plan revision for the

Nez-Perce Clearwater National Forest presents multiple alternative scenarios in which sharp increases in even-aged harvest (i.e., up to 3–4 × 2010–2020 timber harvest volumes) are utilized to alter forest composition on the scale of 100,000–300,000 acres per decade (USDA, 2019). In combination, the significant impacts to NRM forest ecosystems from novel climate, natural disturbances, and human disturbances drive a need for the study of potential 21st century landscape function and vulnerability.

Here, we demonstrate a novel approach to modeling 21st century NRM forest vulnerability to loss of biomass and function resulting from climate change and disturbance using CLM-FATES (the Community Land Model with the Functionally Assembled Terrestrial Ecosystem Simulator; Fisher et al., 2015; Lawrence et al., 2018), a cohort-based VDM (FATES) coupled to an ESM (CLM). We employ CLM-FATES due to the model's prognostic mortality mechanisms (fire, carbon starvation, hydraulic failure, and freezing); due to its representation of cohorts of trees with crown spatiality and mass allocated to cohorts with distinct individual counts, species, and organ sizes; and due to its sub-grid cell patches that represent areas of distinct disturbance, functional gaps, and recovery. In this study, modeled NRM forest trajectories from 2025–2100 are assessed via forest mortality, growth, canopy cover, carbon stocks, and carbon fluxes under changing climate, fire, and management. We examine outcomes under both business-as-usual (BAU) scenarios and increased harvest scenarios based on current U.S. national forest management plans in the NRM region. Modified management scenarios include increased regeneration harvest rates that are intended to reduce forest vulnerability to disturbance via prescribed shifts in forest structure and composition. We ask:

1. Does climate change diminish landscape carbon stocks and forest cover in the NRM through 2100?
2. How do changing climate and disturbance impact ecosystem stress, production, and mortality across forest types?
3. Do prescribed composition shifts via increased regeneration harvest (active management) effectively reduce landscape vulnerability to climate change?

Materials and methods

Modeling framework

Simulations were performed with the Functionally Assembled Terrestrial Ecosystem Simulator (FATES; Fisher et al., 2015) coupled with the Community Land Model 5.0 (CLM; Lawrence et al., 2018) of the Community Earth Systems Model (CESM). With this configuration, FATES modifies CLM vegetation surface representation to include vegetation demographics via cohorts of trees occupying patches defined by disturbance history. CLM represents land surface biogeophysics, biogeochemistry, and human land impacts across gridded domains. FATES has been tested and evaluated for sensitivities, parameterization strategies, and predominantly site-scale analyses (Koven et al., 2019; Lawrence et al., 2019; Huang et al., 2020; FATES Development Team, 2022; Lambert et al., 2022).

Functionally Assembled Terrestrial Ecosystem Simulator cohorts represent groups of trees defined by common size, canopy position, and plant functional type (PFT). Cohort processes include photosynthesis, respiration, transpiration, recruitment, growth, reproduction, and mortality driven by climate, light, soil moisture, and disturbance. Cohorts occupy patches within each site that are generated by disturbances. PFTs are defined by common sets of functional traits that correspond to physiology and structure. Surface processes are calculated at a half-hourly time step and include soil-leaf-atmosphere exchanges (e.g., mass and energy fluxes; photosynthesis, respiration, transpiration). Daily time-step processes include recruitment, growth, disturbance, turnover to surface and soil pools, and cohort/patch fusion/fission. Within patches, cohorts compete for light via vertical canopy position (layer), dependent on tree height and total crown area per patch. Net Primary Production (NPP) is the balance between photosynthesis and autotrophic respiration. Growth is in turn dependent on a NPP allocation scheme in which tissue turnover and carbon stores are first replenished, allometric deficits are diminished, and then, if possible, tissues grow concurrently according to allometric targets. Event-based mortality can result from prescribed harvest and prognostic fire impacts mediated by cohort size, bark thickness, and canopy variables. 'Treefall' mortality includes hydraulic failure, carbon starvation (based on carbon balance), cold stress, and a background mortality rate per PFT. Within FATES, a SPITFIRE-based model (Thonicke et al., 2010) simulates daily patch fire initiation, ignition, spread, intensity, and effects based on lightning strikes (here, spatially variable), patch fuel conditions (mass, size distribution, moisture), fire weather, and cohort characteristics (FATES Development Team, 2022; "FATES SPITFIRE description" in the **Supplementary material**).

We modified FATES to enable several processes that were important in our study scenarios (full description in the **Supplementary material**). Modifications included the following: (1) the addition of regeneration harvest as a management option (e.g., harvest and then planting of selected PFTs) and the addition of parameters controlling combustion fraction of harvest slash; (2) the addition of standing dead (i.e., "snag") pools and treefall fluxes to better reflect post-mortality fuel structure and emissions timing (Edburg et al., 2011; Stenzel et al., 2019); (3) the addition of cohort fine root depth based on tree size and PFT to differentiate soil water access based on tree structural growth and PFT strategy (Law et al., 2003; Irvine et al., 2004, 2008; Law and Berner, 2015); and (4) the inclusion of cold stress mortality thresholds for small trees and the calculation of cold stress from daily minimum temperatures, rather than averages. Modifications 3 and 4 were intended to better generate PFT fundamental niches by representing recruit mortality from extreme conditions.

Terminology

Carbon cycle terms include Gross Primary Production (GPP), Autotrophic (plant) respiration (R_a), Heterotrophic respiration (R_h) and Net Primary Production (NPP = GPP–R_a) (Chapin et al., 2006). The balance of ecosystem production and respiratory fluxes define Net Ecosystem Production (NEP = NPP–R_h). The

Net Ecosystem Carbon Balance (NECB) represents the total site carbon balance, subtracting from NEP any additional horizontal fluxes and vertical non-respiratory fluxes (here, NECB = NEP– fire C emissions–harvest removals). Crown area refers to the ratio of forest canopy cover to ground area. Soil moisture stress, used here in place of the CLM-FATES variable "β-Transpiration," refers to model stress-response scaling (0–1) of stomatal conductance and photosynthesis based on soil water matric potential and plant wilting point (FATES Development Team, 2022). Carbon use efficiency (CUE) is the site ratio of GPP to NPP and reflects the efficiency with which modeled photosynthate from GPP is converted to live biomass pools (vs. plant respiration).

Study domain and forests

Simulations were performed within ∼ 2.5 million hectares of US national forest land in the Northern Rocky Mountain (NRM) ecoregion and the northern portion of the Idaho Batholith ecoregion of Idaho (Figure 1; hereafter referred to simply as NRM; Omernik and Griffith, 2014) through the year 2100. We focus on the Idaho Panhandle (IPNF) and Nez-Perce Clearwater National (NPCNF) forests due to their recently revised or in-revision forest management plans, which seek desired conditions of altered forest composition in the context of changing climate and disturbance.

The study domain (Figure 1) ranges in elevation from ∼450–2,500 m, rising primarily from west to east. The climate of the region is spatially complex; climatic gradients (warm-dry to cold-wet) correspond to strong elevation gradients and latitude, but climate generally consists of relatively dry summers and a maritime influence that leads to high forest productivity compared to drier portions of the Rocky Mountains to the south. The western side of the ecoregion is characterized by a stronger maritime influence, and the domain includes Koppen climate zones Dsb, Dsc, Dfb, and Dfc (Mediterranean-influenced and continental warm-summer and subarctic climates). Much of the domain experiences growing season drought. July, August, and September are typically both the hottest and driest months (Figure 1); during this dry period, precipitation is often less than 10% of the yearly total. Forest soil moisture typically decreases to multi-month minimums by the month of August, while tree sap flow, secondary growth, stomatal conductance, and leaf water potential demonstrate marked downregulation and stress (Baker et al., 2019; Stenzel et al., 2021).

The NRM of Idaho is 88% forested, with the largest portion of forest land administered by the US Forest Service (USFS) (Walsh and Hudiburg, 2019). The pre-20th century forest landscape experienced ∼ 50% mixed fire regimes, with lesser proportions of non-lethal and stand-replacing events, but modern regimes have been altered by combinations of fire suppression, timber harvest, and climate (Arno et al., 2000; Morgan et al., 2008; Naficy et al., 2010). Study plant functional types (PFTs) correspond to forest type distributions from previous CLM studies (Buotte et al., 2019), and include types defined by both single and multiple species. PFTs include ponderosa pine (PP, *Pinus ponderosa*), Douglas fir (DF; *Pseudotsuga menziesii*), mixed mesic fir/cedar/hemlock (MC; Douglas fir; grand fir, *Abies grandis*; western redcedar, *Thuja plicata*;

western hemlock, *Tsuga heterophylla*), lodgepole pine (LP; *Pinus contorta*), and subalpine fir/spruce (SF; *Abies lasiocarpa*, *Picea engelmannii*). Grand fir and Douglas fir represent ∼ 50% of tree mass in the domain (USDA, 2015, 2019; Walsh and Hudiburg, 2021), dominating warm and cool moist sites. Cold site forests are composed of subalpine Spruce/fir and lodgepole pine types.

Historical timber harvest on the two national forests increased rapidly in the mid 20th century, peaked at over 30,000 acres per year by the 1980s, then declined to an average of ∼5,000 acres per year after 2000 (USDA, 2022). In the first half of the century, high-grade harvests often selectively removed large and commercially valuable trees (Gruell, 1982, 1983; Smith and Arno, 1999; Brown et al., 2004; Naficy et al., 2010). Beginning in the 1950s and until the 1980s, even-aged harvest (e.g., clear cuts) increased drastically on USFS lands. Combined with white pine blister rust, regeneration harvest methods served to increase the prevalence of species such as Douglas fir and grand fir, while western white pine (*Pinus monticola)* was nearly eliminated from the landscape (USDA, 2015, 2019).

Historically, large portions of forest within both present-day national forests burned in wildfires, including the >5,000 km^2 "Big Burn" of 1910 (Bartowitz et al., 2022). Modern burned area has been relatively low in the Idaho Panhandle National forest, with < 300 km^2 (<2.5%) total burned area from 1985–2020 (Eidenshink et al., 2007). In the Nez Perce-Clearwater National Forest, ∼ 3600 km^2 (∼ 22%) of forest area has burned during the same period. In the 21st century, harvest has replaced fire as the primary stand-replacing agent in the Idaho panhandle despite annual timber harvest that is an order of magnitude lower than its 20th century maximum (USDA, 2022). To the south, in the Clearwater Basin of north-central Idaho, >20% of forest area was within burned perimeters from 2000–2019 (Finco et al., 2012; Picotte et al., 2020). In both areas, root diseases from fungi (e.g., *Armillaria*, laminated root rot) are estimated to represent the largest source of non-stand replacing turnover and afflict the greatest areas of Douglas and grand fir forests (USDA, 2015, 2019). Beetle mortality has had the greatest effect on lodgepole pine (mountain pine beetle) in the NRM, though mortality rates are generally lower than in Montana, Colorado, and Wyoming (Berner et al., 2017).

The USFS completed a revised forest management plan for a portion of the NRM (Idaho Panhandle National Forest; IPNF) in 2015, while a second plan for the Nez Perce-Clearwater National Forest (NPCNF) is currently in draft form (USDA, 2015, 2019). Both plans stress that regional forests deviate from historical and desired structure and composition. Revision plan desired conditions aim to increase forest resilience to climate change, including direct (fire, drought) and indirect (susceptibility to insects, pathogens) impacts on tree mortality and growth rates. Desired conditions from the management plans of both national forests include sharp composition shifts, increasing the prevalence of early seral, shade intolerants (e.g., pine species) that can have higher tolerance to fire, drought, windthrow, and/or root disease than more shade-tolerant, mid or late seral mesic forest species.

Desired composition changes include large decreases in Douglas fir and grand fir forest types (USFS definition: USDA, 2019) and increases in ponderosa pine types at warm-dry and warm-moist sites. In the 2019 draft environmental impact
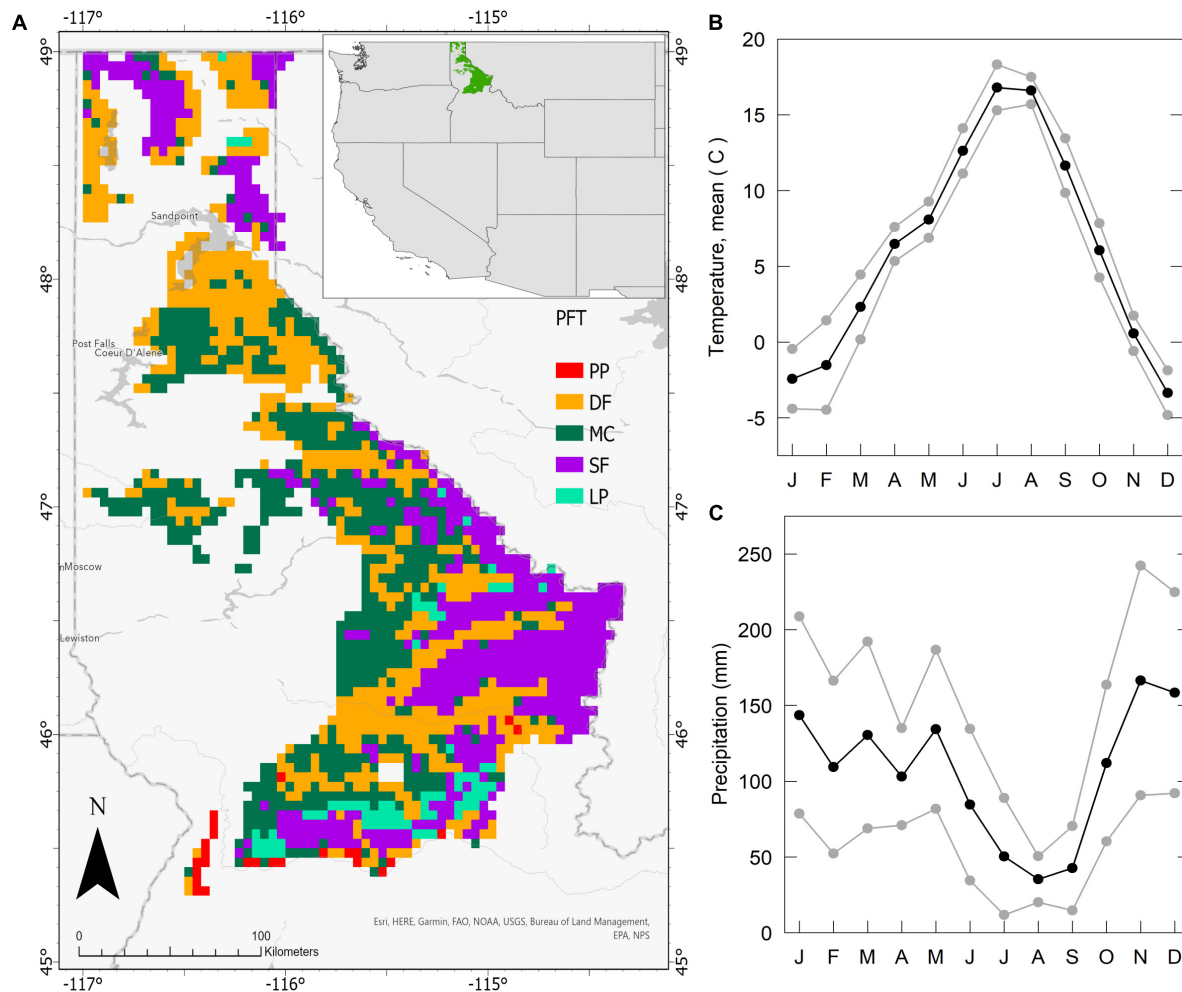
FIGURE 1
Domain location, PFTs, and monthly near-future climate (2025–2035, MIROC climate). **(A)** Domain 4 × 4 km grid cells (*n* = 1,811) and initial Plant Functional Type (PFT) distribution. PFTs include ponderosa pine (PP), Douglas fir (DF), mixed mesic conifer (MC), subalpine fir and Engelmann spruce (SF), and lodgepole pine (LP). The domain is located in the Idaho Panhandle and Nez Perce–Clearwater National Forests of northern Idaho, USA (see inset). **(B)** MIROC5 mean (± sd) monthly temperature (2025–2034) and **(C)** precipitation.

statement for the NPCNF, for instance, desired conditions include 75–90% and 70–85% reductions in Douglas fir and grand fir/western redcedar forest types for warm-moist sites, which support the largest and most productive forests sites in the region (vs. warm-dry and cold). For the same sites, increases in ponderosa pine forest types of 400–900% are desired. Across NPCNF draft plan alternatives, these conditions would be sought in part with timber harvest increases of ∼40–400% across alternative scenarios (up to 55,000 ha yr^{-1}).

Parameterization

PFT trait data

Tree species trait data informing FATES PFT parameter ranges included observations from the tree trait database compiled in Buotte et al. (2021), the TRY Database (Kattge et al., 2020), the NACP TERRA-PNW Forest database (Law and Berner, 2015), and additional literature (see also attached parameter reference file; Hudiburg et al., 2009, 2013; Buotte et al., 2019).

Parameter selection

For each FATES PFT, we generated parameter set ensembles in which key functional traits were varied within observed ranges (Buotte et al., 2021). To further constrain parameter value, PFT competitive strategies were defined (**Supplementary Table 1**) and final parameters across PFTs were constrained by relative differences in strategies. Where PFT-specific observations were not available, parameters were generally held constant between species.

We first generated 72-member parameter set ensembles for each of 3 generic PFTs, corresponding to a range of tree ecological strategies within the study domain (**Supplementary Table 1**). Initial PFTs included: (1) A shade-intolerant, drought-avoidant, fire-resistant PFT (PINE; corresponding to ponderosa pine forest); (2) A more shade-tolerant, less drought-tolerant, less fire-resistant PFT (FIR; corresponding to regional mesic mixed conifer forest); and (3) A cold-tolerant, fire-intolerant PFT with subalpine canopy architecture (SUB; corresponding to subalpine fir/Engelmann spruce forest). We first defined parameters that would not vary in ensembles (e.g., PFT wood density, stem allometry). Next, key PFT

parameters were varied to represent the range of PFT strategies (**Supplementary Table 1**). Fire resistance was determined by bark thickness (*bark*) and canopy height allometry (*canopy_ht*). Shade tolerance was determined by specific leaf area at the top of the canopy (SLA_{top}), maximum specific leaf area (SLA_{max}), maximum rate of carboxylation (V_{cmax}), leaf nitrogen stoichiometry (*Leaf_N*; affects leaf respiration), leaf biomass allometry (*d2bl1*; affects leaf respiration and LAI), and leaf longevity (*leaf_life*; impacts foliage turnover replacement costs and availability of carbon for structural growth under low carbon-supply conditions). Drought avoidance was controlled by the soil matric potential of stomatal closure (*SMPSC*), stomatal slope (*stoma*; affects water use efficiency via regulating stomatal conductance in relation to photosynthesis, soil moisture stress, and VPD), and minimum and maximum fine root depth (*root_min*, *root_max*; also affects the rate of root depth growth). Cold tolerance was determined by the seedling cold temperature threshold (*cold_tol_seedling*). SUB PFT crown area (*d2ca*) was decreased relative to PINE and FIR, though we note that FATES does not include mechanics that make narrow, dense tree crowns advantageous due to snow or wind effects. Each initial ensemble member parameter set was generated through random selection of each parameter within a uniform distribution spanning each parameter's observed range.

Calibration

Iterative 72-member single-PFT ensembles for the initial 3 PFTs were run for 150–400 years each across three core sites. Core sites (single grid cells) were characterized by varying ratios of precipitation to potential evapotranspiration (P: PET) and included DRY, WET, and moderate moisture (MOD) sites. PFT ensembles members were filtered (i.e., selected for or against) according to a series of ecological expectations at each site [based on Buotte et al. (2021); see **Supplementary Table 1** for expectations; **Supplementary Figures 18–22** for example results]. The DRY site (PET > P) filtered PFT capability for drought avoidance/tolerance, including the ability of shallow-rooted recruits to avoid carbon starvation or hydraulic dysfunction, and the ability of mature forest to maintain near-canopy closure in the absence of mass disturbance events. At the MOD site (PET ≈ P), PFTs were filtered based on successful formation of near-closed forest canopies under higher site moisture availability than the DRY site. Yearly hydraulic failure mortality of mature trees was selected against. At the WET site (P < PET) carbon starvation mortality was selected for in shade-intolerant PINE PFT recruits under shade-intolerant (and low LAI) FIR PFT canopies. Partial survival and growth of shade-intolerant FIR recruits under low-LAI PINE canopies was selected for. All PFT ensembles were also calibrated to estimated ranges of local biomass by stand age, and carbon fluxes (GPP, NPP) where relevant monitoring ground-based data existed (Law et al., 2001a,b; Irvine et al., 2004; Sun et al., 2004; Stenzel et al., 2021; **Supplementary Figures 18–22**). To develop the final five domain PFT parameterizations (i.e., non-generic; PP, MC, DF, LP, SF), ensemble members that passed initial ecological filters were varied relative to observed ranges for common component species, maintaining PFT-relative parameter relationships. All parameterizations were again evaluated against C stock and flux filters at each site.

Sub-regional wildfire calibrations proceeded with 72-cell simulations. Six (6) grid cells were randomly selected for each of 12 PFT x climate type combinations. For grid cells of each PFT (n = 5), climate types (2–4 per PFT) were assigned via multivariate cluster analysis (Multivariate Clustering, Arcgis Pro; Scott and Janikas, 2009) with mean annual precipitation, T_{min}, and T_{max} from 1979–2014 historical input climate data (Abatzoglou, 2013; Buotte et al., 2021). Wildfire calibration assessed the sensitivity of FATES SPITFIRE to parameter variation, ultimately focusing on variation to the 'drying ratio' parameter (personal communication P Buotte; Thonicke et al., 2010). Final PFT parameterizations were selected by area burned per forest type for the period of 2001–2020 compared to observation-based burn area (Eidenshink et al., 2007; Finco et al., 2012; Picotte et al., 2020). Parameterizations were additionally selected to be within one standard deviation of FIA-based PFT-average aboveground live tree carbon density (Hudiburg et al., 2019) for the period of 2007–2016 and to maintain the relative order of observed stock densities across forest types.

Regional scenarios

Domain-scale scenarios were run across 1811, 4 × 4 km grid cells (~28,000 km^2 of national forest land) for 600 years each (400-year spin-up, 200-year historical and future from 1900–2099). Six future scenarios (**Table 1**) were run from 2020–2099 and were defined by regionally warmer and cooler RCP 8.5 climate forcings for each of three timber harvest intensities (business-as-usual, moderate harvest increase, high harvest increase; see detailed descriptions below).

Surface datasets defined land variables, including soil texture, color, slope, depth to bedrock, and PFT area distribution (from Lawrence et al., 2018; Buotte et al., 2021). FATES 'fixed biogeography' mode was enabled and a single initial PFT was prescribed per site based on Buotte et al. (2019) dominant gridcell PFTs (by area). Fixed biogeography mode was selected because the aggregated soil water pools within and across patches in CLM FATES limit spatially variable impacts of different soil water use strategies across multiple site PFTs (see discussion section) in the seasonally dry domain. For each scenario, FATES mass stocks and fluxes were spun-up for 400 years under repeated historical climate (1950–1979). This spin-up period length was sufficient for all PFTs to reach equilibrium ecosystem carbon stocks (live and dead tree, soil C), fluxes (NPP, GPP, R_a, R_h) and site dynamics (crown area, mortality, size structure) under a recycled 30 year climate. Domain live tree, litter, and woody debris pools each changed by ≤ 1% across the final 100 years of spin-up. Soil C stocks increased by ~0.1% yr^{-1} by spin-up year 400. Historical and then future periods were simulated with 1950–2099 climate inputs (see climate details below).

Historical harvest fraction by grid cell and year was prescribed via the CLM "land-use timeseries" harvest dataset according to USFS records (**Supplementary Figure 2**; Hurtt et al., 2020; USDA, 2022). Currently, FATES does not allow spatiotemporal variation in selective harvest parameters that interact with CLM harvest areas. We therefore prescribed harvests that removed the overstory ("clearcuts") within dynamic harvest areas, both with and without planting. While this represents a simplification of

TABLE 1 Future regional scenarios.

Name	RCP	Description	CO2	Source	
Climate					
MIROC	8.5	'Cooler'. From MIROC5 GCM. 1/24° (4 km), 3 h.	Constant, yr 2000	Buotte et al., 2019	
IPSL	8.5	'Warmer'. From IPSL-CM5A-MR GCM. 1/24° (4 km), 3 h.	Constant, yr 2000	Buotte et al., 2019	
Name	**Description**	**Area (ac yr^{-1})**	**Distribution**	**Methods**	**Source**
Timber harvest					
BAU	Business-As-Usual	∼ 4,500	2001–2020 grid cell harvest proportions	Regen Harvest, only stands with cohorts > 20 cm DBH	USDA, 2022
AC1	Moderate Harvest Increase	∼ 12,000	2001–2020 grid cell proportions, redistributed if > 100% by 2100	see above	USDA, 2015, USDA, 2019 scenarios "W" and "X"
AC2	High Harvest Increase	∼ 23,000	2001–2020 grid cell proportions, redistributed if > 100% by 2100	see above	USDA, 2015, USDA, 2019 scenarios "W" and "X"

Six 2020–2099 scenarios were simulated from 3 timber harvest intensities under each of 2 climate forcings. Values indicate mean (sd) of 1811 gridcell decadal means, with single years referring to decadal end years (e.g., 2029 for 2020–2029). The dead C pool aggregates aboveground (litter, woody debris, snag) and belowground (fine and course roots) dead biomass. Drought mortality is the sum of hydraulic failure mortality and carbon starvation mortality.

actual harvest prescriptions experienced on the landscape, harvest records (USDA, 2022) indicate that less than 25% of regional harvests from 2001–2020 were selective. Further, while additional even-aged techniques were not represented (e.g., shelterwood, seed tree), many of the regeneration benefits those techniques provide (seeding, protection from plant competition) are realized by seedlings in FATES regardless.

Based on USFS management plans from the Idaho Panhandle and the Nez Perce-Clearwater National forests, future harvest scenarios were generated to represent business-as-usual (BAU; from 2001–2020 harvest averages; ∼ 4,500 acre yr^{-1}), moderately accelerated harvest (AC1 ∼ 12,000 acre yr^{-1}) and highly accelerated harvest (AC2; ∼ 23,000 acre yr^{-1}). AC1 and AC2 primarily reflect variable potential contributions from the NPCNF draft forest plan scenarios "W" and "X," and were calculated from estimated timber harvest production (USDA, 2019). For all harvest scenarios, yearly grid cell harvest area as a proportion of yearly domain harvest followed observed cell harvest proportions from 2001–2020 (USDA, 2022). In cases where >100% of grid cell area would be harvested during the 2025–2100 future simulations due to increased rates, harvest area above 100% was allocated to cells with <100% period harvest. As with historical prescriptions, even-aged harvests were prescribed in the future. Both forest revision plans list regeneration harvest and selective harvest as "possible actions." However, given the large desired species composition shifts and a modeled dependence on regeneration harvest methods in the Nez Perce-Clearwater plan (USDA, 2019), non-selective harvests were simulated. To represent even age regeneration harvest practices rather than selective harvest, FATES code was modified to only harvest on patches that contained cohorts of trees with > 20 cm DBH. For

forest pixels that had not been classified as cold-wet or cold-dry during calibration (from calibration climate-type analysis), non-BAU harvest scenarios implemented regeneration harvest-based composition shifts via planting of the PP PFT following harvest.

Two future climate scenarios were defined by 1/24° × 1/24° (∼ 4 km × 4 km), 3-hourly climate input data derived from the MIROC5 (MIROC) and IPSL-CM5A-MR (IPSL) general circulation models under historical and RCP 8.5 greenhouse gas concentrations (1950–2099) (Abatzoglou, 2013 (datasets from Rupp et al., 2017; Buotte et al., 2019). The climate data was previously downscaled and disaggregated to force 4 × 4 km CLM 4.5 simulations. RCP 8.5 climate forcings were selected due to similarity to global emissions trajectories (Peters et al., 2013; Buotte et al., 2019). The two climate models were selected due to necessary variable availability and continuity. Regionally, future MIROC climate is cooler and wetter than IPSL climate (**Supplementary Figure 1**; see Buotte et al., 2021 supplemental information for detailed climate model comparison and dataset methodology). The 4 × 4 km inputs included air temperature, humidity, incoming solar radiation, windspeed, and precipitation. Scenarios were forced by transient climate but constant CO_2 (year 2000). During initial study simulations and under constant climate, transient CO_2 experiments led to > 50% increases from equilibrium live PFT biomass in 50–100 years, also disrupting PFT strategies that had been defined via PFT calibration (e.g., shade-intolerant pine began to survive under full canopy cover). Excessive CO_2 fertilization relative to observations was possibly the result of the current FATES version not representing gross and primary production limitations aside from those associated with carbon and water supply (e.g., only representing carbon cycling, excessive C

supply invariably resulting in increased structural growth; Körner et al., 2005; Anderson-Teixeira et al., 2013).

FATES SPITFIRE was driven by spatiotemporally variable forest processes (prognostic) and climate (prescribed). A future natural (lightning, 0.5°, 3-hourly) ignitions dataset was repeated yearly and based on 1995–2013 averages. Human population density (0.5°) from the year 2000 drove future human ignition rates. Fire suppression has not been implemented in CLM FATES to date; we implemented a constant fire area suppression factor (0.61) in non-wilderness grid cells based on CLM5 socioeconomic suppression formulas for the region (from population density and GDP; Lawrence et al., 2019). For additional details on FATES SPITFIRE dynamics and documentation references, see the Supporting Material section "FATES SPITFIRE description."

Model outputs were scaled by percent forest cover to account for non-forest regions within the actual domain (Ruefenacht et al., 2008). Modeled live and dead carbon stocks across non-calibration grid cells were evaluated per PFT in comparison to FIA-based live tree carbon stock estimates (Supplementary Table 2; Gray et al., 2012; Hudiburg et al., 2019). Carbon fluxes were assessed across the domain in comparison to MODIS NPP and GPP within MODIS product grid cells classified as 'Evergreen Needleleaf Conifer' (ENF) (Running and Zhao, 2021). Total modeled burned area was evaluated relative to combined low, moderate, and high severity burn areas recorded from the Monitoring Trends in Burn Severity (MTBS) project for the historical period (Eidenshink et al., 2007). MTBS has known caveats (Kolden et al., 2015) and reflects the full fire suppression strategy employed by USFS, but is the most accurate representation of contemporary area burned.

Results

Model evaluation

Calibration

Final PFT parameter set selections passed all site-scale PFT filters at DRY, MOD, and WET locations (Supplementary Table 1) during site calibrations (Supplementary Figures 18–22). The DRY site supported recruit establishment of the calibrated ponderosa pine (PP) PFT but not the mesic fir PFT, which faced high hydraulic failure mortality. DRY site PP simulation outputs were within observed variable ranges from local eddy covariance site and chronosequence plots (Supplementary Figure 21), including total live tree C across stand ages, NPP, and GPP. At the MOD site, both generic pine and fir PFT were able to successfully initiate, with high NPP and biomass accumulation of young pine stands relative to the DRY site that was within observed ranges (Supplementary Figure 22). Due to carbon starvation from light limitation and consistent with site observations, the MOD site did not support a persistent understory. The WET site experienced the highest rates of site biomass accumulation for both PFTs from bare ground (Supplementary Figure 20). There, site FIR recruit presence persisted under a PINE canopy, passing the FIR PFT filter of moderate shade tolerance. In the absence of fire or harvest, WET site mean 100-year stand tree C was between FIA plot-based means and maximums for ponderosa pine and mixed conifer forests.

Validation

Across all PFTs, mean modeled aboveground tree C stocks were within one standard deviation of FIA plot-based calculations within the domain (2007–2017 period. Mean modeled: 63–103 Mg C ha^{-1}; mean observed: 53–108 Mg C ha^{-1}) (Supplementary Table 3; Supplementary Figure 17) and followed the same order of carbon stock densities. Mean modeled subalpine fir/spruce (SF), lodgepole pine (LP), and Douglas fir (DF) tree stocks exceeded FIA-based means by 10, 18, and 22% in 2010. Ponderosa pine (PP) and mixed conifer (MC) means were 4 and 5% lower than observations. Yearly simulated burn fractions for PP, DF, and MC also fell within one standard deviation of MTBS-based averages for the period of 2001–2017 (modeled means: 0.38–2.59% yr^{-1}; observed means: 0.31–2.33% yr^{-1}). SF and LP mean burn fractions of 0.14% yr^{-1} underestimated the observed 1.02% yr^{-1} for 2001–2017 due to inadequate fuel dryness. The 0.14% yr^{-1} 2001–2017 modeled burn fraction was similar to the 1985–2000 rate of 0.15% yr^{-1}. Observed changes to SF and LP burn fractions from the late 20th to early 21st centuries ($\sim$ 1000%) were higher than other PFTs (from MTBS).

In comparison to MODIS GPP estimates of 955–1,117 g C m^{-2} yr^{-1} across PFT site-types, modeled GPP means of 837–1178 g m^{-2} yr^{-1} were 8–18% higher (PP, DF, MC) and 13–24% lower (LP, SF) (Table 2; Supplementary Figure 17). All MODIS PFT NPP means (558–628 g C m^{-2} yr^{-1}) were higher than modeled NPP (398–495 g C m^{-2} yr^{-1}). As a result, mean MODIS CUE (NPP/GPP) across PFT domains of 0.54–0.59 exceeded modeled CUE means of 0.39–0.48. Nonetheless, modeled CUE ranges overlapped with previously observed ranges for temperate coniferous forests (DeLucia et al., 2007).

Future forests

Across all transient climate and management scenarios, live and dead carbon stocks decreased between 2025 and 2099 (Table 2, Figure 2). Total domain live tree carbon stocks decreased by 5–29%, with greater losses incurred under the hotter IPSL climate scenarios and with increasing timber harvest. In all scenarios, GPP, NPP, and NECB decreased by the late 21st century (Figure 3) due to a combination of: (1) high intermittent mortality from fire, hydraulic failure, and carbon starvation during hot and dry years (Figures 4–8) that led to decreases in crown area and GPP but not heterotrophic respiration (Figures 3); (2) tree stress from increased VPD and decreased VWC (Supplementary Figure 1) that led to decreases in GPP and carbon use efficiency (NPP/GPP; Figures 3, 6); and, (3) decreased replacement of killed crown area due to increased mortality of recruits and decreased allocation to seed biomass as NPP declined (positive feedback) (Figure 5).

Within the domain, IPSL 2050–2059 and 2090–2099 mean annual temperature (MAT) was 0.9 and 1.7°C higher than MIROC (Supplementary Figure 1). Domain MAT under IPSL and MIROC increased 5.5 C and 3.9 C, respectively, between 2026–2030 and 2095–2099. Future annual precipitation increased in both scenarios before declining from 2080–2090. Relative to MIROC, the hotter IPSL BAU scenario experienced ~250% greater burned area from 2025–2100 (Table 2). Large burned area differences between climate forcings resulted from extreme fire years, particularly from the 2050 and later (Figure 4). From 2026–2099, IPSL and MIROC

TABLE 2 Domain forest stocks and fluxes by climate and management scenario.

Climate	Harvest	Period	Tree C	Dead C	Crown area	NPP	NECB	Mortality total	Mortality harvest	Mortality drought	Mortality fire	Burned fraction
			$Mg\ ha^{-1}$	$Mg\ ha^{-1}$	$m^2\ m^{-2}$	$g\ m^{-2}\ yr^{-1}$	$g\ m^{-2}\ yr^{-1}$	$g\ m^{-2}\ yr^{-1}$	$g\ m^{-2}\ yr^{-1}$	$g\ m^{-2}\ yr^{-1}$	$g\ m^{-2}\ yr^{-1}$	$m^2\ m^{-2}\ yr^{-1}$
MIROC5	BAU	2029	131 (40)	56 (30)	65 (16)	460 (119)	1 (0)	164 (39)	6 (9)	2 (1)	5 (15)	0.16 (0.39)
		2059	133 (40)	54 (29)	66 (16)	463 (121)	−8 (45)	167 (41)	6 (9)	2 (7)	5 (8)	0.17 (0.27)
		2099	126 (39)	51 (28)	61 (17)	349 (107)	−78 (47)	176 (47)	6 (9)	13 (44)	11 (14)	0.31 (0.35)
		2025–2099	132 (40)	54 (28)	65 (16)	428 (114)	−19 (40)	170 (39)	6 (9)	4 (9)	7 (8)	0.2 (0.29)
	AC2	2059	124 (43)	53 (28)	61 (18)	442 (134)	−56 (93)	190 (50)	41 (58)	2 (7)	4 (7)	0.14 (0.22)
		2099	113 (49)	48 (29)	59 (22)	380 (176)	−70 (78)	187 (52)	38 (57)	10 (34)	10 (13)	0.31 (0.34)
		2025–2099	122 (44)	52 (28)	61 (18)	425 (134)	−48 (74)	192 (48)	41 (58)	3 (7)	6 (7)	0.18 (0.24)
	AC1	2059	129 (41)	54 (29)	64 (17)	454 (124)	−30 (58)	178 (43)	22 (34)	2 (7)	4 (7)	0.16 (0.26)
		2099	122 (43)	50 (28)	55 (20)	378 (160)	−66 (70)	184 (49)	22 (35)	12 (40)	10 (14)	0.26 (0.3)
		2025–2099	128 (41)	53 (28)	63 (17)	432 (126)	−30 (51)	181 (42)	22 (34)	4 (8)	7 (8)	0.2 (0.27)
IPSL	BAU	2029	128 (38)	58 (31)	61 (15)	460 (117)	−9 (47)	170 (42)	6 (8)	2 (6)	14 (16)	0.29 (0.27)
		2059	119 (37)	55 (30)	58 (16)	348 (107)	−97 (46)	190 (60)	5 (8)	7 (28)	40 (37)	0.63 (0.49)
		2099	105 (37)	46 (26)	51 (18)	286 (113)	−157 (42)	220 (89)	5 (8)	38 (107)	59 (56)	1.24 (0.71)
		2025–2099	119 (37)	52 (28)	57 (17)	369 (111)	−82 (36)	174 (45)	5 (8)	8 (19)	24 (17)	0.51 (0.34)
	AC2	2059	111 (39)	54 (30)	54 (18)	338 (121)	−132 (77)	208 (61)	37 (53)	6 (25)	37 (36)	0.56 (0.42)
		2099	95 (46)	42 (27)	49 (23)	311 (186)	−152 (77)	216 (85)	35 (54)	23 (75)	53 (55)	1.12 (0.72)
		2025–2099	110 (41)	51 (28)	54 (18)	367 (135)	−108 (66)	192 (51)	38 (54)	6 (15)	22 (17)	0.46 (0.31)
	AC1	2059	115 (37)	55 (30)	56 (17)	344 (113)	−113 (55)	199 (60)	20 (31)	7 (27)	38 (36)	0.6 (0.47)
		2099	102 (42)	44 (26)	51 (21)	311 (170)	−148 (71)	220 (85)	20 (34)	31 (92)	55 (54)	1.19 (0.7)
		2025–2099	115 (38)	51 (28)	56 (17)	373 (126)	−92 (47)	183 (47)	21 (32)	7 (17)	23 (17)	0.49 (0.33)
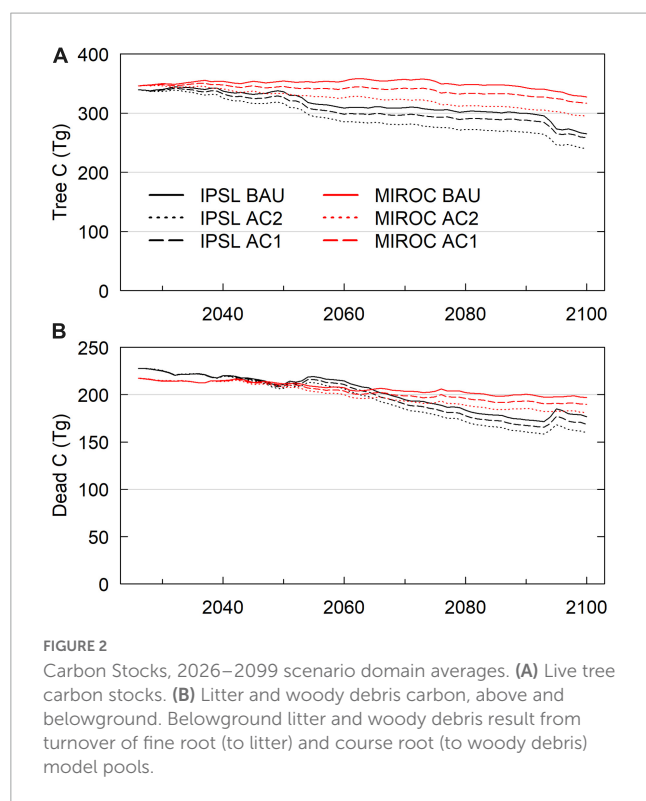
FIGURE 2
Carbon Stocks, 2026–2099 scenario domain averages. **(A)** Live tree carbon stocks. **(B)** Litter and woody debris carbon, above and belowground. Belowground litter and woody debris result from turnover of fine root (to litter) and course root (to woody debris) model pools.

burned areas were ∼10,000 km² and ∼4,000 km², or 38% and 15% of domain area. IPSL burned fraction approximately doubled between 2000–2049 and 2050–2099 (∼ 0.33% yr⁻¹ to 0.6% yr⁻¹), while mean MIROC burned fraction remained consistent (∼ 0.22% yr⁻¹ to 0.21% yr⁻¹). A lack of strong MIROC burn area increase resulted from large fuel losses to combustion during large early 2000s fire events as well as increases in precipitation that buffered fuel moisture (**Figure 4**).

Domain climate impacts, business-as-usual

Under BAU management, the hotter IPSL climate scenario experienced earlier and more extreme decreases in carbon stocks, greater burned area, and higher mortality compared to cooler MIROC scenario (**Table 2**). IPSL scenario live and dead carbon stocks decreased throughout the 21st century, with 24% vegetation C stock decreases between 2020–2029 and 2090–2099 (**Figure 2**). Extreme fire and drought years resulted in intermittent, sharp declines in live tree carbon. High fire years were associated with a combination of high burn fractions, high fire intensity, and low fuel moisture that overwhelmed negative feedbacks from lower fuel availability (**Figure 4**). During these acute mortality years, by mass, fire became the dominant source of tree mortality, followed by hydraulic and carbon starvation mortality from drought (**Figures 7, 8**).

IPSL domain annual NECB declined sharply during the periods of 2020–2050 and 2080–2100, leading to negative NECB after ∼ 2030 (**Figure 3**). Tree crown area, GPP, NPP, and NECB fell following high mortality years (**Figure 8**) due to greater declines in primary production than heterotrophic respiration. However, across the century, declining VWC (**Supplementary Figure 1**) also continually depressed NPP, NECB, and CUE via decreased stomatal conductance and GPP (carbon supply relative to autotrophic and

heterotrophic respiration) (**Figures 3, 6**). Decreased forest area and decreased NPP led to decreases in seed production and a resulting 37% decrease in recruitment between 2020–2029 and 2090–2099 (**Figure 5**). Notably, forest losses stabilized for a period after the mid-century (∼2060–2080) due to a combination of increased precipitation (**Supplementary Figure 1**) and decreased forest cover (**Figure 5**). Early period mortality resulted in increased moisture availability on a crown area basis (a negative feedback) and decreased moisture stress (**Figure 6**).

In contrast to the BAU IPSL climate scenario, MIROC BAU live tree C stocks did not begin to decline until the onset of high fire and drought mortality years in the late 21st century (>2075, >2090) (**Figures 2, 7**). Under this relatively cool climate scenario, domain total tree C stocks instead increased modestly from ∼2010–2075 following a gradual decline during the peak harvest years of the mid 20th century. From 2008 –2075, mean live tree carbon pools increased from 126 Mg ha⁻¹ to a maximum of 135 Mg ha⁻¹ (similar to early 20th century levels). By 2100, live carbon stocks had decreased to 124 Mg ha⁻¹, with a consistent and steep decline from 2085 onwards. MIROC scenario NEP, GPP, and NPP was on average 50%, 17%, and 22% higher than the IPSL BAU scenario during 2090–2099. Early to mid-century increases in MIROC live tree carbon stocks occurred despite gradual increases in autotrophic respiration that drove decreases in NPP, NECB, and CUE (**Figure 3**). Combined warmer and wetter conditions led to increases in heterotrophic respiration; decreases in litter, CWD, and snag carbon pools; and approximately balanced total domain total carbon stocks (<1% decrease).

The cooler MIROC BAU scenario experienced relatively low fire and drought-related mortality (**Figures 7, 8**) through much of the 21st century. After the highest mortality year of the 21st century in 2075 (>300% the century average mortality rate), crown area then decreased ∼9% through 2100, precipitating a transition to late-century, continual decreases in NPP, GPP, NEP, and live and total carbon stocks (**Figures 2, 3**).

Both scenarios experienced continual forest biomass declines (**Figure 2**) by the 2090s due to late century increases in plant water and carbon balance stress (**Figure 6**). Continual increases in soil moisture stress and temperature decreased stomatal conductance and tree C stores. Stress responses in turn led to decreases in NEP and the first occurrences of years in which drought mortality (carbon starvation and hydraulic failure) became the highest source of prognostic mortality for canopy trees (**Figures 7, 8**).

Under both BAU scenarios from 2025–2100, the highest mortality rates by tree count resulted from mortality of newly recruited, small trees. In decreasing order, the greatest number of trees were killed by hydraulic failure, background mortality, freezing, and carbon starvation. In contrast, mortality by mass for both IPSL and MIROC climate scenarios (**Table 2**) resulted most from background mortality (1.4 and 1.7 Mg C ha⁻¹ yr⁻¹, respectively), followed by fire (0.24 and 0.05 Mg C ha⁻¹ yr⁻¹), harvest (0.04 and 0.05 Mg C ha⁻¹ yr⁻¹) and hydraulic failure mortality (0.07 and 0.04 Mg C ha⁻¹ yr⁻¹). However, hot and dry year natural disturbance mortality (combined fire, hydraulic failure, and carbon starvation) was responsible for the highest mortality years of the century, which exceeded average rates by maximums of ∼300–400% (**Figures 7, 8**). During these years, the abrupt decreases in live tree mass generated losses of ecosystem GPP and NPP via reductions in crown area. A subsequent lack
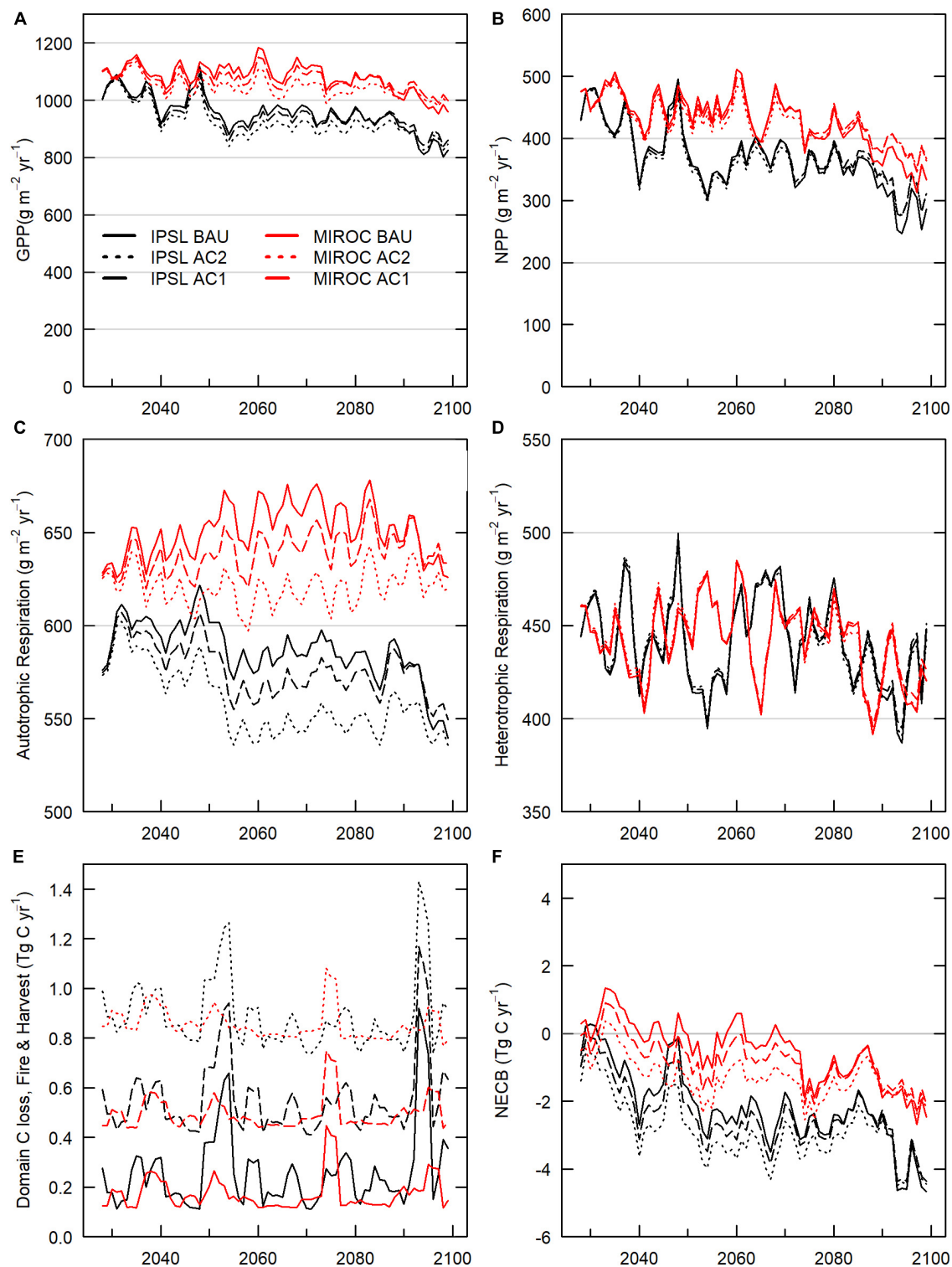
FIGURE 3

Carbon fluxes, 2026–2099 scenario domain averages. **(A)** GPP. **(B)** NPP. **(C)** Autotrophic respiration, **(D)** Heterotrophic respiration **(E)** Domain C losses (outfluxes from domain) from wildfire fire emissions, harvest slash emissions, and harvest removals. **(F)** NECB.

of crown area and primary production recovery resulted from previously depressed NPP, growth, seed allocation, and recruitment rates. IPSL BAU scenario mean and maximum yearly mortality rates (1.5 and 6.3% of live tree mass) exceeded MIROC BAU mortality rates (1.3 and 2.6%).

PFT responses, business-as-usual

Throughout the 21st century, intermittent, acute mortality occurred during high fire and drought years (**Figures 8**, **9**; **Supplementary Figures 12–16**), yet intensified for most PFTs and climate scenarios in the 2090s. As a proportion of live site
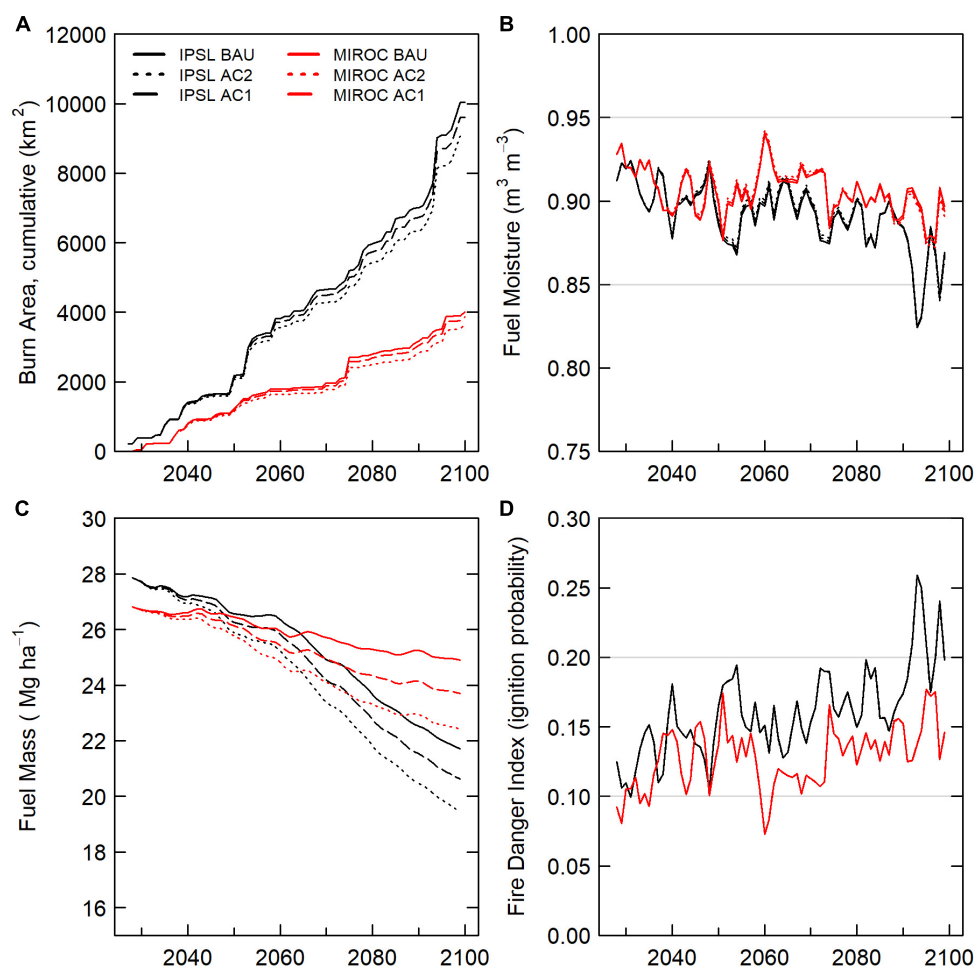
FIGURE 4
Wildfire dynamics, 2026−2099 scenario domain averages. **(A)** Cumulative wildfire burned area by scenario. **(B)** Fuel moisture. **(C)** Fuel Mass. **(D)** Fire danger index.

mass, PFT-average 2090–2099 mortality under MIROC climate increased over 2020–2029 mortality by 4% (PP), 24% (DF), 12% (MC), 8% (SF), and 59% (LP). IPSL climate scenario mortality rates increased by 385% (PP), 106% (DF), 47% (MC), 39% (SF), and 61% (LP). By 2090, all PFTs under both climate scenarios experienced years in which drought-related mortality (hydraulic failure and carbon starvation) exceeded mortality from fire or harvest as temperatures increased, precipitation decreased from mid-century maximums, and VWC decreased (**Supplementary Figure 1**). In contrast, during the spin-up and historical periods, hydraulic failure largely affected shallow-rooted recruits and was not a large source of canopy mortality or mortality by biomass. In the 2090s, dry PP sites were the only site-type on which carbon starvation mortality exceeded hydraulic failure mortality. Despite greater burned area extremes after 2050, average fire mortality and burned area did not continually increase across the century under MIROC climate for DF, MC, and SF and under both climate scenarios for dry PP and LP sites (**Supplementary Figures 3–7, 12–16**). In contrast, DF, MC, and SF burned area under IPSL climate increased over earlier 21st century burn area maximums by the 2090s.

Average BAU live tree carbon, dead carbon, and crown area decreased across most PFT site types and climate scenarios after 2075 (**Figure 9**; **Supplementary Figures 12–16**). Between 2025 and 2099, PFT-site tree C for IPSL and MIROC scenarios, respectively, decreased by 42% and 9% (PP), 23 and 10% (DF) 17% and 4% (MC), 23% and −1% (SF), and 40% and 14% (LP). Crown cover decreased by 26% and 21% (PP), 21% and 10% (DF), 24% and 11% (MC), 22% and −1% (SF), and 30% and 8% (LP). Litter and woody debris C decreased by 26% and 21% (PP), 21% and 10% (DF), 24% and 11% (MC), 22% and −1% (SF), 30% and 8% (LP). MC, DF, SF, and LP relative tree carbon deficits under IPSL versus MIROC climate continually widened from 2025–2099 (**Figures 2, 9**).

Between 2025 and 2075, MIROC MC and SF site tree carbon increased modestly (3% and 6%) under moderately warmer and wetter climate (**Figure 9**; **Supplementary Figures 15, 16**). Continued MC and SF stock growth through the mid century was the result of relatively low R_a and leaf turnover costs, higher NPP, and/or higher allocation to wood versus PP and DF on drier sites. MC and SF stock growth occurred despite comparatively low GPP. Reflecting this trend, MC and SF CUE under IPSL and MIROC decreased by 19% and 18% (MC) and 15% and 13% (SF), while
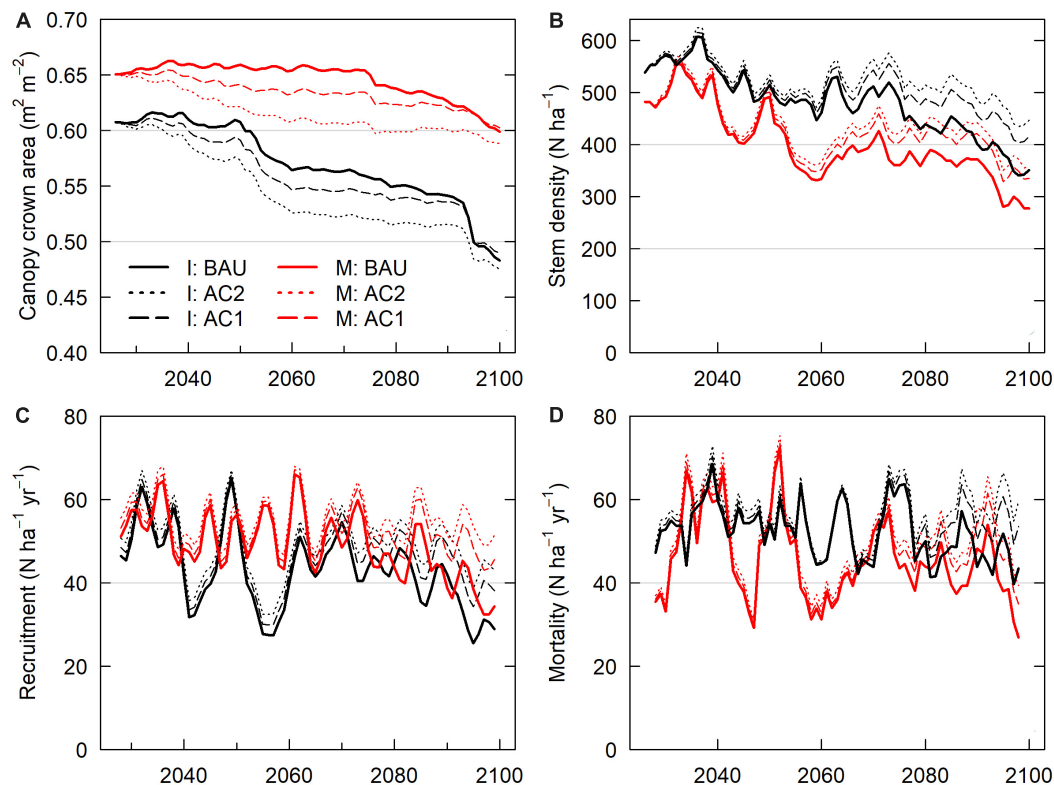
FIGURE 5
Forest structure and turnover, 2026–2099 scenario domain averages. **(A)** Canopy layer crown area. Canopy crown area < 1.0 implies site patches with bare ground. **(B)** Stem density. **(C)** Recruitment of new seedlings from seed stock. Note: Recruitment values include tree planting with regeneration harvest. **(D)** Tree stem mortality.

PP, DF, and LP CUE decreased by 24–31% (IPSL) and 18–28% (MIROC).

Ponderosa pine site C Stocks under the hotter IPSL climate did not decrease below MIROC stocks until the 2050s and then remained 5–10% lower until declining sharply in the 2090s (Figure 9). Despite higher fire and drought mortality, IPSL PP-site GPP, NPP, and crown area did not decline below MIROC values during this period due to higher ISPL PP tree C stocks and NPP In the early 21st century under moderate warming (Supplementary Figure 12).

Management impacts

By 2100, increased harvest scenarios (moderate: AC1; high: AC2) had lowered domain live carbon by 2.5–3.2% (AC1; 6.5–10.5 Tg C) and 9–10% (AC2; ∼ 24–32 Tg C, from 327 Tg C BAU) by 2100 (Table 2; Figure 2; Supplementary Figure 9). Within active harvest grid cells only, 2099 increased harvest tree carbon was 4–11% lower (AC1) and 16–18% lower (AC2) than under BAU. Year 2100 BAU-relative deficits of AC1 scenarios decreased from maximum deficits of 12.4–15.6 Tg C in the 2070s. Increased harvests decreased average crown coverage by ∼ 3–7% during the mid century (Figure 5; Supplementary Figure 10). AC1 harvest scenario crown area then reached approximate parity with BAU scenarios by 2100 due to harvest feedbacks with fire and tree stress (Figure 7). Increased harvest scenarios decreased burn area mortality due to decreased average fuel mass and decreased late-period water stress due to lowered transpiration (higher VWC

and lesser downregulation of stomatal conductance). In the 2090s, Increased harvest scenario NECB exceeded that of BAU scenarios (Table 2). Lower 2090s BAU NECB resulted from a combination of lower GPP (higher water stress) and higher R_a (higher live biomass), not higher mortality (Figure 3).

AC2 and AC1 harvest scenarios increased total mortality mass over BAU by increasing harvest mortality (Figures 7, 8), ultimately killing additional tree mass of 18–22 Tg C (AC1) and 37–44 Tg C (AC2) from 2026–2099. Increased harvest scenarios decreased 2026–2100 fire and drought-related mortality (hydraulic failure and carbon starvation) mass by 1.5–4.5 Tg C (AC1) and 2.9–8.6 Tg C (AC2). Burned area was also reduced by 4–9%, with the greatest reduction in the IPSL climate scenario. Decreases in burned area and total mortality resulted from 5–10% decreases in fuel mass (Figure 4) and resulting decreases in fire intensity. Decreases in fuel mass were the result of both the direct removal of live woody biomass that would otherwise have reached dead surface pools and via reductions in site NPP_{wood} and NPP_{leaf}.

Ponderosa pine PFT-site tree and ecosystem C was higher in BAU scenarios than AC2 and AC1 through 2100 (Supplementary Figure 12). However, during high fire and drought mortality years of the 2090s, AC2 NPP at PP sites exceeded that of BAU and AC1 scenarios. AC2 crown area deficits also shrank. For IPSL scenarios near 2100, lower AC1 and BAU NPP resulted from higher canopy mortality. During the 2090s, PP sites first began to experience years in which carbon starvation was the leading source of mortality by mass (Supplementary Figure 3). For MIROC

FIGURE 6
Tree stress and efficiency, 2026−2099 scenario domain averages.
(A) Tree carbon storage as a proportion of leaf carbon. This
proportion is used by FATES to determine the onset of cohort
carbon starvation as well as low-storage maintenance respiration
reductions. **(B)** Carbon Use Efficiency (CUE), or NPP/GPP.
Decreases in carbon use efficiency imply relative increases in
autotrophic respiration vs GPP. **(C)** Soil H_2O in the top 10 cm of soil.
(D) β-Transpiration, soil moisture stress scalar affecting stomatal
conductance. β-Transpiration reflects PFT response to soil matric
potential (0−1 = low−high conductance).

scenarios in the 2090s, PP ecosystem GPP across management
scenarios converged due to moisture limitation (**Supplementary
Figure 12**). In conjunction, higher live PP biomass and R_a in
MIROC AC1 and BAU scenarios led to lower NPP and CUE.

MC grid cells were the only PFT site-type on which moderately
increased harvest (AC1) tree C stocks converged with BAU stocks
by 2100 (**Supplementary Figure 14**). In both AC1 and AC2
scenarios, planting of the more drought and fire-tolerant PP PFT
on warmer MC-sites led to increased GPP and R versus BAU. As a
result, late-century NPP and NEP of both AC2 and AC1 scenarios
faced low declines relative to BAU. Nonetheless, high AC2 harvest
led to live and total site carbon that remained lower than BAU.

Discussion

Business-as-usual

Domain

By 2100, business-as-usual (BAU) live and dead forest carbon
stocks in northern Idaho Rocky Mountain forests declined across
RCP 8.5 climate scenarios and across plant functional types (PFT).
However, declines in domain-scale forest carbon stocks of 22%
(warmer, IPSL) and 6% (cooler, MIROC) did not result from an
increase to average mortality rates through most of the period.
Rather, we found that long-term stocks declines were characterized
by declines in gross primary production (GPP) and net primary
production (NPP) under contemporary levels of tree biomass

and canopy area. Modeled forests experienced declining NPP
and carbon use efficiency (CUE) that contributed to declining,
negative net ecosystem carbon balance (NECB), and in turn the
failure of forest canopy recovery following intermittent high fire
and drought mortality years. Under increasing temperatures, NPP
and NECB decline resulted from respiratory fluxes that were less
sensitive to climate changes than primary production, consistent
with previous research (Ciais et al., 2005; Schwalm et al., 2010). In
the late 21st century, pronounced decreases to GPP resulted from
increasing vapor pressure deficit (VPD), declining soil moisture,
and decreasing stomatal conductance. 2090–2099 was the first
decade in which drought-related forest mortality rates consistently
increased across forest types and across climate model scenarios.

The forecasted declines of forest carbon stocks, crown area,
and NECB in the region differed in timing and magnitude between
climate scenarios under BAU management, indicating uncertainty
as to whether forest carbon stock decline should be expected before
the late 21st century (2080–2099). Annual precipitation increased
under both climate scenarios, but was sufficient to prevent early
to mid century NPP and NECB decline under moderate MIROC
warming only. Further, 2025–2099 MIROC burned area was ∼40%
of IPSL area due to non-linear impacts of fuel moisture on fire
dynamics, causing average and maximum yearly MIROC tree
fire mortality to be considerably lower. Despite the characteristic
summer drought of much of the domain, these differing results
indicate that the degree to which this relatively productive forest
region of the WUSA will be increasingly vulnerable to direct
negative impacts of warming though the mid-century (e.g., 1–
3°C warming) is unclear, varying by climate scenario and also
dependent on precipitation shifts. This result is consistent with
recent modeling research with CLM 4.5, indicating higher relative
fire and drought vulnerability in the southwest U.S. and Sierra
Nevada than in the northern Rocky Mountains (Buotte et al.,
2019). Previous LANDIS II simulations have also indicated delays
in future C stock declines in the forests of the Northern Rocky
Mountains (NRM) and Greater Yellowstone Ecosystem, in part due
to increased precipitation (Henne et al., 2021; Walsh and Hudiburg,
2021). However, a NRM LANDIS II study also projected more
distinct mid-century increases in burned area under RCP 8.5 (note:
partially overlapping domain; Walsh and Hudiburg, 2021). This
contrast highlights future vulnerability uncertainty arising from
differing fire and vegetation dynamics across models as well as from
differing climate model inputs and resolutions (Stenzel et al., 2019).

Plant functional type

Proportional decreases in year 2100 BAU tree C stocks, NPP,
CUE, and crown cover were greatest for dry pine sites (PP and LP).
While pine PFT traits (parameters. E.g., stomatal slope, root depth,
bark depth, crown depth etc.) conferred relative drought and fire
tolerance, tree carbon balance for shade-intolerant pine PFT-sites
declined due to relatively high maintenance costs (e.g., respiration,
leaf turnover). PP sites of this study represent the lower boundary
of tree cover in the domain (Walsh and Hudiburg, 2021), generally
occupying the hottest and driest forest land. Results support the
notion that this drought-tolerant species (Martnez-Vilalta et al.,
2004; Sala et al., 2005; Kwon et al., 2018) is nonetheless vulnerable
to extended periods of drought and that negative drought impacts
may be highest at hotter, lower elevation sites (Stevens-Rumann
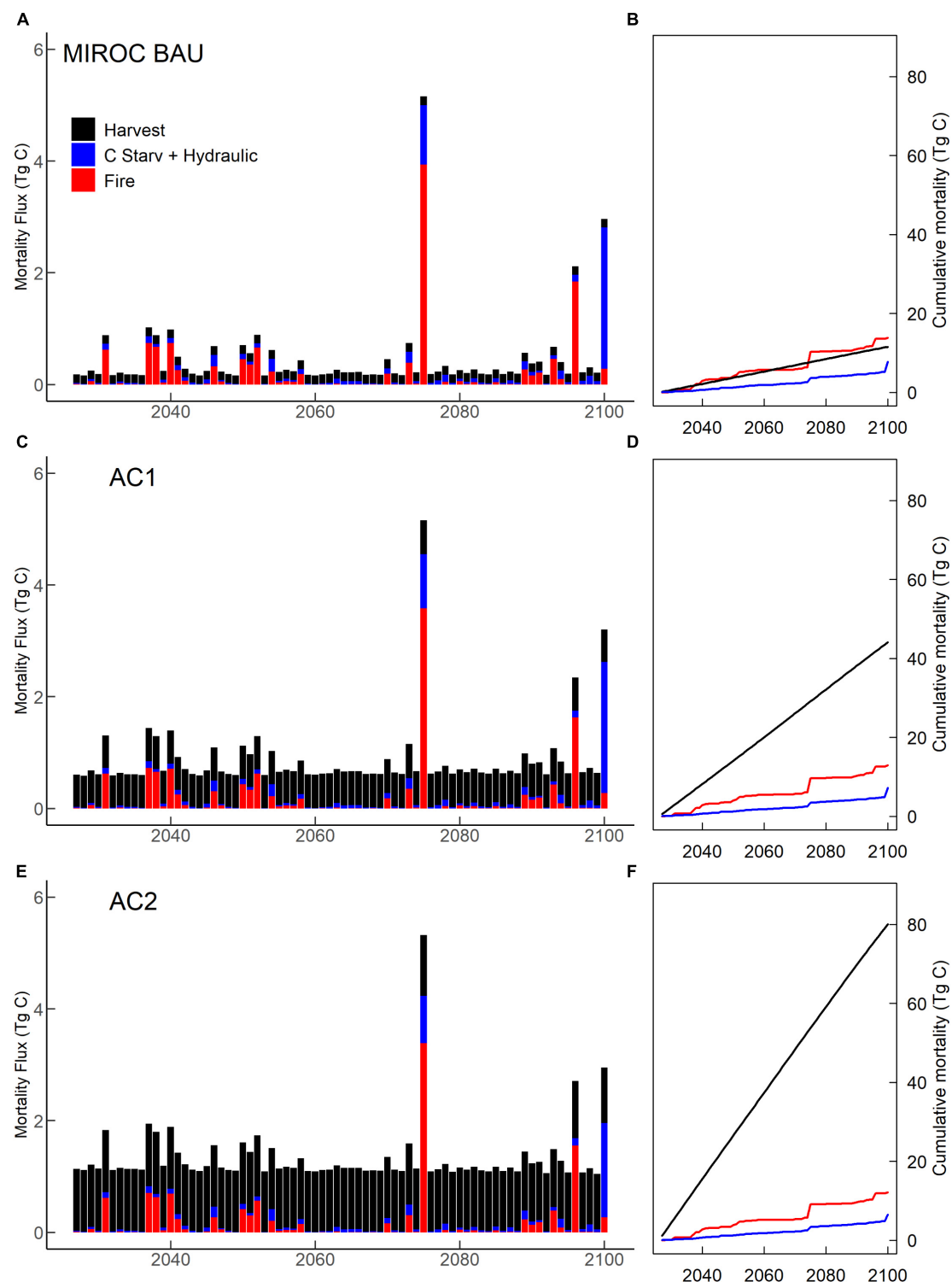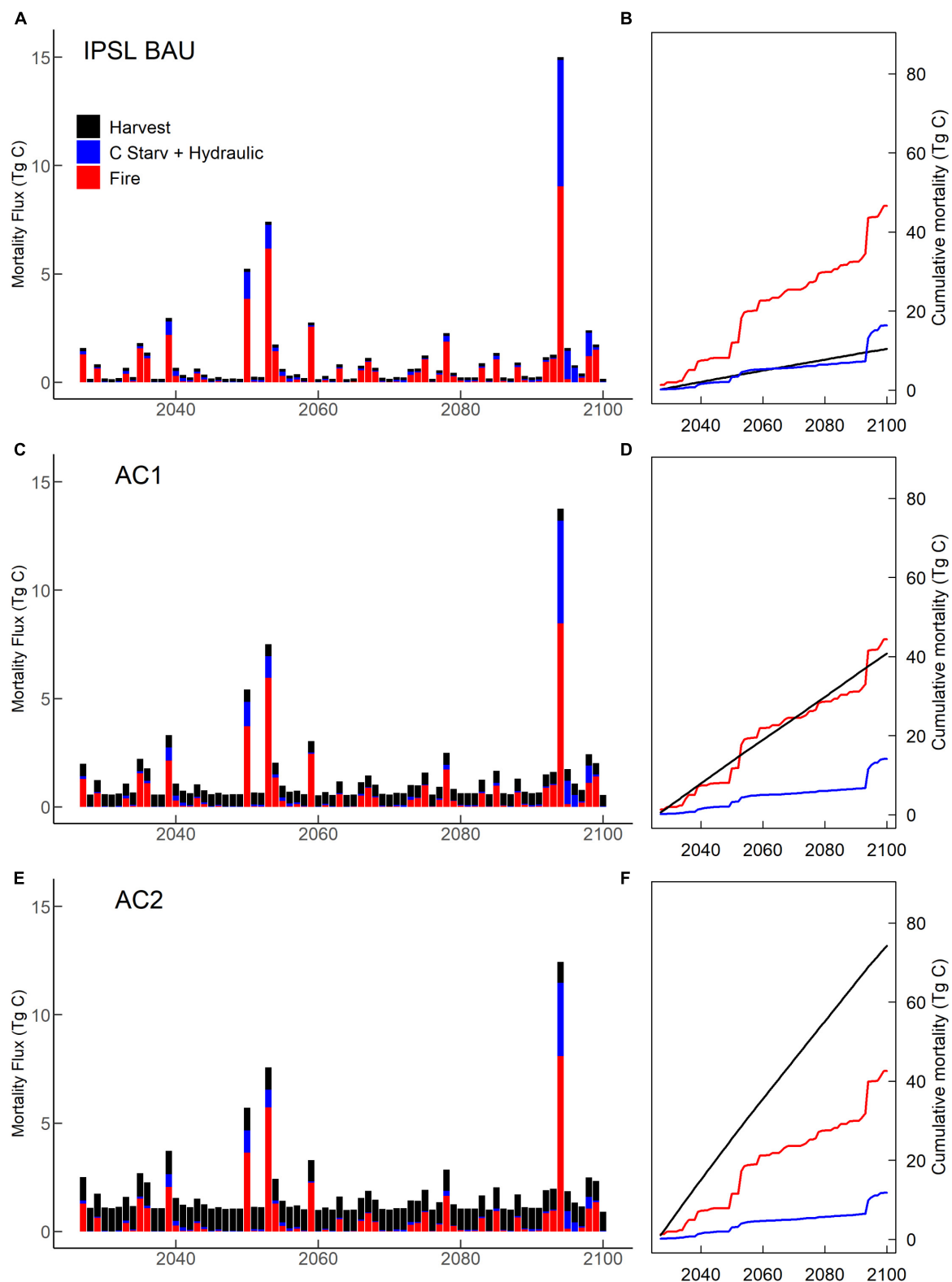et al., 2017; Walsh and Hudiburg, 2021). Carbon starvation, rather

FIGURE 7
MIROC climate scenario tree mortality. **(A,C,E)** Annual mortality; and **(B,D,F)** cumulative mortality from wildfire, harvest, hydraulic failure and carbon starvation. **(A,B)** Business-as-usual (BAU). **(C,D)** Moderate harvest increase (AC1). **(E,F)** High harvest increase (AC2).

than hydraulic dysfunction, contributed to acute 2090s mortality of PP under IPSL climate (Sevanto et al., 2014). Higher typical moisture on MC and SF PFT-sites and lower maintenance costs delayed or prevented 21st century declines in PFT C stocks. Observed increases in burned area and mortality on DF, MC, and

SF sites in the 2090s highlight an eventual projected reduction in fuel moisture limitations in moist, high biomass forests of the region (Arno, 1980; Arno et al., 2000). In contrast, the lack of modeled increase in PP and LP burned area resulted from lower fuel moisture, declining NPP, relatively low fire return intervals,

FIGURE 8
IPSL climate scenario tree mortality. **(A,C,E)** Annual mortality; and **(B,D,F)** cumulative mortality from wildfire, harvest, hydraulic failure and carbon starvation. **(A,B)** Business-as-usual (BAU). **(C,D)** Moderate harvest increase (AC1). **(E,F)** High harvest increase (AC2).

and declining fuel mass through the 21st century. End-of-century increases in drought related mortality for pine sites and burned area for moister mixed conifer and fir sites suggest that shifts in

northern Idaho forest dynamics are primarily predicted in the long-term. However, we highlight that PFT distributions in this study are static across grid cells (i.e., fixed biogeography), leading to possible
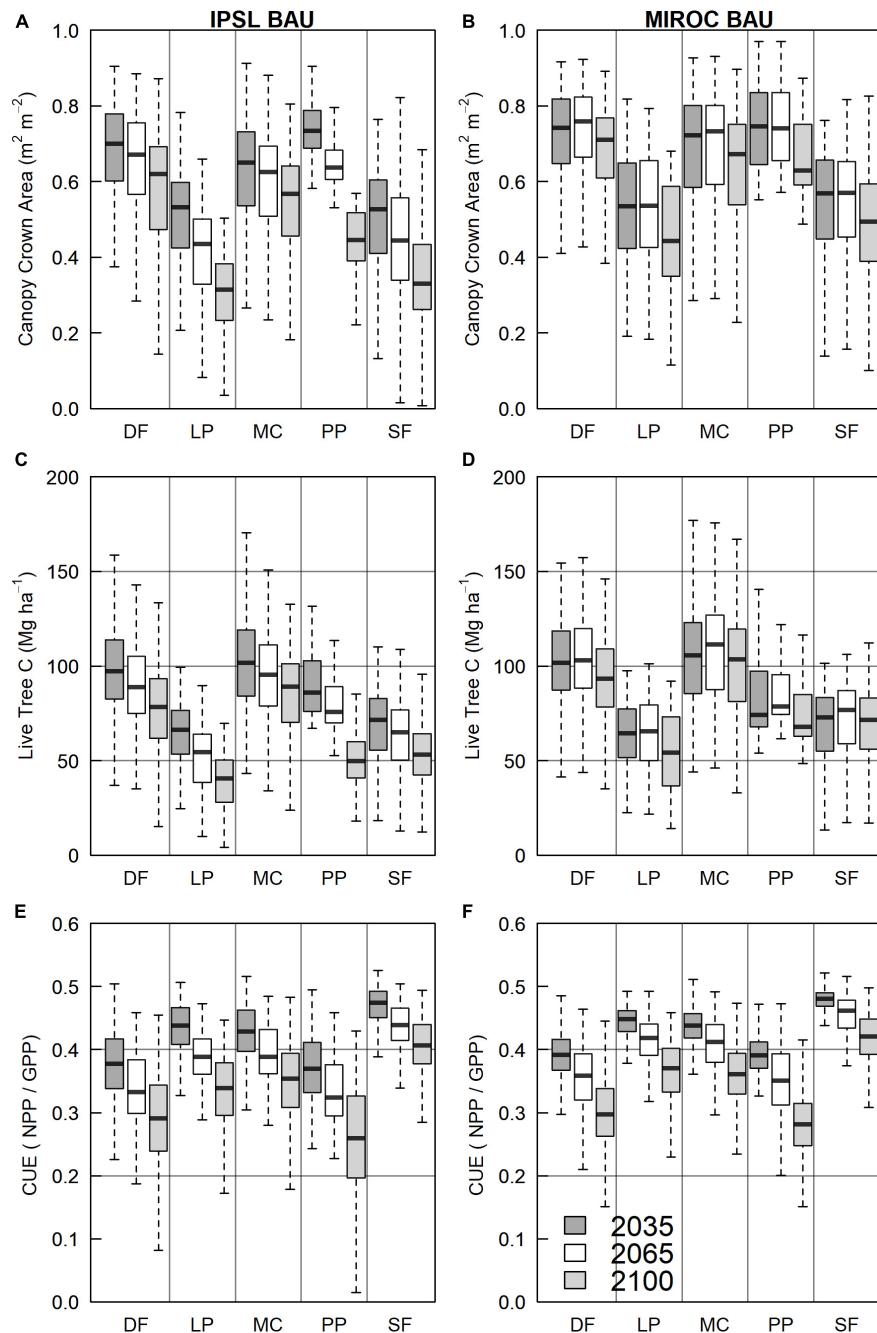
FIGURE 9
BAU forest structure and function by PFT site-type and climate scenario, 2025−2099. **(A,C,E)** IPSL climate; and **(B,D,F)** MIROC climate. **(A,B)** Canopy layer crown area. **(C,D)** Live tree carbon. **(E,F)** Carbon use efficiency (CUE). Boxes denote the interquartile range (IQ), horizontal bars show medians, and whiskers extend to extreme values within 1.5 times the IQ.

understatements of site resilience to stress via regional species diversity (DellaSala et al., 2013; Franklin and Johnson, 2013).

Increased harvest

We implemented moderate (AC1) and high (AC2) increased harvest scenarios to reflect large potential increases in timber harvest being considered on NRM USFS lands. In particular, the draft revision plan for the Nez Perce-Clearwater National Forest

presents management alternatives that could implement multifold increases in regeneration harvest (i.e., even-aged harvest with post-harvest planting) (USDA, 2019). The high harvest scenario implemented in this study shifted future harvest levels near to 20th century maximums (USDA, 2022).

Across climate scenarios, both intensities of increased harvest resulted in domain carbon stock losses, forest cover losses, and increased total tree mortality relative to BAU through 2100. Consistent with previous research on the positive relationship between harvest intensity and ecosystem carbon

storage (Law et al., 2013, 2018; James et al., 2018), losses increased with harvest intensity. Higher increased harvest scenario mortality (by mass) occurred despite reductions in burned area and fire mortality, as lower fuel mass was achieved indirectly via impactful even-aged harvest. However, after 2060, reductions in residual forest stress under increased harvest also became evident, including reduced soil moisture limitation, increased stored carbon fraction, and increased CUE. Nonetheless, through approximately 2090, increased harvest scenario component carbon fluxes (GPP, NPP, R_a) remained lower than BAU scenarios due to reduced forest canopy area. After 2090, however, average GPP, NPP, and NECB of increased harvest scenarios exceeded BAU fluxes, while forest canopy cover converged with BAU at moderate harvest intensity (AC1). This pattern indicated that late 21st century climate stress began to lower the density of domain forest cover supported on the landscape, leading to greater impacts on higher biomass density BAU forests. Even so, total regional carbon stock deficits from increased harvest persisted through the entire simulation period. This suggests that increased even-aged harvest will not protect *in situ* stocks under near-term climate change and is consistent with previous research in the U.S. Pacific Northwest (Law et al., 2018, 2021).

The greatest benefit from increased harvest was experienced at the warmer and drier subset of mixed conifer PFT sites. There, moderate harvest increases (AC1) with planting of drought tolerant pine led to approximately equal tree biomass stocks and higher crown area in year 2100 than under BAU. Further, despite the higher maintenance costs of the ponderosa pine PFT (associated with parameters conferring relative shade-intolerance in FATES), deeper water access and more isohydric stomatal behavior (via stomatal slope) led to higher annual GPP, NPP, and CUE on such sites after 2090. However, convergence of mixed conifer site biomass levels across BAU and AC1 scenarios occurred late in the simulation period, leading to average increases in simulation period harvest C stock deficits versus BAU.

The management scenario results in this study demonstrate a tradeoff in which 21st century forest biomass and canopy area removal losses were incurred in return for a reduction in potential forest vulnerability in the 22nd century. Increased harvest and planting of fire and drought tolerant species increased NRM forest disturbance, mortality, and function loss through much of the 21st century, with little apparent reduction in vulnerability to natural stressors (fire, drought) in the short-term future. Only late-century increases in tree moisture stress fed back to lower growth, lower recruitment, and natural mortality rates in higher biomass-density BAU forests. Through 2100, however, all PFTs under all increased management scenarios demonstrated total live and dead biomass stocks that were lower than BAU stocks. The possible 22nd century convergence of management scenario biomass stocks and the likely positive impacts of planting drought and fire tolerant species on forest resilience are beyond the scope of this study. However, 21st century results indicate a need for further research into whether different management timing (e.g., later in the century) or methods could reduce late-century forest stress and decline while incurring lower time-averaged ecosystem carbon deficits (Hessburg et al., 2021; Prichard et al., 2021; Stenzel et al., 2021). Our management scenarios only implement the significant intensifications of regeneration harvest considered in draft NRM forest management plans (USDA,

2019). Changes to harvest levels in conjunction with prescribed fire, selective harvest, or other strategies are not modeled. This may in part explain the lack of near-term management benefits found in comparison to previous western U.S. modeling studies that implemented lower-mortality treatments such as selective harvest (Hurteau et al., 2016; Liang et al., 2018; McCauley et al., 2019).

Model discussion

Model advantages

A primary motivation for our use of CLM-FATES was its representation of distinct cohort crown areas within patches that can leave light gaps when individuals die. Patch post-disturbance recovery can then depend on the establishment and growth of new cohorts in available canopy space. Decreasing canopy area provides a spatial mechanism for forest function decline within grid cells (Fisher et al., 2015; Koven et al., 2019; FATES Development Team, 2022). These dynamics are not present in homogenous LAI models (i.e., non-spatial) like CLM 5.0 (Lawrence et al., 2018) or various successions extensions of LANDIS II (NECN, PnET; Scheller et al., 2011; De Bruijn et al., 2014), which represent vegetated column surfaces on which shrinking or expanding leaf biomass pools determine site leaf area index, rather than crown area. FATES representation of canopy space was essential to our results in U.S. Northern Rocky Mountain forests. Declining forest cover and biomass under climate change resulted from a combination of canopy mortality and gap generation; decreased carbon allocation to growth and seed production; and decreased tree recruitment and survival to maturity. Underlying the need for model functional gaps, the northern Idaho forest domain of this study has contemporary, observation-based tree canopy cover estimates of <60% (LANDFIRE Existing Vegetation Cover; DOI and USDA, 2022), with most of the remainder associated with post-forest disturbance canopy gaps. In this study, simulated primary production patterns emerged in large part from modeled gaps in forested canopy cover (60–65% in 2020, **Supplementary Figure 10**) that increased through 2100. While selective harvest was not explored as a forest treatment in this study, the gap dynamics of FATES would possibly refine previous thinning study results that represent modified forest stress via site LAI (Liang et al., 2018; Stenzel et al., 2021).

Model limitations

CLM-FATES lack of explicit cohort root area (vs depth) or root constraint within grid cell patches represents an important deficiency in this study's representation of forest response to soil moisture limitations under seasonal drought. As noted in the methods section, CLM-FATES does not represent separate soil water pools for FATES vegetated patches and instead aggregates soil water fluxes within grid cells. These dynamics can preclude water availability thresholds below which grid cells will no longer support a given PFT (i.e., fall outside PFT fundamental niche space). Grid cell canopy cover reductions instead lead to continual increases in per-tree soil water availability (negative feedback) and per-tree soil area can exceed feasible horizontal root spread. In this study, this dynamic was

potentially responsible for overestimated per-tree water availability, unconstrained negative feedbacks between tree density and stress, and forest resilience, rather than ecological tipping points, under warming climate.

Possible study overestimates of regional forest resilience to climate change stress may also have resulted from model seed distribution dynamics. FATES timestep seed production is aggregated across patches and then distributed in proportion to patch area. For this reason, FATES cannot represent limitations to disturbed patch seeding and regeneration that could realistically result from significant distances between live seed sources and disturbed areas. Within the NRM, observed forest gaps on the scale of hectares to square kilometers can persist for years to decades as a result of mass forest mortality from wildfire, bark beetles, and timber harvest (DOI and USDA, 2022).

Finally, forest plan revision documents for the domain's Idaho Panhandle and Nez Perce-Clearwater National Forests (USDA, 2015, 2019) also highlight observed and anticipated mortality resulting from biotic agents (insects and pathogens), particularly in productive, mid elevation, mixed conifer forests that include Douglas fir and grand fir. However, our study only represents the contribution of biotic agents to calibrated rates of recent species mortality (McNellis et al., 2021) via PFT-dependent background mortality rate parameters, and thus does not simulate prognostic changes to vulnerability to biotic-agent stress and mortality. Forest management revision plan alternatives that would cause species composition shifts (e.g., towards drought tolerant pine) at the scale of hundreds of thousands of acres per decade would create novel vegetation-stressor interactions and resulting species mortality rates would almost certainly shift (Das et al., 2016).

Conclusion

While much recent ecological research in western U.S. forest focuses on severe climate impacts such as increasing wildfire area (Westerling et al., 2006; Westerling, 2016; Abatzoglou et al., 2021), tree die-off (Anderegg et al., 2012; Allen et al., 2015), and cover conversions (Davis et al., 2019; Coop et al., 2020), it is also essential to highlight where and why lower vulnerability might occur. This is especially true in low vulnerability regions with high forest carbon density, where preservation priority is high (Law et al., 2018, 2021; Buotte et al., 2020). Based on our study's lack of intensifying forest vulnerability to drought and fire before 2050 and disagreement on post-mid-century decline across climate projections, we conclude that Idaho NRM forests represent one such moderate vulnerability region under BAU. This conclusion is supported by the low or moderate vulnerability to 21st century disturbance and carbon stock loss that has been reported in forest modeling studies in other subregions of the northwest U.S. (Henne et al., 2021; Walsh and Hudiburg, 2021), and contrasts with the greater vulnerability of drier or warmer portions of western U.S. forest (Buotte et al., 2019).

Uncertainties in global climate model projections are high at the end of the 21st century (IPCC, 2022). Further, climate model temperature-precipitation trends diverge from observations in the western U.S. (Abatzoglou et al., 2022), yet are essential to simulations of vegetation stress. In this study, climate uncertainty was reflected in divergent climate impacts to NRM forests. Highly

variable scenario forest carbon stock decline timing and magnitude after 2050 resulted from the interaction of relatively high (IPSL) versus low (MIROC) RCP 8.5 warming with increases in annual precipitation. Because acute and consistent forest function loss was restricted to the late century, our confidence in increased 21st century NRM forest vulnerability is low.

The moderate vulnerability and high carbon density of modeled NRM forests indicates the persistent value of maintaining existing forest function through the 21st century (Buotte et al., 2020). In the context of low-certainty, long-term climate risks, conservative management strategies would seek to bolster forest resilience while minimizing landscape biomass and function losses to the extent possible. The 21st century increased harvest scenarios in this study instead implement a 'hard reset' approach that prescribes novel landscape compositions (USDA, 2019) and results in long-term forest cover and carbon stock losses. While the reduced forest cover density of increased harvest scenarios led to reduced moisture stress on a portion of the domain by 2100, high harvest mortality prevented ecosystem biomass stock parity with BAU.

This study represents the first regional application of CLM-FATES in the productive forests of the northwest U.S. and is an early application of the model towards applied research topics (Huang et al., 2020). With FATES coupling of CLM surface processes to heterogenous grid cell patches occupied by tree cohorts, we demonstrate 21st century climate and variable disturbance impacts that depend on declining forest cover in addition to declining biomass pool density (e.g., Walsh and Hudiburg, 2021). Our study implements a fixed PFT biogeography (i.e., PFT distribution across grid cells) and we highlight that limited spatiality to root water access (in contrast to spatial canopy light access) may limit the ability of the model to simulate competitive outcomes of variable PFT hydraulic strategies in moisture limited environments. Nonetheless, the capability of FATES to model shifting forest canopy area and the negative feedbacks between patch canopy density and tree stress were essential to projecting the mixed vulnerability of NRM forests to 21st century climate change.

Data availability statement

The data that support the findings of this study are openly available in the University of Idaho repository at https://doi.org/10.7923/2kee-sq55. Datasets include model inputs/outputs (FATES parameter set, domain, surfdat, land use, and history files). The FATES source code used in these experiments is available at: https://github.com/jestenzel/fates/releases/tag/nrockies_1.0.

Author contributions

JS, CK, and TH designed the study. JS implemented FATES code modifications and simulations. PB provided extensive model training and advice. All authors prepared the manuscript and approved the submitted version.

Funding

Acknowledgments

Conflict of interest

The authors declare that the research was conducted in the absence of any commercial or financial relationships that could be construed as a potential conflict of interest.

Publisher's note

All claims expressed in this article are solely those of the authors and do not necessarily represent those of their affiliated organizations, or those of the publisher, the editors and the reviewers. Any product that may be evaluated in this article, or claim that may be made by its manufacturer, is not guaranteed or endorsed by the publisher.

Supplementary material

The Supplementary Material for this article can be found online at: https://www.frontiersin.org/articles/10.3389/ffgc.2023.1146033/full#supplementary-material

References

Abatzoglou, J. T. (2013). Development of gridded surface meteorological data for ecological applications and modelling. *Int. J. Climatol.* 33, 121–131.

Abatzoglou, J. T., and Williams, A. P. (2016). Impact of anthropogenic climate change on wildfire across western US forests. *Proc. Natl. Acad. Sci. U.S.A.* 113, 11770–11775. doi: 10.1073/pnas.1607171113

Abatzoglou, J. T., Battisti, D. S., Williams, A. P., Hansen, W. D., Harvey, B. J., and Kolden, C. A. (2021). Projected increases in western US forest fire despite growing fuel constraints. *Commun. Earth Environ.* 2:227.

Abatzoglou, J. T., Marshall, A. M., Lute, A. C., and Safeeq, M. (2022). Precipitation dependence of temperature trends across the contiguous US. *Geophys. Res. Lett.* 49, 1–10. doi: 10.1007/s00704-022-04232-z

Allen, C. D., Breshears, D. D., and McDowell, N. G. (2015). On underestimation of global vulnerability to tree mortality and forest die-off from hotter drought in the Anthropocene. *Ecosphere* 6, 1–55.

Allen, C. D., Macalady, A. K., Chenchouni, H., Bachelet, D., McDowell, N., Vennetier, M., et al. (2010). A global overview of drought and heat-induced tree mortality reveals emerging climate change risks for forests. *For. Ecol. Manag.* 259, 660–684.

Anderegg, W. R., Berry, J. A., Smith, D. D., Sperry, J. S., Anderegg, L. D., and Field, C. B. (2012). The roles of hydraulic and carbon stress in a widespread climate-induced forest die-off. *Proc. Natl. Acad. Sci. U.S.A.* 109, 233–237.

Anderegg, W. R. L., Trugman, A. T., Wang, J., and Wu, C. (2022). Open science priorities for rigorous nature-based climate solutions. *PLoS Biol.* 20:e3001929. doi: 10.1371/journal.pbio.3001929

Anderson-Teixeira, K. J., Miller, A. D., Mohan, J. E., Hudiburg, T. W., Duval, B. D., and DeLucia, E. H. (2013). Altered dynamics of forest recovery under a changing climate. *Glob. Change Biol.* 19, 2001–2021. doi: 10.1111/gcb.12194

Arno, S. F. (1980). Forest fire history in the northern rockies. *J. For.* 78, 460–465.

Arno, S. F., Parsons, D. J., and Keane, R. E. (2000). Mixed-severity fire regimes in the northern rocky mountains: Consequences of fire exclusion and options for the future. *USDA For. Serv. Proc.* 5, 225–232.

Baker, K. V., Tai, X., Miller, M. L., and Johnson, D. M. (2019). Six co-occurring conifer species in northern idaho exhibit a continuum of hydraulic strategies during an extreme drought year. *AoB Plants* 11, 1–13. doi: 10.1093/aobpla/plz056

Bartowitz, K. J., Higuera, P. E., Shuman, B. N., McLauchlan, K. K., and Hudiburg, T. W. (2019). Post-fire carbon dynamics in subalpine forests of the Rocky Mountains. *Fire* 2:58.

Bartowitz, K. J., Walsh, E. S., Stenzel, J. E., Kolden, C. A., and Hudiburg, T. W. (2022). Forest carbon emission sources are not equal: Putting fire, harvest, and fossil fuel emissions in context. *Front. For. Glob. Change* 5:867112. doi: 10.3389/ffgc.2022.867112

Berner, L. T., Law, B. E., Meddens, A. J. H., and Hicke, J. A. (2017). Tree mortality from fires, bark beetles, and timber harvest during a hot and dry decade in the western United States (2003–2012). *Environ. Res. Lett.* 12:65005.

Bollenbacher, B. L., Graham, R. T., and Reynolds, K. M. (2014). Regional forest landscape restoration priorities: Integrating historical conditions and an uncertain future in the northern rocky mountains. *J. For.* 112, 474–483.

Bonan, G. (2019). *Climate change and terrestrial ecosystem modeling*. Cambridge: Cambridge University Press.

Bonan, G. B. (2008). Forests and climate change: Forcings, feedbacks, and the climate benefits of forests. *Science* 320, 1444–1449.

Brown, R. T., Agee, J. K., and Franklin, J. F. (2004). Forest restoration and fire: Principles in the context of place. *Conserv. Biol.* 18, 903–912.

Buotte, P. C., Koven, C. D., Xu, C., Shuman, J. K., Goulden, M. L., Levis, S., et al. (2021). Capturing functional strategies and compositional dynamics in vegetation demographic models. *Biogeosciences* 18, 4473–4490. doi: 10.1186/1475-2875-9-228

Buotte, P. C., Law, B. E., Ripple, W. J., and Berner, L. T. (2020). Carbon sequestration and biodiversity co-benefits of preserving forests in the western United States. *Ecol. Appl.* 30, 1–11. doi: 10.1002/eap.2039

Buotte, P. C., Levis, S., Law, B. E., Hudiburg, T. W., Rupp, D. E., and Kent, J. J. (2019). Near-future forest vulnerability to drought and fire varies across the western United States. *Glob. Change Biol.* 25, 290–303. doi: 10.1111/gcb.14490

Case, M. J., Johnson, B. G., Bartowitz, K. J., and Hudiburg, T. W. (2021). Forests of the future: Climate change impacts and implications for carbon storage in the Pacific Northwest, USA. *For. Ecol. Manag.* 482:118886.

Chapin, F. S., Woodwell, G. M., Randerson, J. T., Rastetter, E. B., Lovett, G. M., Baldocchi, D. D., et al. (2006). Reconciling carbon-cycle concepts, terminology, and methods. *Ecosystems* 9, 1041–1050.

Ciais, P., Reichstein, M., Viovy, N., Granier, A., Ogée, J., Allard, V., et al. (2005). Europe-wide reduction in primary productivity caused by the heat and drought in 2003. *Nature* 437, 529–533. doi: 10.1038/nature03972

Coop, J. D., Parks, S. A., Stevens-Rumann, C. S., Crausbay, S. D., Higuera, P. E., Hurteau, M. D., et al. (2020). Wildfire-driven forest conversion in western North American landscapes. *BioScience* 70, 659–673. doi: 10.1093/biosci/biaa061

Das, A. J., Stephenson, N. L., and Davis, K. P. (2016). Why do trees die? Characterizing the drivers of background tree mortality. *Ecology* 97, 2616–2627. doi: 10.1002/ecy.1497

Davis, K. T., Dobrowski, S. Z., Higuera, P. E., Holden, Z. A., Veblen, T. T., Rother, M. T., et al. (2019). Wildfires and climate change push low-elevation forests across

a critical climate threshold for tree regeneration. *Proc. Natl. Acad. Sci. U.S.A.* 116, 6193–6198. doi: 10.1073/pnas.1815107116

De Bruijn, A. M., Gustafson, E. J., Sturtevant, B. R., Foster, J. R., Miranda, B. R., Lichti, N. I., et al. (2014). Toward more robust projections of forest landscape dynamics under novel environmental conditions: Embedding PnET within LANDIS-II. *Ecol. Model.* 287, 44–57.

DellaSala, D. A., Anthony, R. G., Bond, M. L., Fernandez, E. S., Frissell, C. A., Hanson, C. T., et al. (2013). Alternative views of a restoration framework for federal forests in the Pacific Northwest. *J. For.* 111, 420–429.

DeLucia, E. H., Drake, J. E., Thomas, R. B., and Gonzalez-Meler, M. (2007). Forest carbon use efficiency: Is respiration a constant fraction of gross primary production?. *Glob. Change Biol.* 13, 1157–1167. doi: 10.1093/treephys/tpz034

DOI and USDA (2022). *LANDFIRE: LANDFIRE existing vegetation type layer. Online.* Available online at: https://www.landfire.gov/evc.php (accessed October 16, 2022).

Edburg, S. L., Hicke, J. A., Lawrence, D. M., and Thornton, P. E. (2011). Simulating coupled carbon and nitrogen dynamics following mountain pine beetle outbreaks in the Western United States. *J. Geophys. Res. Biogeosci.* 116, 1–15.

Eidenshink, J., Schwind, B., Brewer, K., Zhu, Z.-L., Quayle, B., and Howard, S. (2007). A project for monitoring trends in burn severity. *Fire Ecol.* 3, 3–21.

Evangelista, P. H., Kumar, S., Stohlgren, T. J., and Young, N. E. (2011). Assessing forest vulnerability and the potential distribution of pine beetles under current and future climate scenarios in the interior west of the US. *For. Ecol. Manag.* 262, 307–316.

Evans, M. E. K., Merow, C., Record, S., McMahon, S. M., and Enquist, B. J. (2016). Towards process-based range modeling of many species. *Trends Ecol. Evol.* 31, 860–871.

FATES Development Team (2022). *FATES documentation. Release d2*, eds R. A. Fisher, R. G. Knox, C. D. Koven, G. Lemieux, C. Xu, B. Christofferson, et al. Available online at: https://fates-users-guide.readthedocs.io/_/downloads/tech-doc/en/stable/pdf/

Finco, M., Quayle, B., Zhang, Y., Lecker, J., Megown, K. A., and Brewer, C. K. (2012). "Monitoring trends and burn severity (MTBS): Monitoring wildfire activity for the past quarter century using LANDSAT data," in *Proceedings: Moving from status to trends: Forest inventory and analysis (FIA) symposium; 2012 December 4-6; Baltimore, MD*, eds R. Morin and G. Liknes (Newtown Square, PA: U.S. Department of Agriculture, Forest Service, Northern Research Station), 222–228.

Fisher, R. A., and Koven, C. D. (2020). Perspectives on the future of land surface models and the challenges of representing complex terrestrial systems. *J. Adv. Model. Earth Syst.* 12:e2018MS001453.

Fisher, R. A., Koven, C. D., Anderegg, W. R. L., Christoffersen, B. O., Dietze, M. C., Farrior, C. E., et al. (2018). Vegetation demographics in earth system models: A review of progress and priorities. *Glob. Change Biol.* 24, 35–54. doi: 10.1111/gcb.13910

Fisher, R. A., Muszala, S., Verteinstein, M., Lawrence, P., Xu, C., McDowell, N. G., et al. (2015). Taking off the training wheels: The properties of a dynamic vegetation model without climate envelopes, CLM4.5(ED). *Geosci. Model Dev.* 8, 3593–3619.

Franklin, J. F., and Johnson, K. N. (2013). A restoration framework for federal forests in the Pacific Northwest. *J. For.* 110, 429–439.

Gibson, C. E., and Morgan, P. (2005). *Fire history polygons for northern rockies: 1889–2003. Vector digital data.* Moscow, ID: University of Idaho.

Gray, A., Brandeis, T., Shaw, J., McWilliams, W., and Miles, P. (2012). Forest inventory and analysis database of the United States of America (FIA). *Biodivers. Ecol.* 4, 225–231.

Gruell, G. E. (1982). *Seventy years of vegetative change in a managed ponderosa pine forest in Western Montana–implications for resource management*, Vol. 130. Ogden, UT: US Department of Agriculture, Forest Service, Intermountain Forest and Range.

Gruell, G. E. (1983). *Fire and vegetative trends in the northern rockies: Interpretations from 1871-1982 Photographs. General technical report.* Washington, DC: US Department of Agriculture, Forest Service (INT-158).

Hanbury-Brown, A. R., Ward, R. E., and Kueppers, L. M. (2022). Forest regeneration within earth system models: Current process representations and ways forward. *New Phytol.* 235, 20–40. doi: 10.1111/nph.18131

Henne, P. D., Hawbaker, T. J., Scheller, R. M., Zhao, F., He, H. S., Xu, W., et al. (2021). Increased burning in a warming climate reduces carbon uptake in the greater yellowstone ecosystem despite productivity gains. *J. Ecol.* 109, 1148–1169.

Hessburg, P. F., Prichard, S. J., Hagmann, R. K., Povak, N. A., and Lake, F. K. (2021). Wildfire and climate change adaptation of western North American forests: A case for intentional management. *Ecol. Appl.* 31:e02432.

Higuera, P. E., and Abatzoglou, J. T. (2021). Record-setting climate enabled the extraordinary 2020 fire season in the Western United States. *Glob. Change Biol.* 27, 1–2. doi: 10.1111/gcb.15388

Huang, M., Xu, Y., Longo, M., Keller, M., Knox, R. G., Koven, C. D., et al. (2020). Assessing impacts of selective logging on water, energy, and carbon budgets and ecosystem dynamics in amazon forests using the functionally assembled terrestrial ecosystem simulator. *Biogeosciences* 17, 4999–5023.

Hudiburg, T. W., Higuera, P. E., and Hicke, J. A. (2017). Fire-regime variability impacts forest carbon dynamics for centuries to Millennia. *Biogeosciences* 14, 3873–3882.

Hudiburg, T. W., Law, B. E., and Thornton, P. E. (2013). Evaluation and improvement of the community land model (CLM4) in oregon forests. *Biogeosciences* 10, 453–470.

Hudiburg, T. W., Law, B. E., Moomaw, W. R., Harmon, M. E., and Stenzel, J. E. (2019). Meeting GHG reduction targets requires accounting for all forest sector emissions. *Environ. Res. Lett.* 14:095005.

Hudiburg, T., Law, B., Turner, D. P., Campbell, J., Donato, D., and Duane, M. (2009). Carbon dynamics of oregon and Northern California forests and potential land-based carbon storage. *Ecol. Appl.* 19, 163–180. doi: 10.1890/07-2006.1

Hurteau, M. D., Liang, S., Martin, K. L., North, M. P., Koch, G. W., and Hungate, B. A. (2016). Restoring forest structure and process stabilizes forest carbon in wildfire-prone southwestern ponderosa pine forests. *Ecol. Appl.* 26, 382–391. doi: 10.1890/15-0337

Hurtt, G. C., Chini, L., Sahajpal, R., Frolking, S., Bodirsky, B. L., Calvin, K., et al. (2020). Harmonization of global land-use change and management for the period 850-2100 (LUH2 for CMIP6. *Geosci. Model Dev. Discuss.* 13, 5425–5464.

IPCC (2022). "Climate change 2022: Impacts, adaptation, and vulnerability," in *Contribution of working group II to the sixth assessment report of the intergovernmental panel on climate change*, eds B. R. H.-O. Pörtner, D. C. Roberts, M. Tignor, E. S. Poloczanska, K. Mintenbeck, A. Alegría, et al. (Cambridge: Cambridge University Press).

Irvine, J., Law, B. E., Kurpius, M. R., Anthoni, P. M., Moore, D., and Schwarz, P. A. (2004). Age-related changes in ecosystem structure and function and effects on water and carbon exchange in ponderosa pine. *Tree Physiol.* 24, 753–763. doi: 10.1093/treephys/24.7.753

Irvine, J., Law, B. E., Martin, J. G., and Vickers, D. (2008). Interannual variation in Soil CO2 efflux and the response of root respiration to climate and canopy gas exchange in mature ponderosa pine. *Glob. Change Biol.* 14, 2848–2859.

James, J. N., Kates, N., Kuhn, C. D., Littlefield, C. E., Miller, C. W., Bakker, J. D., et al. (2018). The effects of forest restoration on ecosystem carbon in western North America: A systematic review. *For. Ecol. Manag.* 429, 625–641.

Kattge, J., Bönisch, G., Díaz, S., Lavorel, S. I, Prentice, C., Leadley, P., et al. (2020). TRY plant trait database – enhanced coverage and open access. *Glob. Change Biol.* 26, 119–188. doi: 10.1111/gcb.14904

Koch, E. (1942). *History of the 1910 forest fires in Idaho and Western Montana.* Moscow: University of Idaho Library.

Koch, E. (1978). *When the mountains roared: Stories of the 1910 fire.* Washington, DC: US Department of Agriculture, Forest Service.

Kolden, C. A., Smith, A. M. S., and Abatzoglou, J. T. (2015). Limitations and utilisation of monitoring trends in burn severity products for assessing wildfire severity in the USA. *Int. J. Wildland Fire* 24, 1023–1028.

Körner, C., Asshoff, R., Bignucolo, O., Hättenschwiler, S., Keel, S. G., Peláez-Riedl, S., et al. (2005). Ecology: Carbon flux and growth in mature deciduous forest trees exposed to elevated CO2. *Science* 309, 1360–1362. doi: 10.1126/science.1113977

Koven, C., Knox, R., Fisher, R., Chambers, J., Christoffersen, B., Davies, S., et al. (2019). Benchmarking and parameter sensitivity of physiological and vegetation dynamics using the functionally assembled terrestrial ecosystem simulator (FATES) at Barro Colorado Island, Panama. *Biogeosci. Discuss.* 17, 3017–3044.

Kwon, H., Law, B. E., Thomas, C. K., and Johnson, B. G. (2018). The influence of hydrological variability on inherent water use efficiency in forests of contrasting composition, age, and precipitation regimes in the Pacific Northwest. *Agric. For. Meteorol.* 249, 488–500.

Lambert, M. S. A., Tang, H., Aas, K. S., Stordal, F., Fisher, R. A., Fang, Y., et al. (2022). Inclusion of a cold hardening scheme to represent frost tolerance is essential to model realistic plant hydraulics in the Arctic – Boreal Zone in CLM5 . 0-FATES-Hydro. *Geosci. Model Dev. Discuss.* [preprint]. doi: 10.5194/gmd-2022-136

Law, B. E., and Berner, L. T. (2015). *NACP TERRA-PNW: Forest plant traits, NPP, biomass, and soil properties, 1999-2014.* Oak Ridge, TN: ORNL DAAC.

Law, B. E., Berner, L. T., Buotte, P. C., Mildrexler, D. J., and Ripple, W. J. (2021). Strategic forest reserves can protect biodiversity in the Western United States and mitigate climate change. *Commun. Earth Environ.* 2, 1–13.

Law, B. E., Hudiburg, T. W., and Luyssaert, S. (2013). Thinning effects on forest productivity: Consequences of preserving old forests and mitigating impacts of fire and drought. *Plant Ecol. Divers.* 6, 73–85.

Law, B. E., Hudiburg, T. W., Berner, L. T., Kent, J. J., Buotte, P. C., and Harmon, M. E. (2018). Land use strategies to mitigate climate change in carbon dense temperate forests. *Proc. Natl. Acad. Sci. U.S.A.* 115, 3663–3668. doi: 10.1073/pnas.1720064115

Law, B. E., Moomaw, W. R., Hudiburg, T. W., Schlesinger, W. H., Sterman, J. D., and Woodwell, G. M. (2022). Creating strategic reserves to protect forest carbon and reduce biodiversity losses in the United States. *Land* 11, 1–15.

Law, B. E., Thornton, P. E., Irvine, J., Anthoni, P. M., and Van Tuyl, S. (2001a). Carbon storage and fluxes in ponderosa pine forests at different developmental stages. *Glob. Change Biol.* 7, 755–777.

Law, B. E., Van Tuyl, S., Cescatti, A., and Baldocchi, D. D. (2001b). Estimation of leaf area index in open-canopy ponderosa pine forests at different successional stages and management regimes in oregon. *Agric. For. Meteorol.* 108, 1–14.

Law, B., Sun, O. J., Campbell, J., Van Tuyl, S., and Thornton, P. (2003). Changes in carbon storage and fluxes in a chronoseuence of ponderosa pine. *Glob. Change Biol.* 4, 510–524.

Lawrence, D. M., Fisher, R. A., Koven, C. D., Oleson, K. W., Swenson, S. C., Bonan, G., et al. (2019). The community land model version 5: Description of new features, benchmarking, and impact of forcing uncertainty. *J. Adv. Model. Earth Syst.* 11, 4245–4287.

Lawrence, D., Fisher, R., Koven, C., Oleson, K., Swenson, S., and Vertenstein, M. (2018). *Technical description of version 5.0 of the community land model (CLM)*. Boulder, CO: National Center for Atmospheric Research.

Liang, S., Hurteau, M. D., and Westerling, A. L. (2018). Large-scale restoration increases carbon stability under projected climate and wildfire regimes. *Front. Ecol. Environ.* 16:207–212. doi: 10.1002/fee.1791

Lutz, J. A., Larson, A. J., Swanson, M. E., and Freund, J. A. (2012). Ecological importance of large-diameter trees in a temperate mixed-conifer forest. *PLoS One* 7:e36131. doi: 10.1371/journal.pone.0036131

Martnez-Vilalta, J., Sala, A., and Piol, J. (2004). The hydraulic architecture of pinaceae–review. *Plant Ecol.* 171, 3–13.

McCauley, L. A., Robles, M. D., Woolley, T., Marshall, R. M., Kretchun, A., and Gori, D. F. (2019). Large-scale forest restoration stabilizes carbon under climate change in Southwest United States. *Ecol. Appl.* 29:e01979. doi: 10.1002/eap.1979

McNellis, B. E., Smith, A. M. S., Hudak, A. T., and Strand, E. K. (2021). Tree mortality in Western U.S. Forests forecasted using forest inventory and random forest classification. *Ecosphere* 12:e03419.

Morgan, P., Heyerdahl, E. K., and Gibson, C. E. (2008). Multi-season climate synchronized forest fires throughout the 20th century, Northern Rockies, USA. *Ecology* 89, 717–728. doi: 10.1890/06-2049.1

Muthukrishnan, R., Hayes, K., Bartowitz, K., Cattau, M. E., Harvey, B. J., Lin, Y., et al. (2022). Harnessing NEON to evaluate ecological tipping points: Opportunities, challenges, and approaches. *Ecosphere* 13, 1–16.

Naficy, C., Sala, A., Keeling, E. G., Graham, J., and DeLuca, T. H. (2010). Interactive effects of historical logging and fire exclusion on ponderosa pine forest structure in the Northern Rockies. *Ecol. Appl.* 20, 1851–1864. doi: 10.1890/09-0217.1

Nagy, R. C., Balch, J. K., Bissell, E. K., Cattau, M. E., Glenn, N. F., Halpern, B. S., et al. (2021). Harnessing the NEON data revolution to advance open environmental science with a diverse and data-capable community. *Ecosphere* 12:e03833.

Omernik, J. M., and Griffith, G. E. (2014). Ecoregions of the conterminous united states: Evolution of a hierarchical spatial framework. *Environ. Manag.* 54, 1249–1266. doi: 10.1007/s00267-014-0364-1

Parks, S. A., and Abatzoglou, J. T. (2020). Warmer and drier fire seasons contribute to increases in area burned at high severity in Western US forests from 1985 to 2017. *Geophys. Res. Lett.* 47, 1–10.

Peters, G. P., Andrew, R. M., Boden, T., Canadell, J. G., Ciais, P., Le Quéré, C., et al. (2013). The challenge to keep global warming below 2C. *Nat. Clim. Change* 3, 4–6. doi: 10.3390/nano13142050

Picotte, J. J., Bhattarai, K., Howard, D., Lecker, J., Epting, J., Quayle, B., et al. (2020). Changes to the monitoring trends in burn severity program mapping production procedures and data products. *Fire Ecol.* 16:16.

Prichard, S. J., Hessburg, P. F., Hagmann, R. K., Povak, N. A., Dobrowski, S. Z., Hurteau, M. D., et al. (2021). Adapting Western North American forests to climate change and wildfires: Ten common questions. *Ecol. Appl.* 31:E02433. doi: 10.1002/eap.2433

Ramsfield, T. D., Bentz, B. J., Faccoli, M., Jactel, H., and Brockerhoff, E. G. (2016). Forest health in a changing world: Effects of globalization and climate change on forest insect and pathogen impacts. *Forestry* 89, 245–252.

Ruefenacht, B., Finco, M. V., Czaplewski, R., Helmer, E., Blackard, J., Holden, G. R., et al. (2008). Mapping using forest inventory and analysis data. *Photogramm. Eng. Remote Sensing* 74, 1379–1388.

Running, S., and Zhao, M. (2021). MODIS/Terra net primary production gap-filled yearly L4 Global 500m SIN grid V061 [Dataset]. NASA EOSDIS land processes DAAC. Available online at: https://doi.org/10.5067/MODIS/MOD17A3HGF.061 (accessed October 1, 2022).

Rupp, D. E., Abatzoglou, J. T., and Mote, P. W. (2017). Projections of 21st century climate of the columbia river basin. *Clim. Dyn.* 49, 1783–1799.

Sala, A., Peters, G. D., McIntyre, L. R., and Harrington, M. G. (2005). Physiological responses of ponderosa pine in western montana to thinning, prescribed fire and burning season. *Tree Physiol.* 25, 339–348.

Scheiter, S., Langan, L., and Higgins, S. I. (2013). Next-generation dynamic global vegetation models: Learning from community ecology. *New Phytol.* 198, 957–969. doi: 10.1111/nph.12210

Scheller, R. M., Hua, D., Bolstad, P. V., Birdsey, R. A., and Mladenoff, D. J. (2011). The effects of forest harvest intensity in combination with wind disturbance on carbon dynamics in lake states mesic forests. *Ecol. Model.* 222, 144–153.

Schimel, D., Kittel, T. G. F., Running, S., Monson, R., Turnipseed, A., and Anderson, D. (2002). Carbon sequestration studied in Western U.S. mountains. *Eos* 83, 445–449.

Schwalm, C. R., Williams, C. A., Schaefer, K., Arneth, A., Bonal, D., Buchmann, N., et al. (2010). Assimilation exceeds respiration sensitivity to drought: A FLUXNET synthesis. *Glob. Change Biol.* 16, 657–670.

Schwalm, C. R., Williams, C. A., Schaefer, K., Baldocchi, D., Black, T. A., Goldstein, A. H., et al. (2012). Reduction in carbon uptake during turn of the century drought in Western North America. *Nat. Geosci.* 5, 551–556.

Scott, L. M., and Janikas, M. V. (2009). "Spatial statistics in ArcGIS," in *Handbook of applied spatial analysis: Software tools, methods and applications* (Heidelberg: Springer Berlin Heidelberg), 27–41.

Sevanto, S., Mcdowell, N. G., Dickman, L. T., Pangle, R., and Pockman, W. T. (2014). How do trees die? A test of the hydraulic failure and carbon starvation hypotheses. *Plant Cell Environ.* 37, 153–161. doi: 10.1111/pce.12141

Smith, H. Y., and Arno, S. F. (1999). *Eighty-eight years of change in a managed ponderosa pine forest*. Ogden, UT: US Department Agriculture, Forest Service, Rocky Mountain Research Station.

Smith, J. E., Domke, G. M., Nichols, M. C., and Walters, B. F. (2019). Carbon stocks and stock change on federal forest lands of the United States. *Ecosphere* 10:e02637. doi: 10.1073/pnas.1512542112

Stenzel, J. E., Bartowitz, K. J., Hartman, M. D., Lutz, J. A., Kolden, C. A., Smith, A. M. S., et al. (2019). Fixing a snag in carbon emissions estimates from wildfires. *Glob. Change Biol.* 25, 3985–3994. doi: 10.1111/gcb.14716

Stenzel, J. E., Berardi, D. M., Walsh, E. S., and Hudiburg, T. W. (2021). Restoration thinning in a drought-prone idaho forest creates a persistent carbon deficit. *J. Geophys. Res. Biogeosci.* 126, 1–18.

Stevens-Rumann, C. S., Kemp, K. B., Higuera, P. E., Harvey, B. J., Rother, M. T., Donato, D. C., et al. (2017). Evidence for declining forest resilience to wildfires under climate change. *Ecol. Lett.* 21, 243–252.

Sun, O. J., Campbell, J., Law, B. E., and Wolf, V. (2004). Dynamics of carbon stocks in soils and detritus across chronosequences of different forest types in the Pacific Northwest, USA. *Glob. Change Biol.* 10, 1470–1481.

Thonicke, K., Spessa, A., Prentice, I. C., Harrison, S. P., Dong, L., and Carmona-Moreno, C. (2010). The influence of vegetation, fire spread and fire behaviour on biomass burning and trace gas emissions: Results from a process-based model. *Biogeosciences* 7, 1991–2011.

Thurner, M., Beer, C., Santoro, M., Carvalhais, N., Wutzler, T., Schepaschenko, D., et al. (2014). Carbon stock and density of northern boreal and temperate forests. *Glob. Ecol. Biogeogr.* 23, 297–310. doi: 10.1002/eap.1749

Turner, M. G., Braziunas, K. H., Hansen, W. D., and Harvey, B. J. (2019). Short-interval severe fire erodes the resilience of subalpine lodgepole pine forests. *Proc. Natl. Acad. Sci. U.S.A.* 166, 11319–11328. doi: 10.1073/pnas.1902841116

USDA (2015). *Idaho panhandle national forests land management plan, 2015 Revision*. Washington, DC: USDA.

USDA (2019). *Draft land management plan for the nez perce-clearwater national forests*. Washington, DC: USDA.

USDA (2022). *Forest service activity tracking system*. Washington, DC: USDA.

VanderWeide, B. L., and Hartnett, D. C. (2011). Fire resistance of tree species explains historical gallery forest community composition. *For. Ecol. Manag.* 261, 1530–1538.

Walsh, E. S., and Hudiburg, T. W. (2019). An integration framework for linking avifauna niche and forest landscape models. *PLoS One* 14:e0217299. doi: 10.1371/journal.pone.0217299

Walsh, E. S., and Hudiburg, T. W. (2021). Response of avian cavity nesters and carbon dynamics to forest management and climate change in the Northern Rockies. *Ecosphere* 12:e03636.

Westerling, A. L. (2016). Increasing western US forest wildfire activity: Sensitivity to changes in the timing of spring. *Philos. Trans. R. Soc. B Biol. Sci.* 371:20150178.

Westerling, A. L., Hidalgo, H. G., Cayan, D. R., and Swetnam, T. W. (2006). Warming and earlier spring increase western U.S. forest wildfire activity. *Science* 313, 940–943.

Zhao, M., and Running, S. W. (2010). Drought-induced reduction in global. *Science* 329, 940–943.

Local-scale mapping of tree species in a lower mountain area using Sentinel-1 and -2 multitemporal images, vegetation indices, and topographic information

Iosif Vorovencii[1], Lucian Dincă[2], Vlad Crișan[2]*,
Ruxandra-Georgiana Postolache[2,3], Codrin-Leonid Codrean[1],
Cristian Cătălin[2], Constantin Irinel Greșiță[1], Sanda Chima[1] and
Ion Gavrilescu[1]

[1]Faculty of Silviculture and Forest Engineering, Transilvania University of Brașov, Brașov, Romania,
[2]National Institute for Research and Development in Forestry "Marin Drăcea", Brașov, Romania,
[3]Forestry Faculty, Stefan cel Mare University of Suceava, Suceava, Romania

Introduction: Mapping tree species is an important activity that provides the information necessary for sustainable forest management. Remote sensing is a effective tool that offers data at different spatial and spectral resolutions over large areas. Free and open acces Sentinel satellite imagery and Google Earth Engine, which is a powerful cloud computing platform, can be used together to map tree species.

Methods: In this study we mapped tree species at a local scale using recent Sentinel-1 (S-1) and Sentinel-2 (S-2) time-series imagery, various vegetation indices (Normalized Difference Vegetation Index - NDVI, Enhanced Vegetation Index - EVI, Green Leaf Index - GLI, and Green Normalized Difference Vegetation Index - GNDVI) and topographic features (elevation, aspect and slope). Five sets of data were used, in different combinations, together with the Random Forest classifier in order to determine seven tree species (spruce, beech, larch, fir, pine, mixed, and other broadleaves [BLs]) in the studied area.

Results and discussion: Dataset 1 was a combination of S-2 images (bands 2, 3, 4, 5, 6, 7, 8, 8a, 11 and 12), for which an overall accuracy of 76.74% was obtained. Dataset 2 comprised S-2 images and vegetation indices, leading to an overall accuracy of 78.24%. Dataset 3 included S-2 images and topographic features, which lead to an overall accuracy of 89.51%. Dataset 4 included S-2 images, vegetation indices, and topographic features, that have determined an overall accuracy of 89.36%. Dataset 5 was composed of S-2 images, S-1 images (VV and VH polarization), vegetation indices, and topographic features that lead to an overall accuracy of 89.68%. Among the five sets of data, Dataset 3 produced the most significant increase in accuracy, of 12.77%, compared to Dataset 1. Including the vegetation indices with the S-2 images (Dataset 2) gave an accuracy increase of only 1.50%. By combining the S-1 and S-2 images, vegetation indices and topographic features (Dataset 5) there was an accuracy increase of only 0.17%, compared with the S-2 images plus topographic features combination (Dataset 3). However, the input brought by the S-1 images was apparent in the increase in classification accuracy for the mixed and other BL species that were mostly found in hilly locations. Our findings confirm the potential of S-2 images, used together with other variables, for classifying tree species at the local scale.

1. Introduction

Mapping forest species is crucial for sustainable forest management, biodiversity assessment, monitoring, and forest ecosystem conservation and protection (Vihervaara et al., 2017; Hościło and Lewandowska, 2019). Knowing the forest at a tree species of species groups level, as well as their distribution, plays an important role in maintaining an ecological balance (Wang et al., 2018). Identifying tree species precisely is necessary in forest management planning, in applying silvicultural treatments, in forest certification and other forest applications (Persson et al., 2018). Furthermore, tree species information is necessary for the operational and tactical planning of forest resources (Persson et al., 2018). Obtaining information regarding tree species is important for both forest districts and at a national level, for knowing the surface occupied by tree species as well as their distribution. Precise and up-to-date information regarding the health and type of the forest, the spatial distribution, area, composition, and extension can be obtained from satellite images. Using remote sensing and its methods requires less time and ensures a larger studied area as well as access to inaccessible areas (Fassnacht et al., 2016; Sedliak et al., 2017; Grabska et al., 2019).

Previous studies on mapping forest species have used multispectral images, especially those from the Landsat satellite program (Schmitt and Ruppert, 1996; Mickelson et al., 1998). The main limitation of these images is their intermediate spatial resolution, which poses a challenge when using satellite images like Landsat in areas with mixed forests due to the occurrence of mixed pixels (Griffiths et al., 2014; Madonsela et al., 2017; Grabska et al., 2019). Generally speaking, images with intermediate and low spatial resolution have generally been used for mapping different forests over large areas, without realizing classification at the tree species level (Townshend et al., 2012; Immitzer et al., 2016). In addition to the limitation posed by intermediate spatial resolution, the relatively low temporal resolution (16 days) can also constrain their use in vegetation mapping. The issues are more significant when the period of interest falls within a rainy season, during which clouds reduce the image quality (Xie et al., 2008).

The Sentinel-2 (S-2) satellite is equipped with a MultiSpectral Instrument (MSI) for capturing images (processed during the Copernicus mission), which significantly improves forest mapping because data is acquired across 12 bands, three (Bands 5–7) being red-edge bands used especially for obtaining information concerning vegetation, such as chlorophyll content. Furthermore, with its five-day temporal resolution, S-2A, together with its twin satellite, S-2B, it acquires dense time-series imagery (Grabska et al., 2019).

The use of S-2 satellite images for mapping tree species has been the focus of several studies, some realized at the local scale or on single-forest estates. In one such, Immitzer et al. (2016) classified four species of resinous tree and two broadleaves (BLs) in Bavarian forests, obtaining an overall accuracy of 66%. They have used S-2 images (single image for forest and single image for cropland) with a spatial resolution of 10 m and 20 m, with the last ones resampled at 10 m, and RF algorithms for classification. In another study on a Bavarian forest, Wessel et al. (2018) distinguished beech from oak trees using a hierarchical classification

approach and multitemporal S-2 images. The authors used two machine-learning algorithms – support vector machines (SVMs) and random forest (RF) – finding only small differences between these, but with the SVMs performing slightly better than the RF. They have evaluated 54 different setups and obtained the best overall accuracy (91%) by using the SVM algorithm applied to bands 8, 2, and 3 belonging to the May image. An user's accuracy of 94% and a producer's accuracy of 79% was obtained for beech, while the oak trees user's accuracy and producer's accuracy was of 100%. Persson et al. (2018) used all the bands from the four multitemporal S-2 imagery in different combinations, achieving an overall accuracy of 88.2% in discriminating five species (Scots pine, spruce, larch, birch, and pedunculate oak). The study was performed on a mature forest in Central Sweden; the RF method was used for the classification. The user's accuracies were: 95.6% for birch, 85.2% for larch, 97.3% for pedunculate oak, 70.9% for Scots pine and 90.8% for spruce. Karasiak et al. (2017) used multitemporal S-2 images to classify 14 tree species in southwestern France through three classification algorithms (SVMs, RF, and Gradient Boosted Trees [GBT]), revealing that black pine and douglas fir were the most-confused species, while aspen and red oak were the best predicted. Even though the classification performance was improved, moving from 4-bands dataset to 10-bands dataset, the tree species hierarchy for their identification has remained the same. As such, based on the F1-score in the case of 10-bands dataset, black pine had an F1-score of 0.81 and 0.74 for douglas fir; aspen and red oak had a F1-score equal to 0.99, as cypress. All other species had the following F1-scores: 0.98 (silver birch, oak, European ash), 0.97 (eucalyptus), 0.95 (black locust), 0.90 (willow), 0.98 (Corsican pine and maritime pine), and 0.91 (silver fir). The overall accuracy of the classification was between 91.02 and 97.40%, depending on the dataset and algorithm considered. Stoffels et al. (2015) classified five species (beech, sessile and pedunculate oak, spruce, duglas fir, and Scots pine) using SPOT-4 and SPOT-5 multitemporal satellite images, together with multitemporal RapidEye and airborne LiDAR data, obtaining an overall accuracy of 83.5%. The maximum likelihood classification based on locally optimized training data was used for identifying tree species. The results obtained by the authors show an user's accuracy of 79.5% for beech, 84.0% for sessile and pedunculate oak, 91.6% for spruce, 76.6% for douglas fir, and 85.9% for Scots pine.

On the other hand, radar sensors provide a continuous data stream with a lower signal-to-noise ratio (SNR), as well as terrain- and observation-geometry-related artifacts (Lechner et al., 2022). The two S-1 satellites (S-1A and S-1B) capture microwave imagery with higher spatial resolution and high temporal resolution. Radar data is freely available, and their independence from weather conditions and daytime usage makes them frequently employed in assessing forest attributes worldwide (Waser et al., 2021).

Some conducted studies have shown that S-1 images are suitable for differentiating between deciduous and coniferous trees (Dostálová et al., 2021; Waser et al., 2021). Based on multitemporal S-1 data, Udali et al. (2021) conducted a classification of forest types and forest tree species in a test area in southern Sweden and achieved overall accuracies of 94 and 66%, respectively. Rüetschi et al. (2017), in a test size in Switzerland, obtained an overall accuracy of 86% in classifying

forest types and 72% in distinguishing between three species (European beech - *Fagus sylvatica*, oak - *Quercus robur* and *Quercus petraea*, and Norway spruce - *Picea abies*).

In a small number of other studies, forest compositions have been determined over large areas at regional and national scales (Hościło and Lewandowska, 2019). Forest mapping using remote-sensing methods over large mountainous areas has also been limited. In these cases, the digital elevation model (DEM) can be used because it can enhance the overall accuracy of the species classification. Adding the DEM variable in the classification leads to good results for regions where vegetation distribution follows topographic data. Dorren et al. (2003) showed that, by applying topographic corrections and using the DEM method, or other characteristics derived from this in combination with spectral data, can increase the overall classification accuracy for steep mountain terrains in Austria (ranging from 600 to 3,000 m a.s.l.). In another study, undertaken on a large regional scale in south-central China by Liu et al. (2018), four tree species and mixed forest types were mapped from both flat and mountainous areas (up to 850 m a.s.l.). The authors obtained the highest accuracy (82.8%) by combining Landsat-8, S-2, and a Shuttle Radar Topography Mission (SRTM) DEM. Furthermore, the authors showed that the overall accuracy was increased by 15.2% by combining satellite images with terrain features, compared with using a single image.

The combination of S-1 and S-2 imagery with topographic data has opened up new opportunities for the classification of forested landscape. Waser et al. (2021) used S-1 and S-2 imagery in combination with topographic data for classifying dominant leaf types, employing both RF and deep learning (UNET) algorithms, resulting in significantly higher accuracies (kappa coefficient around 0.95). Their research also highlighted that the combined use of S-1, S-2, and topographic predictors effectively mitigate issues related to terrain topography and shadow, surpassing the performance of using S-1 and DEM or S-2 and DEM data separately. Liu et al. (2023) employed a combination of S-1, S-2, and topographic data for mapping tree species diversity in temperate montane forests, and found that this combination yielded the highest accuracy (species richness: $R2 = 0.562$, $RMSE = 1.502$; Shannon-Wiener diversity: $R2 = 0.628$, $RMSE = 0.231$). The combination of S-1, S-2, and topographic data was also identified by Xie et al. (2021) as providing the highest overall accuracy (77.5%) in classifying six dominant tree species (*Pinus tabuliformis*, *Quercus mongolia*, *Betula* spp., *Populus* spp., *Larix* spp., and *Armeniaca sibirica*) and one residual class.

Hyperspectral imagery contains more information about vegetation and can be used for more accurate mapping of tree species. The essential condition is that the tree species exhibit significant differences in spectral reflectance measured across multiple spectral bands (Farreira et al., 2016; Hycza et al., 2018). The capability to succesfully classify tree species using such data has been demonstrated in equatorial forests, where classifications of seven tree species achieved accuracies ranging from 80 to 100% (Clark et al., 2005; Peerbhay et al., 2013). Additionally, hyperspectral data has been used in tropical and subtropical regions, where tree species classifications achieved accuracies of over 90% (Dian et al., 2014; Ballanti et al., 2016). Tree species classifications have also been conducted in temperate regions, with accuracies ranging from 74 to 93% (Dian et al., 2014; Dmitriev, 2014; Richter et al., 2016).

The main purpose of this study was to map local-scale tree species located on mountainous terrain with a heterogeneous landscape, using S-1 and S-2 dense-image series, vegetation indices (VIs), and topographic features. The analysis were realised at a local scale, taking into account the size of forest management units and the size of patches located inside the villages. The specific objectives of the study were: (i) to investigate the performance of time-series S-1 and S-2 images, VIs, and topographic features (DEM, aspect, and slope) combined into five datasets for mapping tree species and analyzing the variable importance used in the classification; (ii) identifying seven tree species (spruce, beech, larch, fir, pine, mixed species, and other BLs) based on the best combination of data in order to achieve the highest classification accuracy; and (iii) analyzing the importance of tree species identification on satellite images in the context of global change. We compiled five datasets with different variable combinations in order to achieve our research objectives and provide more-detailed information on the results. Google Earth Engine (GEE) cloud computing and a RF machine-learning algorithm were directed at achieving these objectives.

2. Materials and methods

2.1. Study area

The studied area covered 8,519 ha of the Prahovei Valley (Romania), located in the southern part of the Bucegi Mountains (Figure 1). This included forests located in hilly and mountainous areas. The minimum altitude was 530 m, and the maximum altitude reached 1,340 m a.s.l. in the northwestern part of the studied area. The average slope was approximately 26°, although slopes with a higher inclination (over 30°) were also present. The most common ones were steep slopes (77%), followed by less steep slopes (18%). The average annual temperature was +6.8°C, while the average annual precipitation was approximately 770 mm.

Of the entire surface of the studied area, 34.54% was forest, managed by the National Forest Administration, 43.33% was private compact or dispersed forests, and 22.13% was built-up surfaces (buildings, roads, parking lots, etc.), pasture, and hay. The woodlands were dominated by common beech (*Fagus sylvatica*), Norway spruce (*Picea abies*), silver fir (*Abies alba*), European larch (*Larix decidua*), Scots pine (*Pinus sylvestris*), and black pine (*Pinus nigra*), which represented about 89% of the total forest species. The other tree species were sessile oak (*Quercus petraea*), European hornbeam (*Carpinus betulus*), grey alder (*Alnus incana*), black alder (*Alnus glutinosa*), silver birch (*Betula pendula*), sycamore maple (*Acer pseudoplatanus*), European ash (*Fraxinus excelsior*), aspen (*Populus tremula*), and willow (*Salix caprea*).

The proportions of these forest tree species in the overall species composition differed in various parts of the studied area. The main species (beech, spruce, fir, pine, and larch) were generally present in compact stands, but were also found, rarely, in built-up areas. Parts of the stands were pure, while others were mixed, composed of two to three main species. The basal area threshold for distinguishing between pure and mixed stands is 80%; if the basal area exceeds this percentage for a single tree species, then the stand is considered pure, and if it falls below this percentage, the stand is considered mixed. In certain stands, the main species were accompanied, in a small percentage (10–20%), by sycamore maple, ash, sessile oak, and hornbeam. In the southern and middle part of the studied area, built-up areas were present at low altitudes, alternating with pastures and meadows. These areas contained groups of tree species or fruit trees grouped together or growing in rows and along the edges of private properties that were not included in any forest management plans. Here and there in the built-up area, the vegetation occurred as shrubs or was in a different stage of development.

FIGURE 1
Location of the study area.
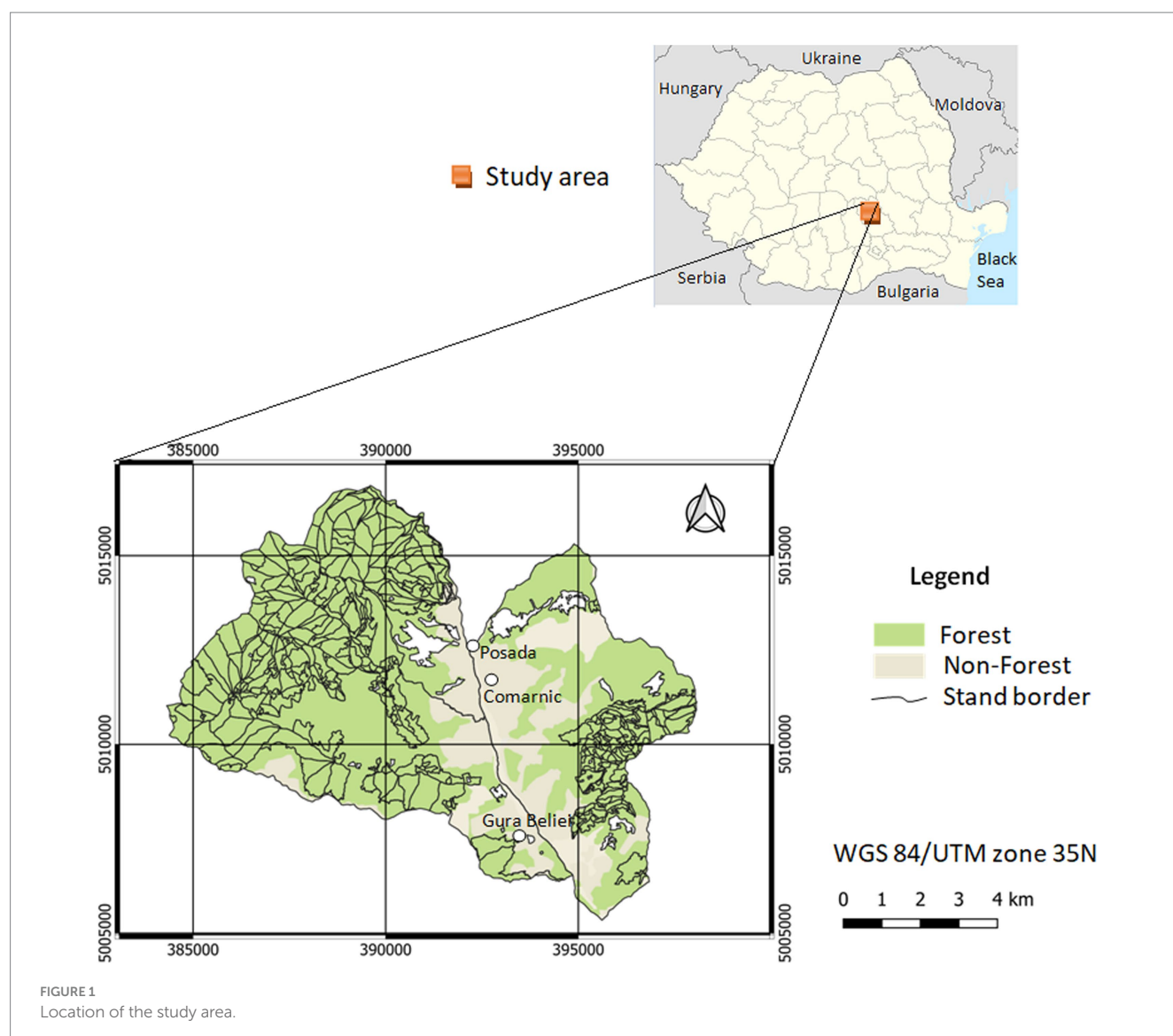
2.2. Data and data preprocessing

We employed the JavaScript API within the GEE code editor to analyze the data. GEE is a cloud computing platform launched by Google in 2010. It enables users to conduct geospatial analysis and is the most popular platform for processing large geospatial datasets. It includes various built-in algorithms, such as those for classification, allowing for global-scale data analysis and facilitating the development of custom algorithms by researchers. The Earth Engine Data Catalog contains a diverse range of standard Earth science raster datasets that are freely accessible. Additionally, users have the option to upload their own raster or vector data for private use or sharing in scripts. In this study, we used the preprocessed archives of S-1, S-2, and DEM data available on GEE. These preprocessed datasets had already been corrected for atmospheric and topographic effects, which significantly streamlined the data acquisition and preprocessing task, saving us valuable time and effort.

2.2.1. Sentinel-1 imagery

We used 224 S-1 images, gathered in 2021 and 2022. These were ground range detected (GRD) (Level-1) interferometric wide (IW)

swath-mode acquisitions that had already been preprocessed, using multi-looking and projection, to the ground range using an Earth ellipsoid model (Copernicus, 2014; Table 1). The spatial resolution of this dataset was measured at 10 m. The S-1 GRD data was processed by thermal noise removal, and radiation and terrain correction, and the 10-m dual bands, VV and VH, of the IW swath mode was selected for further processing to match the resolution of S-2. Because S-1 data were collected from both ascending and descending passes, the VV and VH data were co-registered.

The S-1 images in VV and HV polarization were divided into three temporal intervals for 2021 and 2022. Each temporal interval was specific, from a phenological perspective, to a certain season: April 1 – May 31 (start of the growing season), June 1 – August 31 (peak growing season), and September 1 – November 15 (end of the growing season). In this way, we obtained 12 stock layers (median) that were then compiled individually (Table 1).

2.2.2. Sentinel-2 imagery

We used a set of multispectral data, composed of 15 S-2 surface reflectance images with no cloud cover, acquired in 2021 and 2022 between April 10 and November 26, distributed irregularly over the

TABLE 1 Main characteristics of S-1 imagery used in study and the temporal intervals for calculating seasonal composites in 2021 and 2022.

Collection and Instrument mode	Stock acronim used in study	Period of images acquisition	Orbit properties pass	Polarisation	Number of images
COPERNICUS/S1_GRD Interferometric Wide	VV1_2021	April 1 – May 31	Ascending	VV	20
	VH1_2021		Descending	VH	20
	VV1_2022		Ascending	VV	10
	VH1_2022		Descending	VH	10
	VV2_2021	June 1 – August 31	Ascending	VV	30
	VH2_2021		Descending	VH	30
	VV2_2022		Ascending	VV	15
	VH2_2022		Descending	VH	15
	VV3_2021	September 1 – November 15	Ascending	VV	24
	VH3_2021		Descending	VH	24
	VV3_2022		Ascending	VV	13
	VH3_2022		Descending	VH	13
Total					224

TABLE 2 Description of the S-2 images used in study.

Collection		Date acquired	Relative orbit number	Tile number
COPERNICUS/S2_SR	2021	April 10, May 10, July 29, August 8, August 23, October 27, November 11, November 21, November 26	50	T35TLL
	2022	April 5, April 15, May 20, June 29, October 17, November 1		

study periods. The images were downloaded free from Copernicus Data Hub (Table 2). Because tree species analysis depends on phenology, we selected images that had recorded forests in different phenological phases (Hościło and Lewandowska, 2019). In this regard, for both years, we used images acquired at the beginning of spring (when BL species begin to green-up), in the summer (when photosynthetic activity is high), and in the fall (when the leaves begin to color steadily and differently for each tree species). In this way, we chose to include three seasons in the analysis because the signatures exposed in the 15 images during the vegetation season could offer a unique spectral model that could not be obtained by any single image. Unfortunately, we did not find any suitable images for early autumn (September).

The downloaded images were orthorectified and atmospherically and topographically corrected at Level-2A (spectral reflectance). For this study, we omitted three bands–coastal (0.43–0.45 μm), water vapor (0.93–0.95 μm), and cirrus bands (1.36–1.39 μm)–because of their sensitivity to atmospheric interference (Stych et al., 2019; Fundisi et al., 2022). The other 10 bands used were red, green, blue, near infrared (NIR), vegetation red edge (VRE), and shortwave infrared (SWIR). They covered a wavelength of 0.41–2.28 μm. The spatial resolution of the S-2 images was 10 m (blue, green, red, and NIR) and 20 m (VRE bands, narrow NIR, SWIR bands). The S-2 bands with the 20-m spatial resolution were resampled to 10 m using the nearest-neighbor resampling method. The resampling was carried out in order to have the same spatial resolution. The images are in WGS84 projection, Zone 35 N.

2.2.3. Digital elevation model

The topographic variables were derived from the SRTM DEM, which is a free product obtained from interferometric radar. The

SRTM provided a near-global DEM between 60°N and 56°S latitude and was realized based on data collected from 11 days in February 2000 by a specially modified radar system onboard the Space Shuttle Endeavour. The SRTM DEM is available globally at 1 arcsecond at about a 30-m spatial resolution. The SRTM DEM was cut on the studied contour and resampled to 10 m (S-2 resolution) using the bilinear resampling method. Based on the SRTM DEM we obtained two topographic variables – slope and aspect – that, together with the elevation, were added to the data stock without any adjustment. In the GEE, the scaling was executed automatically, and all the bands used in different combinations were overlaid correctly.

2.2.4. Vegetation indices

The high spectral resolution of the S-2 images allowed us to obtain different features connected to the green cover. Based on the literature review, we selected four VIs – the Normalized Difference Vegetation Index (NDVI), Enhanced Vegetation Index (EVI), Green Leaf Index (GLI), and Green Normalized Difference Vegetation Index (GNDVI; Table 3). The NDVI is an indicator of the greenness of the vegetation. High values indicate a rich and healthy vegetation. The EVI was developed because it is more sensitive to changes in areas with high biomass (Bhatnagar et al., 2021). The GLI is intended to measure the quantity of greenery, with positive values representing green leaves and stems. The GNDVI is a modified NDVI, capable of detecting variations in chlorophyll concentration by replacing the red band with the green band (Gitelson et al., 1996).

They were selected to offer a comprehensive understanding of various facets of vegetation as these indices offer diverse viewpoints on vegetation health, density, and chlorophyll concentration,

TABLE 3 Vegetation indices used in the study.

Vegetation Indices	Formula	Application from S-2
NDVI	$\dfrac{B_8 - B_4}{B_8 + B_4}$	Map vegetation in a complex and mixed vegetation cover (Mohammadpour et al., 2022) Vegetation mapping (Dobrinić et al., 2021) Mapping forest cover and forest types (Waśniewski et al., 2020)
EVI	$\dfrac{B_8 - B_4}{B_8 + (6 \times B_4) - (7.5 \times B_2) + 1} \times 2.5$	Vegetation mapping (Dobrinić et al., 2021)
GLI	$\dfrac{(2 \times B_3) - B_2 - B_4}{(2 \times B_3) + B_2 + B_4}$	Crop classification (Sonobe et al., 2018)
GNDVI	$\dfrac{B_8 - B_3}{B_8 + B_3}$	Map vegetation in a complex and mixed vegetation cover (Mohammadpour et al., 2022) Tree species classification (Lechner et al., 2022)

B2, B3, B4, and B8 are the correspondence S-2 bands.

inclusively vegetation phenology. By integrating these indices as input variables for classification, the goal was to capture a comprehensive view of vegetation characteristics for the purpose of identifying tree species.

2.2.5. Boundaries and stand polygons

All the images and topographic features used were clipped on the contour of two production units from within the Sinaia Forest District – Forest Management Unit (FMU) I Comarnic and FMU II Posada. The exact geolocations of the boundaries are stored in a GIS database and were provided by the "Marin Drăcea" National Institute for Research and Development in Forestry (NIRDF). These boundaries and stand polygons were converted from Stereografic 1970, the official projection of Romania, in WGS84 projection, Zone 35 N (Greșiță, 2011; Greșiță, 2013). The boundaries of the 2 units (shapefile format) were merged in QGIS and imported into the GEE *via* Google fusion tables. The obtained contour was used in clipping images and topographic features on the studied area. In addition, all stand polygons were imported in QGIS and the GEE.

2.3. Classification approach and reference data

2.3.1. Random forest

The classification process was divided into two levels of forest detail: (i) mapping forest covers; and (ii) classifying tree species. The RF classifier was used for both levels.

The RF is a machine-learning algorithm that uses multiple self-learning decision trees to parameterize models (Hościło and Lewandowska, 2019). In this algorithm, several decision trees are built based on a random subsample of the data used. Each decision tree is produced independently, with no cut, while each node is divided using a defined number of characteristics (Mtry) that were selected randomly (Belgiu and Drăguț, 2016). By increasing the forest to a defined level of usage by using the number of trees (Ntree), the algorithm creates trees that have a higher variance level and a low bias (Breiman, 2001). The final classification decision is taken by obtaining an arithmetical average of the attribution probabilities calculated by all the trees produced (Belgiu and Drăguț, 2016).

The RF classification was carried out using the GEE – a powerful cloud computing platform. The parameterization of the model was performed on 500 single trees in the forest, with the minimum

number of samples in a node set to one. Setting Ntree at the 500 level was realized in accordance with the specialist literature, which explains that the errors stabilize before this number of trees are classified (Lawrence et al., 2006). In addition, this value is set as a default value in the R package for RFs (Belgiu and Drăguț, 2016). Mtry parameter was tested from 1 to 9 using a single interval and null value (default in GEE) which means no limits. The last value was considered the best because the overall accuracy was high.

After performing the classification using the RF algorithm, the importance of the variables was estimated through GEE by computing the normalized and raw variable importance. For each classification result, we calculated the importance of the variables.

2.3.2. Forest mask

At the first level, we performed a forest mask by extracting forest areas from all the S-2 images acquired in 2021 and 2022 (Table 2) using the RF classifier. In the non-forested class, we included built-up surfaces (buildings, roads, parking lots, etc.), non-wooded vegetation, agricultural lands (pasture, hay, arable), and water. A 'No Data' value was assigned to all pixels not covered by the forest polygons or outside the forested areas mask. The 'No Data' pixels were not used for tree species identification. Thus, only pixels with forest and inside the forested areas mask were used.

2.3.3. Tree species classification

At the second level, we used different subsets that included various combinations of the two satellite systems, S-1 and S-2, topographic features, and VIs (Table 4). In this stage, we obtained a tree species separation inside the forest mask. All datasets from the second level were classified using the same samples. Figure 2 presents the flowchart of the different classification scenarios.

For this study, we focused on five main stand tree species that collectively represented more than 89% of the total forest of FMU I Comarnic and FMU II Posada–that is, spruce, beech, larch, fir, and pine. Together with these main species, we also identified two groups of species–mixed and other BLs. The mixed species class included both resinous and BL species (including fruit trees) located in urban areas and on private properties, spread on meadows and pastures that were not included in forest management plans. The way in which these patches were grouped was intimate, with the species not being separated based on their components. The other BL species class included species such as oak, maple, sycamore maple, silver birch, European ash, aspen, and willow that were present in small

TABLE 4 Scenarios evaluated using different combinations of S-1, S-2, VIs, and DEM.

Nr. crt.	Subsets (acronim)	Features	Description
1	Dataset 1	10	S-2 bands: 2, 3, 4, 5, 6, 7, 8, 8a, 11, and 12
2	Dataset 2	14	S-2 bands: 2, 3, 4, 5, 6, 7, 8, 8a, 11, and 12 VIs: NDVI, EVI, GLI, and GNDVI
3	Dataset 3	13	S-2 bands: 2, 3, 4, 5, 6, 7, 8, 8a, 11, and 12 DEM: elevation, slope, and aspect
4	Dataset 4	17	S-2 bands: 2, 3, 4, 5, 6, 7, 8, 8a, 11, and 12 DEM: elevation, slope, and aspect VIs: NDVI, EVI, GLI, and GNDVI
5	Dataset 5	241	S-2 bands: 2, 3, 4, 5, 6, 7, 8, 8a, 11, and 12 DEM: elevation, slope, and aspect VIs: NDVI, EVI, GLI, and GNDVI S-1 GRD: 224 images with VV and VH polarization

percentages in both the stands and the urban area. They were localized *via* groups of species. The other BL species were included in forest management plans but located outside those.

2.3.4. Reference data

2.3.4.1. For forest mask

Reference data for generating the forest mask were sourced from multiple references, including forest management plan maps, orthophotoplans provided by the National Agency for Cadastre and Land Registration, as well as Google Earth images. Sample selection employed a stratified random sampling approach, where strata were defined by thematic classes. These samples were evenly distributed across the entire study area. For the training and validation datasets, samples were visually chosen from both forested and non-forested polygons, resulting in a total of 193 samples – comprising 84 forested and 109 non-forested areas. These training and validation samples accounted for 7.49% of the forested area and 4.49% of the non-forested area. The average polygon size for forested area was 5.90 ha, while for non-forested areas, it was 0.78 ha. The smaller size on non-forested areas, compared to forested areas, was primarily due to landscape fragmentation.

2.3.4.2. For tree species classification

All training and validation data regarding stand compositions were automatically drawn from the official forestry database of the state forest administration received from the "Marin Drăcea" National Institute for Research and Development in Forestry. This offered detailed information on species composition, stand characteristics (e.g., stand structure, stand density, age, height, medium diameter, and volume), site characteristics (e.g., soil, geology, slope, and orientation), as well as many other types of information (Tereşneu et al., 2016). Forest management plans are updated every 10 years, but major changes, such as stand cutting, plantations and windthrows are recorded annually (Tudoran, 2013). In this way, all the changes that affect stands are recorded in forest management plans at the moment when they are produced. As such, the database is updated and contains all the changes suffered by each stand. The minimum recorded unit is the forest unit, created as a homogenous surface from a silvicultural perspective: to be comprised of a single ecosystem unit or stational unit; the same consistency or differences smaller than 0.2 (on a scale

from 0 to 1); the same composition, with difference that do not exceed 20% (on a scale from 0 to 100) for the main species; the average age should not differ more than 20 years; the same type of structure (same age, relatively same age, relativ plurien, plurien); a single productivity category. These criteria were taken into account in the forest inventory in order to demarcate homogeneous stands. Each management unit is demarcated by a polyline that has known coordinates and by marking trees with paint (Tereşneu, 2019; Tudoran and Zotta, 2020). In this study, the stand polygons ranged in size from 0.20 to 44.34 ha (average 5.89 ha) for FMU I Comarnic and from 0.11 to 31.81 ha (average 7.67 ha) for FMU II Posada (Forest Research and Management Institute, 2013a,b).

FMU consists of more forest units. FMU I Comarnic consists of 355 forest units, while FMU II Posada has 111 forest units, all included in the updated database (Forest Research and Management Institute, 2013a). Besides these forest units, approximately 60 forest units belonging to forest owners were also analyzed FMU I Comarnic has a surface of 2091.60 ha (state forest), completed by 907.7 ha (private forests that were retroceded). FMU II Posada has 850.9 ha, completed by retroceded forests (Forest Research and Management Institute, 2013b). The limits of the 2 units are materialized on the field by paint and are represented by natural details (peaks, valleys, waters) or artificial details (roads, railroads etc.). Forest clusters are found inside FMU, on different sizes located within cities.

A forest stand may include, in some cases, five or six different tree species, although the average is usually two, three or four main tree species in a mixture. The tree species composition share in a forest stand is recorded in the forest management plan during the forest inventory. For the present study, we used this share for each management unit. For species with a small share, they were considered together, leading to a distinct class classification (for example, other BL species and mixed species).

Training and validation samples were performed by screen digitization. Each sample was from inside a management unit, with a priority placed on stands with a pure species composition (e.g., with a species share of 100%). Where stands were not pure (i.e., where the share was not 100%), we followed those stands in which the respective species had the largest share.

For tree species that are widespread across the entire analyzed area (such as beech, spruce, and mixed species), the reference sample were evenly distributed throughout the study area. However, for tree species

FIGURE 2
Flowchart of the research.
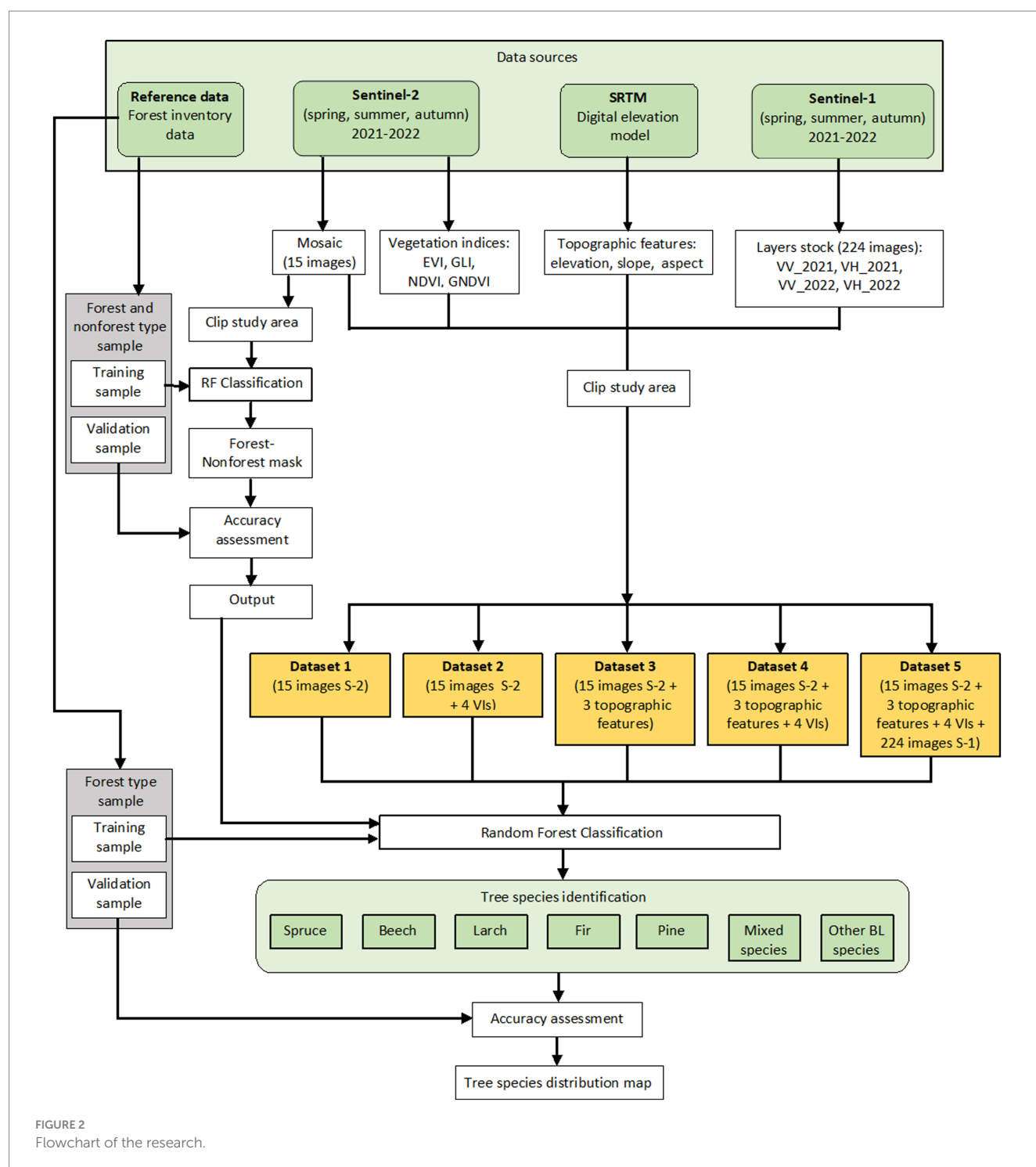
with a more limited distribution (including larch, fir, pine, and other BL species), the reference sample were selectively collected in the specific areas where these tree species are known to occur. In all cases, the selection of reference samples was carried out using a stratified random sampling approach. Table 5 provides detailed information regarding the number of polygons, total area covered, and average polygon size for reference data. Notably, the mixed species class exhibited the smallest average polygon size due to the close proximity of these tree species and their relatively smaller total area. Conversely, the beech class displayed the largest average polygon size, as it typically

forms compact stands that extend over a larger geographic area. The choice of remote sensing data used for generating the dataset varied depending on the specific combination (Table 4).

In order to validate the data, we used ortophotoplans present in the database from the National Agency for Cadastre and Land Registration, as well as Google Earth images.

2.3.5. Accuracy assessment

The reference samples were randomly divided–80% were used for training and 20% for accuracy assessment purposes.

TABLE 5 Characteristics of reference samples.

Tree species	Number of polygons	Area (ha)	Average polygon size (ha)
Spruce	79	71.83	0.91
Beech	94	121.32	1.29
Larch	38	13.15	0.35
Fir	45	20.60	0.46
Pine	42	18.08	0.43
Mixed species	48	10.89	0.23
Other BL species	51	22.98	0.45
Total	397	278.85	0.70

TABLE 6 Error matrix for forest and non-forest classification.

Reference data	Classification data			
	Classes	Forest	Non-forest	Total (number of pixels)
	Forest	2,453	7	2,460
	Non-forest	8	436	444
Total (number of pixels)		2,461	443	2,904

We selected 14,525 pixels for the forest/non-forest map, of which 11,621 pixels were for training and 2,904 for validation. The total number of pixels was 6,971 for the tree species classification, of which 5,577 were for training and 1,395 for validation. To ensure that the tree species proportions are maintained in both datasets, namely the training and validation data, the facilities provided by GEE were used.

An accuracy assessment was performed based on a confusion matrix from which we calculated the overall accuracy indices, in addition to a producer's accuracy, user's accuracy, Kappa statistic, and F1 score. Overall accuracy is expressed in percentages and represents the relation between the correctly classified pixels and the total of pixels used for verification. Producer's accuracy is calculated by dividing the number of correctly classified pixels for a given class by the total number of pixels that belong to that class in the reference dataset. User's accuracy is calculated by dividing the number of correctly classified pixels for a given class by the total number of pixels that were classified as that class on the map. The Kappa statistic evaluates how well the classification performs in comparison with the random attribution of values. The F1 score is the harmonic mean of precision and recall.

Establishing samples for accuracy assessment was realized through stratified proportional random sampling. Through this method, the total number of pixels was distributed in each class, in report with the surface of the tree species from the analyzed surface. The strata were represented by the tree species present in the classified images. Within each strata, validation data were sampled using a random method. The sampling units were individual pixels. The accuracy assessment was carried out individually for each classification result.

3. Results

3.1. Forest classification

The result of the forest/non-forest classification derived from all the multitemporal S-2 images using the RF approach showed a high level of agreement with the forest status on the ground. The overall accuracy of the forest/non-forest map was 99.48%, with a Kappa coefficient of 98.01%. The producer's accuracy for the forest was 99.71, and 98.20% for the non-forest. The user's accuracy for the forest was

99.67, and 98.42% for the non-forest (Table 6). Because we obtained a high accuracy, we used the output of the RF classification derived from combination with the S-2 images to calculate the forest area for the study area and the forest mask. Under these conditions, the surface covered by forest was 6,634 ha, representing 77.87% of the studied surface. Of this forest surface, 2,942 ha (44.35%) were managed by the state, while 3,692 ha (55.65%) represented private property.

3.2. Tree species classification

The results regarding the overall accuracy of the tree species classification, based on the five sets of data, are presented in Figure 3. A very close overall accuracy was obtained for three of these combinations (Datasets 3–5). The best result was obtained for Dataset 5, with an overall accuracy of 89.68%, followed by Dataset 3, with 89.51%, and Dataset 4, with 89.36% (Figure 3A). The lowest result was obtained by Dataset 1, which included only S-2 satellite images, and had an overall accuracy of 76.74%.

Evaluation of the classification performance for Dataset 5 among the individual tree species showed good results for spruce (93.82%), larch (93.44%), and fir (92.96%). These three species corresponded quite well to the forest stands. For spruce, 16 pixels were confused with beech, while for larch, 7 pixels were confused with beech, for fir, 15 pixels were confused with beech and 11 pixels with spruce (Table 7). Slightly weaker results were obtained for mixed species (86.96%) and other BL species (87.06%). For mixed species, 9 pixels were classified as beech and 33 pixels for other BL species.

The results obtained after calculating the F1 score for each tree species show that they are close for the 3–5 Dataset. Spruce is best discriminated in Dataset 3, with an F1 score equal to 0.96, while beech is best discriminated in all three data sets, with an F1 score of 0.93 (Figure 3B). As for larch, the best discrimination is in Dataset 4, as well as in the other four datasets, while F1 varies from 0.83 (Dataset 1) to 0.89 (Dataset 4). Fir is identified better in Dataset 5, with an F1 score of 0.89. Mixed species (F1 = 0.70) and other BL species (F1 = 0.73) are the two group of species with the less confidence (Figure 3B).

Based on the evaluation of the overall accuracy of the classification, we created the final map with tree species from the best combination–Dataset 5 (Figure 4).

3.3. Variable importance

The importance of the variables used in the classification of the tree species is presented in Figure 5. These were prioritized based on importance level. The DEM contributed the most toward classifying
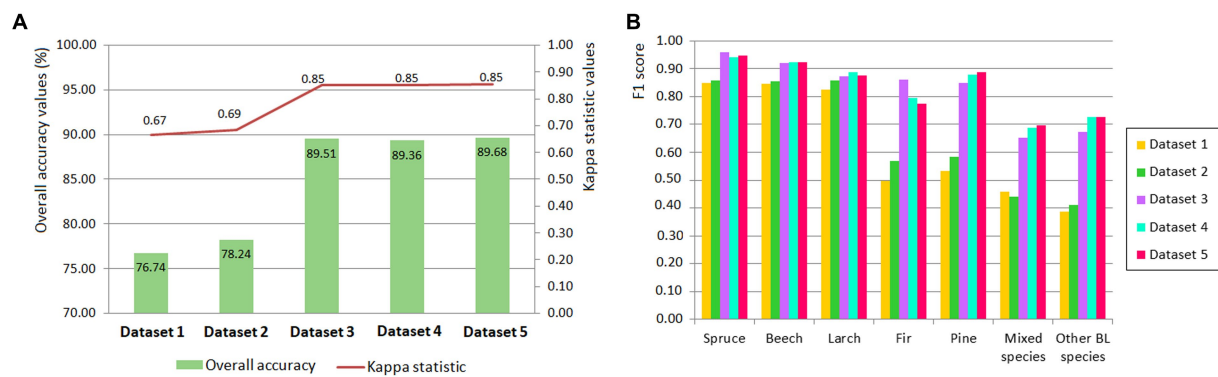
FIGURE 3
Overall accuracies and Kappa statistics for the five datasets used in tree species identification **(A)** and F1 score **(B)**.

TABLE 7 Confusion matrixs for RF classification of seven tree species inside of forest mask using dataset 5.

Reference data	Classification data							
	Classes	Spruce	Beech	Larch	Fir	Pine	Mixed species	Other BL species	Total (number of pixels)
	Spruce	**334**	16	1	2	0	0	0	353
	Beech	2	**602**	2	1	3	1	0	611
	Larch	0	7	**57**	0	0	0	1	65
	Fir	11	15	1	**65**	0	0	1	93
	Pine	4	6	0	0	**79**	0	1	90
	Mixed species	0	9	0	0	1	**40**	8	58
	Other BL species	5	33	0	2	6	5	**74**	125
Total (number of pixels)		356	688	61	70	89	46	85	**1,395**

The bold value on the main diagonal represents the pixels correctly classified in each class.

the datasets (Datasets 3–5). Together with elevation, aspect and slope proved to be the most important variables. They also determined an evident increase in the overall accuracy. With regard to the S-2 spectral bands, B12 and B11 (SWIR) were the most important contributors in separating the tree species in all the datasets. Band 8 (NIR) obtained the lowest scores in the tree datasets. The inclusion of VIs in three of the datasets, combined with the S-2 bands, DEM, and S-1 bands, did not produce a high rate when compared with DEM, aspect, and slope. The GLI and EVI indices made the highest contribution of all the VIs, while the NDVI contributed the least. Even though we used many S-1 images, their contribution to classifying the tree species was minimal.

4. Discussion

4.1. Dataset performance and variable importance

We mapped tree species using different combinations of dense S-1 and S-2 time-series images, VIs derived from optical S-2 bands, and topographic features derived from a DEM. The S-1 and S-2 images were taken in two growing seasons (2021 and 2022), allowing us to obtain detailed information about the spectral-temporal patterns of the studied species. This study was performed on an area with a heterogeneous distribution of vegetation, including both dense forests

on massifs and tree species grouped in patches of different sizes that alternated with built-up areas, pasture, and hay.

Combining the 15 S-2 images taken from the two vegetation seasons led to an overall accuracy of 76.74%. In this combination, SWIR bands (B11 and B12) had the highest importance, while B8 and B7 had the lowest (Figure 5A). The low importance of Bands B8 and B7 can be explained by the fact that many of the S-2 images were acquired during spring and autumn, not during summer, when the photosynthetic activity is strong and the reflectance in NIR is also high. However, the sun's elevation angle is low during early spring and late autumn–an effect that could lead to a decrease in the classification's accuracy (Hościło and Lewandowska, 2019).

The results regarding the overall accuracy of the tree species classification, based on the five sets of data, are presented in Figure 3. A very close overall accuracy was obtained for three of these combinations (Datasets 3–5). The best result was obtained for Dataset 5, with an overall accuracy of 89.68%, followed by Dataset 3, with 89.51%, and Dataset 4, with 89.36%. The weakest result was obtained by Dataset 1, which included only S-2 satellite images, and had an overall accuracy of 76.74%.

By including the VIs in the classification, together with the S-2 images (Dataset 2), the overall accuracy reached 78.24%, increasing by only 1.5%. This result is similar to that of Mohammadpour et al. (2022), who mentioned that a slight accuracy increase was obtained by combining four VIs with S-2 images, compared with only using spectral bands. Another study (Spracklen and Spracklen, 2019)
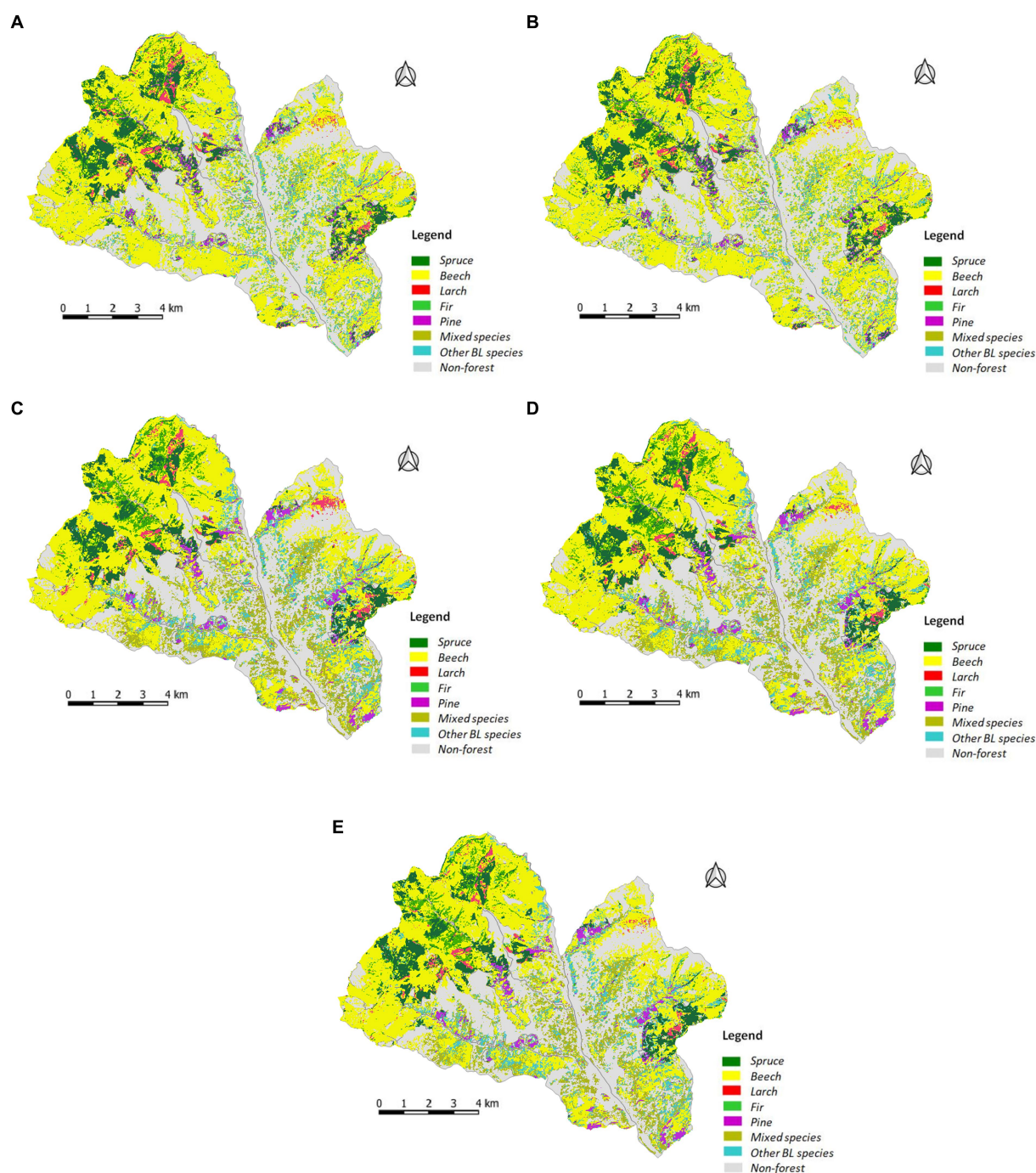
FIGURE 4
Tree species identification maps generated using RF classification for: **(A)** Dataset 1; **(B)** Dataset 2; **(C)** Dataset 3; **(D)** Dataset 4; **(E)** Dataset 5.

showed that adding six VIs to identifying European old-growth forests led to a worse performance from using them in combinations instead of the S-2 bands, resulting in the overall accuracy being reduced by 0.3%. On examining the relative importance of the variables, we can see that, in this case as well, Bands B11 and B12 were in first place, followed by the GLI and EVI. The GNDVI and NDVI contributed the least among all the indices. The low importance of the NDVI in classifying tree species has also been signaled by other studies (Pouteau et al., 2018; Silveira et al., 2018).

Choosing VIs in emphasising the vegetation phenology is important. EVI and GLI proved to be the most suitable in identifying phenological changes as they are more strongly correlated with the crown's foliage. The high separability on which it is based derives from spectral bands with blue, green and near infrared reflectance. EVI emphasises better the phenology, compared with NDVI in surfaces with both dense and sparse vegetation (Tian et al., 2021). Furthermore, Bolton et al. (2020) have shown the high two-band EVI (EVI2) capacity in emphasising the phenology of ecosystems with a strong
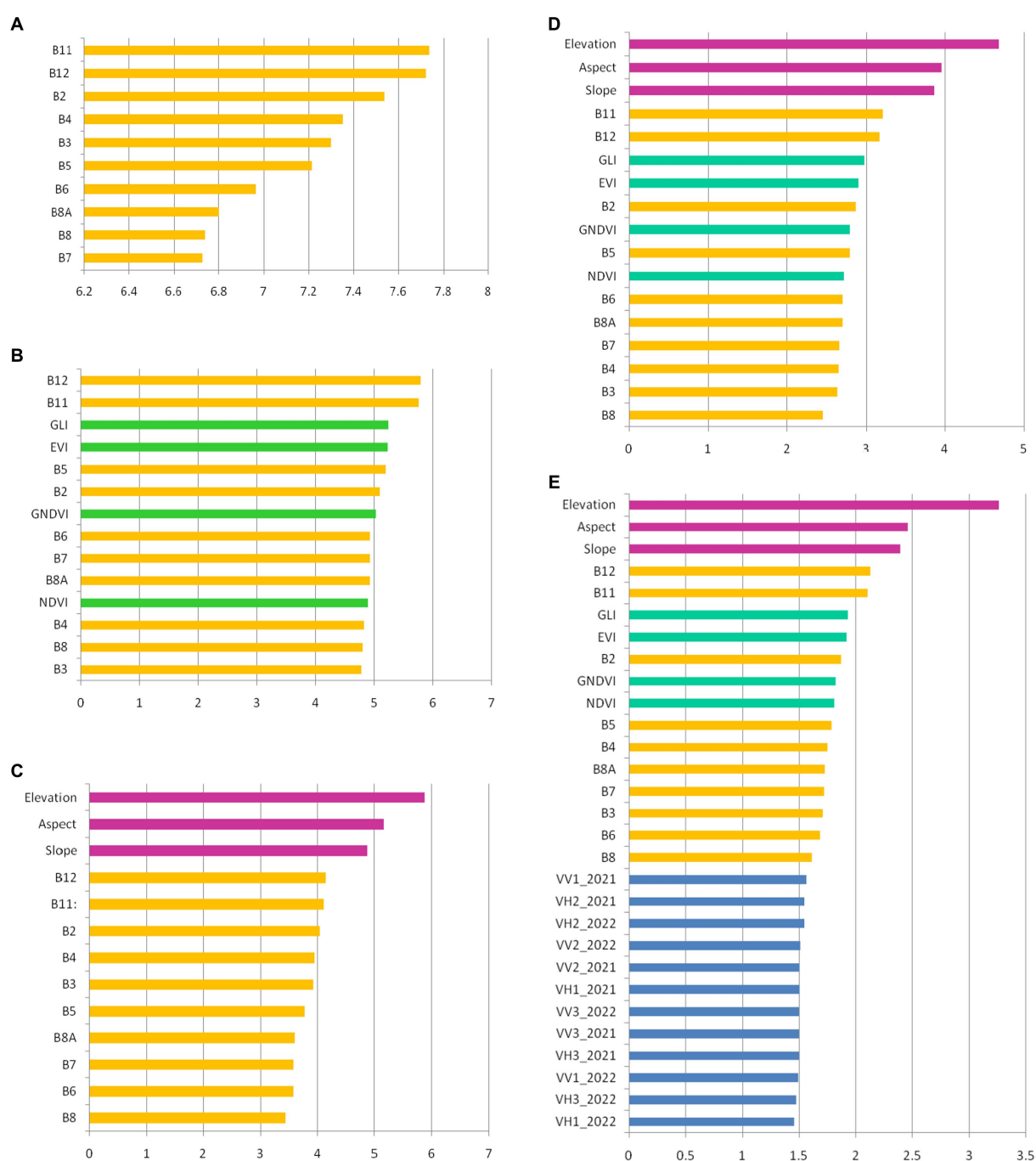
FIGURE 5
The variable importance for tree species classification: **(A)** Dataset 1 (S-2 images); **(B)** Dataset 2 (S-2 images and VIs); **(C)** Dataset 3 (S-2 images and topographic features); **(D)** Dataset 4 (S-2 images, VIs and topographic features); **(E)** Dataset 5 (S-2 images, VIs, topographic features, and S-1 images). The colors are as follows: orange – spectral bands of S-2 images; green – VIs; magenta – topographic features; blue – layer stacks of S-1 images (according Table 1).

seasonality, namely deciduous trees species, and less for those with evergreen species. The share brought by VIs in identifying resinous species was marginal because the crown is green all year long. NDVI-derived phenology is uncertain for surfaces covered with resinous trees where the seasonal amplitudes are small (Tian et al., 2021).

An important leap in overall accuracy came from adding topographic features to the S-2 images (Dataset 3), when 89.51% was obtained. The results obtained in this study are in line with those from

other studies. Hościło and Lewandowska (2019) classified eight tree species with an accuracy of 75.6% using only S-2 data. By adding a DEM, slope, and aspect, an accuracy of 81.7% was reached by classifying all species together, with 89.5% achieved for a stratified classification. In Liu et al. (2018), the importance of slope derived from a DEM was demonstrated in the classification of four common species and four mixed forests located in China. The importance of a DEM in classifying species and obtaining high accuracy has also been

reported in other studies (Waśniewski et al., 2020; Dobrinić et al., 2021). In the present study, we proved that the DEM contributed the most, followed by aspect and slope (Figure 5C). This means that the presence of species in the studied area was highly dependent on elevation.

The S-1 images, VIs, and topographic features combination (Dataset 4) decreased the accuracy by 0.15%, compared with the S-2 plus topographic features combination (Dataset 3). These results are similar to those from other studies that showed that adding the NDVI led to a decrease in accuracy of 8% (Mohammadpour et al., 2022). Other studies have shown that adding the NDVI to a combination of S-2 images and a DEM leads to a decrease in accuracy of 3% (Waśniewski et al., 2020). In the present case, the decrease in overall accuracy can be associated with a decrease in user accuracy for spruce, beech, larch, and other BL species (Figure 3).

In the S-1, S-2, VIs, and topographic features combination (Dataset 5), we obtained an overall accuracy of 89.69%. Compared with the overall accuracy resulting from combining S-2 images with topographic features (Dataset 2), the overall accuracy increased by only 0.17%, and by 0.32% compared with the S-2, VIs, and topographic features combination (Dataset 4). By analyzing the contributions of the variables, we can see that the importance of the S-1 images was minimal, even though their number was high when compared with the other variables (Figure 5E).

The results obtained from this study are very close to the ones obtained by Lechner et al. (2022), where, by adding 250 S-1 images for 14 S-2 images taken from a vegetation season, the accuracy was only 0.5%. Liu et al. (2018) demonstrated that adding backscattering features from VV images of S-1 to the combination of S-2, DEM, and Landsat 8 provided only a modest 2.65% improvement in classifying forest types, compared to the same combination without S-1. Furthermore, the additional of VV and HV features from S-1 to the combination with S-2, DEM, and Landsat 8 actually resulted in a 1.32% decrease in accuracy when compared to using the combination of S-2, DEM, and Landsat 8 alone. This indicates that VV polarization images are more effective in discriminating forest types than VH polarization data. Additionally, the fusion of S-2 with S-1 yielded only a marginal 1.5% increase in overall accuracy for forest mapping (Hirschmugl et al., 2018). In another study, it was found that using S-1 images in combination with S-2 images to distinguish between plantations and natural forests led to a slight decrease in accuracy, from 92.5% achieved using S-2 alone to 92.3% for S-1 and S-2 combination (Spracklen and Spracklen, 2021). Therefore, integrating S-1 data with S-2 did not significantly enhance accuracy and, in some cases, even resulted in a slight reduction of 0.2%. Consequently, the addition of S-1 images only marginally improves accuracy or may potentially lead to a decrease in accuracy.

Achieving only a marginal increase in accuracy through the combination of S-1 with S-2 images can be attributed to several factors. For instance, S-1 images capture data that reflect surface properties such as its structure and roughness. Lechner et al. (2022) found that within the conifer group, when separated using S-1 images, achieving satisfactory accuracy may be related to the more pronounced roughness of conifer crowns compared to those of deciduous trees. Furthermore, in comparison to the multispectral data of S-2 images, S-1 data do not provide so much detailed information about the biometric and spectral characteristics of vegetation. Additionally, S-1 images can be influenced by factors such as soil moisture and

vegetation density, which can lead to variations in captured signals and more complex data interpretation. In the study conducted by Xi et al. (2023), it is shown that the contribution of S-1 images to forest diversity estimation was found to be rather limited, possibly due to the relatively short frequency of the C-band, making it less sensitive to characterizing dense forest canopies. Moreover, C-band radar waves are strongly attenuated by tree canopies, causing intensities to be similar for plant types with subtle structural differences (Ienco et al., 2019; Slagter et al., 2020). Furthermore, physiologically similar tree species cannot be differentiated using S-1 data (Heckel et al., 2020). In such cases, the spectral response of tree species recorded in S-2 images is more valuable in distinguishing between them, with less contribution from S-1 images.

4.2. Tree species identification

The forest of the study area was divided into seven classes. Sampling data was collected by visually interpreting images and ortophotoplans, and by comparing these with Google Earth images. The sampling size was approximately 3.4% for training and 0.8% for testing from the total surface (Table 8). Dividing them in training (80%) and validation (20%) samples was made randomly, according to the code written in GEE. According to the specialty literature, the sample size was indicated to be between 0.2 and 3.0% of the total data (Blatchford et al., 2021). Therefore, the samples were sufficient for training classifiers and were relatively uniformly spread across the entire studied area.

For Dataset 1, by using only the S-2 multitemporal images, the tree species that had low user accuracy values were fir (61.54%), pine (60.00%), mixed species (62.50%), and other BL species (52.38%). By using only the S-2 images, Immitzer et al. (2016) obtained the same user accuracy for pine, while spruce reached a user's accuracy of 77%, fir 71%, and larch 64%. The discrimination capacity for these species substantially increased after adding elevation, slope, and aspect as variables to the S-2 images (Dataset 3). By adding topographic features, the most substantial increases in accuracy for the tree species were (Figure 6) 26.30% (fir), 22.29% (pine), 11.31 (mixed species), and 33.70% (other BL species). Smaller accuracy increases were observed for other tree species–spruce (11.54%), beech (9.86%), and larch (12.00%).

TABLE 8 The size of training and validation samples for each of the tree species.

Tree species	Size of training samples (ha)	Size of validation samples (ha)	Total size (training and validation) (ha)
Spruce	57.46	14.37	71.83
Beech	97.06	24.26	121.32
Larch	10.52	2.63	13.15
Fir	16.48	4.12	20.6
Pine	14.46	3.62	18.08
Mixed species	8.71	2.18	10.89
Other BL species	18.38	4.60	22.98
Total	223.07	55.78	278.85

However, using an increasing number of variables in the classification did not necessarily lead to greater accuracy for all tree species (Figure 6). This was particularly notable for spruce, larch, and other BL species when, by adding VIs in combination with S-2 images and topographic features (Dataset 3), the user accuracy decreased by 3.14, 0.19, and 1.70%, respectively (Figure 6).

Looking globally, the overall accuracy increase from 76.74% (Dataset 1) to 89.68% (Dataset 5) was resulted from increasing the discrimination capacity for fir, pine, mixed species, and other BL species. The user accuracy increases were 31.32% (fir), 28.76% (pine), 24.42% (mixed species), and 34.68% (other BL species). As has already been shown, these increases were not linear (Figure 6). In the case of spruce, by adding new bands to the classification, apart from the S-2 bands, the increase in user accuracy was 9.18%, with 9.56% for beech, and 11.5% for larch – considerably lower than for the other species. For example, the accuracy increase was 9.53% for spruce, 5.3% for beech, and 4.59% for larch. Important increases were recorded for fir (28.65%), pine (41.63%), mixed species (31.32%), and other BL species (28.64%).

At the conifer/BL level, the results showed that coniferous species were classified better than BLs. In terms of the separation of coniferous tree species, the best user's accuracy was obtained for spruce (93.82%), larch (93.44%), fir (92.96%), and pine (88.86%). Stoffels et al. (2015) obtained a user's accuracy of 91.6% for spruce, which is close to the value from the present study. Hościło and Lewandowska (2019) applied the stratified approach to the S-2 multitemporal images and topographic features, obtaining separation accuracy of 85% for spruce, 84.1% for pine, and almost 80% for larch and fir. Lower accuracy was obtained by Immitzer et al. (2012) for spruce (80.4%), pine (85.1%), larch (70.4%), and fir (82.3%) using very high spatial resolution 8-band Worldview-2 satellite data. In the case of the BLs, the highest

user's accuracy was obtained by beech (87.50%), followed by other BL species, with a user's accuracy of 87.06%, and mixed species, with 86.96%. Immitzer et al. (2016), using S-2 images, recorded a user's accuracy of 73.8% for beech and 51.4% for BL species. Hościło and Lewandowska (2019) used S-2 images and topographic features, achieving a beech user's accuracy of 92.3%.

According to the classification for which the highest overall accuracy was obtained (Dataset 5), the most widespread species in the study area were beech (56.21%), mixed species (13.30%), and spruce (10.27%). The order of decrease in the occupied surface was BLs (9.15%), fir (5.47%), pine (3.36%), and larch (2.24%; Figure 7). The obtained surfaces could not be verified because we lacked forest evidence from outside the forest management plan and for the private areas.

Mapping tree species using multitemporal data S-2 are generally based on leaf seasonality, and the main phenophases such as budburst, leaf unfolding, autumn colouring, and abscission. In the case of deciduous trees, seasonal variations in the efficiency of the photosynthetic activity are strongly emphasised during autumn, through the senescence process which is strongly connected with leaf colouring. The importance of the six S-2 images from autumn (October and November), when the leaf colouring process appeared, is crucial in separating tree species, especially deciduous trees. However, the very similar spectral signatures for beech, hornbeam, sessile oak, grey alder, sycamore maple, and European ash have led to a lower accuracy of mixed species and other BL species. This phenomenon was also emphasised by other studies (Hill et al., 2010; Pasquarella et al., 2018; Grabska et al., 2019). Furthermore, the phenological differences were difficult to capture for species characterised by very close phenological phases (for example, between beech and hornbeam). This situation was also reported by other
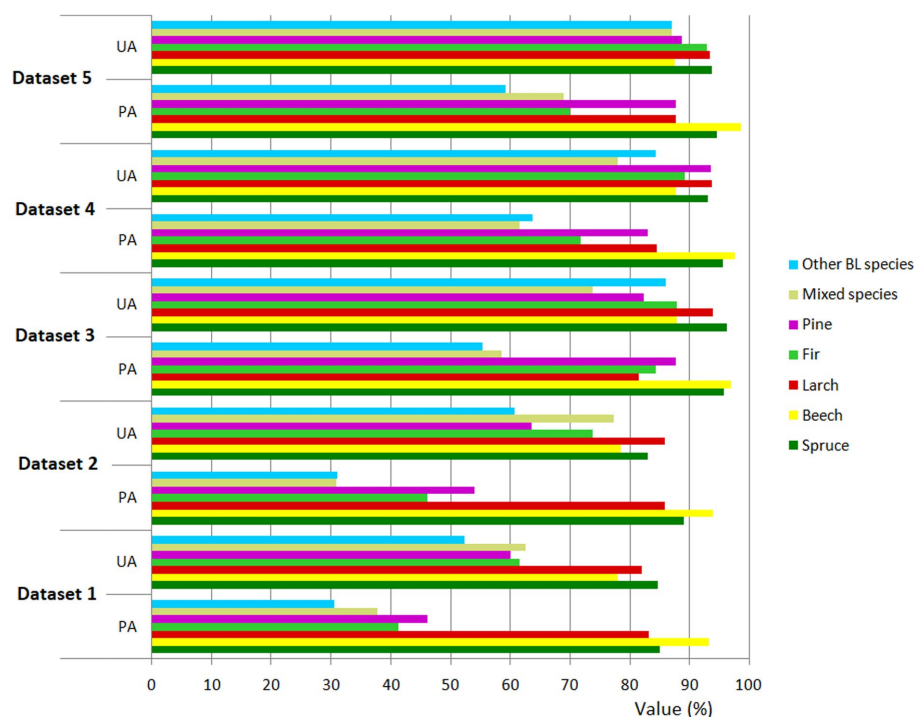
FIGURE 6
Class level accuracy assessment (producer's accuracy – PA and user's accuracy - UA) for all tree species and datasets mapped by RF classification.
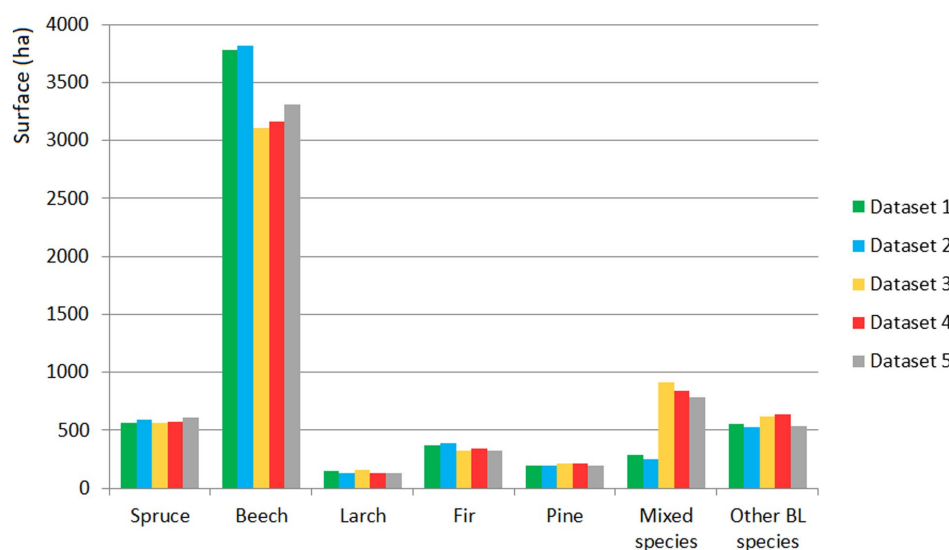
FIGURE 7
The areas occupied by tree species according to of the RF classification for the five datasets.

studies (Schieber et al., 2009). The five images used in the study and acquired during spring (April and May), are depicting tree species phenology through different moments of leaf green colouring. The species located at lower altitudes have greened faster than the ones located at higher altitudes. Both cases depend on the temperature. For example, beech foliation depended on temperatures from March, at lower altitudes and on April temperatures as the altitude increases.

The photosynthetic activity of resinous species is rather hard to quantify based on satellite images, but seasonal changes can be quantified in the visible spectra (Gamon et al., 2016). Generally speaking, the spectral behaviour of spruce and fir is similar, but differs significantly from pine, indicating a difference between the phenology of pines and other resinous species. Larch, the only resinous species from the present study, has shown a spectral signature closed to deciduous trees that increased during autumn in the visible and SWIR bands. All the other resinous did not have obvious phenological phases, but needle appearance during spring can be an indicator of growth start that can be seen on spring images.

The classification errors could have different causes. Using samples based on data from forest management plans could be one of them. Even though stand composition is established through forest inventory, disparities can occur. The small training dataset could also be the reason for some of the confusion in classifying the tree species. To some degree, this failed to provide a coherent spectral reflectance. This was the case for species such as larch and pine that were present in small percentages (10–20%) in the composition of some stands. Another cause could be the inclusion of pixels that represented other species in the samples. This was found to be the case for beech and hornbeam mixtures, oak, sycamore maple, ash, aspen, silver birch, grey alder, and black alder. These were disseminated in the stands and, because of their similar spectral behaviors, confusions appeared where the accuracy was lower for mixed and other BL species. Furthermore, obtaining samples for the same species in stands of different ages likely led to selecting some different spectral signatures. For example, beech had a very high intensity signature in some samples and a dark signature in others, leading to its classification as resinous.

4.3. Importance of tree species identification

Global change and tree species identification are interconnected topics that play a crucial role in understanding and addressing the challenges facing our planet's forests. Tree forest identification through satellite imagery and remote sensing techniques allows for continuous monitoring of forest an global scale. It is essential for monitoring changes in forest cover, understanding the distribution of tree species, and assessing the health and resilience of forests. Global change factors, such as rising temperatures, altered precipitation patterns, and increase frequency of extreme weather events, influence the growth, reproduction, and survial of tree species. Consequently, certain trees my encounter difficulties in adapting to this conditions, leading to shifts in forest composition and distribution. All the forests in the analyzed area are categorized as forests with special protection functions. Understanding the composition and distribution of tree species in such an area is crucial for ensuring the forest's functions as designated in the forest management plan.

In the context of global change, tree species identification is crucial for identifying areas that have undergone deforestation or degradation. By knowing the original species composition, efforts to restore this forests can focus on reintroducing the right tree species and promoting ecosystem resilience. In the studied area, these forests are categorized within the forest management plan as tree stands situated on rocky outcrops, scree slope, lands with deep erosion, or on terrain with a slope exceeding 35 degrees. In this way, strategies for planting and regenerating forests can be developed in accordance with the requirements of the species (Abrudan, 2006), thus preventing the negative effects of planting in unsuitable areas, such as fungal and insect attacks.

Different tree species have varying abilities to sequester carbon dioxide from the atmosphere, making tree species identification crucial for estimating carbon stocks in forests. In this sense, forests play a critical role in mitigating climate change by acting as carbon sinks, capturing and storing significant amounts of carbon (Goetz et al., 2009). Additionally, in the case of urban forests and rapid

urbanization, it is essential to investigate the role of these forests in maintaining air quality, biodiversity, and the quality of life in cites, and to develop policies for managing these changing ecosystems. This applies to the forests in the lower and middle parts of the studied area, encompassing 257.9 ha, which are designated in the forest management plan as forests with recreational and social significance.

Tree species identification is vital for conservation efforts. By knowing the tree species present in a forest, conservationists can develop targeted strategies to protect and restore specific habitats, especially those of threatened or endemic species. Certainly, within the studied area, 442.09 ha of FMU II Posada are encompassed by the Natura 2000 site ROSCI0013 Bucegi. The encountered Romanian habitat types consist of Southeastern Carpathian forests featuring spruce, beech, and fir with *Pulmonaria rubra*, as well as Southeastern Carpathian beech forests with *Symphytum cordatum*, both of which require conservation efforts. Furthermore, an additional 285.85 ha of forest serve as buffer zones for the reserves within the Bucegi Natural Park. Additionally, 94.73 ha of forests are designated as reserves for seed production and the preservation of the forest gene pool. It also aids in planning sustainable forest management practices that consider the needs of different species. By understanding changes in tree species distribution, forest managers and policymakers can adapt their strategies to address emerging challenges posed by global change. In the analyzed area, several essential activities are required to support natural regeneration, maintain an optimal mix of tree species, control invasive tree species, and manage mature forest to preserve a high level of biodiversity.

Additionally, identifying tree species on satellite images helps to identity fire-prone areas and monitor illegal logging activities. By monitoring tree species, strategies for fire risk management and effective firefighting can be developed (Jaiswal et al., 2002). Moreover, by identifying tree species through remote sensing data, the impact of human activities on forests, such as excessive logging, agricultural expansion, and urban development, can be analysed. In this way, appropriate measures for protection and ecological restoration can be taken. The analysed area also serves as a tourist destination, featuring human settlements in its central region. This necessitates vigilant monitoring of human activities within the forested areas and urban development.

Overall, tree species identification using satellite images is an essential tool for understanding the impact of global change on forests and developing effective strategies for conservation, adaptation, and sustainable management. It helps us to make informed decisions to protect and preserve our valuable forest ecosystems in the face of ongoing environmental challenges.

5. Conclusion

In this study, the performance of S-1 and S-2 images, VIs, and topographic features in various combinations were investigated as tools for tree species mapping. Seven tree species–four coniferous and three deciduous–located in a complex mountain area characterized by compact forests and forests fragmented by private property, were classified using the RF algorithm. The accuracy of the classification was compared for five different combinations (datasets) of input variables. This showed the importance of phenology, together with topographic features (elevation, aspect, and slope), in improving the performance of the RF classifier in the classification of tree species.

Using topographic features also guaranteed that a sample belonged to a particular tree species based on its precise altitudinal distribution.

Because phenology varies with species, it is important to select S-2 images that represent the phenological cycle of the studied tree species when mapping tree species. Seasonal S-2 composites have advantages over monotemporal classifications, but preference should be given to a combination of S-2 images and topographic features. Bands B11, B12, and B2 contributed the most among the S-2 bands used in this study, allowing the capturing of differences among the species during the growing season, and analyzing their temporal patterns. The S-2 satellite has numerous advantages, such as high temporal resolution and being able to provide data more frequently than other medium-resolution sensors.

Combining VIs with the S-2 images did not bring a substantial accuracy advantage, but GLI and EVI made the largest contribution. By bringing together S-1 images combined with S-2 images, VIs, and topographic features, the effect was only marginal, while the accuracy was very low. However, the results have indicated that introducing S-1 images into the classification caused a shift in the contributing features. As such, they had a more important role in classifying groups of species from BL species and mixed species. This approach has allowed us to establish that the lowest accuracy was obtained in the hill area, where there was less forest cover and more forest fragmented by private property, and around the margins of stands that contained different species. The highest accuracy was obtained from compact, pure, and homogenous stands from mountain areas, where the degree of forest coverage was very high.

Data availability statement

The original contributions presented in the study are included in the article, further inquiries can be directed to the corresponding author.

Author contributions

IV supervised and coordinated the research and wrote the manuscript. LD, CV, RGP, and CC helped with the study conception and design, performed material preparation, data collection and analysis, read and commented on previous versions of the manuscript. CLC, CIG, SC, and IG participated in data validation. All authors contributed to the article and approved the submitted version.

Acknowledgments

Conflict of interest

The authors declare that the research was conducted in the absence of any commercial or financial relationships that could be construed as a potential conflict of interest.

Publisher's note

All claims expressed in this article are solely those of the authors and do not necessarily represent those of their affiliated organizations, or those of the publisher, the editors and the reviewers. Any product that may be evaluated in this article, or claim that may be made by its manufacturer, is not guaranteed or endorsed by the publisher.

References

Abrudan, I. V. (2006). *Afforestation (in Romanian)*. Brașov: Transilvania University Publishing House.

Ballanti, L., Blesius, L., Hinnes, E., and Kruse, B. (2016). Tree species classification using hyperspectral imagery: a comparison of two classifiers. *Remote Sens.* 8, 445–463. doi: 10.3390/rs8060445

Belgiu, M., and Drăguţ, L. (2016). Random forest in remote sensing: a review of applications and future directions. *ISPRS J. Photogramm. Remote Sens.* 114, 24–31. doi: 10.1016/j.isprsjprs.2016.01.011

Bhatnagar, S., Gill, L., Regan, S., Waldren, S., and Ghosh, B. (2021). A nested drone-satellite approach to monitoring the ecological conditions of wetlands. *ISPRSJ. Photogramm. Remote Sens.* 174, 151–165. doi: 10.1016/j.isprsjprs.2021.01.012

Blatchford, M. L., Mannaerts, C. M., and Zeng, Y. (2021). Determining representative sample size for validation of continuous, large continental remote sensing data. *Int. J. Appl. Earth Obs. Geoinf.* 94:102235. doi: 10.1016/j.jag.2020.102235

Bolton, D. K., Gray, J. M., Melaas, E. K., Moon, M., Eklundh, L., and Friedl, M. A. (2020). Continental-scale land surface phenology from harmonized Landsat 8 and Sentinel-2 imagery. *Remote Sens. Environ.* 240:111685. doi: 10.1016/j.rse.2020.111685

Breiman, L. (2001). Random forest. *Mach. Learn.* 45, 5–32. doi: 10.1023/A:1010933404324

Clark, M., Roberts, D., and Clark, D. (2005). Hyperspectral discrimination of tropical rain forest tree species at leaf to crown scales. *Remote Sens. Environ.* 96, 375–398. doi: 10.1016/j.rse.2005.03.009

Copernicus (2014). *Sentinel-1 Data Access and Products* European Space Agency. Available at: https://dataspace.copernicus.eu/explore-data/data-collections/sentinel-data/sentinel-1 (Accessed March 18, 2023).

Dian, Y., Li, Z., and Pang, Y. (2014). Spectral and texture features combined for forest tree species classification with airborne hyperspectral imagery. *Indian Soc Remote Sens* 43, 101–107. doi: 10.1007/s12524-014-0392-6

Dmitriev, E. (2014). Classification of the forest cover of Tver oblast using hyperspectral airborne images. *Izv. Atmos. Ocean. Phys.* 50, 929–942. doi: 10.1134/S0001433814090072

Dobrinić, D., Gašparović, M., and Medak, D. (2021). Sentinel-1 and 2time-series for vegetation mappingusing random forest classification: a case study of northern Croatia. *Remote Sens.* 13:2321. doi: 10.3390/rs13122321

Dorren, L. K. A., Maier, B., and Seijmonsbergen, A. C. (2003). Improved landsat-based forest mapping in steep mountainous terrain using object-based classification. *For. Ecol. Manag.* 183, 31–46. doi: 10.1016/S0378-1127(03)00113-0

Dostálová, A., Lang, M., Ivanovs, J., Waser, L. T., and Wagner, W. (2021). European wide forest classification based on Sentinel-1 data. *Remote Sens.* 13:337. doi: 10.3390/rs13030337

Farreira, M. P., Zortea, M., Zanotta, D. C., Shimabukuro, Y. E., and de Souza Filho, C. R. (2016). Mapping tree species in tropical seasonal semi-deciduous forests with hyperspectral and multispectral data. *Remote Sens. Environ.* 179, 66–78. doi: 10.1016/j.rse.2016.03.021

Fassnacht, F. E., Latifi, H., Stereńczak, K., Modzelewska, A., Lefsky, M., Waser, L. T., et al. (2016). Review of studies on tree species classification from remotely sensed data. *Remote Sens. Environ.* 186, 64–87. doi: 10.1016/j.rse.2016.08.013

Forest Research and Management Institute (2013a). *Forest Management Plan of Forest Management Unit I Comarnic (in Romanian)*. Brașov, Romania: Marin Dracea, ICAS. 156 p.

Forest Research and Management Institute (2013b). *Forest Management Plan of Forest Management Unit II Posada (in Romanian)*. Brașov, Romania: Marin Dracea, ICAS. 148 p.

Fundisi, E., Tesfamichael, S. G., and Ahmed, F. (2022). A combination of Sentinel-1 RADAR and Sentinel-2 multispectral data improves classification of morphologically similar savanna woody plants. *Eur. J. Remote Sens.* 55, 372–387. doi: 10.1080/22797254.2022.2083984

Gamon, J. A., Huemmrich, K. F., Wong, C. Y. S., Ensminger, I., Garrity, S., Hollinger, D. Y., et al. (2016). A remotely sensed pigment index reveals photosynthetic phenology in evergreen conifers. *Proc. Natl. Acad. Sci.* 113, 13087–13092. doi: 10.1073/pnas.1606162113

Gitelson, A. A., Kaufman, Y. J., and Merzlyac, M. N. (1996). Use of a green channel in remote sensing of global vegetation from EOS-MODIS. *Remote Sens Environ.* 58, 289–298. doi: 10.1016/S0034-4257(96)00072-7

Goetz, S. J., Baccini, A., Laporte, N. T., Johns, T., Walker, W., Kellndorfer, J., et al. (2009). Mapping and monitoring carbon stocks with satellite observations: a comparison of methods. *Carbon Balance Manag.* 4, 1–7. doi: 10.1186/1750-0680-4-2

Grabska, E., Hostert, P., Pflugmacher, D., and Ostapowicz, K. (2019). Forest stand species mapping using the Sentinel-2 time series. *Remote Sens.* 11:1197. doi: 10.3390/rs11101197

Greșiță, C. I. (2011). Expert system used for monitoring the behaviour of hydrotechnical constructions. *REVCAD J. Geod. Cadastre* 11, 75–84.

Greșiță, C. I. (2013). *Surveying Methods to Studying the Behaviour of Dams (in Romanian)*. Iași: Tehnopress Publishing House.

Griffiths, P., Kuemmerle, T., Baumann, M., Radeloff, V. C., Abrudan, I. V., Lieskovsky, J., et al. (2014). Forest disturbances, forest recovery, and changes in forest types across the carpathian ecoregion from 1985 to 2010 based on Landsat image composites. *Remote Sens. Environ.* 151, 72–88. doi: 10.1016/j.rse.2013.04.022

Heckel, K., Urban, M., Schratz, P., Mahecha, M. D., and Schmullius, C. (2020). Predicting forest cover in distinct ecosystems: the potential of multi-source Sentinel-1 and −2 data fusion. *Remote Sens.* 12:302. doi: 10.3390/rs12020302

Hill, R. A., Wilson, A. K., George, M., and Hinsley, S. A. (2010). Mapping tree species in temperate deciduous woodland using time-series multi-spectral data. *Appl. Veg. Sci.* 13, 86–99. doi: 10.1111/j.1654-109X.2009.01053.x

Hirschmugl, M., Sobe, C., Deutscher, J., and Schardt, M. (2018). Combined use of optical and synthetic aperture radar data for REDD+ applications in Malawi. *Land* 7:116. doi: 10.3390/land7040116

Hościło, A., and Lewandowska, A. (2019). Mapping forest type and tree species on a regional scale using multi-temporal Sentinel-2 data. *Remote Sens.* 11:929. doi: 10.3390/rs11080929

Hycza, T., Stereńczak, K., and Bałazy, R. (2018). Potential use of hyperspectral data to classify forest tree species. *N. Z. J. For. Sci.* 48:18. doi: 10.1186/s40490-018-0123-9

Ienco, D., Interdonato, R., Gaetano, R., and Tong Minh, D. H. (2019). Combining Sentinel-1 and Sentinel-2 satellite image time series for land cover mapping via a multi-source deep learning architecture. *ISPRS J. Photogramm. Remote Sens.* 158, 11–22. doi: 10.1016/j.isprsjprs.2019.09.016

Immitzer, M., Atzberger, C., and Koukal, T. (2012). Tree species classification with random Forest using very high spatial resolution 8-band WorldView-2 satellite data. *Remote Sens.* 4, 2661–2693. doi: 10.3390/rs4092661

Immitzer, M., Vuolo, F., and Atzberger, C. (2016). First experience with Sentinel-2 data for crop and tree species classifications in Central Europe. *Remote Sens.* 8:166. doi: 10.3390/rs8030166

Jaiswal, R. K., Mukherjee, S., Raju, K. D., and Saxena, R. (2002). Forest fire risk zone mapping from satellite imagery and GIS. *Int. J. Appl. Earth Obs. Geoinf.* 4, 1–10. doi: 10.1016/S0303-2434(02)00006-5

Karasiak, N., Sheeren, D., Fauvel, M., Willm, J., Dejoux, J.-F., and Monteil, C. (2017). "Mapping tree species of forests in Southwest France using Sentinel-2 image time series" in IEEE (Ed.) *In Proceedings of the 9th International Workshop on the Analysis of Multitemporal Remote Sensing Images (MultiTemp)* (Belgium: Brugge), 27–29.

Lawrence, R. L., Wood, S. D., and Sheley, R. L. (2006). Mapping invasive plants using hyperspectral imagery and Breiman cutler classifications (random Forest). *Remote Sens. Environ.* 100, 356–362. doi: 10.1016/j.rse.2005.10.014

Lechner, M., Dostálová, A., Hollaus, M., Atzberger, C., and Immitzer, M. (2022). Combination of Sentinel-1 and Sentinel-2 data for tree species classification in a central European biosphere reserve. *Remote Sens.* 14:2687. doi: 10.3390/rs14112687

Liu, X., Frey, J., Munteanu, C., Still, N., and Koch, B. (2023). Mapping tree species diversity in temperate montane forests using Sentinel-1 and Sentinel-2 imagery and topography data. *Remote Sens. Environ.* 292:113576. doi: 10.1016/j.rse.2023.113576

Liu, Y. A., Gong, W. S., Hu, X. Y., and Gong, J. Y. (2018). Forest type identification with random Forest using sentinel-1A, sentinel-2A, multi-temporal Landsat-8 and DEM data. *Remote Sens.* 10:946. doi: 10.3390/rs10060946

Madonsela, S., Cho, M. A., Mathieu, R., Mutanga, O., Ramoelo, A., Kaszta, Z., et al. (2017). Multi-phenology WorldView-2 imagery improves remote sensing of savannah tree species. *Int. J. Appl. Earth Obs. Geoinf.* 58, 65–73. doi: 10.1016/j.jag.2017.01.018

Mickelson, J. G., Civco, D. L., and Silander, J. A. (1998). Delineating forest canopy species in the northeastern United States using multi-temporal TM imagery. *Photogramm. Eng. Remote. Sens.* 64, 891–904.

Mohammadpour, P., Viegas, D. X., and Viegas, C. (2022). Vegetation mapping with random Forest using sentinel 2 and GLCM texture feature - a case study for Lousã region, Portugal. *Remote Sens.* 14:4585. doi: 10.3390/rs14184585

Pasquarella, V. J., Holden, C. E., and Woodcock, C. E. (2018). Improved mapping of forest type using spectral-temporal Landsat features. *Remote Sens. Environ.* 210, 193–207. doi: 10.1016/j.rse.2018.02.064

Peerbhay, K. Y., Mutanga, O., and Ismail, R. (2013). Commercial tree species discrimination using airborne AISA eagle hyperspectral imagery and partial least squared discriminant analysis (PLS-DA) in KwaZulu-Natal - South Africa. *Remote Sens.* 79, 19–28. doi: 10.1016/j.isprsjprs.2013.01.013

Persson, M., Lindberg, E., and Reese, H. (2018). Tree species classification with multi-temporal Sentinel-2 data. *Remote Sens.* 10:1794. doi: 10.3390/rs10111794

Pouteau, R., Gillespie, T. W., and Birnbaum, P. (2018). Predicting tropical tree species richness from normalized difference vegetation index time series: the devil is perhaps not in the detail. *Remote Sens.* 10:698. doi: 10.3390/rs10050698

Richter, R., Reu, B., Wirth, C., Doktor, D., and Vohland, M. (2016). The use of airborne hyperspectral data for tree species classification in a species-rich central European forest area. *Int. J. Appl. Earth Obs. Geoinf.* 52, 464–474. doi: 10.1016/j.jag.2016.07.018

Rüetschi, M., Schaepman, M., and Small, D. (2017). Using multitemporal Sentinel-1 C-band backscatter to monitor phenology and classify deciduous and coniferous forests in northern Switzerland. *Remote Sens.* 10:55. doi: 10.3390/rs10010055

Schieber, B., Janík, R., and Snopková, Z. (2009). Phenology of four broad-leaved forest trees in a submountain beech forest. *J. For. Sci.* 55, 15–22. doi: 10.17221/51/2008-JFS

Schmitt, U., and Ruppert, G. S. (1996). Forest classification of multitemporal mosaicked satellite images. *Int. Arch. Photogramm. Remote Sens.* 31, 602–605.

Sedliak, M., Sačkov, I., and Kulla, L. (2017). Classification of tree species composition using a combination of multispectral imagery and airborne laser scanning data. *Cent. Eur. For.* 63, 1–9. doi: 10.1515/forj-2017-0002

Silveira, E. M. O., Bueno, I. T., Acerbi, F. W., Mello, J. M., Scolforo, J. R. S., and Wulder, M. A. (2018). Using spatial features to reduce the impact of seasonality for detecting tropical forest changes from Landsat time series. *Remote Sens.* 10:808. doi: 10.3390/rs10060808

Slagter, B., Tsendbazar, N. E., Vollrath, A., and Reiche, J. (2020). Mapping wetland characteristics using temporally dense Sentinel-1 and Sentinel-2 data: a case study in the St. Lucia wetlands, South Africa. *Int. J. Appl. Earth Obs. Geoinf.* 86:102009. doi: 10.1016/j.jag.2019.102009

Sonobe, R., Yamaya, Y., Tani, H., Wang, X., Kobayashi, N., and Mochizukie, K. (2018). Crop classification from Sentinel-2 derived vegetation indices using ensemble learning. *J. Appl. Remote. Sens.* 12:026019. doi: 10.1117/1.JRS.12.026019

Spracklen, B. D., and Spracklen, D. V. (2019). Identifying european old-growth forests using remote sensing: a study in the Ukrainian Carpathians. *Forests* 10:127. doi: 10.3390/f10020127

Spracklen, B., and Spracklen, D. V. (2021). Synergistic use of Sentinel-1 and Sentinel-2 to map natural forest and acacia plantation and stand ages in north-Central Vietnam. *Remote Sens.* 13:185. doi: 10.3390/rs13020185

Stoffels, J., Hill, J., Sachtleber, T., Mader, S., Buddenbaum, H., Stern, O., et al. (2015). Satellite-based derivation of high-resolution forest information layers for operational forest management. *Forests* 6, 1982–2013. doi: 10.3390/f6061982

Stych, P., Jerabkova, B., Lastovicka, J., Riedl, M., and Paluba, D. (2019). A comparison of WorldView-2 and Landsat 8 images for the classification of forests affected by bark beetle outbreaks using a support vector machine and a neural network: a case study in the Sumava mountains. *Geosciences* 9:396. doi: 10.3390/geosciences9090396

Tereșneu, C. C. (2019). *Computer Aided Graphics (in Romanian)*. Brașov: Transilvania University Press.

Tereșneu, C. C., Clinciu, I., Vasilescu, M. M., and Biali, G. (2016). Using the GIS tools for a sustainable forest management. *Environ. Eng. Manag. J.* 15, 461–472. doi: 10.30638/eemj.2016.049

Tian, F., Cai, Z., Jin, H., Hufkens, K., Scheifinger, H., Tagesson, T., et al. (2021). Calibrating vegetation phenology from Sentinel-2 using eddy covariance, PhenoCam, and PEP725 networks across Europe. *Remote Sens. Environ.* 260:112456. doi: 10.1016/j.rse.2021.112456

Townshend, J. R., Masek, J. G., Huang, C., Vermote, E. F., Gao, F., Channan, S., et al. (2012). Global characterization and monitoring of forest cover using Landsat data: opportunities and challenges. *Int. J. Digit. Earth* 5, 373–397. doi: 10.1080/17538947.2012.713190

Tudoran, G. M. (2013). Regulations regarding the management of forests included in natural protected areas. Bulletin of the Transilvania University of Brașov, series II: forestry. *Wood. Industry. Agric. Food Eng.* 55, 35–38.

Tudoran, G. M., and Zotta, M. (2020). Adapting the planning and management of Norway spruce forests in mountain areas of Romania to environmental conditions including climate change. *Sci. Total Environ.* 698:133761. doi: 10.1016/j.scitotenv.2019.133761

Udali, A., Lingua, E., and Persson, H. J. (2021). Assessing forest type and tree species classification using Sentinel-1 C-band SAR data in southern Sweden. *Remote Sens.* 13:3237. doi: 10.3390/rs13163237

Vihervaara, P., Auvinen, A.-P., Mononen, L., Törmä, M., Ahlroth, P., Anttila, S., et al. (2017). How essential biodiversity variables and remote sensing can help national biodiversity monitoring. *Glob. Ecol. Conserv.* 10, 43–59. doi: 10.1016/j.gecco.2017.01.007

Wang, D., Wan, B., Qiu, P., Su, Y., Guo, Q., Wang, R., et al. (2018). Evaluating the performance of Sentinel-2, Landsat 8 and Pléiades-1 in mapping mangrove extent and species. *Remote Sens.* 10:1468. doi: 10.3390/rs10091468

Waser, L. T., Rüetschi, M., Psomas, A., Small, D., and Rehush, N. (2021). Mapping dominant leaf type based on combined Sentinel-1/−2 data - challenges for mountainous countries. *ISPRS J. Photogramm. Remote Sens.* 180, 209–226. doi: 10.1016/j.isprsjprs.2021.08.017

Waśniewski, A., Hościło, A., Zagajewski, B., and Moukétou-Tarazewicz, D. (2020). Assessment of Sentinel-2 satellite images and random Forest classifier for rainforest mapping in Gabon. *Forests* 11:941. doi: 10.3390/f11090941

Wessel, M., Brandmeier, M., and Tiede, D. (2018). Evaluation of different machine learning algorithms for scalable classification of tree types and tree species based on Sentinel-2 data. *Remote Sens.* 10:1419. doi: 10.3390/rs10091419

Xi, Y., Zhang, W., Brandt, M., Tian, Q., and Fensholt, R. (2023). Mapping tree species diversity of temperate forests using multi-temporal Sentinel-1 and -2 imagery. *Sci. Remote Sens.* 8:100094. doi: 10.1016/j.srs.2023.100094

Xie, B., Cao, C., Xu, M., Duerler, R. S., Yang, X., Bashir, B., et al. (2021). Analysis of regional distribution of tree species using multi-seasonal Sentinel-1 & 2 imagery within Google earth engine. *Forests* 12:565. doi: 10.3390/f12050565

Xie, Y., Sha, Z., and Yu, M. (2008). Remote sensing imagery in vegetation mapping: a review. *J. Plant Ecol.* 1, 9–23. doi: 10.1093/jpe/rtm005

Check for updates

Response of radial growth of *Pinus sylvestris* var. *mongolica* of different stand ages to climate and extreme drought events in the semi-arid region of western Liaoning, Northeast China

Ping Liu[1,2], Shiyu Hu[1,2], Hongxu Wei[3], Wenting He[1,2], Yiming Zhou[1,2] and Yutao Wang[1,2]*

[1]College of Forestry, Shenyang Agricultural University, Shenyang, China, [2]Key Laboratory for Silviculture of Liaoning Province, Shenyang Agricultural University, Shenyang, China, [3]Northeast Institute of Geography and Agroecology, Chinese Academy of Sciences, Changchun, China

The frequency and severity of drought events are increasing under a changing climate, trees of different stand ages respond differently to drought events, which has a great impact on the stability of forest ecosystems. In this study, we measured radial growth (RG) in cored trees from 49 forests including young stands (20–30a) and middle-aged stands (31–50a) of *Pinus sylvestris* var. *mongolica* plantations in a semi-arid area of western Liaoning, China. We evaluated the response of RG of *P. sylvestris* to long-term climate, and calculate three response indicators: resistance (Rt), recovery (Rc) and resilience (Rs), so as to measure the growth response of trees to drought events. Results showed that a negative correlation was detected between RG of young stands and the monthly highest temperature (MHT) in April and May. Positive correlations were found between RG of young stands and the monthly lowest temperature (MLT) across periods from September to November, when RG of young stands was also positively correlated with Palmer Drought Severity Index (PDSI) across whole-years. There was a positive correlation between RG of middle-aged stands and MLT in September, and PDSI from June to December. After the first drought event, most pine trees recovered their RG (Rc > 1, Rs > 1). However, after three consecutive drought events, Rt, Rc, and Rs of pine trees decreased significantly ($p < 0.05$), and Rt and Rs were less than 1. In summary, younger pine trees are more sensitive to climate change, and spring drought is more inhibitory to growth of pine trees than high summer temperatures. Pine trees have a compensation effect after experiencing drought events, but the cumulative effect of multiple drought events will gradually offset the compensation effect of trees and eventually decline in pine tree growth, while the resistance and resilience of young stands after continuous drought events were significantly lower than those of middle-aged stands, and have a higher risk of death.

1. Introduction

In recent decades, with global warming, drought events have become more frequent and drought severity has increased (Allen et al., 2010; Field et al., 2012), which has become a serious challenge for forest ecosystems (Bolte et al., 2009; Lindner et al., 2010). Studies have shown that forests are adaptive to drought events and can achieve self-regulation within the corresponding range (Adams, 2009; Lloret et al., 2011; Longo et al., 2018). However, extreme drought events beyond the range of adaptation can affect tree survival and thus the productivity and biodiversity of forest ecosystems (Bolte et al., 2009; van Mantgem et al., 2009; Allen et al., 2010). Therefore, an accurate assessment of the adaptability of trees to drought events is helpful for understanding and predicting the survival risk of forests under future climate change, which is of great importance for maintaining sustainable forest management (Oliver et al., 2015).

Dendrochronology is an important method for studying the response of tree radial growth (RG) to climate change with temporal certainty and annual continuity (Martín-Benito et al., 2008; Fritts, 2012). Studies have shown that temperature and precipitation are important drivers of tree growth. In both tropical and cold regions, low temperature in winter, rainfall during the growing season, and snowfall in winter promote tree growth (Bigelow et al., 2014; Yuanqiao et al., 2021; Jing et al., 2022; Ning et al., 2023). High summer temperatures often have a significant inhibitory effect on RG of trees (Gantois, 2022; Jing et al., 2022). To quantify the response of RG to climate change, Lloret et al. (2011) proposed three indicators resistance (Rt), recovery (Rc) and resilience (Rs) to evaluate the tolerance of trees to drought events. Studies have shown that forests with low stand density have stronger resistance and recovery to drought events than forests with high stand density, and reducing stand density contributes to tree growth (Hollunder et al., 2021; Ovenden et al., 2021). Trees in different ecological environments respond differently to drought events. Compared to arid areas, trees in humid areas generally grow better and recover faster (Gazol et al., 2017; Longo et al., 2018). The Rt, Rc, and Rs of different tree species to drought events also differ (Zang et al., 2014; Vitali et al., 2017), but there is still controversy about the response of the same tree species of different sizes to drought events: Some studies have found that large trees have a poor recovery capacity, while small trees have a stronger adaptability to dry environments (Pretzsch et al., 2018; Trugman et al., 2018), but other studies have shown that small trees are more susceptible (Colangelo et al., 2017; Versace et al., 2022). Age, as an important ecological indicator of forest community structure, affects the growth status of trees and the assessment of forest ecosystems (Law et al., 2001; Song and Woodcock, 2003; Tang et al., 2017). Trees of different ages respond differently to drought events and also affect the stability of forest ecosystems. The high mortality of small trees is likely to alter the trajectory of ecosystem succession, while the high mortality of large trees will disrupt the balance of the ecosystem (Lucas-Borja et al., 2021). In addition, some studies have found that some trees recover quickly after experiencing drought events and even exceed the original growth level, but some trees cannot recover to the previous growth level and are still affected by the legacy effect of drought events for a long time (Serra-Maluquer et al., 2018; Kannenberg et al., 2019). The ability of trees to recover quickly from drought events has a significant impact on forest ecosystems.

In order to prevent and control dust storms, soil desertification, soil erosion, etc., China started to implement the Three-North Shelter Forest Program in the late 1970s (Zhang et al., 2016). *Pinus sylvestris* has become one of the main afforestation tree species in the shelter forest due to its excellent characteristics of cold resistance, drought resistance, barren resistance, suitable sandy soil and fast growth. Zhanggutai Town, Zhangwu County, western Liaoning Province, is the first area in China to introduce *P. sylvestris*, and it is also the most important experimental demonstration base for sand-fixing afforestation of *P. sylvestris* (Yuzhang, 1990). After that, the introduction area of *P. sylvestris* continued to expand southward and westward, covering the entire "Three North" project area. Therefore, whether the widely planted *P. sylvestris* plantation can grow healthily directly affects the effectiveness of afforestation, windbreak and sand fixation in western Liaoning. As a typical semi-arid area in China, western Liaoning may face more severe climate challenges in the future, and trees will be exposed to multiple drought events (Allen et al., 2010; Zuidema et al., 2022). Therefore, it is very important to explore the response characteristics of *P. sylvestris* plantations of different stand ages to climatic factors, and to study the response ability of *P. sylvestris* of different stand ages to continuous multiple drought events. It is conducive to maintaining the stability of forest ecosystems in the context of climate change, improving forest management and forecasting, and understanding forest dynamics in the context of future global change.

In this study, *P. sylvestris* plantations in the semi-arid area of western Liaoning were taken as the research object, and the long-term climate change and sudden extreme drought events were combined to evaluate the differences in growth dynamic characteristics of *P. sylvestris* plantations at different stand ages under different climatic conditions. We hypothesized that: (1) RG of *P. sylvestris* in different age stands responds differently to climatic factors; (2) drought events have legacy effect and cumulative effect; (3) the Rt, Rc and Rs of *P. sylvestris* in different age stands were significantly different.

2. Materials and methods

2.1. Study sites

The study area is located in Zhangwu County, Liaoning Province, in the southeastern edge of Khorchin Sandy Land, which is a typical semi-arid area. The geographical location is between 121° 53 'and 122° 58 'east longitude, 42° 07 'and 42° 51 'north latitude, with an average altitude of 255 m. The main feature of the landform is that the dunes overlap each other, and there are wind erosion lowlands between the hills. It belongs to the temperate continental monsoon climate, and the main climate characteristics are drought and wind. The representative plants are *Pinus sylvestris*, *Pinus tabuliformis, Ulmus pumila*, etc. The meteorological data of the last decades show that the extreme lowest temperature is −36.3°C, the extreme highest temperature is 38.4°C, and the average annual temperature is 7.93°C. The hottest season appears in July, with an average temperature of 24.2°C. The coldest month is January, with an average temperature of −11.5°C (Figure 1). The average annual precipitation is 570.8 mm, the maximum annual precipitation is 1,390 mm, and the minimum annual precipitation is 295.1 mm. The seasonal distribution of precipitation is uneven, and the annual precipitation is concentrated in June, July and August. There is less snow in winter, spring precipitation is low, and spring drought is common (Figure 2).

2.2. Field sampling and sample processing

2.2.1. Sample plot selection and annual ring sample collection

The sample plot of *P. sylvestris* artificial shelter forest is located in the experimental forest farm of Shenyang Agricultural University in Aer Township, Zhangwu County. According to the National Forestry Administration (2017), in the artificial shelter forest of *P. sylvestris*,
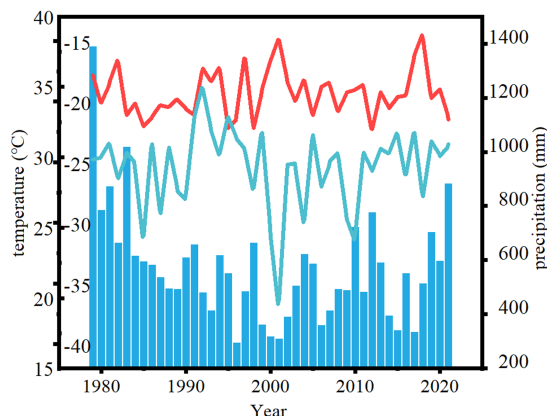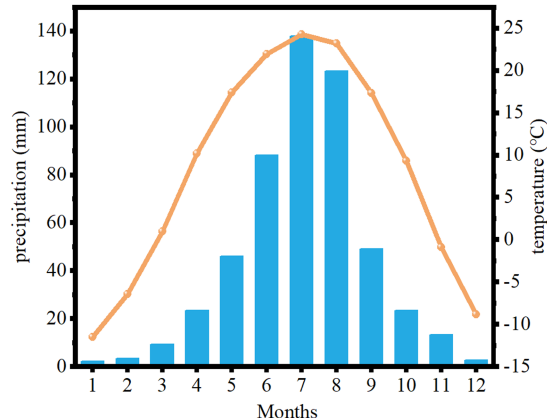
young stands (≤ 30a) and middle-aged stands (31a~50a) with basically the same site conditions (Supplementary Table S1), the dominant trees with straight trunks, no pests and diseases, no scars, and good growth were selected. The diameter at breast height, tree height, and crown width of each tree were measured by breast height rule, height meter, and tape measure (Table 1). To study RG of tree rings, we used an increment borer with a diameter of 5.15 mm to drill two tree cores at breast height (1.3 m) of each tree. When drilling, the increment borer is perpendicular to the trunk, avoiding trunk deformation and depression, and only the core without breakage is retained.

2.2.2. Tree-ring sample treatment and determination

The tree core was loaded into a special plastic tube, numbered, and returned to the laboratory. In the laboratory, the tree core was fixed in a wooden trough with white emulsion and paper tape for natural air drying. After air drying, the tree rings were polished in the laboratory with 240, 320, 400, and 600 mesh sandpaper in turn in the laboratory until the bright and clear tree ring contour could be seen under the microscope. The polished tree ring was placed under the microscope for preliminary marking and dating. Then the width of each annual ring is measured with a LINTAB. Six measuring instrument with an accuracy of 0.001 mm. Finally, the COFECHA software was used to check and correct the measurement and dating results in order to ensure the accuracy of the dating, to remove the sequence of poor quality, and finally 98 cores were kept, including 38 in the young stands and 60 in the middle-aged stands.

To eliminate the influence of the trees' own physiological factors, we used negative exponential curve or linear regression to fit the growth trend of the trees and detrend the ring-width series in the ARSTAN program, and the mean standard chronologies for each age stand were calculated as the bi-weight robust mean of the detrended individual series. Finally, the standard chronology of each age stand was obtained and used to analyze the response of stand growth to climate. Express population signal (EPS) values of the two stand ages were greater than 0.85, mean sensitivity (MS)of young stands and middle-aged stands were 0.211 and 0.208, respectively. And serial correlation were 0.505 and 0.449, respectively. In addition, to more accurately quantify the growth of individual *P. sylvestris*, we used the tree-ring width to calculate the basal area increment (BAI) of each sample tree to better analyze the response of its RG to extreme drought events. The calculation formula is as follows:

$$BAI\left(cm^2\right) = \pi\left(R_t^2 - R_{t-1}^2\right)$$

In the formula, R_t and R_{t-1} are the radius of the tree corresponding to year t and year t-1, respectively. The tree radius is calculated from the tree-ring width.

TABLE 1 Basic information of *Pinus sylvestris* var. *mongolica* in different agestands.

Stands	Number of sample trees (trees)	Number of sample cores (trees)	Mean diameter (cm)	Mean tree height (m)	Mean crown width (m)
Young stands	19	38	25.62	8.44	7.77
Middle-aged stands	30	60	29.23	10.43	8.10
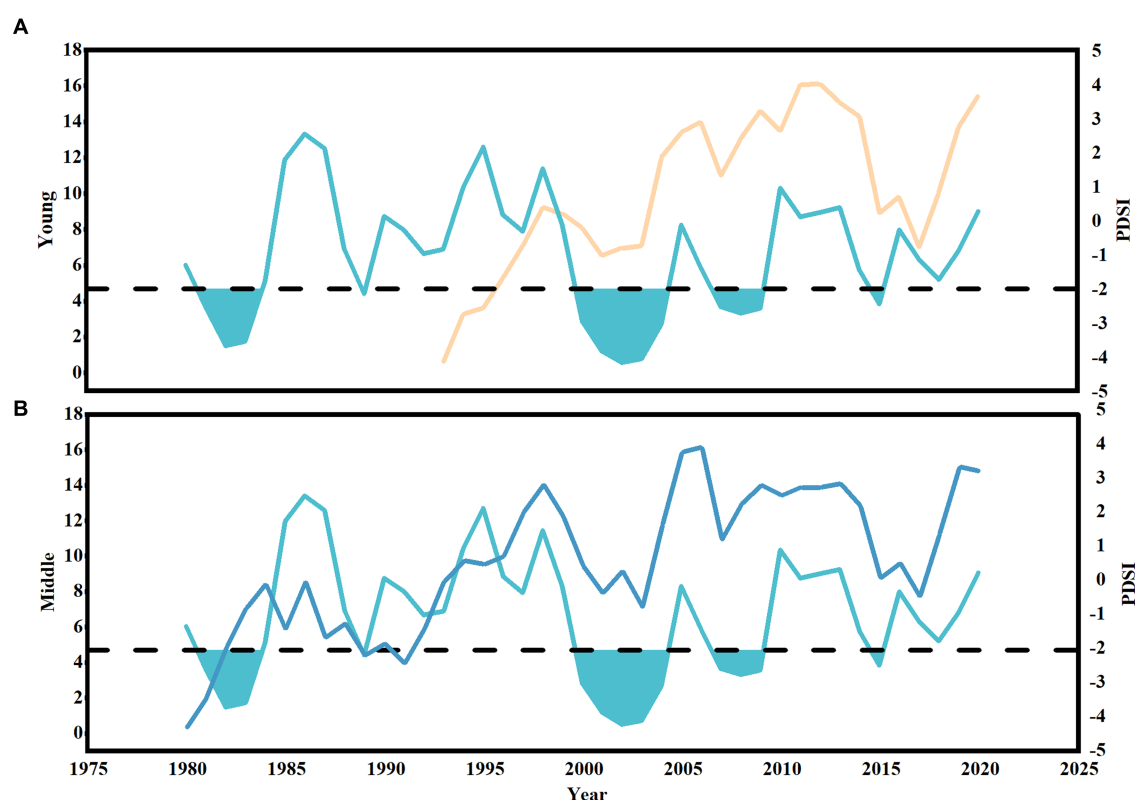
FIGURE 3
Drought event screening. The changes of BAI growth and annual average Palmer Drought Severity Index (PDSI) with time in young stands **(A)** and middle-aged stands **(B)**. The yellow and dark blue lines represent the annual BAI growth of young and middle-aged *Pinus sylvestris* var. mongolica, respectively. The light blue line represents the annual average PDSI value change, and the blue filling part is the year of drought event.

2.3. Climate data

The daily lowest temperature, daily highest temperature, daily average temperature and daily precipitation data were obtained from the Zhangwu County Meteorological Bureau (42 ° 38 'N, 122 ° 55 'E) closest to the sampling site. In addition, the Palmer Drought Severity Index (PDSI) grid data are obtained using the data sharing network[1] of the KNMI Climate Explorer. PDSI data set is CRU self-calibrated data with a spatial resolution of $0.5° \times 0.5°$. Compared to other drought indices, PDSI takes into account temperature, precipitation, soil moisture, and water evaporation (Palmer, 1965). Since it was proposed by Palmer in 1965, it has been used as one of the most widely used indices for the study and detection of meteorological drought (Sun et al., 2012; Yan et al., 2014; Smerdon et al., 2015). In order to analyze the differences in the response of growth of *P. sylvestris* plantations of different stand ages to climate, this paper selected the public period of growth of *P. sylvestris* plantations for growth-climate response analysis, that is, 1980–2021.

2.4. Identification of drought events

In order to exclude the reduction in tree growth caused by non-drought and to more accurately select drought events,

we combined PDSI with the trend of change in tree basal area growth. We define that if the annual average PDSI is moderate drought and below (Supplementary Table S2), and the BAI of trees has a significant downward trend, the year is a drought year, that is, a drought event (Figures 3A,B), and defined drought events lasting more than 2 years as extreme drought events. Finally, the drought events in the study area since the 1980s were determined to be 1981, 1982, 1983, 1989, 2000, 2001, 2002, 2003, 2004, 2007, 2008, 2009, and 2015 (Figures 3A,B). In order to compare the drought events of different stand ages in the same period, the drought years 2000, 2001, 2002, 2003, 2004, 2007, 2008, 2009, and 2015 were selected during the public period of young and middle-aged stands. In fact, after the severe spring, summer, fall and winter drought in 2000, the study area was still a four-season continuous drought in 2001, 2002, 2003, and 2004. Therefore, 2000–2004 was considered as an extreme drought event for 60 consecutive months, and 2007, 2008 and 2009 were also extreme drought events for 36 consecutive months. Therefore, three drought events (2000–2004, 2007–2009, 2015) occurred in the last 20 years (2000–2020) during the growth of trees in the study area were selected for the study (Figures 3A,B).

2.5. Resistance, recovery and resilience indices

Following the method of Lloret et al. (2011), we quantified the response of RG of trees of different stand ages to drought stress in

1 http://climexp.knmi.nl/
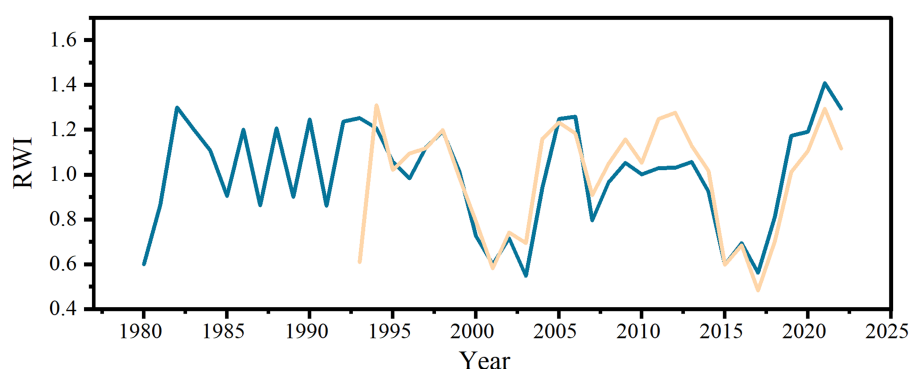
FIGURE 4
Change of ring-width index (RWI) of young and middle-aged stands The yellow line represents the RWI of young stands, and the blue line represents the RWI of middle-aged stands.

different indicators: Rt, Rc and Rs. The calculation formula is as follows:

$$Rt = G_d \, / \, G_{prev}$$

$$Rc = G_{post} \, / \, G_d$$

$$Rs = G_{post} \, / \, G_{prev}$$

Among them, G_{prev} and G_{post} are the BAI of trees in 3 years before and after the drought event, G_d is the BAI in the drought year, and if the drought event exceeds 1 year, it is the average BAI during the drought event. Rt quantifies the intensity of tree growth inhibition in the drought event (G_d) relative to the predrought event (G_{prev}). The higher the value, the stronger the resistance of trees. When Rt = 1, it indicates that the drought event does not limit the growth of trees. Rt > 1 indicates that the growth of trees in drought years is better than in non-drought years, and the resistance of trees is strong. Rt < 1 indicates that tree growth decreases during drought events. Rc is defined as the ratio of the BAI of trees after the drought event (G_{post}) to that in the year of the drought event (G_d). Rc = 1 means that trees grow normally after the drought event and are not affected. Rs is defined as the ratio of tree growth after the drought event (G_{post}) to that in the year before the drought event (G_{prev}). Rs = 1 indicates that trees are not affected by drought events and return to their original growth level. Rs > 1 indicates that the growth rate of trees exceeds the growth rate before drought events and that tree resilience is strong. Rs < 1 indicates that trees do not return to the growth level before drought events (Lloret et al., 2011). Considering the 'legacy effect' of trees after drought, the reference period before and after drought was set to 3 years in this study. All these indicators were calculated at the individual tree level.

2.6. Statistical analyses

Pearson correlation analysis was used to test the correlation between the ring-width index (RWI) of *P. sylvestris* and climatic factors

(monthly lowest temperature, MLT; monthly highest temperature, MHT; monthly average temperature, MAT; monthly precipitation; monthly PDSI). Considering the lag effect of climate, the climate data of the previous year and the current year were selected. Single factor analysis of variance and significance test were used to compare the differences in resistance, recovery, resilience among different ages of stands of *P. sylvestris.* All statistical analysis levels: α = 0.05. All statistical analyses were performed using SPSS Statistics 26.

3. Results

3.1. Ring width index of different stand ages

Ring width index (RWI) represents the growth of tree rings. It can be seen from Figure 4 that the RWI of young and middle-aged stands are basically the same from 1995 to 2021. The RWI of the two ages of stands decreased significantly in 2000–2004, 2007–2009, 2015 and 2018, indicating that RG of *P. sylvestris* plantation may be affected by extreme climate change.

3.2. Relationship between RWI of *Pinus sylvestris* in different stand ages and climate

The RWI of young stands was positively correlated with MLT in November of the previous year and September–November of the current year (Figure 5A), and negatively correlated with MHT in September of the previous year, April and May of the current year (Figure 5B). It was positively correlated with precipitation in August of the previous year, July and November of the current year (Figure 5D), and positively correlated with PDSI in 12 months of the current year (Figure 5E). The RWI of the middle-aged stands was positively correlated with MLT in October of the previous year (Figure 5A), but not correlated with MHT (Figure 5B). It was negatively correlated with precipitation in December of the previous year (Figure 5D), and positively correlated with PDSI from June to December of the current year (Figure 5E).
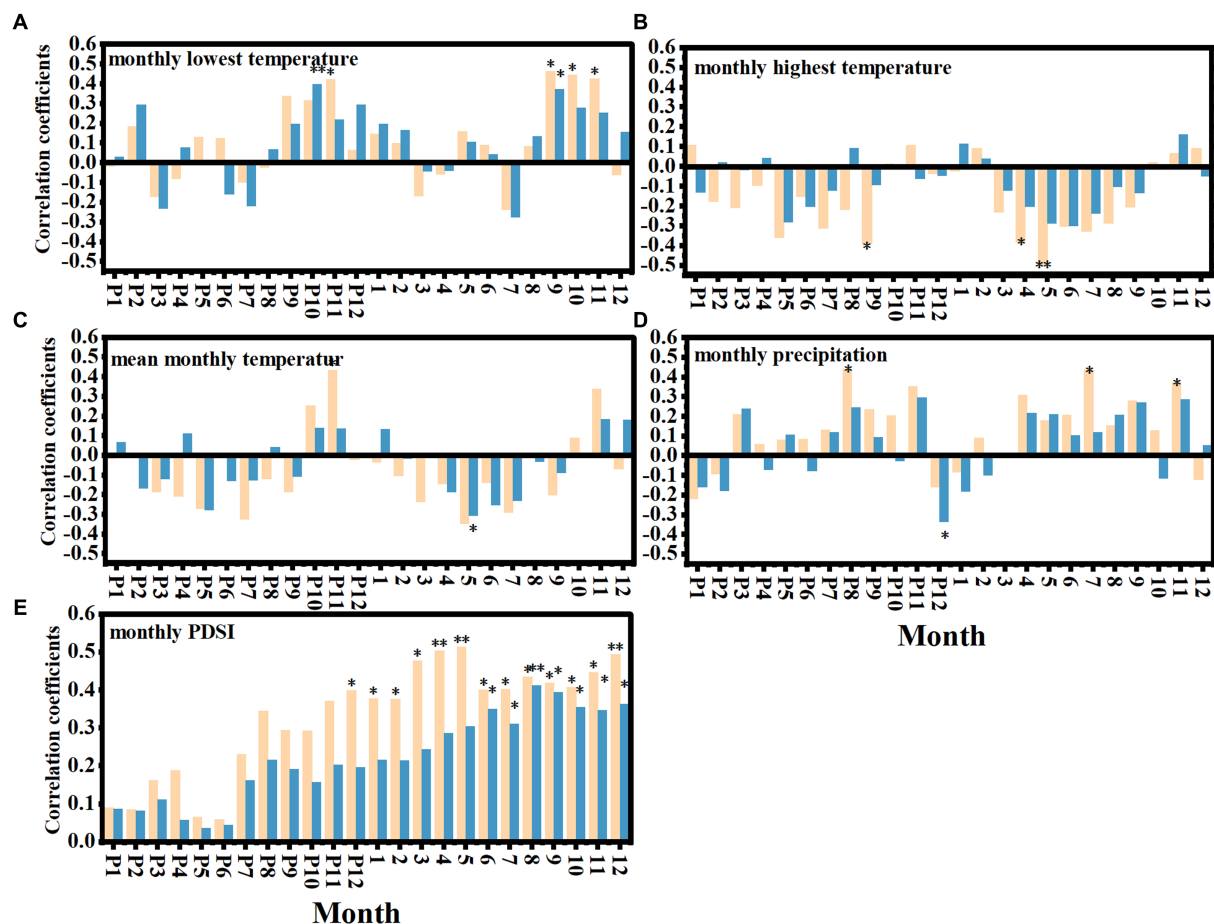
FIGURE 5
Correlation between different age stands and climatic factors. The correlation between different age stands and monthly lowest temperature (MLT) **(A)**, monthly highest temperature(MHT) **(B)**, monthly average temperature (MAT) **(C)**, monthly precipitation **(D)**, monthly average PDSI **(E)**. The yellow and blue bar charts represent the correlation coefficients between the RWI of young and middle-aged stands and climatic factors, respectively. The letter P represents the month of the previous year, * indicates that there are significant differences between different age stands ($p < 0.05$), ** indicates that there are extremely significant differences between different age stands ($p < 0.01$).

3.3. The changes of Rt, Rc and Rs in different drought events

There was no significant difference in Rt between the first two drought events in the two stand ages, and it was significantly lower than the first two in the third drought event (Figures 6A,D). Rc in the first drought event was significantly higher than that in the second and third drought events, but there was no difference between the latter two (Figures 6B,E). The Rs of the young stands decreased significantly in the three drought events, and the Rs of the latter two drought events of the middle-aged stands were significantly lower than that of the first drought event, but there was no significant difference between the latter two ($p < 0.05$) (Figures 6C,F). During the first drought event, the average value of Rt in the young stands was greater than 1, and the average values of Rc and Rs in the two-aged stands were also greater than 1. However, after three drought events, only the average value of RC was greater than 1, while the average values of Rt and Rs were less than 1, indicating that most trees can recover radial growth level after the first drought. However, multiple consecutive drought events have a serious impact on the resistance and resilience of trees. Although the growth after the drought event will be better than that of the year in which the drought occurred, it will not return to the growth level before the drought event. Multiple drought events have seriously reduced the radial growth level of trees.

3.4. The changes of Rt, Rc and Rs after multiple drought events in different stand ages

The average Rc values of the young stands and the middle-aged stands after the three drought events were 1.23 and 1.27 ($p < 0.05$), respectively, and there was no significant difference between the two stands (Figure 7B). The average Rt values of the young stands and the middle-aged stands after the three drought events were 0.55 and 0.66 ($p < 0.05$), respectively, and the average Rs values were 0.61 and 0.78 ($p < 0.05$), respectively, and there were significant differences in Rt and Rs between the two stands.

The Rt and Rs of the young stands were significantly lower than those of the middle-aged stands (Figures 7A,C), indicating that the resistance and resilience of the young stands were worse, and the adaptability of the middle-aged stands to extreme drought was better.
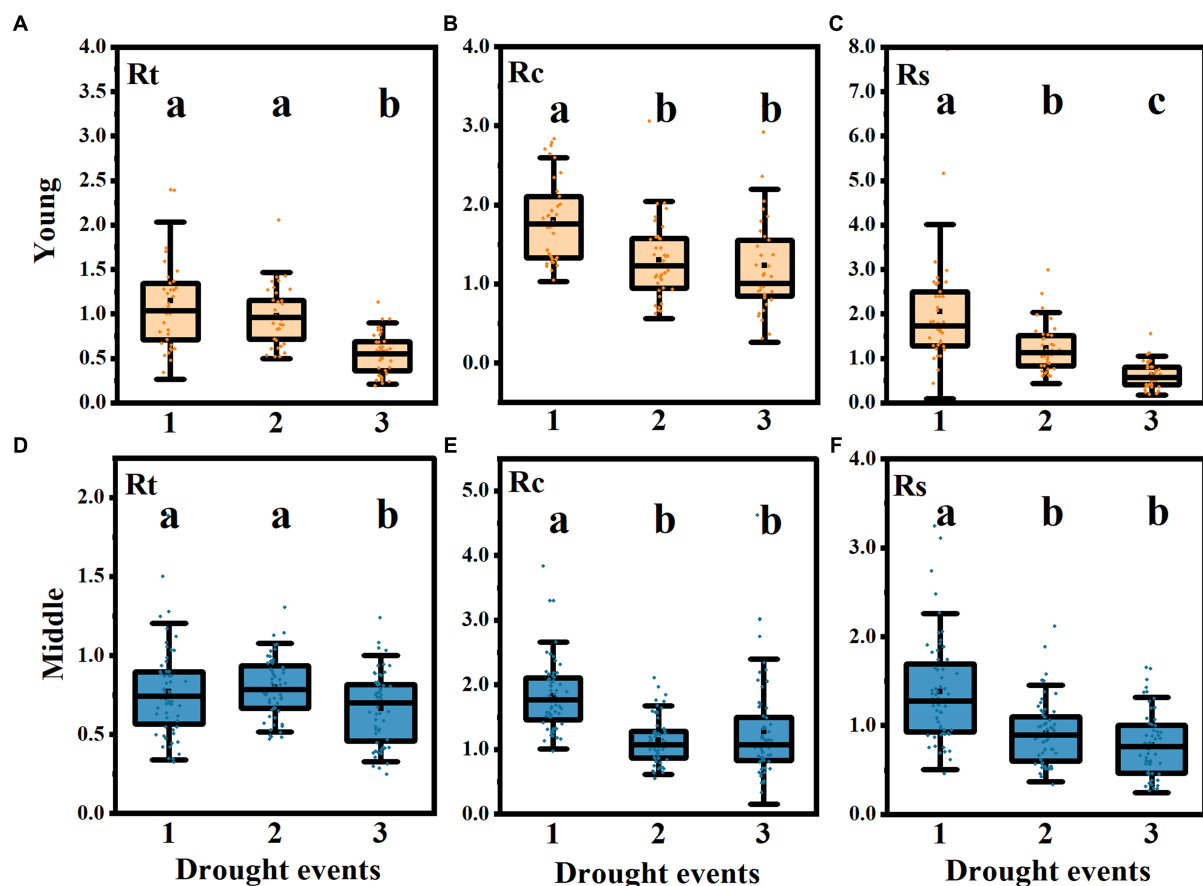
FIGURE 6
Difference analysis of Rt, Rc and Rs under different drought events. The changes of resistance (Rt) **(A)**, recovery (Rc) **(B)**, and resilience (Rs) **(C)** in young group and Rt **(D)**, Rc **(E)**, Rs **(F)** in middle-aged stands in three drought events. Black dots represent the median; the bottom and top of the box represent the first and third quartiles, respectively. The extension line represents the most extreme data points in the 1.5 times quartile range (the same below). Different letters indicated that there were significant differences between drought events ($p < 0.05$).

4. Discussion

4.1. RG of *Pinus sylvestris* in different stand ages and its response to climate

Although the overall growth trends of young and middle-aged *P. sylvestris* are similar (Figure 4), the correlation between the two stand ages and climate is not the same. The RWI of young stands was negatively correlated with MHT in April and May of the current year, while the RWI of middle-aged stands was not correlated with the MHT. The RWI of the young stands was positively correlated with precipitation in August of the previous year, July and November of the current year, while the RWI of the middle-aged stands was only negatively correlated with precipitation in December of the previous year. The RWI of the young stands was positively correlated with PDSI of the 12 months of the current year, and the RWI of the middle-aged stands was positively correlated with PDSI only from June to December of the current year. The above results indicate that the young stands are more sensitive to high temperature, precipitation and PDSI than the middle-aged stands (Figure 5), which supports our first hypothesis and is consistent with the results of many studies

(vieira et al., 2006; kontera et al., 2016; Christopoulou et al., 2022). Arco Molina et al. (2016) and Gurskaya and Shiyatov (2006) found that the bark of trees thickened with age, resulting in a stronger insulation and protective capacity, thereby reducing the sensitivity of older trees to climate change. In addition, the soil desertification in the semi-arid area of western Liaoning is severe, the surface water retention capacity is low, the root system of young stands is shallow, and less groundwater available than in middle-aged forests. When the temperature increases and precipitation decreases, the available water of young trees is less, which also explains why young stands are more sensitive to climate change (Haijun, 2015). The RWI of young stands was negatively correlated with MHT in April and May in the spring of the year. This may be due to the fact that in the semi-arid area of western Liaoning, although the temperature was relatively high in June, July and August, it concentrated more than 66% of the annual precipitation (Figure 2), which can alleviate the inhibitory effect of high temperature on tree growth. In April and May, the precipitation is less, but the temperature is second only to June, July and August, which is more prone to spring drought (Mingshu et al., 2016). The increase in temperature will increase the evaporation of soil moisture and increase the evapotranspiration of trees. If the
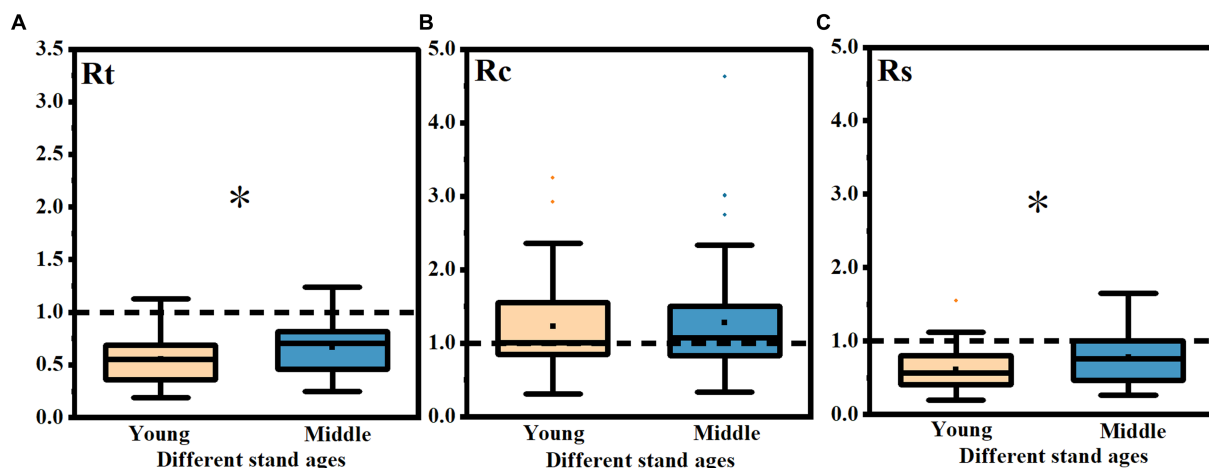
FIGURE 7
Difference analysis of Rt, Rc and Rs in different age stands after three drought events. The differences of Rt **(A)**, Rc **(B)** and Rs **(C)** in different age stands after three drought events. * indicated that there were significant differences between different age stands ($p < 0.05$).

precipitation is not timely, or the precipitation is low and the soil moisture is not sufficient, the trees are susceptible to drought stress. Therefore, the high temperature and low precipitation in April and May inhibited the growth of young stands more than that in June, July and August. Similarly, the growth of young stands was positively correlated with MLT in the fall of the year, and the growth of middle-aged stands was positively correlated with MLT in September of the year. It was also because the low temperature reduced the transpiration of trees and reduced the evaporation of water, which was beneficial to the growth of trees. This is similar to the spring drought of pines in France (Merlin et al., 2015). However, the study of Peng et al. (2018) showed that pine trees were subjected to high temperature stress in summer, which was different from our research results. The possible reason is that its research is located in the humid climate zone of central China, and the annual rainfall is abundant. Even if the temperature rises, the trees still have enough water to maintain normal growth and are not affected by drought.

4.2. The compensation effect and cumulative effect of drought events

In the growth process of *P. sylvestris*, there were multiple growth reductions in the young and middle-aged stands (Figure 4), and its growth reduction corresponded to the reduction of PDSI (Figure 3), indicating that drought events had a certain negative effect on the growth of trees. However, our study found that most trees recovered their radial growth level 3 years after the first drought event (RS > 1, Figure 6), which is different from the first part of our second hypothesis. This may be due to the compensation effect of trees (Arend et al., 2016). Compensatory growth is a typical physiological response or domestication strategy of trees to compensate for losses during drought. When the drought event ends and growth conditions become favorable, trees will grow faster to compensate for the lack of drought, which also shows that trees have some resistance and resilience. Compensatory growth effects are widespread in forests

around the world (Granda et al., 2013; Bose et al., 2021; Ovenden et al., 2021), which also shows that many studies are consistent with our findings. However, our study also found that when pine trees experienced multiple consecutive drought events, their resistance and resilience decreased rapidly, especially after the third drought event, almost all pine trees could not recover to the pre-drought level (Rt < 1, Rs < 1, Figure 6), which is consistent with the research conclusions of Serra-Maluquer et al. (2018) and Mueller et al. (2005), which is also consistent with the cumulative effect of our second hypothesis. Serra-Maluquer et al. (2018) and Mueller et al. (2005) believe that the failure to recover to the previous level after multiple drought events is related to the previous drought events. The compensation effect of trees is not infinite. The cumulative effect of continuous drought events will offset the compensation effect of drought events and damage the resistance of species to disasters and the ability to resilience after drought. We speculate that this phenomenon is caused by drought-induced xylem cavitation damage in trees. This change reduces the available water in trees, and continuous drought events aggravate the hydraulic degradation caused by xylem cavitation. Even if the drought event passes, the hydraulic degradation is irreversible and has long-term effects, eventually preventing the tree from returning to its original growth level (Anderegg et al., 2013). At the same time, we also found that although the third drought event was only a moderate drought, its severity and duration were much smaller than the first and second extreme droughts, but the Rs was still significantly reduced in the young groups, indicating that the cumulative effect of the drought events was very severe. We speculate that the resilience of trees will be more affected when drought events occur again. With the increase of drought events in the future, the cumulative effect will continue to increase until the trees die and the forests decline on a large scale.

4.3. Differences in response to drought events in different stand ages

After three events, there were significant differences in Rt and Rs between the two stand ages (Figure 7), which was consistent

with our third hypothesis. The Rt and Rs of the middle-aged stands were significantly higher than those of the young stands, indicating that the middle-aged stands had stronger adaptability to extreme drought events, which was consistent with the results of Colangelo et al. (2017) and Versace et al. (2022), which is also consistent with our first part of the conclusion. Studies have shown that with the increase of tree age, the greater the dependence on water storage in the body, the stronger the water storage capacity of trees. During the drought period, the water that trees can absorb from the soil is limited, so the water stored in trees is very important. The more water stored in trees, the less affected by drought events (Phillips et al., 2003; Scholz et al., 2011). In addition, the stomatal closure ability of large trees is often better than that of small trees, which helps to reduce the risk of water evaporation and xylem cavitation during drought (Niinemets, 2002), which may also explain why the resistance and resilience of middle-aged stands are greater than those of young stands. However, the study by Loïc et al. (2021) shows that the age of trees has a negative effect on their resilience, contrary to our findings. This may be due to the different study sites. Their research site is located in Switzerland, which has a temperate maritime climate. Unlike semi-arid areas, where trees rely mainly on their own stored water during droughts, Switzerland has a mild climate and high annual precipitation. The water-holding capacity of the soil is better than that of the desertified sandy land. Even during droughts, groundwater is more abundant and trees are less dependent on stored water in the body. In the same stand, small trees were shaded by large trees, which reduced water evaporation (pretzsch et al., 2018; Loïc et al., 2021), so small trees were less affected in his study.

5. Conclusion

Based on the method of dendrochronology, this study investigated the response of *P. sylvestris* plantations in different age stands to climate change and drought events, and drew the following conclusions: Young stands display a greater sensitivity to climate change and drought events compared to middle-aged stands. In the semi-arid area, the spring drought has a more significant inhibitory impact on the growth of pine trees compared to the high summer temperatures. While pine trees have some compensation effect after drought events, the cumulative effect of repeated drought events will gradually offset the trees' compensation effect, leading to reduced growth and death in some cases. Global warming has resulted in more frequent drought events. As a consequence, young trees are at a higher risk of death compared to middle-aged trees. In order to prevent the decay or death of trees, it is necessary to focus on the growth of young trees. In the process of forest construction, we should pay attention to the age structure of the stand, strengthen manual management and tending, and create a forest ecological environment with strong resistance and strong recovery ability.

Conflict of interest

The authors declare that the research was conducted in the absence of any commercial or financial relationships that could be construed as a potential conflict of interest.

Publisher's note

All claims expressed in this article are solely those of the authors and do not necessarily represent those of their affiliated organizations, or those of the publisher, the editors and the reviewers. Any product that may be evaluated in this article, or claim that may be made by its manufacturer, is not guaranteed or endorsed by the publisher.

Supplementary material

The Supplementary material for this article can be found online at: https://www.frontiersin.org/articles/10.3389/ffgc.2023.1272477/full#supplementary-material

References

Adams, J. (2009). *Vegetation-climate interaction: How plants make the global environment*. Berlin, New York, Chichester: Springer in association with Praxis.

Allen, C. D., Macalady, A. K., Chenchouni, H., Bachelet, D., McDowell, N., Vennetier, M., et al. (2010). A global overview of drought and heat-induced tree

mortality reveals emerging climate change risks for forests. *For. Ecol. Manag.* 259, 660–684. doi: 10.1016/j.foreco.2009.09.001

Anderegg, W. R. L., Plavcová, L., Anderegg, L. D. L., Hacke, U. G., Berry, J. A., and Field, C. B. (2013). Drought's legacy: multiyear hydraulic deterioration underlies

widespread aspen forest die-off and portends increased future risk. *Glob. Change Biol.* 19, 1188–1196. doi: 10.1111/gcb.12100

Arco Molina, J. G., Domínguez, D. P., Roig, F. A., and Martín, A. H. (2016). Tree age and bark thickness as traits linked to frost ring probability on *araucaria araucana* trees in northern Patagonia. *Dendrochronologia* 37, 116–125. doi: 10.1016/j.dendro.2016.01.003

Arend, M., Sever, K., Pflug, E., Gessler, A., and Schaub, M. (2016). Seasonal photosynthetic response of european beech to severe summer drought: limitation, recovery and post-drought stimulation. *Agric. For. Meteorol.* 220, 83–89. doi: 10.1016/j.agrformet.2016.01.011

Bigelow, S. W., Papaik, M. J., Caum, C., and North, M. P. (2014). Faster growth in warmer winters for large trees in a mediterranean-climate ecosystem. *Clim. Chang.* 123, 215–224. doi: 10.1007/s10584-014-1060-0

Bolte, A., Ammer, C., Lof, M., Madsen, P., Nabuurs, G., Schall, P., et al. (2009). Adaptive forest management in central europe: climate change impacts, strategies and integrative concept. *Scand. J. For. Res.* 24, 473–482. doi: 10.1080/02827580903418224

Bose, A. K., Scherrer, D., Camarero, J. J., Ziche, D., Babst, F., Bigler, C., et al. (2021). Climate sensitivity and drought seasonality determine post-drought growth recovery of quercus petraea and quercus robur in europe. *Sci. Total Environ.* 784:147222. doi: 10.1016/j.scitotenv.2021.147222

Christopoulou, A., Sazeides, C. I., and Fyllas, N. M. (2022). Size-mediated effects of climate on tree growth and mortality in mediterranean brutia pine forests. *Sci. Total Environ.* 812:151463. doi: 10.1016/j.scitotenv.2021.151463

Colangelo, M., Camarero, J. J., Borghetti, M., Gazol, A., Gentilesca, T., and Ripullone, F. (2017). Size matters a lot: drought-affected italian oaks are smaller and show lower growth prior to tree death. *Front. Plant Sci.* 8:135. doi: 10.3389/fpls.2017.00135

Field, C. B., Barros, V., Stocker, T. F., and Dahe, Q. (2012). *Managing the risks of extreme events and disasters to advance climate change adaptation: Special report of the intergovernmental panel on climate change.* Cambridge: Cambridge University Press.

Fritts, H. (2012). *Tree rings and climate.* Elsevier: Amsterdam, The Netherlands

Gantois, J. (2022). New tree-level temperature response curves document sensitivity of tree growth to high temperatures across a US-wide climatic gradient. *Glob. Chang. Biol.* 28, 6002–6020. doi: 10.1111/gcb.16313

Gazol, A., Camarero, J. J., Anderegg, W., and Vicente-Serrano, S. (2017). Impacts of droughts on the growth resilience of northern hemisphere forests. *Glob. Ecol. Biogeogr.* 26, 166–176. doi: 10.1111/geb.12526

Granda, E., Camarero, J. J., Gimeno, T. E., Martinez-Fernandez, J., and Valladares, F. (2013). Intensity and timing of warming and drought differentially affect growth patterns of co-occurring mediterranean tree species. *Eur. J. Forest Res.* 132, 469–480. doi: 10.1007/s10342-013-0687-0

Gurskaya, M. A., and Shiyatov, S. G. (2006). Distribution of frost injuries in the wood of conifers. *Russ. J. Ecol.* 37, 7–12. doi: 10.1134/S1067413606010024

Haijun, Z. (2015). Vigorously promote agricultural mechanization to improve rural ecological environment. *Agri. Technol.* 9, 46–48. doi: 10.11974/nyyjs.20150932011

Hollunder, R. K., Mariotte, P., Carrijo, T. T., Holmgren, M., Luber, J., Stein-Soares, B., et al. (2021). Topography and vegetation structure mediate drought impacts on the understory of the south american Atlantic forest. *Sci. Total Environ.* 766:144234. doi: 10.1016/j.scitotenv.2020.144234

Jing, M., Zhu, L., Liu, S., Cao, Y., Zhu, Y., and Yan, W. (2022). Warming-induced drought leads to tree growth decline in subtropics: evidence from tree rings in Central China. *Front. Plant Sci.* 13:964400. doi: 10.3389/fpls.2022.964400

Kannenberg, S. A., Maxwell, J. T., Pederson, N., D'Orangeville, L., Ficklin, D. L., and Phillips, R. P. (2019). Drought legacies are dependent on water table depth, wood anatomy and drought timing across the eastern US. *Ecol. Lett.* 22, 119–127. doi: 10.1111/ele.13173

Kontera, O., Buentgenb, U., Carrere, M., Timonenf, M., and Espera, J. (2016). Climate signal age effects in boreal tree-rings: lessons to be learned for paleoclimatic reconstructions. *Quat. Sci. Rev.* 142, 164–172. doi: 10.1016/j.quascirev.2016.04.020

Law, B., Thornton, P., Irvine, J., Anthoni, P., and Van Tuyl, S. (2001). Carbon storage and fluxes in ponderosa pine forests at different developmental stages. *Glob. Chang. Biol.* 7, 755–777. doi: 10.1046/j.1354-1013.2001.00439.x

Lindner, M., Maroschek, M., Netherer, S., Kremer, A., Barbati, A., Garcia-Gonzalo, J., et al. (2010). Climate change impacts, adaptive capacity, and vulnerability of european forest ecosystems. *For. Ecol. Manag.* 259, 698–709. doi: 10.1016/j.foreco.2009.09.023

Lloret, F., Keeling, E. G., and Sala, A. (2011). Components of tree resilience: effects of successive low-growth episodes in old ponderosa pine forests. *Oikos* 120, 1909–1920. doi: 10.1111/j.1600-0706.2011.19372.x

Loïc, G., Forrester, D. I., Bottero, A., Andreas, R., and Mathieu, L. (2021). Tree neighbourhood diversity has negligible effects on drought resilience of european beech, silver fir and Norway spruce. *Ecosystems* 24, 20–36. doi: 10.1007/s10021-020-00501-y

Longo, M., Knox, R. G., Levine, N. M., Alves, L. F., Bonal, D., Camargo, P. B., et al. (2018). Ecosystem heterogeneity and diversity mitigate amazon forest resilience to frequent extreme droughts. *New Phytol.* 219, 914–931. doi: 10.1111/nph.15185

Lucas-Borja, M. E., Bose, A. K., Andivia, E., Candel-Pérez, D., Plaza-Álvarez, P. A., and Linares, J. C. (2021). Assessing tree drought resistance and climate-growth relationships under different tree age classes in a *Pinus nigra* Arn ssp. salzmannii forest. *Forests* 12:1161. doi: 10.3390/f12091161

Martín-Benito, D., Cherubini, P., del Río, M., and Cañellas, I. (2008). Growth response to climate and drought in *Pinus nigra* Arn. Trees of different crown classes. *Trees* 22, 363–373. doi: 10.1007/s00468-007-0191-6

Merlin, M., Perot, T., Perret, S., Korboulewsky, N., and Vallet, P. (2015). Effects of stand composition and tree size on resistance and resilience to drought in sessile oak and scots pine. *For. Ecol. Manag.* 339, 22–33. doi: 10.1016/j.foreco.2014.11.032

Mingshu, C., Baoli, S., and Ke, S. (2016). Analysis of causes of spring drought in Fuxin area and defense countermeasures. *Friends of Farmers Getting Rich.* 2:294. doi: 10.3969/j.issn.1003-1650.2016.02.280

Mueller, R. C., Scudder, C. M., Porter, M. E., Trotter, R. T. III, Gehring, C. A., and Whitham, T. G. (2005). Differential tree mortality in response to severe drought: evidence for long-term vegetation shifts. *J. Ecol.* 93, 1085–1093. doi: 10.1111/j.1365-2745.2005.01042.x

National Forestry Administration (2017). *Age-class and age-group of main tree species.* Beijing: China Standard Press.

Niinemets, Ü. (2002). Stomatal conductance alone does not explain the decline in foliar photosynthetic rates with increasing tree age and size in Picea abies and *Pinus sylvestris*. *Tree Physiol.* 22, 515–535. doi: 10.1093/treephys/22.8.515

Ning, P., Zhang, M., Bai, T., Zhang, B., Yang, L., Dang, S., et al. (2023). Dendroclimatic response of *pinus tabuliformis* carr. Along an altitudinal gradient in the warm temperate region of China. *Front. Plant Sci.* 14:1147229. doi: 10.3389/fpls.2023.1147229

Oliver, T. H., Heard, M. S., Isaac, N. J. B., Roy, D. B., Procter, D., Eigenbrod, F., et al. (2015). Biodiversity and resilience of ecosystem functions. *Trends Ecol. Evol.* 30, 673–684. doi: 10.1016/j.tree.2015.08.009

Ovenden, T. S., Perks, M. P., Clarke, T.-K., Mencuccini, M., and Jump, A. S. (2021). Life after recovery: increased resolution of forest resilience assessment sheds new light on post-drought compensatory growth and recovery dynamics. *J. Ecol.* 109, 3157–3170. doi: 10.1111/1365-2745.13576

Palmer, W. C. (1965), *Meteorological drought.* Weather Bureau Research Paper 45, U.S. Dep. of Commerce, Washington, D. C.

Peng, J. F., Peng, K. Y., and Li, J. B. (2018). Climate-growth response of Chinese white pine (*Pinus armandii*) at different age groups in the Baiyunshan National Nature Reserve, Central China. *Dendrochronologia* 49, 102–109. doi: 10.1016/j.dendro.2018.02.004

Phillips, N. G., Ryan, M. G., Bond, B. J., McDowell, N. G., Hinckley, T. M., and Cermák, J. (2003). Reliance on stored water increases with tree size in three species in the pacific northwest. *Tree Physiol.* 23, 237–245. doi: 10.1093/treephys/23.4.237

Pretzsch, H., Schütze, G., and Biber, P. (2018). Drought can favour the growth of small in relation to tall trees in mature stands of Norway spruce and european beech. *For. Ecosyst.* 5, 1–19. doi: 10.1186/s40663-018-0139-x

Scholz, F. G., Phillips, N. G., Bucci, S. J., Meinzer, F. C., and Goldstein, G. (2011). "Hydraulic capacitance: biophysics and functional significance of internal water sources in relation to tree size" in *Size-and age-related changes in tree structure and function* (Dordrecht: Springer), 341–361.

Serra-Maluquer, X., Mencuccini, M., and Martínez-Vilalta, J. (2018). Changes in tree resistance, recovery and resilience across three successive extreme droughts in the northeast iberian peninsula. *Oecologia* 187, 343–354. doi: 10.1007/s00442-018-4118-2

Smerdon, J. E., Cook, B. I., Cook, E. R., and Seager, R. (2015). Bridging past and future climate across paleoclimatic reconstructions, observations, and models: A hydroclimate case study*. *J. Clim.* 28, 3212–3231. doi: 10.1175/JCLI-D-14-00417.1

Song, C., and Woodcock, C. E. (2003). A regional forest ecosystem carbon budget model: impacts of forest age structure and landuse history. *Ecol. Model.* 164, 33–47. doi: 10.1016/S0304-3800(03)00013-9

Sun, Y., Liu, Y., Sun, B., and Wang, R. (2012). Tree-ring based PDSI reconstruction since 1853 AD in the source of the fenhe river basin, Shanxi province, China. *Sci. China: Earth Sci.* 55, 1847–1854. doi: 10.1007/s11430-012-4369-4

Tang, X., Li, H., Ma, M., Yao, L., Peichl, M., Arain, A., et al. (2017). How do disturbances and climate effects on carbon and water fluxes differ between multi-aged and even-aged coniferous forests? *Sci. Total Environ.* 599-600, 1583–1597. doi: 10.1016/j.scitotenv.2017.05.119

Trugman, A. T., Detto, M., Bartlett, M. K., Medvigy, D., Anderegg, W. R. L., Schwalm, C., et al. (2018). Tree carbon allocation explains forest drought-kill and recovery patterns. *Ecol. Lett.* 21, 1552–1560. doi: 10.1111/ele.13136

van Mantgem, P., Stephenson, N. L., Byrne, J. C., Daniels, L. D., Franklin, J. F., Fulé, P. Z., et al. (2009). Widespread increase of tree mortality rates in the western United States. *Science* 323, 521–524. doi: 10.1126/science.1165000

Versace, S., Bräuning, A., Cherubini, P., Febbraro, M. D., Häusser, M., Lombardi, F., et al. (2022). New evidence for population-specific responses to drought events from tree ring chronologies of *pinus nigra ssp. laricio* across the entire distribution range. *Agric. For. Meteorol.* 323:109076. doi: 10.1016/j.agrformet.2022.109076

Vieira, J., Campelo, F., and Nabais, C. (2006). Age-dependent responses of tree-ring growth and intra-annual density fluctuations of *pinus pinaster* to mediterranean climate. *Trees* 23, 257–265. doi: 10.1007/s00468-008-0273-0

Vitali, V., Büntgen, U., and Bauhus, J. (2017). Silver fir and Douglas fir are more tolerant to extreme droughts than Norway spruce in South-Western Germany. *Glob. Chang. Biol.* 23, 5108–5119. doi: 10.1111/gcb.13774

Yan, H., Wang, S., Lu, H., Yu, Q., Zhu, Z., Myneni, R. B., et al. (2014). Development of a remotely sensing seasonal vegetation-based palmer drought severity index and its application of global drought monitoring over 1982-2011. *J. Geophys. Res. Atmos.* 119, 9419–9440. doi: 10.1002/2014JD021673

Yuanqiao, L., Xiuchen, W., Huang, Y., Li, X., Fangzhong, S., Zhao, S., et al. (2021). Compensation effect of winter snow on larch growth in Northeast China. *Clim. Chang.* 164, 1–17. doi: 10.1007/s10584-021-02998-1

Yuzhang, Z. (1990). Liaoning Jilin, Heilongjiang Province, Zhangzi pine plantation investigation report. *J. Liaoning For. Sci. Technol.* 2, 52–57.

Zang, C., Hartl-Meier, C., Dittmar, C., Rothe, A., and Menzel, A. (2014). Patterns of drought tolerance in major european temperate forest trees: climatic drivers and levels of variability. *Glob. Chang. Biol.* 20, 3767–3779. doi: 10.1111/gcb.12637

Zhang, Y., Peng, C., Zhang, G., Liu, G., Chen, H., Wang, J., et al. (2016). Multiple afforestation programs accelerate the greenness in the 'three north' region of China from 1982 to 2013. *Ecol. Indic.* 61, 404–412. doi: 10.1016/j.ecolind.2015.09.041

Zuidema, P. A., Flurin, B., Groenendijk, P., Valerie, T., Abrham, A., Acuña-Soto, R., et al. (2022). Tropical tree growth driven by dry-season climate variability. *Nat. Geosci.* 15, 269–276. doi: 10.1038/s41561-022-00911-8

Invasive behaviour of oak lace bug in forest ecosystems: a comparative analysis between thermophilous and mesophilous oak forests

Flavius Bălăcenoiu [1], Constantin Nețoiu[1], Dragoș Toma[1,2]* and Ion Cătălin Petrițan [2]

[1]National Institute for Research and Development in Forestry "Marin Dracea", Voluntari, Romania, [2]Faculty of Silviculture and Forest Engineering, Transilvania University of Brașov, Brașov, Romania

Forest ecosystems provide invaluable ecological, economic, and social benefits, making them essential for global well-being. However, these ecosystems face various threats, including biological invasions by alien species. Among these, the oak lace bug (OLB), an invasive North American insect, has rapidly spread in Europe, impacting oak forests and raising concerns about its adaptation to new environments. OLB feeds on the undersides of oak leaves, extracting sap and causing chlorotic discoloration. Severe infestations lead to premature defoliation, increased susceptibility to diseases or pests and can also result in a substantial reduction in photosynthesis activity. This study aims to analyse OLB's invasive behaviour in Romanian forest ecosystems, with a specific focus on the differences between thermophilous and mesophilous oak forests. The analysis covers 6 years of data and reveals critical insights. In the initial 4 years, OLB predominantly inhabited the extracarpathian regions of Romania, with concentrated presence in the southern, western, and northwestern areas. Forest ecosystems mainly affected between 2017 and 2020 were characterized by thermophilous oak forests in southern and western regions. However, in the last 2 years (2021−2022), OLB presence increased, particularly in lowland ecosystems, albeit with reduced damage intensity. The analysis also unveiled an adaptation and expansion of OLB in mesophilous forest ecosystems. Climatic factors, specifically temperature and precipitation, significantly influenced OLB's behaviour, points with severe attacks exhibiting specific climatic conditions. In summary, this study provides crucial insights into OLB's behaviour, emphasizing the role of climatic and environmental factors in its invasive tendencies.

KEYWORDS

biological invasions, forest health, oak forests, habitat disruption, ecological resilience

1 Introduction

Forest ecosystems have immeasurable value for our planet, providing a multitude of ecological, social, and economic benefits. In terms of ecological benefits, forests play a vital role in climate regulation at both local and global levels, contributing to the mitigation of weather phenomena, regulating the hydrological cycle, and safeguarding watersheds. Forest ecosystems hold significant ecological importance due to the diversity of functional groups

within them (Haq et al., 2023a), as well as for their capacity to sequester carbon (Haq et al., 2023b). They serve as habitats for a remarkable diversity of species and constitute reservoirs of genetically important information, with many of these species yet to be discovered (Pearce, 2001). Some of these ecosystem services, such as climate regulation, soil formation, water resource management, and water supply, make significant contributions to human society, even in the absence of direct monetary valuation (Costanza et al., 1997). Furthermore, the total annual value of ecosystem services globally averages around 33 trillion USD, with global forests contributing approximately 969 USD per hectare (Costanza et al., 1997).

From an economic standpoint, forests are fundamental for poverty eradication and economic development, providing food, fiber, wood, and other essential forest products for sustenance and income generation (Jenkins and Schaap, 2018). In terms of the social benefits of ecosystem services provided by forests, they manifest in ensuring human health and well-being, providing a high-quality living environment, offering outdoor recreation and tourism opportunities, aesthetic values, facilitating outdoor education, and promoting knowledge about forests and the environment. Additionally, forests serve as sources of intellectual and spiritual inspiration, contributing to cultural identity and our cultural heritage (de Groot et al., 2010).

Disturbances caused by factors such as insect outbreaks, phytopathogens, wind, precipitation, or wildfires can affect the ability of forest ecosystems to fulfill multiple functions. In addition to these factors, forest ecosystems are threatened by various phenomena, including pollution, climate change (Lindner et al., 2010) and most notably, biological invasions caused by alien species (Trumbore et al., 2015). In the context of the global expansion of invasive species, accelerated by processes of globalization, it is evident that invasions of foreign species have generated diverse consequences for the environment, economy, and human health (Pimentel et al., 2000; Lovell et al., 2006; Meyerson and Mooney, 2007; Vilà et al., 2010, 2011; Jeschke et al., 2013; Simberloff et al., 2013; Blackburn et al., 2014; Hulme, 2014; Schindler et al., 2015). Through the forecast of forest ecosystem health, the results could aid in the assessment and evaluation of ecosystem goods and services (Haq et al., 2022). This, in turn, might support the development of forest conservation plans, aiming to restore the ecology in areas affected by invasions (Haq et al., 2023c).

Among alien species with a significant impact on ecosystems in Europe and, consequently, Romania, *Corythucha arcuata* (Say, 1832) (Hemiptera, Tingidae) stands out as an invasive insect of particular relevance. Also known as the oak lace bug (OLB), this North American-origin insect was first reported in Europe in 2000, in Italy (Bernardinelli and Zandigiacomo, 2000). This insect species feeds on the underside of host leaves, typically oaks, by piercing the epidermis and extracting cellular sap material (Mutun et al., 2009), resulting in chlorotic discoloration of the leaves (Bernardinelli, 2006; Mutun et al., 2009; Paulin et al., 2020). In cases of severe infestation, this pest can cause premature defoliation of the host or increase its susceptibility to various diseases or pests (Connell and Beacher, 1947), as well as affect photosynthesis activity by up to 58.8% (Nikolic et al., 2019). Although the general public and stakeholders in the forestry sector of countries facing the invasion caused by OLB believe that the insect's attack can lead to tree mortality (Bălăcenoiu et al., 2021a) to our knowledge, there is no research on the impact of the insect on local ecosystems and biodiversity.

Regarding its invasion into the Eurasian territory, within just 2 years following its first report, in 2002, the species was recorded in both Switzerland (Forster et al., 2005), and Turkey (Mutun, 2003). Due to its potential to cause significant damage and its rapid spread, OLB was included on the Alert List of the European and Mediterranean Plant Protection Organization in March 2001 (EPPO, 2001) and remained on this list until 2007 (EPPO, 2007), when it became evident that administrative efforts could not halt its expansion. In 2012, the species was first reported in Bulgaria (Dobreva et al., 2013) and in 2013, its presence was confirmed in three other countries: Hungary (Csóka et al., 2013), Croația (Hrašovec et al., 2013) și Serbia (Pap et al., 2015; Poljaković-Pajnik et al., 2015). Furthermore, its presence is currently documented in various other European countries as a result of its invasion, including Russia (Neimorovets et al., 2017), Romania (Don et al., 2016; Chireceanu et al., 2017), Albania (Csóka et al., 2019), Slovenia (Jurc and Jurc, 2017), Bosnia and Herzegovina (Dautbašić et al., 2018), France (Streito et al., 2018), Ukraine (Meshkova, 2022), Greece (Csóka et al., 2019), Slovakia (Zúbrik et al., 2019), and Austria (Sallmannshofer et al., 2019).

Following the first recording of the insect in several countries, including Turkey, Hungary, Bulgaria, and Romania, the phenomenon did not remain limited to the stage of appearance, with subsequent reports confirming the other phases of a biological invasion, namely, its spread and establishment within the respective territories (Mutun et al., 2009; Csepelényi et al., 2017; Simov et al., 2018; Tomescu et al., 2018). The invasion in many European countries is likely due to the fact that the majority of European and Asian forests provide favourable conditions for its establishment (Csóka et al., 2019). In 2019, the oak lace bug infested an estimated combined area of over 1.7 million hectares of oak forests in just five European countries: Croatia, Hungary, Romania, the European part of Russia, and Serbia (Paulin et al., 2020). However, the chemical control method has not yielded efficient results (Bălăcenoiu et al., 2021b). Nevertheless, trials conducted in Turkey (Sönmez et al., 2016) and Croatia (Kovač et al., 2020, 2021) provide a glimmer of hope for a potential future biological control program for the insect.

Considering that oak forests in Romania constitute 16% of the country's forested area (NFI, 2018), their susceptibility to the invasive oak lace bug (OLB) is of paramount importance. The scale of these ecosystems makes them a critical component of Romania's biodiversity and ecological balance. Given the findings of Tomescu et al. (2018), which demonstrated that OLB had reached altitudes of 534 meters in Romania just 2 years after its initial report and had shown survival in locations where the average temperature of the coldest month was 0.8°C, this situation could potentially pose future challenges to montane forest ecosystems. The aim of this study is to analyse the invasive behaviour of the oak lace bug in the forest ecosystems of Romania, with a particular focus on the differences between thermophilous oak forests and mesophilous oak forests. Therefore, the study aims to address two crucial questions: (i) Are there significant differences in the invasive behaviour of the oak lace bug between these environments (thermophilous and mesophilous), and if so, what are these differences? (ii) What role do climatic factors play in the expansion and intensification of the oak lace bug invasion in the forest ecosystems of Romania? By examining how this insect has evolved in these distinct environments, our goal is to contribute to a deeper understanding of the dynamics of biological invasion and its impact on forest ecosystems.

FIGURE 1
Standardized scale for assessing damage intensity through leaf discoloration.

2 Material and method

2.1 Data collection

To study the invasive behaviour of the Oak Lace Bug (OLB) in the forest ecosystems of Romania, we focused on monitoring the temporal evolution of damage in the oak forests of Romania. Given that the OLB was first reported in the national forest fund starting in 2016 (Tomescu et al., 2018), we established the reference period for understanding the temporal evolution of damage caused by the insect in oak forests in Romania as the interval between 2017 and 2022.

Information regarding the location and damage intensity during this period was extracted from the internal databases of the National Research and Development Institute for Forestry "Marin Drăcea" pertaining to the status of attacks produced by *C. arcuata* in Romanian oak forests. We employed the methodology outlined in Tomescu et al. (2018) to gauge the extent of insect attack. This involved a visual assessment of the extent of foliage discoloration relative to the typical colour of oak leaves on the host trees. The damage intensity was quantified using percentages of discoloration in multiples of 5, with a range spanning from 0% (indicating no attack) to 100% (indicating a severe attack). To ensure clarity and consistency in our assessments, we established a standardized scale with five degrees of damage intensity (Figure 1).

2.2 Mapping attacks produced by OLB

To highlight the relationship between the intensity of attacks and the invaded ecosystem units, we conducted the mapping of damage caused by OLB on the Forest Map of Romania – based on forest ecosystem types (Doniță et al., 2008).

In this manner, each forest where the damage caused by *C. arcuata* was recorded was assigned a point of a specific colour corresponding to the level of attack (See Figure 1).

Maps throughout this paper were created using ArcGIS® 10.3 software by Esri.

2.3 Description of studied forest ecosystem formations

Our study focused on the analysis and characterization of a set of forest ecosystems in Romania where OLB is present. These ecosystem formations were initially described by Doniță et al. (2008) and represent a diverse range of forest habitats that are of particular importance to the biodiversity and ecological functioning of the region. The ecosystem formations in which OLB was identified in Romania are presented in Table 1.

2.4 Climatic data

Due to the incompleteness of local climate data, we used gridded climatic data (annual monthly temperature and average daily precipitation) to generate the annual mean temperature, annual winter temperature, overwinter temperature, annual total precipitation, winter precipitation and overwinter precipitation, but also temperature and precipitation during the growing season for each monitoring point for each year of the 2017–2022 period. This dataset was downloaded from the KNMI Climate Explorer (E-OBS, https://climexp.knmi.nl/) and corresponds to interpolated data obtained from measured values recorded by a dense network of local meteorological stations, and gridded onto a 0.25° network (0.25° 1950-now: E-OBS v25.0e Tg (Europe), 0.25° 1950-now: E-OBS v25.0e precip (Europe)). E-OBS is a daily gridded observational dataset for main climatic parameters (e.g., precipitation and temperature, used in current research) in Europe based on ECA&D (European Climate Assessment & Dataset) information and currently it is maintained and by the Copernicus Climate Change Services. We acknowledge the E-OBS dataset from the Copernicus Climate Change Service (C3S, https://surfobs.climate.copernicus.eu) and the data providers in the ECA&D project.[1] More detail on interpolation method could be found in Cornes et al. (2018). We have decided to use E-OBS dataset mainly

---

1 https://www.ecad.eu

TABLE 1 Characterization of forest ecosystems with oak lace bug.

Forest ecosystem formation		Number of OLB points	Altitude range (m)
Code [According to Doniţă et al., 2008]	Name		
4	Mesophilous hill beech (*Fagus sylvatica* L.) forests	82	91–984
5	Mesophilous and thermophilous sessile oak (*Quercus petraea* (Matt.) Liebl)forests	75	75–618
6	Mesophilous and thermophilous oak (*Quercus robur* L.,) forests	74	29–526
7	Thermophilous Turkey oak (*Quercus cerris* L.) and Hungarian oak (*Quercus frainetto* Ten.) forests	139	59–462
8	Thermophilous grayish oak (*Quercus pedunculiflora* K. Koch) and downy oak (*Quercus pubescens* Wild.) forests	42	0–207
9	Alluvial and wetland deciduous broad-leaved forests	64	7–375

due to higher provided resolution (0.25°) compared to of that other similarly products existed on Europe level (>0.5°).

2.5 Data analysis

To comprehensively evaluate the climatic conditions leading to significant attacks by OLB in all the examined ecosystems, we conducted a 2D scatterplot frequency analysis. This analysis primarily concentrated on severe attacks, which encompassed strong and very strong instances (refer to Figure 1), considering two pivotal climatic factors: (i) the average annual temperature and annual precipitation, and (ii) the average temperature during the growing season (May–October) and the corresponding precipitation.

To determine the key factors influencing the migration of OLB into mesophilous forest ecosystems, we employed Principal Components Analysis (PCA), using the following variables: damage intensity, the year in which it occurred, altitude, average annual temperature and precipitation, average temperature and precipitation during the growing season (May–October), average temperature and precipitation during the insect's overwintering period (November–April), and average temperature and precipitation during winter (December–February).

Although the important factors (temperature and precipitation) influencing insect damages are well represented by Principal Component Analysis, a quantitative analysis (e.g., correlation analysis or regression analysis) of their impact on insect damages should be considered to obtain a deeper explanation of such variables. Finally, a correlation analysis was preferred over regression analysis or GLM analysis mainly due to the presence of autocorrelation between different climatic variables that cannot be included as explanatory variables in the same model simultaneously. Thus, a Spearman correlation coefficient was calculated between insect damages and every climatic variable (average annual temperature and precipitation, overwintering temperature and precipitation but also during growing season temperature and precipitation). Spearman rank correlation coefficient calculation was performed because the assumptions necessary for Pearson correlation coefficients were violated (lack of data normality and discrete character of damage values).The relationship between climatic factors and severe attacks caused by OLB (2D scatterplot frequency analysis), but also principal component analysis and correlation analysis was performed using STATISTICA 8.0 software (StatSoft Inc., 2007).

3 Results

3.1 Analysis of oak lace bug spread: concentration and expansion in forest ecosystems

The study, conducted from 2017 to 2022, focused on analysing the spread of the OLB in Romanian forest ecosystems (Figure 2). The data analysis reveals that in the first 4 years of observation, the spread of the oak lace bug was predominantly confirmed to the extra Carpathian regions of Romania, concentrating in the southern, western, and northwestern parts of the country, with a recent expansion into the eastern region. During the period of 2017–2020, the most affected forest ecosystems were characterized by termophilous Turkey oak and Hungarian oak forests, termophilous pedunculate oak forests, as well as alluvial and wetland deciduous broad-leaved forests (where there are also grey oak forests), located mainly at low altitudes in the southern and western regions of Romania. In the final 2 years of the analysis (2021–2022), there is a noticeable increase in the frequency of insect presence, especially in lowland ecosystems, accompanied by a decline in damage intensity in these forests. During this period, attacks with severe leaf damage have been reported in forest ecosystems consisting of mesophilous sessile oak forests and mixed beech-oak forests, located mainly at high altitudes. Additionally, during this period, the insect was reported within the forested area of the Carpathian arc for the first time, albeit with a very low damage intensity. Notably, in the last year of the study, data analysis indicates that most points (55%) with very high damage intensity are situated in forest ecosystems consisting of mesophilous sessile oak forests and mixed beech-oak forests.

3.2 Assessing the climatic range and major OLB attacks

The analysis of the climate data reveals that most of the locations where OLB caused significant damage can be characterized by average annual temperatures ranging between 10 and 14°C and annual precipitation between 300 and 700 mm. Additionally, the most frequent severe damage were situated between 12 and 13°C and 450–600 mm of annual precipitation (Figure 3A). Regarding the analysis of climate characteristics during the growing season,
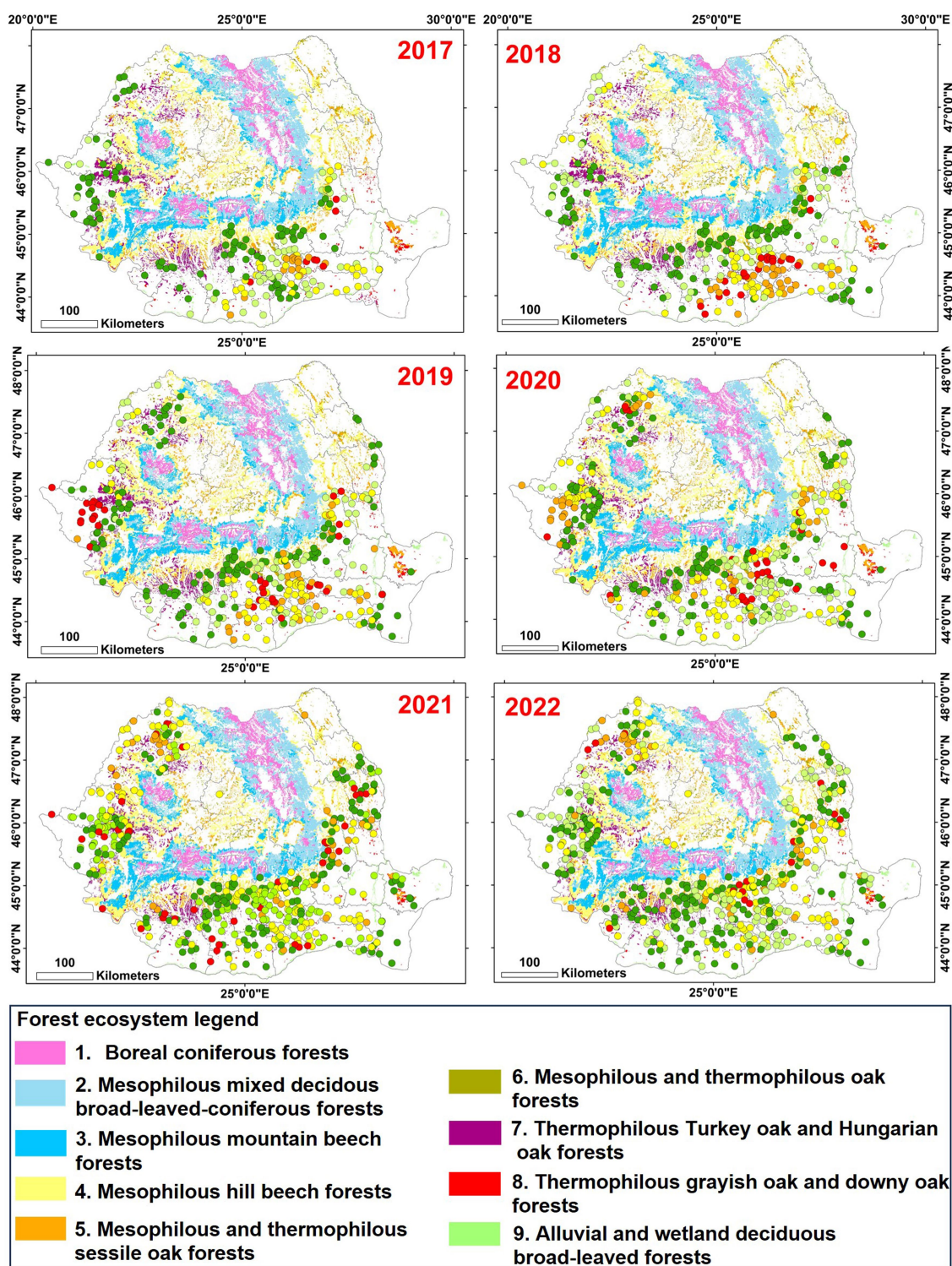
FIGURE 2
Yearly distribution patterns of oak lace bug (2017–2022) in Romanian forest ecosystems.

the data analysis indicates that most points where OLB caused major damages can be characterized by average temperatures during the vegetation season ranging between 17 and 21.5°C and precipitation between 150–450 mm during the vegetation season (Figure 3B). The most frequent severe attacks are produced around values of 19 and 20.5°C and 300–400 mm of precipitation during the growing season.

3.3 Impact trends in varying ecosystem contexts

As for the analysis of each ecosystem individually, it is noted that forest ecosystems in which oak lace bug was present during the analysed period can be divided into two main clusters: thermophilous
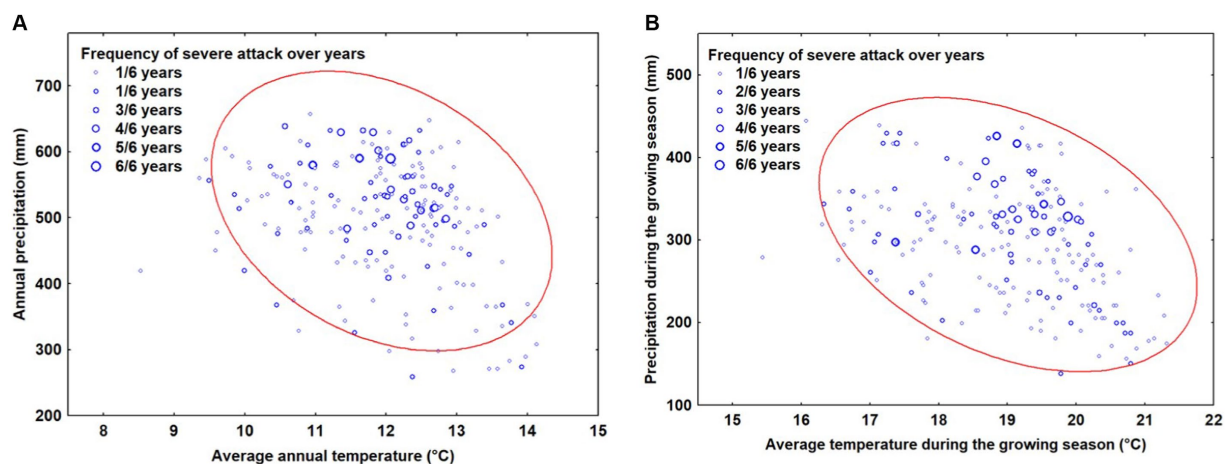
FIGURE 3
The relationship between climatic factors and severe attack caused by OLB: **(A)** analysis of annual mean temperatures and precipitation **(B)** analysis of mean temperatures and precipitation during the growing season. The ellipse represents 95% confidence.

located mainly at low altitudes in the lowland regions and mesophilous forest ecosystems that are mainly found at higher altitudes, in mountainous areas (Figure 4).

Within thermophilous forest ecosystems, the dynamics of damage intensity during the period of 2017–2022 exhibit an oscillating pattern, where the number of points with strong and very strong attacks showed an increase until the year 2019, when it reached its peak. Subsequently, starting from 2020, a steady decrease was observed, and by 2022, oak lace bug caused very few attacks with strong intensity. In parallel, within mesophilous forest ecosystems, a distinct pattern of damage intensity dynamics during the period of 2017–2023 becomes evident. This can be described as an increase in the number of points where the insect caused major attacks, concurrently with a decrease in the number of points where the insect caused weak damages as time progressed. This trend suggests a significant adaptation and expansion of the oak lace bug in mountainous environments, exerting an increasingly pronounced impact on forest ecosystems in this area.

3.4 Determinants factors on the migration of oak lace bug in mesophilous forest ecosystems

The PCA results provide a profound insight into the influence of climatic factors on the invasive behaviour of the insect, highlighting a direct correlation between rising temperatures, decreasing precipitation, and the increasing number of recorded points with severe attacks in both ecosystem 4 (Figure 5A) and ecosystem 5 (Figure 5B). Data analysis suggests that, as the number of recorded points with major attacks increases, there is a noticeable upward trend in temperature-related factors, while precipitation rates exhibit a decreasing trend in the mesophilous ecosystems over the study period (2017–2022). In particular, the average winter temperature and the annual precipitation mean to be determinants in this evolution.

Furthermore, altitude plays a crucial role in the insect's attack pattern. The higher the altitude, the fewer attacks seem to occur. This

observation suggests that OLB appears to favour lower areas within mesophilous ecosystems, where climatic and altitude conditions may be more favourable for its development and survival.

The correlation analysis (Table 2) revealed that the average annual temperature and the average temperature during the growing season positively influenced the intensity of insect damage. Meanwhile, the altitude and annual precipitation had a significant negative impact on insect damage intensity. Spearman values did not indicate any significant relationship between insect damage intensity and precipitation during the growing season, overwintering temperature, overwintering precipitation, average winter precipitation, and average winter temperature.

4 Discussions

This study aimed to investigate the invasive behaviour of the oak lace bug in the forest ecosystems of Romania, with a focus on the differences between thermophilous and mesophilous environments.

During the study period, a distinctive pattern of OLB invasion emerges, predominantly in the extra-Carpathian regions of Romania, with recent expansion into the eastern region. In contrast, the central part of the country has remained relatively protected from this invasion. An intriguing aspect to highlight is how the Carpathian Mountain range has played a crucial role in shaping the spatial distribution of OLB. These major geographical features have acted as natural barriers, delimiting the distribution of native insects and posing significant obstacles to the invasion of alien insects (Haran et al., 2015). These geographical barriers have created environmental variability, which, in turn, can influence the adaptability and invasiveness of species. A relevant example of this phenomenon is the different climate in mountainous areas, which can inhibit the activity and development of insects (Mellanby, 1939; Bale, 2002; Sinclair et al., 2003; Jaworski and Hilszczański, 2013). Temperature, in particular, has proven to be a key factor in the success or failure of invasion by several alien species (Kang et al., 2009; Ju et al., 2017; Ward et al., 2019). In the same context, another important aspect that could
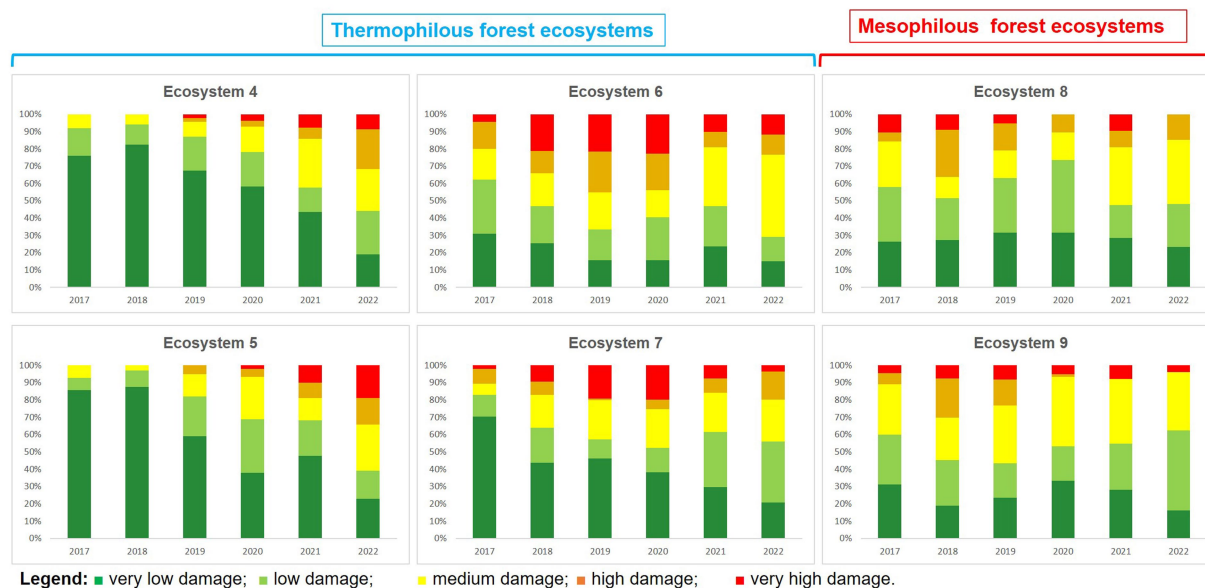
FIGURE 4

Assessing oak lace bug damage trends (2017−2022) in Romanian thermophilous and mesophilous ecosystems.
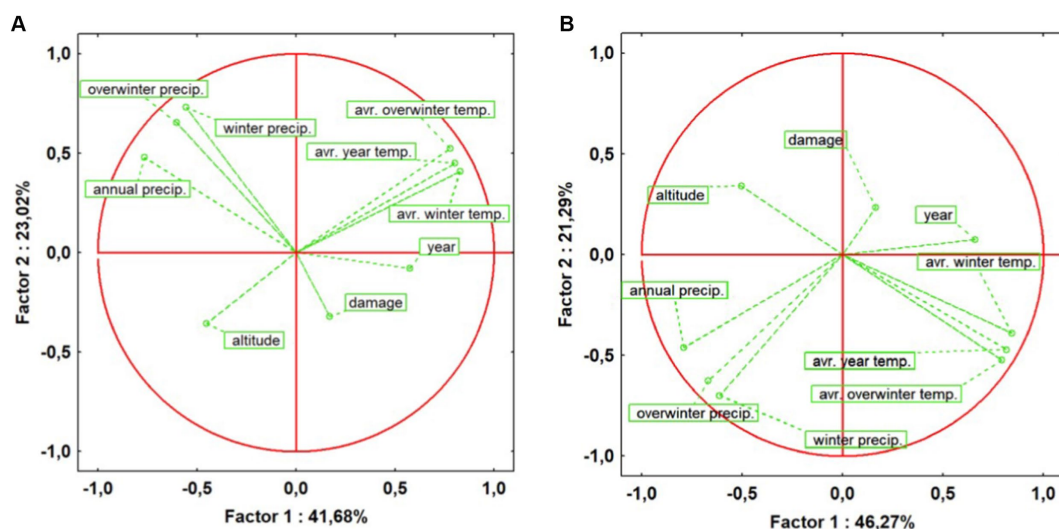

FIGURE 5

Assessing factors influencing oak lace bug attack patterns in mesophilous forest ecosystems: **(A)** Ecosystem 4 − Mesophilous hill beech forests; **(B)** Ecosystem 5 − Mesophilous and thermophilous sessile oak forests.

be relevant to the influence of the mountain range on OLB invasion is related to landscape heterogeneity, including habitat composition and configuration (With, 2002; O'Reilly-Nugent et al., 2016). Furthermore, the host species range should not be underestimated in its influence on OLB invasion, primarily represented by oak species (Tomescu et al., 2018; Csóka et al., 2019; Paulin et al., 2020). In the Carpathian region, the food resources available to this insect are limited, which may significantly contribute to the creation of a natural barrier to OLB's spread, at least for the time being.

Regarding forest ecosystems, in the initial years of the study (2017–2020), thermophilous forest ecosystems, especially those featuring termophilous Turkey oak and Hungarian oak forests, termophilous pedunculate oak forests, and grey oak forests, proved to be the most affected. This finding aligns with the results of a Eurasian study (Csóka et al., 2019), which identified *Quercus cerris* L., *Q. petraea* (Matt.) Liebl., *Q. pubescens* Willd. and particularly *Q. robur* L. as the species that suffered the most significant attacks across all the countries studied. Furthermore, Marković et al. (2021) demonstrated that by studying OLB's preference for different oak species in field conditions, the insect exhibited the greatest preference for the Hungarian oak and the least for pedunculate oak. Additionally, in terms of the spatial distribution of the invasion, it is evident that

TABLE 2 Correlation analysis of insect damage with altitudinal and climatic variables.

Pair of variables	Spearman R value	Value of p
Damage & altitude	−0.2486	0.0000
Damage & average year temperature	0.0648	0.0031
Damage & average winter temperature	0.0232	0.2909
Damage & average overwinter temperature	0.0247	0.2601
Damage & annual precipitation	−0.0444	0.0427
Damage & winter precipitation	0.0342	0.1190
Damage & overwinter precipitation	−0.0063	0.7755
Damage & average growing season temperature	0.0857	0.0001
Damage & growing season precipitation	0.0125	0.5704

Bold values indicate statistically significant correlations.

during this period, the forests in the western part of the country, particularly in the south, experienced more severe impacts than other regions. This trend can be attributed to the initial reports of the insect in these two regions (Don et al., 2016; Chireceanu et al., 2017), making the southern part of the country one of the most severely affected areas in Romania (Tomescu et al., 2018).

In the last years of the study period, we observe an expansion of locations where the insect is present in thermophilous ecosystems, coupled with a reduction in the severity of damage in the forests of these regions. This suggests that the areas with strong attacks are diminishing in intensity, while the number of areas with mild damage is increasing. Simultaneously, we notice that OLB has extended its range to higher altitudes, infiltrating montane environmentals and predominantly establishing in mesophilic oak forests. In the final year of the study, most of the points with very strong attacks are in sessile oak forests or mixed beech-oak forests. This phenomenon might indicate a potential adaptation of OLB to new conditions, including the insect's ability to colonize and explore new environments, progressively overcoming natural barriers. These results are consistent with another study (Paulin et al., 2023), which suggests that OLB is adapted to surviving Central European winter conditions, with low winter temperatures not being a major limiting factor for its expansion in the invaded regions, as supported by previous observations in Hungary (Csepelényi et al., 2017; Paulin et al., 2021).

It is worth noting that these findings align with research by Robinet and Roques (2010), which posits that climate change can play a pivotal role in the rapid spread of invasive insects. Rising temperatures enable the introduction of species into areas where they could not survive previously (Walther et al., 2009). For instance, Régnière et al. (2009) provide a compelling example of the invasive species Lymantria dispar (Linnaeus, 1758) (Lepidoptera, Erebidae) in Canada, showcasing its close correlation with favourable climatic conditions. Increasing temperatures have allowed this insect to expand its population north-westward in the country. Moreover, research by Jaworski and Hilszczański (2013) suggests that invasive species such as Parectopa robiniella Clemens, 1863 and Phyllonorycter robiniella (Clemens, 1859), (both Lepidoptera: Gracillariidae), introduced in Southern Europe from North America during the latter half of the 20th century, have

extended their range northward on the continent primarily due to temperature increases. These examples underscore the importance of considering climate change when assessing the behaviour of invasive species like OLB.

Overall, the analysis of major attacks in forest ecosystems suggests that climate changes can play a crucial role in the expansion and intensification of the OLB invasion in mesophilous forest ecosystems in Romania. Increasing temperatures and decreasing precipitation in these ecosystems may have contributed to increased stress on host trees, rendering them more susceptible to OLB attacks. Furthermore, based on prior observations (Bălăcenoiu et al., 2021c), we have highlighted that the daily and seasonal dynamics of the OLB population are significantly influenced by climatic factors. In this context, it becomes increasingly plausible that OLB is developing adaptive capabilities and thriving in mountainous environments, establishing itself as a remarkable and challenging invasive species for the forest ecosystems of Romania. "Studies have shown that rising winter temperatures have allowed some species to extend their ranges. For example, rising winter temperatures allowed the southern pine beetle Dendroctonus frontalis Zimmermann, 1868 (Coleoptera, Curculionidae) to extend its range to northern latitudes (Ungerer et al., 1999). Similarly, warmer winters enabled the expansion of species like Operophtera brumata (Linnaeus, 1758) and Epirrita autumnata (Borkhausen, 1794) (both Lepidoptera, Geometridae) northward into Scandinavia (Jepsen et al., 2008). Certainly, temperature increases not only lead to latitudinal range extensions but also to altitudinal ones. A striking example is the Mediterranean species, the pine processionary moth Thaumetopoea pityocampa (Denis and Schiffermüller, 1775) (Lepidoptera, Notodontidae), which expanded its range into the mountainous regions of the Alps, reaching altitudes exceeding 1,400 meters due to the rising temperatures in both the winter and the flight period of females (Battisti et al., 2006).

The PCA analysis reveals a significant influence of climatic factors on the expansion and intensification of the Oak Lace Bug (OLB) invasion in the Romanian mesophilous ecosystems. The substantial increase in temperatures and the decrease in precipitation are closely associated with the heightened intensity of attacks, suggesting increased activity of the insect in these ecosystems and enhanced efficiency in attacking their hosts. These climatic factors may lead to a drier environment in mountainous ecosystems, potentially contributing to the water stress experienced by host trees. By the end of the century, European forests could undergo remarkable changes due to the climate change phenomenon, which will substantially alter the current distribution of climatically suitable areas for the majority of European tree species (Buras and Menzel, 2019; Mauri et al., 2022). In this context, harmful effects for several insect guilds, such as the OLB, can be expected, as the new microclimates may also become more favorable for certain insect groups (Sallé et al., 2021). Regarding our results, this additional climatic stress renders the trees more vulnerable to OLB attacks, which can explain the notable rise in the attack levels under these conditions. These findings align with the results of another study (Ju et al., 2011), which indicates an increase in both average fecundity and the success rate of passing through all developmental stages in Corythucha ciliata (Say, 1832) (Hemiptera, Tingidae), a closely related species to the one studied here, in response to rising temperatures. Additionally, similar conclusions have been drawn by Lu et al. (2019), who observed a significant impact of air

temperature on the flight distance of *C. ciliata*. Our research primarily focuses on the study of select climatic and environmental factors that influence the invasion of the oak lace bug, as it is essential to gain a deeper understanding of this invasion's dynamics in Romania and to formulate effective management strategies for this invasive species. While human-mediated introduction of potentially invasive species is a well-recognized factor (Brockerhoff et al., 2006; Skarpaas and Økland, 2009), our present work dedicates particular attention to elucidating the critical ecological and climatic aspects of this invasion. It is worth noting that invasive species' movement and establishment can be influenced by a complex interplay of factors beyond climate, environment, and human activities (e.g., habitat availability, host tree diversity, predator–prey relationships, and more). Therefore, our study underscores the importance of continued monitoring and research efforts to comprehensively grasp the evolution of the OLB's presence in Romania and to devise robust strategies for its management.

Nevertheless, it is essential to acknowledge certain limitations in our study that may impact the robustness and generalizability of the findings. Firstly, the relatively short duration of the study period, spanning from 2017 to 2022, might limit our ability to conclusively assert the influence of climatic factors on the behaviour of the OLB. Climate patterns exhibit long-term trends, and our study may not capture the full spectrum of these influences. Recognizing this, we intend to continue monitoring OLB behaviour in subsequent years to enhance our understanding of its relationship with climatic conditions. Secondly, the reliance on visual assessment for determining the extent of foliage discoloration introduces potential biases in data collection. While visual inspections are a widely used method, the subjectivity inherent in human judgment may lead to variations in assessing the severity of OLB damage. The current study attempted to mitigate this limitation by categorizing the damage caused by OLB into five distinct levels. However, it is essential to recognize that advancements in Artificial Intelligence data processing may enhance the objectivity of remote sensing technologies in the future. Exploring these technological advancements could further refine and standardize the methodology for quantifying OLB-induced foliage discoloration, addressing concerns about potential biases associated with visual assessments.

5 Conclusion

Geographical spread: initially, oak lace bug was mainly observed in the extra Carpathian regions of Romania, particularly in the southern, western, and northwestern parts. However, there has been a recent expansion into the eastern region.

Change in attack patterns: in recent years (2021–2022), OLB presence has become more frequent, especially in thermophilous ecosystems, coinciding with a decrease in damage intensity.

Mountain environment impact: in the last year of the study, most points with very strong OLB attacks were observed in mountain environments, particularly within mesophilous sessile oak and mixed beech-oak forests.

Climate influence: climate analysis indicated that OLB's major attacks were associated with specific temperature and precipitation ranges, suggesting that climatic factors play a significant role in its behaviour.

Altitude: there was an inverse relationship between altitude and OLB attacks, with lower elevations in mesophilous ecosystems being more prone to severe attacks. This relationship may be associated with both abiotic factors such as precipitation and temperature, as well as the distribution of oak species in those specific altitudinal ranges.

Data availability statement

The original contributions presented in the study are included in the article/supplementary material, further inquiries can be directed to the corresponding author.

Author contributions

FB: Conceptualization, Formal analysis, Investigation, Methodology, Writing – original draft. CN: Conceptualization, Funding acquisition, Methodology, Project administration, Writing – review & editing. DT: Conceptualization, Data curation, Investigation, Writing – review & editing. IP: Formal analysis, Writing – review & editing.

Funding

Acknowledgments

Conflict of interest

The authors declare that the research was conducted in the absence of any commercial or financial relationships that could be construed as a potential conflict of interest.

Publisher's note

All claims expressed in this article are solely those of the authors and do not necessarily represent those of their affiliated organizations, or those of the publisher, the editors and the reviewers. Any product that may be evaluated in this article, or claim that may be made by its manufacturer, is not guaranteed or endorsed by the publisher.

References

Bălăcenoiu, F., Japelj, A., Bernardinelli, I., Castagneyrol, B., Csóka, G., and Glavendekić, M. (2021a). Corythucha arcuata (say, 1832) (Hemiptera, Tingidae) in its invasive range in Europe: perception, knowledge and willingness to act in foresters and citizens. *NeoBiota* 69:133. doi: 10.3897/neobiota.69.71851

Bălăcenoiu, F., Neţoiu, C., Tomescu, R., Simon, D. C., and Buzatu, A. (2021b). Chemical control of Corythucha arcuata (say, 1832), an invasive alien species, in oak forests. *Forests* 12:770. doi: 10.3390/f12060770

Bălăcenoiu, F., Simon, D. C., Neţoiu, C., Toma, D., and Petriţan, I. C. (2021c). The seasonal population dynamics of Corythucha arcuata (say, 1832) (Hemiptera: Tingidae) and the relationship between meteorological factors and the diurnal flight intensity of the adults in Romanian oak forests. *Forests* 12:1774. doi: 10.3390/f12121774

Bale, J. S. (2002). Insects and low temperatures: from molecular biology to distributions and abundance. *Philos. Trans. R. Soc. Lond. Ser. B Biol. Sci.* 357, 849–862. doi: 10.1098/rstb.2002.1074

Battisti, A., Stastny, M., Buffo, E., and Larsson, S. (2006). A rapid altitudinal range expansion in the pine processionary moth produced by the 2003 climatic anomaly. *Glob. Chang. Biol.* 12, 662–671. doi: 10.1111/j.1365-2486.2006.01124.x

Bernardinelli, I. (2006). Potential host plants of Corythucha arcuata (Het., Tingidae) in Europe: a laboratory study. *J. Appl. Entomol.* 130, 480–484. doi: 10.1111/j.1439-0418.2006.01098.x

Bernardinelli, I., and Zandigiacomo, P. (2000). Prima segnalazione di Corythucha arcuata (say) (Heteroptera, Tingidae) in Europa. *Inf Fitopatol* 50, 47–49.

Blackburn, T. M., Essl, F., Evans, T., Hulme, P. E., Jeschke, J. M., and Kühn, I. (2014). A unified classification of alien species based on the magnitude of their environmental impacts. *PLoS Biol.* 12:e1001850. doi: 10.1371/journal.pbio.1001850

Brockerhoff, E. G., Liebhold, A. M., and Jactel, H. (2006). The ecology of forest insect invasions and advances in their management. *Can. J. For. Res.* 36, 263–268. doi: 10.1139/x06-013

Buras, A., and Menzel, A. (2019). Projecting tree species composition changes of European forests for 2061–2090 under RCP 4.5 and RCP 8.5 scenarios. *Front. Plant Sci.* 9:1986. doi: 10.3389/fpls.2018.01986

Chireceanu, C., Teodoru, A., and Chiriloaie, A. (2017). First record of oak lace bug Corythucha arcuata (Tingidae: Heteroptera) in Romania. 7th ESENIAS Workshop with Scientific Conference

Connell, W. A., and Beacher, J. H. (1947). *Life history and control of the oak lace bug.*

Cornes, R. C., Van Der, S. G., Van Den, B. E. J. M., and Jones, P. D. (2018). An ensemble version of the E-OBS temperature and precipitation data sets. *J. Geophys. Res. Atmos.* 123, 9391–9409. doi: 10.1029/2017JD028200

Costanza, R., d'Arge, R., de Groot, R., Farber, S., Grasso, M., and Hannon, B. (1997). The value of the world's ecosystem services and natural capital. *Nature* 387, 253–260. doi: 10.1038/387253a0

Csepelényi, M., Hirka, A., Szénási, Á., Mikó, Á., and Szőcs, L. (2017). Az inváziós tölgy csipkéspoloska Corythucha arcuata (say, 1832) gyors terjeszkedése és tömeges fellépése Magyarországon=rapid area expansion and mass occurrences of the invasive oak lace bug Corythucha arcuata (say 1932) in Hungary. *Erdészettudományi Közlemények* 7, 127–134. doi: 10.17164/EK.2017.009

Csóka, G., Hirka, A., Mutun, S., Glavendekić, M., Mikó, Á., and Szőcs, L. (2019). Spread and potential host range of the invasive oak lace bug Corythucha arcuata (say, 1832)-Heteroptera: Tingidae in Eurasia. *Agric. For. Entomol.* 22, 61–74. doi: 10.1111/afe.12362

Csóka, G., Hirka, A., and Somlyai, M. (2013). A tölgy csipkéspoloska (Corythuca arcuata Say, 1832-Hemiptera, Tingidae) első észlelése Magyarországon. *Novenyvedelem* 49, 293–296.

Dautbašić, M., Zahirović, K., Mujezinović, O., and Margaletić, J. (2018). Prvi nalaz hrastove mrežaste stjenice (Corythucha arcuata) u Bosni i Hercegovini. *Sumar List* 142, 179–181. doi: 10.31298/sl.142.3-4.6

de Groot, R. S., Alkemade, R., Braat, L., Hein, L., and Willemen, L. (2010). Challenges in integrating the concept of ecosystem services and values in landscape planning, management and decision making. *Ecol. Complex.* 7, 260–272. doi: 10.1016/j.ecocom.2009.10.006

Dobreva, M., Simov, N., Georgiev, G., et al. (2013). First record of Corythucha arcuata (say) (Heteroptera: Tingidae) on the Balkan peninsula. *Acta Zool Bulg* 65, 409–412.

Don, I., Don, C. D., and Sasu, L. R. (2016). Insect pests on the trees and shrubs from the Macea botanical garden. *Studia Universitatis Vasile Goldis Arad* 11, 23–28.

Doniţă, N, Bândiu, C, and Biriş, IA, (2008). *Harta forestieră a României pe unităţi ecosistemice, scara 1: 500 000/Forest Map of Romania-based on forest ecosystem types, scale 1: 500 000. Editura Silvică, Bucureşti*

EPPO. (2001). *Introduction of Corythucha arcuata in Italy. Addition to the EPPO alert list. EPPO [global database] reporting service no. 03–2001.Num. Article 2001/057*

EPPO. (2007). *EPPO [global database] (2007) mini data sheet on Corythucha arcuata*

Forster, B., Giacalone, I., Moretti, M., et al. (2005). die amerikanische eichennetzwanze Corythucha arcuata (Say) (Heteroptera, Tingidae) hat die Sudschweiz erreicht. *Mitteilungen-Schweizerische entomologische gesellschaft* 78:317.

Haq, S. M., Amjad, M. S., Waheed, M., and Bussmann, R. W. (2022). The floristic quality assessment index as ecological health indicator for forest vegetation: a case study from Zabarwan Mountain range, Himalayas. *Ecol. Indic.* 145:109670. doi: 10.1016/j.ecolind.2022.109670

Haq, S. M., Khoja, A. A., Lone, F. A., Waheed, M., and Bussmann, R. W. (2023a). Floristic composition, life history traits and phytogeographic distribution of forest vegetation in the Western Himalaya. *Front Forests Global Chang* 6:1169085. doi: 10.3389/ffgc.2023.1169085

Haq, S. M., Rashid, I., Waheed, M., and Khuroo, A. A. (2023b). From forest floor to tree top: partitioning of biomass and carbon stock in multiple strata of forest vegetation in Western Himalaya. *Environ. Monit. Assess.* 195:812. doi: 10.1007/s10661-023-11376-6

Haq, S. M., Waheed, M., Khoja, A. A., Amjad, M. S., and Bussmann, R. W. (2023c). Measuring forest health at stand level: a multi-indicator evaluation for use in adaptive management and policy. *Ecol. Indic.* 150:110225. doi: 10.1016/j.ecolind.2023.110225

Haran, J., Roques, A., Bernard, A., Robinet, C., and Roux, G. (2015). Altitudinal barrier to the spread of an invasive species: could the Pyrenean chain slow the natural spread of the pinewood nematode? *PLoS One* 10:e0134126. doi: 10.1371/journal.pone.0134126

Hrašovec, B., Posarić, D., Lukić, I., and Pernek, M. (2013). Prvi nalaz hrastove mrežaste stjenice (Corythucha arcuata) u Hrvatskoj. *Sumar List* 137, 499–503.

Hulme, P. E. (2014). Invasive species challenge the global response to emerging diseases. *Trends Parasitol.* 30, 267–270. doi: 10.1016/j.pt.2014.03.005

Jaworski, T, and Hilszczański, J. (2013). The effect of temperature and humidity changes on insects development their impact on forest ecosystems in the context of expected climate change.

Jenkins, M., and Schaap, B. (2018). Forest ecosystem services. Background analytical study 1. Available at: https://www.un.org/esa/forests/wp-content/uploads/2018/05/UNFF13_BkgdStudy_ForestsEcoServices.pdf (Accessed November 13, 2023).

Jepsen, J. U., Hagen, S. B., Ims, R. A., and Yoccoz, N. G. (2008). Climate change and outbreaks of the geometrids Operophtera brumata and Epirrita autumnata in subarctic birch forest: evidence of a recent outbreak range expansion. *J. Anim. Ecol.* 77, 257–264. doi: 10.1111/j.1365-2656.2007.01339.x

Jeschke, J. M., Keesing, F., and Ostfeld, R. S. (2013). Novel organisms: comparing invasive species, GMOs, and emerging pathogens. *Ambio* 42, 541–548. doi: 10.1007/s13280-013-0387-5

Ju, R.-T., Gao, L., Wei, S.-J., and Li, B. (2017). Spring warming increases the abundance of an invasive specialist insect: links to phenology and life history. *Sci. Rep.* 7:14805. doi: 10.1038/s41598-017-14989-3

Ju, R.-T., Wang, F., and Li, B. (2011). Effects of temperature on the development and population growth of the sycamore lace bug, Corythucha ciliata. *J. Insect Sci.* 11, 1–12. doi: 10.1673/031.011.0116

Jurc, M., and Jurc, D. (2017). The first record and the beginning the spread of oak lace bug, Corythucha arcuata (say, 1832) (Heteroptera: Tingidae), in Slovenia. *Sumar List* 141:488. doi: 10.31298/sl.141.9-10.5

Kang, L., Chen, B., Wei, J.-N., and Liu, T.-X. (2009). Roles of thermal adaptation and chemical ecology in Liriomyza distribution and control. *Annu. Rev. Entomol.* 54, 127–145. doi: 10.1146/annurev.ento.54.110807.090507

Kovač, M., Gorczak, M., Wrzosek, M., Tkaczuk, C., and Pernek, M. (2020). Identification of entomopathogenic fungi as naturally occurring enemies of the invasive oak lace bug, Corythucha arcuata (say) (Hemiptera: Tingidae). *Insects* 11:679. doi: 10.3390/insects11100679

Kovač, M., Linde, A., Lacković, N., Bollmann, F., and Pernek, M. (2021). Natural infestation of entomopathogenic fungus Beauveria pseudobassiana on overwintering Corythucha arcuata (say) (Hemiptera: Tingidae) and its efficacy under laboratory conditions. *For. Ecol. Manag.* 491:119193. doi: 10.1016/j.foreco.2021.119193

Lindner, M., Maroschek, M., Netherer, S., Kremer, A., Barbati, A., and Garcia-Gonzalo, J. (2010). Climate change impacts, adaptive capacity, and vulnerability of European forest ecosystems. *For. Ecol. Manag.* 259, 698–709. doi: 10.1016/j.foreco.2009.09.023

Lovell, S. J., Stone, S. F., and Fernandez, L. (2006). The economic impacts of aquatic invasive species: a review of the literature. *J. Agric. Resour. Econ.* 35, 195–208. doi: 10.1017/S1068280500010157

Lu, S. H., Wei, M. C., Yuan, G. J., Cui, J. X., and Gong, D. F. (2019). Flight behavior of the sycamore lace bug, Corythucha ciliata, in relation to temperature, age, and sex. *J. Integr. Agric.* 18, 2330–2337. doi: 10.1016/s2095-3119(19)62624-9

Marković, Č., Dobrosavljević, J., and Milanović, S. (2021). Factors influencing the oak lace bug (Hemiptera: Tingidae) behavior on oaks: feeding preference does not mean better performance? *J. Econ. Entomol.* 114, 2051–2059. doi: 10.1093/jee/toab148

Mauri, A., Girardello, M., Strona, G., Beck, P. S. A., and Forzieri, G. (2022). EU-Trees4F, a dataset on the future distribution of European tree species. *Scient Data* 9:37. doi: 10.1038/s41597-022-01128-5

Mellanby, K. (1939). Low temperature and insect activity. *Proc R Soc London B* 127, 473–487. doi: 10.1098/rspb.1939.0035

Meshkova, V. (2022). Insecte fitofage invazive din arboretele și parcurile din Ucraina. *Bucovina Forestiera* 22:29. doi: 10.4316/bf.2022.004

Meyerson, L. A., and Mooney, H. A. (2007). Invasive alien species in an era of globalization. *Front. Ecol. Environ.* 5:199. doi: 10.1890/1540-9295(2007)5[199:IASIAE]2.0.CO;2

Mutun, S. (2003). First report of the oak lace bug, Corythucha arcuata (say, 1832) (Heteroptera: Tingidae), from Bolu, Turkey. *Isr. J. Zool.* 49, 323–324.

Mutun, S., Ceyhan, Z., and Sözen, C. (2009). Invasion by the oak lace bug, Corythucha arcuata (say) (Heteroptera: Tingidae), in Turkey. *Turk J. Zool.* 33, 263–268. doi: 10.3906/zoo-0806-13

Neimorovets, V. V., Shchurov, V. I., Bondarenko, A. S., et al. (2017). First documented outbreak and new data on the distribution of Corythucha arcuata (say, 1832) (Hemiptera: Tingidae) in Russia. *Acta Zool Bulg* 9, 139–142.

NFI. (2018). National Forest inventor results – cycle II 2013–2018: Forest. Web: Available at: http://roifn.ro/site/rezultate-ifn-2/ (Accessed November 13, 2023).

Nikolic, N., Pilipovic, A., Drekic, M., Kojic, D., and Poljakovic-Pajnik, L. (2019). Physiological responses of pedunculate oak (Quercus robur L.) to Corythucha arcuata (say, 1832) attack. *Arch Biol Sci* 71, 167–176. doi: 10.2298/ABS180927058N

O'Reilly-Nugent, A., Palit, R., Lopez-Aldana, A., and Medina-Romero, M. (2016). Landscape effects on the spread of invasive species. *Curr Landsc Ecol Rep* 1, 107–114. doi: 10.1007/s40823-016-0012-y

Pap, P., Drekić, M., Poljaković-Pajnik, L., et al. (2015). Monitoring zdravstvenog stanja šuma na teritoriji Vojvodine u 2015. godini. *Topola* 195, 117–133.

Paulin, M. J., Eötvös, C. B., Zabransky, P., Csóka, G., and Schebeck, M. (2023). Cold tolerance of the invasive oak lace bug, Corythucha arcuata. *Agric. For. Entomol.* 25, 612–621. doi: 10.1111/afe.12585

Paulin, M., Hirka, A., Csepelényi, M., Fürjes-Mikó, Á., Tenorio-Baigorria, I., and Eötvös, C. (2021). Overwintering mortality of the oak lace bug (Corythucha arcuata) in Hungary – a field survey. *Lesnicky Casopis* 67, 108–112. doi: 10.2478/forj-2020-0024

Paulin, M., Hirka, A., Eötvös, C. B., Gáspár, C., and Fürjes-Mikó, Á. (2020). Known and predicted impacts of the invasive oak lace bug (Corythucha arcuata) in European oak ecosystems – a review. *Folia Oecologica* 47, 131–139. doi: 10.2478/foecol-2020-0015

Pearce, D. W. (2001). The economic value of forest ecosystems. *Ecosyst. Health* 7, 284–296. doi: 10.1046/j.1526-0992.2001.01037.x

Pimentel, D., Lach, L., Zuniga, R., and Morrison, D. (2000). Environmental and economic costs of nonindigenous species in the United States. *Bioscience* 50, 53–65. doi: 10.1641/0006-3568(2000)050[0053:EAECON]2.3.CO;2

Poljaković-Pajnik, L., Drekić, M., Pilipović, A., et al. (2015). Pojava velikih šteta od Corythucha arcuata (Say) (Heteroptera: Tingidae) u šumama hrasta u Vojvodini. XIII savetovanje o zaštiti bilja. *Zbornik radova str*:63.

Régnière, J., Nealis, V., and Porter, K. (2009). Climate suitability and management of the gypsy moth invasion into Canada. *Diabetologia* 10, 135–148. doi: 10.1007/978-1-4020-9680-8_10

Robinet, C., and Roques, A. (2010). Direct impacts of recent climate warming on insect populations. *Integr Zool* 5, 132–142. doi: 10.1111/j.1749-4877.2010.00196.x

Sallé, A., Cours, J., Le Souchu, E., Lopez-Vaamonde, C., and Pincebourde, S. (2021). Climate change alters temperate forest canopies and indirectly reshapes arthropod communities. *Front Forests Global Change* 4:710854. doi: 10.3389/ffgc.2021.710854

Sallmannshofer, M., Ette, S., Hinterstoisser, W., et al. (2019). Erstnachweis der Eichennetzwanze, Corythucha arcuata, in Österreich. *Aktuell* 66, 1–6.

Schindler, S., Staska, B., Adam, M., Rabitsch, W., and Essl, F. (2015). Alien species and public health impacts in Europe: a literature review. *NeoBiota* 27:1. doi: 10.3897/neobiota.27.5007

Simberloff, D., Martin, J.-L., Genovesi, P., Maris, V., Wardle, D. A., and Aronson, J. (2013). Impacts of biological invasions: what's what and the way forward. *Trends Ecol. Evol.* 28, 58–66. doi: 10.1016/j.tree.2012.07.013

Simov, N., Grozeva, S., Langourov, M., et al. (2018). Rapid expansion of the oak lace bug Corythucha arcuata (say, 1832) (Hemiptera: Tingidae) in Bulgaria. *Hist Nat Bulg* 27, 51–55.

Sinclair, B. J., Vernon, P., Klok, C. J., and Chown, S. L. (2003). Insects at low temperatures: an ecological perspective. *Trends Ecol. Evol.* 18, 257–262. doi: 10.1016/S0169-5347(03)00014-4

Skarpaas, O., and Økland, B. (2009). Timber import and the risk of forest pest introductions. *J. Appl. Ecol.* 46, 55–63. doi: 10.1111/j.1365-2664.2008.01561.x

Sönmez, E., Demirbağ, Z., and Demir, I. (2016). Pathogenicity of selected entomopathogenic fungal isolates against the oak lace bug, Corythucha arcuata say. (Hemiptera: Tingidae), under controlled conditions. *Turk. J. Agric. For.* 40, 715–722. doi: 10.3906/tar-1412-10

Streito, J.-C., Balmès, V., Aversenq, P., et al. (2018). Corythucha arcuata (Say, 1832) et Stephanitis lauri Rietschel, 2014, deux espèces invasives nouvelles pour la faune de France (Hemiptera Tingidae). *L'Entomologiste* 74, 133–136.

StatSoft Inc. (2007). *STATISTICA (data analysis software system). Version, 8.0. www.statsoft.com.*

Tomescu, R., Olenici, N., Netoiu, C., Balacenoiu, F., and Buzatu, A. (2018). Invasion of the oak lace bug Corythucha arcuata (say.) in Romania: a first extended reporting. *Ann. For. Res.* 61, 161–170. doi: 10.15287/afr.2018.1187

Trumbore, S., Brando, P., and Hartmann, H. (2015). Forest health and global change. *Science* 349, 814–818. doi: 10.1126/science.aac6759

Ungerer, M. J., Ayres, M. P., and Lombardero, M. J. (1999). Climate and the northern distribution limits of Dendroctonus frontalis Zimmermann (Coleoptera: Scolytidae). *J. Biogeogr.* 26, 1133–1145. doi: 10.1046/j.1365-2699.1999.00363.x

Vilà, M., Basnou, C., Pyšek, P., Josefsson, M., Genovesi, P., and Gollasch, S. (2010). How well do we understand the impacts of alien species on ecosystem services? A pan-European, cross-taxa assessment. *Front. Ecol. Environ.* 8, 135–144. doi: 10.1890/080083

Vilà, M., Espinar, J. L., Hejda, M., Hulme, P. E., Jarošík, V., and Maron, J. L. (2011). Ecological impacts of invasive alien plants: a meta-analysis of their effects on species, communities and ecosystems. *Ecol. Lett.* 14, 702–708. doi: 10.1111/j.1461-0248.2011.01628.x

Walther, G.-R., Roques, A., Hulme, P. E., Sykes, M. T., Pysek, P., and Kühn, I. (2009). Alien species in a warmer world: risks and opportunities. *Trends Ecol. Evol.* 24, 686–693. doi: 10.1016/j.tree.2009.06.008

Ward, S. F., Venette, R. C., and Aukema, B. H. (2019). Cold tolerance of the invasive larch casebearer and implications for invasion success. *Agric. For. Entomol.* 21, 88–98. doi: 10.1111/afe.12311

With, K. A. (2002). The landscape ecology of invasive spread. *Conserv. Biol.* 16, 1192–1203. doi: 10.1046/j.1523-1739.2002.01064.x

Zúbrik, M., Gubka, A., Rell, S., Kunca, A., Vakula, J., and Galko, J. (2019). First record of Corythucha arcuata in Slovakia-short communication. *Plant Prot. Sci.* 55, 129–133. doi: 10.17221/124/2018-PPS

Integrating monetary and non-monetary valuation for ecosystem services in Piatra Craiului national park, Southern Carpathians: a comprehensive approach to sustainability and conservation

Serban Chivulescu[1], Mihai Hapa[1,2]*, Diana Pitar[1],
Adrian Lorenţ[1,2], Luminita Marmureanu[1], Stefan Leca[1],
Raul Radu[1], Roxana Cazacu[1], Alexandru Claudiu Dobre[1],
Ionut Silviu Pascu[1], Cristiana Marcu[1], Mircea Verghelet[3],
Constantin Vezeanu[3], Tudor Racoviceanu[4,5] and
Ovidiu Badea[1,2]

[1]National Institute for Research and Development in Forestry "Marin Drăcea," Voluntari, Romania,
[2]Faculty of Silviculture and Forest Engineering, "Transilvania" University of Braşov, Braşov, Romania,
[3]Piatra Craiului National Park Administration, RNP-ROMSILVA, Zărneşti, Romania, [4]Research Centre in
Systems Ecology and Sustainability, Faculty of Biology, University of Bucharest, Bucharest, Romania,
[5]IHS-Romania SRL, Bucharest, Romania

The concept of ecosystem services and their valuation has gained significant attention in recent years due to the profound interdependence and interconnectedness between humans and ecosystems. As several studies on valuation of forest ecosystem services have stressed the human-nature interactions lately, in the research study area, the environmental conditions shows rapid changes while human pressures on forests intensify. Thus, the research questions are as follows: (i) what are the the monetary and non-monetary value of ecosystem services provided by forests in Piatra Craiului National Park and (ii) their relationship with other variables, focusing on identifying differences and resemblances between each approach. The R PASTECS package was utilized to analyze primary statistical indicators for both monetary and non-monetary values, revealing significant variability in the results (s% monetary 141% and s% non-monetary 62%). Both monetary and non-monetary assessments were computed at the management unit level and the data used was provided by the Forest Management plans and photograph analysis which have significant value as indicators of ecosystem services. The correlation between nature and culture was assessed through social-media based method, highly known to stimulate participant engagement while the quantitative data was assessed through forest data computation and PCA method for visualization. The research highlighted that, in monetary terms, the minimum value of identified ecosystem services was €34 and the maximum value exceeded €570,000 at management unit level and in non-monetary terms, the values ranged from 1 to 5 (kernel score). The research

reveals a substantial variability in both types of valuations. Strong associations between certain variables (monetary value with carbon stock and stand volume), moderate connections (slope with stand productivity), and weaker relationships (non-monetary value with altitude, age with slope, type of flora with altitude, and altitude with stand productivity) were revealed. The findings provided valuable insights for policymakers, land managers, and stakeholders involved in natural resource management and conservation, emphasizing the importance of considering both economic and non-economic benefits in decision-making processes. The integrated approach of this study shows how we can better assess the mixed value of ecosystem services, contributing to the ongoing actions of raising awareness and social responsibility.

1 Introduction

The concept of ecosystem services has garnered significant attention in recent years due to its recognition of the profound interdependence and interconnectedness between humans and ecosystems (Zhang et al., 2021), which plays a vital role in supporting human wellbeing and sustainability (Costanza et al., 2014). Moreover, this concept has been emphasized in the past by the Millennium Ecosystem Assessment (MEA), in 2005, which sought to alter public perceptions of natural ecosystems by raising awareness and enhancing knowledge about the services they provide. This breakthrough not only showed us the value of nature but also highlighted how nature's services directly impact our wellbeing. The MEA aimed at mitigating degradation (Millennium Ecosystem Assessmen, 2005; Carpenter et al., 2009; Reyers et al., 2013) and addressing the impacts of climate change on society as a whole. It emphasized that the emergence of ecosystem services as a framework can serve as a valuable tool in decision-making processes (Martínez Pastur et al., 2016; Bell-James, 2020), reinforcing the need for considering nature's contributions in various policy and management strategies.

Since ecosystem services encompasses the bundles of benefits to humans and society such as provisioning of essential resources and regulating its involved processes (pollination, decomposition, water purification, erosion and flood control, and carbon storage and climate regulation) (Millennium Ecosystem Assessmen, 2005), they fundamentally link ecology, economics and social wellbeing together (Everard, 2013). Nevertheless, researchers such as Luck et al. (2012) and Schröter et al. (2014) have examined various concerns related to ethical perceptions of valuing nature based on its utility rather than its intrinsic value. There is a spectrum of perspectives on the concept of ecosystem services, with some favoring its general application, while others advocate for a distinct approach that involves separation, monetization, and treating it as a commodity, as discussed by Bell-James (2020). Even though the concept of ES framework has been shown to emphasize the multiple ways of dependency between humans and nature, the framework is believed to have failed due to continuous ecosystem loss and ecological breakdown, attributed to the core foundations of modern Western culture (Muradian and Gómez-Baggethun, 2021).

To highlight the role of ecosystem services, for a correct valuation Spangenberg and Settele (2010) suggested the use of adequate methods integrating monetary and non-monetary valuation of ES (traditional economic valuation techniques such as cost-benefit analysis and stated preference methods for monetary valuation, alongside qualitative assessments, multi-criteria analysis, and integrated models to capture non-monetary values).

Monetary valuation has been widely utilized as a direct method to assess the economic value of ecosystem services (Baveye et al., 2013). This approach involves assigning a monetary value to goods and services provided by ecosystems, based on market prices or other valuation techniques (Turner et al., 2003; Baveye et al., 2013; Selivanov and Hlaváčková, 2021). It provides policymakers with quantifiable information that can be integrated into cost-benefit analyses and policy-making processes, providing a deeper understanding of the real contributions of nature to human wellbeing (Balmford et al., 2002; Jiang et al., 2021). Nevertheless, monetary valuation often overlooks the inherent non-monetary aspects of ecosystem services, such as cultural and social values, which are challenging to capture in monetary terms. Thus, methods are often pondered, and a combination of them might provide greater reliability (Daily et al., 2009; Custódio et al., 2020). The dimension of knowledge regarding ecosystem services as a means of a possible non-monetary evaluation depends on the values of the civil society correlated with certain locations or environmental areas (Paracchini et al., 2014; Martínez Pastur et al., 2016; Sharma et al., 2022). However, cultural ecosystem services are tricky to address, requiring a multidisciplinary and comprehensive approach because, ultimately, it is about the access right and right to nature as some argue (Tenerelli et al., 2016; Kosanic and Petzold, 2020). Thus, establishing a comprehensive approach toward the space of cultural ecosystem services (CES) has to take into account the connectivity between capacity building and raising awareness, besides the evaluation per-se (Scholte et al., 2015).

To capture the diversity of values correlated with nature, the non-monetary approach looks into the values, preferences,

perceptions, demands, and experiences of the people who benefit from ecosystem services, demonstrating the pluralistic value of nature and its close connection to the ES framework (Chan et al., 2013; Custódio et al., 2020). These methods typically involve surveys, interviews, social-media based approaches, or other concepts from the citizen science principles to collect data on people's perceptions and willingness to pay for ecosystem services (Boyd and Banzhaf, 2007; Cabana et al., 2020; Isse et al., 2021; Peri et al., 2022; Sharma et al., 2022). Non-monetary valuation recognizes the diverse range of values (biodiversity conservation, cultural significance, aesthetic enjoyment, recreational opportunities) associated with ecosystems and offers a more comprehensive understanding of the benefits they provide (Díaz et al., 2018; Sharma et al., 2022).

For the area where the research was carried out, respectively, Romania, several studies have been conducted to assess forest ecosystem services, including carbon sequestration (Chivulescu and Schiteanu, 2017; Dobre et al., 2021; Nichiforel et al., 2021; Pache et al., 2021; Pitar et al., 2021; Chivulescu et al., 2022) water purification (Petz et al., 2012; Platon et al., 2015), and recreational value (Hartel et al., 2014; Bogdan et al., 2019; Tudoran et al., 2022). However, as environmental conditions evolve and human pressures on forests intensify, further research is necessary to comprehensively understand the changing dynamics of these services and devise effective conservation measures (Chivulescu et al., 2020; Leca et al., 2023).

The aim of this research is to valuate ecosystems services in Piatra Craiului National Park, using both monetary and non-monetary valuation methods, harmonize quantitative data [obtained from forest management plans for monetary valuation, incorporating market prices and other economic indicators (Costanza et al., 2014)] and qualitative data [collected from the general public visiting the national park, capturing their perspectives and preferences regarding ecosystem services (Vedeld et al., 2004; Sharma et al., 2022)], and to explore relationships among identified ecosystem services indicators and different characteristics of ecosystems.

Consequently, the research paper answers to following research questions: (i) which are the ecosystem services provided by a national park (Piatra Craiului National Park-Southern Carpathians Mountains), and which is their monetary and non-monetary value and (ii) which is the relationship between values obtained from monetary and non-monetary valuations and other variables (ecosystem characteristics), with a specific focus on identifying dissimilarities and resemblances between each approach.

2 Materials and methods

2.1 Location and description of the study area

The study area is located in the Southern Carpathians Mountains, specifically in Piatra Craiului National Park (Figure 1) part of the Romanian Long Term Ecological Research Network (RO-LTER) (Badea et al., 2012; Badea, 2021). This area is characterized by a temperate continental climate, with slightly small topo climates typically found at medium and high altitudes. The annual rainfall ranges between 800 and 1200 mm, while the annual temperature averages from 3 to 4 degrees Celsius, with a high annual variation ($\pm$ 3 degrees Celsius). The park encompasses a forested area of over 11,400 hectares, consisting predominantly of spruce, beech, pure and mix stands. Historically, the National Park was designated a nature reserve in 1938, and the management practices at that time focused on preserving the constituent habitats. Moreover, in 1990, it was designated as a national park, and the current management plan focuses on the conservation of representative ecosystems in their natural state, as well as the establishment of the prerequisites for recreational activities, visitation, and education while ensuring minimal impact on these ecosystems.

Currently, the study area is divided into 4 different areas: a strict protection zone, which covers 43% of the total area; an integral protection zone occupying 1%; a sustainable conservation area of 46%; and a sustainable development zone on the remaining 10%.

This zonal configuration within the park is the focal point of a comprehensive management investigation, which involves stratification of the woodland based on forest management methods, topographical attributes, climatic conditions, and ecosystem classification. Two types of management practices are distinguished based on the forest management plans information and the designated management areas: forest conservation and forest wood production.

2.2 Models and methods

2.2.1 Analytical frameworks and contextual insights

The Forest Management plans rely on international terminology as outlined by Carcea and Dissescu (2014) and encompass various parameters essential for effective management. These parameters include stand productivity (indicative of potential wood volume production and yield class), stand density (standing volume per unit area), slope (average land slope or gradient), altitude (average elevation above sea level), type of flora (plant species characteristic of the forest type), age (average age of component trees at the management unit level), forest type (homogeneous forest parts requiring consistent silvicultural measures), annual stand growth (current yearly volume increment of the stand), and stand volume (total timber volume of the stand). Both Monetary and Non-monetary assessments were computed at the management unit level, where a management unit represents a designated area of forest land managed and treated as a single entity for sustainable forest management purposes. This unit serves as a distinct ecological and administrative planning entity utilized by forestry authorities or administrators/owners to implement comprehensive forest management practices. Data used from Forest Management plans and photograph analysis have significant value as indicators of ecosystem services. These variables are related to indicators found in ecosystem service classifications (Haines-Young and Potschin-Young, 2018). In particular, each variable from both sources is associated with one or more ecosystem services. In our study, we selected these variables based on correlation matrix analysis.
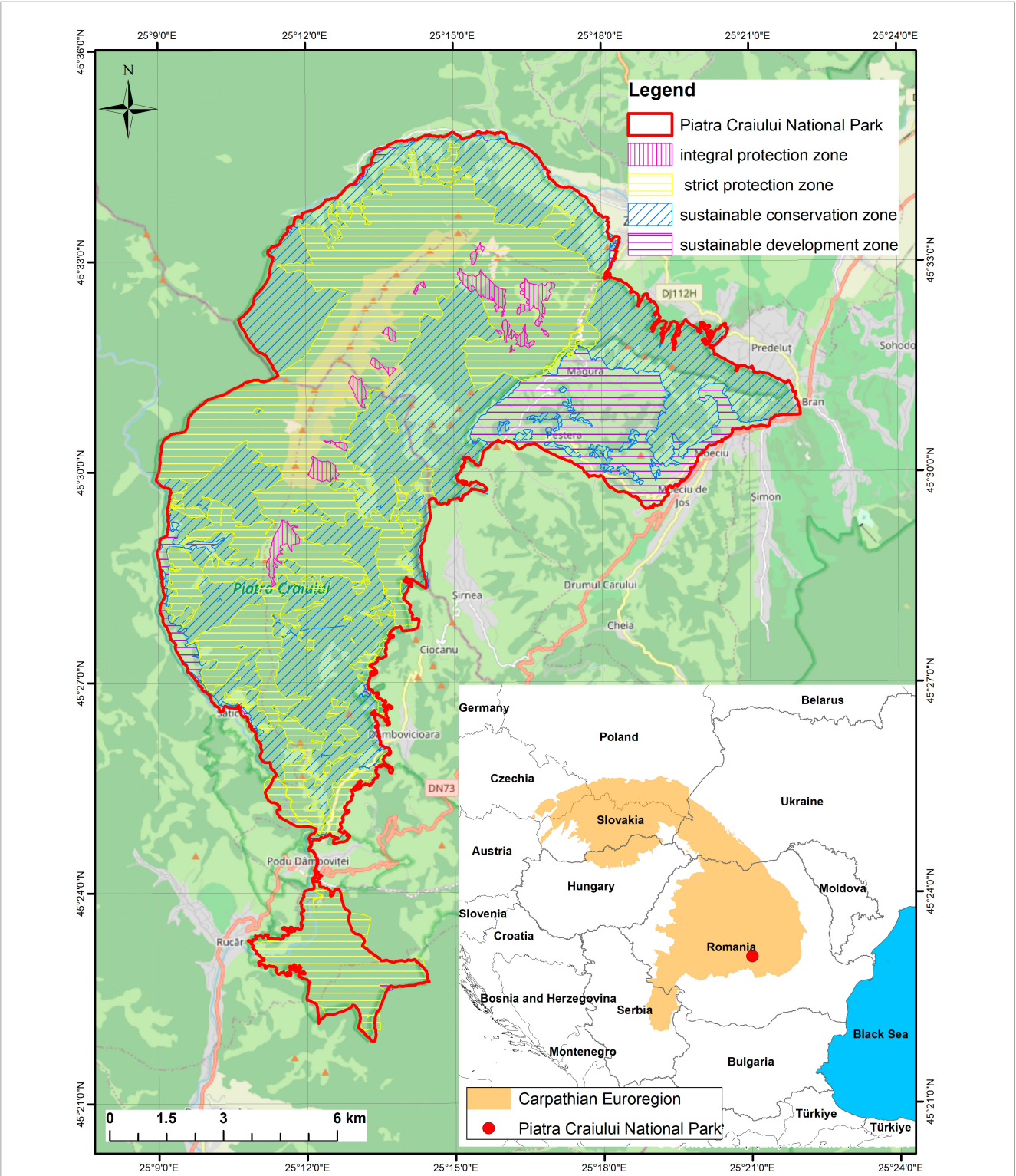
FIGURE 1
Administrative map of the Piatra Craiului National Park. The hatched area indicates the designated management plans for the park. The small square represents the location of Piatra Craiului National Park (red dot) within the Carpathian Mountains (dark yellow).

2.2.2 Non-monetary valuation

Assessing cultural ecosystem services overall took into consideration the spreading of knowledge based on scientific data (quantitative data) in such a way that any user of such ecosystem services can acknowledge and understand the principles

and requirements of CES. For this reason, the correlation between nature and culture was assessed through a mixture between specific communication instruments, easy to understand, regarding the classification of cultural ecosystem services types in the sense of subjective value-based judgments with the help of imagery data.

In order to evaluate CES, using non-monetary methods, social innovations such as the social-media based method were used. This approach was chosen for the non-monetary valuation because of its ability to stimulate participant engagement, obtain qualitative information, overcome language barriers and promote a holistic understanding of ecosystem services. It contributes to a more comprehensive and culturally sensitive assessment, with the added benefit of simplified data collection. With the help of photographs taken by the public and posted on the photograph-sharing platform Flickr (last accessed on 01.10.2019), we assessed each image and its respective correlation with the ecosystem services it offers, following the methodology presented in Tenerelli et al. (2016).

In the present research endeavor, an assemblage of 1288 photographic records, captured within the confines of Piatra Craiului National Park's geographical expanse, was procured from the digital imagery exchange platform Flickr. Among this corpus, a discernment emerged indicating that a total of 998 entries were concomitant with explicit geolocation metadata. Subsequent to meticulous scrutiny, it was ascertained that 489 of these instances delineate instances of non-monetary contributions, thus furnishing pivotal spatial and elaborative data of significance for subsequent analytical undertakings.

The ecosystem services identified in the photographs encompass groups of services like aesthetic, existence, land use/land cover, intellectual, and recreational. Additionally, some provisioning services were observed and various wood and non-wood forest products. After the categorization process, assessments were carried out for each ecosystem service. These results were then digitally represented, taking spatial distribution into account.

Under the classification of ecosystem services (Millennium Ecosystem Assessmen, 2005), photographs were grouped according to their content. The "Existence" group included images of vertebrate wild animals, non-vertebrate wild animals, and vegetation. The "Aesthetic" group comprised visually pleasing photographs. The "Recreational" group contained images depicting various activities such as hiking, mountain walking, freeskiing, biking, camping, barbecuing, picnicking, etc. The "Intellectual" group consisted of photographs related to local identity, cultural heritage, education, and scientific exploration. Similarly, the "Land use/land cover" group encompassed images representing different land types, including forests, sparse forests, transitional woodlands, shrub areas, grasslands, moors, bare rocks, rivers, and streams, among others. Each of these groups facilitated the classification and organization of the diverse photographs based on their respective characteristics and themes.

We utilized Kernel Density Estimation (KDE) to convert point data from photographs into a continuous surface across the Piatra Craiului National Park for comparable results with monetary value ES estimation. KDE provides a non-parametric estimate of the underlying unknown intensity function (Waller and Gotway, 2004). Widely employed in various scientific disciplines, such as fire science for defining patterns of fire occurrence (Kuter et al., 2011; Oliveira et al., 2012; Mallinis et al., 2019), wildlife ecology (Fieberg, 2007; Fleming and Calabrese, 2017), and crime incident analysis (Levine and Associates., 2013), KDE ensures a comprehensive representation of the landscape. In kernel density analysis, bandwidth selection is crucial, often surpassing the significance of choosing the kernel function (Kuter et al., 2011). We determined the optimal bandwidth by calculating the average

k-th nearest neighborhood distances between points, using the k-nearest neighbors' algorithm (Williamson et al., 1999). After multiple tests, we identified the optimal k value as 40 through visual examination, ensuring accurate and meaningful outcomes. To treat observations consistently across diverse concentrations, we employed the normal distribution kernel function with a fixed bandwidth, ensuring standardized data handling across the national park.

For each of the 5 ecosystem service categories (aesthetic, existence, intellectual, recreational and land use/land cover), we generated individual kernel density maps. Additionally, a cumulative kernel density map, representing non-monetary values, was produced by spatially intersecting all categories. This map was then overlaid onto forest management units, and the average kernel value for each unit, indicating the non-monetary score, was calculated, and assigned to all 1127 management units.

Subsequent to conducting an analysis employing kernel functions, an allocated kernel score was attributed to individual forest management units situated within the confines of Piatra Craiului National Park. This procedure consequently engendered a model of comparability between the realms of pecuniary and non-pecuniary valuations.

2.2.3 Monetary valuation

To assess the value of ecosystem services that forests have to offer, various methods have been considered according to the area studied. Thus, the methods used (described below) have taken into account reliable ways to evaluate the available harvestable wood volume, the carbon stock in above-ground biomass, and the provision of non-woody products (medicinal plants and berries).

Leveraging data from forest management plans, we assessed wood volume through primary harvesting procedures like shelterwood, conservation, and secondary cutting for stand management. The monetary value of stands with specified logging rules (regeneration felling) was determined by multiplying the average firewood price (Statistics, 2019) with harvestable wood volume. For estimating the above-ground tree biomass carbon stock in the Piatra Craiului National Park, we relied on standing tree volumes, net growth, and national emission factors from the forest management plans. The carbon stock estimation followed the Intergovernmental Panel on Climate Change Guidelines (IPCC, 2006), and the 2019 Refinement on forestland use equations:

$$AGB = AG \text{ volume} * WD\ i * BEF \qquad (1)$$

Where:

AGB—aboveground biomass, in tones;

AG *volume*—aboveground volume of forest stands provided by forest management plans in m^3;

WD—wood density for each main species expressed, tones/m^3, i represents the main species (**Table 1**);

BEF—biomass expansion factor (1 for broadleaves and 1.15 for conifers).

The biomass expansion factor is needed to correctly add the biomass of branches to the stem to estimate the overall tree AGB. Nevertheless, due to the fact that the volume provided by the management plan is estimated with an allometric equation (Giurgiu, 2004) that estimates the all-aboveground volume in broadleaves species (i.e., BEF equal to one), it was used only for

Sp.	WD	Sp.	WD
Picea abies in the areal	0.353	*Quercus petraea*	0.568
Picea abies outside the areal	0.346	*Quercus robur*	0.571
Abies alba	0.335	*Tilia cordata*	0.440
Larix decidua	0.460	*Salix alba*	0.390
Pinus sylvestris	0.406	*Ulmus minor*	0.530
Pseudotsuga menziesii	0.460	*Fraxinus excelsior*	0.560
Pinus nigra	0.466	*Acer campestre*	0.510
Pinus strobus	0.300	*Carpinus betulus*	0.620

conifers. The value of BEF was 1.15 for conifers used for temperate forests by various countries, which have shown to provide reliable results (IPCC, 2006). The root to shoot was considered to be 0.2 for all species (Giurgiu, 2004).

The total carbon stock, for each forest stand, considering also the below ground biomass was ultimately estimated, using the equation provided by the IPCC (2006) guidelines:

$$C = AGB * (1 + R) * CF \qquad (2)$$

where:

C - carbon stock expressed in tones;

AGB—above-ground biomass expressed in tones.

R - root to shoot factor, dimensionless;

CF—carbon fraction.

We used a default factor for carbon fraction of 0.5 (IPCC, 2006). The carbon amount was transformed to CO_2 and expressed in metric tons, which was then multiplied by the pre-established reference value of 42.05 €/tCO_2, which represents the average market value of CO_2 at the time the study was conducted to evaluate the monetary values of existing carbon stock.

For valuing non-woody products, such as medicinal plants and berries, we relied on a methodology guided by expert studies (INCDS Marin Dracea, 2020a,b). This approach establishes permissible harvesting quantities based on forest types (**Table 2**). To assign monetary value to medicinal plants and berries, an average price was applied—0.76 euro/kg for medicinal plants and 0.80 euro/kg for berries—representing reference prices excluding exploitation, packaging, and transport costs (Statistics, 2019).

2.2.4 Descriptive statistics

The statistical parameters to describe both Monetary and Non-monetary values were calculated utilizing the R PASTECS package available in R software (Grosjean and Ibanez, 2004). In the context of ecosystem service valuation, the application of statistical metrics serves the purpose of providing a succinct overview and assessing the quality of monetary and non-monetary values, thereby increasing transparency and even facilitating informed decision-making.

2.2.5 PCA assessment

The Principal Component Analysis (PCA) method was utilized to reduce the dimensionality of the datasets and gain a more detailed visualization (Mudrov and Proch, 2005; Greenacre et al., 2022). The R packages used for this analysis include *corrr* (Kuhn et al., 2020), *ggcorrplot* (Kassambara, 2022), *FactoMineR* (Lê et al., 2008), and *factoextra* (Kassambara and Mundt, 2020) from the R studio application (R Core Team, 2023). In more specific terms, it can be defined that the "corrr" package allows exploration of correlations, "ggcorrplot" facilitates the visualization of correlation plots, "FactoMineR" performs factor analysis and PCA, while "factoextra" aids in extracting and visualizing multivariate analysis results in R.

The PCA analysis utilized primary data from management plans, including stand productivity, density, slope, altitude, flora type, age, annual growth, and volume. Additional data, such as carbon stock and monetary and non-monetary values, were incorporated. Areas in imagery data were digitized using GIS. Qualitative results from social media and Kernel interpolation were compared with monetary valuation at the management unit level. All datasets were standardized using R packages and visually represented. The study employs both monetary and non-monetary methods to offer a comprehensive understanding of ecosystem service values. Valuing services from ordinary people's perspectives through non-monetary methods provides insights into social values. The research assesses the reliability of a hybrid method combining both approaches, contributing to the discourse on comprehensive ecosystem service valuation. A mixed-methods approach combines quantitative monetary analysis with qualitative non-monetary analysis, emphasizing the need for a combined view in forest policy (Krott, 2005). Incorporating qualitative data into decision-making processes, as suggested by (Kenter, 2018) and (Maca-Millán et al., 2021) has proven to be effective. This approach involves meticulous data preparation, using quantitative facts presented in summary tables and graphical representations to emphasize key points, especially as policy-briefs for decision-makers. The use of inferential statistics goes beyond raw data to explore investigative questions based on hypotheses (Smith et al., 2011). The study's findings provide reasonable arguments for policymakers, land managers, and stakeholders involved in park management, emphasizing the importance of combining factual and value judgments for effective problem-solving.

3 Results

3.1 Non-monetary valuation

The photographs extracted from the Flickr proxy were used to represent five distinct groups of ecosystem services, namely aesthetic, existence, land use/land cover, intellectual, and recreational services, as depicted in **Figure 2**.

It should also be mentioned that using Kernel analysis, each management unit in the research area has been assigned a kernel value (score) for non-monetary services.

Since the non-monetary methods have shown a significant increased use in scientific research as compared to the monetary ones, the results in this study reveal high preferences toward the

TABLE 2 Quantity of herbs/berries that can be harvested according to the type of forest (dry quantity expressed in kg/hectare) (INCDS Marin Dracea, 2020a,b).

Forest type	Herbs		Berries	
	Scientific name	Dry quantity	Scientific name	Dry quantity
Spruce	*Sambucus nigra*	48	*Vaccinium myrtillus*	200
	Vaccinium myrtillus	180	*Vaccinium vitis idaea*	100
	Arctium lappa	3.8	*Rubus idaeus*	100
	Taraxacum officinale	0.6	*Rubus fruticosus*	100
Beech	*Achillea millefolium*	0.207	*	*
	Equisetum arvense	2.14	*	*
	Primula officinalis	3.2	*	*
	Hypericum perforatum	3.89	*	*
	Taraxacum officinale	5.4	*	*
	Urtica dioica	9.69	*	*
	Sambucus nigra	9.31	*	*
	Vaccinium myrtillus	29.87	*	*

*No information was available.

aesthetic and existence ecosystem services, as well as land use/ land cover (Figures 2A–C). The graphic representation of the most considered non-monetary ecosystem services has shown that they generally overlap in the north part of the National Park in the case of each service. The overlapping is more visible in the case of intellectual, recreational, and land use/land cover ecosystem services.

To this matter, these respective ecosystem services were classified into 5 importance classes, using the kernel function in ArcGIS, resulting in a combined reliable value of them.

According to the Kernel Function classification of the ES, the average combined percentage cover is around 9% in the case of the classes 3–5 (moderate, high, and very high), while in the case of the classes very low and low, respectively, 1–2, the average combined percentage cover falls just a bit under 36% from the total area.

In the case of aesthetic services, the coverage is rather low, most of it being situated in the northern part, covering 14% of the total area of Piatra Craiului National Park from the Southern Carpathians Mountains, the rest being of low interest, especially on 75% coverage in the south of the mountains. Nevertheless, such ecosystem services are predominantly located in the main tourist sites within the area, strategically positioned along the frequently visited tourist routes, and with information easily accessible through online platforms (Figure 2A). Additionally, locations featuring caves or canyons (e.g., Zarnestiului canyon) are highly sought after and greatly appreciated by visitors, due mostly to their scenery and accessibility.

Similar Kernel function coverage can be found in the case of existence services (Figure 2B) where most of its importance is located in the Northern part as well, covering almost 18% of the total area of the park while the remaining area being taken as granted by observers, under the presupposition and believe that the right to nature is equal with other fundamental rights.

Closely related to other services, intellectual (Figure 2D) and recreational (Figure 2E) services cover similar percentages of the total of the park, the former accounting for barely 35% while the

latter just topping 24%, perceived to express the low interest in such values of the community and society as a whole.

According to graphical representation, it was found that the most valued services are located in the northern part of the research area, grouped into four cores. The respective cores are close to the main infrastructure road network, allowing fairly easy access to the forest, a fact that might have motivated users to express their interests in such core areas.

For valuing *Natural Capital between currency and intrinsic appraisal*, the multidisciplinary approach was used to provide the reliable outcomes for monetary valuation. The analysis is carried out with high respect to the comprehensive methodology on ecosystem service provision. Monetary values are expressed in euros for each case of provisioning service. The monetary values are represented in fact by: the volume of harvestable wood, stored carbon, harvestable medicinal plants, and harvestable berries, whereas the non-monetary values foresee the cultural ecosystem service categories (aesthetic, existence, land use and land cover, intellectual, and recreational services). Moreover, through the use of Geographic information system (GIS), the values were analyzed and displayed graphically by means of a thematic map (Figure 3A), in which the summed values of these monetary services have been plotted in relation to their geographically referenced information. Simultaneously, non-monetary values, expressed as the sum of Kernel scores, were graphed to illustrate the ecosystem services of existence, aesthetic, recreational, intellectual, and land use/land cover (Figure 3B) for the purpose of comparison.

Thus, for the forests in Piatra Craiului National Park, a value of 2.6 million euros was determined for the harvestable wood, and the value of the carbon stock was 49.7 million euros. Following the application of the methodology for determining the production capacity of medicinal plants and forest fruits in relation to the types of forest, a value of 71 thousand euros and 17 thousand euros was determined. The total value of all these monetary services was 53.2 million euros, calculated with prices at the time of the research in the year 2021. Figure 3A displays a few regions where the
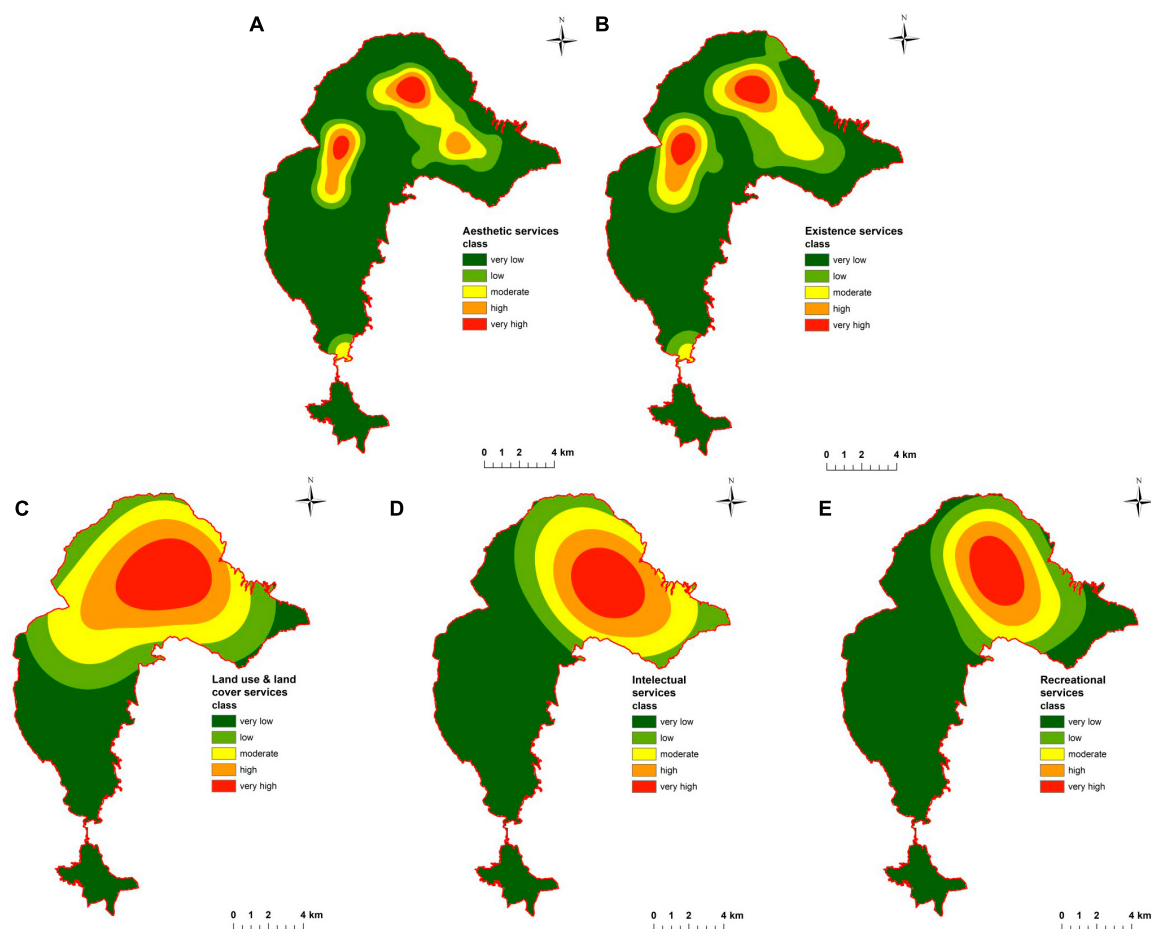
FIGURE 2
Map of Non-monetary valuation [**(A)** aesthetic services, **(B)** existence services, **(C)** land use/land cover services, **(D)** intellectual services, **(E)** recreational services].

monetary value of ecosystem services surpasses 400 thousand euros (evidenced by the red color). These areas predominantly consist of old-growth forests with substantial wood volume, covering extensive plots (more than 30 hectares). Generally, the distribution of monetary values remains consistent across the entire survey area, with the exception of a few "white" areas. These "white" areas represent locations devoid of forest vegetation, such as cliffs and mountain hollows, which were excluded from our analysis.

Forested areas were classified into five importance classes using the kernel function in ArcGIS, resulting in a combined value of them, and after the graphical representation, it was determined that the most important of them are located in the northern part of the research area (**Figure 3B**), grouped in four cores.

As it is well known, an ecosystem can provide several ecosystem services at the same time, as seen in this research, where more than 2400 records of ecosystem services provided by forests in Piatra Craiului National Park were found. About 25% of these were existence ES, 29% aesthetic ES, 3% recreational ES, 11% intellectual ES and about 32% land use/land cover ES.

For exploring the relationship between currency and intrinsic values, a correlation matrix of the parameters analyzed in this study was built that reveals some significant associations among the variables (**Figure 4**).

The highest correlation is observed between monetary values, stand volume (0.87), and carbon stock (0.92). This strong correlation is expected, given that wood can be rapidly capitalized, making it economically important in the short term. We also found notable negative correlations between stand productivity and slope (−0.41) and altitude (−0.32), indicating that accessibility and climatic conditions can be limiting factors for forest productivity.

Furthermore, the correlation analysis revealed weak relationships between several variables, including age and slope (0.22) and stand density and productivity (0.17). In addition, the correlation matrix analysis shows a weak correlation between non-monetary values and altitude (0.24), slope (0.14), and age (0.14).

Based on the aforementioned methodology, we also explored the relationship between non-monetary and monetary values. The correlation coefficient of −0.055 indicates a lack of a significant linear relationship between these variables. As expected, we did not identify robust correlations, as there is no direct causality between monetary and non-monetary factors, nor between provisioning, regulating, and cultural ecosystem services.

Due to the lack of strong correlations found between monetary and non-monetary values, we do not have sufficient evidence to make robust predictions or draw significant conclusions.

FIGURE 3

Compared monetary and non-monetary evaluation [**(A)** monetary evaluation, **(B)**- non-monetary evaluation summarized].
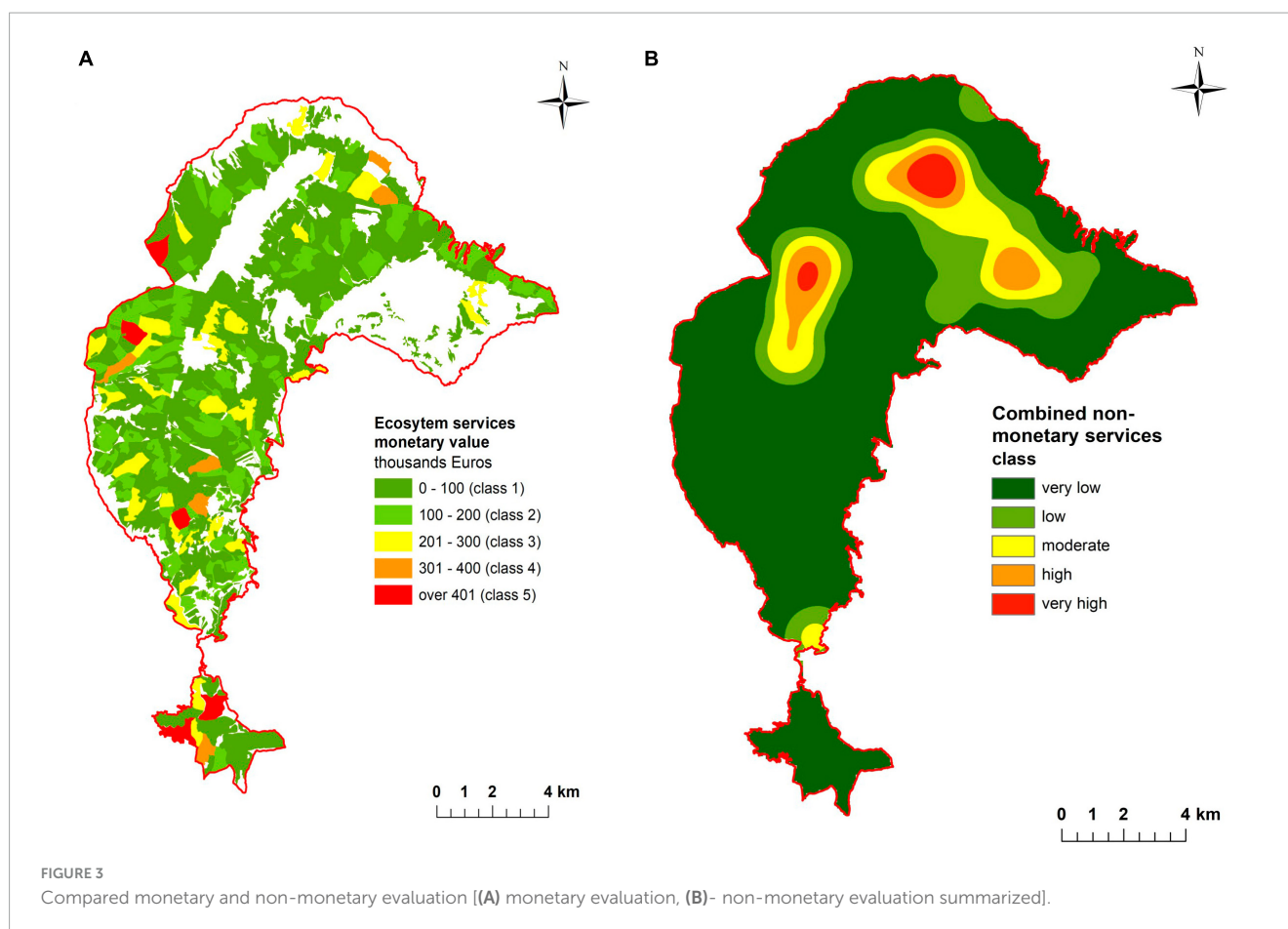
Therefore, further investigation and consideration of other factors are necessary to gain a more comprehensive understanding of the relationships between these variables.

The examination of the primary statistical indicators for both monetary and non-monetary values of selected ES reveal a substantial amount of data for both types of assessments (**Table 3**). The minimum value for monetary valuations is 34 euros, while for non-monetary valuations, it is 1 (kernel score). On the upper end of the scale, the maximum values slightly surpass 570 thousand euros for monetary valuations and 5 (kernel score) for non-monetary valuations. The average for monetary valuations exceeds 47 thousand euros, whereas for non-monetary valuations, the average stands at 1.38 (kernel score).

The significantly high standard deviation values reflect a high level of variability in the monetary values across the research area. In contrast, the standard deviation for non-monetary valuations indicates a more moderate level of variability in the dataset. Furthermore, the coefficient of variation reveals very high values, emphasizing the pronounced variability in both the monetary and non-monetary values of ES.

Considering the absence of strong correlations between monetary and non-monetary relationships, we pursued a *Principal Component Analysis (PCA)* as the next step. PCA analysis (**Figure 5**) was employed to reduce data dimensionality while retaining a substantial portion of the variance. According to PCA analyses, the first two dimensions explained 43.3% of the total

variability. The first component (Dim 1) accounts for 26.5% while the second component (Dim 2) accounts for 16.8%.

In PCA analysis, the first dimension of the data is represented by a linear combination of the monetary value, carbon stock, and stand volume (**Figure 5**). Also, the uniform angle index between them indicates a maximized variance, suggesting that they are well-distributed and effectively contribute to the formation of the first principal component.

The total variance of the second principal component exhibits positive loadings for slope, altitude, age, and non-monetary value. On the other hand, stand density, stand productivity, type of flora, and annual stand growth have negative loadings in Dim 2. This means that higher values of these variables are associated with lower values of Dim 2.

The absence of correlation between monetary-related values loaded by Dim 1 and the second principal component related to aesthetic or cultural aspects (Dim 2) suggests that Dim 1 and Dim 2 represent distinct patterns of variability in the data. This highlights the independence of the two principal components based on the information analyzed in the present study.

4 Discussion

The values provided by ecosystem services play a crucial role in fostering awareness within society (Daily et al., 2009; Badea et al., 2013; Kosanic and Petzold, 2020; Tsirintanis et al., 2022). To achieve
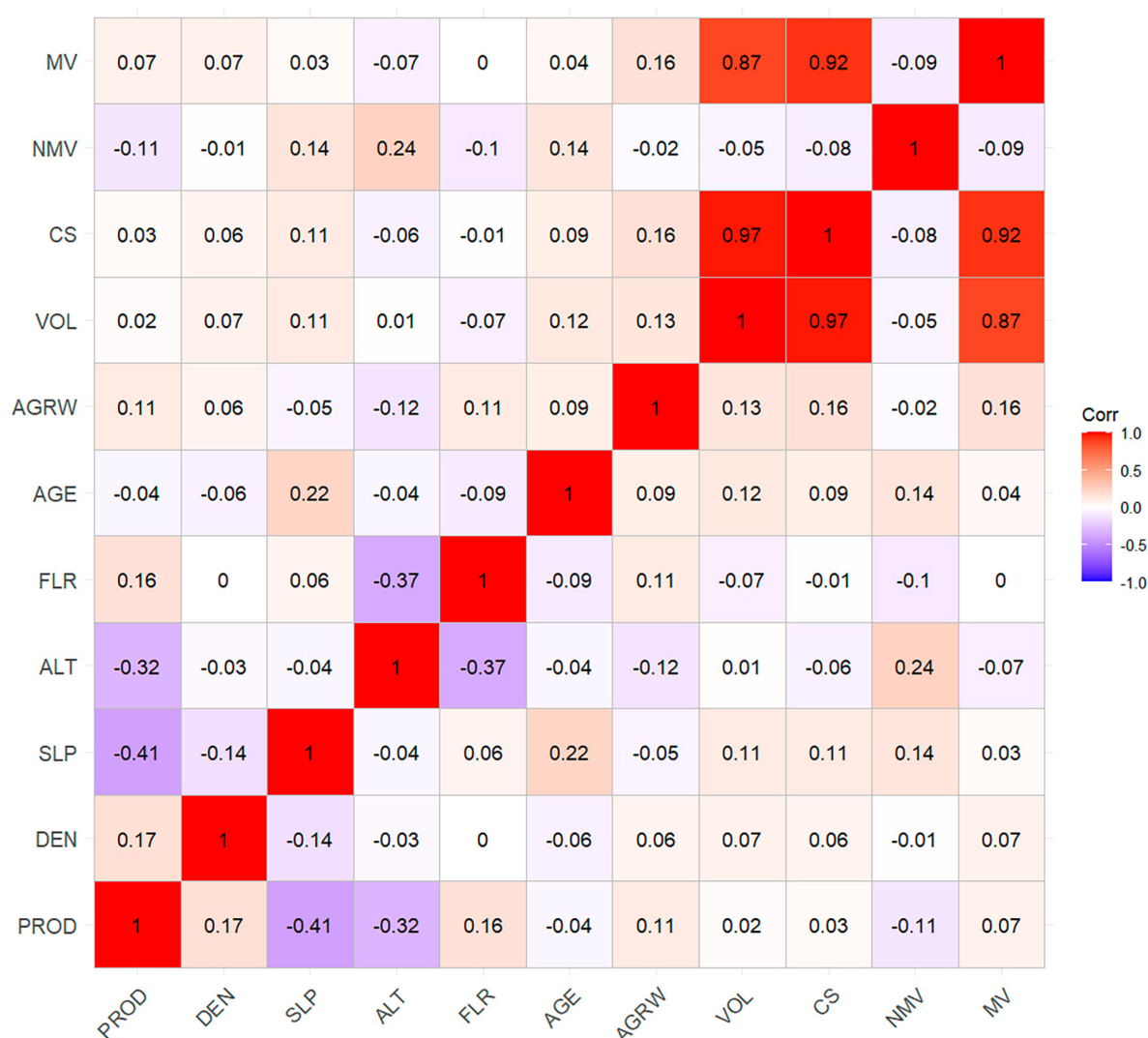
FIGURE 4
Correlation matrix of main variable PROD, stand productivity; DEN, stand density; SPL, slope; ALT, altitude; FLR, type of flora; AGE, stand age; AGRW, annual stand growth; VOL, stand volume; CS, carbon stock; NMV, non-monetary value; MV, monetary value.

TABLE 3 Descriptive statistics of type of valuation method.

Type of evaluation	No. val.	Min.	Max.	Mean	(s)	(s%)
Monetary values	1127	34	571521	47230	67052.40	141.90
Non-monetary values	1127	1	5	1.38	0.86	61.95

(No. val -number of samples, Min–minimum value of monetary evaluation) (expressed in Euro/management unit) and minimum value of non-monetary evaluation (expressed in Kernel score/management unit), Max–maximum value of monetary evaluation (expressed in Euro/management unit) and maximum value of non-monetary evaluation (expressed in Kernel score/management unit), Mean–average value of monetary evaluation (expressed in Euro/management unit) and the average value of non-monetary evaluation (expressed in Kernel score/management unit), (s)–standard deviation value of monetary evaluation (expressed in Euro) and standard deviation value of non-monetary evaluation (expressed in Kernel score), (s %)–coefficient of variance of monetary evaluation (expressed in Euro) and coefficient of variance value of non-monetary evaluation (expressed in Kernel score).

this, a comprehensive and multidimensional approach is essential. This involves integrating social science methods with GIS analysis and statistics to make informed decisions (Apostol et al., 2018; Cabana et al., 2020), especially for policy-makers (Jones et al., 2022).

Given the challenge of economically assessing non-monetary services, the study employed a combination of the "document method" and the "social media-based method" (Cheng et al., 2019). By examining revealed preferences through images and other

materials, along with structured identification of ecosystem services using Flickr uploaded images, qualitative insights were captured (Donaire et al., 2014; Barchiesi et al., 2015; Hartmann et al., 2022).

The research identified strong preferences for aesthetic, existence, and land use/land cover ecosystem services in the northern part of the National Park. The reason behind the popularity of the northern area lies in its strong appeal to tourists due to the abundance of natural monuments. This can be

FIGURE 5
Principal component analysis PROD, stand productivity; DEN, stand density; SPL, slope; ALT, altitude; FLR, type of flora; AGE, stand age; AGRW, annual stand growth; VOL, stand volume; CS, carbon stock; NMV, non-monetary value; MV, monetary value.
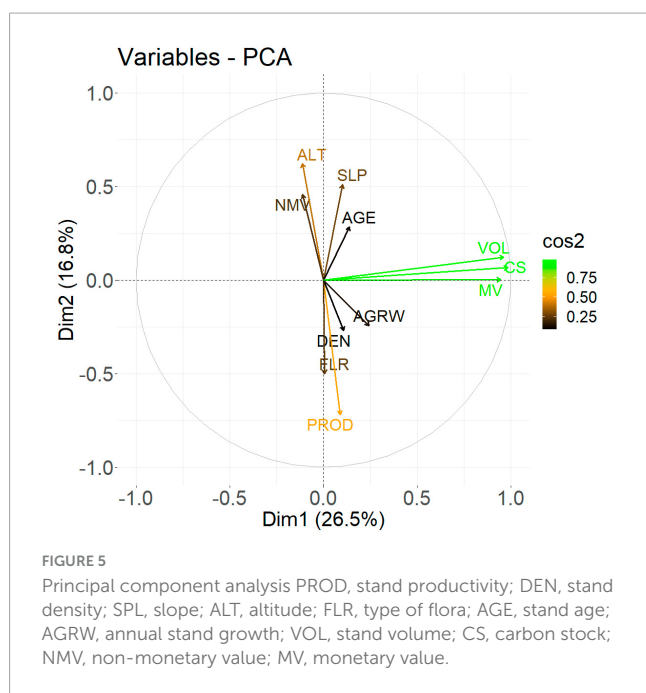
attributed to the region's excellent accessibility, thanks to numerous access roads and well-established tourist trails. Additionally, its proximity to larger towns further enhances its attractiveness as a tourist destination.

These services were highly valued by visitors for their scenic beauty and accessibility (Parga-Dans et al., 2020; Yang et al., 2022). The Kernel distribution provided insights into the varying degrees of importance and perceived value of different ecosystem services across the research area.

Although recreational and intellectual ecosystem services were less identified by experts (Paracchini et al., 2014; Inácio et al., 2022), their overlapping with other non-monetary forest ecosystem services suggests the complexity of ecosystems (Christie et al., 2012; Raihan, 2023) as a whole. Benefits for recreation were highly correlated with aesthetic and intellectual values (Calcagni et al., 2022) and diverse land use services. This highlights the societal valuation of ecosystem services in the context of climate change and the importance of nature (Daily, 1997; Hermann et al., 2011; Costanza, 2020; Weiskopf et al., 2020).

Also, the identification of substantial monetary values linked to diverse forest-related services in Piatra Craiului National Park is vital for evidence-based decision-making (Maes et al., 2012), public awareness (Acharya et al., 2019), guiding sustainable environmental management practices (Meraj et al., 2022), and fostering a deeper understanding of the economic significance of nature's contributions to society (Sangha et al., 2019). It provides a robust foundation for interdisciplinary approaches to conservation and land-use planning (Delgado-Aguilar et al., 2019; César et al., 2021), encouraging the adoption or redistribution of responsible policies and actions to protect priceless natural assets and promote biodiversity conservation on a broader scale (Ola and Benjamin, 2019).

The analysis revealed significant variability in both monetary and non-monetary valuations of ecosystem services (Martin and Mazzotta, 2018; Torres et al., 2021). This wide range of values

reflects the diverse economic and non-market attributes associated with these services, a situation also found in state forest institutions, where there is a high discrepancy between policy goals formulated in official documents and their on-field fulfillment, many focusing on economic terms rather than non-monetary services (Chudy et al., 2016; Romanazzi et al., 2023). To make well-informed decisions about ecosystem management and conservation, it is vital to consider both monetary and non-monetary aspects (Wanek et al., 2023).

Using correlation matrix analysis, we thoroughly examined the relationships between monetary and non-monetary valuations of ecosystem services. The results indicated a lack of notable connections between these two types of valuations (Acharya et al., 2019; Taye et al., 2021). This observation can be attributed to several factors, including the intricate nature of ecosystem services, making it challenging to precisely quantify their economic value. Additionally, the subjective aspects involved in non-monetary valuations, such as perceptions and preferences of different individuals and communities, contribute to the disparities (Czembrowski et al., 2016). Furthermore, diverse perspectives and purposes from stakeholders involved in the evaluation process can lead to contrasting assessments (Gos and Lavorel, 2012; Vallet et al., 2018; Aryal et al., 2022). Methodological challenges in quantifying and comparing both monetary and non-monetary values also play a significant role in the observed disconnection between these two evaluation approaches.

Our research revealed strong associations between certain variables (monetary value with carbon stock and stand volume), moderate connections (slope with stand productivity), and weaker relationships (non-monetary value with altitude, age with slope, type of flora with altitude, and altitude with stand productivity). This week correlation suggest that mature ecosystems located at higher altitudes are more likely to be positively appreciated by tourists.

These unexpected findings provide valuable insights into ecosystem dynamics and offer important guidance for developing more effective, integrated and sustainable natural resource management policies and practices. Understanding these intricate interrelationships empowers us to enhance our understanding of ecosystems and undertake appropriate and custom-tailored decisions to protect and preserve the environment.

The finding of the Principal Component Analysis (PCA) highlights the independence of monetary and non-monetary values, offering crucial insights into the complex interplay of ecosystem variables, guiding future research for comprehensive ecosystem management and conservation strategies.

While the study offers valuable insights, it has certain limitations. Conducted within a national park, the research's small geographic area may limit generalizability to larger regions or different ecosystems. Quantifying non-monetary values remains challenging due to their subjective nature (Hammermann and Mohnen, 2014; Márquez et al., 2023). The non-monetary valuation approach employed captures qualitative insights but lacks straightforward conversion into monetary values (Christie et al., 2012; Scholte et al., 2015; Hardy et al., 2022).

Despite these limitations, the study has notable strengths. It utilized accurate and reliable field data, ensuring credibility in the monetary valuation results. Additionally, the inclusion of perspectives from ordinary people visiting the park enhanced

the non-monetary valuation component. The hybrid approach combining monetary and non-monetary methods allowed for a more holistic understanding of ecosystem services' value (Dunford et al., 2018; Cazacu et al., 2020) and the importance of enhancing, preserving and listening to local communities' wisdom. By capturing the perspectives and preferences of ordinary people, decision makers can align management strategies with stakeholder expectations, fostering a sense of ownership and stewardship.

This research holds practical implications for decision-making in ecosystem management and conservation. By considering both economic and non-economic dimensions, decision-makers can formulate proper policy instruments for well-informed choices (Campbell, 2020) that balance sustainability and societal needs. The methodology used in this study can be valuable for assessing cultural ecosystem services in regions with limited data and challenging field accessibility. Also, the multidisciplinary approach employed in this study demonstrates the potential for a more comprehensive and integrated evaluation of ecosystem services.

Therefore, this study, with its strengths and weaknesses, enhances our comprehension of ecosystem services within a national park context, and beyond. The findings have significant implications for stakeholders and decision makers, empowering them to advocate for conservation, align management strategies with stakeholder preferences, and promote sustainability under a circular economy. Future research should address valuation method limitations to achieve a more comprehensive and integrated approach to ecosystem service assessment.

5 Conclusion

This research provides valuable insights into the valuation of ecosystem services through the integration of monetary and non-monetary valuation methods. By examining a specific national park, this study sheds light on the economic and non-economic dimensions of ecosystem services, contributing to a comprehensive understanding of their value.

While the size of the study may limits its applicability, the robustness of the findings is strengthened by the accurate and reliable field data collected, thus minimizing this limitation. The utilization of actual data from forest management plans and the inclusion of grassroots perspectives ensures a more accurate on-field representation of the monetary and non-monetary values associated with ecosystem services.

The adoption of a hybrid approach that combines monetary and non-monetary valuation techniques presents a practical advantage. This integrated approach allows decision makers to consider both the economic and non-economic benefits of ecosystem services, enabling them to make more informed choices that balance environmental sustainability with social and economic needs.

The findings of this research have important implications for stakeholders and decision makers involved in the sustainable management and conservation of natural resources. The economic valuation results serve as a compelling argument for the preservation and sustainable management of national parks

and other natural areas. They provide quantifiable information that can be integrated into cost-benefit analyses and policy-making processes.

In conclusion, this research contributes to the ongoing discourse on the evaluation of ecosystem services by providing insights into the economic and non-economic dimensions of their value. Future research should continue to address the limitations of valuation methods and strive for a more comprehensive and integrated approach to ecosystem service assessment.

Data availability statement

The datasets presented in this article are not readily available because datasets belong to the host institution. Requests to access the datasets should be directed to not applicable.

Author contributions

Funding

Conflict of interest

The authors declare that the research was conducted in the absence of any commercial or financial relationships that could be construed as a potential conflict of interest.

Publisher's note

All claims expressed in this article are solely those of the authors and do not necessarily represent those of their affiliated organizations, or those of the publisher, the editors and the reviewers. Any product that may be evaluated in this article, or claim that may be made by its manufacturer, is not guaranteed or endorsed by the publisher.

References

Acharya, R. P., Maraseni, T., and Cockfield, G. (2019). Global trend of forest ecosystem services valuation – an analysis of publications. *Ecosyst. Serv*. 39:100979.

Apostol, B., Chivulescu, S., Ciceu, A., Petrila, M., Pascu, I.-S., Apostol, E. N., et al. (2018). Data collection methods for forest inventory: a comparison between an integrated conventional equipment and terrestrial laser scanning. *Ann. For. Res.* 61:189.

Aryal, K., Maraseni, T., and Apan, A. (2022). How much do we know about trade-offs in ecosystem services? a systematic review of empirical research observations. *Sci. Total Environ.* 806:151229.

Badea, O. (2021). Climate change and air pollution effect on forest ecosystems. *Forests* 12:1642.

Badea, O., Bytnerowicz, A., Silaghi, D., Neagu, S., Barbu, I., Iacoban, C., et al. (2012). Status of the Southern Carpathian forests in the long-term ecological research network. *Environ. Monit. Assess.* 184, 7491–7515.

Badea, O., Silaghi, D. M., Neagu, S., Taut, I., and Leca, S. (2013). Forest monitoring - assessment, analysis and warning system for forest ecosystem status. *Not. Bot. Hort. Agrobot. Cluj* 41, 613–625.

Balmford, A., Bruner, A., Cooper, P., Costanza, R., Farber, S., Green, R. E., et al. (2002). Ecology: economic reasons for conserving wild nature. *Science* 297, 950–953.

Barchiesi, D., Moat, H. S., Alis, C., Bishop, S., and Preis, T. (2015). Quantifying international travel flows using Flickr. *PLoS One* 10:e0128470. doi: 10.1371/journal. pone.0128470

Baveye, P. C., Baveye, J., and Gowdy, J. (2013). Monetary valuation of ecosystem services: it matters to get the timeline right. *Ecol. Econ.* 39, 321–335.

Bell-James, J. (2020). Ecosystem services as a metaphor in environmental law. *Univer. Queensland Law J.* 39, 525–548.

Bogdan, S. M., Stupariu, I., Andra-Topârceanu, A., and Năstase, I. I. (2019). Mapping social values for cultural ecosystem services in a mountain landscape in the Romanian Carpathians. *Carpathian J. Earth Environ. Sci.* 14, 199–208.

Boyd, J., and Banzhaf, S. (2007). What are ecosystem services? the need for standardized environmental accounting units. *Ecol. Econ.* 63, 616–626.

Cabana, D., Ryfield, F., Crowe, T. P., and Brannigan, J. (2020). Evaluating and communicating cultural ecosystem services. *Ecosyst. Serv.* 42:101085.

Calcagni, F., Nogué Batallé, J., Baró, F., and Langemeyer, J. (2022). A tag is worth a thousand pictures: a framework for an empirically grounded typology of relational values through social media. *Ecosyst. Serv.* 58:101495.

Campbell, D. E. (2020). "Environmental goods and services: economic and non-economic methods for valuing," in *Terrestrial Ecosystems and Biodiversity*, ed. Y. Wang (Boca Raton, FL: CRC Press), 205–211.

Carcea, F., and Dissescu, R. (2014). Forest Management Terminology. Terms and Definitions in Romanian [Terminologia Amenajarii Pădurilor. Termeni si definiții in Limba Romana]. IUFRO 4.04.07 SilvaPlan and SilvoVoc. Available Online at: https://www.iufro.org/uploads/media/ws9-ro.pdf (accessed June 21, 2023).

Carpenter, S. R., Mooney, H. A., Agard, J., Capistrano, D., Defries, R. S., Diaz, S., et al. (2009). Science for managing ecosystem services: beyond the millennium ecosystem assessment. *Proc. Natl. Acad. Sci. U S A.* 106, 1305–1312.

Cazacu, R., Baciu, G., Chivulescu, Ş, Pitar, D., Dobre, A. C., Apostol, B., et al. (2020). Identifying and selecting methods for ecosystem services valuation-A case study in Piatra Craiului National Park. *Revista de Silvicultura si Cinegetica* 24, 49–55.

César, R. G., Belei, L., Badari, C. G., Viani, R. A. G., Gutierrez, V., Chazdon, R. L., et al. (2021). Forest and landscape restoration: a review emphasizing principles, concepts, and practices. *Land* 10:28.

Chan, K. M. A., Goldstein, J., Satterfield, T., Hannahs, N., Kikiloi, K., Naidoo, R., et al. (2013). "Cultural services and non-use values," in *Natural Capital*, ed. k. Peter (Oxford: Oxford University Press).

Cheng, X., Van Damme, S., Li, L., and Uyttenhove, P. (2019). Evaluation of cultural ecosystem services: a review of methods. *Ecosyst. Serv.* 37:100925.

Chivulescu, S., Ciceu, A., Leca, S., Apostol, B., Popescu, O., and Badea, O. (2020). Development phases and structural characteristics of the Penteleu-Viforta virgin forest in the curvature Carpathians. *iForest* 13, 389–395.

Chivulescu, Ş, and Schiteanu, I. (2017). Estimation of carbon stock in south of western Carpathians from Moldova Noua forest district using GIS data from managements plans. *Poljoprivreda i Sumarstvo* 63, 39–46.

Chivulescu, Ş, Pitar, D., Apostol, B., Leca, Ş, and Badea, O. (2022). Importance of dead wood in virgin forest ecosystem functioning in Southern Carpathians. *Forests* 13:409.

Christie, M., Fazey, I., Cooper, R., Hyde, T., and Kenter, J. O. (2012). An evaluation of monetary and non-monetary techniques for assessing the importance of biodiversity and ecosystem services to people in countries with developing economies. *Ecol. Econ.* 83, 67–78.

Chudy, R., Stevanov, M., and Krott, M. (2016). Strategic options for state forest institutions in poland: evaluation by the 3L model and ways ahead. *Int. For. Rev.* 18, 387–411.

Costanza, R. (2020). Valuing natural capital and ecosystem services toward the goals of efficiency, fairness, and sustainability. *Ecosyst. Serv.* 43:101096.

Costanza, R., de Groot, R., Sutton, P., van der Ploeg, S., Anderson, S. J., Kubiszewski, I., et al. (2014). Changes in the global value of ecosystem services. *Glob. Environ. Change* 26, 152–158.

Custódio, M., Villasante, S., Calado, R., and Lillebø, A. I. (2020). Valuation of ecosystem services to promote sustainable aquaculture practices. *Rev. Aquacult.* 12, 392–405.

Czembrowski, P., Kronenberg, J., and Czepkiewicz, M. (2016). Integrating non-monetary and monetary valuation methods – SoftGIS and hedonic pricing. *Ecol. Econ.* 130, 166–175.

Daily, G. C. (1997). "Nature's services: societal dependence on natural ecosystems," in *Nature's Services: Societal Dependence On Natural Ecosystems*, ed. G. C. Daily (Washington, DC: Island Press).

Daily, G. C., Polasky, S., Goldstein, J., Kareiva, P. M., Mooney, H. A., Pejchar, L., et al. (2009). Ecosystem services in decision making: time to deliver. *Front. Ecol. Environ.* 7:21–28. doi: 10.1890/080025

Delgado-Aguilar, M. J., Hinojosa, L., and Schmitt, C. B. (2019). Combining remote sensing techniques and participatory mapping to understand the relations between forest degradation and ecosystems services in a tropical rainforest. *Appl. Geogr.* 104, 65–74.

Díaz, S., Pascual, U., Stenseke, M., Martín-López, B., Watson, R. T., Molnár, Z., et al. (2018). Assessing nature's contributions to people. *Science* 359, 270–272.

Dobre, A. C., Pascu, I.-S., Leca, S., Garcia-Duro, J., Dobrota, C.-E., Tudoran, G. M., et al. (2021). Applications of TLS and ALS in evaluating forest ecosystem services: a Southern Carpathians case study. *Forests* 12:1269.

Donaire, J. A., Camprubí, R., and Galí, N. (2014). Tourist clusters from Flickr travel photography. *Tour. Manag. Perspect.* 11, 26–33.

Dunford, R., Harrison, P., Smith, A., Dick, J., Barton, D. N., Martin-Lopez, B., et al. (2018). Integrating methods for ecosystem service assessment: experiences from real world situations. *Ecosyst. Serv.* 29, 499–514.

Everard, M. (2013). *Ecosystem Services Key issues*. Milton Park: Routledge.

Fieberg, J. (2007). Utilization distribution estimation using weighted kernel density estimators. *J. Wildlife Manag.* 71, 1669–1675.

Fleming, C. H., and Calabrese, J. M. (2017). A new kernel density estimator for accurate home-range and species-range area estimation. *Methods Ecol. Evol.* 8, 571–579.

Giurgiu, V. (2004). *Silvologie: Gestionarea durabilă a pădurilor României*. Romania: Editura Academiei Române.

Gos, P., and Lavorel, S. (2012). Stakeholders' expectations on ecosystem services affect the assessment of ecosystem services hotspots and their congruence with biodiversity. *Int. J. Biodiver. Sci. Ecosyst. Serv. Manag.* 8, 93–106.

Greenacre, M., Groenen, P. J. F., Hastie, T., D'Enza, A. I., Markos, A., and Tuzhilina, E. (2022). Principal component analysis. *Nat. Rev. Methods Prim.* 2:100.

Grosjean, P., and Ibanez, F. (2004). *Package for analysis of space-time ecological series. PASTECS version 1.2-0 for R v. 2.0. 0 & version 1.0-1 for S+ 2000 rel.*

Haines-Young, R., and Potschin-Young, M. (2018). Revision of the common international classification for ecosystem services (CICES V5. 1): a policy brief. *One Ecosyst.* 3:e27108.

Hammermann, A., and Mohnen, A. (2014). The pric(z)e of hard work: different incentive effects of non-monetary and monetary prizes. *J. Econ. Psychol.* 43, 1–15.

Hardy, C., de Rivera, C., Bliss-Ketchum, L., Butler, E. P., Dissanayake, S., Horn, D. A., et al. (2022). Ecosystem connectivity for livable cities: a connectivity benefits framework for Urban planning. *Ecol. Soc.* 27, 1–25.

Hartel, T., Fischer, J., Câmpeanu, C., Milcu, A. I., Hanspach, J., and Fazey, I. (2014). The importance of ecosystem services for rural inhabitants in a changing cultural landscape in Romania. *Ecol. Soc.* 19:9.

Hartmann, M. C., Schott, M., Dsouza, A., Metz, Y., Volpi, M., and Purves, R. S. (2022). A text and image analysis workflow using citizen science data to extract relevant social media records: combining red kite observations from Flickr, eBird and iNaturalist. *Ecol. Informatics* 71:101782.

Hermann, A., Schleifer, S., and Wrbka, T. (2011). The concept of ecosystem services regarding landscape research: a review. *Living Rev. Landsc. Res.* 5, 1–37.

Inácio, M., Gomes, E., Bogdzevič, K., Kalinauskas, M., Zhao, W., and Pereira, P. (2022). Mapping and assessing coastal recreation cultural ecosystem services supply, flow, and demand in Lithuania. *J. Environ. Manag.* 323:116175.

INCDS Marin Dracea (2020a). *Assessment Study for the year 2021 of the State of the Biological Resources of Medicinal and Aromatic Plants of the Wild (spontaneous) Flora of the State-Owned Forest Land Administered by the NATIONAL FOREST MANAGEMENT COMPANY ROMSILVA - in romanian [Studiul de evaluare pentru anul 2021 a stării resurselor biologice de plante medicinale și aromatice din flora sălbatică (spontană) a fondului forestier proprietate publică a statului administrat de REGIA NAȚIONALă A PăDURILOR ROMSILVA]*. Voluntari: INCDS.

INCDS Marin Dracea (2020b). *Assessment Study for the Year 2021 of the Status of the Biological Resources of Berries From Wild Flora (spontaneous) of the State-Owned Forest Land Administered by the REGIA NAȚIONALă A PăDURILOR ROMSILVA - in romanian [Studiul de evaluare pentru anul 2021 a stării resurselor biologice de fructe de pădure din flora sălbatică (spontană) a fondului forestier proprietate publică a statului administrat de REGIA NAȚIONALă A PăDURILOR ROMSILVA]*. Voluntari: INCDS.

IPCC (2006). *Intergovernmental Panel on Climate Change 2006 IPCC Guidelines for National Greenhouse Gas inventories*. Hayama: Institute for Global Environmental Strategies.

Isse, N., Tachibana, Y., Kinoshita, M., and Fetters, M. D. (2021). Evaluating outcomes of a social media-based peer and clinician-supported smoking cessation program in preventing smoking relapse: mixed methods case study. *JMIR Formative Res.* 5:e25883.

Jiang, W., Wu, T., and Fu, B. (2021). The value of ecosystem services in China: a systematic review for twenty years. *Ecosyst. Serv.* 52:101365.

Jones, N., McGinlay, J., Kontoleon, A., Maguire-Rajpaul, V. A., Dimitrakopoulos, P. G., and Gkoumas, V. (2022). Understanding public support for European protected areas: a review of the literature and proposing a new approach for policy makers. *Land* 11:733.

Kassambara, A. (2022). *ggcorrplot: Visualization of a Correlation Matrix Using "ggplot2." R package version 0.1.4.1.*

Kassambara, A., and Mundt, F. (2020). *factoextra: Extract and Visualize the Results of Multivariate Data Analyses. Package Version 1.0.7. R package version.*

Kenter, J. O. (2018). "Deliberative and non-monetary valuation," in *Handbook of Ecosystem Services*, eds R. Haines-Young, M. Potschin, R. Fish, and R. K. Turner (Milton Park: Routledge).

Kosanic, A., and Petzold, J. (2020). A systematic review of cultural ecosystem services and human wellbeing. *Ecosyst. Serv.* 45:101168.

Krott, M. (2005). *Forest Policy Analysis*. Berlin: Springer.

Kuhn, M., Jackson, S., and Cimentada, J. (2020). *Corrr: Correlations in R. 2020. R package version 0.4 2, 3–3.*

Kuter, N., Yenilmez, F., and Kuter, S. (2011). Forest fire risk mapping by kernel density estimation. *Croatian J. For. Eng. J. Theory Appl. For. Eng.* 32, 599–610.

Lê, S., Josse, J., and Husson, F. (2008). FactoMineR: an R package for multivariate analysis. *J. Stat. Softw.* 25, 1–8.

Leca, Ş, Popa, I., Chivulescu, Ş, Popa, A., Pitar, D., Dobre, A.-C., et al. (2023). Structure and diversity in a periurban forest of Bucharest, Romania. *Ann. For. Res.* 66, 139–153.

Levine, N., and Associates. (2013). CrimeStat IV: a spatial statistics program for the analysis of crime incident locations (V. 4). *J. Chem. Information Modeling*.

Luck, G. W., Chan, K. M. A., Eser, U., Gómez-Baggethun, E., Matzdorf, B., Norton, B., et al. (2012). Ethical considerations in on-ground applications of the ecosystem services concept. *BioScience* 62, 1020–1029.

Maca-Millán, S., Arias-Arévalo, P., and Restrepo-Plaza, L. (2021). Payment for ecosystem services and motivational crowding: experimental insights regarding the integration of plural values via non-monetary incentives. *Ecosyst. Serv.* 52:101375.

Maes, J., Egoh, B., Willemen, L., Liquete, C., Vihervaara, P., Schägner, J. P., et al. (2012). Mapping ecosystem services for policy support and decision making in the European Union. *Ecosyst. Serv.* 1, 31–39.

Mallinis, G., Petrila, M., Mitsopoulos, I., Lorenţ, A., Neagu, Ş, Apostol, B., et al. (2019). Geospatial patterns and drivers of forest fire occurrence in Romania. *Appl. Spatial Analy. Policy* 12, 773–795.

Márquez, L. A. M., Rezende, E. C. N., Machado, K. B., do Nascimento, E. L. M., Castro, J. D. A. B., and Nabout, J. C. (2023). Trends in valuation approaches for cultural ecosystem services: a systematic literature review. *Ecosyst. Serv.* 64:101572.

Martin, D. M., and Mazzotta, M. (2018). Non-monetary valuation using multi-criteria decision Analysis: sensitivity of additive aggregation methods to scaling and compensation assumptions. *Ecosyst. Serv.* 29, 13–22.

Martínez Pastur, G., Peri, P. L., Lencinas, M. V., García-Llorente, M., and Martín-López, B. (2016). Spatial patterns of cultural ecosystem services provision in Southern Patagonia. *Landsc. Ecol.* 8, 15–34.

Meraj, G., Singh, S. K., Kanga, S., and Islam, M. N. (2022). Modeling on comparison of ecosystem services concepts, tools, methods and their ecological-economic implications: a review. *Modeling Earth Syst. Environ.* 8, 15–34.

Millennium Ecosystem Assessmen (2005). *Ecosystems and Human Well-Being, Synthesis Report*. Available Online at: https://www.millenniumassessment.org/documents/document.356.aspx.pdf (accessed June 21, 2023).

Mudrov, M., and Proch, A. (2005). *Principal Component Analysis in Image Processing*. Prague: Institute of Chemical Technology.

Muradian, R., and Gómez-Baggethun, E. (2021). Beyond ecosystem services and nature's contributions: is it time to leave utilitarian environmentalism behind? *Ecol. Econ.* 185:107038.

Nichiforel, L., Duduman, G., Scriban, R. E., Popa, B., Barnoaiea, I., and Drăgoi, M. (2021). Forest ecosystem services in Romania: orchestrating regulatory and voluntary planning documents. *Ecosyst. Serv.* 49:101276.

Ola, O., and Benjamin, E. (2019). Preserving biodiversity and ecosystem services in West African forest, watersheds, and wetlands: a review of incentives. *Forests* 10:479.

Oliveira, S., Oehler, F., San-Miguel-Ayanz, J., Camia, A., and Pereira, J. M. C. (2012). Modeling spatial patterns of fire occurrence in mediterranean Europe using multiple regression and random forest. *Forest Ecol. Manag.* 275, 117–129.

Pache, R. G., Abrudan, I. V., and Niţă, M. D. (2021). Economic valuation of carbon storage and sequestration in Retezat National Park, Romania. *Forests* 12:43.

Paracchini, M. L., Zulian, G., Kopperoinen, L., Maes, J., Schägner, J. P., Termansen, M., et al. (2014). Mapping cultural ecosystem services: a framework to assess the potential for outdoor recreation across the EU. *Ecol. Ind.* 12: 2138.

Parga-Dans, E., González, P. A., and Enríquez, R. O. (2020). The social value of heritage: balancing the promotion-preservation relationship in the Altamira World Heritage site, Spain. *J. Destination Mark. Manag.* 18: 100499.

Peri, P. L., Rosas, Y. M., and Pastur, G. M. (2022). Human appropriation of net primary production related to livestock provisioning ecosystem services in Southern Patagonia. *Sustainability* 14:7617.

Petz, K., Minca, E. L., Werners, S. E., and Leemans, R. (2012). Managing the current and future supply of ecosystem services in the Hungarian and Romanian Tisza River Basin. *Regional Environ. Change* 12, 689–700.

Pitar, D., Pitar, D., Chivulescu, Ş, Badea, O., Apostol, B., Alimpesc, A., et al. (2021). Evaluarea monetară/non-monetară a serviciilor ecosistemice selectate furnizate de pădurile din PN Grădiştea Muncelului–Cioclovina. *Revista de Silvicultura si Cinegetica* 26:68.

Platon, V., Frone, S., and Constantinescu, A. (2015). New developments in assessing forest ecosystem services in Romania. *Proc. Econ. Finance* 22, 45–54.

R Core Team (2023). *R Core Team 2023 R: a Language and Environment for Statistical Computing.*. Vienna: R Foundation for Statistical Computing.

Raihan, A. (2023). A review on the integrative approach for economic valuation of forest ecosystem services. *J. Environ. Sci. Econ.* 2, 1–18.

Reyers, B., Biggs, R., Cumming, G. S., Elmqvist, T., Hejnowicz, A. P., and Polasky, S. (2013). Getting the measure of ecosystem services: a social-ecological approach. *Front. Ecol. Environ.* 11, 268–273.

Romanazzi, G. R., Koto, R., De Boni, A., Palmisano, G. O., Cioffi, M., and Roma, R. (2023). Cultural ecosystem services: a review of methods and tools for economic evaluation. *Environ. Sustainabil. Ind.* 37:100304.

Sangha, K. K., Russell-Smith, J., and Costanza, R. (2019). Mainstreaming indigenous and local communities' connections with nature for policy decision-making. *Glob. Ecol. Conserv.* 19:e00668.

Scholte, S. S. K., van Teeffelen, A. J. A., and Verburg, P. H. (2015). Integrating socio-cultural perspectives into ecosystem service valuation: a review of concepts and methods. *Ecol. Econ.* 114, 67–78.

Schröter, M., van der Zanden, E. H., van Oudenhoven, A. P. E., Remme, R. P., Serna-Chavez, H. M., de Groot, R. S., et al. (2014). Ecosystem services as a contested concept: a synthesis of critique and counter-arguments. *Conserv. Lett.* 7, 514–523.

Selivanov, E., and Hlaváčková, P. (2021). Methods for monetary valuation of ecosystem services: a scoping review. *J. For. Sci.* 67, 499–511.

Sharma, S., Hussain, S., and Singh, A. N. (2022). Evaluation methods for cultural ecosystem services: a systematic review. *Proc. Int. Acad. Ecol. Environ. Sci.* 12, 194–210.

Smith, R. I., Dick, J. M., and Scott, E. M. (2011). The role of statistics in the analysis of ecosystem services. *Environmetrics* 22, 608–617.

Spangenberg, J. H., and Settele, J. (2010). Precisely incorrect? monetising the value of ecosystem services. *Ecol. Complexity* 7, 237–337.

Statistics (2019). *Statistics of Forestry Activities in Romania*. Available online at: https://insse.ro/cms/sites/default/files/field/publicatii/statistica_activitatilor_din_silvicultura_in_anul_2019_1.pdf

Taye, F. A., Folkersen, M. V., Fleming, C. M., Buckwell, A., Mackey, B., Diwakar, K. C., et al. (2021). The economic values of global forest ecosystem services: a meta-analysis. *Ecol. Econ.* 89:107145.

Tenerelli, P., Demšar, U., and Luque, S. (2016). Crowdsourcing indicators for cultural ecosystem services: a geographically weighted approach for mountain landscapes. *Ecol. Ind.* 64, 237–248.

Torres, A. V., Tiwari, C., and Atkinson, S. F. (2021). Progress in ecosystem services research: a guide for scholars and practitioners. *Ecosyst. Serv.* 49:101267.

Tsirintanis, K., Azzurro, E., Crocetta, F., Dimiza, M., Froglia, C., Gerovasileiou, V., et al. (2022). Bioinvasion impacts on biodiversity, ecosystem services, and human health in the Mediterranean sea. *Aquatic Invasions* 17, 308–352.

Tudoran, G. M., Cicşa, A., Cicşa, M., and Dobre, A. C. (2022). Management of recreational forests in the Romanian Carpathians. *Forests* 13:1369.

Turner, R. K., Paavola, J., Cooper, P., Farber, S., Jessamy, V., and Georgiou, S. (2003). Valuing nature: lessons learned and future research directions. *Ecol. Econ.* 46, 493–510.

Vallet, A., Locatelli, B., Levrel, H., Wunder, S., Seppelt, R., Scholes, R. J., et al. (2018). Relationships between ecosystem services: comparing methods for assessing tradeoffs and synergies. *Ecol. Econ.* 150, 96–106.

Vedeld, P., Angelson, A., Sjaastad, E., Berg, G., Angelsen, A., Sjaastad, E., et al. (2004). Counting on the environment. forest incomes and the rural poor. *Environ. Econ. Ser.* 1, 869–879.

Waller, L. A., and Gotway, C. A. (2004). *Applied Spatial Statistics for Public Health Data*. Hoboken, NJ: John Wiley & Sons.

Wanek, E., Bartkowski, B., Bourgeois-Gironde, S., and Schaafsma, M. (2023). Deliberately vague or vaguely deliberative: a review of motivation and design choices in deliberative monetary valuation studies. *Ecol. Econ.* 208: 107820.

Weiskopf, S. R., Rubenstein, M. A., Crozier, L. G., Gaichas, S., Griffis, R., Halofsky, J. E., et al. (2020). Climate change effects on biodiversity, ecosystems, ecosystem services, and natural resource management in the United States. *Sci. Total Environ.* 733:137782.

Williamson, D., McLafferty, S., Goldsmith, V., Mollenkopf, J., and McGuire, P. (1999). *A Better Method to Smooth Crime Incident Data. ESRI ArcUser Magazine*. Available online at: http://www.esri.com/news/arcuser/0199/crimedata.html

Yang, W., Chen, Q., Huang, X., Xie, M., and Guo, Q. (2022). How do aesthetics and tourist involvement influence cultural identity in heritage tourism? the mediating role of mental experience. *Front. Psychol.* 13:990030. doi: 10.3389/fpsyg.2022.990030

Zhang, S., Paterson, J. S., and Hujala, T. (2021). Sustaining forest ecosystem services through social enterprises: motivations and challenges from a case study in Scotland. *Small Scale For.* 20, 627–647.

Radial growth response of *Pinus Yunnanensis* to climate in high mountain forests of northwestern Yunnan, southwestern China

Siyu Xie[1], Tao Yan[1], Xueyi Sun[2], Hai Chen[3], Mei Sun[1] and Yun Zhang[1]*

[1]National Plateau Wetlands Research Center, Wetlands College, Southwest Forestry University, Kunming, China, [2]Anji Yinjiang Agriculture Development Co., Ltd., Anji, China, [3]Changxing Forestry Technology Extension Center, Changxing, China

Understanding the relationship between tree growth and environmental conditions is essential to elucidating the impact of global climate change on forest ecosystems. We used the dendrochronology method to examine the growth sensitivity of a typical conifer to climate change in mountain forests of Central Hengduan Mountain. The study involved the establishment of tree ring width chronologies of *Pinus yunnanensis* in both Haba Snow Mountain (HB) and Yulong Snow Mountain (YL) in northwestern Yunnan, enabling the detection of the relationship between its radial growth and climates, i.e., monthly total precipitation, monthly temperatures (average minimum, mean and maximum) and monthly Palmer Drought Severity Index (PDSI). Response function and redundancy analysis (RDA) were used to identify correlations between climate variables and radial growth, and moving interval analysis was applied to determine the stability of climate-growth relationship. The findings demonstrated that the growth of *P. yunnanensis* had similar response patterns to climate change at two sites, exhibiting growth synchronization and common signals. Specifically, the radial growth of *P. yunnanensis* was negatively correlated with May temperature, while temperature in current October significantly promoted radial growth. Precipitation in June was the common climate variable with inverse effects between two sites, with positive impacts on YL and negative impacts on HB. The results of moving interval analysis were consistent with response function and RDA, presenting significant correlations in many years for those climatic variables significantly affecting tree growth. Stability analysis also revealed that the climate-growth relationship could fluctuate over a small range of time scales, induced by an abrupt change in climate. A forecast of strengthen in growth of *P. yunnanensis* forests was expected, since increases in precipitation and temperature of most months would benefit tree growth, and negative impacts of May temperature would be offset by the increase of precipitation in the corresponding month. These results could provide a basis for developing sustainable strategies of forest management under the climate change.

KEYWORDS

tree ring, conifer, dendroclimatology, climate change, climate-growth relationships

1 Introduction

Global surface temperature will continue to increase until at least mid-century. Global warming will exceed 1.5°C to 2°C during the 21st century unless deep reduction measures of CO_2 and other greenhouse gas emissions will be carried out in the coming decades (IPCC, 2021). In southwestern China, the climate has been warming and drying, with a tendency of intensification since the beginning of the 21st century (Su et al., 2014). Climate change has a massive impact on the structure and function of terrestrial ecosystems. For forest ecosystems, the largest component of the terrestrial ecosystem, climate change has greatly influenced its composition, structure, productivity, carbon storage capability, and ecological function (Zhang et al., 2017; Fan et al., 2019). Tree radial growth is sensitive to climate variation and mainly affected by climate factors, thus, a better understanding of climate effects on tree growth will help predict growth dynamics of forests under global climate change.

Climate warming is expected to enhance tree growth at alpine treelines (Camarero et al., 2021). Nevertheless, these positive influences need to be considered alongside water availability (Martínez-Vilalta et al., 2008), as high temperatures may lead to an increase in the frequency and intensity of droughts. If water availability is insufficient, the impact of drought stress on tree physiological processes will worsen, and consequently lead to a reduction of tree growth (Aber et al., 2001). Recent studies have revealed that droughts widely affected tree and forests growth over the world and even determined the survival of trees. For instance, a study found that consecutive hotter droughts posed a threat to forests under climate change in Central European floodplain forests, even with comparably high levels of water supply (Schnabel et al., 2022). Years with more intense drought corresponded with larger growth reductions and increased tree mortality rates in California forests, North America (Young et al., 2017; Bohner and Diez, 2021). Studies in Tibetan Plateau have shown that water deficit was the main factor controlling the resistance of juniper trees and higher drought frequency caused the decline of junipers' growth, which was due to a lower tolerance to extreme drought events (Fang et al., 2021). In South America, predicted increases in drought frequency and intensity can have negative consequences for the functioning of the Amazon Forest (Van Passel et al., 2022).

Tree ring width is commonly used as a tree ring parameter and a measure of tree increment, which has contributed to the largest proportion of dendroclimatological research worldwide (He et al., 2019). Due to its precision as a proxy of recording climate information up to the millennium scale (Shen et al., 2020), it has been a useful tool in evaluating growth sensitivity to climate change and assessing the impact of future climate change on the radial growth of tree species and forests (Huang et al., 2010).

The Central Hengduan Mountains (CHM) is located in southeastern margin of Tibetan Plateau, which is a sensitive region to global climate change (Zhang et al., 2020). It is rich in biodiversity and covered by extensive forests composed of various species, covering their altitude distributional range and forming different treeline types. Therefore, the area is considered an excellent location to conduct a dendroclimatology study (Fan et al., 2009). Many efforts have been made to reconstruct historical climate and to find key climate factors affecting tree growth by using tree ring data of typical coniferous tree species in CHM, such as for *Abies georgei* (Fan et al., 2009; Liang et al.,

2010; Panthi et al., 2018), *Larix potaninii* (Zhang et al., 2017, 2020), *Picea brachytyla* (Fan et al., 2008; Li et al., 2012; Yue et al., 2022), *Picea likiangensis* (Wang et al., 2018; Yu et al., 2018; Du et al., 2020), and *Tsuga dumosa* (Guo G. et al., 2009; Li et al., 2011; Aryal et al., 2020). These studies found that tree radial growth was influenced by both temperature and precipitation, but the growth response pattern was depended on species characteristics and site conditions. These studies provide an opportunity to understand climate-growth relationships for tree species and forests in high-altitude areas, and their connection to large-scale climate models (He et al., 2019).
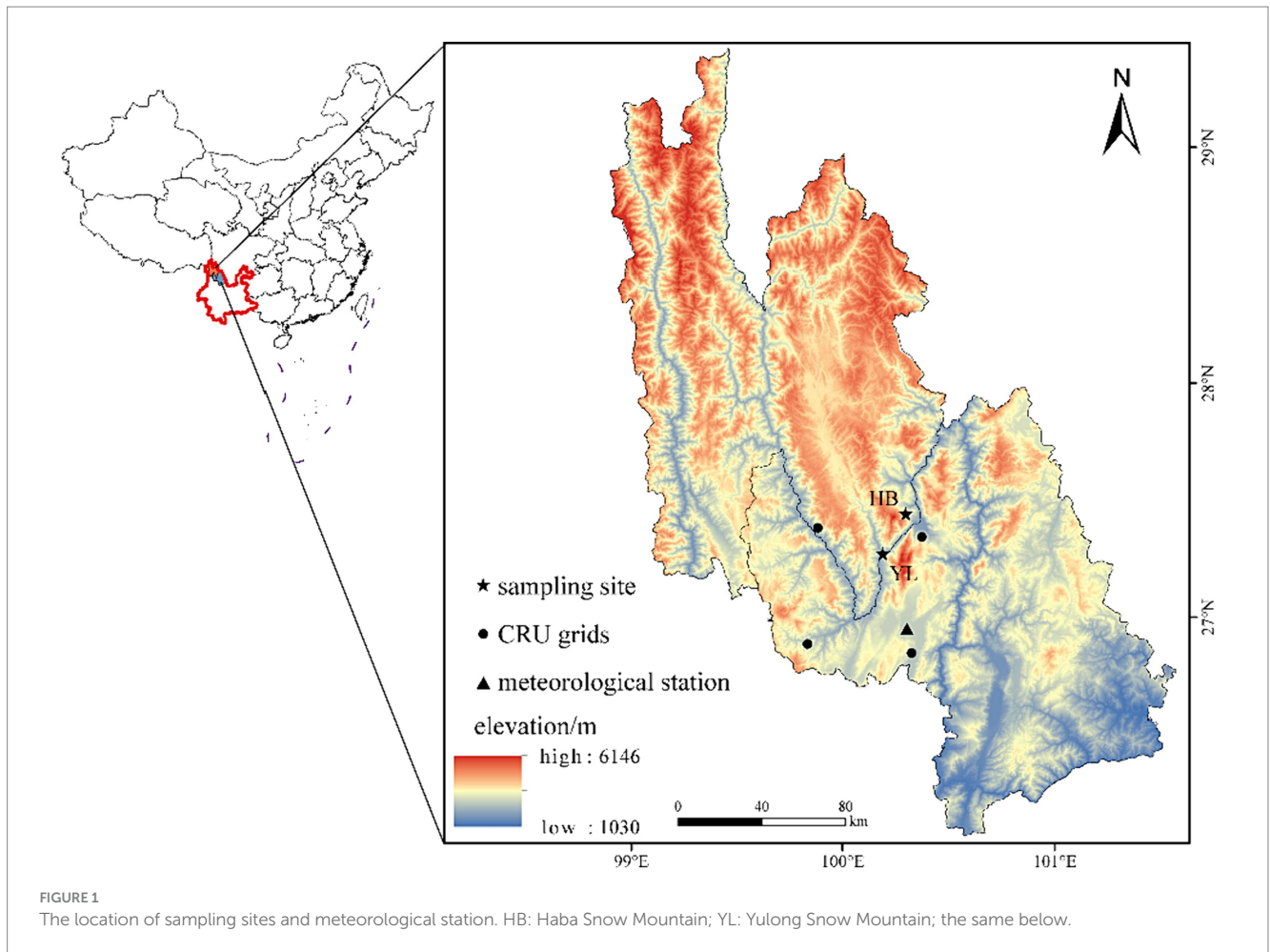
Pinus yunnanensis forests are mainly distributed in Yunnan-Guizhou Plateau and in the southeastern edge of the Tibetan Plateau, and are important timber forests in southwestern China (Fu et al., 1999). *P. yunnanensis* is a shade-intolerant and deep-rooted coniferous species growing at altitudes between 1800 to 3,200 m a.s.l. in CHM (Deng et al., 2014; Shen et al., 2020). The species has strong adaptability to arid climate and barren soil, with red soil as the representative soil type. It grows best on well-drained north slopes with adequate light. The concurrent climate conditions in CHM are consistent with the climate background of global warming, which makes this typical species particularly interesting for studying the growth response to climate change. Tree ring studies of *P. yunnanensis* have been carried out at high (Yang et al., 2018, 2022), medium (Shen et al., 2020), and low altitudes in southwestern China (Sun et al., 2020). However, its growth responses to climate change in CHM is not well understood.

In this paper, we utilized dendrochronology methods to study the relationship between the radial growth of *P. yunnanensis* and climate by establishing tree ring width chronologies and detecting its growth response to climate factors on Haba Snow Mountain (HB) and Yulong Snow Mountain (YL) in CHM. We aim to (1) identify the critical climate factors affecting the growth of *P. yunnanensis* in the area, and (2) analyze the temporal stability of climate-growth relationships to determine whether the growth response to annual climate factors is smooth over time. It was hypothesized that temperature and precipitation interacted temporally, and negative impacts of temperature on growth were expected in dry periods. Furthermore, we explored the impact of future climate change on *P. yunnanensis* forests growth based on climate-growth relationships results and climate models.

2 Materials and methods

2.1 Study area

HB with the peak of 5,396 m a.s.l. and YL with the peak of 5,596 m a.s.l. are two typical snow-capped mountains in the Central Hengduan Mountain (CHM), separated by the Jinsha River (Figure 1). Different vegetation types are formed along the altitudinal gradient in CHM. The dry valleys are usually covered by scrublands. Warm-temperate coniferous forests, dominated by *P. yunnanensis* and *Pinus armandii*, are mainly distributed at altitudes between 1,000 m a.s.l. and 3,300 m a.s.l. *Pinus densata* is a dominant species at altitudes of 2,600 to 3,500 m a.s.l. on the southern slope. Cold-temperate coniferous forests are dominated by spruce (*P. brachytyla*, *P. likiangensis*), fir (*A. georgei*, *Abies forrestii*) and larch species (*L. potaninii*), at elevations ranging from 3,000 m a.s.l. to 4,200 m a.s.l. (Fan et al., 2009).

FIGURE 1
The location of sampling sites and meteorological station. HB: Haba Snow Mountain; YL: Yulong Snow Mountain; the same below.
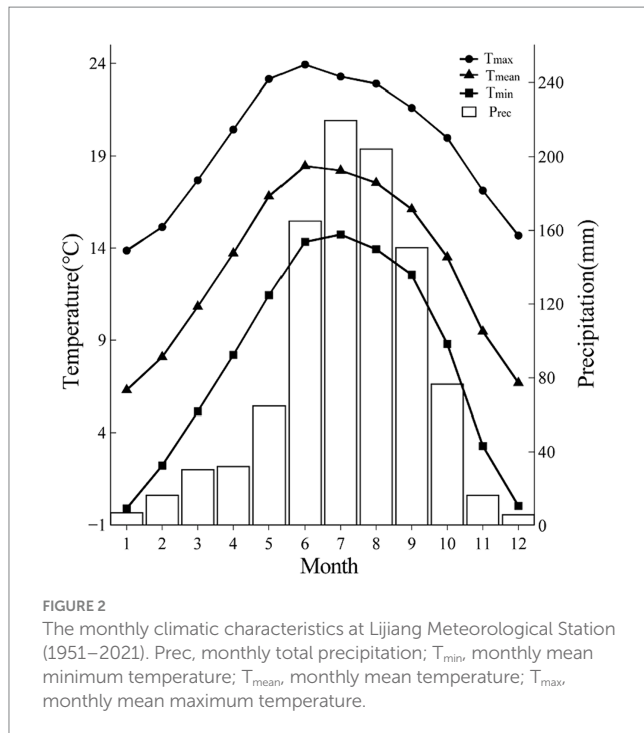
Although vegetation types along the altitudinal gradient were similar in both HB and YL, the distribution range of *P. yunnanensis* was a bit different. The species is mainly distributed from 2000 m a.s.l. to 3,500 m a.s.l. in HB, while the distribution of *P. yunnanensis* in YL ranged from 2000 m a.s.l. to 3,000 m a.s.l. In HB, the soil texture is predominantly loamy, distributed from 1800 to 3,450 m a.s.l., transitioning from red soils to yellow and then brown soils. Above 3,900 m a.s.l., podzolic soil and meadow soil prevail. In YL, the soil texture is dominated by loam and clay, with a gradual transition from clay and loamy clay to sandy clay, sandy loam, and loam as the altitude increases from low to high.

The climate in CHM is strongly influenced by the southeast monsoon and southwest monsoon, with the monsoon climate characteristics of simultaneous rain and heat, and distinct dry and wet seasons. According to the meteorological data (1951–2021) of Lijiang meteorological station (26°51′N, 100°13′E, 2380.9 m a.s.l., Figure 2), annual mean temperature was 12.97°C, while annual maximum temperature (23.92°C) and annual minimum temperature (−0.11°C) appeared in June and January, respectively. The annual total precipitation was 988.93 mm, mainly occurring in summer, as the precipitation from June to September accounted for 75% of the total precipitation. Over the last three decades, the climate of the study area has been characterized by noticeable warming and drying, with a significant increasing trend in temperature (particularly during the period from 1990 to 2016) and a decreasing trend in Palmer Drought

Severity Index (PDSI) between 1951 and 2021, while precipitation did not show a significant decreasing trend (Figure 3).

2.2 Tree-ring sampling and chronology development

We sampled mature and healthy trees without insect damage at undisturbed forest communities at two adjacent sites with similar climate conditions and growth environments (Table 1). The cores were drilled at the trees' breast height (1.3 m) with a 5.15-mm-diameter increment borer, one or two cores were extracted per tree from the opposite direction parallel to the contour to avoid growth reaction to the slope. Obtained cores were labelled and placed in plastic straws. In the laboratory, the cores were put into wooden tanks by using white latex and tape. The samples were polished by sandpaper with gradually finer particle sizes (200 mesh to 1,000 mesh) until the growth rings were visible. Then, the cores were visual cross-dating under a microscope and scanned by EPSON (Expression11000XL) scanner. The scanner parameters were set to 24-bit full-color professional mode image types, with a resolution of 2000 dpi. The dated cores were measured using the CDendro and CooRecorder ver. 9.8.1 software at a precision of 0.001 mm to obtain the ring widths. Furthermore, the results of cross-dating were examined by the COFECHA program (Holmes, 1983), and those cores with inadequate quality were

FIGURE 2
The monthly climatic characteristics at Lijiang Meteorological Station (1951–2021). Prec, monthly total precipitation; T_{min}, monthly mean minimum temperature; T_{mean}, monthly mean temperature; T_{max}, monthly mean maximum temperature.

removed based on the testing results. Ultimately, 62 trees from 112 cores remained for the further analysis.

To remove the growth trend caused by genetic factors or individual interference while preserving more climate signals, a negative-exponential curve function was applied to standardize the ring width series. Residual chronologies (Figure 4) were developed after autoregressive modelling performed on per standardized series to remove potential autocorrelation and retain high-frequency climate change. Further, all residual series were averaged on a site-by-site basis utilizing the bi-weight robust mean (Cook, 1985), to minimize the influence of outliers. All procedures were executed using the ARSTAN Program (Cook, 1985) and two residual chronologies were generated with chronological eigenvalue (Table 2), including mean sensitivity (MS), signal-to-noise ratio (SNR), standard deviation (SD), and expressed population signal (EPS), etc.

The MS quantifies the degree of inter-annual variation in ring width, serving as an indicator of the sensitivity of tree growth to climate change. A higher value indicates a greater inter-annual variation in ring width, suggesting that the trees are highly responsive to environmental changes. The SNR serves as an indicator of the proportion of climatic signals to non-climatic noise within the ring width data. A high SNR signifies that the ring-width data contains a richer climatic information. The SD is a statistical measure that assesses the dispersion of tree ring width data, reflecting the variation in ring width across different growth years. The EPS is a statistical metric that assesses the representativeness of a sample. A high value of EPS means that the sample data are well represented and can be used to infer growth and climate change in broader regions.

2.3 Climate data

Monthly mean maximum temperature (T_{max}), monthly mean temperature (T_{mean}), and monthly mean minimum temperature (T_{min}),

sourced from the neareast Lijiang Meteorological Station (26°50′N, 100°13′E, 2,382 m a.s.l), were acquired through the National Oceanic and Atmospheric Administration (NOAA).[1] Precipitation data were obtained from the Climatic Research Unit (CRU TS v. 4.07; https://crudata.uea.ac.uk/cru/data/hrg) at a resolution of 0.5° × 0.5° (Harris et al., 2020). The PDSI is a comprehensive meteorological drought index that considers precipitation, temperature, evapotranspiration, and drought duration (Alley, 1985). The PDSI data was extracted from the monthly data set compiled by the global CRU grids[2] at 0.5° × 0.5° spatial resolution (Dunn et al., 2022). Its index ranges from −4 (indicating extremely dry conditions) to +4 (indicating extremely wet conditions), where a smaller value represents a more severe relative drought.

2.4 Data analysis

To capture the lag effect of climate on tree radial growth (Fritts et al., 1965), each tree ring was paired with 14 months of climate data spanning from the previous year's September through the following October. The climate timeseries interval was from 1987 to 2017 for the data analysis. Five climate variables were selected for analyzing relation to tree radial growth, including T_{mean}, T_{max}, T_{min}, the monthly total precipitation, and PDSI.

The response function was applied to analyze correlations between climate variables and chronologies by using DendroClim2002 (Biondi and Waikul, 2004). The coefficients of the response function are multivariate estimates from a principal component regression model (Morzuch and Ruark, 1991) and the method solves the inter-correlation problems among climatic variables (Fritts et al., 1971). To further identify common climate variables affecting the radial growth of *P. yunnanensis*, the redundancy analysis (RDA) was also conducted using CANOCO 5.0 software. RDA is the canonical form of principal component analysis (PCA) and constitutes the direct extension of multiple regressions applied to multivariate data (Legendre and Legendre, 1998). In RDA, the ordination axes are constrained to be linear combinations of supplied environmental variables (ter Braak, 1994), and it is an effective method in quantifying the relationship between tree-ring width and climate variables (Girardin et al., 2004; Drobyshev et al., 2013; Zhang et al., 2020). Like the response function, T_{mean}, T_{max}, T_{min}, the monthly total precipitation, and PDSI were selected for RDA. Following a Monte Carlo permutation test involving 999 random permutations, only those climate variables showing significant correlations ($p < 0.05$) with the two residual chronologies were presented in the RDA.

For tracing the dynamic relationship over time between the annual ring width index and climate, the Moving Forward method (with a window of 36 years) in the Evolutionary and Moving Response and Correlation module of DendroClim 2002 software was also applied to calculate temporal stability of relationships between chronologies and climate variables. The Special Report on Emissions Scenarios (SRES) B2 scenario was considered as future changes in temperature and precipitation, it was published by the Intergovernmental Panel on Climate Change to provide an assessment
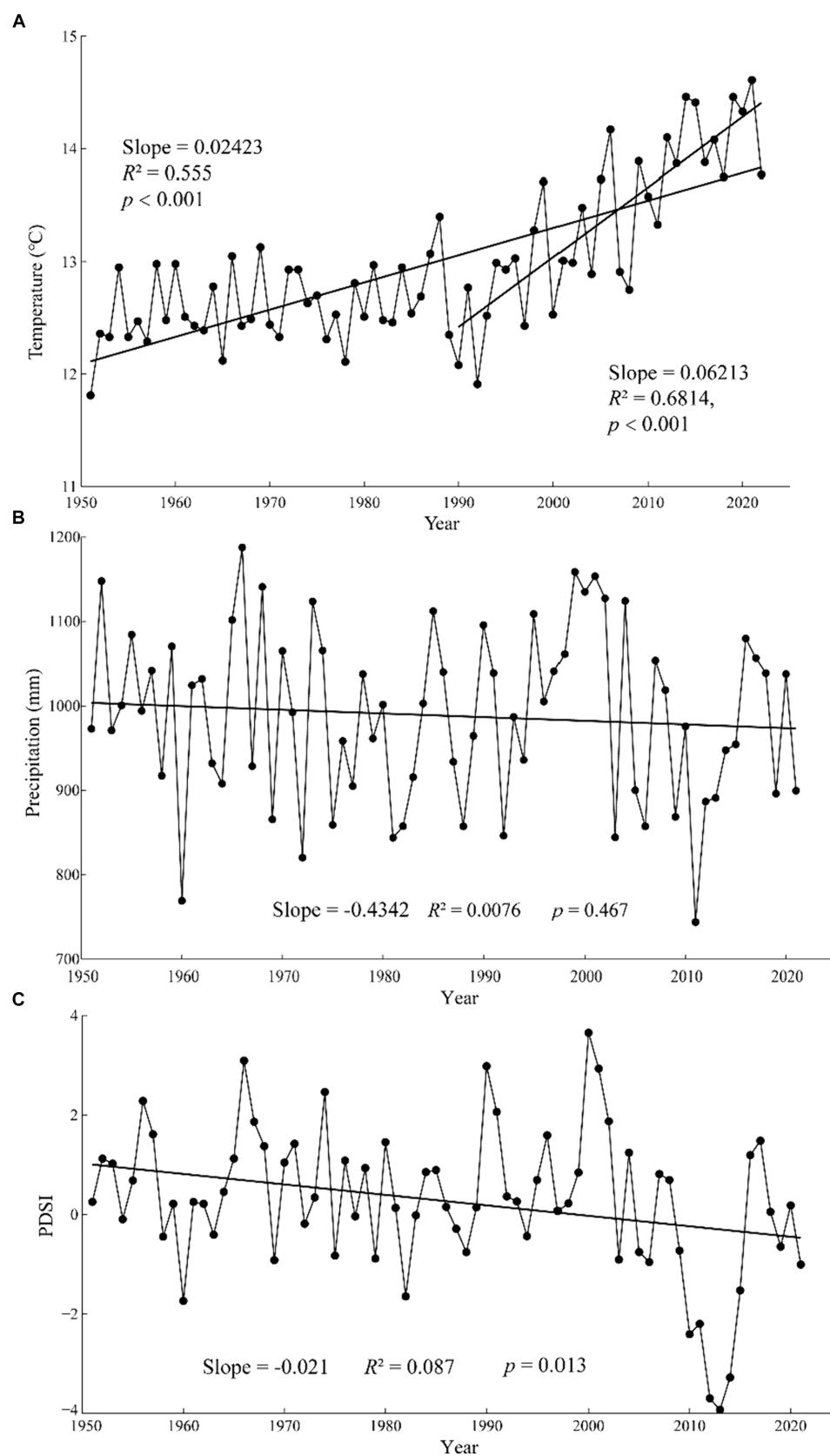

FIGURE 3
Annual trends of mean temperature **(A)**, precipitation **(B)** and Palmer Drought Severity Index (PDSI) **(C)** at Lijiang Meteorological Station (1951–2021).

TABLE 1 Sampling sites information.

Sampling site	Longitude	Latitude	Altitude (m)	No. (trees/cores)
HB	100°09′50.18″	27°20′34.02″	3,214	32/62
YL	100°04′16″	27°09′48″	2,935	30/56

HB, Haba Snow Mountain; YL, Yulong Snow Mountain; the same below.
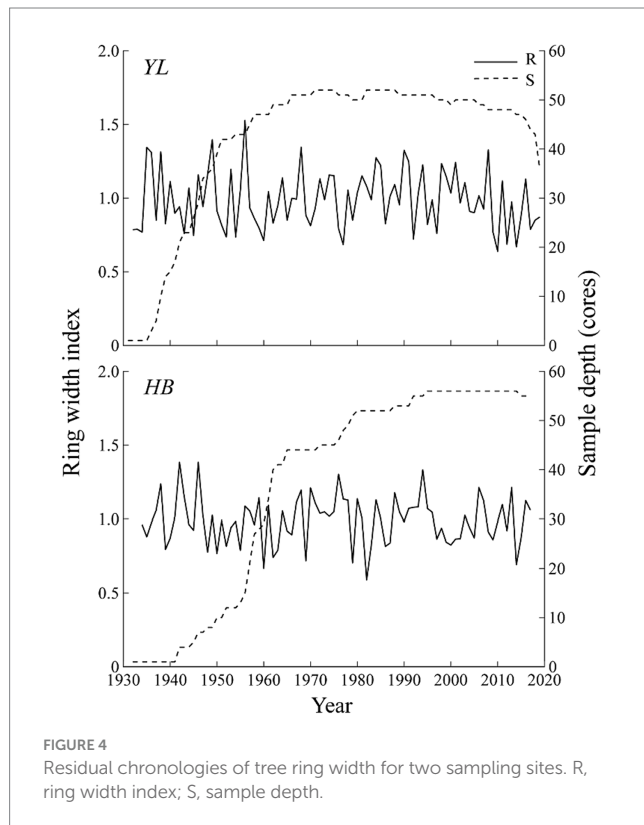
FIGURE 4
Residual chronologies of tree ring width for two sampling sites. R, ring width index; S, sample depth.

of the climate change. The graphs were plotted using the ggplot2 program package in R.

3 Results

3.1 Tree-ring chronologies

Both residual chronologies with high values of SNR and variance in first eigenvector contained large climate information (Table 2). Tree growing in YL with greater MS and SD showed higher interannual fluctuations than those in HB (Table 2). The high EPS (>0.85) confirmed that the sampled population for each site was well-represented, and two residual chronologies could reflect the overall growth characteristics of *P. yunnanensis* in the study area and then the chronologies could be applied to conduct correlation analysis with climate variables.

3.2 Climate-growth relationship

We showed correlations between radial growth and climate variables in Figure 5. In HB, the radial growth of *P. yunnanensis* was

TABLE 2 Statistics of tree ring width residual chronologies.

Statistic characters	HB	YL
Sample depth (trees/cores)	32/56	30/56
Time span (A.D)	1932–2017	1931–2019
Common interval analysis	1966–2016	
Mean sensitivity (MS)	0.18	0.24
Standard deviation (SD)	0.16	0.20
Signal-to-noise ratio (SNR)	20.67	21.10
Expressed population signal (EPS)	0.95	0.96
Variance in first eigenvector (%)	36.23	39.54

significantly associated with T_{max} in May and precipitation in February, by showing negative and positive correlations, respectively. In addition, PDSI in the previous September negatively affected *P. yunnanensis* growth. In YL, the radial growth was significantly and negatively correlated with May and June temperatures (both T_{mean} and T_{max}), and significantly and positively correlated with T_{mean} and T_{min} of the current October. While *P. yunnanensis* radial growth was found to be positively correlated with precipitation in May and June, and previous October. For PDSI, significant and positive correlations were found in June and July.

3.3 Redundancy analysis

The results of RDA (Figure 6) revealed that three climate variables significantly affected the radial growth of *P. yunnanensis*. Specifically, May T_{mean}, current October T_{mean}, and June precipitation explained 17.9, 6.7, and 4.7% of the radial growth, respectively. The first axis and the second axis accounted for 24.49 and 4.85% of the response variables, respectively. May T_{mean} exerted the most considerable influence on radial growth with negative impacts at both sites, while current October T_{mean} positively affected the radial growth. June precipitation presented inverse impacts on tree growth at two sites, by showing negative and positive influences in HB and YL, respectively.

3.4 Dynamic relationships analysis

The moving response analysis results (Figures 7A,C,E) showed that the growth response of *P. yunnanensis* to precipitation in May remained relatively stable in HB, by showing positive correlations over the decade with significant periods between 1987 and 1999. The negative response to May temperature reached a significant level before 2000 ($p < 0.05$) and then weakened. The drought condition in previous September was likely to affect *P. yunnanensis* growth, as the negative influences of PDSI strengthened in recent 20 years.

In YL, the response of *P. yunnanensis* to precipitation (positive) and temperature (negative) in current May, temperature in current October (positive), and PDSI (negative) in current October were stable, by showing significant correlations at many years. For current June, the negative impacts of temperature and positive effects of precipitation on tree growth were enhanced after 1992. In Addition, the positive response to PDSI in current June and July fluctuated due
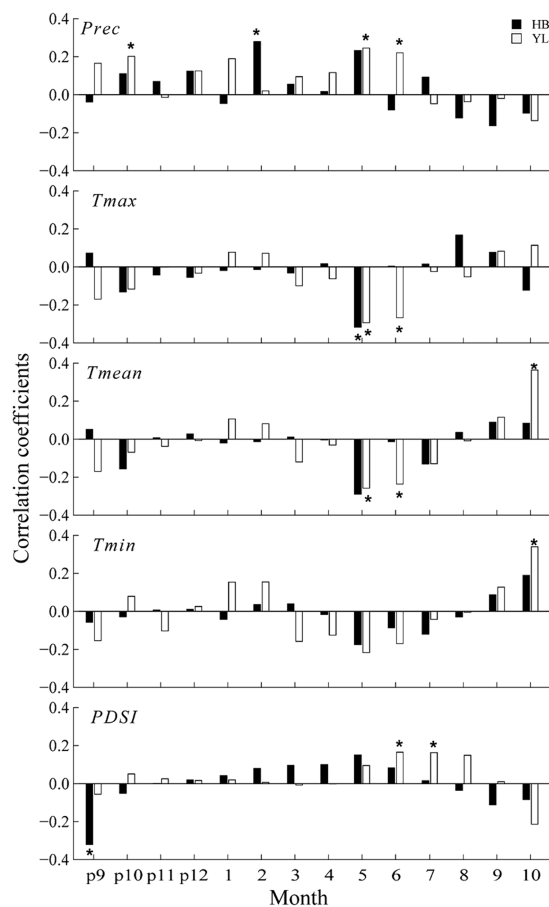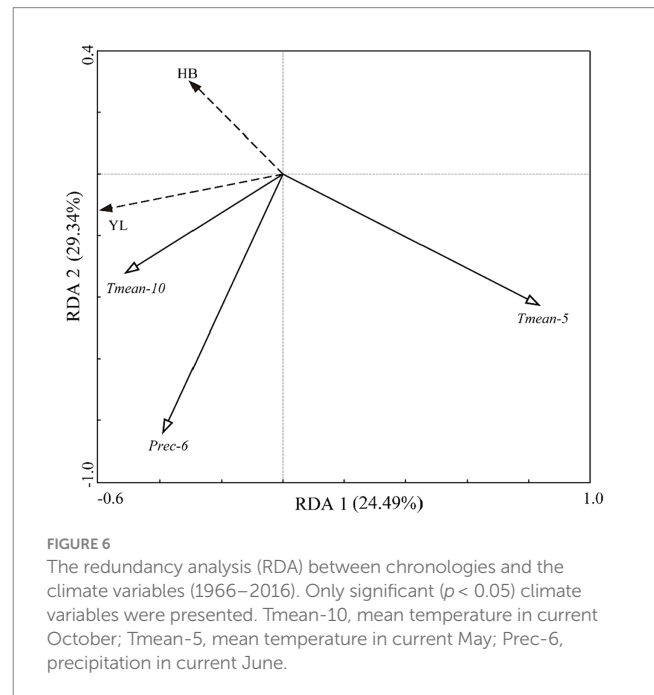
rapid increase in temperature with high evaporation, consequently alleviate the plant transpiration and avoid stomatal closure. Moreover, the increase in precipitation could supply soil moisture for xylem cell production and the onset of xylogenesis (Shen et al., 2020) during the cambium active period of tree growth in the early growing season (Rossi et al., 2016).

Current October T_{mean} positively affected the radial growth of *P. yunnanensis* (Figure 6), suggesting the importance of the impact of post-growing season temperature on tree growth. During the post-growing season, cambial activity tended to be weakened (Gričar et al., 2007). However, elevated temperatures could stimulate photosynthesis and generate nutrients for tree growth, and prolong the growing season, consequently leading to the formation of wider annual ring widths (Dawadi et al., 2013). Similar results have also been found in the growth of *A. georgei* (Sun et al., 2021) in HB and *Abies fargesii* (Kharal et al., 2017) in adjacent Manan River Valley of central Himalayas.

The common climate variables with inverse effects between two sites were also observed. Excessive precipitation in June had negative impacts on *P. yunnanensis* growth in HB. Tree began to fast growth in June on HB and would benefit from high temperature for photosynthesis (Zhang et al., 2020). However, greater precipitation is generally combined with enhanced cloudiness, reduced solar radiation input, and lower temperatures, which might decrease the photosynthetic process (Fan et al., 2019). The constraints of early summer precipitation on tree growth have also been reported in previous studies in four conifers (Zhang et al., 2020), *P. yunnanensis* (Shen et al., 2020), and *A. georgei* (Yin et al., 2018) in CHM. In comparison with HB, the sampling site is about 300 m lower in YL, water availability was more important than temperature at lower elevation sites (Fan et al., 2009). Xylem cell production benefits from energy and soil moisture during the cambium active phase (Liang et al., 2014) and enough precipitation can satisfy the water demand of the tree growth in the growing season. This was also demonstrated by growth reaction to PDSI in YL, presenting significant and positive correlations with PDSI in current June (Figure 5).
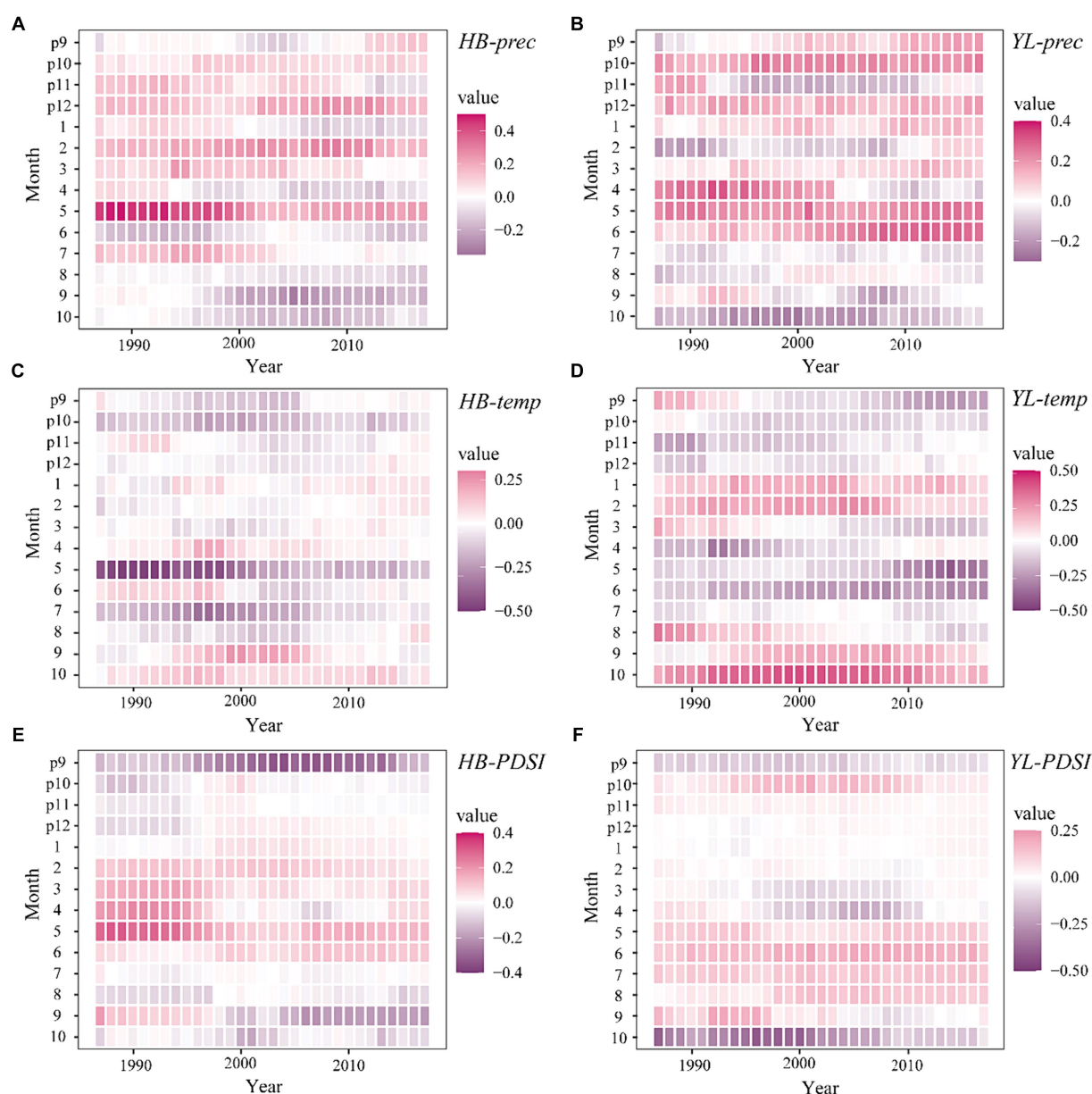
to climate change and reached a significant level from 2012 to 2016 (Figures 7B,D,F).

4 Discussion

4.1 Common response to climate

Both response function analysis and RDA revealed that high temperature (T_{max}) in May restricted the radial growth of *P. yunnanensis* at two sites (Figures 5, 6). In general, temperatures rose rapidly during the early growing season (April to May), but the region does not experience a rapid increase in precipitation during these months (Figure 2). This may cause drought stress for tree growth induced by the acceleration of plant transpiration and soil moisture evaporation, which lead to insufficient water supply (Denmead and Shaw, 1962). Similar results have been reported in other conifers in CHM, such as the *A. georgei* in HB (Sun et al., 2021), *A. forrestii* and *P. likiangensis* in YL (Yang et al., 2022), and *T. dumosa* in YL (Guo G. et al., 2009), indicating the importance of sufficient moisture condition of this period on tree growth in the area. This water-demand effect was also supported by the results of response function analysis, by showing positive relation to May precipitation (Figure 5). High precipitation could compensate for the loss of soil water caused by

Moving interval analysis between chronologies and the monthly total precipitation (prec) **(A)**, monthly mean temperature (temp) **(C)** and Palmer Drought Severity Index (PDSI) **(E)** in HB, and (prec) **(B)**, (temp) **(D)**, (PDSI) **(F)** in YL from previous September to current October (1987–2017). p: previous year.

Furthermore, the observed inverse response can be attributed to variations in soil conditions. The soil is relatively infertile with low organic matter due to steep slopes and shallow soil layers in HB (Su and Wang, 2020), elevated precipitation may trigger soil erosion and therefore endanger its growth. While in YL, the soil is comprised of loam and clay with a higher organic matter content, abundant precipitation may create moist soil conditions for tree growth (Guo L. N. et al., 2009).

4.2 Site-specific climate response

The radial growth of *P. yunnanensis* was affected by winter precipitation in HB (Figure 5). The rise in February precipitation facilitated the formation of a thicker snow cover, effectively shielding

roots from potential damage induced by low temperatures and harsh winds at higher altitudes (Zhang et al., 2020). As the snow melted, the heightened soil moisture further supported roots in optimizing water and nutrient uptake, ultimately promoting tree growth (Su and Wang, 2020). The positive effects of winter temperature on tree growth were also highlighted by previous studies at high elevations in the area (Fan et al., 2009; Zhang et al., 2018).

Favorable soil moisture conditions in July promoted the radial growth of *P. yunnanensis* in YL, since adequate soil moisture could accelerate nutrient dissolution and transport, as well as facilitate root absorption, enriching trees with essential nutrients and alleviating drought stress. A similar response pattern to soil moisture was observed by Sun et al. (2020) in Hengduan Mountains, where *P. yunnanensis* tree rings were positively correlated with summer moisture availability.

4.3 The stability dynamics

In general, the results of moving interval analysis approved the findings obtained through response function and RDA, by showing significant correlations in many years for those months (e.g., May, June, July, and October), which presented significant relations to tree growth. Furthermore, the stability of climate-growth relationships exhibited variability on an interannual scale. For example, the strongest correlation between tree growth and May temperature in HB was detected from 1990 to 2000, then the strength of the relationship became weakened after the 21st century. This may be attributed to the noticeable temperature surge in Lijiang during that 10-year period (Figure 3), correspondingly, there was a notable strengthening of the positive correlation between growth and May precipitation during this period. The increased precipitation seemed to alleviate the drought stress caused by the sharp temperature rise. Similar results were also presented by the relationship between tree growth and June precipitation, temperature, and PDSI in YL, and other studies that showed the stability of climate-growth relationships varied with warming periods and abrupt climatic changes in the region (Shen et al., 2020).

4.4 Future tree and forest growth

According to the future climate simulation under the Special Report on Emissions Scenarios (SRES) B2 scenario, the mean temperature in spring, summer, autumn, and winter in Southwest China is projected to increase by 2.6°C, 3.1°C, 2.7°C, and 3.1°C, and precipitation will relatively increase by 8, 7, 6, and 8% in 2071–2,100 (Xu et al., 2005). Incorporating the climate response of tree growth and the prediction of future climate conditions, the productivity of *P. yunnanensis* forests would likely be enhanced. The radial growth of *P. yunnanensis* will benefit from increases in precipitation since precipitation is all positively correlated with tree growth (except June precipitation in HB). Although higher temperature in spring and early summer will inhibit tree growth, increases in precipitation of the corresponding seasons is likely to offset the negative impact. Therefore, the growth of *P. yunnanensis* forests was expected to enhance under future climate change in the area.

5 Conclusion

We studied the climate-growth relationships of *P. yunnanensis* in CHM and predicted the growth of its predominant forest. Both temperature and precipitation affected its growth, and tree growth showed common and site-specific responses to climate change. Moisture conditions in May would be the most critical factor influencing its growth, while June precipitation and current October temperature were other two common factors affecting *P. yunnanensis* growth. Although intense warming of spring and early summer months in the future may exacerbate drought stress on forests, we believe that a high percentage of increased precipitation would offset insufficient water supply induced by warming. According to the results, the radial growth of

P. yunnanensis may increase under future climate conditions in our study area. Further studies on species' drought response mechanism are required and sustainable strategies of forest management should be focused on improving resistance to drought.

Data availability statement

The original contributions presented in the study are included in the article/supplementary material, further inquiries can be directed to the corresponding author.

Conflict of interest

XS was employed by Anji Yinjiang Agriculture Development Co., Ltd.

The remaining authors declare that the research was conducted in the absence of any commercial or financial relationships that could be construed as a potential conflict of interest.

Publisher's note

All claims expressed in this article are solely those of the authors and do not necessarily represent those of their affiliated organizations, or those of the publisher, the editors and the reviewers. Any product that may be evaluated in this article, or claim that may be made by its manufacturer, is not guaranteed or endorsed by the publisher.

References

Aber, J., Neilson, R. P., McNulty, S., Lenihan, J. M., Bachelet, D., and Drapek, R. J. (2001). Forest processes and global environmental change: predicting the effects of individual and multiple stressors. *Bioscience* 51, 735–751. doi: 10.1641/0006-3568(2001)051[0735,FPAGEC]2.0.CO;2

Alley, W. M. (1985). The palmer drought severity index as a measure of hydrological drought. *J. Am. Water Resour. Assoc.* 21, 105–114. doi: 10.1111/j.1752-1688.1985.tb05357.x

Aryal, S., Gaire, N. P., Pokhrel, N. R., Rana, P., Sharma, B., Kharal, D. K., et al. (2020). Spring season in western Nepal Himalaya is not yet warming: a 400-year temperature reconstruction based on tree-ring widths of Himalayan hemlock (*Tsuga dumosa*). *Atmos.* 11:132. doi: 10.3390/atmos11020132

Biondi, F., and Waikul, K. (2004). DENDROCLIM2002: A C++ program for statistical calibration of climate signals in tree-ring chronologies. *Comput. Geosci.* 30, 303–311. doi: 10.1016/j.cageo.2003.11.004

Bohner, T., and Diez, J. (2021). Tree resistance and recovery from drought mediated by multiple abiotic and biotic processes across a large geographic gradient. *Sci. Total Environ.* 789:147744. doi: 10.1016/j.scitotenv.2021.147744

Camarero, J. J., Gazol, A., Sánchez-Salguero, R., Fajardo, A., McIntire, E. J. B., and Liang, E. (2021). Tree growth and treeline responses to temperature: different questions and concepts. *Glob. Chang. Biol.* 27, e13–e14. doi: 10.1111/gcb.15728

Cook, E. R. (1985). *A time series analysis approach to tree ring standardization.* University of Arizona, Tucson, AZ, USA.

Dawadi, B., Liang, E., Tian, L., Devkota, L. P., and Yao, T. (2013). Pre-monsoon precipitation signal in tree rings of timberline Betula utilis in the Central Himalayas. *Quat. Int.* 283, 72–77. doi: 10.1016/j.quaint.2012.05.039

Deng, X. Q., Huang, B. L., Wen, Q. Z., Hua, C. L., Tao, J., and Zheng, J. X. (2014). Dynamic of *Pinus yunnanensis* forest resources in Yunnan. *J. Nat. Resour.* 29, 1411–1419. doi: 10.11849/zrzyxb.2014.08.013

Denmead, O. T., and Shaw, R. H. (1962). Availability of soil water to plants as affected by soil moisture content and meteorological conditions. *Agron. J.* 54, 385–390. doi: 10.2134/agronj1962.00021962005400050005x

Drobyshev, I., Gewehr, S., Berninger, F., and Bergeron, Y. (2013). Species specific growth responses of black spruce and trembling aspen may enhance resilience of boreal forest to climate change. *J. Ecol.* 101, 231–242. doi: 10.1111/1365-2745.12007

Du, Q., Rossi, S., Lu, X., Wang, Y., Zhu, H., Liang, E., et al. (2020). Negative growth responses to temperature of sympatric species converge under warming conditions on the southeastern Tibetan plateau. *Trees* 34, 395–404. doi: 10.1007/s00468-019-01924-4

Dunn, R. J. H., Aldred, F., Gobron, N., Miller, J. B., Willett, K. M., Ades, M., et al. (2022). Global climate. *Bull. Am. Meteorol. Soc.* 103, S11–S142. doi: 10.1175/BAMS-D-22-0092.1

Fan, Z. X., Bräuning, A., and Cao, K. F. (2008). Annual temperature reconstruction in the central Hengduan Mountains, China, as deduced from tree rings. *Dendrochronologia* 26, 97–107. doi: 10.1016/j.dendro.2008.01.003

Fan, Z. X., Bräuning, A., Cao, K. F., and Zhu, S. D. (2009). Growth-climate responses of high-elevation conifers in the central Hengduan Mountains, southwestern China. *For. Ecol. Manag.* 258, 306–313. doi: 10.1016/j.foreco.2009.04.017

Fan, Z. X., Bräuning, A., Fu, P. L., Yang, R. Q., Qi, J. H., Grießinger, J., et al. (2019). Intra-annual radial growth of *Pinus kesiya* var. *langbianensis* is mainly controlled by moisture availability in the Ailao Mountains, southwestern China. *Forests* 10:899. doi: 10.3390/f10100899

Fang, O., Zhang, Q. B., Vitasse, Y., Zweifel, R., and Cherubini, P. (2021). The frequency and severity of past droughts shape the drought sensitivity of juniper trees on the Tibetan plateau. *For. Ecol. Manag.* 486:118968. doi: 10.1016/j.foreco.2021.118968

Fritts, H. C., Blasing, T. J., Hayden, B. P., and Kutzbach, J. E. (1971). Multivariate techniques for specifying tree-growth and climate relationships and for reconstructing anomalies in paleoclimate. *J. Appl. Meteorol.* 10, 845–864. doi: 10.1175/1520-0450(1971)010<0845:MTFSTG>2.0.CO;2

Fritts, H. C., Smith, D. G., Cardis, J. W., and Budelsky, C. A. (1965). Tree-ring characteristics along a vegetation gradient in northern Arizona. *Ecology* 46, 393–401. doi: 10.2307/1934872

Fu, L. G., Li, N., and Robert, R. M. (1999). "Pinus" in *Flora of China*. eds. Z. Y. Wu and P. H. Raven (Beijing: Science Press), 11–25.

Girardin, M. P., Tardif, J., Flannigan, M. D., and Bergeron, Y. (2004). Multicentury reconstruction of the Canadian drought code from eastern Canada and its relationship with paleoclimatic indices of atmospheric circulation. *Clim. Dyn.* 23, 99–115. doi: 10.1007/s00382-004-0417-x

Gričar, J., Zupančič, M., Čufar, K., and Primož, O. (2007). Regular cambial activity and xylem and phloem formation in locally heated and cooled stem portions of Norway spruce. *Wood Sci. Technol.* 41, 463–475. doi: 10.1007/s00226-006-0109-2

Guo, L. N., He, Z. J., Long, X. Z., Wang, J. Z., Wang, L. D., and Li, C. X. (2009). Genetic characteristics and taxonomy of soil in the Yulong Snow Mountain. *J. South. Agric.* 40, 1177–1183.

Guo, G., Li, Z. S., Zhang, Q. B., Ma, K. P., and Mu, C. (2009). Dendroclimatological studies of *Picea Likiangensis* and *Tsuga Dumosa* in Lijiang, China. *IAWA J.* 30, 435–441. doi: 10.1163/22941932-90000230

Harris, I., Osborn, T. J., Jones, P., and Lister, D. (2020). Version 4 of the CRU TS monthly high-resolution gridded multivariate climate dataset. *Sci. Data* 7:109. doi: 10.1038/s41597-020-0453-3

He, M., Yang, B., Bräuning, A., Rossi, S., Ljungqvist, F. C., Shishov, V., et al. (2019). Recent advances in dendroclimatology in China. *Earth Sci. Rev.* 194, 521–535. doi: 10.1016/j.earscirev.2019.02.012

Holmes, R. L. (1983). Computer-assisted quality control in tree-ring dating and measurement. *Tree-Ring Bull.* 43, 69–78.

Huang, J., Tardif, J. C., Bergeron, Y., Denneler, B., Berninger, F., and Girardin, M. P. (2010). Radial growth response of four dominant boreal tree species to climate along a latitudinal gradient in the eastern Canadian boreal forest. *Glob. Chang. Biol.* 16, 711–731. doi: 10.1111/j.1365-2486.2009.01990.x

IPCC (2021). "Summary for Policymakers" in *Climate Change 2021: The Physical Science Basis. Contribution of Working Group I to the Sixth Assessment Report of the Intergovernmental Panel on Climate Change.* eds. V. Masson-Delmotte, P. Zhai, A. Pirani, S. L. Connors, C. Péan and S. Berger et al. (Cambridge, United Kingdom and New York, NY, USA: Cambridge University Press), 3–32.

Kharal, D. K., Thapa, U. K., George, S. S., Meilby, H., Rayamajhi, S., and Bhuju, D. R. (2017). Tree-climate relations along an elevational transect in Manang Valley, Central Nepal. *Dendrochronologia* 41, 57–64. doi: 10.1016/j.dendro.2016.04.004

Legendre, P., and Legendre, L. (1998). *Numerical ecology*. New York: Elsevier.

Li, Z., Shi, C., Liu, Y., Zhang, J., and Ma, K. (2011). Winter drought variations based on tree-ring data in Gaoligong Mountain, northwestern Yunnan, China, A. D. 1795-2004. *Pak. J. Bot.* 43, 2469–2478.

Li, Z. S., Zhang, Q. B., and Ma, K. (2012). Tree-ring reconstruction of summer temperature for A.D. 1475-2003 in the central Hengduan Mountains, northwestern Yunnan, China. *Clim. Chang.* 110, 455–467. doi: 10.1007/s10584-011-0111-z

Liang, E., Dawadi, B., Pederson, N., and Eckstein, D. (2014). Is the growth of birch at the upper timberline in the Himalayas limited by moisture or by temperature? *Ecology* 95, 2453–2465. doi: 10.1890/13-1904.1

Liang, E., Wang, Y., Xu, Y., Liu, B., and Shao, X. (2010). Growth variation in *Abies georgei* var. *smithii* along altitudinal gradients in the Sygera Mountains, southeastern Tibetan plateau. *Trees* 24, 363–373. doi: 10.1007/s00468-009-0406-0

Martínez-Vilalta, J., López, B. C., Adell, N., Badiella, L., and Ninyerola, M. (2008). Twentieth century increase of Scots pine radial growth in NE Spain shows strong climate interactions: recent changes in scots pine radial growth. *Glob. Chang. Biol.* 14, 2868–2881. doi: 10.1111/j.1365-2486.2008.01685.x

Morzuch, B. J., and Ruark, G. A. (1991). Principal components regression to mitigate the effects of multicollinearity. *For. Sci.* 37, 191–199. doi: 10.1093/forestscience/37.1.191

Panthi, S., Bräuning, A., Zhou, Z. K., and Fan, Z. X. (2018). Growth response of *Abies georgei* to climate increases with elevation in the central Hengduan Mountains, southwestern China. *Dendrochronologia* 47, 1–9. doi: 10.1016/j.dendro.2017.11.001

Rossi, S., Anfodillo, T., Čufar, K., Cuny, H. E., Deslauriers, A., Fonti, P., et al. (2016). Pattern of xylem phenology in conifers of cold ecosystems at the northern hemisphere. *Glob. Change Biol. Bioenergy.* 22, 3804–3813. doi: 10.1111/gcb.13317

Schnabel, F., Purrucker, S., Schmitt, L., Engelmann, R. A., Kahl, A., Richter, R., et al. (2022). Cumulative growth and stress responses to the 2018-2019 drought in a European floodplain forest. *Glob. Chang. Biol.* 28, 1870–1883. doi: 10.1111/gcb.16028

Shen, J. Y., Li, Z. S., Gao, C. J., Li, S. F., Huang, X. B., Lang, X. D., et al. (2020). Radial growth response of *Pinus yunnanensis* to rising temperature and drought stress on the Yunnan plateau, southwestern China. *For. Ecol. Manag.* 474:118357. doi: 10.1016/j.foreco.2020.118357

Su, H., and Wang, P. (2020). Vertical differentiation of soil organic matter in Haba Snow Mountain nature reserve. *Yunnan Geogr. Environ. Res.* 32, 65–76.

Su, X. C., Wang, L., Li, Q. L., and Teng, C. (2014). Study of surface dry and wet conditions in Southwest China in recent 50 years. *J. Nat. Resour.* 29, 104–116.

Sun, L., Cai, Y., Zhou, Y., Shi, S., Zhao, Y., Gunnarson, B. E., et al. (2020). Radial growth responses to climate of *Pinus yunnanensis* at low elevations of the Hengduan Mountains, China. *Forests* 11:1066. doi: 10.3390/f11101066

Sun, M., Li, J., and Zhang, Y. (2021). Climate-growth relations of *Abies georgei* along an altitudinal gradient in Haba Snow Mountain, southwestern China. *Forests* 12:1569. doi: 10.3390/f12111569

ter Braak, C. J. F. (1994). Canonical community ordination. Part I: basic theory and linear methods. *Écoscience* 1, 127–140. doi: 10.1080/11956860.1994.11682237

Van Passel, J., De Keersmaecker, W., Bernardino, P. N., Jing, X., Umlauf, N., Van Meerbeek, K., et al. (2022). Climatic legacy effects on the drought response of the Amazon rainforest. *Glob. Chang. Biol.* 28, 5808–5819. doi: 10.1111/gcb.16336

Wang, Y., Zhang, Y., Fang, O., and Shao, X. (2018). Long-term changes in the tree radial growth and intrinsic water-use efficiency of Chuanxi spruce (*Picea likiangensis*

var. *balfouriana*) in southwestern China. *J. Geog. Sci.* 28, 833–844. doi: 10.1007/s11442-018-1508-7

Xu, Y. L., Huang, X. Y., Zhang, Y., Lin, W. T., and Lin, E. D. (2005). Statistical analyses of climate change scenarios over China in the 21st century. *Adv. Clim. Chang. Res.* 1, 80–97.

Yang, R. Q., Fan, Z. X., Li, Z. S., and Wen, Q. Z. (2018). Radial growth of *Pinus yunnanensis* at different elevations and their responses to climatic factors in the Yulong Snow Mountain, Northwest Yunnan, China. *Acta Ecol. Sin.* 38, 8983–8991. doi: 10.5846/stxb201805311214

Yang, R. Q., Fu, P. L., Fan, Z. X., Panthi, S., Gao, J., Niu, Y., et al. (2022). Growth-climate sensitivity of two pine species shows species-specific changes along temperature and moisture gradients in Southwest China. *Agric. For. Meteorol.* 318:108907. doi: 10.1016/j.agrformet.2022.108907

Yin, D. C., Xu, D., Tian, K., Xiao, D., Zhang, W., Sun, D., et al. (2018). Radial growth response of *Abies georgei* to climate at the upper timberlines in central Hengduan Mountains, southwestern China. *Forests* 9:606. doi: 10.3390/f9100606

Young, D. J. N., Stevens, J. T., Earles, J. M., Moore, J., Ellis, A., Jirka, A. L., et al. (2017). Long-term climate and competition explain forest mortality patterns under extreme drought. *Ecol. Lett.* 20, 78–86. doi: 10.1111/ele.12711

Yu, J., Liu, Q., Meng, S., Zhou, G., Shah, S., and Xu, Z. (2018). Summer temperature variability inferred from tree-ring records in the central Hengduan Mountains, southeastern Tibetan plateau. *Dendrochronologia* 51, 92–100. doi: 10.1016/j.dendro.2018.08.004

Yue, W., Zhao, X., Chen, F., Khan, A., and Gao, Z. (2022). Reconstructed precipitation in the Lohit River basin, southern Tibetan plateau since 1720 CE and its weak linkages with monsoon-season Brahmaputra discharge. *Int. J. Climatol.* 42, 3793–3808. doi: 10.1002/joc.7445

Zhang, Y., Cao, R. J., Yin, J., Tian, K., Xiao, D. R., Zhang, W. G., et al. (2020). Radial growth response of major conifers to climate change on Haba Snow Mountain, southwestern China. *Dendrochronologia* 60:125682. doi: 10.1016/j.dendro.2020.125682

Zhang, Y., Yin, D. C., Sun, M., Wang, H., Tian, K., Xiao, D. R., et al. (2017). Variations of climate-growth response of major conifers at upper distributional limits in Shika Snow Mountain, northwestern Yunnan plateau, China. *Forests* 8:377. doi: 10.3390/f8100377

Zhang, Y., Yin, D. C., Tian, K., Zhang, W. G., He, R. H., He, W. Q., et al. (2018). Radial growth responses of *Picea likiangensis* to climate variabilities at different altitudes in Yulong Snow Mountain, Southwest China. *Chin. J. Plant Ecol.* 42, 629–639. doi: 10.17521/cjpe.2018.0003

Patterns and drivers of tree species diversity in a coniferous forest of northwest China

Wendong Wang[1], Jingjing Zhao[2]*, Baojiang Zhang[3], Gang Deng[3], Alimu Maimaiti[1] and Zhongjun Guo[1]

[1]Institute of Forest Ecology, Xinjiang Academy of Forestry, Urumqi, China, [2]School of Ecology, Sun Yat-sen University, Shenzhen, China, [3]Management Committee of Kanas State-level Nature Reserve, Altay, China

Introduction: Understanding the pattern of species diversity and underlying ecological determinants driving a forest ecosystem is fundamental to conservation biology and forest management. Boreal forests play an irreplaceable role in providing ecosystem services and maintaining the carbon cycle globally, yet research attention remains disproportionately limited and lacking throughout time.

Methods: Based on field measurement data from a large (25 ha) fully-mapped coniferous forest plot, the present study quantified patterns of species diversity and their determinants in Kanas of Xinjiang, northwest China. We applied linear regression analysis to test the effects of biotic and soil factors on alpha-diversity and local contribution of beta diversity (LCBD), and then we adopted path analysis to test the determinants that affected the species diversity index.

Results and discussion: Our results revealed that alpha-diversity indices did not vary greatly across different subplots, and richness value (between 2 and 6) was low in Kanas. Noteworthy is the discerned negative association between the average diameter at breast height (DBH) and species richness, suggesting that areas with smaller DBH values tend to harbor greater species richness. For beta-diversity, a higher value was observed in the substory layer (0.221) compared to both the canopy layer (0.161) and the understory layer (0.158). We also found that the species abundance distance matrix of biological and soil environmental factors were significantly correlated with species geographic distance matrices. More importantly, our results showed that average DBH and soil pH would affect the alpha diversity indices, and average DBH, soil Ph, average height and soil total Phosphorous would affect the beta diversity indices. Soil pH also indirectly affected the LCBDunder, LCBDsub, and LCBDcan ($p \leq 0.001$), upon mediation of alpha diversity indices. Overall, our results provide crucial revelations about species diversity patterns in boreal forests, and insights that can support the protection of forest biodiversity in China.

1 Introduction

Seeking explanation on mechanisms of species coexistence, which determine the spatial patterns of species and dynamics of communities of a forest ecosystem (Shaheen et al., 2023; Haq et al., 2023c), has been a longtime endeavor within community ecology research (Whittaker, 1960). Although several studies have sought to explain species coexistence and

community structure (Gravel et al., 2011; Levine et al., 2017), and the relationships between biodiversity and ecosystem functioning, it is still a great challenge to interpret how biotic and abiotic factors affect plant diversity functions (Sanaei et al., 2021). These factors are not exclusively influential but rather mutually correlated, rendering it challenging to discern the specific role of each in shaping community structure (Pyšek et al., 2005; He et al., 2022). Hence, a detailed study on the relationship between forest species diversity and environmental factors is vital to shed light on key influential factors and underlying ecological mechanisms (He et al., 2022).

Species diversity remains one of the central topics in contemporary ecology and the subject of various studies, from community to landscape-level, and in all types of ecosystems (Pyšek et al., 2005; Bhat et al., 2020; Legesse and Negash, 2021; Thakur et al., 2022; Haq et al., 2023a). Understanding the patterns and determinants of species diversity in forest ecosystems are fundamental to our knowledge of ecological processes, biological conservation and forest management (Socolar et al., 2016; Haq et al., 2023b). In the 1960s, an ecologist proposed three scales to measure biological diversity - alpha-diversity, beta-diversity, and gamma-diversity (Whittaker, 1972). Alpha (α) diversity mainly explores species diversity within a community, while beta (β) diversity focuses on species diversity between communities (Socolar et al., 2016; He et al., 2022). Both alpha-diversity and beta-diversity are crucial for understanding what species are composited and how biotic communities are structured (Socolar et al., 2016). Importantly, as a supplement to species richness, understanding the pattern of beta-diversity in different communities plays an important role in guiding conservation strategies, and determining priorities for regional conservation (Bergamin et al., 2017; He et al., 2020). However, most current research only recognizes patterns of alpha-diversity (Pyšek et al., 2005; Bhat et al., 2020), whereas those of beta-diversity has often been overlooked.

In a forest ecosystem, the plant compartment is composed of canopy, substory and understory strata, which are hierarchically structured (Barrufol et al., 2013; Haq et al., 2022; Basham et al., 2023). It is generally well-known that canopy strata can shape the function and structure of understory strata by regulating available resources, including light and nutrients (Barrufol et al., 2013; Araujo et al., 2020). Although exploring the complex the vertical structure in a stable forest community is crucial, especially when linked to the partitioning of beta-diversity, the studies mostly overlooked the variations in the vertical structure (Mori et al., 2013).

It has also been widely reported that interactions between plants and environmental conditions are regulating community spatial patterns of various vegetation types in different climatic regions (Sanaei et al., 2021). Localized environmental conditions may further affect tree growth and distribution, which may determine resource availability for plant growth and survival (Barrufol et al., 2013; Lu et al., 2021). For example, nitrogen is considered as the key nutrient for plant survival and growth in terrestrial ecosystems, particularly in cold temperate soil (Liu et al., 2021; Chang et al., 2022; Chen et al., 2022). Additionally, some studies found that soil pH can directly or indirectly impact plant species diversity and community composition (Ste-Marie and Pareâ, 1999; Ouyang et al., 2022). In summary, changes in soil properties caused by plants would definitely improve the availability of nutrient, thereby affecting plant diversity and performance (Pyšek et al., 2005; Sanaei et al., 2021). Furthermore, some studies have identified topographic variables as key explanatory factors for species richness, highlighting the significance of site-specific habitat factors in driving spatial variation in species richness at the local scale (Irl et al., 2015; Zellweger et al., 2015). Yet the process of how soil factors affect plant growth and community construction is still unclear.

Although some ecologists have studied species diversity and its determinants, most of these were carried out in subtropical and tropical forests (Phillips et al., 1994; Japan et al., 2004; Hill et al., 2011). Despite boreal forests accounting for 11% of the total forested area, and thus represents the largest vegetation type around the world (Gauthier et al., 2015), research on boreal forests remain sparse. It is therefore crucial to study existing patterns of species diversity and its drivers, to help us better understand community assemblies and diversity maintenance under current global environmental changes (Liu et al., 2021). In Kanas, forests are commonly dominated by diverse species, which differ from other forests in central North Asia that are dominated by a single canopy (Liu et al., 2021). Yet the interaction between the plant species and environment in kanas forest is still unclear.

In this study, we aim to explore the potential factors influencing species diversity through the perspective of vertical stratification within forest community. Specifically, we first collected data-relevant variables from a 25-ha permanent forest plot in the Kanas National Nature Reserve (KNNR) within the Xinjiang Uygur Autonomous Region in Northwest China, calculated the alpha-diversity and beta-diversity, and partitioned the local contributions to beta diversity (LCBD). We then tested the linkages between LCBD and environment factor by regressing on related explanatory variables. Our study aims to answer the next four questions: (a) what are the alpha-diversity and beta-diversity patterns of the boreal coniferous forest in KNNR; (b) what is the relationship between environmental variables and plant diversity; (c) do environmental factors affect the alpha-diversity and beta-diversity patterns; and (d) how do soil environmental variables, topographic variables, biological variables and plant diversity indices interact with each other? what is the specific impact path process? By studying the potential impact factors of species diversity from the aspect of vertical stratification of forest communities, this study may present novelty in revealing the mechanism of forest biodiversity conservation and species coexistence.

2 Materials and methods

2.1 Study area

The study area is located in the middle of Altai Mountain (48° 35′-49° 11′ N, 86° 54′-87° 54′ E) at KNNR (Figure 1), which has a temperate continental climate, with temperature extremes between summer and winter. The temperature ranges from −37°C to 29.3°C with an annual average at −0.2°C, and mean annual precipitation at about 1,000 mm. Elevation within the KNNR ranges from 1,241 m to 4,381 m. The Forest cover in the Altai mountains of China is considered typical of boreal forests found regionally, with coverage dominated by over four plant species, including *Larix sibirica* Ledeb., Picea obovata Ledeb., *Pinus sibirica* (Loud.) Mayr, and *Betula pendula* (Loud.) Mayr (Liu et al., 2020).
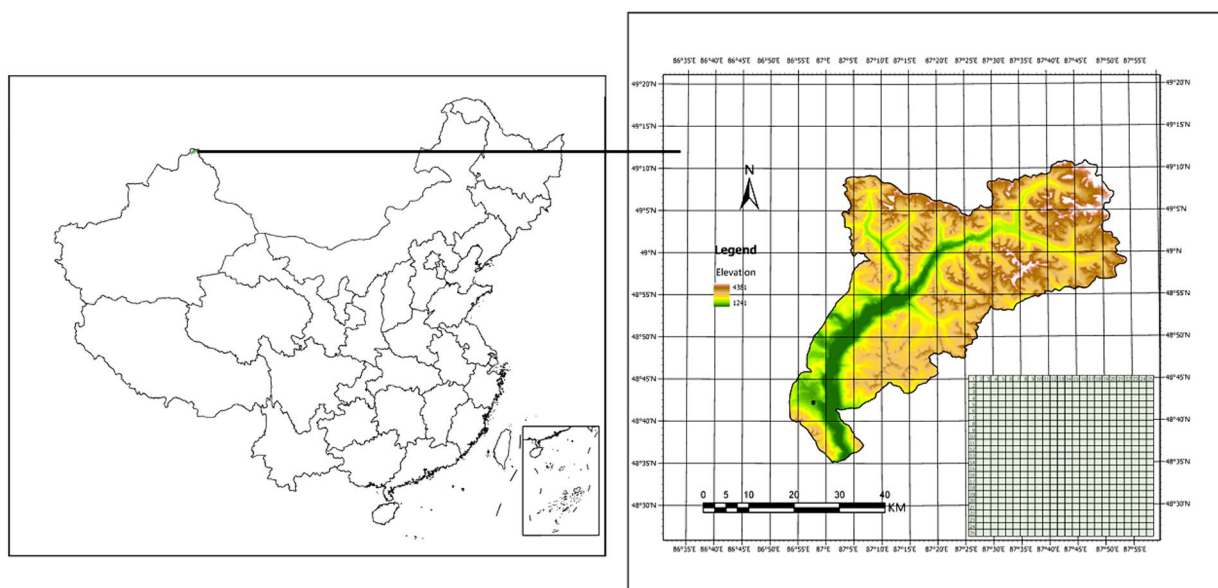
FIGURE 1
The location and Digital elevation map (DEM) of the study area in the Altay Mountains, north-west China.
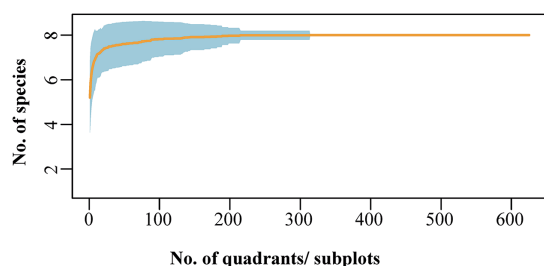

FIGURE 2
Species−area curve for woody plants in KNNR 25 ha forest dynamics plot.

2.2 Data collection

In the summer of 2019 and 2020, we collected data from a 25 ha (500 m*500 m) permanent forest plot, established in a coniferous forest of northwest China. We inventoried the plants in our study area according to the standard field protocol of the Center for Tropic Forest Sciences (CTFS; Condit 1998). Marking the southwest corner as the origin of the coordinates, the 25-ha plot was divided into 625 subplots at 20 m*20 m, and each subplot was then subdivided into 16 quadrats at 5 m*5 m. Within each quadrat, we recorded all living species with a diameter at breast height (DBH) ≥ 1 cm (Bagchi et al., 2011).

After removing litter and stones, the top soil (0–15 cm) of these plant species was taken to laboratory and soil characteristics were analyzed. We also measured nine soil environmental factors, which included soil pH value, bulk density, alkaline hydrolysable nitrogen (AHN), soil organic carbon (SOC), total nitrogen (N), total phosphorus (P), C:N ratio, C:P ratio and N:P ratio for each subplot. Soils were sampled both at the center and at the four quadrat corners

(Bao, 2000). For each soil property, the mean of all five samples (center and four corners) was calculated. We also calculated four topographic traits for each subplot, including aspect, convexity, elevation and slope (He et al., 2022).

Within the plot at KNNR, the number of species increased rapidly during initial stages when the sampling area was small, and gradually plateaued with further increase in sampling area (Figure 2). This indicated that the 625 subplot is sufficient to explain the species composition in KNNR.

In total, we recorded 28,321 plant individuals for analysis. Based on the 10 cm DBH intervals, the forest vertical stratum was divided into three categories, the understory layer (0-10 cm), substory layer (10-20 cm) and canopy layer (>20 cm) (He et al., 2022).

2.3 Measures of alpha-diversity and beta-diversity

We calculated four alpha-diversity indices in each of the 625 subplots across the KNNR forest plot, including species Richness, Shannon entropy, Simpson index and Pielou evenness indices. The alpha-diversity indices calculations were conducted using the 'vegan' R package in R 4.0.3 software (Oksanen et al., 2018). The species 330 richness is the total count of species types within a subplot, while the 331 specific calculations for the other three alpha-diversity indices are as follows (Eqs. 1–3):

$$Shannon\ entropy = -\sum_{i=1}^{S} P_i \log(P_i) \qquad (1)$$

where N_i represents the abundance of species i, and N_0 is the sum of the individual number of all species.

$$Simpson\ index = 1 - \sum_{i=1}^{S} P_i^2 \qquad (2)$$

$$Pielou\ evenness = H\ /\ logS \qquad (3)$$

On beta diversity, as the total variance of the Hellinger-transformed community composition, the beta-diversity statistic (BDTotal) was calculated (Eq. 4). We than partitioned Beta-diversity into Local Contribution to Beta Diversity (LCBD, Eq. 5). The beta-diversity calculation was performed using the 'adespatial' R package in R 4.0.3 software (Dray et al., 2012).

$$BD_{Total} = Var\left(Y_{Hel}\right) = {SS_{Total}}\Big/{\left(n-1\right)} \qquad (4)$$

where SS_{Total} refers to the total sum of the squared deviations from the column means of the whole Y_{Hel} matrix, and BD_{Total} represents the unbiased form of the total variance.

$$LCBD_i = LCBD_i = SS_i\ /\ SS_{Total} \qquad (5)$$

where SS_i represents the sum of squares corresponding to the i_{th} subplot (i.e., the contribution of subplot i to the overall beta-diversity). $LCBD_i$ is the reflection of the degree of the compositional uniqueness of the subplots which can be compared with each other.

2.4 Data analysis

We first adopted the mantel test to identify whether there a relationship between species diversity indics and environmental factors. Mantel test was carried out using the 'LinkET' R package in R 4.0.3 software (Huang, 2021).

We used general linear models (LM) to analyse how soil environment factors affected the species diversity indices. We identified Richness index (model 1), Shannon index (model 2), Simpson index (model 3), Pielou evenness index (model 4), $LCBD_{layer}$ (model 5), $LCBD_{und}$ (model 6), $LCBD_{sub}$ (model 7) and $LCBD_{can}$ (model 8) as response variables. In order to assess multicollinearity among the predictor variables in the model, we conducted VIF (Variance Inflation Factor) tests using the 'car' package in R (Fox and Weisberg, 2019). The results indicated that all VIF values were below 10, suggesting the absence of severe multicollinearity issues within the model. The model selection process produced 33 and 40 top-ranked models (ΔAIC≤2), respectively, which we averaged into a final model. Model selection was performed using the 'MuMIn' R package (Barto, 2023), whereas the LM analysis was conducted using the 'lme4' R package in R 4.0.3 software (Bates, 2005).

Furthermore, we used path analysis to explore influences from the constructs of the species diversity. We selected significant variables from the LM models, and subsequently tested for relationships between biological variables, soil environmental variables, alpha diversity indices and LCBD. Path analyses were carried out using the 'Lavvan' R package in R 4.0.3 software (Rosseel, 2012).

3 Results

3.1 The patterns of alpha-diversity and beta-diversity

A total of 28,321 woody individuals, representing 4 families, 7 genera, and 7 species, were recorded and analyzed in this study. We mapped the spatial distributions of the alpha-diversity value for each subplot (Figure 3). The range of species richness for each subplot varied between 2 and 6 with a coefficient of variation (CV) at 19.42%, whereas the range of the exponential of Shannon entropy for each subplot varied from 0.229 to 2.152 (CV = 19.18%). The average Simpson and Pielou value for each subplot was 0.604 and 0.779, respectively, (CV = 17.92) (Figure 3).

Our results showed that there were higher values for species composition in the substory layer than the other two forest layers, which corresponded to the observed higher beta-diversity value in the substory layer (0.221) relative to the canopy (0.161) and understory layers (0.158) (Table 1). We found the highest beta-diversity value for the substory layer, which reflected the greatest compositional dissimilarities between its sampled subplots.

LCBD measures the contribution of local environmental factors to beta diversity, indicating how much species composition differs between neighboring locations within the forest. In our result, we observed the highly predictable pattern of LCBD value. The value of LCBD among three layers were different across the three forest vertical strata, with an average value of $1.77*10^{-3}$ in the understory layer, $1.60*10^{-3}$ in the substory layer, and $1.76*10^{-3}$ in the canopy layer (Figure 4). This highlighted variations in local environmental conditions and species composition across these strata.

3.2 Relationship between species diversity indices and soil environmental variables

We used the Mantel test to explore the relationship between species diversity indices values and soil environmental factors. The test results showed that the distance matrix on alpha-diversity and beta-diversity in the community had a significant positive correlation with the distance matrix of soil pH, soil SOC, total N, AHN, N:P and C:P ($p < 0.001$), and also a significant positive correlation between average DBH and average height of tree plants ($p < 0.001$; Figure 5). In addition, total N, C:N ratio, aspect, convexity, elevation, and slope showed no significant correlation with biodiversity indices. Specifically, soil pH, SOC, total N, AHN, N:P ratio, and C:P ratio were significantly positively correlated with species Richness, Shannon, Simpson, and Pielou indices, while they were significantly negatively correlated with LCBD, $LCBD_{und}$ and $LCBD_{sub}$; The average DBH were significantly positively correlated with species richness, while they were significantly negatively correlated with $LCBD_{und}$.

3.3 Effects of soil environmental variables on species diversity indices

We used LM to further explore whether the soil feature and plant biological factors would directly affect the alpha-diversity indices and LCBD value (Figure 6; Tables 2, 3). Our results showed that average
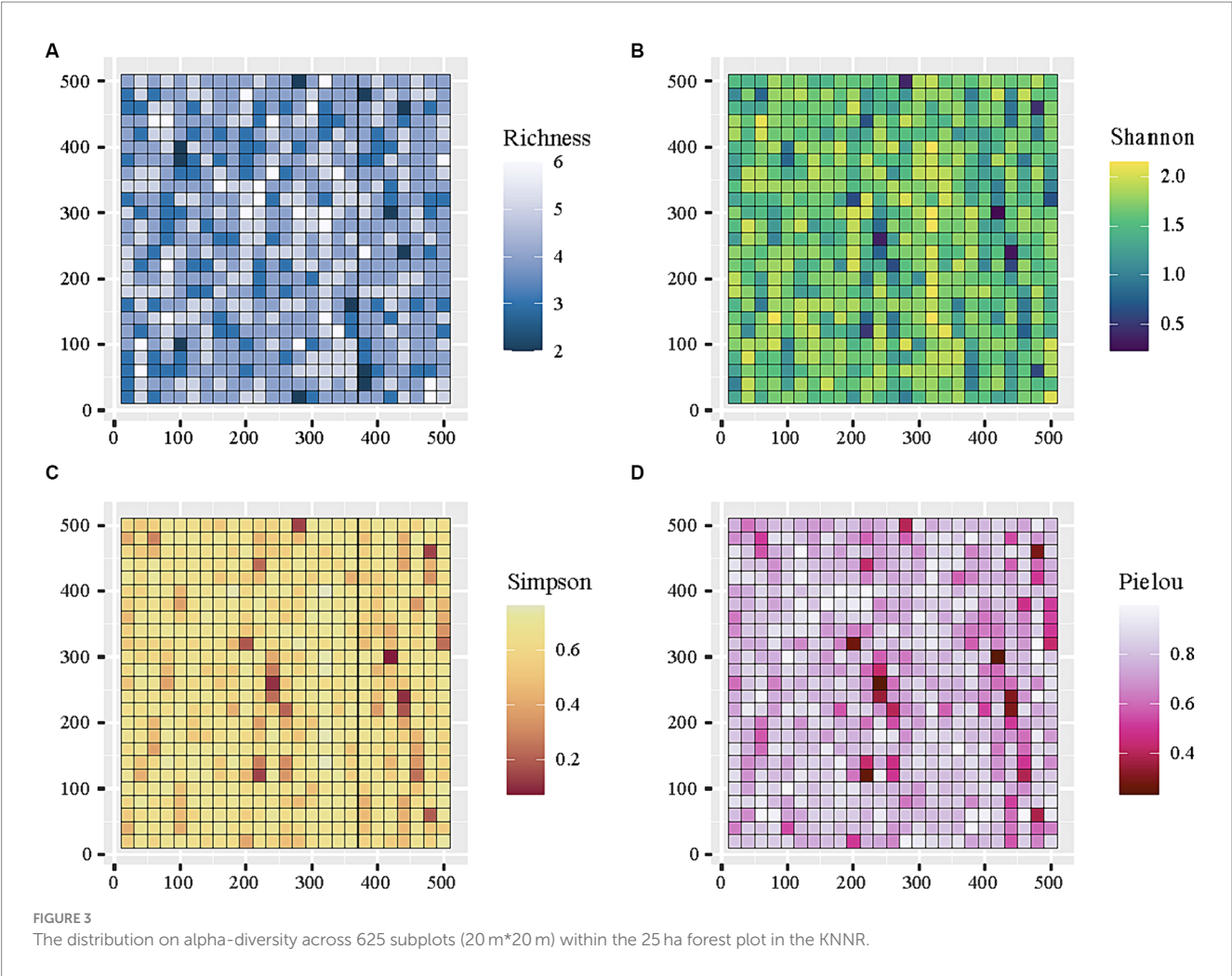
FIGURE 3
The distribution on alpha-diversity across 625 subplots (20 m*20 m) within the 25 ha forest plot in the KNNR.

TABLE 1 The statistical results of beta diversity in a coniferous forest of northwest China.

	Size range	Species	Individuals	Beta-diversity
Understory layer	DBH ≤ 10 cm	7	10,804	0.158
Substory layer	10 cm < DBH ≤ 20 cm	7	10,292	0.221
Canopy layer	DBH > 20 cm	6	7,225	0.161
Layer		7	28,321	0.247

DBH had significant positive impact on the Pielou index, and significant negative impact on the Richness (Figure 6A). Particularly, soil pH values had significant negative impacts on the Shannon, Simpson and Pielou indices values, and soil N:P had significant negative impacts on the Simpson index (Figure 6A). Regarding local contribution to beta-diversity, the average DBH, average height, soil pH, soil total N and soil total p values were found to affect LCBD values (Figure 6B). Specifically, the $LCBD_{und}$ was significantly positively impacted by average height and soil pH. $LCBD_{sub}$ was significantly positively impacted by average DBH, whereas $LCBD_{can}$ was significantly negatively impacted by average DBH, total N and soil total P (Figure 6B). Our results indicated that topographic variables (aspect, convexity, elevation and slope) and soil factors including SOC, AHN, C:N and C:P did not show any significant influence on the alpha and beta indices.

3.4 Determinants of the local contribution to beta diversity

We used path analysis to test the determinants that affected the species diversity index. Our path analyses showed that soil pH and N:P ratio had positive direct and indirect effects on the alpha-diversity indices and LCBD ($p \leq 0.001$; Figure 7A). Specifically, N:P ratio and pH influenced Richness and Pielou indices by affecting average DBH, ultimately impacting LCBD (Figure 7A). PH directly affected the LCBD, mediating by the Simpson index (Figure 7A).

For $LCBD_{und}$, N:P ratio and pH influence Richness and Pielou indices by affecting average DBH, ultimately impacting $LCBD_{und}$. Average height directly affected $LCBD_{und}$ (Figure 7B). For $LCBD_{sub,}$ pH indirectly affected the $LCBD_{sub}$, mediating by Shannon, Simpson and
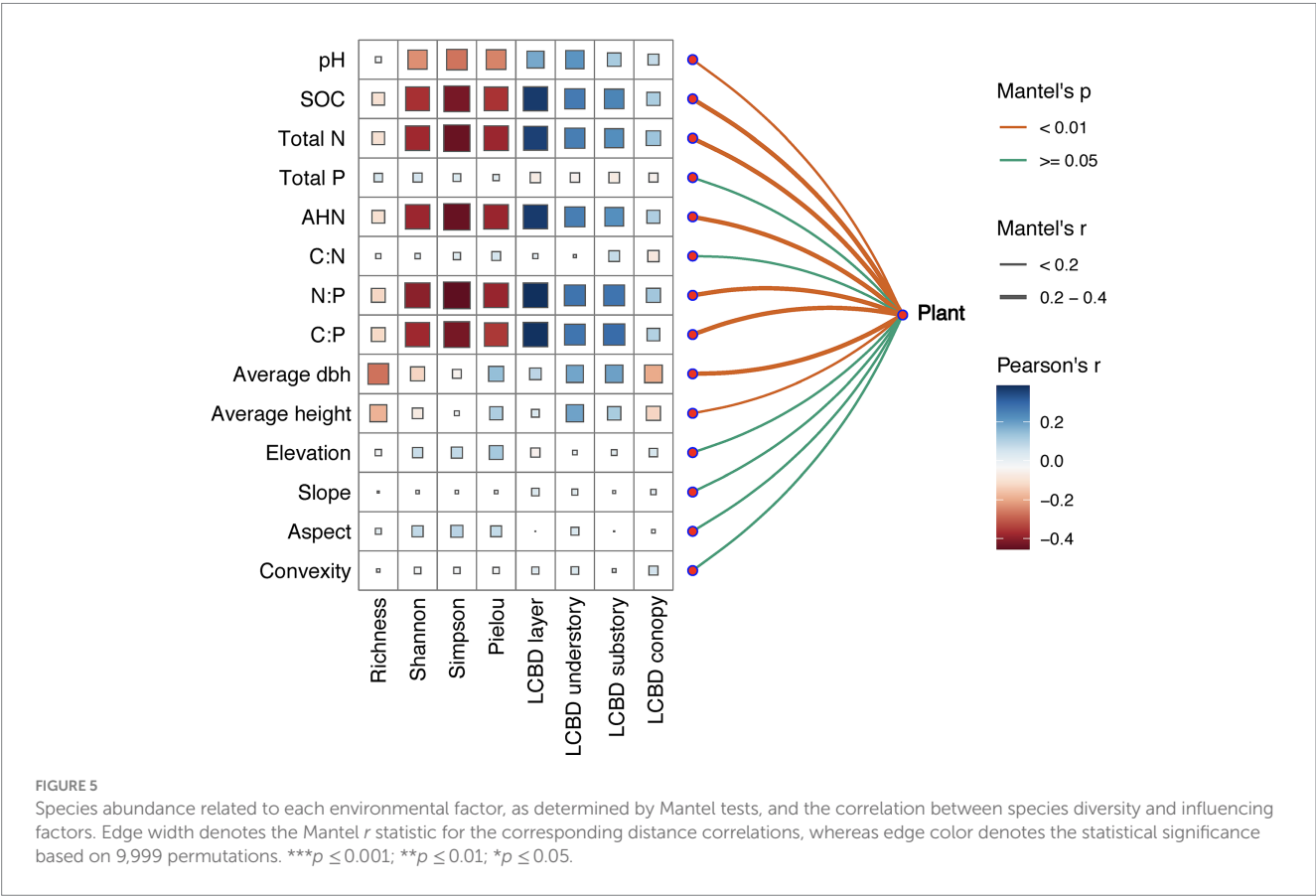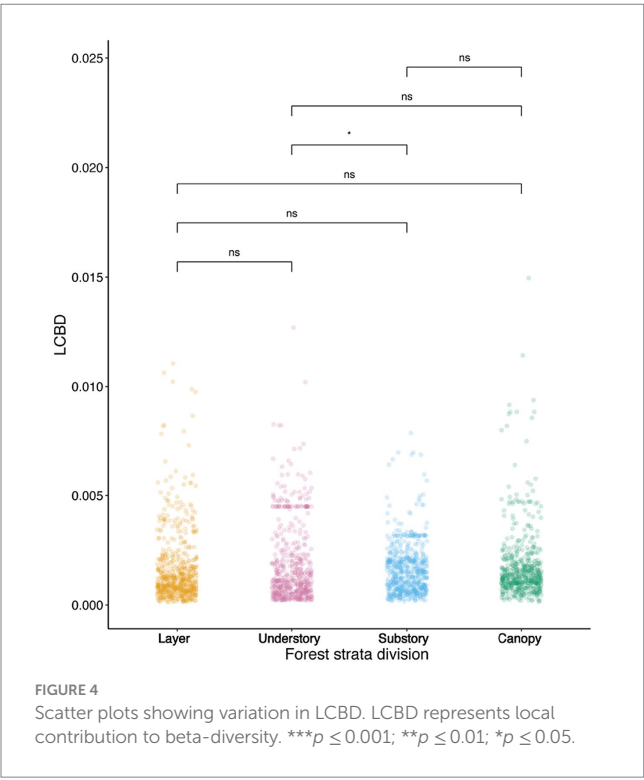
Pielou indices. While N:P ratio indirectly influenced LCBD$_{sub}$ through the effect of the Pielou index (Figure 7C). LCBD$_{can}$ was directly influenced by total P, while total P, total N, N:P ratio and pH also indirectly influenced Richness, Shannon, Simpson Pielou and LCBD$_{can}$ through average DBH (Figure 7D).

4 Discussion

Our results demonstrated that the species distance matric of biological factors and soil environmental factors were significantly correlated with species geographic distance matrices (Figure 5), suggesting that the tree species community in KNNR diverges with environmental conditions and biological features. Previous studies have shown that the colonization and extinction processes of forest communities are mainly determined by environmental heterogeneity and species competition (Lu et al., 2021; He et al., 2022; Thakur et al., 2022). Due to the different sensitivities from species to environmental changes, threatened species are prone to disappearing in habitats with high environmental pressure by selective extinction (Socolar et al., 2016; Legesse and Negash, 2021). In that case, if a species has high tolerance to environmental changes, it can survive in vary habitats (Xie et al., 2019; Liu et al., 2020; He et al., 2022). For the dominant species of Kanas, they show excellent resilience and adaptability to environmental changes. These species can withstand fluctuations in temperature, precipitation and soil conditions, their ability to tolerate a wide range of environmental conditions allows them to occupy various niches and outcompete other species (Liu et al., 2020, 2021).

This study found that among the 625 sub-plots, the highest value of species richness was only 6, and the lowest value was only 2 (Figure 3A), indicating that the species richness in the forest

FIGURE 4
Scatter plots showing variation in LCBD. LCBD represents local contribution to beta-diversity. ***$p \leq 0.001$; **$p \leq 0.01$; *$p \leq 0.05$.

FIGURE 5
Species abundance related to each environmental factor, as determined by Mantel tests, and the correlation between species diversity and influencing factors. Edge width denotes the Mantel r statistic for the corresponding distance correlations, whereas edge color denotes the statistical significance based on 9,999 permutations. ***$p \leq 0.001$; **$p \leq 0.01$; *$p \leq 0.05$.

FIGURE 6
Summary of LM averaged model estimates for **(A)** alpha-diversity and **(B)** beta-diversity values, under different forest strata (N = 625). ***p ≤ 0.001; **p ≤ 0.01; *p ≤ 0.05.

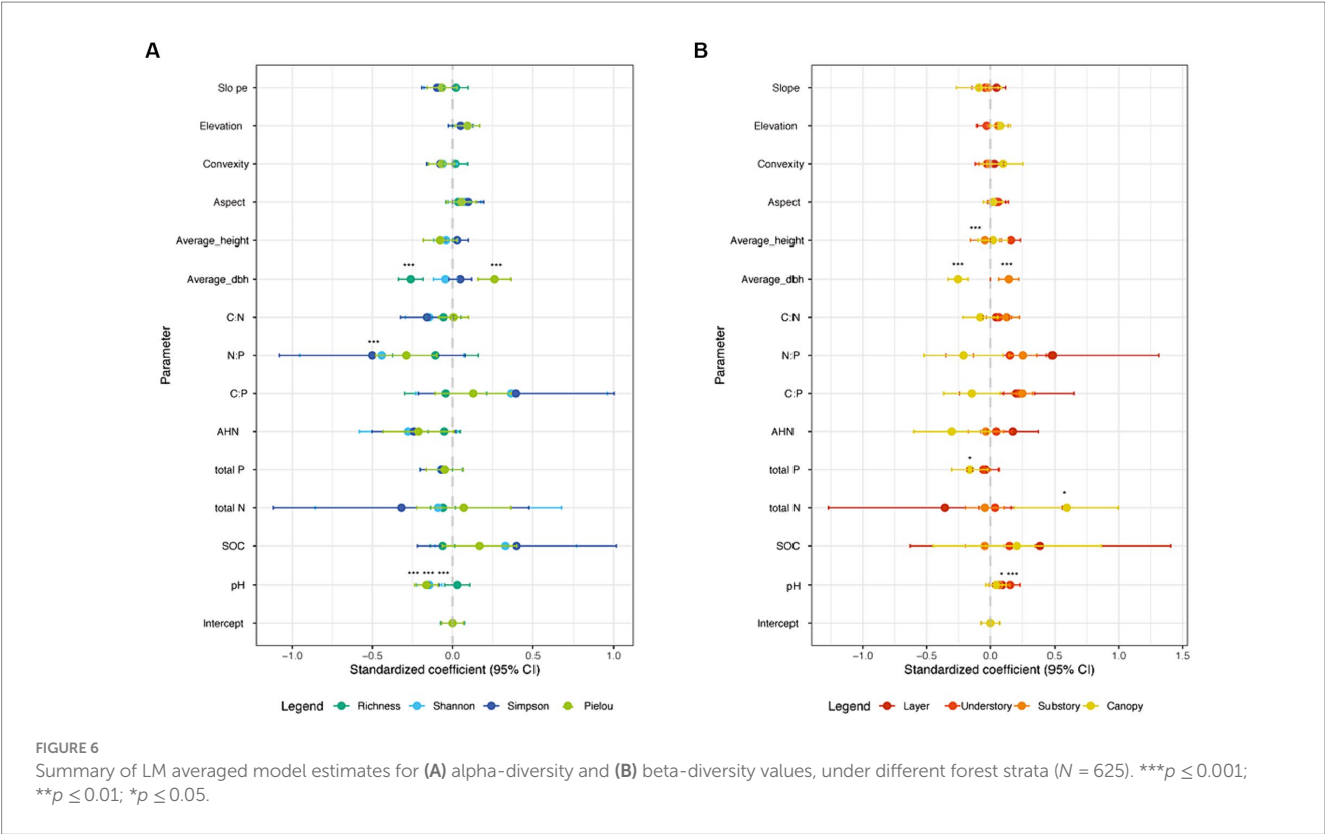**TABLE 2** Summary of LM averaged model estimates for alpha-diversity. ***p ≤ 0.001; **p ≤ 0.01; *p ≤ 0.05.

Covariate	Model 1 Richness	Model 2 Shannon	Model 3 Simpson	Model 4 Pielou
Average DBH	−0.26***(0.04)	0.00(0.04)	0.02(0.03)	0.26***(0.05)
Average height	-	−0.00(0.02)	0.00(0.01)	−0.04(0.05)
C:N	−0.01(0.04)	−0.13(0.09)	−0.13(0.10)	0.00(0.01)
N:P	−0.03(0.09)	−0.44(0.27)	−0.48(0.30)	−0.28**(0.10)
C:P	−0.02(−0.09)	0.13(0.25)	0.19(0.29)	0.02(0.07)
AHN	−0.01(0.03)	−0.26(0.16)	−0.24(0.13)	−0.21(0.11)
Total N	−0.01(0.02)	−0.02(0.18)	−0.08(0.25)	0.00(0.03)
Total P	-	−0.00(0.02)	−0.00(0.02)	−0.00(0.02)
SOC	−0.00(0.02)	0.21(0.24)	0.19(0.29)	0.07(0.11)
pH	0.01(0.01)	−0.15***(0.03)	−0.16***(0.04)	−0.16***(0.04)
Aspect	0.00(0.02)	0.03(0.05)	0.08(0.06)	0.01(0.04)
Convexity	0.00(0.01)	−0.01(0.03)	−0.01(0.03)	−0.04(0.05)
Elevation	-	0.01(0.02)	0.01(0.03)	0.09(0.04)
Slope	0.00(0.01)	−0.02(0.04)	−0.06(0.06)	−0.01(0.04)
Intercept	−0.00(0.04)	−0.01(0.04)	0.00(0.03)	0.00(0.03)

The value within closed bracket represents the standard error. AHN represents the alkaline hydrolysable nitrogen, C represents the soil organic carbon, N represents the total nitrogen and P represents the total phosphorus.

community in this study area is relatively low. The Kanas region is overall a typical boreal forest, with forest cover mostly dominated by a single species (Gauthier et al., 2015; Liu et al., 2021). Although our research in the Kanas region has also found coverage by multiple species, species richness is still at a lower level compared to tropical

and subtropical forest regions (Liu et al., 2020). This characteristic is largely attributed to the extreme environmental conditions prevalent in boreal regions, such as cold temperatures, short growing seasons, and nutrient-poor soils, which limit the diversity of plant species (Bonan, 1989; Venier et al., 2014). It suggests that the environmental

TABLE 3 Summary of LM averaged model estimates for LCBD. ***$p \leq 0.001$; **$p \leq 0.01$; *$p \leq 0.05$.

Covariate	Model 5 Layer	Model 6 Understory	Model 7 Substory	Model 8 Canopy
Average DBH	–	–	0.15***(0.04)	−0.25***(0.05)
Average height	–	0.16***(0.04)	−0.00(0.02)	0.00(0.01)
C:N	0.01(0.02)	0.01(3.54)	0.11(0.06)	−0.02(0.05)
N:P	0.07(0.23)	0.02(0.08)	0.19(0.12)	−0.08(0.14)
C:P	0.18(0.22)	0.18(0.11)	0.07(0.11)	−0.05(0.10)
AHN	0.18(0.10)	0.00(0.02)	−0.00(0.02)	−0.29(0.16)
Total N	--0.08(0.27)	0.00(0.02)	0.00(0.02)	0.56*(0.24)
Total P	−0.01(0.02)	−0.01(0.03)	–	−0.16*(0.08)
SOC	0.05(0.23)	0.03(0.08)	−0.00(0.02)	0.03(0.15)
pH	0.09* (0.04)	0.16***(0.04)	0.05(0.05)	0.01(0.02)
Aspect	0.01(0.03)	0.04(0.04)	0.00(0.01)	0.00(0.01)
Convexity	0.00(0.01)	−0.00(0.01)	−0.00(0.01)	0.06(0.08)
Elevation	−0.00(0.02)	−0.00(0.01)	0.03(0.04)	0.07 (0.05)
Slope	0.01(0.03)	−0.00(0.01)	−0.00(0.01)	−0.03(0.07)
Intercept	−0.00(0.04)	0.00(0.04)	0.00(0.04)	0.00(0.04)

The value within closed bracket represents the standard error. AHN represents the alkaline hydrolysable nitrogen, C represents the soil organic carbon, N represents the total nitrogen and P represents the total phosphorus.

conditions in the Kanas region may be particularly challenging for supporting a diverse array of species. This can inform targeted conservation strategies should aim at preserving and restoring biodiversity in boreal forest habitats, not only in the Kanas region but also in similar ecosystems globally.

Generally, the values of DBH noted living individuals also infer on the degree of competition between species communities (Yao et al., 2016; Lu et al., 2021). Among the two biological feature factors, average DBH had the highest interpretation power across various species richness and Pielou indices (Figure 5), which implies that tree species in the boreal forest exhibit strong species competition. This aligns with the Janzen-Connell hypothesis, when an individual is surrounded by high-density homogeneous neighbors, or when an individual is proximate to homogeneous neighbors, the strong intraspecific competition of host specific natural enemies for resources and infections will reduce recruitment and survival rate (Janzen, 1970). This provides more recruitment and survival space for other plant species, thereupon then regulating population dynamics and promoting species coexistence in vary plant communities (Janzen, 1970; Volkov et al., 2005; Yao et al., 2016).

Moreover, our study area showed that the value of total beta-diversity in the canopy and understory layers were slightly lower than the substory layer (Table 1), indicating that the species composition in the substory were more unique or distinctive compared to the average species composition of the entire area. The reason is the substory layer has access to abundant resources like light, water, and nutrients, compared to the shaded understory layers and resource-limited canopy layer (Gravel et al., 2010; De Lombaerde et al., 2019). As our results found the value of LCBD$_{und}$ higher than the LCBD$_{can}$ and LCBD$_{sub}$ (Figure 4), this may be owing to the chosen site itself, compared with other sites, which possibly result in a different species composition from other layers. Because the value of LCBD value express the level of ecological uniqueness of the site relative to other

sites within the specific area (Hill et al., 2011; Xia et al., 2022). The distribution of understory species is highly hinging on the niche process. Some studies have proved the strong relationship between biological factors (i.e., DBH and height), and this had a significant effect on LCBD in each vertical stratum of in our study area (He et al., 2022).

Particularly, our results tested that DBH had a significant effect on the variations of LCBD values in the canopy layer and substory layer (Table 3; Figure 6), and that soil pH value captured significant positive variations of LCBD$_{under.}$ This implies that subplots with complex environmental conditions and acidic soil conditions would increase the uniqueness of the species composition. Additionally, several studies have indicated that low soil P availability was associated with high species diversity, which was consistent with our findings that P had a significant negative correlation with LCBD in the canopy layer (Olde Venterink, 2011; Wu et al., 2019). This might be attributable to the fact that the survival of woody plants in the studied forest is generally nitrogen-phosphorus co-limited (Liu et al., 2021), which is consistent with previous studies reporting that species richness in a plant community under low soil fertility is primarily driven by competition for limited nutrient resources (Gravel et al., 2011; Sanaei et al., 2021; He et al., 2022).

With limited available knowledge, understanding the stability of both ecosystem structure and function is particularly vital for biodiversity conservation (Socolar et al., 2016). However, as the external environment (biotic and abiotic) in which biological communities live and exist in is not static, the spatial composition of biological communities will also change dynamically over time (Zhou et al., 2019; He et al., 2022). Therefore, abiotic factors such as soil environment and topography will inevitably affect biological community results, whether through potential direct or indirect pathways. In this study, we found that soil characteristics would indirectly affect the beta-diversity index of the community by affecting biotic variables, such as average DBH,
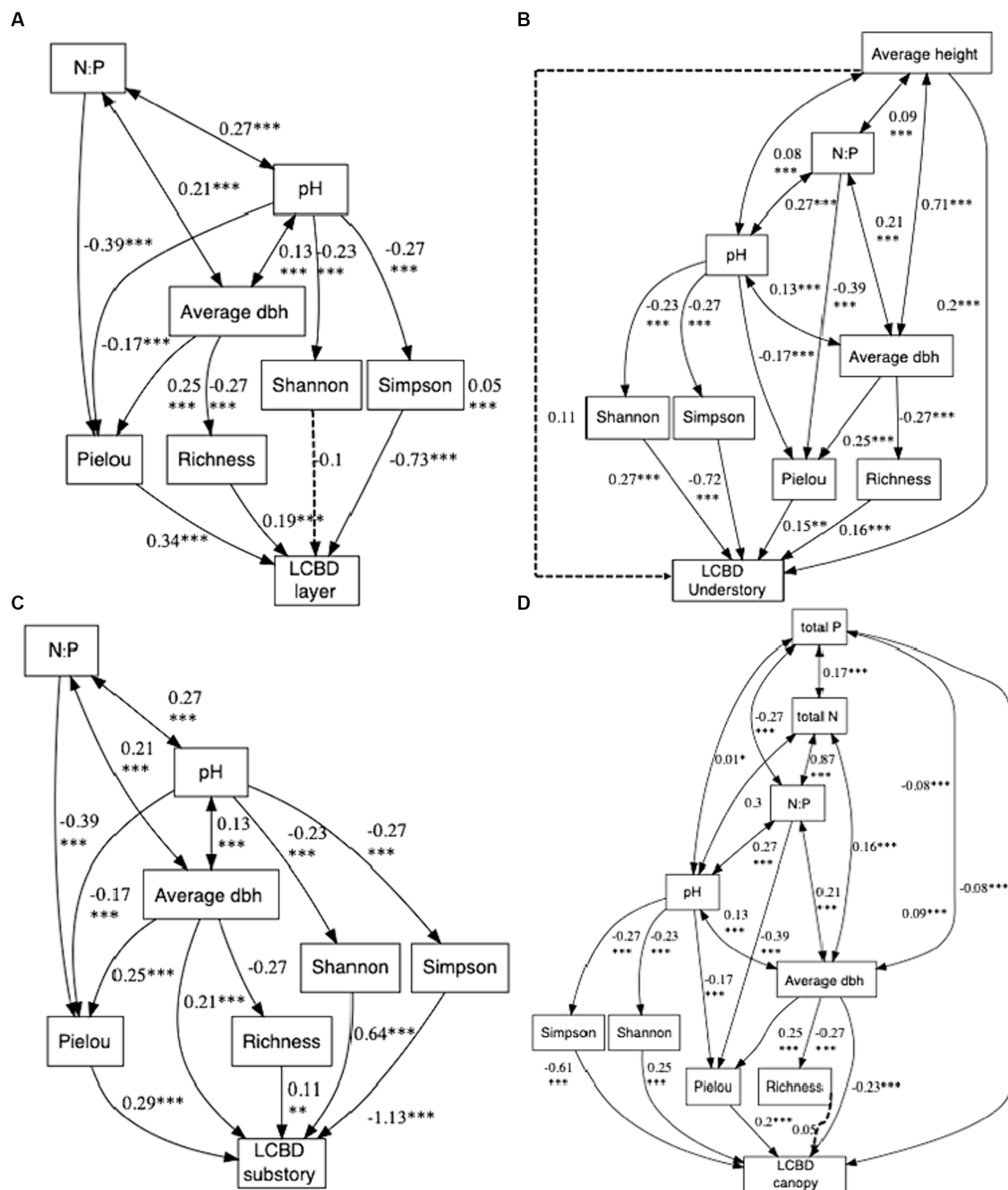
FIGURE 7
summarizes the results of path analysis on the LCBD (*N* = 625). Panel **A** illustrates the path analysis among influencing factors for all layer LCBDs, Panel **B** is for understory, Panel **C** is for substory, and Panel **D** is for canopy. Path estimates are standardized coefficients. The solid line indicates significant relationship between variables, and the dotted line insignificant relationship between variables. ***$p \leq 0.001$; **$p \leq 0.01$; *$p \leq 0.05$.

species richness and evenness (Figure 7). Indeed, plants absorb nutrients from the soil, thus would affect the growth rate of plant species in the community (Chen et al., 2022). Moreover, some studies have reported that soil pH could correlate with plant species richness at both regional and local scales (Ste-Marie and Pareâ, 1999). Being that the soil in our study area was slightly acidic, our study observations on alpha indices values of species diversity showed a significant negative trend with the gradual acidification of soil. This is may be due to low pH in the soil preventing germination or establishment of plants species, by obstructing roots from reaching the soil (Hill et al., 2011). Moreover, we found the SOC and AHN no significant effect on alpha

diversity and beta diversity indices. The influence of SOC and AHN on species diversity may vary depending on local site conditions and ecosystem characteristics (Dawud et al., 2016). Our study area may have specific soil and environmental conditions that influence the relative importance of different factors on species diversity, leading to nonsignificant contributions from SOC and AHN. Additionally, our study revealed that the influence of topographical variables on alpha and beta diversity was not statistically significant. This lack of significance could potentially be attributed to the limited spatial extent of our study area and the minimal variability in topographical changes (Japan et al., 2004).

In addition to abiotic factors, the value of LCBD can be also directly related to biotic variables, including average height, average DBH and alpha diversity (Figure 7). Larger DBH and height trees may imply an advantage in resource acquisition and ecological competition (Forrester, 2019). This could lead to their dominance at specific sites, exerting a greater influence on species composition and ecological processes at those locations, thereby increasing the LCBD value (Forrester, 2019). Previous studies have found that the values of LCBD are usually negatively correlated with species richness in broad-leaved forest ecosystem (He et al., 2022). This negative linkage indicates that the trade-off between species richness and ecological uniqueness can be take into account in conservation planning, since even species-poor communities can make great impact on the overall beta-diversity (Xia et al., 2022). Future conservation planning should aim to protect and manage these sites to preserve their distinct biodiversity, even if they have lower species richness.

5 Conclusion

In conclusion, our study sheds light on the patterns of species diversity within the boreal forests of Kanas, Xinjiang, northwest China. Concretely, our findings indicated that the negative linkage between average DBH and species richness, suggesting that areas with smaller DBH tend to harbor greater species richness. Furthermore, our analysis of beta-diversity demonstrated higher values in the substory layer compared to both the canopy and understory layers. Notably, average DBH and soil pH were found to influence alpha diversity indices, while average DBH, soil pH, average height, soil total nitrogen and soil total phosphorous affected beta diversity indices. Soil pH also indirectly influenced LCBD through mediating of alpha diversity indices. These findings provide crucial insights into species diversity patterns in boreal forests and offer valuable guidance for the protection of forest biodiversity in China. By understanding the ecological determinants driving species diversity, policymakers and forest managers can implement targeted conservation strategies to preserve the invaluable ecosystem services provided by boreal forests.

Data availability statement

The raw data supporting the conclusions of this article will be made available by the authors, without undue reservation.

Author contributions

WW: Conceptualization, Data curation, Funding acquisition, Investigation, Project administration, Resources, Software, Validation, Visualization, Writing – original draft, Writing – review & editing. JZ: Conceptualization, Formal analysis, Methodology, Software, Supervision, Writing – original draft, Writing – review & editing. BZ: Data curation, Investigation, Methodology, Writing – review & editing. GD: Data curation, Investigation, Methodology, Writing – review & editing. AM: Data curation, Investigation, Methodology, Writing – review & editing. ZG: Data curation, Investigation, Methodology, Writing – review & editing.

Funding

Acknowledgments

Conflict of interest

The authors declare that the research was conducted in the absence of any commercial or financial relationships that could be construed as a potential conflict of interest.

Publisher's note

All claims expressed in this article are solely those of the authors and do not necessarily represent those of their affiliated organizations, or those of the publisher, the editors and the reviewers. Any product that may be evaluated in this article, or claim that may be made by its manufacturer, is not guaranteed or endorsed by the publisher.

References

Araujo, R. F., Chambers, J. Q., Celes, C. H. S., Muller-Landau, H. C., dos Santos, A. P. F., Emmert, F., et al. (2020). Integrating high resolution drone imagery and forest inventory to distinguish canopy and understory trees and quantify their contributions to forest structure and dynamics. *PLoS One* 15:e0243079. doi: 10.1371/journal.pone.0243079

Bagchi, R., Henrys, P. A., Brown, P. E., Burslem, D. F. R. P., Diggle, P. J., Gunatilleke, C. V. S., et al. (2011). Spatial patterns reveal negative density dependence and habitat associations in tropical trees. *Ecology* 92, 1723–1729. doi: 10.1890/11-0335.1

Bao, S.N., (2000). *Soil agrochemical analysis*. Beijing: China Agricultural Press, 20–38.

Barrufol, M., Schmid, B., Bruelheide, H., Chi, X., Hector, A., Ma, K., et al. (2013). Biodiversity promotes tree growth during succession in subtropical forest. *PLoS One* 8:e0081246. doi: 10.1371/journal.pone.0081246

Barto, K, (2023). Package "MuMIn": Multi-Model Inference.Madison, USA: Springer.

Basham, E. W., Baecher, J. A., Klinges, D. H., and Scheffers, B. R. (2023). Vertical stratification patterns of tropical forest vertebrates: a meta-analysis. *Biol. Rev.* 98, 99–114. doi: 10.1111/brv.12896

Bates, D.M., (2005). lme4: mixed-effects modeling with R. R package version 1.47.5.

Bergamin, R. S., Bastazini, V. A. G., Vélez-Martin, E., Debastiani, V., Zanini, K. J., Loyola, R., et al. (2017). Linking beta diversity patterns to protected areas: lessons from the Brazilian Atlantic rainforest. *Biodivers. Conserv.* 26, 1557–1568. doi: 10.1007/s10531-017-1315-y

Bhat, J. A., Kumar, M., Negi, A. K., Todaria, N. P., Malik, Z. A., Pala, N. A., et al. (2020). Species diversity of woody vegetation along altitudinal gradient of the Western Himalayas. *Glob Ecol Conserv* 24:e01302. doi: 10.1016/j.gecco.2020.e01302

Bonan, G.B., (1989). *Environmental factors and ecological processes controlling vegetation patterns in boreal forests*, Landscape Ecology. SPB Academic Publishing, 3, 111–130,

Chang, Y., Zhong, Q., Yang, H., Xu, C., Hua, W., and Li, B. (2022). Patterns and driving factors of leaf C, N, and P stoichiometry in two forest types with different stand ages in a mid-subtropical zone. *Forest Ecosystem* 9:100005. doi: 10.1016/j.fecs.2022.100005

Chen, C., Nelson, A. S., Shaw, T., and Kimsey, M. (2022). Effects of fertilization on the growth dominance of inland northwest forests of the United States. *Forest Ecosystem* 9:100038. doi: 10.1016/j.fecs.2022.100038

Dawud, S. M., Raulund-Rasmussen, K., Domisch, T., Finér, L., Jaroszewicz, B., and Vesterdal, L. (2016). Is tree species diversity or species identity the more important driver of soil carbon stocks, C/N ratio, and pH? *Ecosystems* 19, 645–660. doi: 10.1007/s10021-016-9958-1

De Lombaerde, E., Verheyen, K., Van Calster, H., and Baeten, L. (2019). Tree regeneration responds more to shade casting by the overstorey and competition in the understorey than to abundance per se. *For. Ecol. Manag.* 450:117492. doi: 10.1016/J.FORECO.2019.117492

Dray, S., Pélissier, R., Couteron, P., Fortin, M. J., Legendre, P., Peres-Neto, P. R., et al. (2012). Community ecology in the age of multivariate multiscale spatial analysis. *Ecol. Monogr.* 82, 257–275. doi: 10.1890/11-1183.1

Forrester, D. I. (2019). Linking forest growth with stand structure: tree size inequality, tree growth or resource partitioning and the asymmetry of competition. *For. Ecol. Manag.* 447, 139–157. doi: 10.1016/J.FORECO.2019.05.053

Fox, J., and Weisberg, S. (2019). *An R companion to applied regression. 3rd Edn.* New York, USA: SAGE Publications.

Gauthier, S., Bernier, P., Kuuluvainen, T., Shvidenko, A. Z., and Schepaschenko, D. G. (2015). Boreal forest health and global change. *Science* 349, 819–822. doi: 10.1126/science.aaa9092

Gravel, D., Canham, C. D., Beaudet, M., and Messier, C. (2010). Shade tolerance, canopy gaps and mechanisms of coexistence of forest trees. *Oikos* 119, 475–484. doi: 10.1111/j.1600-0706.2009.17441.x

Gravel, D., Guichard, F., and Hochberg, M. E. (2011). Species coexistence in a variable world. *Ecol. Lett.* 14, 828–839. doi: 10.1111/j.1461-0248.2011.01643.x

He, R., Hu, M., Shi, H., Zhou, Q., Shu, X., Zhang, K., et al. (2022). Patterns of species diversity and its determinants in a temperate deciduous broad-leaved forest. *Forest Ecosystem* 9:100062.

Haq, S. M., Amjad, M. S., Waheed, M., Bussmann, R. W., and Proćków, J. (2022). The floristic quality assessment index as ecological health indicator for forest vegetation: a case study from Zabarwan Mountain range, Himalayas. *Ecol. Indicators* 145:109670. doi: 10.1016/j.ecolind.2022.109670

Haq, S. M., Khoja, A. A., Lone, F. A., Waheed, M., Bussmann, R. W., Mahmoud, E. A., et al. (2023a). Floristic composition, life history traits and phytogeographic distribution of forest vegetation in the Western Himalaya. *Front. Forests Glob. Change* 6:1169085. doi: 10.3389/ffgc.2023.1169085

Haq, S. M., Rashid, I., Waheed, M., and Khuroo, A. A. (2023b). From forest floor to tree top: partitioning of biomass and carbon stock in multiple strata of forest vegetation in Western Himalaya. *Environ. Monit. Assess.* 195:812. doi: 10.1007/s10661-023-11376-6

Haq, S. M., Waheed, M., Khoja, A. A., Amjad, M. S., Bussmann, R. W., Ali, K., et al. (2023c). Measuring forest health at stand level: a multi-indicator evaluation for use in adaptive management and policy. *Ecol. Indic.* 150:110225. doi: 10.1016/j.ecolind.2023.110225

He, C., Fang, L., Xiong, X., Fan, F., Li, Y., He, L., et al. (2022). Environmental heterogeneity regulates species-area relationships through the spatial distribution of species. *Forest Ecosystem* 9:100033. doi: 10.1016/j.fecs.2022.100033

He, R., Hu, M., Shi, H., Zhou, Q., Shu, X., Zhang, K., et al. (2022). Patterns of species diversity and its determinants in a temperate deciduous broad-leaved forest. *Forest Ecosystem* 9:100062. doi: 10.1016/j.fecs.2022.100062

He, C., Jia, S., Luo, Y., Hao, Z., and Yin, Q. (2022). Spatial distribution and species Association of Dominant Tree Species in Huangguan plot of Qinling Mountains, China. *Forests* 13:866. doi: 10.3390/f13060866

He, J., Lin, S., Kong, F., Yu, J., Zhu, H., and Jiang, H. (2020). Determinants of the beta diversity of tree species in tropical forests: implications for biodiversity conservation. *Sci. Total Environ.* 704:135301. doi: 10.1016/j.scitotenv.2019.135301

Hill, J. K., Gray, M. A., Khen, C. V., Benedick, S., Tawatao, N., and Hamer, K. C. (2011). Ecological impacts of tropical forest fragmentation: how consistent are patterns in species richness and nestedness? *Phil. Trans. Royal Soc. B* 366, 3265–3276. doi: 10.1098/rstb.2011.0050

Huang, Houyun, (2021). linkET: everything is linkable. R package version 0.0.3.

Irl, S. D. H., Harter, D. E. V., Steinbauer, M. J., Gallego Puyol, D., Fernández-Palacios, J. M., Jentsch, A., et al. (2015). Climate vs. topography - spatial patterns of plant species diversity and endemism on a high-elevation island. *J. Ecol.* 103, 1621–1633. doi: 10.1111/1365-2745.12463

Jost, L., (2006). Entropy and diversity. *Oikos* 113, 363–375.

Janzen, D. H. (1970). Herbivores and the number of tree species in tropical forests. *Am. Nat.* 104, 501–528. doi: 10.1086/282687

Japan, S., Kubota, Y., Murata, H., and Kikuzawa, K. (2004). Effects of topographic heterogeneity on tree species richness and stand dynamics in a subtropical Forest in Okinawa Island, southern Japan. *J. Ecol.* 92, 230–240. doi: 10.1111/j.0022-0477.2004.00875.x

Legendre, P., and De Caceres, M., (2013). Beta diversity as the variance of community data: dissimilarity coefficients and partitioning. *Ecology Letters* 16, 951–963.

Legesse, A., and Negash, M. (2021). Species diversity, composition, structure and management in agroforestry systems: the case of Kachabira district, Southern Ethiopia. *Heliyon* 7:e06477. doi: 10.1016/j.heliyon.2021.e06477

Levine, J. M., Bascompte, J., Adler, P. B., and Allesina, S. (2017). Beyond pairwise mechanisms of species coexistence in complex communities. *Nature* 546, 56–64. doi: 10.1038/nature22898

Liu, P., Wang, W., Bai, Z., Guo, Z., Ren, W., Huang, J., et al. (2020). Competition and facilitation co-regulate the spatial patterns of boreal tree species in kanas of Xinjiang, Northwest China. *For. Ecol. Manag.* 467:118167. doi: 10.1016/j.foreco.2020.118167

Liu, L., Zeng, F., Song, T., Wang, K., and Du, H. (2020). Stand structure and abiotic factors modulate karst forest biomass in Southwest China. *Forests* 11:443. doi: 10.3390/F11040443

Liu, P., Wang, W., Bai, Z., Guo, Z., Ren, W., Huang, J., et al. (2021). Nutrient loads and ratios both explain the coexistence of dominant tree species in a boreal forest in Xinjiang, Northwest China. *Forest Ecol. Manag.* 491:119198. doi: 10.1016/j.foreco.2021.119198

Lu, M., Du, H., Song, T., Peng, W., Su, L., Zhang, H., et al. (2021). Effects of density dependence in an evergreen-deciduous broadleaf karst forest in Southwest China. *For. Ecol. Manag.* 490:119142. doi: 10.1016/j.foreco.2021.119142

Ma, M. A., and Liu, Y. M. (1994). Measurement of biotic community diversity. I. α diversity (Part 2). *Chin. Biodivers* 2:231–239 (in Chinese).

Mori, A. S., Shiono, T., Koide, D., Kitagawa, R., Ota, A. T., and Mizumachi, E. (2013). Community assembly processes shape an altitudinal gradient of forest biodiversity. *Glob. Ecol. Biogeogr.* 22, 878–888. doi: 10.1111/geb.12058

Oksanen, J., Blanchet, F. G., and Minchin, P. R., (2018). *Vegan: Community ecology package*. R package version 2.6.4.

Olde Venterink, H. (2011). Does phosphorus limitation promote species-rich plant communities? *Plant Soil* 345, 1–9. doi: 10.1007/s11104-011-0796-9

Ouyang, M., Tian, D., Pan, J., Chen, G., Su, H., Yan, Z., et al. (2022). Moso bamboo (*Phyllostachys edulis*) invasion increases forest soil pH in subtropical China. *Catena* 215:106339. doi: 10.1016/j.catena.2022.106339

Pielou, E. C., (1975). *Ecological Diversity*. Wiley, New York.

Phillips, L., Hall, P., Gentry, A. H., Sawyer, S. A., and Vasquez, R. (1994). Dynamics and species richness of tropical rain forests. *Proc. Natl. Acad. Sci.* 91, 2805–2809. doi: 10.1073/pnas.91.7.2805

Pyšek, P., Jarošík, V., Kropáč, Z., Chytrý, M., Wild, J., and Tichý, L. (2005). Effects of abiotic factors on species richness and cover in central European weed communities. *Agric. Ecosyst. Environ.* 109, 1–8. doi: 10.1016/j.agee.2005.02.018

Rosseel, Y. (2012). Lavaan: an R package for structural equation modeling. *J. Stat. Softw.* 48, 1–36. doi: 10.18637/jss.v048.i02

Sanaei, A., Yuan, Z., Ali, A., Loreau, M., Mori, A. S., Reich, P. B., et al. (2021). Tree species diversity enhances plant-soil interactions in a temperate forest in Northeast China. *For. Ecol. Manag.* 491:119160. doi: 10.1016/j.foreco.2021.119160

Shaheen, H., Aziz, S., Nasar, S., Waheed, M., Manzoor, M., Siddiqui, M. H., et al. (2023). Distribution patterns of alpine flora for long-term monitoring of global change along a wide elevational gradient in the Western Himalayas. *Glob. Ecol. Conserv.* 48:e02702. doi: 10.1016/j.gecco.2023.e02702

Socolar, J. B., Gilroy, J. J., Kunin, W. E., and Edwards, D. P. (2016). How should Beta-diversity inform biodiversity conservation? *Trends Ecol. Evol.* 31, 67–80. doi: 10.1016/j.tree.2015.11.005

Ste-Marie, C., and Pareâ, D. (1999). Soil, pH and N availability effects on net nitrification in the forest floors of a range of boreal forest stands. *Soil Biol. Biochem.* 31, 1579–1589. doi: 10.1016/S0038-0717(99)00086-3

Thakur, S., Negi, V. S., Dhyani, R., Bhatt, I. D., and Yadava, A. K. (2022). Influence of environmental factors on tree species diversity and composition in the Indian western Himalaya. *For. Ecol. Manag.* 503:119746. doi: 10.1016/j.foreco.2021.119746

Venier, L. A., Thompson, I. D., Fleming, R., Malcolm, J., Aubin, I., Trofymow, J. A., et al. (2014). Effects of natural resource development on the terrestrial biodiversity of Canadian boreal forests. *Environ. Rev.* 22, 457–490. doi: 10.1139/er-2013-0075

Volkov, I., Banavar, J. R., He, F., Hubbell, S. P., and Maritan, A. (2005). Density dependence explains tree species abundance and diversity in tropical forests. *Nature* 438, 658–661. doi: 10.1038/nature04030

Whittaker, R.H., (1960). Vegetation of the Siskiyou Mountains, *Ecological Monographs*, 30, 279–338. doi: 10.2307/1943563

Whittaker, R. H. (1972). Evolution and measurement of species diversity. *Taxon* 21, 213–251. doi: 10.2307/1218190

Wu, H., Xiang, W., Ouyang, S., Forrester, D. I., Zhou, B., Chen, L., et al. (2019). Linkage between tree species richness and soil microbial diversity improves phosphorus bioavailability. *Funct. Ecol.* 33, 1549–1560. doi: 10.1111/1365-2435.13355

Xia, Z., Heino, J., Yu, F., He, Y., Liu, F., and Wang, J. (2022). Spatial patterns of site and species contributions to β diversity in riverine fish assemblages. *Ecol. Indic.* 145:109728. doi: 10.1016/j.ecolind.2022.109728

Xie, F., Zhou, Q., Shi, H., Shu, X., Zhang, K., Li, T., et al. (2019). Species composition and community characteristics of a 25 ha forest dynamics plot in deciduous broad-leaved forest, Qinling mountains, north-Central China. *Biodivers. Sci.* 27, 439–448. doi: 10.17520/biods.2018326

Yao, J., Zhang, X., Zhang, C., Zhao, X., and Von Gadow, K. (2016). Effects of density dependence in a temperate forest in northeastern China. *Scientific Report* 6:32944. doi: 10.1038/srep32844

Zellweger, F., Braunisch, V., Morsdorf, F., Baltensweiler, A., Abegg, M., Roth, T., et al. (2015). Disentangling the effects of climate, topography, soil and vegetation on stand-scale species richness in temperate forests. *For. Ecol. Manag.* 349, 36–44. doi: 10.1016/j.foreco.2015.04.008

Zhou, Q., Shi, H., Shu, X., Xie, F., Zhang, K., Zhang, Q., et al. (2019). Spatial distribution and interspecific associations in a deciduous broad-leaved forest in north-Central China. *J. Veg. Sci.* 30, 1153–1163. doi: 10.1111/jvs.12805

Competition and density dependence in arid mountain forest stands: revealing the complex process from spatial patterns

Junlong Yang[1,2]*†, Jian Yu[3]†, Guangping Wang[1] and Xiaowei Li[1,4]*

[1]College of Forestry and Prataculture, Ningxia University, Yinchuan, China, [2]State Key Laboratory of Efficient Production of Forest Resources, Yinchuan, China, [3]School of Landscape Architecture, Jiangsu Vocational College of Agriculture and Forestry, Jurong, China, [4]State Key Laboratory Breeding Base of Land Degradation and Ecological Restoration of Northwest China, Ningxia University, Yinchuan, China

Understanding the spatial patterns and interaction of trees is crucial for exploring forest dynamics. However, limited research has explored the spatial pattern and interactions between adult trees and their offspring population in arid mountain forest ecosystems. We investigated the spatial distribution and interaction of recruitment, survival, and mortality at different size classes in the *Populus davidiana* forest in the Luoshan Mountains (Ningxia, China), to gain insights into its stand dynamics. (1) This demonstrated the characteristic shift from an aggregated to random distribution as seedlings grew and developed into adult trees. (2) The adult trees exhibited strong positive and weak negative spatial associations with seedlings and saplings, respectively, with an increasing spatial scale, yet both stages underwent stark transitions from negative (1–15 m scales) to positive (> 20 m scale) associations. (3) Generally, the closer the individual trees were to each other, the greater the negative impact of neighboring trees on the size of an individual tree. (4) Additionally, adult trees strongly increased the risk of seedling mortality across the spatial scale of 0–50 m. (5) Live seedlings were less than the dead ones around dead seedlings. There was a stronger aggregation of dead seedlings than live seedlings. Moreover, the density-dependent mortality in our study rejected the random mortality hypothesis. In summary, these results suggest that spatial separation occurs between dead and live seedlings of *P. davidiana*. Under adult trees, negative dependence plays an important role in the arid mountain forest recruitment. Our findings will contribute to the restoration and conservation of arid mountain forests and provide theoretical support for forest management.

KEYWORDS

arid mountain forest, spatial point pattern, *Populus davidiana*, density-dependent mortality, competition

Introduction

The patterns and scales of tree distribution influence forest structure and dynamics through complex interactions involving crown architecture differences between species (Haq et al., 2023), soil properties (Waheed et al., 2022), water availability constraints on tree height (Klein et al., 2015), disturbance effects (Zhang et al., 2022), and the integration of dynamics

across various spatial scales within forest ecosystems (Mitchell et al., 2023). Changing spatial patterns can strengthen or weaken interactions within and among tree populations, and between them and their environment (Kuehne et al., 2018). Several empirical studies have found that spatial patterns significantly influence forest recruitment rates (Yang et al., 2008; Hai et al., 2014; Rendenieks et al., 2022). In a forest, the spatial arrangement of different-sized stems within tree populations can influence competition for resources, which, in turn, affects tree growth and mortality rates (Beyns et al., 2021). In particular, stem aggregation or dispersion could explain the certain spatial processes observed (e.g., density dependence, thinning, and predation) in a forest through spatial point pattern analysis (Nguyen et al., 2022; Salas-Eljatib et al., 2022; Muñoz-Gallego et al., 2023).

The spatial point pattern analysis is a fundamental tool for exploring the spatial processes and patterns of an ecosystem (Illian et al., 2008). In a spatial point pattern analysis, every single tree can be considered a point (Ripley, 1976), which allows the estimate of the spatial distribution of individual trees mapped in a given area (Diggle, 2003; Wiegand and Moloney, 2004; Illian et al., 2008; Law et al., 2009; Wiegand and Moloney, 2014). Therefore, by analyzing spatial point patterns, we may infer certain properties or behaviors of related or underlying spatial processes involved (Baddeley et al., 2015; Xin et al., 2022). However, different ecological mechanisms and processes such as competition and disturbance may result in the same spatial patterns (Detto and Muller-Landau, 2013). Exploring the underlying ecological dynamics that drive these spatial patterns remains a significant challenge in ecology.

In forest stands, density dependence is an important mechanism that could change the spatial distribution of trees (Piao et al., 2013; Kuang et al., 2017; Miao et al., 2018; Ma et al., 2024). As the density of recruits increases beyond the maximum threshold that the environment can support, resource competition occurs. Thereafter, negative density dependence leads to a lower probability of survival close to parent trees. For instance, in pure Norway spruce forests in Switzerland, the small dead trees tend to gather close to large trees, and this aggregation effect decreases as the distance increases (Bianchi et al., 2021). A study of Japanese larch forests revealed that density dependence did not play a role, and the further away seedlings were from the seed tree, the greater their survival rates (Im et al., 2023). However, in tropical mountain rainforests, the densities of saplings and small and medium trees increased and then decreased with the distance from old-growth trees, which exhibited a consistent pattern of density dependence (Miao et al., 2018). In Barro Colorado Island forests, the research found a high probability of recruitment in the vicinity of adult trees of other species (Condit et al., 1992). Consequently, further research is needed to investigate whether density dependence is consistent across different forest stands and under various environmental conditions.

Arid mountain forests harbor a significant proportion of global biodiversity, acting as reservoirs for diverse species and providing essential ecosystem services such as soil protection and habitat creation (Zhang et al., 2023). In this study, we aimed to examine the arid mountain forest ecosystem of the Luoshan Mountains in Ningxia, northwest China, situated in the transitional zone between grassland and desert. The forest stands in this area are dominated by Qinghai spruce (*Picea crassifolia*), Chinese pine (*Pinus tabulaeformis*), and Aspen (*Populus davidiana*) (Liang, 2018). *P. davidiana*, a common

pioneer species that emerges in the aftermath of human disturbances, is known to function as effective sites for seedling recruitment (Bouchard et al., 2018). Unlike *P. crassifolia* and *P. tabulaeformis* (seedlings from seed germination), *P. davidiana* reproduces asexually through root sprouting, and this method can result in more dense individual trees around adult trees. We aimed to investigate how the spatial correlation of different sizes distributes in *P. davidiana* stands in this arid mountain forest. We also sought to determine whether there is density dependence between recruits and adult trees, and if the death of seedlings is random or density-dependent? Therefore, we aimed to answer these questions from five perspectives.

1 We use the univariate *O*-ring statistic $O_{11}(r)$ under the heterogeneous Poisson null model to analyze whether the spatial distributions of various *P. davidiana* size classes transition from an aggregated pattern to a uniform or random pattern. As tree sizes increase, stems should exhibit more regular spatial patterns at small scales, due to self-thinning resulting from competition (Salas-Eljatib et al., 2022).

2 Then, by using the bivariate *O*-ring statistic $O_{12}(r)$ under an antecedent condition null model (Wiegand and Moloney, 2004), we could analyze the spatial associations among different size classes. The antecedent condition null model conveys the relationships between living adult trees and saplings or seedlings (Wiegand et al., 1999), enabling us to examine the influence of adult trees upon seedlings and saplings across a range of spatial scales.

3 The mark-correlation functions could quantify the similarity or dissimilarity between neighboring trees in terms of their attributes (such as size, height, and biomass). Researchers can identify patterns of positive or negative associations among tree attributes at different spatial scales. Positive correlations indicate that similar tree attributes tend to cluster together, while negative correlations suggest a tendency for dissimilar attributes to be spatially segregated. By using mark-correlation functions $k_{m1m1}(r)$ under the independent marking null model, we could test the similarity of two neighboring trees separated by distance (Illian et al., 2008; Wiegand and Moloney, 2014).

4 The trivariate random labeling null model enables the study of how an extra (previous) pattern affects the processes associated with a distinctly identified pattern (Holík et al., 2021). Within this method, pairs of points are chosen based on a set distance r, with the initial point originating from the primary pattern (adult tree) and the subsequent point from another clearly defined pattern (whether the seedlings and saplings are dead or alive). The cumulative non-normalized r-mark correlation function $C^{cum}_{,,m2}$ based on a trivariate random labeling null model was applied to examine the impact of living adult trees on seedling mortality (Wiegand, 2014).

5 We aimed to test the random mortality hypothesis, which posits that individual mortality events occur randomly in space (Wang et al., 2019). According to this hypothesis, spatial correlations between individual mortality events should not be observed, and the mortality of adjacent individual trees should not increase in response to neighborhood density. In contrast, we propose that the spatial positioning of individual trees may have an impact on the mortality of its neighboring trees. To test this alternative hypothesis, we employed the g12, g22-g11, and g2, 1 + 2-g1, 1 + 2 functions under the random labeling null model (Stoyan and Stoyan, 1994; Raventós et al., 2010; Wiegand and Moloney, 2014).

Methods

Study area

The study area is located in the Luoshan National Nature Reserve in the arid region of central Ningxia, China (37°11′–37°25′ N, 106°04′–106°24′ E). Since the Luoshan Mountains of the reserve are located within the ecotone between grassland and desert biomes, they provide a variety of species in this ecosystem. The reserve protects the arid mountain forest ecosystems (*Picea crassifolia*, *Pinus tabulaeformis*, and *Populus davidiana*) in Ningxia, northwest China. The elevation spans from 1560.0 m to 2624.5 m in the study area, with an average annual temperature of 8.8°C, annual precipitation ranging from 151.4 to 485.4 mm, and annual evaporation of 2,325 mm (Liang, 2018).
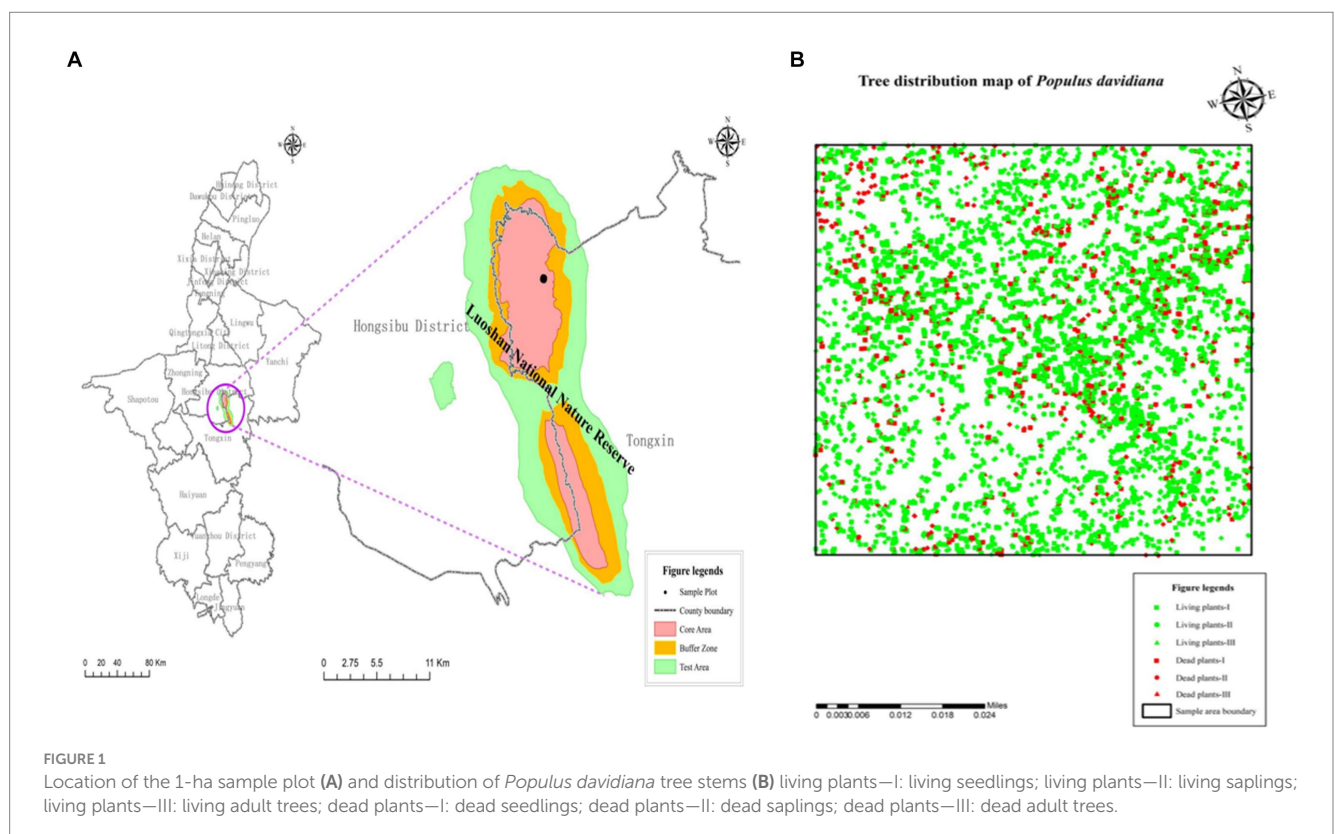
Data collection

In October 2022, a 100-m × 100-m plot (1 ha) was set up in a forest stand dominated by *P. davidiana* in the Luoshan National Nature Reserve. The geocoordinates of each tree were recorded using the real-time kinematic (RTK) GPS (Hi-Target, D8 VR, China), along with the measurements of their diameter of breast height (DBH) and seedling basal diameter, as well as their status (live or dead). A total of 6,830 individual trees were surveyed in the plot (see Figure 1). Based on the size of *P. davidiana*, the conspecific individual trees in the sampled population were divided into three size classes as a proxy of growth stages: seedling, DBH ≤ 6 cm; sapling, 6 cm < DBH ≤ 15 cm; and adult tree, DBH > 15 cm.

Data analysis

Ripley's K or L function is a method used to analyze the spatial patterns of species in a circle of radius r centered at one point (Wiegand and Moloney, 2004; Getzin et al., 2006). However, as the radius increases, it includes information from all smaller scales, which can confound effects at large scales with those at small scales (Condit et al., 2000; Wiegand and Moloney, 2004; George et al., 2006). In contrast, O-ring statistics replaces circles with rings and uses the mean number of neighboring trees in a ring of radius r and ring width around an individual, isolating specific distance classes (Stoyan and Stoyan, 1994; Wiegand and Moloney, 2004). This allows for the analysis of spatial patterns deriving from ecological processes easily and intuitively. O-ring statistics includes both univariate and bivariate statistics, with univariate statistics used for analyzing the spatial pattern of one object and bivariate statistics used for analyzing the spatial association of two objects (Wiegand and Moloney, 2004).

Analysis 1

In our research, we utilized the univariate O-ring statistic $O_{11}(r)$ to examine the spatial distribution patterns of the size classes. To determine the basic null model for the univariate O-ring statistic, we first visualized the stem distribution of trees at different size classes. If there was no evidence of strong clustering (indicated by clearly visible clusters in the pattern), we chose complete spatial randomness (CSR) as the null model, which assumes that the spatial distribution of a given species is completely random and devoid of underlying biological processes (Ebert et al., 2016). However, the pattern was heterogeneous (e.g., only distributed in part of the plot) (Velázquez et al., 2016), therefore, we chose the heterogeneous Poisson null model

FIGURE 1
Location of the 1-ha sample plot **(A)** and distribution of *Populus davidiana* tree stems **(B)** living plants—I: living seedlings; living plants—II: living saplings; living plants—III: living adult trees; dead plants—I: dead seedlings; dead plants—II: dead saplings; dead plants—III: dead adult trees.

as an alternative to CSR. For univariate point patterns, $O_{11}(r)$ inside the envelope indicates a random distribution of trees at scale r; while $O_{11}(r)$ above the envelope's upper bound indicates clumping and $O_{11}(r)$ below the envelope's lower bound indicates regularity.

Analysis 2

For the bivariate O-ring statistic, we hypothesized that higher-size classes would inhibit the recruitment and growth of lower ones, but that lower-size classes would not affect higher ones. An antecedent condition null model randomizes the locations of the lower-size classes while keeping the locations of the higher ones constant (Cipriotti and Aguiar, 2005). Therefore, we utilized the bivariate pairwise correlation function $O_{12}(r)$ to analyze the spatial associations between different-sized individual trees of *P. davidiana* under the antecedent condition null model. In the correlation analysis, when $O_{12}(r)$ is inside the envelope, there is no significant correlation between the two size classes at scale r; when $O_{12}(r)$ is above the envelope's upper bound, the two size classes have a significant positive correlation at scale r; when $O_{12}(r)$ is below the envelope's lower bound, the two size classes showed a significant negative correlation at scale r (Wiegand and Moloney, 2004).

Analysis 3

In addition to point pattern locations, other information called "mark" such as the tree size can be analyzed. We choose an independent marking null model, which randomly shuffles the marks over all trees; thus, means sizes are independent of individual locations (Wiegand and Moloney, 2014). The influence of neighboring trees' size on individual growth could be analyzed using mark-correlation functions $k_{m1m1}(r)$ (Stoyan and Stoyan, 1994). When the $k_{m1m1}(r) > 1$, it indicates that two trees have a larger size than average when they are nearby (positive correlation); conversely, when $k_{m1m1}(r) < 1$, it means that individual trees tend to have a smaller size (negative correlation), and if $k_{m1m1}(r) = 1$, there is no significant correlation between individual trees (Illian et al., 2008; Wiegand and Moloney, 2014).

Analysis 4

Trivariate random labeling is useful for testing how an additional antecedent pattern influences the processes for producing marks in a qualitatively marked pattern (Wiegand, 2014). We calculated the cumulative non-normalized r-mark correlation function $C^{cum}_{.,m2}$ to estimate the proportion of dead seedlings among all seedlings that are located within a distance r of adult trees. This summary function explores the effect of an antecedent focal pattern (i.e., adult trees) on the process that distributes a qualitative mark (i.e., live as type 1 and dead as type 2) on a second pattern (i.e., seedlings). When the $C^{cum}_{.,m2}(r) > 1$, this indicates that adult trees increase the mortality of seedlings; conversely, when $C^{cum}_{.,m2}(r) < 1$, adult trees tend to increase the survival proportion, and if $C^{cum}_{.,m2}(r) = 1$, there is no mortality impact of seedlings coming from adult trees. Therefore, the influence of adult trees on the mortality of seedlings could be investigated by using cumulative non-normalized r-mark correlation function $C^{cum}_{.,m2.}$

Analysis 5

The test of the random mortality hypothesis under the random labeling null model.

1 Testing the spatial aggregation of live and dead trees.

$g_{21}(r)$ may be used to statistically analyze spatial patterns of tree survival and mortality (Goreaud and Pélissier, 2003). $g_{21}(r)$ falls below

a simulation envelope when there are fewer dead neighboring trees at distance r from an arbitrary live tree than expected under the random labeling null model (Goreaud and Pélissier, 2003). This means that live and dead seedlings tend to be negatively correlated at distance r (i.e., segregated). Conversely, dead seedlings are considered positively correlated with dead seedlings when $g_{21}(r)$ lies above the envelope.

Furthermore, the function $g_{21}(r)$-$g_{22}(r)$ is applied to explore if the live seedlings around dead seedlings have the same density as the dead seedlings around the dead ones at scale r ($g_{21}(r)$-$g_{22}(r) = 0$). If $g_{21}(r)$-$g_{22}(r) > 0$, it indicates that the neighborhood density of live seedlings around dead seedlings outnumbers the dead seedlings around dead seedlings. If g $g_{21}(r)$-$g_{22}(r) < 0$, it suggests that there are fewer live seedlings than dead seedlings around the dead seedlings.

2 Comparing the clustering of live and dead trees.

The univariate functions g_{22} and g_{11} under the random labeling null model can show the clustering of dead (type 2) and live (type 1) seedlings, respectively. In this study, we examine which of those two clusters is denser by using the function g_{22}-g_{11}. If g_{22}-g_{11} falls above the envelope, it indicates dead trees are more clustered than surviving ones, and vice versa if g_{22}-g_{11} falls below the envelope.

3 Testing for density-dependent mortality of seedlings.

We employed the statistic $g_{2,1+2}$-$g_{1,1+2}$ to assess density-dependent mortality effects (Miao et al., 2018). This $g_{2,1+2}$-$g_{1,1+2}$ function compares the density of dead and live seedlings ($1 + 2$) around dead seedlings (pattern 2) and their density around live seedlings (pattern 1). Under the random labeling null model, the expected value is zero. However, under density-dependent mortality, we expect dead seedlings to occur more often in areas with high live seedlings density (i.e., $g_{2,1+2}$-$g_{1,1+2} > 0$).

Programita 2018 software was used to run every spatial two-dimensional coordinate analysis. For this purpose, the spatial scale was set to 0–50 m in the plot (step size: 1 m). In total, 199 Monte Carlo random simulations were performed to generate the 95% confidence envelopes; the goodness-of-fit (GoF) test was used to assess the ability of the null models to reflect the data (Loosmore and Ford, 2006). Both SPSS 25 and Excel 2007 were used for the statistical analysis of the data, while two other programs such as ArcGIS10.0 and Origin 2021 were used to graph the spatial trends found.

Results

Testing for environmental heterogeneity from spatial patterns of trees

As shown in Figure 2, the spatial Poisson distribution after removing environmental heterogeneity revealed that *P. davidiana* seedlings and saplings were aggregated at the smallest scale of 1 m and were then transitioned to a random distribution as the spatial scale increased (Figures 2A,B). Adult trees had a random distribution across all spatial scales investigated (0–50 m) (Figure 2C). This demonstrated the characteristic shift of aggregated distribution to random distribution with greater tree size.

Influence of adult trees on seedlings and saplings

Overall, the curve evidently above the upper envelope (Figure 3A) indicated that adult trees were positively correlated with seedlings at
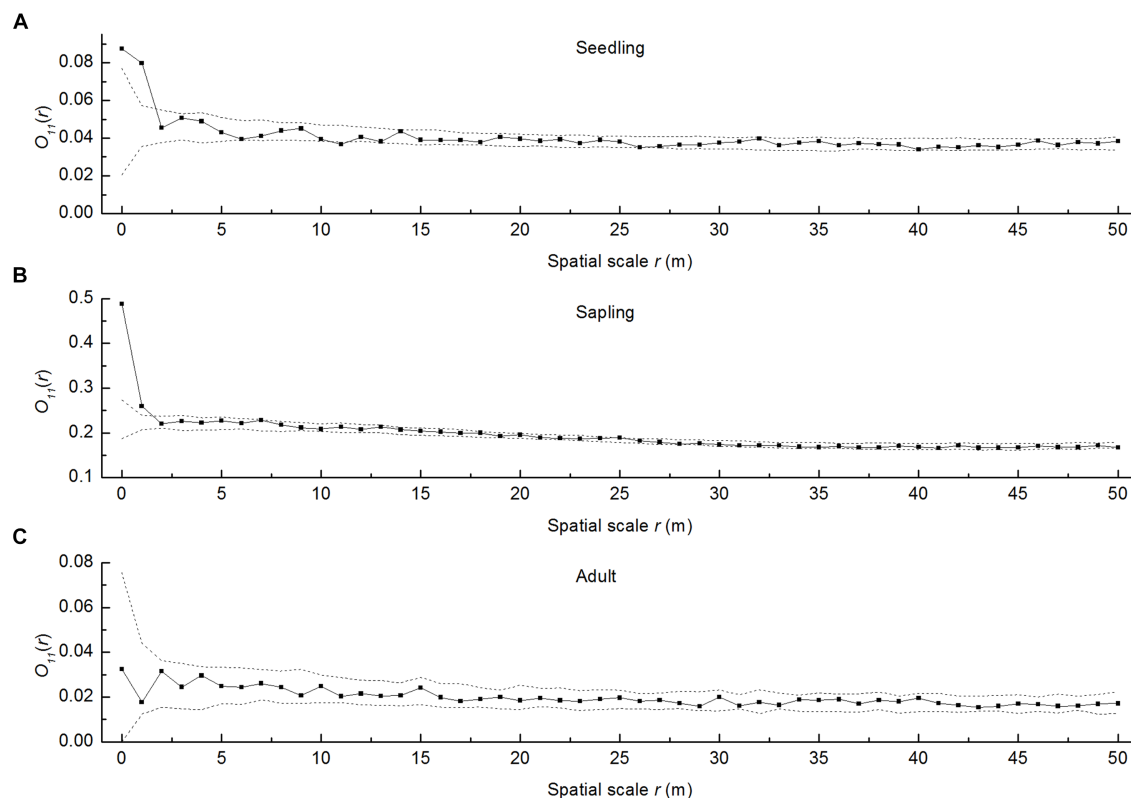
FIGURE 2
Spatial patterns of *P. davidiana* seedlings, saplings, and adult trees under the heterogeneous Poisson model. The solid lines indicate obtained values for the ring statistic $O_{11}(r)$; dashed lines indicate the upper and lower limits of the 95% simulation envelope for the heterogeneous Poisson null model. The points above an envelope indicate a cluster pattern, the points within an envelope indicate spatial independence, and the points below an envelope indicate a segregation pattern, **(A)** the seedlings of *Populus davidiana*; **(B)** the saplings of *P. davidiana*; **(C)** the adult trees of *P. davidiana*.

all spatial scales examined. However, adult trees and saplings were negatively correlated at scales of 1–14 m, beyond which their relationship was random (Figure 3B). Saplings and seedlings displayed a significant negative correlation at scales of 1–14 m, which shifted to a positive correlation beyond 20 m (Figure 3C). These results showed the existence of significant spatial differences and scale dependence in the spatial distribution of *P. davidiana* saplings and seedlings.

Mark-correlation function analysis

According to the mark-correlation functions $k_{m1m1}(r)$, the resulting trend of $k_{m1m1}(r)$ was below 1, indicating a significant negative correlation across scales of 0–50 m (Figure 4A), but this correlation diminished with increasing scale. This showed that *P. davidiana* trees were smaller in size than the average size around neighboring living trees. The closer the spatial distance between individual trees, the greater the negative impact on their size.

The impact of adult trees on seedling mortality was evaluated using the non-normalized r-mark correlation function $C^{cum}_{.,m2}$ under the trivariate random labeling null model. It revealed that adult trees augment the risk of seedling mortality at almost all distances (Figure 4B).

As shown in Figure 5A, the g_{21} trend indicated that the spatial association was mostly random between live and dead seedlings in the studied *P. davidiana* population. According to the results for the g_{21}-g_{11} function—testing whether the number of dead seedlings around live seedlings exceeds that around dead seedlings—there were

fewer live seedlings near dead seedlings than dead seedlings around the dead ones (Figure 5B), suggesting the aggregation of the latter. Furthermore, the g_{22}-g_{11} trend also showed a stronger aggregation for dead seedlings than for live seedlings (Figure 5C). In most spatial scale r, $g_{2,1+2}$-$g_{1,1+2} > 0$ convinced density-dependent mortality (Figure 5D), while rejecting the random mortality hypothesis.

Discussion

For Analysis1, our comparison of the spatial distributions $O_{11}(r)$ of different-sized *Populus davidiana* trees is consistent with earlier findings of Miao et al. (2009) and lends further support to the hypothesis that tree population's spatial distribution transitions from aggregated to random through ontogeny in most temperate forests.

Based on the spatial association results of $O_{12}(r)$, we found a high positive correlation between conspecific adult trees and seedlings (Analysis 2). This is easily explained because *P. davidiana* seedlings originate from root sprouts of reproductive individual trees and are therefore expected to exhibit strong positive spatial correlations with these adult trees (Qin and Shangguan, 2006). However, for Analysis 3, as the seedlings grow and recruit into saplings, the stem density-related limitations and greater competition for the resource (i.e., light, water, and nutrient) strongly influenced the distance and size of individual trees, especially asymmetrically vis-à-vis taller neighboring trees (Figure 4A). Therefore, at a spatial position away from adult trees
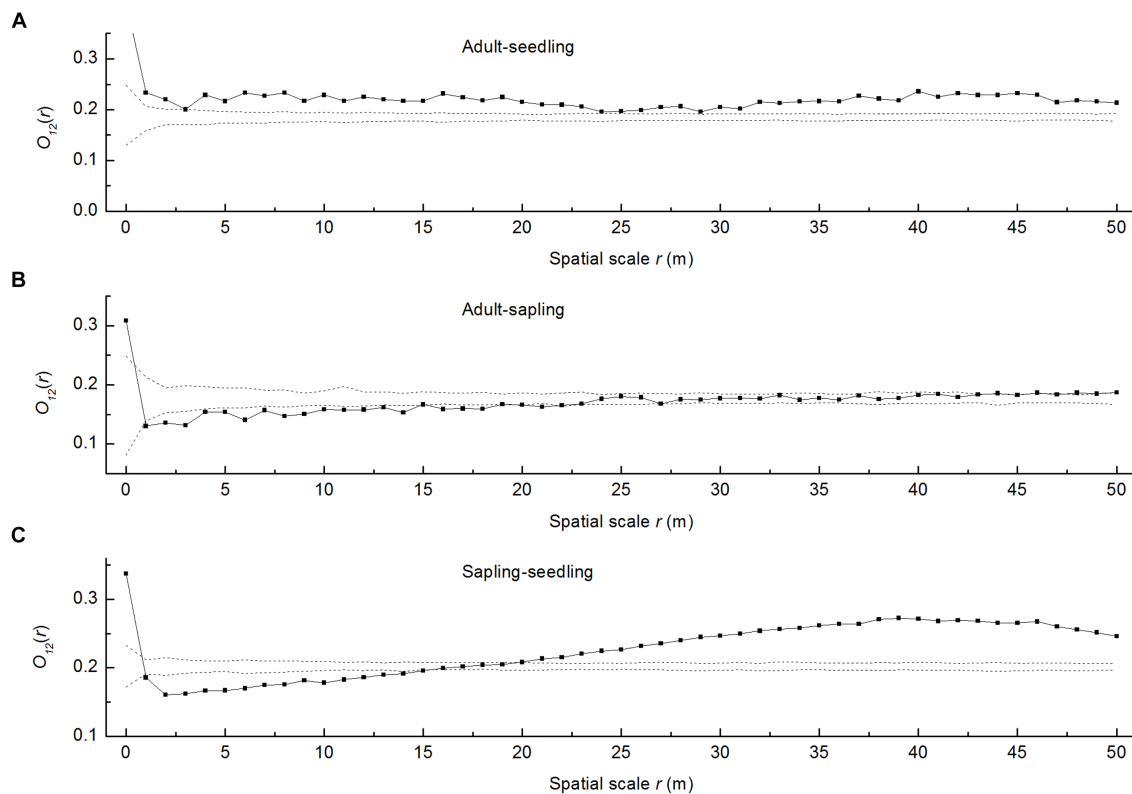
FIGURE 3
Spatial associations of *P. davidiana* adult trees, seedlings, and saplings. The solid lines indicate ring statistics $O_{12}(r)$; dotted lines indicate the upper and lower limits of the 95% simulation envelope of the heterogeneous Poisson null model. The points lying above the upper envelope indicate positive associations, the points lying between the envelopes indicate spatial independence, and the points lying below the lower envelope indicate negative associations, **(A)** Spatial association of adult trees to seedlings **(B)** Spatial association of adult trees to saplings **(C)** Spatial association of saplings to seedlings.

(1-14 m in our result, Figure 3B), seedlings tend to have a better potential to reach the sapling stage (Shao et al., 2011; Gao et al., 2014), which, in turn, enhances their prospects for adult recruitment into the canopy.

To explore the possible reasons for seedling mortality of *P. davidiana*, we hypothesized that it was the outcome of an excessively high local density, leading to intense intraspecific competition and self-thinning effects (Analysis 4 and Analysis 5). Although g_{21} did not detect a significant negative spatial correlation between dead and live seedlings, the function $g_{2,1+2} - g_{1,1+2} > 0$ indicated that the mortality of seedlings was density-dependent (Figure 5D). As a result of high-density seedlings from root sprouting, *P. davidiana* adult trees showed a positive association with seedlings (Figure 3A). Therefore, the seedling mortality is density dependent due to the presence of adult trees. The results from $C^{cum}_{.,m2}$ evidenced that adult trees contribute to a higher risk of seedling mortality that nonetheless declines with distance (Figure 4B). As seedlings were negatively correlated with saplings at both medium and small spatial scales, the initially high density of seedlings may have led to higher post-dispersal mortality risks faced by *P. davidiana* at the stage when its individual trees are most vulnerable. Thus, the closer the seedlings are to an adult tree, the stronger the negative conspecific impact in the form of higher mortality (Liang et al., 2016).

The g_{21}-g_{22} and g_{22}-g_{11} functions together discover the dead seedlings that emerged more cluster around dead ones and depart with live seedlings (Figures 5B,C). For *P. davidiana*, its dead seedlings display higher aggregation than the surviving seedlings, which

rejected the random mortality hypothesis. However, we did not investigate why having an excessive density of seedlings makes them prone to die off in a clustered spatial pattern. Additionally, we did not know the maximum density limit that causes mortality at the seedling. Seedling mortality is a result of a complex causes. At different scales, different dominant causes lead to their death. For instance, forest research on negative density-dependent dynamics in trees has confirmed that local high densities of the progeny of the same species could lead to disproportionately high levels of seedling mortality caused by soil pathogens (Janzen-Connell hypothesis) (Liu et al., 2007). Such a negative density-dependent feedback driven by the soil microbial community is actually common and ecologically important in many temperate tree species (Packer and Clay, 2000; Liang et al., 2016; Jevon et al., 2020). Moreover, Yamazaki et al. (2009) found that vertebrate herbivores (mainly rodents) were the major cause of mortality for large-seeded tree species, whereas the disease was most important for small-seeded species. Therefore, further investigation is needed on where and how the density impacts seedling mortality in arid mountain forests.

Conclusion

The spatial patterns of trees in an arid region, such as the Luoshan Mountains in China, are influenced by plant competition. To gain insights into the stand dynamics and guide regeneration
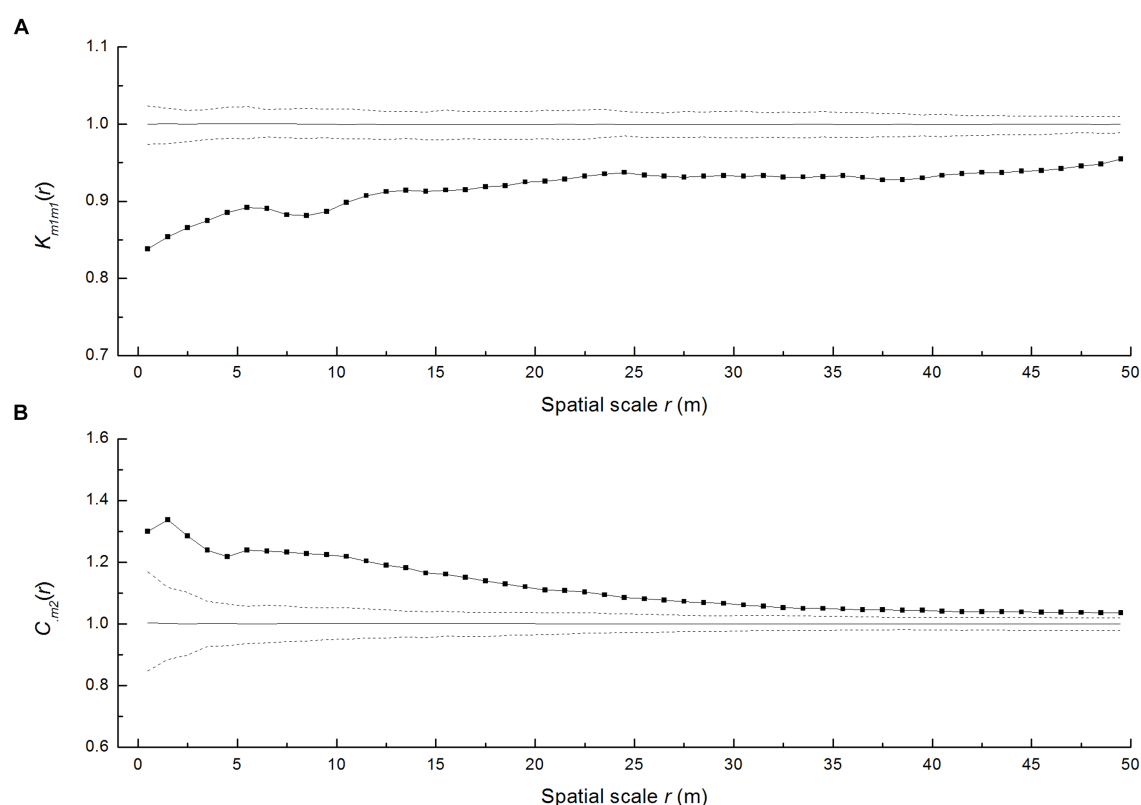
FIGURE 4
(A) Univariate mark function $k_{m1m1}(r)$ of *P. davidiana* and **(B)** trivariate random labeling on the mark-correlation function $C_{.m2}$ of *P. davidiana*. The solid line indicates the empirical curve, the gray line indicates the expected value under the random labeling null model, and the dashed lines indicate the limits of 199 Monte Carlo simulation envelopes.

strategies, we investigated the spatial distribution of individual trees at different growth stages (sizes) in *P. davidiana* forest in the Luoshan Mountains.

Spatial point pattern analysis confirmed that the spatial distribution of individual trees shifted from an aggregated distribution to random distribution as seedlings grew and developed into adult trees. Additionally, we found that more seedlings emerged around adult trees while high seedlings' mortality happened in clusters. Further research is arguably needed to elucidate the causes of *P. davidiana* mortality, and the close relationship between its adult trees, seedling density, and seedling mortality was prominent in this arid mountain forest.

Data availability statement

The raw data supporting the conclusions of this article will be made available by the authors, without undue reservation.

Author contributions

JuY: Conceptualization, Funding acquisition, Project administration, Software, Writing – original draft, Writing – review & editing. JiY: Funding acquisition, Resources, Writing – review & editing. GW: Investigation, Methodology, Visualization, Writing

– review & editing. XL: Conceptualization, Project administration, Resources, Writing – review & editing.

Conflict of interest

The authors declare that the research was conducted in the absence of any commercial or financial relationships that could be construed as a potential conflict of interest.
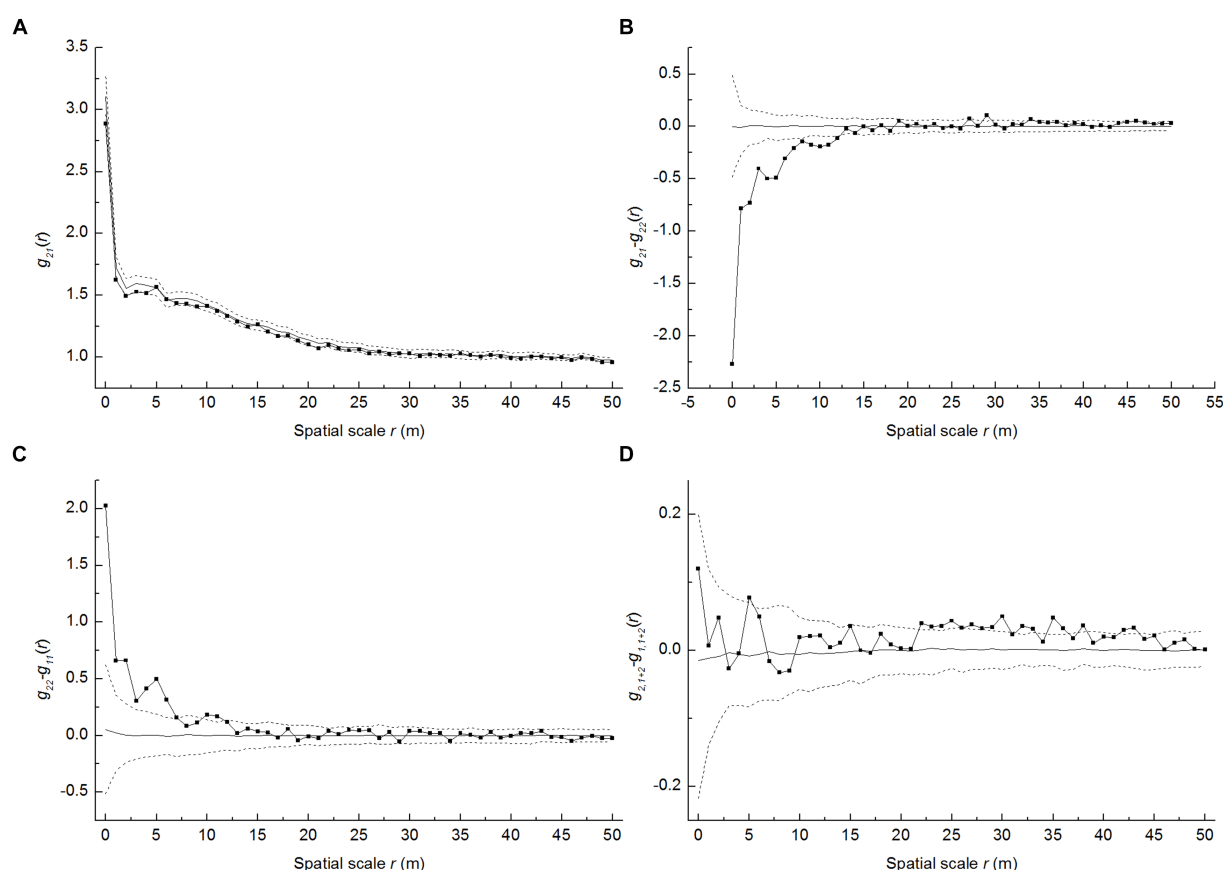
FIGURE 5
Spatial analysis of random mortality of *P. davidiana* seedlings. The solid line indicates the empirical curve, the gray line indicates the expected value under the random labeling null model, and the dashed lines indicate the limits of 199 Monte Carlo simulation envelopes, **(A)** g21 function of live and dead seedlings; **(B)** g21-g11 function of live and dead seedlings; **(C)** g21-g22 function of live and dead seedlings **(D)** g2,1+2-g1,1+2 function of live and dead seedlings.

Publisher's note

All claims expressed in this article are solely those of the authors and do not necessarily represent those of their affiliated organizations, or those of the publisher, the editors and the reviewers. Any product that may be evaluated in this article, or claim that may be made by its manufacturer, is not guaranteed or endorsed by the publisher.

References

Baddeley, A., Rubak, E., and Turner, R. (2015). *Spatial point patterns: methodology and applications with R-London*. New York: Chapman and Hall/ CRC Press.

Beyns, R., Bauman, D., and Drouet, T. (2021). Fine-scale tree spatial patterns are shaped by dispersal limitation which correlates with functional traits in a natural temperate forest. *J. Veg. Sci.* 32:e13070. doi: 10.1111/jvs.13070

Bianchi, E., Bugmann, H., Hobi, M. L., and Bigler, C. (2021). Spatial patterns of living and dead small trees in subalpine Norway spruce forest reserves in Switzerland. *For. Ecol. Manag.* 494:119315. doi: 10.1016/j.foreco.2021. 119315

Bouchard, H., Guittonny, M., and Brais, S. (2018). Early recruitment of boreal forest trees in hybrid poplar plantations of different densities on mine waste rock slopes. *For. Ecol. Manag.* 429, 520–533. doi: 10.1016/j.foreco.2018.07.003

Cipriotti, P. A., and Aguiar, M. R. (2005). Effects of grazing on patch structure in a semi-arid two-phase vegetation mosaic. *J. Veg. Sci.* 16, 57–66. doi: 10.1111/j.1654 -1103.2005.tb02338.x

Condit, R., Ashton, P. S., Baker, P., Bunyavejchewin, S., Gunatilleke, S., Gunatilleke, N., et al. (2000). Spatial patterns in the distribution of tropical tree species. *Science* 288, 1414–1418. doi: 10.1126/science.288.5470.1414

Condit, R. S. T. R., Hubbell, S. P., and Foster, R. B. (1992). Recruitment near conspecific adults and the maintenance of tree and shrub diversity in a neotropical forest. *Am. Nat.* 140, 261–286. doi: 10.1086/285412

Detto, M., and Muller-Landau, H. C. (2013). Fitting ecological process models to spatial patterns using Scalewise variances and moment equations. *Am. Nat.* 181, E68– E82. doi: 10.1086/669678

Diggle, P. (2003) *Statistical analysis of spatial point patterns, 2nd*. London: Arnold.

Ebert, A., Brito Da Costa, R., and Brondani, G. E. (2016). Spatial distribution pattern of Mezilaurus itauba (Meins.) Taub. Ex mez. In a seasonal forest area of the southern Amazon, Brazil. *IForest (Viterbo)* 9, 497–502. doi: 10.3832/ifor1427-008

Gao, L. S., Zhao, X. H., Wang, X. M., and Zhang, C. Y. (2014). Sexual differences in climatic response of dioecious Populus davidiana tree. *Ying Yong Sheng Tai Xue Bao* 25, 1863–1869.

George, L. W. P., Miller, B. P., and Enright, N. J. (2006). A comparison of methods for the statistical analysis of spatial point patterns in plant ecology. *Plant Ecol.* 181, 59–82. doi: 10.1007/s11258-006-9133-4

Getzin, S., Dean, C., He, F., Trofymow, J. A., Wiegand, K., and Wiegand, T. (2006). Spatial patterns and competition of tree species in a Douglas-fir chronosequence on Vancouver Island. *Ecography* 29, 671–682. doi: 10.1111/j.2006.0906-7590.04675.x

Goreaud, F., and Pélissier, R. (2003). Avoiding misinterpretation of biotic interactions with the intertype K12-function: population independence vs. random labelling hypotheses. *J. Veg. Sci.* 14, 681–692. doi: 10.1111/j.1654-1103.2003.tb02200.x

Hai, N. H., Wiegand, K., and Getzin, S. (2014). Spatial distributions of tropical tree species in northern Vietnam under environmentally variable site conditions. *J. For. Res.* 25, 257–268. doi: 10.1007/s11676-014-0457-y

Haq, S. M., Rashid, I., Waheed, M., and Khuroo, A. A. (2023). From forest floor to tree top: partitioning of biomass and carbon stock in multiple strata of forest vegetation in Western Himalaya. *Environ. Monit. Assess.* 195:812. doi: 10.1007/s10661-023-11376-6

Holík, J., Janík, D., and Adam, D. (2021). Light can modify density-dependent seedling mortality in a temperate forest. *J. Veg. Sci.* 32:e12992. doi: 10.1111/jvs.12992

Illian, J., Penttinen, A., and Stoyan, H. (2008). *Statistical analysis and modelling of spatial point patterns*. Chichester: John Wiley & Sons Ltd.

Im, C., Chung, J., Kim, H. S., Chung, S., and Yoon, T. K. (2023). Are seed dispersal and seedling establishment distance- and/or density-dependent in naturally regenerating larch patches? A within-patch scale analysis using an eigenvector spatial filtering approach. *For. Ecol. Manag.* 531:120763. doi: 10.1016/j.foreco.2022.120763

Jevon, F. V., Record, S., Grady, J., Lang, A. K., Orwig, D. A., Ayres, M. P., et al. (2020). Seedling survival declines with increasing conspecific density in a common temperate tree. *Ecosphere* 11:e03292. doi: 10.1002/ecs2.3292

Klein, T., Randin, C., and Korner, C. (2015). Water availability predicts forest canopy height at the global scale. *Ecol. Lett.* 18, 1311–1320. doi: 10.1111/ele.12525

Kuang, X., Zhu, K., Yuan, Z., Lin, F., Ye, J., Wang, X., et al. (2017). Conspecific density dependence and community structure: insights from 11 years of monitoring in an old-growth temperate forest in Northeast China. *Ecol. Evol.* 7, 5191–5200. doi: 10.1002/ece3.3050

Kuehne, C., Weiskittel, A., Pommerening, A., and Wagner, R. G. (2018). Evaluation of 10-year temporal and spatial variability in structure and growth across contrasting commercial thinning treatments in spruce-fir forests of northern Maine, USA. *Ann. For. Sci.* 75, 1–12. doi: 10.1007/s13595-018-0697-7

Law, R., Illian, J., Burslem, D., Gratzer, G., Gunatilleke, C. V. S., and Gunatilleke, I. A. U. N. (2009). Ecoogical information from satial patterns of plants: insights from point process theory. *J. Ecol.* 97, 616–628. doi: 10.1111/j.1365-2745.2009.01510.x

Liang, Z. (2018). Variation pattern of physicochemical properties along altitudes of Luoshan Mountain in Ningxia-world. *J. For.* 7, 19–31. doi: 10.12677/wjf.2018.71004

Liang, M., Liu, X., Gilbert, G. S., Zheng, Y., Luo, S., Huang, F., et al. (2016). Adult trees cause density-dependent mortality in conspecific seedlings by regulating the frequency of pathogenic soil fungi. *Ecol. Lett.* 19, 1448–1456. doi: 10.1111/ele.12694

Liu, D., Kelly, M., Gong, P., and Guo, Q. (2007). Characterizing spatial–temporal tree mortality patterns associated with a new forest disease. *For. Ecol. Manag.* 253, 220–231. doi: 10.1016/J.FORECO.2007.07.020

Loosmore, N. B., and Ford, E. D. (2006). Statistical inference using the g or K point pattern spatial statistics. *Ecology* 87, 1925–1931. doi: 10.1890/0012-9658(2006)87[1925:SIUTGO]2.0.CO;2

Ma, R., Li, J., Guo, Y., Wang, B., Xiang, W., Li, D., et al. (2024). Recruitment dynamics in a tropical karst seasonal rain forest: revealing complex processes from spatial patterns. *For. Ecol. Manag.* 553:121610. doi: 10.1016/j.foreco.2023.121610

Miao, N., Liu, S. R., Shi, Z. M., Yu, H., and Liu, X. L. (2009). Spatial patterns of dominant tree species in sub-alpine Betula-Abies forest in West Sichuan of China. *Ying Yong Sheng Tai Xue Bao* 20, 1263–1270.

Miao, N., Xu, H., Moermond, T. C., Li, Y., and Liu, S. (2018). Density-dependent and distance-dependent effects in a 60-ha tropical mountain rain forest in the Jianfengling mountains, Hainan Island, China: spatial pattern analysis. *For. Ecol. Manag.* 429, 226–232. doi: 10.1016/j.foreco.2018.07.013

Mitchell, J. C., Kashian, D. M., Chen, X., Cousins, S., Flaspohler, D., Gruner, D. S., et al. (2023). Forest ecosystem properties emerge from interactions of structure and disturbance. *Front. Ecol. Environ.* 21, 14–23. doi: 10.1002/fee.2589

Muñoz-Gallego, R., Wiegand, T., Traveset, A., and Fedriani, J. M. (2023). From seed dispersal service to reproductive collapse: density-dependent outcome of a palm–mammal interaction. *Oikos* 2023:e10002. doi: 10.1111/oik.10002

Nguyen, V. A. T., Blardoni, F., Manh, H. B., Schlicht, R., and Wagner, S. (2022). Disentangling the regeneration niche of Vatica odorata (Griff.) Symington using point pattern analysis. *Ecologies* 3, 336–360. doi: 10.3390/ecologies3030026

Packer, A., and Clay, K. (2000). Soil pathogens and spatial patterns of seedling mortality in a temperate tree. *Nature (London)* 404, 278–281. doi: 10.1038/35005072

Piao, T., Comita, L. S., Jin, G., and Kim, J. H. (2013). Density dependence across multiple life stages in a temperate old-growth forest of Northeast China. *Oecologia* 172, 207–217. doi: 10.1007/s00442-012-2481-y

Qin, J., and Shangguan, Z. (2006). Physiological-ecological effects of Populus davidiana--Quercus liaotungensis mixed forest in Ziwuling forest area. *Ying Yong Sheng Tai Xue Bao* 17, 972–976.

Raventós, J., Wiegand, T., and Luis, M. D. (2010). Evidence for the spatial segregation hypothesis: a test with nine-year survivorship data in a Mediterranean shrubland. *Ecology* 91, 2110–2120. doi: 10.1890/09-0385.1

Rendenieks, Z., Liepa, L., and Nikodemus, O. (2022). Spatial patterns and species composition of new forest areas present challenges for forest management in Latvia. *For. Ecol. Manag.* 509:120097. doi: 10.1016/j.foreco.2022.120097

Ripley, B. D. (1976). The second-order analysis of stationary point processes. *J. Appl. Probab.* 13, 255–266. doi: 10.2307/3212829

Salas-Eljatib, C., Riquelme-Alarcón, J., Donoso, P. J., Ponce, D., and Soto, D. P. (2022). Analysing changes in spatial point patterns: A proposal using data from a forest thinning experiment. *For. Ecosyst.* 9, 878–887. doi: 10.1016/j.fecs.2022.100081

Shao, F. L., Yu, X. X., Song, S. M., and Zhao, Y. (2011). Spatial structural characteristics of natural Populus davidiana - *Betula platyphylla* secondary forest. *Ying Yong Sheng Tai Xue Bao* 22, 2792–2798.

Stoyan, D., and Stoyan, H. (1994). *Fractals, random shapes and point fields. Methods of geometrical gtatistics.* - Chichester, Wiley.

Velázquez, E., Martínez, I., Getzin, S., Moloney, K. A., and Wiegand, T. (2016). An evaluation of the state of spatial point pattern analysis in ecology. *Ecography* 39, 1042–1055. doi: 10.1111/ecog.01579

Waheed, M., Arshad, F., Majeed, M., Fatima, S., Mukhtar, N., Aziz, R., et al. (2022). Community structure and distribution pattern of Woody vegetation in response to soil properties in semi-arid Lowland District Kasur Punjab, Pakistan. *Land* 11:2145. doi: 10.3390/land11122145

Wang, Q., Chi, X., Tang, Z., and Jiang, M. (2019). Analysing tree–neighbourhood interactions in ecotones of montane evergreen and deciduous forests in China. *J. Veg. Sci.* 30, 654–663. doi: 10.1111/jvs.12737

Wiegand, T. (2014). *User manual for the Programita software.*, Germany.

Wiegand, T., and Moloney, K. A. (2004). Rings, circles, and null-models for point pattern analysis in ecology. *Oikos* 104, 209–229. doi: 10.1111/j.0030-1299.2004.12497.x

Wiegand, T., and Moloney, K. (2014). *Handbook of spatial point-pattern analysis in ecology-USA.* Boca Raton, FL: Chapman and Hall/CRC Press.

Wiegand, T., Moloney, K. A., Naves, J., and Knauer, F. (1999). Finding the missing link between landscape structure and population dynamics: a spatially explicit perspective. *Am. Nat.* 154, 605–627. doi: 10.1086/303272

Xin, H., Jackson, T., Cao, Y., Zhang, H., Lin, Y., and Shenkin, A. (2022). Spatial pattern analysis of forest trees based on the vectorial mark. *J. For. Res.* 33, 1301–1315. doi: 10.1007/s11676-021-01417-6

Yamazaki, M., Iwamoto, S., and Seiwa, K. (2009). Distance- and density-dependent seedling mortality caused by several diseases in eight tree species co-occurring in a temperate forest. *Plant Ecol.* 201, 181–196. doi: 10.1007/s11258-008-9531-x

Yang, J., He, H. S., and Shifley, S. R. (2008). Spatial controls of occurrence and spread of wildfires in the Missouri Ozark highlands. *Ecol. Appl.* 18, 1212–1225. doi: 10.1890/07-0825.1

Zhang, Y., Tariq, A., Hughes, A. C., Hong, D., Wei, F., Sun, H., et al. (2023). Challenges and solutions to biodiversity conservation in arid lands. *Sci. Total Environ.* 857:159695. doi: 10.1016/j.scitotenv.2022.159695

Zhang, M., Wang, J., and Kang, X. (2022). Spatial distribution pattern of dominant tree species in different disturbance plots in the Changbai Mountain. *Sci. Rep.* 12:14161. doi: 10.1038/s41598-022-18621-x

Frontiers in
Forests and Global Change

**Informs and promotes sustainable management
of the world's forests**

An innovative journal that places forests at the
forefront of attention for scientists, policy makers
and the public. It advances our understanding of
how forests 'work', spanning from molecules to
ecosystems to the biosphere.

Discover the latest
Research Topics

See more →

frontiers | Research Topics